Cenozoic climate reconstructions via the prism of the organic geochemistry of IODP recovered sediments from the southern Pacific, northern Atlantic, and northern Indian Ocean

Sophia Aharonovich

A thesis submitted in fulfilment
of the requirements for the degree of
Doctor of Philosophy

2017

Department of Earth and Planetary Sciences
Faculty of Science
Macquarie University
Sydney, Australia

Statement of Authenticity

I hereby declare that this thesis entitled: "Cenozoic climate reconstructions via the prism of the organic geochemistry of IODP recovered sediments from the southern Pacific, northern Atlantic, and northern Indian Ocean" has not been submitted for the award of a higher degree at any other university or institution other than Macquarie University. I also certify that this thesis is an original piece of research that has been written by me and that the help in preparing this study and all sources used have been appropriately acknowledged. Four chapters are in the form of a series of in-preparation papers of which I am the primary author. Information on author and co-authors contribution are clearly stated for each of these chapters.

This thesis is a study sponsored by Macquarie University (Australia) and the Australian and New Zealand International Ocean Discovery Program Consortium (ANZIC) under the supervision of Prof. Simon George, Prof. Leanne Armand (Macquarie University, Australia), and Dr. Kelsie Dadd (Program Director of Curious Mind, Australia).

Sophia Aharonovich

Acknowledgements

This thesis is the product of a PhD project supervised by Prof. Simon C. George and co-supervised by A/Prof. Kelsie Dadd and A/Prof. Leanne Armand. This is the first PhD thesis from the Department of Earth and Planetary Sciences in collaboration with the Australia and New Zealand International Ocean Discovery Program Consortium (ANZIC). Analytical work for this research was funded by Macquarie University and by competitive ANZIC funding schemes. ANZIC supported my participation on board the JOIDES Resolution, a US drilling vessel, as an organic geochemist during the IODP Expedition 355 between March 31st and May 31st, 2015 . The thesis is a product of the department's organic geochemistry laboratory and group, led by Prof. Simon George. This thesis benefits from the organic geochemical expertise at Macquarie University and many international collaborations created during the IODP expeditions. These include Dr. Julius Lipp (MARUM, Germany), Prof. Peter Clift (Louisiana State University, USA), Prof. Sergio Ando (Milan–Bicocca University, Italy), A/Prof. Sarah J. Feakins (University of Southern California, USA), Prof. Stephan Steinke (University of Xiamen, China), Dr. Denise K. Kulhanek (Texas A&M University, USA), Dr. Manish Tiwari (National Centre for Antarctic and Ocean Research , India), and Prof. B. K. Kim (Pusan National University, Republic of Korea).

Abstract

This thesis presents detailed geochemical, hydrocarbon and biomarker analyses carried out on cored marine sediments from three International Ocean Discovery Program (IODP) Expeditions. IODP Expedition 313, New Jersey continental shelf, U.S. middle Atlantic margin (New Jersey–Delaware–Maryland), IODP Expedition 317, Canterbury Basin, New Zealand, and IODP Expedition 355, in the Arabian Sea, Indian Ocean. The three expeditions have been a focus of attention for an extensive study of eustasy, global climatic variations, and local tectonic activity controls on the regional depositional processes. The correlation between preserved organic matter in marine sediments and climate fluctuations has been widely discussed in the scientific community. While the ability to separate between influences of local and global events on the accumulated organic matter remains challenging, the current thesis aims to look into hydrocarbon and biomarker data from the three expeditions to compare these events.

The main purpose of IODP Expedition 317 was to compare the relative influence of local tectonics and global sea level changes on sediments accumulated on the continental shelf and slope off the east coast of the Southern Island of New Zealand. Cored sediments were recovered from Early Oligocene to Holocene sequences, with a particular focus on the sequence stratigraphy of the last 19 million years, when global sea level changes were dominated by glacio-eustasy. Sediments drilled in a transect of two sites on the continental shelf (Sites U1351 and U1353) and one on the continental slope (Site U1352) were used in two studies. The first study provided the first examination of the organic geochemical record from Sites U1351, U1352, and U1353 using bulk geochemistry together with hydrocarbon and biomarker distributions for early Oligocene to early Pliocene samples. Based on these it is suggested that local tectonic activity has had a rapid and significant influence on the accumulation of organic matter on the continental shelf and slope.

Samples for the second study were taken from early Oligocene to Holocene sediments from the same three drilling sites, with geochemical and lipid analysis carried out to identify the source of the organic matter, and reconstruct changes in sea surface temperature (SST), soil pH, and mean annual air temperatures (MAT) in the area influenced by local tectonic activity or global climatic events. A global climatic optimum and temperature increase at the early/middle Miocene boundary, combined with the increasing land mass of the sub-continent based on an increase in sedimentation rates since the middle Miocene, suggests gradual intensification in the amount of land vegetation. Interpretation of global eustatic and climatic

transformations confirms cooler Neogene SSTs were coupled with a decrease in global sea levels. A comparison study between IODP Expedition 317 Site 1352 samples and IODP Expedition 313 Sites M0027A and M0028A samples was performed. Overall, 43 samples from Expedition 313, dated from late Miocene to early Oligocene, were analysed for hydrocarbon and biomarker content. The hydrocarbon data as well as reconstructed SST, soil pH, and MAT from the New Jersey expedition were compared with results from 55 IODP Expedition 317 samples dated from early Oligocene to late Miocene. There is a decreasing SST trend from the early Miocene to the middle Miocene at both locations. Moreover, both sites show significant soil pH decreases during the mid-Miocene Climatic Optimum, and an increase in MAT during the same geological period.

The last research project is based on IODP Expedition 355 drilling Site U1456 samples from the Laxmi Basin, Arabian Sea. Multi-proxy data has enabled reconstruction of the evolving provenance of deep sea sediments in the basin, by the use of heavy minerals, bulk isotopic data, bulk and molecular geochemistry, and biomarker and compound specific isotope analyses. The results show that the Indus River was the main source of the sediment into the basin for the last eight million years. Palaeothermometry of the last ten million years based on glycerol dialkyl glycerol tetraethers (GDGTs) and long chain unsaturated alkenones show SST fluctuations during this time. Our data indicate a significant increase of C_3 vegetation input to the eastern Arabian Sea around 8 Ma, and increased erosion from the Himalayas around 6 Ma. Variation in precipitation patterns are shown by the δD data set as well as by other geochemical and biomarker parameters, and can be attributed to variation in Asian monsoon precipitation patterns.

The results show warm water environments for the first part of the Neogene and a significant temperature decrease in the SST in the New Zealand region from ~15 Ma that can be coupled with decrease in global sea levels. Comparison between New Jersey and New Zealand samples suggest strong eustatic influence for the New Jersey region and local tectonic influence on the organic matter accumulation in New Zealand during Miocene. At the same time, the Arabian sea data shows relatively warm late Miocene that is characterised by increasing precipitation levels influenced by Asian monsoon precipitation patterns.

Table of Contents

List of Figures

List of Tables

1. Introduction

Climate variations during the Cenozoic Era are a source of broad debate in scientific circles (Haq et al., 1987; Zachos et al., 2001), and of a great interest to the general public. Variations in global sea level (eustasy) as well as continental tectonic shifts are among the major factors influencing the climatic shifts for the last 65 million years (e.g., Vail and Mitchum Jr, 1979; Haq et al., 1987; Raymo and Ruddiman, 1992). Marine sediments contain a stratigraphic record of these shifts are usually well preserved. Organic material that accumulated in the marine sediments, including kerogen, organic compounds, and specific biomarkers from terrestrial and oceanic input, carries an imprint of the climate variations through its influence on living organisms.

Previous studies have shown strong correlations between variations in climate and tectonic activity (Kennett, 1977; Stickley et al., 2009; Passchier et al., 2013). In particular positioning of the Antarctic continent near the southern pole and its isolation after the opening of the Southern Ocean (Kennett, 1977) led to the start of massive ice accumulation on the eastern part of the continent from the Early Eocene to the Middle Miocene (e.g., Langebroek et al., 2010; Pross et al., 2012; Knorr and Lohmann, 2014). Development of the Antarctic Circumpolar Current (ACC) around Antarctica caused local cooling and further ice accumulation, and influenced global climate (Kennett, 1977). Low ACC temperatures influenced the global sea surface temperature (SST) by circulating cold water towards the Pacific, Atlantic, and Indian oceans.

The International Ocean Discovery Program (IODP) provides an opportunity to work on marine sedimentary records from around the globe using cored rocks and sediments. This PhD thesis is based on the recovery of organic biogeochemistry data from three expeditions. The sedimentary records worked on are from (1) IODP Expedition 317, Canterbury Basin, New Zealand, (2) IODP Expedition 313, New Jersey continental margin, and (3) IODP Expedition 355, Arabian Sea Monsoon. The geological material analysed dates from the

Eocene to the Holocene from three different oceans (Mountain et al., 2010; Fulthorpe et al., 2011; Pandey et al., 2016). The results show major changes in organic matter input into recovered sediments influenced by local tectonic activity, eustasy, and global climate changes.

In addition to the continental isolation during the Cenozoic, two major continental collisions have occurred. The first one was when India and Asia collided, which started around the Eocene (Garzanti et al., 1987; Rowley, 1996). The collision started the uplift of the Tibetan plateau and the Himalaya mountains, causing the development of the global precipitation circulation system known as the Asian Monsoon (Kroon et al., 1991; Prell and Kutzbach, 1992) and the Thermohaline circulation (Wyrtki, 1961). This circulation system potentially had a huge influence on the global climate by decreasing Indian Ocean salinity levels by increasing precipitation around the Indian Ocean region, including in the western Himalayas, Indonesia, and India (Duplessy, 1992). The second major continental collision happened between the northern part of Africa and central Asia, leading to the separation of the Palaeo-Tethys Ocean into the Indian Ocean and Mediterranean Sea (Metcalfe, 2013). The disappearance of the big water mass in the west-northern part of the Indian Ocean caused aridification in the North African and Pakistan regions during the Late Miocene (Feakins and Eglinton, 2005).

1.1. Palaeoenvironmental research in the Cenozoic

The Cenozoic is the latest Era in Phanerozoic geological eras, and covers the last 66 million years (Cohen et al., 2013). The Cenozoic consist of three geological periods: the Paleogene (66.00–23.03 Ma), the Neogene (23.03–2.58 Ma), and the Quaternary (2.58–present). The Paleogene is subdivided into three epochs: the Paleocene (66.0–56.0 Ma), the Eocene (56.0–33.9 Ma), and the Oligocene (33.9–23.03 Ma). The Neogene is subdivided into two epochs:

the Miocene (23.03–5.33 Ma) and the Pliocene (5.33–2.58 Ma). The Quaternary is the most recent geological period and it is divided into two epochs: the Pleistocene (2.58 Ma – 11.7 thousand years ago [ka]) and the Holocene (11.7 ka to present) (Cohen et al., 2013). The Cenozoic era is characterised by significant climate variations (Zachos et al., 2001). The temperature variations were driven by different cycles. On the 10^5 to 10^7 year scale, tectonic activity is the major factor; and on the 10^4 to 10^6 years scale, climatic cyclicity is driven by orbital processes (e.g., Ehrmann and Mackensen, 1992; Laskar et al., 1993; Crowley and Burke, 1998).

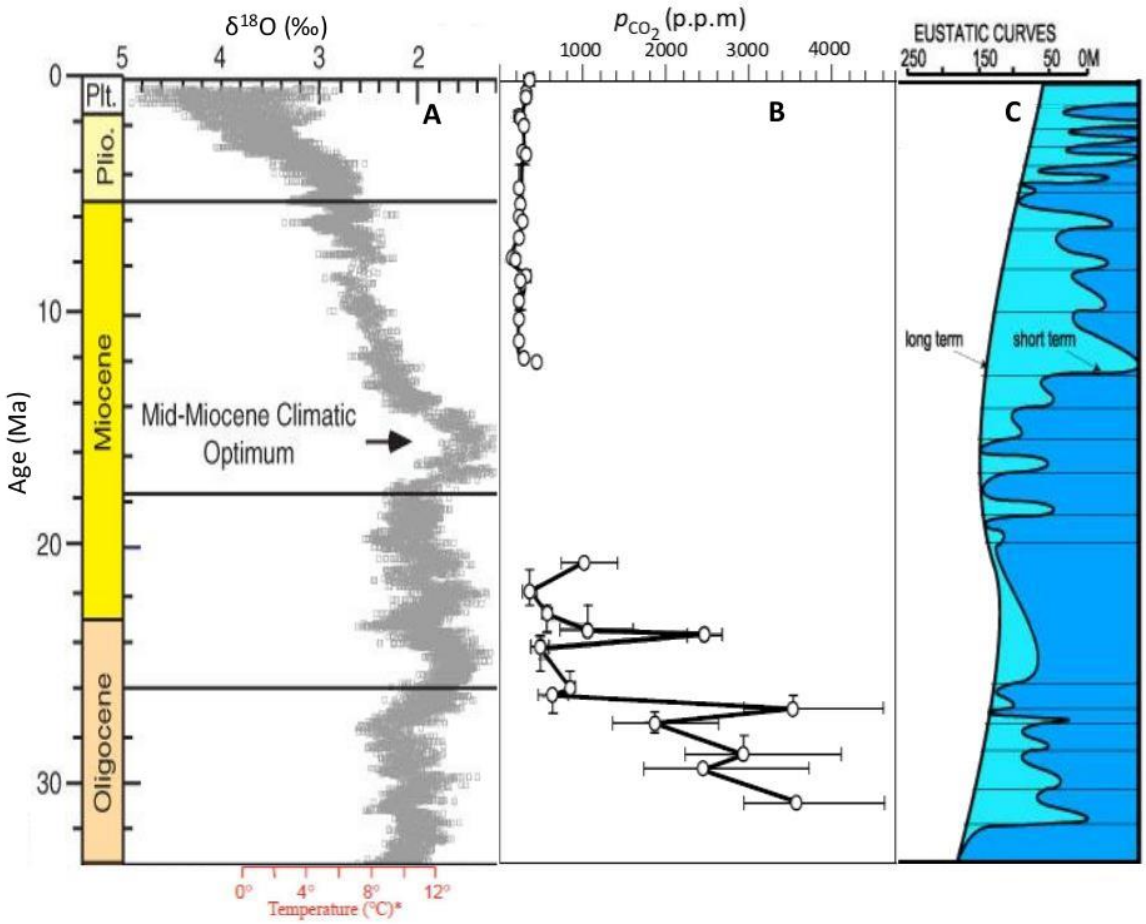

Figure 1.1: 30 Ma temperature variations recorded in deep-sea oxygen isotope records based from DSDP and ODP sites (**A**) (after Zachos et al., 2008); carbon dioxide levels in Cenozoic (**B**) (Pearson and Palmer, 2000); Cenozoic sea level curve (**C**) (Haq et al., 1987; Miller et al., 2005).

Global deep sea oxygen isotope ($\delta^{18}O$) measurements show a significant temperature decrease through the Cenozoic (Fig. 1.1), with several climatic optimums at every epoch showing temporary temperature increases (Zachos et al., 2008 and references within). The Cenozoic era from the early Oligocene is characterised by Antarctic ice sheets accumulation (Francis, 1988; Hambrey et al., 1992). Expansion of the Antarctic ice sheet started in the Oligocene, and was characterised by an increase of mass up to ~50% of today's levels. This accumulation caused cooling of the southern deep water currents followed by ~4ºC decrease in global ocean temperatures (Zachos et al., 1993; Zachos et al., 2001; Zachos et al., 2008). The Late Oligocene warming (Fig. 1.1) decreased Antarctic ice levels significantly, and it remained at this level until the end of the Middle Miocene Climatic Optimum (Miller et al., 1991). During this ten million year period the oceanic temperatures were slightly higher than before (Fig. 1.1) (Miller et al., 1991; Wright and Miller, 1993; Zachos et al., 2001; Zachos et al., 2008). The Southern Hemisphere ice expansion after the Middle Miocene Climatic Optimum was followed by intensification of Northern Hemisphere glaciation from ~2.7 Ma (Shackleton, 1977; Shackleton and Pisias, 1985; Vorren and Thiede, 1994). This accumulation was later called the Northern Hemisphere Glaciation (Shackleton, 1977; Shackleton and Pisias, 1985; Maslin et al., 1996).

The ice accumulation record in the Cenozoic was recorded through various proxies. For example, benthic foraminifera Mg/Ca ratios have been used to record changes in ocean temperature (Saraswat et al., 2005). In addition, the $\delta^{18}O$ deep ocean records provide a high resolution record through the Cenozoic (Billups et al., 2002; Bohaty and Zachos, 2003; Pälike et al., 2006). Variations in $\delta^{18}O$ have been attributed to variations in ocean temperature and ice accumulations. Heavy $\delta^{18}O$ values have been attributed to low temperatures and a synchronous increase in ice volume (Billups et al., 2002; Bohaty and Zachos, 2003; Pälike et al., 2006). Raymo et al. (1988), Berner (1990) and later on Pearson and Palmer (2000) suggest correlation between decreasing pCO_2 levels and global Cenozoic cooling. However, the

inability to correlate between pCO_2 levels and the cooling event around 22 Ma (Foster and Rohling, 2013; Foster et al., 2017) makes this theory rather controversial.

1.2. Eustasy

During geological history, the global sea levels varied significantly in a process called eustasy (Haq et al., 1987; Van Sickel et al., 2004). These variations played a major role in the climate evolution of the planet and in particular in the coastline development, creating a wider coast line during the low sea level periods. The coastline is the meeting point between the lithosphere, biosphere, and atmosphere, so is strongly affected by eustasy (Vail and Mitchum Jr, 1979). Therefore, it is important to understand the ways mass and energy are moving around. Distinguishing eustasy from the effects of subsidence and changing sediment supply requires a fundamental understanding of passive margin response to sedimentation, regional tectonic activity, and mantle dynamics in the area (Mountain et al., 2010). Although local tectonics play a major role in shaping the continental margins, it has been suggested that continental margins around the globe respond similarly to eustatic sea level variations (Bartek et al., 1991). Glacio-eustatic changes have been analysed through the $\delta^{18}O$ records (Miller et al., 1991; Miller et al., 1998; Miller et al., 2005), but these estimations are not precise (Miller et al., 2005; Mountain et al., 2010), mainly because of the problematic correlation between $\delta^{18}O$ based temperature reconstructions and the ice levels correlated to these fluctuations. Continental margin sediments have also been used to estimate eustasy levels (Vail and Mitchum Jr, 1979; Haq et al., 1987), but the full effect of eustasy on passive margins and continental shelves is still poorly understood The major factors influencing eustatic fluctuations are tectonic activity and mantle dynamics. Dating can also play a significant role in correlation between the events.

1.3. Total organic carbon

Organic carbon content in the marine environment is usually produced in situ by microalgae, or transported from the continents by rivers, wind, and ice (Brassell et al., 1978). Organic material can be of either direct or indirect biological origin, following the variation in the depositional processes. The organic matter (OM) can be incorporated directly into the sediment and used as precursors for various organisms, or may be modified by biological or chemical alteration during diagenesis (Summons, 1993).

The abundance of organic matter in sediments is usually expressed as dry weight percentage of total organic carbon (TOC). However, the correlation between measured TOC and abundance of organic matter in sediment can vary according to the characteristics of the organic matter and a conversion factor that can range between 1.7–1.9 (Tyson, 1995). In general, the relationship is characterised by decreasing the TOC from the continental shelf to the abyssal depths. However, these trends are heavily influenced by regional activity (Tyson, 1995).

There are numerous environmental factors that control TOC values in marginal sediments. Some commonly considered regional environmental factors include primary productivity, the biological and chemical content of the water column, the oxicity of the bottom water, the sediment accumulation rate and particle size, and bioturbation processes and post depositional processes (e.g. Henrichs, 1992, 1993; Meyers and Ishiwatari, 1993a, b).

One of the common ways to distinguish between primary TOC production and secondary terrestrial input is the relative presence of TOC and total nitrogen (TN) in the sediments (Henrichs, 1992; Meyers and Ishiwatari, 1993a). Marine organisms such as zooplankton (Prahl et al., 1980), benthic organisms (Prahl et al., 1980), diatoms (Meyers, 1990) and algae (Bourbonniere, 1980) have TOC/TN ratios <10, with typical values between 4 and 10, based on the lack of cellulose in the cells. In contrast, vascular land plants containing cellulose

common have a TOC/TN ratio of 20 or higher (Meyers and Ishiwatari, 1993a). Under ideal conditions, the continental shelf areas are characterised by high TOC/TN values, whereas the abyssal plain sediments will dominantly have TOC/TN values below 10.

1.4. Organic compounds and biomarkers

Organic compounds and biomarkers are produced by living organisms as part of biogeochemical cycles. They are abundant in oceans, lakes, and sedimentary rocks, but are often overlooked for palaeo-oceanographic reconstructions (Summons, 1993; Peters et al., 2005). The amount and diversity of organic compounds and biomarkers in sediments and rocks enables reconstruction of the regional palaeo-presence of specific organisms (e.g., Simoneit, 1977; Brassell, 1993; Meyers and Ishiwatari, 1993a; Meyers, 1997; Volkman et al., 1998).

Ideal palaeoclimatological biomarkers should fulfil several criteria: they must be unique to an organism or group of organisms that inhabit a specific ecological niche, and should be influenced by a single climatological variable such as SST or mean annual air temperature (MAT). The organic compounds should also have good preservation potential and undergo only slight geological alteration during deposition and post deposition. Ideally, biological function of these compounds in the pattern organism should be identified. The compounds should be deposited quantitatively and in high amounts that allow accurate measurements. Moreover, the transport mechanisms and diagenetic history of the compounds need to be well established. The biomarker signal should be analysed by known and well established techniques, which are reproducible in the laboratory under specific conditions (Peters and Moldowan, 1993; Rosell-Melé et al., 1994; Peters et al., 2005).

Several organic compounds fulfil most of the required conditions to be reasonable palaeoenvironmental indicators. Some compounds such as *n*-alkanes are recognised as the

structural compounds of plants and allow correlation between their abundance and source of the organic material (Bray and Evans, 1961; Eglinton and Hamilton, 1967). Others, such as hopanes and steranes can be attributed to different types of organisms and indicate palaeoclimatic variations through their presence or absence (Hedges and Oades, 1997). Biological sources of some lipids (e.g. alkenones and glycerol dialkyl glycerol tetraethers - GDGTs) are restricted to specific organisms and their production is influenced by environmental changes (Schouten et al., 2013). None of these compounds fulfil all the ideal biomarker requirements. Therefore, a multi-proxy approach of multiple biomarker analyses together with other organic geochemical, stratigraphical, and palaeo-lithological data are the strongest tools for carrying out palaeoenvironmental reconstructions. For chemical structure of the compounds see Appendix 6.1.

1.4.1. *n*-Alkanes

n-Alkanes are organic compounds constructed of a straight saturated chain of carbons. These compounds are very abundant and ubiquitous, and can be found in continental and marine sediments (Bray and Evans, 1961). *n*-Alkanes are structural compounds present in algae, bacteria, and land plant cell walls (Tissot and Welte, 1978). The length of the carbon chain produced by various organisms is different. The presence of long-chain odd-carbon numbered *n*-alkanes (C_{27}, C_{29}, and C_{31}) has been attributed to land-plant epicuticular waxes (Eglinton and Hamilton, 1967; Barnes and Barnes, 1978), whereas the presence of the C_{15} and C_{17} *n*-alkanes can be attributed to an algal/planktonic origin (Cranwell, 1984; Meyers and Ishiwatari, 1993b). Pelagic zooplankton have a dominant carbon chain length of C_{17}, C_{18}, or C_{24} (Giger et al., 1980). Studies of plants from submerged and floating ecosystems show high abundance of C_{21}, C_{23}, and C_{25} *n*-alkanes (Barnes and Barnes, 1978; Cranwell, 1984; Viso et al., 1993). Bacteria synthesise a variety of *n*-alkanes, but their abundance in sediments is

lower than from plants (Comet and Eglinton, 1987). Therefore, a bacterial origin of *n*-alkanes is usually neglected in favour of higher plants and algae. Because of the distinct difference between the higher plant and algae *n*-alkane distributions, it is possible to propose a main source of sedimentary input based on the predominance of specific chain lengths. There are also other potential sources of the ubiquitous *n*-alkanes in sedimentary environments, including from thermal maturation of kerogen, natural oil seeps and anthropogenic pollution.

It is common to assess *n*-alkane distributions using various indices and ratios such as the carbon preference index ($CPI_{(22\text{-}32)}$), terrigenous/aquatic ratio (TAR), relative abundance of submerged/floating aquatic macrophyte (P_{aq}), and average chain length (ACL). The relative odd-over-even carbon number preference for *n*-alkanes is shown by $CPI_{22–32}$ (Eq. 1). A $CPI_{22–32}$ <1 is indicative of a marine environment, whereas a $CPI_{22–32}$ >1 is a characteristic of terrigenous sources of OM. A $CPI_{22–32}$ around unity often indicates high thermal maturity of the sediment (Bray and Evans, 1961).

$$\text{Eq. 1} \qquad CPI_{(22-32)} = \frac{[C_{23}]+[C_{25}]+[C_{27}]+[C_{29}]+[C_{31}]}{[C_{22}]+2*\sum[C_{24-30\,even}]+[C_{32}]}$$

TAR (Eq. 2) is also based on the *n*-alkane carbon number distribution and has been applied to lacustrine (Bourbonniere and Meyers, 1996) and marine environments (Silliman et al., 2000). TARs < 1 indicate strong algal input, whereas higher values indicate a terrigenous OM predominance (Bourbonniere and Meyers, 1996):

$$\text{Eq. 2} \qquad TAR = \frac{C_{27}+C_{29}+C_{31}}{C_{15}+C_{17}+C_{19}}$$

The TAR might over-represent the absolute amount of terrigenous sources, assuming much higher *n*-alkane production by land plants (Cranwell, 1984; Meyers and Ishiwatari, 1993a).

The relative abundance of submerged/floating aquatic macrophyte input relative to the terrigenous input can be represented using the $1/P_{aq}$ ratio, that is defined after Ficken et al. (2000):

Eq. 3 $$1/P_{aq} = \frac{(C_{23}+C_{25}+C_{29}+C_{31})}{(C_{23}+C_{25})}$$

n-Alkanes have been used extensively as indicators of inputs of terrestrial or land derived organic matter to the marine environment (e.g., Kawamura, 1995; Ohkouchi et al., 1997; Huang et al., 2000; Zhao et al., 2003). Moreover, they have been used in lacustrine environments to infer changes in the relative inputs of organic carbon from aquatic algal sources (including eutrophication) and watershed terrestrial biota (Cranwell, 1973; Kawamura and Ishiwatari, 1985; Cranwell et al., 1987; Kawamura et al., 1987; Meyers and Benson, 1988; Meyers and Ishiwatari, 1993a). Therefore, these compounds give an insight to the relative contributions of organic carbon to a basin (lacustrine, coastal etc.) from algal versus terrestrial plant sources. Because of the multiple sources of *n*-alkanes they cannot be used as absolute environmental indicators. The abundance of *n*-alkanes can also be influenced by thermal maturation (Bray and Evans, 1961) as well as by post-depositional biodegradation processes (Wenger and Isaksen, 2002).

1.4.2. Isoprenoids

Isoprenoids are organic compounds build of two or more isoprene units of hydrocarbons. The isoprenoids play an important role in the physiological processes of animals and plants (Peters et al., 2005). For palaeoenvironmental research, the commonly used isoprenoids are pristane (2,6,10,14-tetramethylpentadecane; Pr) and phytane (2,6,10,14-tetramethylhexadecane; Ph). The phytyl side chain of chlorophyll in phototrophic organisms and bacteriophyll from purple sulfur bacteria have been suggested to be the main source for Pr and Ph (Powell and McKirdy, 1973). Anaerobic bacterial degradation (Rontani et al., 2010), thermal degradation (Lao et al., 1989) and clays can catalyse the decay of the chlorophyll phytyl chain (Rontani et al., 2010), leading to increased levels of Pr in sediments. Ph is known to be derived from

methanogens (Rowland, 1990), thermoacidophilic archaea (Tornabene et al., 1979), from anaerobic biodegradation (Grossi et al., 1998), and clay catalysed thermal hydrogenation of isoprenoid alkenes (Gelin et al., 1995).

The relative abundance of Pr and Ph is related to the oxicity of the depositional environment (Didyk, 1978). Pr/Ph < 0.8 is associated with anoxic depositional environments, whereas Pr/Ph > 3.0 usually correlates with oxic depositional environments or terrigenous plant input deposited under oxic or suboxic conditions (Didyk, 1978). The ratio can be positively influenced by high thermal maturity as well (Connan, 1974).

1.4.3. Hopanes, tricyclic terpanes, and tetracyclic terpanes

C_{27} 17α-trisnorhopane (Tm) and C_{27} 18α-trisnorneohopane (Ts) are commonly used as biomarkers for evaluation of thermal maturity (Seifert and Moldowan, 1978; Stephens and Carroll, 1999; Nuzzo et al., 2012). In general, Tm is less thermally stable than Ts. Therefore, the Ts/(Ts+Tm) ratio increases with increasing thermal maturity. Moldowan et al. (1986) showed that the source of OM during early diagenesis can significantly influence the ratio. Moreover, Ts abundance in basin sediments increases relative to Tm with depth in low thermal maturity sediments (Zhi-Hua et al., 1986). The ratio is also sensitive to clay-catalysed reactions.

Sediment thermal maturity levels are usually verified with additional ratios such as C_{31} and C_{32} αβ 22S/(22S+22R) hopanes, and C_{29} and C_{30} hopanes αβ/(αβ+βα (McKirdy et al., 1984). The terpane homohopane isomerisation [22S/(22S+22R)] for the C_{31} αβ homohopane homologues is highly sensitive to maturity variations in the immature to early oil generation range (Ensminger et al., 1975; Peters et al., 2005), when biologically-produced hopane precursors partially convert from 22R to 22S configuration. The ratio can be calculated for any hopane compounds in the C_{31}-C_{35} range, with equilibrium levels between 0.55–0.62

(Seifert and Moldowan, 1980). Co-elution between the C_{31}-homohopane 22R peak with C_{30}-neohopane can alter the calculated ratio (Subroto et al., 1991). Moreover, Peters and Moldowan (1991) show an increase in abundance of the 22R isomer for bitumens rather than for associated kerogen.

The relative abundance of the 17β,21α(H)-moretanes versus the 17α,21β(H)-hopanes for the C_{29} and C_{30} homologues is also used for thermal maturity characterisation. Both homologues are created from the biological 17β,21β(H)-configuration ($\beta\beta$) of hopanoids (Seifert and Moldowan, 1980), and the βα moretane is less stable than αβ configuration, so decreases with increasing thermal maturity. The C_{30} hopane αβ/(αβ+βα) ratio decreases in thermally mature rocks (Mackenzie et al., 1980; Seifert and Moldowan, 1980). The ratio partially depends on the source of the OM and has higher values for hypersaline environments (Rullkötter and Marzi, 1988). Some influence of terrigenous OM input on the ratio has also been suggested (Isaksen and Bohacs, 1995).

Some organism group-specific compounds such as oleanane and gammacerane are quite indicative biomarkers. Oleanane is a specific biomarker for angiosperm plant input (e.g., Peters, 1986; Moldowan et al., 1994). Its presence in a sediment suggests terrigenous input of the OM. Gammacerane is a specific biomarker for tetrahymanol in ciliates feeding on bacteria (Damsté et al., 1995). When gammacerane is present in high abundance it is indicative of a stratified water column and/or a sulphate-reducing environment. High values of the gammacerane/hopane ratio are indicative of marine carbonates, and the virtual absence of gammacerane is typical of deltaic shales (Peters et al., 2005).

The tricyclic terpanes (Connan, 1974; Aquino et al., 1983) with carbon chain $<C_{30}$ originate from regular isoprenoids (Aquino et al., 1983), and are attributed to the prokaryotic membrane structure (Ourisson et al., 1982). High concentrations of tricyclic terpanes have also been identified as indicators of primitive algae (Volkman et al., 1989; Azevedo et al.,

1992). With unknown specificity, C_{24} tetracyclic terpane, appears to be more resistant to biodegradation than hopanes (Trendel et al., 1982; Peters et al., 2005). Moreover, C_{24} tetracyclic terpanes are more stable in mature oils and sediments than hopanes. High C_{24} tetracyclic/C_{23} tricyclic terpane ratios (>0.6) are indicative of carbonate or evaporate depositional environments (Peters et al., 2005). A high C_{22}/C_{21} tricyclic terpane ratio can help to identify a carbonate source rock as well.

1.4.4. Steranes and diasteranes

Steranes are source-specific compounds. C_{27} steranes are produced by zooplankton, whereas C_{29} steranes were originally suggested to be derived from higher plants (Huang and Meinschein, 1979). Sediments containing high abundances of diatoms, dinoflagellates and coccolithophorids are typically rich in C_{28} steranes (Falkowski et al., 2004). The proportion of C_{28} steranes relative to C_{27} and C_{29} steranes tends to increase with decreasing geological age in the Mesozoic and Cenozoic (e.g. Grantham and Wakefield, 1988). It is now known that there is more complexity in the origins of steranes (e.g.Volkman, 1986, 2005). For example, C_{29} sterols are precursors of C_{29} steranes and have been identified in phytoplankton (Gagosian, 1976) and cyanobacterial mats (Volkman, 1986), as well as in green algal blooms (Kodner et al., 2008).

Despite the multiple biological sources, the use of the C_{27}–C_{28}–C_{29} sterane ternary plot diagram to determine the source of OM and oil-source correlations has been proven to be effective (e.g. Huang and Meinschein, 1979; Moldowan et al., 1985b; Grantham and Wakefield, 1988; Wójcik-Tabol and Ślączka, 2015). In addition, the C_{27}/C_{29} and C_{28}/C_{29} 5α,14α,17α(H) sterane ratios (abbreviated ααα) can be used to define diversification of zooplankton and phytoplankton assemblages (Moldowan et al., 1985a; Moldowan et al.,

1985b). C_{30} *n*-propylcholestanes, when present in sediments, indicates marine algae input (Moldowan et al., 1985b; Moldowan et al., 1985a)

The ratio of regular steranes [C_{27}, C_{28} and C_{29} ααα (20S + 20R) and αββ (20S + 20R) steranes] to αβ -hopanes (C_{29}–C_{33} pseudohomologues) provides information about the relative abundance of eukaryotic versus prokaryotic OM input. High sterane/hopane ratios suggest dominantly marine OM input from planktonic or benthic algae (Moldowan et al., 1985b; Moldowan et al., 1985a).

The C_{27} βα diasterane/C_{27} ααα sterane ratio provides additional information on the source rock. In general, low diasterane/sterane ratios are typical of carbonates or low clay content rocks, whereas high diasterane/sterane ratios indicate clay-rich and/or acid catalysed rocks (Moldowan et al., 1985b; Moldowan et al., 1985a; Peters et al., 2005). However, the diasterane/sterane ratio can be affected by increasing thermal maturation and/or heavy biodegradation (Seifert and Moldowan, 1978).

Thermal maturity related parameters can also be obtained from the isomerisation ratio of C_{29} ααα steranes when the 20S/(20S+20R) isomerisation values vary from 0 to 0.52–0.55 at thermal equilibrium (Seifert and Moldowan, 1986). Thermal maturity information can also be obtained from the C_{29} sterane αββ/(αββ+ααα) ratio, which reaches 0.52 in thermally mature samples (Seifert and Moldowan, 1986).

1.4.5. Alkenones- $U^{K'}_{37}$ and sea surface temperature (SST) calculations

Long-chain ethyl alkenones (alkenones) are long carbon chain (C_{37} and C_{38}) ketones with up to four degrees of unsaturation. Alkenones are synthesized by a limited number of haptophyte microalgae and are commonly used biomarkers in palaeo studies (De Leeuw et al., 1980; Volkman et al., 1980; Marlowe et al., 1984; Conte et al., 1994; Conte et al., 1995; Volkman et al., 1995). The most common biological source of alkenones is the coccolithophorid

Emiliania huxleyi (Volkman et al., 1980). However, this organism only appeared in geological records in the Quaternary, and became the dominant marine haptophyte in the last 50–70 kyr (Flores et al., 1997). Despite this, alkenones have been identified in Eocene sediments (~45 million years), which suggests additional biological precursors (De Leeuw et al., 1980; Volkman et al., 1980; Marlowe et al., 1984). The oldest alkenones have been identified in 100 Ma Cretaceous black shales (Farrimond et al., 1986). The producer of alkenones in pre 260 kyr sediments is not known. However, based on the co-occurrence of coccoliths and alkenones, Marlowe et al. (1990) speculated that species of *Reticulofenestra* may be a source organism.

The relative abundance in sediments of di-unsaturated long chain alkenone ($C_{37:2}$) and tri-unsaturated long chain alkenone ($C_{37:3}$) changes in a systematic way with inferred changes in SST (Marlowe et al., 1984; Brassell et al., 1986a; Brassell et al., 1986b). The temperature dependent nature of the alkenones has been observed in many different environments and regions (Prahl and Wakeham, 1987; Sikes and Volkman, 1993; Sikes et al., 1997; Müller et al., 1998; Sonzogni et al., 1998; Prahl et al., 2000; review by Herbert, 2001). The relative abundances of $C_{37:2}$ and $C_{37:3}$ alkenones are usually represented by $U^{k'}_{37}$ values (Eq. 5; Prahl and Wakeham, 1987):

$$\text{Eq. 4} \qquad U_{37}^{K'} = \frac{C_{37:2}}{C_{37:2}+C_{37:3}}$$

The $U^{K'}_{37}$ values have subsequently been converted into SSTs using an Indian Ocean calibration by Sonzogni et al. (1998); Eq. 6) and a global calibration described by Eglinton et al. (2006); Eq. 7):

$$\text{Eq. 5} \qquad SST(℃) = \frac{U_{37}^{K'} - (0.013 \pm 0.063)}{0.023 \pm 0.004}$$

$$n = 54;\ r^2 = 0.936;\ Temperature\ range\ (℃) = 5 - 30$$

Eq. 6 $$SST(℃) = 29.876\ (U_{37}^{K'}) - 1.334$$

$$n = 592;\ r^2 = 0.97;\ Temperature\ range\ (℃) = -1 - 29$$

The analytical error in these temperature reconstructions is ±1ºC.

Potential disadvantages of analysing alkenones with HPLC–MS could be changes in the relative sensitivity between the di- and tri-unsaturated compounds, and non-linear response factors, as observed with other MS methods, e.g. GC-CI-MS (Chaler et al., 2000; Chaler et al., 2003). However, the quantification limit of the method is ~10 pg, whereas for GC-MS and GC-FID it is generally in the ng range (Villanueva and Grimalt, 1997; Becker et al., 2013).

1.4.6. Glycerol dialkyl glycerol tetraethers (GDGTs)

At first, isoprenoidal glycerol dialkyl glycerol tetraether (iGDGT) lipids were considered to be only synthesised by archaea in extreme environments (De Rosa and Gambacorta, 1988). However, later studies have shown the presence of GDGTs in many phylogenetic Archaeal groups from lacustrine and marine environments without any correlation to extreme environments (Chappe et al., 1979; Chappe et al., 1982; Pauly and Van Vleet, 1986; Schouten et al., 2004).

Further technological development of analytical methods (Hopmans et al., 2000; Sturt et al., 2004; Becker et al., 2013) enabled identification of additional iGDGT groups and a crenarchaeol isomer (Sinninghe Damste et al., 2002)). brGDGTs have been suggested to be mainly derived from lacustrine and terrestrial bacteria and their abundance in marine sediments correlates to levels of terrestrial input through rivers as the main delivery mechanism (Schouten et al., 2002; Schouten et al., 2013). The abundance of brGDGTs has been correlated to environmental input (Pearson et al., 2004), soil pH (Weijers et al., 2007), mean annual air temperature (MAT; (Weijers et al., 2007), and SST (Hopmans et al., 2000;

Schouten et al., 2002; Sinninghe Damste et al., 2002; Kim et al., 2008; Kim et al., 2010; Becker et al., 2013; Schouten et al., 2013; Becker et al., 2015).

The source of the GDGTs in the ocean is mainly from archaea (Schouten et al., 2007; Schouten et al., 2012). It has been noted that the relative abundance of isoprenoidal GDGTs (iGDGTs) in the cell membrane is sensitive to the water temperature it grows in (for review Schouten et al., 2013). This observation enables correlation between SST to iGDGTs abundance using the TEX_{86}^{H} index (Schouten et al., 2002). In warm, tropical pools and coastal environments, the temperature dependence of iGDGT is controversial, and can be heavily influenced by the source of the OM (Hopmans et al., 2004; Schouten et al., 2013).

1.4.6.1. Isoprenoidal GDGTs – TEX^{H}_{86} and sea surface temperature calculations

The use of the TEX_{86} index for correlation between SST and iGDGT abundance was suggested by (Hopmans et al., 2000). The method was initially indicative of a rather limited temperature range, but more recently was recalculated for a wider environmental range (Kim et al., 2008; Kim et al., 2010). For subtropical and greenhouse periods, when temperatures were higher than today, the TEX_{86}^{H} can be calculated from the distribution of iGDGTs using the definition of Kim et al. (2010) for the 10°C to 40°C temperature range:

$$\text{Eq. 7} \qquad TEX_{86}^{H} = \frac{[GDGT-2]+[GDGT-3]+[Cren']}{[GDGT-1]+[GDGT-2]+[GDGT-3]+[Cren']}$$

where the number values refer to the number of rings in the GDGT, and Cren' refers to the crenarchaeol regio isomer. TEX_{86}^{H} can be converted to SST using the correlation for the 10°C - 40°C temperature range with a proposed residual standard error of ±2.5°C (Kim et al., 2010):

Eq. 8 $$SST = 68.4 \times TEX_{86}^{H} + 38.6 \ (r^2 = 0.87, n = 255, p < 0.0001)$$

iGDGT cyclisation can be calculated to evaluate the ring index (Pearson et al., 2004):

Eq. 9 $$Ring\ index = \frac{[GDGT-1]+2\times[GDGT-2]+3\times[GDGT-3]+4\times[GDGT-4]+5\times[Cren+Cren\prime]}{[GDGT-0]+[GDGT-1]+[GDGT-2]+[GDGT-3]+[GDGT-4]+[Cren+Cren\prime]}$$

1.4.6.2. Branched GDGTs – BIT, MBT, CBT, pH, and MAAT

To calculate the relative fluvial input of terrigenous organic matter in the marine environment the branched isoprenoid tetraether (BIT) index is calculated from the brGDGTs (Hopmans et al., 2004):

Eq. 10 $$BIT\ index = \frac{[GDGT-Ia]+[GDGT-IIa]+[GDGT-IIIa]}{[GDGT-Ia]+[GDGT-IIa]+[GDGT-IIIa]+[Cren]}$$

In samples with a BIT index >0.4, the SST reconstructions have been suggested to be problematic (Hopmans et al., 2004; Weijers et al., 2006). High terrigenous sediment input into marine environment introducing high terrestrial iGDGTs from rivers and lakes and altering the TEX^{H}_{86} . Therefore, if BIT index is >0.4, an additional 4ºC is added to the SST reconstruction error range (Weijers et al., 2006).

The methylation index of branched isoprenoid tetraethers (MBT) and the cyclisation index of branched isoprenoid tetraethers (CBT) can be calculated from the brGDGT abundance (Weijers et al., 2007):

Eq. 11 $$MBT = \frac{[GDGT-I]}{\sum[GDGT-I]+\sum[GDGT-II]+\sum[GDGT-III]}$$

Eq. 12 $$CBT = -\log\left(\frac{[GDGT-Ib]+[GDGT-IIb]}{[GDGT-Ia]+[GDGT-IIa]}\right)$$

Mean annual air temperature (MAAT) can be calculated from MBT based on various continental soils, and soil pH was calculated from CBT (Weijers et al., 2007):

Eq. 13 $$MBT = 0.122 + 0.187 \times CBT + 0.020 \times MAAT\ (r^2 = 0.77, n = 134)$$

Eq. 14 $$CBT = 3.33 - 0.38 \times pH\ (r^2 = 0.70, n = 134)$$

1.4.7. Aromatic compounds

The polycyclic aromatic hydrocarbons (PAH) that can be identified in marine sediments include phenanthrene, pyrene, fluoranthene, benzo[a]anthracene, benzo[b]fluoranthene, benzo[k]fluoranthene, benzo[e]pyrene, benzo[a]pyrene, benzo[ghi]perylene and coronene, and their alkylated homologues (Appendix 6.1). Combustion of various plant materials and fossil fuels has been suggested to be one of the major sources of these medium to high molecular-weight PAHs, especially when distributions are dominated by the parent PAH (e.g., Tan and Heit, 1981; Jiang et al., 1998). However, some of these PAH are also found in nearly all marine sediments resulting from the normal maturation of kerogen, and have typically similar amounts of parent PAH and alkylated PAH. For example, fluoranthene and pyrene have been suggested to be major combustion-derived PAHs (Killops and Massoud, 1992). The parent PAH are also abundant in highly over-matured samples (French et al., 2015). The methylphenanthrene index (MPI_1; Eq. 16) that represent a distribution of methyl homologs of phenanthrene (MP), varies with thermal maturity (Radke et al., 1982; Radke, 1988). The methylphenanthrene ratio (MPR (Eq. 17)) is also indicative of thermal maturation.

Eq. 15 $$MPI_1 = \frac{1.5\times((2-MP)+(3-MP))}{Phenanthrene+(1-MP)+(9-MP)}$$

Eq. 16 $$MPR = \frac{2-MP}{1-MP}$$

1.5. Geological settings of the IODP sites

1.5.1. IODP Expedition 313, New Jersey continental margin

The IODP New Jersey continental shelf Expedition 313 took place between 30 April and 17 July 2009 on the U.S. middle Atlantic margin (New Jersey–Delaware–Maryland). The drilling sites were located in an area of tectonic stability, good fossil preservation, and rapid sedimentary deposition (Miller and Mountain, 1994; Mountain et al., 2010), allowing detailed analysis of the global sea level influence on the New Jersey continental shelf sediments during the Cenozoic..

Cored sediments were dated from the Late Eocene to the Upper Pleistocene (Mountain et al., 2010). The expedition continued research from previous drilling expeditions on the New Jersey continental slope and provided a 100 million year chronology of the region (Miller et al., 1998; Miller et al., 2005). These drilling projects enabled correlation of eustatic sea level changes and erosion of the continental margin from the middle Eocene to the middle Miocene epoch using sedimentary erosion pattern, $\delta^{18}O$ records, and biostratigraphy. New results were consistent with previous studies of eustatic variations (Vail and Mitchum Jr, 1979; Haq et al., 1987). The sediments from the IODP Expedition 313 provided a detailed record influenced by eustatic sea level variations, by modelling thermal subsidence on a passive margin. The accumulated data allowed testing of temperature assumptions needed to make glacio-eustatic estimates from $\delta^{18}O$ records and provide an estimate for Oligocene-Miocene sea level calibrations.

Lithostratigraphic data from the drilled Sites M0027 and M0028 showed two main sediment depositional environments. The first one is a mix of storm and river-dominated shelf sediments characterised by well sorted silt and sand deposited in an offshore environment. The silt-rich deposits showed frequent exposure to dysoxia with some cyclical repetition. The second depositional environment is an intra-shelf clinoform rollover and clinoform slope dominated by coarse-grained debris and turbidites with interbedded silt and silty clay (Mountain et al., 2010). No exposure to oxygen was indicated for this deposition type. However, a partial tectonic influence related to large sea level changes was indicated.

Dating of the M0027 and M0028 Sites was achieved based on the biostratigraphy of calcareous nannofossils, planktonic foraminifera, and dinocysts. The lithology of Site M0027A was divided into eight units (Fig. F8 and F10 in Mountain et al., 2010) from the late Eocene to the upper Pleistocene. In general, Unit VII is a poorly sorted sediment with high bioturbation levels from the late Oligocene. The Unit VI sediments, dated from 24–19 Ma, are dominated by thick storm or river-dominated deposits. These are overlain by Unit V, 19–9.5 Ma, comprising poorly sorted glauconitic sands with quartz. The overlying Unit IV, 9.5 – 7.5 Ma, comprises a deepening-upward shore face–offshore transition to offshore succession lacking a regressive facies. This is erosionally truncated by Unit III, dated between 7.5 to ~ 5 Ma, which consists of deepening and shallowing upward silts, with major storm influence. Unit II is characterised by deepening sedimentary cycles that were identified as deposited in a transgressive shoreface with transition deposits. Lastly, Unit I comprises Pleistocene sands and gravels (Mountain et al., 2010).

Palynological data from Site M0027 suggests the presence of the hemlock plants horizon indicating that there were temperate forests and humid conditions on the Atlantic coastal plain during the early Miocene. Middle Miocene pollen assemblages record the expansion of grasses and sedges, indicating increasing aridity at that time. Overall, palynological data support a warm, humid climate during the Eocene–Oligocene transition and the early

Neogene, whereas the Oligocene witnessed intervals of drier and cooler conditions, causing the spread of herbaceous taxa and coniferous forests. The Site M0028 palynological data support previous reconstructions of a warm, humid early Neogene climate (Mountain et al., 2010; Kotthoff et al., 2014).

1.5.2. IODP Expedition 317, Canterbury Basin, New Zealand

IODP Expedition 317 took place between November 2009 and January 2010 in the Canterbury Basin, New Zealand. Its main purpose was to compare the relative influence of local tectonics and global sea level changes on sediments accumulated on the continental shelf and slope off the east coast of New Zealand. One of the scientific objectives was to compare the results with the IODP Expedition 313 conclusions. The regional tectonics and geological history of both sites are different, but it was suggested that during the Neogene, both areas were mainly influenced by eustasy (Fulthorpe et al., 2011).

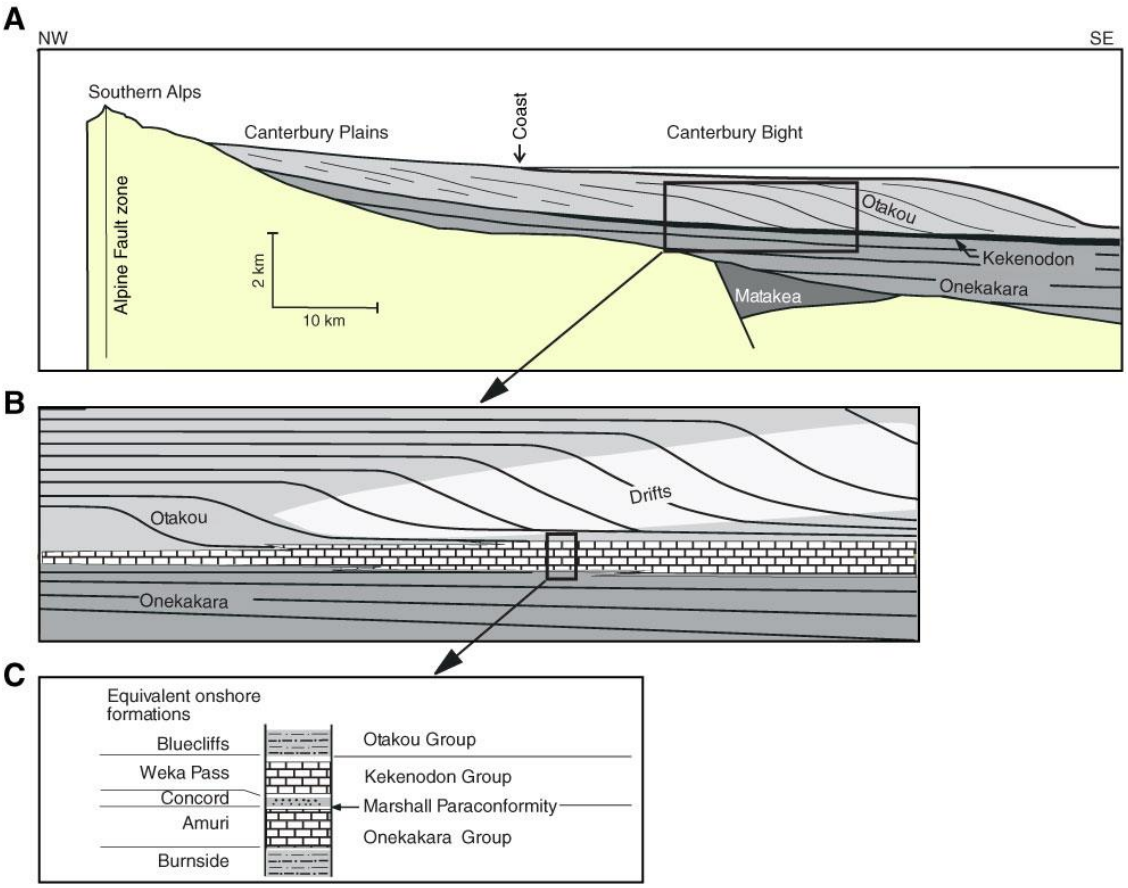

Figure 1.2 Schematic stratigraphy of the Canterbury Basin, drilled during Expedition 317, at three different scales. Modified from Fulthorpe et al. (2011). **A.** Large-scale postrift stratigraphy; **B.** Seismic-scale stratigraphy; **C.** Outcrop-scale stratigraphy across the Marshall Paraconformity.

The regional geology suggests the eastern margin of the South Island of New Zealand is part of a continental fragment that was rifted from Antarctica ~80 Ma, rifting that continued until ~55 Ma (Fulthorpe et al., 2011). The Canterbury Basin lies at the landward edge of the rifted continental fragment and underlies the present-day onshore Canterbury Plains and offshore continental shelf (Browne and Field, 1988). Basin sediments together with onshore rocks show some correlation to uplift and faulting that happened during the latest Miocene (8–5 Ma) that correlated to uplift of the Southern Alps (Adams, 1981; Tippett and Kamp, 1993; Batt et al., 2000). The plate tectonic history of the New Zealand Plateau is recorded in the stratigraphy of the South Island (Mortimer et al., 1999; King, 2000). The Canterbury Basin was part of a passive margin from the Late Cretaceous to the Late Eocene, and the Alpine

Fault was formed by convergence of the Australasian and Pacific plates at ~23 Ma (Wellman, 1971; King, 2000). This tectonic activity possibly increased the sediment supply during this period (Carter and Norris, 1976). Additional uplift of the Southern Alps has been proposed at ~8–5 Ma (Tippett and Kamp, 1993; Batt et al., 2000) or ~10–8 Ma (Carter and Norris, 1976; Norris et al., 1990).

The recovered cored sediments from the Canterbury Basin dated from the Eocene to the Holocene, and there was a particular focus on the sequence stratigraphy of the last 19 million years, when global sea level changes were dominated by glacio-eustasy (Fulthorpe et al., 2011). Sedimentary sequences were drilled in a transect of three sites on the continental shelf (landward to basinward, Sites U1353, U1354, and U1351) and one on the continental slope (Site U1352) (Fulthorpe et al., 2011). The Canterbury Basin sedimentary record (Fig. 1.2) provides a unique opportunity for examining the accumulated biomarker signal in the region. A global climatic optimum and temperature increase at the early/middle Miocene boundary (Nelson and Cooke, 2001), together with the increasing land mass of the sub-continent based on an increase in sedimentation rates since the middle Miocene (Lu et al., 2005), suggest gradual intensification in the amount of land vegetation. Interpretation of global eustatic and climatic transformations suggest that cooler Neogene seawater conditions were coupled with a decrease in global sea levels (Zachos et al., 2001; Van Sickel et al., 2004). Therefore, the influence of this climate shift on the accumulation and preservation of organic matter in the marine sediments is expected.

The study in this thesis is based on a set of sedimentary samples from three drilling sites: U1351, U1352, and U1353. The age model for each site is based on the shipboard study of calcareous nannofossils, diatoms, and planktonic and benthic foraminifera (Fulthorpe et al., 2011). The lithological unit definitions for each of the sites were based on the observed variation in lithology in the cores (Fig. 1.2) (Fulthorpe et al., 2011; Marsaglia et al., accepted 2017). In general, Unit I is heterogeneous, containing a wide variety of facies including

interbedded terrigenous lithologies and many green marls and calcareous beds with sharp (or bioturbated) bases. Unit II is divided into three sub-units (A-C) and is dominated by mud or muddy sand, with lower percentages of carbonate components, and with rare, greenish calcareous beds at Sites U1351 and U1353. The mineralogy suggests a dominant provenance from the southerly Otago Schist (Fulthorpe et al., 2011; Marsaglia et al., accepted 2017). A homogeneous sandy marlstone was identified in Unit II in Site U1352. This unit becomes more lithified with depth because of carbonate cementation. Unit III (Oligocene–Eocene) from Site U1352 is composed of limestone which was deposited in an oceanic environment, with little to no terrigenous sediment input.

Site U1351 was located on the outer continental shelf with lower Pliocene–Late Miocene sediments characterised by low levels of erosion (Fulthorpe et al., 2011). The Miocene section of the site was dated using planktonic foraminifera, which showed a major depositional hiatus of ~3.4 million years between 7.07 and 10.5 Ma. The bottom of Hole B at Site U1351 was dated to 10.6–10.91 Ma.

Site U1352 is located on the upper slope within the Canterbury Basin and is the most basinward site in this study. Good sediment recovery led to an excellent record of the Miocene. The sediments were dated by foraminifera and nannofossil proxies, which show that the Miocene/Pliocene boundary is between 1266 and 1284 meters below sea floor (mbsf). The early Oligocene to Eocene (Unit III) sediments are hemipelagic to pelagic foraminifera-bearing nannofosil limestones, with minor amounts of quartz and clay (Fulthorpe et al., 2011). The latter unit is correlative to the onshore Amuri Limestone (Fulthorpe et al., 2011). One long unconformity from 19–30.1 Ma (1903.29–1916.63 mbsf) is present in Unit III, and the bottom part of Hole C was dated to 35.2–36.0 Ma (Eocene).

The third site, U1353, is the most onshore of the shelf sites from Expedition 317 and is characterised by dark greenish-grey, micaceous very fine sandy-mud and mud samples. The

deepest sample from this site has a biostratigraphical assemblage showing an age of middle to early Miocene, and correlation to other sites places this 510.52–518.66 mbsf interval around 12 Ma. The dominant lithology of the analysed lithological Unit II is dark greenish grey, micaceous fine sandy mud and mud with shells (Fulthorpe et al., 2011).

1.5.3. IODP Expedition 355, Arabian Sea Monsoon

IODP Expedition 355 took place between March and May 2015, and was designed to drill deep into the Indus submarine fan and to sample the underlying basement at two sites. The primary objective was to better understand the erosional and weathering response of the western Himalaya, Karakoram, and Hindu Kush to the changing intensity of the southwest Asian monsoon since the onset of India/Eurasia collision in the early Paleogene (Pandey et al., 2016).

The Arabian Sea in the northern Indian Ocean preserves regional sedimentary records of rifting, tectonic subsidence, and paleoceanographic history and also provides archives of the long-term erosion of the Himalayas since the start of collision between India and Eurasia (Garzanti et al., 1987; Kroon et al., 1991; Prell and Kutzbach, 1992). In addition to being a repository of information about past climate and mountain building, the Arabian Sea also holds potentially illuminating records of continental rifting and breakup tectonics dating from the time of Gondwana fragmentation in the Cretaceous (Heine et al., 2004). Paleogeographic reconstructions based on magnetic anomalies, as well as similarities in structural/tectonic elements, suggest a conjugate relationship between the western continental margin of India and the eastern continental margin of Madagascar and the Seychelles (Storey et al., 1995; Collier et al., 2008). Site U1456 lies within the Laxmi Basin in the eastern Arabian Sea ~475 km west of the Indian coast and ~820 km south from the modern mouth of the Indus River.

The Indus River is presumed to be the primary source of sediment to the area, at least since the Neogene and likely since the Eocene (Clift et al., 2001; Clift et al., 2008).

The cored section at Site U1456 is divided into four lithological units that were dated by calcareous and siliceous microfossils (Pandey et al., 2016). In general, the Pleistocene Unit I consists of light brown to light greenish nannofossil ooze and foraminifera-rich nannofossil ooze interbedded with clay, silt, and sand. Unit II is dated to the late Pliocene to early Pleistocene and consists mainly of massive dark greyish to blackish sand and silt interbedded with thinly bedded nannofossil-rich clay. Unit III consists of semi-indurated to indurated light brown to dark green clay/claystone, light brown to dark gray sand/sandstone, light greenish nannofossil chalk, and light to dark greenish gray nannofossil-rich claystone. It is dated to the upper Miocene to late Pliocene. Lastly, Unit IV is a mix of interbedded lithologies and is dominated by dark gray massive claystone (Pandey et al., 2016).

1.6. Thesis Aims

The aim of this PhD thesis is to reconstruct the climate changes that occurred during the second part of the Cenozoic Era by utilising organic compounds recovered from cored marine sediments. To reach this goal, bulk organic matter information and lipid biomarkers preserved in the marine sediments were used. The primary focus of the research is on *n*-alkanes, hopanes and steranes that were extensively used to reconstruct variations in the source of organic matter. In addition, GDGTs and alkenones were used to reconstruct SSTs and constrain the source of organic matter.

This PhD study provides a detailed Organic Geochemistry record of the cored sediments from three IODP expeditions. IODP Expedition 317 was located in the Canterbury Basin, New Zealand and work was carried out on cores from three of the four sites (U1351, U1352, U1353). IODP Expedition 313 was located on the New Jersey continental shelf and work was carried out on cores from two Sites (M0027A and M0028A). IODP Expedition 355 was located in the Laxmi Basin, eastern Arabian Sea, and work was carried out on three cores from the same site (U1456). Each site represents a separate research project that used a multi-proxy approach to palaeoceanographic reconstructions with organic compounds and biomarkers as the main source of information.

The palaeoceanography of the Canterbury Basin, New Zealand for the last 32 Ma is represented by 115 samples cored at three sites: U1351, inner continental shelf: U1352, continental slope; and U1353, outer continental shelf. The Site U1352 core is the longest analysed sedimentary record ever recovered from 32 Ma to 0.0026 Ma. Tectonic activity and eustasy influences should have a different footprint on the organic matter preserved in the same area. By using these differences, it should be possible to establish which event had a stronger influence on the region though time. These samples were used to correlate between increase in terrestrial OM input and uplift of the New Zealand land mass from the middle

Miocene. The reconstructed SST could be correlated with global climatic events such as appearance of the Antarctic ice sheets and Antarctic Circumpolar Current (ACC).

The organic matter record from the New Jersey continental shelf is represented by 43 samples from two drilling Sites: M0027A, inner part of the continental shelf; and Site M0028A, outer part of the continental shelf. These sediments date from the early to middle Miocene. Global events such as eustasy should have a similar influence on accumulation of the same organic compounds in similar geological records around the globe. The New Jersey record suggests consistent OM input from the land and reconstructed SSTs show a decreasing temperature trend.

Finally, the research in the eastern Arabian Sea region is represented by 20 samples from the U1456 Site, located in the Laxmi Basin, offshore western India. Our hypothesis proposes that increased erosion and precipitation patterns can be attributed to Himalaya Uplift and intensification of the Asian monsoon. The samples cover the last 10 million years of regional history and show variations in OM input attributed to the Himalaya Uplift and changes in Asian Monsoon cyclicity. The palaeoceanographical study did not show any significant SST decrease over the last 10 million years in the north-eastern part of the Indian Ocean.

1.7. Thesis structure

The thesis is divided into seven chapters. The aim of this research is to apply the biomarker and organic matter proxies of environmental change to marine drilling material, and in particular use it as a component of palaeoclimate analysis.

Chapter 1 introduces the background to Cenozoic climate reconstruction, and provides an overview of the organic proxies use in this research.

Chapters 2, 3, 4, and 5 are presented as a series of self-contained chapters that correspond to papers that are ready to be submitted. These chapters are organised as follows:

Chapter 2 is a near final version of a manuscript that will be submitted to *Organic Geochemistry*, in which the results of bulk and Organic Geochemistry analyses on Oligocene and Miocene samples from IODP Expedition 317 are presented and discussed.

Chapter 3 is a near final version of a manuscript that is expected to be submitted to *Marine Geology* that outlines the results of the SSTs based on GDGT and alkenone data from IODP Expedition 317 samples from Oligocene to the recent.

Chapter 4 is a near final version of a manuscript that is expected to be submitted to *Geochimica Cosmochimica Acta* that will discuss a comparison of the IODP Expedition 317 and 313 results, and palaeoclimatic reconstructions made from this comparison.

Chapter 5 is a near final version of a manuscript expected to be submitted to *Geology* which discusses a multi proxy analysis of sediment and organic matter source in the Laxmi Basin, Arabian Sea, IODP Expedition 355.

Chapter 6 lists the main conclusions of this study and presents some perspectives on the applicability of the results for further research.

Chapter 7 biomarker structures, conferences abstracts, and a list of publications.

1.8. References

Adams, C., 1981. Uplift rates and thermal structure in the Alpine fault zone and Alpine schists, Southern Alps, New Zealand. *Geological Society, London, Special Publications* 9, 211-222.

Aquino, N.F., Trendel, J., Restle, A., Connan, J., Albrecht, P., 1983. Occurrence and formation of tricyclic and tetracyclic terpanes in sediments and petroleum. *Advance in Organic Geochemistry. New York: John Wiley and Sons*, 659-676.

Azevedo, D.d.A., Neto, F.A., Simoneit, B., Pinto, A., 1992. Novel series of tricyclic aromatic terpanes characterized in Tasmanian tasmanite. *Organic Geochemistry* 18, 9-16.

Barnes, M., Barnes, W., 1978. Organic compounds in lake sediments, Lakes. Springer, pp. 127-152.
Bartek, L.R., Vail, P., Anderson, J., Emmet, P., Wu, S., 1991. Effect of Cenozoic ice sheet fluctuations in Antarctica on the stratigraphic signature of the Neogene. *Journal of Geophysical Research: Solid Earth* 96, 6753-6778.

Batt, G.E., Braun, J., Kohn, B.P., McDougall, I., 2000. Thermochronological analysis of the dynamics of the Southern Alps, New Zealand. *GSA Bulletin* 112, 250-266.

Becker, K.W., Lipp, J.S., Versteegh, G.J., Wörmer, L., Hinrichs, K.-U., 2015. Rapid and simultaneous analysis of three molecular sea surface temperature proxies and application to sediments from the Sea of Marmara. *Organic Geochemistry* 85, 42-53.

Becker, K.W., Lipp, J.S., Zhu, C., Liu, X.-L., Hinrichs, K.-U., 2013. An improved method for the analysis of archaeal and bacterial ether core lipids. *Organic Geochemistry* 61, 34-44.

Berner, R., 1990. Atmospheric carbon dioxide levels over Phanerozoic time. *Science* 249, 1382-1386.

Billups, K., Channell, J., Zachos, J., 2002. Late Oligocene to early Miocene geochronology and paleoceanography from the subantarctic South Atlantic. *Paleoceanography* 17.

Bohaty, S.M., Zachos, J.C., 2003. Significant Southern Ocean warming event in the late middle Eocene. *Geology* 31, 1017-1020.

Bourbonniere, R., Meyers, P., 1996. Anthropogenic influences on hydrocarbon contents of sediments deposited in eastern Lake Ontario since 1800. *Environmental Geology* 28, 22-28.

Bourbonniere, R.A., 1980. Geochemistry of humic matter in Holocene Great Lakes sediments. University of Michigan.
Brassell, S., Brereton, R., Eglinton, G., Grimalt, J., Liebezeit, G., Marlowe, I., Pflaumann, U., Sarnthein, M., 1986a. Palaeoclimatic signals recognized by chemometric treatment of molecular stratigraphic data. *Organic Geochemistry* 10, 649-660.

Brassell, S., Eglinton, G., Marlowe, I., Pflaumann, U., Sarnthein, M., 1986b. Molecular stratigraphy: a new tool for climatic assessment. *Nature* 320, 129-133.

Brassell, S., Eglinton, G., Maxwell, J., Philp, R., 1978. Natural background of alkanes in the aquatic environment. *Aquatic pollutants: transformation and biological effects*, 69-86.

Brassell, S.C., 1993. Applications of biomarkers for delineating marine paleoclimatic fluctuations during the Pleistocene, Organic Geochemistry. Springer, pp. 699-738.

Bray, E., Evans, E., 1961. Distribution of n-paraffins as a clue to recognition of source beds. *Geochimica et Cosmochimica Acta* 22, 2-15.

Browne, G., Field, B., 1988. A review of Cretaceous-Cenozoic sedimentation and tectonics, east coast, South Island, New Zealand.

Carter, R.t., Norris, R., 1976. Cainozoic history of southern New Zealand: an accord between geological observations and plate-tectonic predictions. *Earth and Planetary Science Letters* 31, 85-94.

Chaler, R., Grimalt, J.O., Pelejero, C., Calvo, E., 2000. Sensitivity Effects in U k '37 Paleotemperature Estimation by Chemical Ionization Mass Spectrometry. *Analytical chemistry* 72, 5892-5897.

Chaler, R., Villanueva, J., Grimalt, J., 2003. Non-linear effects in the determination of paleotemperature U k′ 37 alkenone ratios by chemical ionization mass spectrometry. *Journal of Chromatography A* 1012, 87-93.

Chappe, B., Albrecht, P., Michaelis, W., 1982. Polar lipids of archaebacteria in sediments and petroleums. *Science* 217, 65-66.

Chappe, B., Michaelis, W., Albrecht, P., Ourisson, G., 1979. Fossil evidence for a novel series of archaebacterial lipids. *Naturwissenschaften* 66, 522-523.

Clift, P., Hodges, K., Heslop, D., Hannigan, R., Hoang, L., Calves, G., 2008. Greater Himalayan exhumation triggered by Early Miocene monsoon intensification. *Nat Geosci* 1, 875-880.

Clift, P., Shimizu, N., Layne, G., Blusztajn, J., Gaedicke, C., Schlüter, H.-U., Clark, M., Amjad, S., 2001. Development of the Indus Fan and its significance for the erosional history of the Western Himalaya and Karakoram. *Geological Society of America Bulletin* 113, 1039-1051.

Cohen, K., Finney, S., Gibbard, P., Fan, J.-X., 2013. The ICS international chronostratigraphic chart. *Episodes* 36, 199-204.

Collier, J., Sansom, V., Ishizuka, O., Taylor, R., Minshull, T., Whitmarsh, R., 2008. Age of Seychelles–India break-up. *Earth and Planetary Science Letters* 272, 264-277.

Comet, P., Eglinton, G., 1987. The use of lipids as facies indicators. *Geological Society, London, Special Publications* 26, 99-117.

Connan, J., 1974. Time-temperature relation in oil genesis: geologic notes. *AAPG Bulletin* 58, 2516-2521.

Conte, M., Thompson, A., Eglinton, G., 1994. Primary production of lipid biomarker compounds by Emiliania huxleyi. Results from an experimental mesocosm study in fjords of southwestern Norway. *Sarsia* 79, 319-331.

Conte, M.H., Eglinton, G., Madureira, L.A., Rabouille, C., Labeyrie, L., Mudge, S., 1995. Origin and Fate of Organic Biomarker Compounds in the Water Column and Sediments of the Eastern North Atlantic [and Discussion]. *Philosophical Transactions of the Royal Society of London B: Biological Sciences* 348, 169-178.

Cranwell, P., 1984. Lipid geochemistry of sediments from Upton Broad, a small productive lake. *Organic Geochemistry* 7, 25-37.

Cranwell, P., Eglinton, G., Robinson, N., 1987. Lipids of aquatic organisms as potential contributors to lacustrine sediments—II. *Organic Geochemistry* 11, 513-527.

Cranwell, P.A., 1973. Chain-length distribution of n-alkanes from lake sediments in relation to post-glacial environmental change. *Freshwater Biology* 3, 259-265.

Crowley, T.J., Burke, K., 1998. Tectonic boundary conditions for climate reconstructions. Oxford University Press on Demand.

Damsté, J.S.S., Kenig, F., Koopmans, M.P., Köster, J., Schouten, S., Hayes, J., de Leeuw, J.W., 1995. Evidence for gammacerane as an indicator of water column stratification. *Geochimica et Cosmochimica Acta* 59, 1895-1900.

De Leeuw, J., vd Meer, F., Rijpstra, W., Schenck, P., 1980. On the occurrence and structural identification of long chain unsaturated ketones and hydrocarbons in sediments. *Physics and Chemistry of the Earth* 12, 211-217.

Didyk, B., 1978. Organic geochemical indicators of palaeoenvnonmental conditions of sedimentation. *Nature* 272, 216-222.

Eglinton, G., Hamilton, R.J., 1967. Leaf epicuticular waxes. *Science* 156, 1322-1335.

Eglinton, L.B., Lim, D., Slater, G., Osinski, G.R., Whelan, J.K., Douglas, M., 2006. Organic geochemical characterization of a Miocene core sample from Haughton impact structure, Devon Island, Nunavut, Canadian High Arctic. *Organic Geochemistry* 37, 688-710.

Ehrmann, W.U., Mackensen, A., 1992. Sedimentological evidence for the formation of an East Antarctic ice sheet in Eocene/Oligocene time. *Palaeogeography, Palaeoclimatology, Palaeoecology* 93, 85-112.

Ensminger, A., Albrecht, P., Ourisson, G., Tissot, B., 1975. Evolution of polycyclic alkanes under the effect of burial (Early Toarcian shales, Paris Basin). *Advances in organic geochemistry* 1975, 45-52.

Falkowski, P.G., Schofield, O., Katz, M.E., Van de Schootbrugge, B., Knoll, A.H., 2004. Why is the land green and the ocean red?, Coccolithophores. Springer, pp. 429-453.

Farrimond, P., Eglinton, G., Brassell, S., 1986. Alkenones in Cretaceous black shales, Blake-Bahama Basin, western North Atlantic. *Organic Geochemistry* 10, 897-903.

Feakins, S.J., Eglinton, T.I., 2005. Biomarker records of late Neogene changes in northeast African vegetation. *Geology* 33, 977-980.

Ficken, K.J., Li, B., Swain, D., Eglinton, G., 2000. An n-alkane proxy for the sedimentary input of submerged/floating freshwater aquatic macrophytes. *Organic Geochemistry* 31, 745-749.

Flores, J., Sierro, F., Francés, G., Vázquez, A., Zamarren, I., 1997. The last 100,000 years in the western Mediterranean: sea surface water and frontal dynamics as revealed by coccolithophores. *Marine Micropaleontology* 29, 351-366.

Foster, G.L., Rohling, E.J., 2013. Relationship between sea level and climate forcing by CO2 on geological timescales. *Proceedings of the National Academy of Sciences* 110, 1209-1214.

Foster, G.L., Royer, D.L., Lunt, D.J., 2017. Future climate forcing potentially without precedent in the last 420 million years. *Nature Communications* 8.

Francis, J.E., 1988. A 50-million-year-old fossil forest from Strathcona Fiord, Ellesmere Island, Arctic Canada: evidence for a warm polar climate. *Arctic*, 314-318.

French, K.L., Hallmann, C., Hope, J.M., Schoon, P.L., Zumberge, J.A., Hoshino, Y., Peters, C.A., George, S.C., Love, G.D., Brocks, J.J., 2015. Reappraisal of hydrocarbon biomarkers in Archean rocks. *Proceedings of the National Academy of Sciences* 112, 5915-5920.

Fulthorpe, C.S., Hoyanagi, K., Crundwell, M.P., Dinarès-Turell, J., Ding, X., George, S.C., Hepp, D.A., Jaeger, J., Kawagata, S., Kemp, D.B., 2011. Expedition 317 summary.

Gagosian, R.B., 1976. A detailed vertical profile of sterols in the Sargasso Sea. *Limnol. Oceanogr* 21, 702-710.

Gagosian, R.B., Peltzer, E.T., 1986. The importance of atmospheric input of terrestrial organic material to deep sea sediments. *Organic Geochemistry* 10, 661-669.

Garzanti, E., Baud, A., Mascle, G., 1987. Sedimentary record of the northward flight of India and its collision with Eurasia (Ladakh Himalaya, India). *Geodinamica Acta* 1, 297-312.

Gelin, F., Damsté, J.S.S., Harrison, W.N., Maxwell, J.R., De Leeuw, J.W., 1995. Molecular indicators for palaeoenvironmental change in a Messinian evaporitic sequence (Vena del Gesso, Italy): III. Stratigraphic changes in the molecular structure of kerogen in a single marl bed as revealed by flash pyrolysis. *Organic Geochemistry* 23, 555-566.

Giger, W., Schaffner, C., Wakeham, S.G., 1980. Aliphatic and olefinic hydrocarbons in recent sediments of Greifensee, Switzerland. *Geochimica et Cosmochimica Acta* 44, 119-129.

Grantham, P.J., Wakefield, L.L., 1988. Variations in the sterane carbon number distributions of marine source rock derived crude oils through geological time. *Organic Geochemistry* 12, 61-73.

Grossi, V., Hirschler, A., Raphel, D., Rontani, J.-F., De Leeuw, J., Bertrand, J.-C., 1998. Biotransformation pathways of phytol in recent anoxic sediments. *Organic Geochemistry* 29, 845-861.

Hambrey, M.J., Ehrmann, W.U., Larsen, B., 1992. Cenozoic glacial record of the Prydz Bay continental shelf, East Antarctica. Geological Survey in Denmark.
Haq, B.U., Hardenbol, J., Vail, P.R., 1987. Chronology of fluctuating sea levels since the Triassic. *Science* 235, 1156-1167.

Hedges, J., Oades, J., 1997. Comparative organic geochemistries of soils and marine sediments. *Organic Geochemistry* 27, 319-361.

Heine, C., Müller, R.D., Gaina, C., 2004. Reconstructing the lost eastern Tethys ocean basin: convergence history of the SE Asian margin and marine gateways. *Continent-Ocean Interactions within East Asian Marginal Seas*, 37-54.

Henrichs, S.M., 1992. Early diagenesis of organic matter in marine sediments: progress and perplexity. *Marine Chemistry* 39, 119-149.

Henrichs, S.M., 1993. Early diagenesis of organic matter: the dynamics (rates) of cycling of organic compounds, Organic Geochemistry. Springer, pp. 101-117.
Herbert, T., 2001. Review of alkenone calibrations (culture, water column, and sediments). *Geochemistry, Geophysics, Geosystems* 2.

Hopmans, E.C., Schouten, S., Pancost, R.D., van der Meer, M.T.J., Sinninghe Damste, J.S., 2000. Analysis of intact tetraether lipids in archaeal cell material and sediments by high performance liquid

chromatography/atmospheric pressure chemical ionization mass spectrometry. *Rapid Commun Mass Spectrom* 14, 585-589.

Hopmans, E.C., Weijers, J.W.H., Schefuß, E., Herfort, L., Sinninghe Damsté, J.S., Schouten, S., 2004. A novel proxy for terrestrial organic matter in sediments based on branched and isoprenoid tetraether lipids. *Earth and Planetary Science Letters* 224, 107-116.

Huang, W.-Y., Meinschein, W.G., 1979. Sterols as ecological indicators. *Geochimica et Cosmochimica Acta* 43, 739-745.

Huang, Y., Dupont, L., Sarnthein, M., Hayes, J.M., Eglinton, G., 2000. Mapping of C 4 plant input from North West Africa into North East Atlantic sediments. *Geochimica et Cosmochimica Acta* 64, 3505-3513.

Isaksen, G., Bohacs, K., 1995. Geological controls of source rock geochemistry through relative sea level; Triassic, Barents Sea, Petroleum Source Rocks. Springer, pp. 25-50.
Jiang, C., Alexander, R., Kagi, R.I., Murray, A.P., 1998. Polycyclic aromatic hydrocarbons in ancient sediments and their relationships to palaeoclimate. *Organic Geochemistry* 29, 1721-1735.

Kawamura, K., 1995. Land-derived lipid class compounds in the deep-sea sediments and marine aerosols from North Pacific. *Biogeochemical Processes and Ocean Flux in the Western Pacific*, 31-51.

Kawamura, K., Ishiwatari, R., 1985. Distribution of lipid-class compounds in bottom sediments of freshwater lakes with different trophic status, in Japan. *Chemical Geology* 51, 123-133.

Kawamura, K., Ishiwatari, R., Ogura, K., 1987. Early diagenesis of organic matter in the water column and sediments: microbial degradation and resynthesis of lipids in Lake Haruna. *Organic Geochemistry* 11, 251-264.

Kennett, J.P., 1977. Cenozoic evolution of Antarctic glaciation, the circum-Antarctic Ocean, and their impact on global paleoceanography. *Journal of geophysical research* 82, 3843-3860.

Killops, S., Massoud, M., 1992. Polycyclic aromatic hydrocarbons of pyrolytic origin in ancient sediments: evidence for Jurassic vegetation fires. *Organic Geochemistry* 18, 1-7.

Kim, J.-H., Schouten, S., Hopmans, E.C., Donner, B., Sinninghe Damsté, J.S., 2008. Global sediment core-top calibration of the TEX86 paleothermometer in the ocean. *Geochimica et Cosmochimica Acta* 72, 1154-1173.

Kim, J.-H., Van der Meer, J., Schouten, S., Helmke, P., Willmott, V., Sangiorgi, F., Koç, N., Hopmans, E.C., Damsté, J.S.S., 2010. New indices and calibrations derived from the distribution of crenarchaeal isoprenoid tetraether lipids: Implications for past sea surface temperature reconstructions. *Geochimica et Cosmochimica Acta* 74, 4639-4654.

King, P.R., 2000. Tectonic reconstructions of New Zealand: 40 Ma to the present. *New Zealand Journal of Geology and Geophysics* 43, 611-638.

Knorr, G., Lohmann, G., 2014. Climate warming during Antarctic ice sheet expansion at the Middle Miocene transition. *Nature Geoscience* 7, 376-381.

Kodner, R.B., Pearson, A., Summons, R.E., Knoll, A.H., 2008. Sterols in red and green algae: quantification, phylogeny, and relevance for the interpretation of geologic steranes. *Geobiology* 6, 411-420.

Kotthoff, U., Greenwood, D., McCarthy, F., Müller-Navarra, K., Prader, S., Hesselbo, S., 2014. Late Eocene to middle Miocene (33 to 13 million years ago) vegetation and climate development on the North American Atlantic Coastal Plain (IODP Expedition 313, Site M0027). *Climate of the Past* 10, 1523.

Kroon, D., Steens, T., Troelstra, S.R., 1991. 13. Onset of monsoonal related upwelling in the Western Araibian sea as revealed by planctonic foraminiders.

Langebroek, P., Paul, A., Schulz, M., 2010. Simulating the sea level imprint on marine oxygen isotope records during the middle Miocene using an ice sheet–climate model. *Paleoceanography* 25.

Lao, Y., Korth, J., Ellis, J., Crisp, P., 1989. Heterogeneous reactions of 1-pristene catalysed by clays under simulated geological conditions. *Organic Geochemistry* 14, 375-379.

Laskar, J., Joutel, F., Boudin, F., 1993. Orbital, precessional, and insolation quantities for the Earth from-20 Myr to+ 10 Myr. *Astronomy and Astrophysics* 270, 522-533.

Lu, H., Fulthorpe, C.S., Mann, P., Kominz, M.A., 2005. Miocene–Recent tectonic and climatic controls on sediment supply and sequence stratigraphy: Canterbury basin, New Zealand. *Basin Research* 17, 311-328.

Mackenzie, A., Patience, R., Maxwell, J., Vandenbroucke, M., Durand, B., 1980. Molecular parameters of maturation in the Toarcian shales, Paris Basin, France—I. Changes in the configurations of acyclic isoprenoid alkanes, steranes and triterpanes. *Geochimica et Cosmochimica Acta* 44, 1709-1721.

Marlowe, I., Brassell, S., Eglinton, G., Green, J., 1990. Long-chain alkenones and alkyl alkenoates and the fossil coccolith record of marine sediments. *Chemical Geology* 88, 349-375.

Marlowe, I., Green, J., Neal, A., Brassell, S., Eglinton, G., Course, P., 1984. Long chain (n-C37–C39) alkenones in the Prymnesiophyceae. Distribution of alkenones and other lipids and their taxonomic significance. *British Phycological Journal* 19, 203-216.

Marsaglia, K.M., Browne, G.H., George, S.C., Kemp, D.B., Jaeger, J.M., Carson, D., Richaud, M., Party, a.I.E.S., accepted 2017. The transformation of sediment into rock: insights from IODP Site U1352, Canterbury Basin, New Zealand. . *Journal of Sedimentary Research* 87.

Maslin, M., Haug, G., Sarnthein, M., Tiedemann, R., 1996. The progressive intensification of northern hemisphere glaciation as seen from the North Pacific. *Geologische Rundschau* 85, 452-465.

McKirdy, D.M., Kantsler, A.J., Emmett, J.K., Aldridge, A.K., 1984. Hydrocarbon genesis and organic facies in Cambrian carbonates of the eastern Officer Basin, South Australia.

Metcalfe, I., 2013. Gondwana dispersion and Asian accretion: tectonic and palaeogeographic evolution of eastern Tethys. *Journal of Asian Earth Sciences* 66, 1-33.

Meyers, P.A., 1990. Impacts of late Quaternary fluctuations in water level on the accumulation of sedimentary organic matter in Walker Lake, Nevada. *Palaeogeography, Palaeoclimatology, Palaeoecology* 78, 229-240.

Meyers, P.A., 1997. Organic geochemical proxies of paleoceanographic, paleolimnologic, and paleoclimatic processes. *Organic Geochemistry* 27, 213-250.

Meyers, P.A., Benson, L.V., 1988. Sedimentary biomarker and isotopic indicators of the paleoclimatic history of the Walker Lake basin, western Nevada. *Organic Geochemistry* 13, 807-813.

Meyers, P.A., Ishiwatari, R., 1993a. The Early Diagenesis of Organic Matter in Lacustrine Sediments, in: Engel, M., Macko, S. (Eds.), Organic Geochemistry. Springer US, pp. 185-209.
Meyers, P.A., Ishiwatari, R., 1993b. Lacustrine organic geochemistry—an overview of indicators of organic matter sources and diagenesis in lake sediments. *Organic Geochemistry* 20, 867-900.

Miller, K., Mountain, G., 1994. Global sea-level change and the New Jersey margin, Proceedings of the Ocean Drilling Program. Initial reports. Ocean Drilling Program, pp. 11-19.
Miller, K.G., Kominz, M.A., Browning, J.V., Wright, J.D., Mountain, G.S., Katz, M.E., Sugarman, P.J., Cramer, B.S., Christie-Blick, N., Pekar, S.F., 2005. The phanerozoic record of global sea-level change. *Science* 310, 1293-1298.

Miller, K.G., Mountain, G.S., Browning, J.V., Kominz, M., Sugarman, P.J., Christie-Blick, N., Katz, M.E., Wright, J.D., 1998. Cenozoic global sea level, sequences, and the New Jersey transect: results from coastal plain and continental slope drilling. *Reviews of Geophysics* 36, 569-601.

Miller, K.G., Wright, J.D., Fairbanks, R.G., 1991. Unlocking the ice house: Oligocene-Miocene oxygen isotopes, eustasy, and margin erosion. *Journal of Geophysical Research: Solid Earth* 96, 6829-6848.

Moldowan, J., Peters, K., Carlson, R., Schoell, M., ABUALI, M., 1994. Diverse applications of petroleum biomarker maturity parameters. *Arabian Journal for Science and Engineering* 19, 273-298.

Moldowan, J.M., Seifert, W.K., Gallegos, E.J., 1985a. Biological Marker Variations in Oils from Marine, Nonmarine, and Carbonate Source Rocks. *Abstracts of Papers of the American Chemical Society* 189, 115-GEOC.

Moldowan, J.M., Seifert, W.K., Gallegos, E.J., 1985b. Relationship between petroleum composition and depositional environment of petroleum source rocks. *AAPG bulletin* 69, 1255-1268.

Moldowan, J.M., Sundararaman, P., Schoell, M., 1986. Sensitivity of biomarker properties to depositional environment and/or source input in the Lower Toarcian of SW-Germany. *Organic Geochemistry* 10, 915-926.

Mortimer, N., Tulloch, A., Spark, R., Walker, N., Ladley, E., Allibone, A., Kimbrough, D., 1999. Overview of the Median Batholith, New Zealand: a new interpretation of the geology of the Median Tectonic Zone and adjacent rocks. *Journal of African earth sciences* 29, 257-268.

Mountain, G., Proust, J., McInroy, D., Cotterill, C., 2010. the Expedition 313 Scientists, 2010, Proceedings of the Integrated Ocean Drilling Program.
Müller, P.J., Kirst, G., Ruhland, G., Von Storch, I., Rosell-Melé, A., 1998. Calibration of the alkenone paleotemperature index U 37 K′ based on core-tops from the eastern South Atlantic and the global ocean (60 N-60 S). *Geochimica et Cosmochimica Acta* 62, 1757-1772.

Nelson, C.S., Cooke, P.J., 2001. History of oceanic front development in the New Zealand sector of the Southern Ocean during the Cenozoic - a synthesis. *New Zealand Journal of Geology and Geophysics* 44, 535-553.

Norris, R., Koons, P., Cooper, A., 1990. The obliquely-convergent plate boundary in the South Island of New Zealand: implications for ancient collision zones. *Journal of structural geology* 12, 715-725.

Nuzzo, M., Elvert, M., Schmidt, M., Scholz, F., Reitz, A., Hinrichs, K.-U., Hensen, C., 2012. Impact of hot fluid advection on hydrocarbon gas production and seepage in mud volcano sediments of thick Cenozoic deltas. *Earth and Planetary Science Letters* 341, 139-157.

Ohkouchi, N., Kawamura, K., Kawahata, H., Taira, A., 1997. Latitudinal distributions of terrestrial biomarkers in the sediments from the Central Pacific. *Geochimica et Cosmochimica Acta* 61, 1911-1918.

Ourisson, G., Albrecht, P., Rohmer, M., 1982. Predictive microbial biochemistry—from molecular fossils to procaryotic membranes. *Trends in Biochemical Sciences* 7, 236-239.

Pälike, H., Norris, R.D., Herrle, J.O., Wilson, P.A., Coxall, H.K., Lear, C.H., Shackleton, N.J., Tripati, A.K., Wade, B.S., 2006. The heartbeat of the Oligocene climate system. *Science* 314, 1894-1898.

Pandey, D., Clift, P., Kulhanek, D., Andò, S., Bendle, J., Bratenkov, S., Griffith, E., Gurumurthy, G., Hahn, A., Iwai, M., 2016. Expedition 355 summary. *Pandey, DK, Clift, PD, Kulhanek, DK, and the Expedition* 355.

Passchier, S., Bohaty, S., Jiménez-Espejo, F., Pross, J., Röhl, U., Flierdt, T., Escutia, C., Brinkhuis, H., 2013. Early Eocene to middle Miocene cooling and aridification of East Antarctica. *Geochemistry, Geophysics, Geosystems* 14, 1399-1410.

Pauly, G.G., Van Vleet, E.S., 1986. Acyclic archaebacterial ether lipids in swamp sediments. *Geochimica et Cosmochimica Acta* 50, 1117-1125.

Pearson, A., Huang, Z., Ingalls, A., Romanek, C., Wiegel, J., Freeman, K., Smittenberg, R., Zhang, C., 2004. Nonmarine crenarchaeol in Nevada hot springs. *Applied and Environmental Microbiology* 70, 5229-5237.

Pearson, P.N., Palmer, M.R., 2000. Atmospheric carbon dioxide concentrations over the past 60 million years. *Nature* 406, 695.

Peters, K., 1986. Guidelines for evaluating petroleum source rock using programmed pyrolysis. *AAPG Bulletin* 70, 318-329.

Peters, K.E., Moldowan, J.M., 1991. Effects of source, thermal maturity, and biodegradation on the distribution and isomerization of homohopanes in petroleum. *Organic Geochemistry* 17, 47-61.

Peters, K.E., Moldowan, J.M., 1993. The biomarker guide : interpreting molecular fossils in petroleum and ancient sediments. Prentice Hall, Englewood Cliffs, N.J.
Peters, K.E., Walters, C.C., Moldowan, J.M., 2005. The Biomarker Guide, 2 ed. Press Syndicate of the University of Cambridge.
Powell, T., McKirdy, D., 1973. Relationship between ratio of pristane to phytane, crude oil composition and geological environment in Australia. *Nature* 243, 37-39.

Prahl, F., Herbert, T., Brassell, S., Ohkouchi, N., Pagani, M., Repeta, D., Rosell-Melé, A., Sikes, E., 2000. Status of alkenone paleothermometer calibration: Report from Working Group 3. *Geochemistry, Geophysics, Geosystems* 1.

Prahl, F., Wakeham, S., 1987. Calibration of unsaturation patterns in long-chain ketone compositions for palaeotemperature assessment. *Nature* 330, 367-369.

Prahl, F.G., Bennett, J.T., Carpenter, R., 1980. The early diagenesis of aliphatic hydrocarbons and organic matter in sedimentary particulates from Dabob Bay, Washington. *Geochimica et Cosmochimica Acta* 44, 1967-1976.

Prell, W., Kutzbach, J.E., 1992. Sensitivity of the Indian monsoon to forcing parameters and implications for ‘its evolution. *Nature* 360, 17.

Pross, J., Contreras, L., Bijl, P.K., Greenwood, D.R., Bohaty, S.M., Schouten, S., Bendle, J.A., Röhl, U., Tauxe, L., Raine, J.I., 2012. Persistent near-tropical warmth on the Antarctic continent during the early Eocene epoch. *Nature* 488, 73-77.

Radke, M., 1988. Application of aromatic compounds as maturity indicators in source rocks and crude oils. *Marine and Petroleum Geology* 5, 224-236.

Radke, M., Welte, D.H., Willsch, H., 1982. Geochemical study on a well in the Western Canada Basin: relation of the aromatic distribution pattern to maturity of organic matter. *Geochimica et Cosmochimica Acta* 46, 1-10.

Raymo, M., Ruddiman, W.F., 1992. Tectonic forcing of late Cenozoic climate. *Nature* 359, 117-122.

Raymo, M.E., Ruddiman, W.F., Froelich, P.N., 1988. Influence of late Cenozoic mountain building on ocean geochemical cycles. *Geology* 16, 649-653.

Rontani, J.-F., Nassiry, M., Michotey, V., Guasco, S., Bonin, P., 2010. Formation of pristane from α-tocopherol under simulated anoxic sedimentary conditions: A combination of biotic and abiotic degradative processes. *Geochimica et Cosmochimica Acta* 74, 252-263.

Rosell-Melé, A., Carter, J., Eglinton, G., 1994. Distributions of long-chain alkenones and alkyl alkenoates in marine surface sediments from the North East Atlantic. *Organic Geochemistry* 22, 501-509.

Rowland, S., 1990. Production of acyclic isoprenoid hydrocarbons by laboratory maturation of methanogenic bacteria. *Organic Geochemistry* 15, 9-16.

Rowley, D.B., 1996. Age of initiation of collision between India and Asia: A review of stratigraphic data. *Earth and Planetary Science Letters* 145, 1-13.

Ruddiman, W.F., 2010. Plows, plagues, and petroleum: how humans took control of climate. Princeton University Press.
Rullkötter, J., Marzi, R., 1988. Natural and artificial maturation of biological markers in a Toarcian shale from northern Germany. *Organic Geochemistry* 13, 639-645.

Saraswat, R., Nigam, R., Weldeab, S., Mackensen, A., Naidu, P., 2005. A first look at past sea surface temperatures in the equatorial Indian Ocean from Mg/Ca in foraminifera. *Geophysical Research Letters* 32.

Schouten, S., Hopmans, E.C., Damsté, J.S.S., 2004. The effect of maturity and depositional redox conditions on archaeal tetraether lipid palaeothermometry. *Organic Geochemistry* 35, 567-571.

Schouten, S., Hopmans, E.C., Damsté, J.S.S., 2013. The organic geochemistry of glycerol dialkyl glycerol tetraether lipids: a review. *Organic Geochemistry* 54, 19-61.

Schouten, S., Hopmans, E.C., Schefubb, E., Sinninghe Damste, J.S., 2002. Distributional variations in marine crenarchaeotal membrane lipids:

a new tool for reconstructing ancient sea water temperatures? *Earth and Planetary Science Letters* 204, 265-274.

Schouten, S., Huguet, C., Hopmans, E.C., Kienhuis, M.V., Sinninghe Damsté, J.S., 2007. Analytical methodology for TEX86 paleothermometry by high-performance liquid chromatography/atmospheric pressure chemical ionization-mass spectrometry. *Analytical Chemistry* 79, 2940-2944.

Schouten, S., Pitcher, A., Hopmans, E.C., Villanueva, L., van Bleijswijk, J., Damsté, J.S.S., 2012. Intact polar and core glycerol dibiphytanyl glycerol tetraether lipids in the Arabian Sea oxygen minimum zone: I. Selective preservation and degradation in the water column and consequences for the TEX 86. *Geochimica et Cosmochimica Acta* 98, 228-243.

Seifert, W., Moldowan, J., 1986. Use of biological markers in petroleum exploration. *Methods in geochemistry and geophysics* 24, 261-290.

Seifert, W.K., Moldowan, J.M., 1978. Applications of steranes, terpanes and monoaromatics to the maturation, migration and source of crude oils. *Geochimica et Cosmochimica Acta* 42, 77-95.

Seifert, W.K., Moldowan, J.M., 1980. The effect of thermal stress on source-rock quality as measured by hopane stereochemistry. *Physics and Chemistry of the Earth* 12, 229-237.

Shackleton, N.J., 1977. Oxygen isotope and palaeomagnetic evidence for early Northern Hemisphere glaciation. *Nature* 270, 216-219.

Shackleton, N.J., Pisias, N., 1985. Atmospheric carbon dioxide, orbital forcing, and climate. *The Carbon Cycle and Atmospheric CO: Natural variations Archean to Present*, 303-317.

Sikes, E.L., Volkman, J.K., 1993. Calibration of alkenone unsaturation ratios (Uk'37) for paleotemperature estimation in cold polar waters. *Geochimica et Cosmochimica Acta* 57, 1883-1889.

Sikes, E.L., Volkman, J.K., Robertson, L.G., Pichon, J.-J., 1997. Alkenones and alkenes in surface waters and sediments of the Southern Ocean: Implications for paleotemperature estimation in polar regions. *Geochimica et Cosmochimica Acta* 61, 1495-1505.

Silliman, J., Meyers, P., Ostrom, P., Ostrom, N., Eadie, B., 2000. Insights into the origin of perylene from isotopic analyses of sediments from Saanich Inlet, British Columbia. *Organic Geochemistry* 31, 1133-1142.

Simoneit, B.R., 1977. Diterpenoid compounds and other lipids in deep-sea sediments and their geochemical significance. *Geochimica et Cosmochimica Acta* 41, 463-476.

Sinninghe Damste, J.S., Rijpstra, W.I.C., Hopmans, E.C., Prahl, F.G., Wakeham, S.G., Schouten, S., 2002. Distribution of Membrane Lipids of Planktonic Crenarchaeota in the Arabian Sea. *Applied and Environmental Microbiology* 68, 2997-3002.

Sonzogni, C., Bard, E., Rostek, F., 1998. Tropical sea-surface temperatures during the last glacial period: a view based on alkenones in Indian Ocean sediments. *Quaternary Science Reviews* 17, 1185-1201.

Stephens, N.P., Carroll, A.R., 1999. Salinity stratification in the Permian Phosphoria sea; a proposed paleoceanographic model. *Geology* 27, 899-902.

Stickley, C.E., St John, K., Koç, N., Jordan, R.W., Passchier, S., Pearce, R.B., Kearns, L.E., 2009. Evidence for middle Eocene Arctic sea ice from diatoms and ice-rafted debris. *Nature* 460, 376-379.

Storey, M., Mahoney, J.J., Saunders, A.D., Duncan, R.A., 1995. Timing of hot spot-related volcanism and the breakup of Madagascar and India. *Science* 267, 852.

Sturt, H.F., Summons, R.E., Smith, K., Elvert, M., Hinrichs, K.U., 2004. Intact polar membrane lipids in prokaryotes and sediments deciphered by high-performance liquid chromatography/electrospray ionization

multistage mass spectrometry—new biomarkers for biogeochemistry and microbial ecology. *Rapid Communications in Mass Spectrometry* 18, 617-628.

Subroto, E.A., Alexander, R., Kagi, R.I., 1991. 30-Norhopanes: their occurrence in sediments and crude oils. *Chemical Geology* 93, 179-192.

Summons, R.E., 1993. Biogeochemical cycles, Organic Geochemistry. Springer, pp. 3-21.
Tan, Y., Heit, M., 1981. Biogenic and abiogenic polynuclear aromatic hydrocarbons in sediments from two remote Adirondack lakes. *Geochimica et Cosmochimica Acta* 45, 2267-2279.

Tippett, J.M., Kamp, P.J., 1993. The role of faulting in rock uplift in the Southern Alps, New Zealand. *New Zealand Journal of Geology and Geophysics* 36, 497-504.

Tissot, B., Welte, D., 1978. Petroleum Formation and Occurance: A New Approach to Oil and Gas Exploration. Springer.
Tornabene, T., Langworthy, T., Holzer, G., Oro, J., 1979. Squalenes, phytanes and other isoprenoids as major neutral lipids of methanogenic and thermoacidophilic "archaebacteria". *Journal of Molecular Evolution* 13, 73-83.

Trendel, J.-M., Restle, A., Connan, J., Albrecht, P., 1982. Identification of a novel series of tetracyclic terpene hydrocarbons (C 24–C 27) in sediments and petroleums. *Journal of the Chemical Society, Chemical Communications*, 304-306.

Tyson, R.V., 1995. Abundance of organic matter in sediments: TOC, hydrodynamic equivalence, dilution and flux effects, Sedimentary organic matter. Springer, pp. 81-118.
Vail, P., Mitchum Jr, R., 1979. Global cycles of relative changes of sea level from seismic stratigraphy: resources, comparative structure, and eustatic changes in sea level.

Van Sickel, W.A., Kominz, M.A., Miller, K.G., Browning, J.V., 2004. Late Cretaceous and Cenozoic sea-level estimates: backstripping analysis of borehole data, onshore New Jersey. *Basin Research* 16, 451-465.

Villanueva, J., Grimalt, J.O., 1997. Gas Chromatographic Tuning of the U k '37 Paleothermometer. *Analytical chemistry* 69, 3329-3332.

Viso, A.-C., Pesando, D., Bernard, P., Marty, J.-C., 1993. Lipid components of the Mediterranean seagrass Posidonia oceanica. *Phytochemistry* 34, 381-387.

Volkman, J., Jeffrey, S., Nichols, P., Rogers, G., Garland, C., 1989. Fatty acid and lipid composition of 10 species of microalgae used in mariculture. *Journal of Experimental Marine Biology and Ecology* 128, 219-240.

Volkman, J.K., 1986. A review of sterol markers for marine and terrigenous organic matter. *Organic Geochemistry* 9, 83-99.

Volkman, J.K., 2005. Sterols and other triterpenoids: source specificity and evolution of biosynthetic pathways. *Organic Geochemistry* 36, 139-159.

Volkman, J.K., Barrerr, S.M., Blackburn, S.I., Sikes, E.L., 1995. Alkenones in Gephyrocapsa oceanica: Implications for studies of paleoclimate. *Geochimica et Cosmochimica Acta* 59, 513-520.

Volkman, J.K., Barrett, S.M., Blackburn, S.I., Mansour, M.P., Sikes, E.L., Gelin, F., 1998. Microalgal biomarkers: a review of recent research developments. *Organic Geochemistry* 29, 1163-1179.

Volkman, J.K., Eglinton, G., Corner, E.D., Forsberg, T., 1980. Long-chain alkenes and alkenones in the marine coccolithophorid Emiliania huxleyi. *Phytochemistry* 19, 2619-2622.

Vorren, T.O., Thiede, J., 1994. The marine geology of the Arctic Ocean—Summary. *Marine Geology* 119, 357-361.

Weijers, J.W., Schouten, S., Spaargaren, O.C., Damsté, J.S.S., 2006. Occurrence and distribution of tetraether membrane lipids in soils: implications for the use of the TEX 86 proxy and the BIT index. *Organic Geochemistry* 37, 1680-1693.

Weijers, J.W.H., Schouten, S., van den Donker, J.C., Hopmans, E.C., Sinninghe Damsté, J.S., 2007. Environmental controls on bacterial tetraether membrane lipid distribution in soils. *Geochimica et Cosmochimica Acta* 71, 703-713.

Wellman, H.W., 1971. Age of the Alpine Fault, New Zealand. Proc Int. Geol. Congr, 22nd, 4:148–162. *International Geological Congress* 22, 148-162.

Wenger, L.M., Isaksen, G.H., 2002. Control of hydrocarbon seepage intensity on level of biodegradation in sea bottom sediments. *Organic Geochemistry* 33, 1277-1292.

Wójcik-Tabol, P., Ślączka, A., 2015. Are Early Cretaceous environmental changes recorded in deposits of the Western part of the Silesian Nappe? A geochemical approach. *Palaeogeography, Palaeoclimatology, Palaeoecology* 417, 293-308.

Wright, J.D., Miller, K.G., 1993. Southern Ocean influences on late Eocene to Miocene deepwater circulation. *The Antarctic paleoenvironment: a perspective on global change* 60, 1-25.

Wyrtki, K., 1961. The thermohaline circulation in relation to the general circulation in the oceans. *Deep Sea Research (1953)* 8, 39-64.

Zachos, J., Pagani, M., Sloan, L., Thomas, E., Billups, K., 2001. Trends, rhythms, and aberrations in global climate 65 Ma to present. *Science* 292, 686-693.

Zachos, J.C., Dickens, G.R., Zeebe, R.E., 2008. An early Cenozoic perspective on greenhouse warming and carbon-cycle dynamics. *Nature* 451, 279-283.

Zachos, J.C., Lohmann, K.C., Walker, J.C., Wise, S.W., 1993. Abrupt climate change and transient climates during the Paleogene: A marine perspective. *The Journal of Geology* 101, 191-213.

Zhao, M., Dupont, L., Eglinton, G., Teece, M., 2003. n-Alkane and pollen reconstruction of terrestrial climate and vegetation for NW Africa over the last 160 kyr. *Organic Geochemistry* 34, 131-143.

Zhi-Hua, H., Hui-Xiang, L., Rullkötter, J., Mackenzie, A., 1986. Geochemical application of sterane and triterpane biological marker compounds in the Linyi Basin. *Organic Geochemistry* 10, 433-439.

2. Global sea level changes or local tectonics? First Miocene biomarkers in cored sedimentary rocks from IODP Expedition 317, Canterbury Basin, New Zealand

Sophia Aharonovich[1*], Julius S. Lipp[2], and Simon C. George[1]

[1] Department of Earth and Planetary Sciences and Macquarie Marine Research Centre, Macquarie University, NSW, Australia

[2] MARUM Centre for Marine Environmental Sciences & Department of Geosciences, University of Bremen, 28359 Bremen, Germany, Germany

* corresponding author (e-mail: sophia.aharonovich@mq.edu.au)

Statement of authors' contribution

This Chapter is an article to be submitted to *Organic Geochemistry*. This paper has been formatted to conform to the font and referencing style adopted in this thesis. Section, Figures, and Tables included within the text are prefixed with the chapter number.

I am the primary author (90% of the effort). I extracted the organic material from the samples. I analysed the organic data and created the proposed climate reconstructions. I wrote and designed the structure of the paper. The co-author carefully reviewed and provided feedback and valuable refinements on this version of the manuscript (10%). Neither this manuscript nor one with similar content under our authorship has been published or is being considered for publication elsewhere, except as described above.

Abstract

The influence of global sea level (eustasy) and local tectonic changes on sedimentation processes in continental margin deposits is a fundamental part of sedimentary research. Since the late Miocene global sea level change has been dominated by glacioeustasy. Integrated Ocean Drilling Program (IODP) Expedition 317 to the Canterbury Basin, on the eastern margin of the South Island of New Zealand, provided the opportunity to study sediment geochemistry in contrasting depositional settings, from mid-shelf to upper slope sedimentary rocks from the Eocene to the Holocene. A particular research focus was on the sequence stratigraphy of the sedimentary package, which recorded a time when global sea level change was dominated by glacioeustasy. Late Eocene to Holocene sedimentary sequences were cored in transect of three drilling sites on the continental shelf (Sites U1351, U1353 and U1354) and one on the continental slope (Site U1352).

This paper provides the first examination of the organic geochemical record from Pliocene, Miocene, and Oligocene sediment samples recovered during IODP Expedition 317 from Sites U1351, U1352, and U1353, using bulk geochemistry, and hydrocarbon and biomarker distributions. The hydrocarbon and biomarker data sets are able to record the difference between local tectonic and eustatic influences on the organic reservoirs in the Canterbury Basin sediments. The main aim of this research was to correlate changes in hydrocarbon and biomarker accumulations with local tectonic activity in the area, as well as with the global climatic transformations that occurred during the Miocene epoch.

Total organic carbon content for the samples is generally low (<1 wt. %), with only a few spot samples from the U1352 having higher values. There is good preservation of C_{11} to C_{35} *n*-alkanes, with varying predominance of odd-over-even chain length long-chain *n*-alkanes ($CPI_{(22-32)}$) and a high variation in terrigenous/aquatic ratio (TAR) over the cores. The Pr/Ph ratios (0.7-5.9) for all three cores indicate anoxic to oxic depositional environments. Pr/*n*-C_{17}

and Ph/*n*-C_{18} together with the hopane Ts/(Ts+Tm) ratio indicate low thermal maturities (sub oil window) for all samples. High levels of oleanane, C_{24} tetracyclic terpanes and C_{29} steranes are indicators of terrigenous organic matter input in our samples. A high C_{30} sterane index, and the presence of C_{27} and C_{28} steranes indicate marine organic matter input. Based on these data it is suggested that local tectonic activity had a rapid and significant influence on accumulation of organic matter on the continental shelf and slope, especially during the 14-12 Ma and ~6 Ma periods. The uplift of the Southern Alps and an increase in the continental slope angle could be a possible reason for the increase in terrigenous organic matter input during these periods. The influence of sea level changes and global temperature variations are suggested for periods before 14 Ma, between 12 and 7 Ma, and after 6 Ma.

2.1. Introduction

The Cenozoic era covers the last 66 million years (Ma) of Earth history. Significant climate changes during this period strongly influenced the distribution of flora and fauna in the oceans and on land (e.g. Zachos et al., 2001; Zachos et al., 2008). One of the challenges in Cenozoic climate reconstructions is to understand the main regional triggers of these changes (Zachos et al., 2008). On the one hand, global sea-level changes (eustasy) influenced by high tectonic activity and climate changes (Haq et al., 1987; Van Sickel et al., 2004) with quasi-periodic oscillations in Earth's orbital parameters (eccentricity, obliquity, and precession) have been suggested to be the main sources of the variations (Miller et al., 2005). On the other hand, limited local or regional tectonic activity had very significant controls on the distribution of sediments and life on the continental margins (Van Sickel et al., 2004).

Global marine palaeoclimate reconstructions during the Cenozoic era mostly rely on $\delta^{18}O$ and Mg/Ca ratios from foraminiferal records (Zachos et al., 2008). These data provide information regarding the sea surface temperatures (SST) and changes in global ice volume levels (Keigwin and Keller, 1984; Shackleton and Pisias, 1985; Miller et al., 1991). The oxygen isotope record suggests global SST decreased from the early Eocene all the way through the Neogene (Zachos et al., 2001; Zachos et al., 2008). Correlations between increasing CO_2 concentrations and increases in global SST have been proposed (Zachos et al., 2008). During the Cenozoic, the global climatic optima that are related to high temperature levels, warm poles and no ice cover are associated with high pCO_2 (Zachos et al., 2001). The CO_2 levels were calculated using different proxy data sets such as boron, alkenones, and nahcolites from marine and lacustrine environments (Royer, 2006). Other greenhouse gases such as methane show quite similar trends related to the palaeoclimate reconstructions of the Cenozoic (MacDonald, 1990).

Eustatic sea-level changes are influenced by accumulation and melting of ice sheets around the globe. Both processes are strongly related to temperature variations (Haq et al., 1987; Van

Sickel et al., 2004). The eustatic imprint can be found in regional sedimentary processes mainly on continental margins (Posamentier, 1988; Kominz et al., 1998; Van Sickel et al., 2004). On the one hand, Cenozoic sea level changes models are influenced by large continental ice sheet accumulation which can be responsible for large (>100 m) sea-level fluctuations (Haq et al., 1987; Pitman and Golovchenko, 1991). On the other hand, fluctuations of up to 25 m in sea level can be related to relatively modest climatic changes and ice volume fluctuations (Miller et al., 1998; Miller et al., 2003; Van Sickel et al., 2004). The sequence modelling described by Haq et al. (1987) is widely used nowadays, but it's comparison to later reconstructions based on accumulation of sediments on the Siberian Platform (Sahagian et al., 1996) and the New Jersey Margin (Van Sickel et al., 2004) is limited. The high levels of disagreement between all models for the Cenozoic Era can only be observed during the first half of the Neogene (to 11 Ma). Much higher sea levels are proposed by Haq et al. (1987) during the first part of the Neogene, and very low sea level variations are suggested by Van Sickel et al. (2004) and Miller et al. (2005).

Coastal regions are important sources of the terrigenous organic matter (OM) input derived from the continents that reach marine sediments (Middelburg, 1989; Hedges and Keil, 1995). The terrigenous OM can be transported various ways, such as by river flow, wind, and coastal erosion. However, transport pathways and the fate of terrestrial organic matter in the ocean are not fully understood (Hedges et al., 1997). Changes in sea level strongly influence OM input, especially in coastal regions. Low sea levels expose greater shore areas, causing an increase in erosion of the coastline and an increase in OM input to the oceans. Low sea levels also lead to high exposure of OM to the air, causing higher oxidation of the OM that is delivered to marine sediments (Middelburg, 1989). High sea levels usually decrease the levels of OM input to the sediments, but this OM is better preserved under oxic and suboxic conditions (Middelburg, 1989).

The modern New Zealand (NZ) subcontinent lies at the interface between the southwest Pacific Ocean and the Southern Ocean (Nelson and Cooke, 2001; Tomczak and Godfrey, 2013). Tectonic reconstructions show significant movement of the New Zealand land mass to the north for the last 40 Ma (King, 2000; Nelson and Cooke, 2001). These models also suggest the presence of some New Zealand land mass from the Oligocene (King, 2000) for the South Island, and the first appearance of the Southern Alps as early as the middle Miocene (~11 Ma) (Wood and Stagpoole, 2007). Rapid uplift of the Southern Alps with an associated significant increase of the land mass is proposed from 7-6 Ma (Nelson and Cooke, 2001).

Until the Oligocene, New Zealand was surrounded by tropical and subtropical seas. For example, planktonic foraminifera (Jenkins, 1965) and $\delta^{18}O$ (Shackleton and Kennett, 1975) records suggest warm SSTs at the Oligocene/Miocene boundary for the New Zealand region. During the Neogene, the Antarctic oceanic front developed (Lawver et al., 1992; Nelson and Cooke, 2001). This caused a decrease in the SST around New Zealand from the early Miocene as cooler subtropical paleo-currents and later on the cold intrusions of the sub-Antarctic currents started to influence the ocean temperature, especially around the east coast of New Zealand (Nelson and Cooke, 2001). This influence increased from the middle Miocene, ~ 15 Ma. These reconstructions are supported by land fossil records from New Zealand, which show warm-water environments for the first part of the Neogene (Chaproniere, 1984; Beu et al., 1997).

The main purpose of the Integrated Ocean Discovery Program (IODP) Expedition 317, which occurred from November 2009 to January 2010 in the Canterbury Basin, New Zealand (Fig. 2.1), was to compare the relative influence of local tectonics and global sea level changes on sediments accumulated on the continental shelf and slope off the east coast of the South Island.

Sedimentary sequences (Fig. 2.1) were drilled in a transect of three sites on the continental shelf (landward to basinward, Sites U1353, U1354, and U1351) and one on the continental slope (Site U1352) (Fulthorpe et al., 2011b). The Canterbury Basin sedimentary record provides a unique opportunity for examining the accumulated biomarker signal in the region. A global climatic optimum and temperature increase at the early/middle Miocene boundary (Nelson and Cooke, 2001), together with the increasing land mass of the sub-continent based on an increase in sedimentation rates since the middle Miocene (Lu et al., 2005), would imply gradual intensification in the amount of land vegetation. Interpretation of global eustatic and climatic transformations suggest that cooler Neogene seawater conditions were coupled with a decrease in global sea levels (Zachos et al., 2001; Van Sickel et al., 2004). Therefore, the influence of this climate shift on the accumulation and preservation of organic matter in the marine sediments is expected.

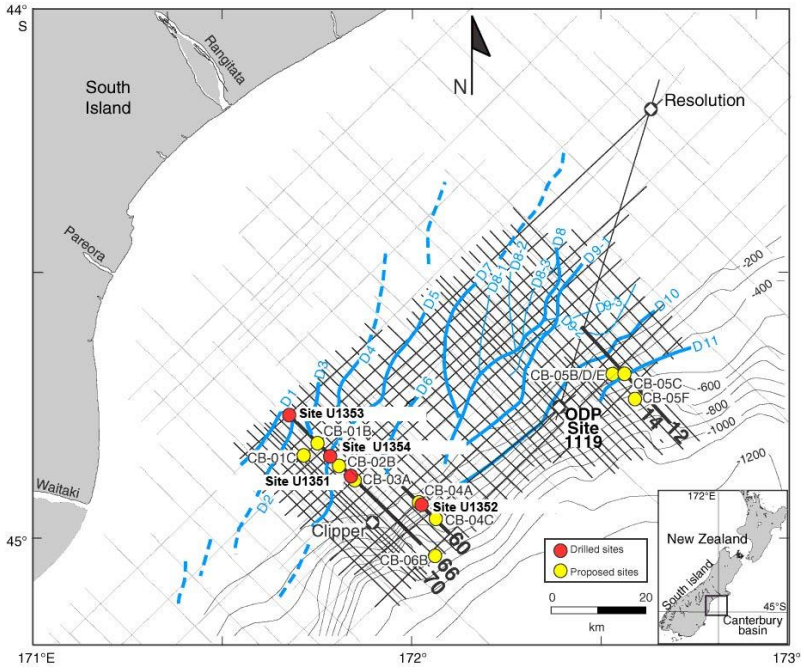

Figure 2.1: Drilled and proposed Expedition 317 sites, with multichannel seismic (MCS) commercial low-resolution grid. Blue curved lines show the distribution of seismically resolvable sediment drifts (Fulthorpe et al., 2011).

This paper provides the first examination of the organic geochemical record from three Pliocene, 72 Miocene, and six Oligocene sediment samples recovered during IODP Expedition 317 from Sites U1351, U1352, and U1353, using bulk geochemistry, and hydrocarbon and biomarker distributions (Tables 1–4). In addition, organic geochemical data are reported for three early Pliocene and six Oligocene samples from Site U1352 (Tables 2–4). The hydrocarbon and biomarker data sets are able to record the difference between local tectonic and eustatic influences on the organic reservoirs in the Canterbury Basin sediments The main aim of this research is to correlate changes in hydrocarbon and biomarker accumulations with local tectonic activity in the area, as well as with the global climatic transformations occurred during the Miocene epoch.

This research assesses the thermal maturity of the sediments in order to test the reliability of the organic proxies used in paleoclimatic reconstructions. In addition, this research distinguishes the source of the organic matter in the Canterbury Basin based on the bulk chemistry and lipid analyses. Samples from IODP Expedition 317 provide a unique opportunity to look at OM accumulated during the second part of the Cenozoic epoch. In addition, comparison between different organic proxies are made so as to establish the reliability of the paleoclimatic reconstructions.

2.2. Materials and methods

2.2.1. Lithology, age/depth model and sample collection

This study is based on a set of sedimentary samples from three drilling sites: U1351, U1352, and U1353 (Fig. 2.1). The age model for each site is based on the shipboard study of calcareous nannofossils, diatoms, and planktonic and benthic foraminiferas (Fulthorpe et al., 2011b). Overall, hydrocarbon and biomarker contents were determined for 81 samples. The lithological unit definitions for each of the sites were based on the observed variation in lithology in the cores (Fulthorpe et al., 2011b).

Site U1351 was located on the outer continental shelf (Fig. 2.1). Lower Pliocene–late Miocene sediments are characterised by low levels of erosion (Fulthorpe et al., 2011b). The Miocene section of the site was mainly dated using planktonic foraminifers, which showed a major depositional hiatus of ~3.4 million years between 7.07 and 10.50 Ma. The bottom of Hole B at the Site U1351 was dated as late Miocene (10.60–10.91 Ma). All ten analysed samples are from U1351 and consist of lithological Unit II, which was deposited in the late Miocene (Table 2.1). Unit II is composed of dark greenish grey to greenish black sandy mud, muddy sand and shell hash. This unit becomes more lithified with depth because of carbonate cementation. The mineralogy suggests a dominant provenance from the southerly Otago Schist (Fulthorpe et al., 2011b).

Site U1352 was located on the upper slope within the Canterbury Basin and is the most basinward site in this study (Fig. 2.1). Good sediment recovery led to an excellent record of the Miocene. The sediments were dated by foraminifera and nannofossil proxies (Table 2.1) which show that the late Miocene/early Pliocene boundary is between 1266 and 1284 meters below sea floor (mbsf). 59 Miocene samples were analysed from lithological unit IIB, and are characterised by hemipelagic and pelagic sedimentation in Hole C (1275–1851 mbsf). The Miocene part of Unit II consists of a low frequency of dark-coloured mudstone beds. There

are also hiatuses in deposition between 1394.62 and 1409.66 mbsf, where at least 5 million years are missing, and between 1486.78 and 1496.91 mbsf, where 1.3 million years are missing. The lower part of Unit II consists of a gradual progression from marlstone to limestone with frequent glauconitic laminae and beds. There is a large unconformity of 11-12 million years between 1851.46 and 1875.46 mbsf (Fulthorpe et al., 2011b). Below this unconformity the early Oligocene to Eocene (Unit III) sediments are hemipelagic to pelagic foraminifer-bearing nannofosil limestones with minor amounts of quartz and clay (Fulthorpe et al., 2011b). The latter unit is correlative to the onshore Amuri Limestone. One long unconformity from 19–30.1 Ma (1903.29–1916.63 mbsf) is present in Unit III, and the bottom part of Hole C was dated to 35.2–36.0 Ma in the Eocene (Fulthorpe et al., 2011b). Six samples representing the early Oligocene from Unit III, below 1875 mbsf, were analysed.

The third set of samples are from Site U1353, which is the most onshore of the shelf sites from Expedition 317 (Fig. 2.1). Hole B at U1353 Site is characterised by dark greenish-grey, micaceous very fine sandy-mud and mud samples. Four samples from this site are from the middle to late Miocene (Fulthorpe et al., 2011b). The Miocene/Pliocene boundary was not detected from the biostratigraphical data. However, stratigraphic correlation to other drilled sites suggest that the 510.52–518.66 mbsf interval could be dated to 12.03 Ma. In addition, the deepest sample from this site has a biostratigraphical assemblage dated to middle to early Miocene. The dominant lithology of the studied lithological Unit II is dark greenish grey, micaceous fine sandy mud and mud with shells. Based /on the proposed stratigraphic correlations, four samples were analysed from this site.

2.2.2. TOC and Source Rock Analyser measurements

Total organic carbon (TOC) and total nitrogen (TN) analyses were performed on board (Methods in Fulthorpe et al., 2011a) Sample data are summarised in Table 2.1. Nominally 10

cm^3 wet volume (about 3 g dry mass) of sediment was selected based on the changes in lithology, with organic-rich lithologies identified based on visual differences. Dried samples were crushed and homogenised to a fine powder. The inorganic carbon (IC) content was determined by a UIC 5011 CO_2 coulometer. About 10 mg of the sample was reacted with 1N HCl.

Total carbon (TC) and the TN content of the sediment samples were determined using a ThermoElectron FlashEA 1112 elemental analyser equipped with a ThermoElectron packed column (CHNS/NCS) and a thermal conductivity detector (TCD). Between 8-12 mg of each sample was mixed with one small spatula of vanadium pentoxide catalyst and the sample was combusted in a stream of oxygen at 900°C. The TOC content was calculated as the difference between TC and IC from coulometry (Table 2.1).

The Rock-Eval parameters *T*max (ºC), production index (PI), hydrogen index (HI) (mg HC/g C) and oxygen index (OI) (mg CO_2/g C) were calculated from pyrolysis values obtained using a Source Rock Analyser (SRA) (Weatherford Laboratories), using between 60 and 150 mg of freeze-dried, ground sediment. All measurements were preceded by a blank and then calibrated to a rock standard from Weatherford Laboratories (99986; PWDR5); the same standard was used for quality control (QC) every 10 samples. Typical precision was assessed using eight replicate analyses of the rock standard. Coefficients of variation for this data set fell between 0.005 (*T*max) and 0.1 (OI). The *T*max and production index provide an estimation of the thermal maturity of the OM, although can be influenced by sample mineralogy (e.g. illite content), kerogen type, and heavy OM fractions in the samples (Espitalié, 1986).

2.2.3. Extraction and fractionation of the soluble organic matter

Two types of samples were extracted. The first group of 11 samples were the "squeeze cake" residues from the pore water analyses (Methods in Fulthorpe et al., 2011a), from which 49–76 g of sediment was extracted (Table 2.2). The second group consists of 70 cut samples that were sampled on-board from the working half of the cores. From these samples 1.6–24.3 g of sediment was extracted (Table 2.2). All samples were hand crushed using a ceramic pestle and mortar and passed through a 125 μm sieve. Samples were mixed ~50:50 with pre-extracted and baked sand (3 hours at 450°C) so as to increase solvent extraction efficiency and were extracted using a Dionex Accelerated Solvent Extractor (ASE 300) using 9:1 dichloromethane (DCM):methanol. Two extraction runs were used, each of which consisted of three cycles of 5 min. preheating, 5 min. static at 1500 bar pressure and 100°C, and 3 min. solvent purging to the collection bottle. Sulphur was removed from the extractable organic matter (EOM) of all samples by refluxing at 40°C with acid-activated copper turnings. The volume of the EOM was reduced to 10 mL using a rotary evaporator (Buchii R-210), and 1 mL was dried in order to obtain the weight of the EOM recovered. The extractability was calculated relative to the weight of sediment used (mg EOM/g sediment) (Table 2.2).

The rest of the EOM was separated using a short silica column into three fractions using organic solvent solutions: aliphatic hydrocarbons (*n*-hexane), aromatic hydrocarbons (n-hexane:DCM, 4:1), and polar compounds (DCM:methanol, 1:1). The polar fraction was dried, weighed and stored. The hydrocarbon fractions were spiked with a mixture of internal standards (IS) of known concentration (terphenyl d14, anthracene d10, and tetracosane d50).

2.2.4. Gas chromatography-mass spectrometry (GC-MS)

The two hydrocarbon fractions were analysed by gas chromatography-mass spectrometry (GC-MS), using an Agilent GC (6890N) coupled to an Agilent Mass Selective Detector

(5975B). 1 μL of solution was injected onto a Programmable Temperature Vaporizing (PTV) inlet at 35°C, followed by a temperature increase at 700°C/min. to 310°C. Separation was performed on a J&W DB5MS UI (60 m x 250 μm x 0.25 μm) column, with helium carrier gas at 1.5 mL/min. constant flow rate and 155 KPa starting pressure. The MS was operated in full-scan mode (50–550 amu) for all samples and fractions. In addition, some of the samples were analysed using two selective ion monitoring (SIM) mode programmes. For the aliphatic fraction the targeting ion masses were: m/z 123.1, 177.2, 191.2, 205.2, 217.2, 218.2, 231.2, 253.2, and 259.2. For the aromatic fraction the targeting ion masses were: m/z 91.1, 106.1, 120.1, 128.1, 134.1, 142.1, 152.2, 154.2, 156.1, 164.2, 166.1, 168.1, 170.1, 178.1, 180.1, 182.1, 192.1, 197.1, 202.1, 206.1, 212.1, 216.1, 220.1, 230.1, 234.1, and 241.1. In addition, SIM ion masses m/z 66.1, 183.2, and 188.1 were added to each programme for IS identification. The target compounds are identified using retention times relative to known standards, and mass spectral comparison to NIST and WILEY library data.

2.3. Results

2.3.1. Bulk geochemistry

The carbonate content of the U1351B Site samples varies from 0.6 to 62.4 wt% (Table 2.1). TOC fluctuates between 0.10 and 0.96 wt%, but is mostly <0.5 wt% and averages around 0.27 wt% (Fig. 2.2A; Table 2.1). The HI (Espitalie et al., 1977) for U1351B Site samples varies from 22 to 51 mg S_2/g TOC with average of 36 mg/g (Fig. 2.2C; Table 2.1) and no particular trend with depth. *T*max (Espitalié, 1986) values vary from 400 to 419°C, with an average of 415°C. The PI (Espitalié, 1986) mostly ranges from 12 to 30, with one higher value (59) at 5.6 Ma (Fig. 2.2F; Table 2.1). The OI (Espitalie et al., 1977) ranges from 25 to 69 mg CO_2/g TOC with the highest value at 5.84 Ma (Fig. 2.2D). These data indicate that the U1351B Site samples are immature and contain large amounts of oxygen-containing functional groups

attached to the kerogen, consistent with the low amount of diagenetic alteration of organic matter expected at these depths (Fig. 2.3A; Table 2.1).

For the U1352C Miocene and early Oligocene samples the TOC varies from 0.03 to 1.5 wt%, with most values <0.5 wt% and an average of ~0.42 wt% (Table 2.1; Fig. 2.2A). The highest TOC values are between 19.27 Ma and 18.69 Ma (reaching 1.5 wt%) and between 14.61 Ma and 13.51 Ma with values as high as 1.4 wt%. TN values are scattered in the range of <0.001–0.09 wt% (Table 2.1), with very low or undetectable levels of TN in the range of 31.67–19.06 Ma, and some higher values of 0.09, 0.06, 0.04, and 0.06 wt% at 19.08, 16.85, 13.51 and 9.25 Ma, respectively (Table 2.1). TOC/TN ratios mostly range from 5 to 50 (Fig. 2.2B), but the age range between 13.77–19.06 Ma has high values of up to 1514, reflecting very low TN contents, mostly in carbonates (Table 2.1). The TOC/TN values increase above 40 in the range of 14.62– 13.77 Ma (Fig. 2.2B).

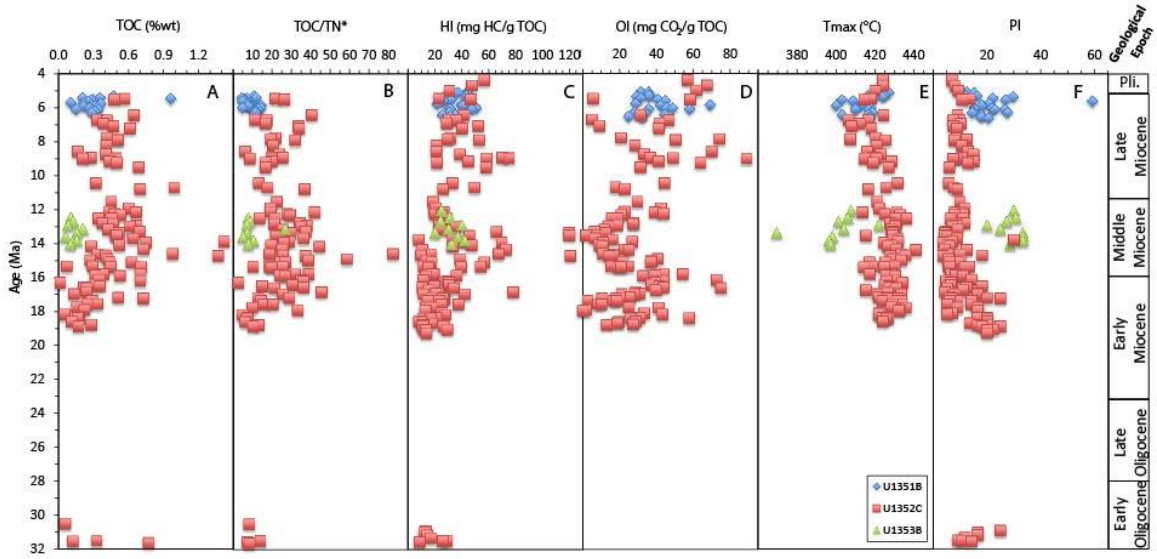

Figure 2.2: On-board acquired bulk geochemistry data (Fulthorpe et al., 2011) for the analysed samples from the outer continental shelf core (U1351, blue), the continental slope core (U1352, red), and the inner continental shelf core (U1353, green). Parameters are plotted against interpreted age from the biostratigraphy (Table 2.1). TOC – total organic carbon, TN – total nitrogen, HI – hydrogen index, OI – oxygen index, Tmax – maximum temperature of S_2 peak, PI – production index, and Pli. – Pliocene. * to keep the presentation to scale all the TOC/TN values above 100 are not plotted, but are shown in Table 2.1.

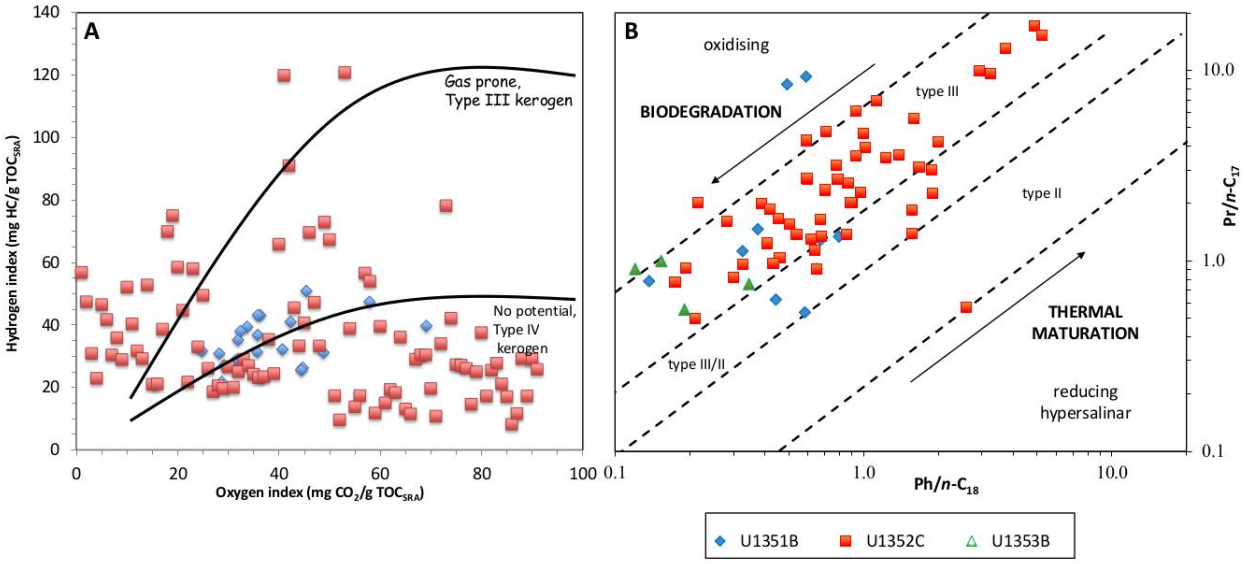

Figure 2.3: **A**. Modified and enlarged van Krevelen diagram based on a cross-plot of hydrogen index vs. oxygen index, showing trend lines for kerogen Types III and IV for U1352C (red) and U1351B (blue), after Fulthorpe et al., 2011. **B**. Kerogen type with biodegradation and maturation levels of EOM based on Ph/n-C_{18} and Pr/n-C_{17} ratios for the U1351 (blue), U1352 (red), and U1353 (green) samples.

The HI of the Miocene and early Oligocene samples in U1352C ranges from 8 to 121 mg S_2/g TOC, with an average of 32.8 mg S_2/g TOC (Table 2.1). The samples can be divided into three major groups based on HI (Fig. 2.2C; Fig. 2.3A): between 31.67–17.16 Ma the samples have low HI values < 38 mg S_2/g TOC, between 16.98–13.17 Ma the HI values vary a lot, reaching a maximum value of 121 at 14.72 Ma, and between 13.17–4.39 Ma the HI values are between 19 and 75 mg S_2/g TOC. The OI is highly variable (2 to 89 mg S_3/g TOC), with an average of 29.5 mg S_3/g TOC (Figs 2D and 3A; Table 2.1). Samples from three age ranges have OI values <15 mg S_3/g TOC: 19.08–18.40 Ma, 16.13–13.51 Ma, and 7.22–5.52 Ma.

The *T*max pyrolysis temperatures of the samples in U1352C range from 406.5°C and 441.1°C with the lowest temperatures calculated for the 7.85–6.70 Ma interval (Table 2.1; Fig. 2.2E). There is a slight increase in *T*max with depth for the Miocene and early Oligocene U1352 samples (Fig. 2.2E). The PI for the U1352C samples is mostly rather low (5–15) for the

Miocene samples <13 Ma, but tends to increase somewhat into the deeper Miocene and Oligocene strata, reaching values of 25 towards the bottom on U1352C (Fig. 2.2F; Table 2.1).

For the Site U1353 Miocene samples the TOC varies between 0.06 to 0.21 wt% with an average of 0.12 wt%, and there is no trend with the depth (Table 2.1; Fig. 2.2A). The TN values are <0.022 wt% and the TOC/TN ratios are mostly <11, with one exception of TOC/TN = 26.9 at 12.90 Ma (Table 2.1; Fig. 2.2B). The HIs range between 20 and 42 mg S_2/g TOC with an average of 31 mg S_2/g TOC (Fig. 2.2C; Table 2.1). No reliable OI was measured for this interval. The *T*max values are generally lower than for similar age samples in Site U1352, and range from 370 to 422 °C (Fig. 2.2E; Table 2.1). The PI averages around 29, with the lowest value of 20 at 12.90 Ma (Fig. 2.2F; Table 2.1).

2.3.2. Extractability

The extractability of the analysed samples is low and does not exceed 0.5 mg EOM/g sediment (Table 2.2). Two depth ranges with higher than average extractability can be identified in U1352 Site between 1750–1580 mbsf and 1390–1245 mbsf. These depths are characterised by darker grey layers of fine sandy mudstone alternating with greenish grey very fine sandy marlstones for the deeper section, and brownish very fine sandy mudstones for the upper section. There is no obvious correlation between extractability and TOC in the sediments. Lithological subunit IIC in U1352C is characterised by many samples with low extractability (<0.1 mg/g) that correlates to recovered sandstone layers. The foraminifera limestone lithology of unit III in U1352C is also characterised by similarly low extractability levels. There is no correlation between the amount of sample extracted and the extractability (Table 2.2).

2.3.3. *n*-Alkanes and isoprenoids

Ten late Miocene samples from the U1351 Site are from the outer continental shelf and contain a low abundance of mid-chain *n*-alkanes and a high abundance of odd carbon-numbered long chain *n*-alkanes (C_{27}, C_{29}, and C_{31}; Table 2.2). Samples from 6.60, 6.41, and 5.76 Ma contain a high relative abundance of *n*-C_{26} (Table 2.2). Parameters summarising the *n*-alkane distributions for the three sites are presented in Fig. 2.4 and Table 2.2. The carbon preference index ($CPI_{(22-32)}$) for this site varies from 0.95–1.8 (Fig. 2.4B). The terrigenous/aquatic ratio (TAR) varies from 11 at 6.60 Ma to 30 at 5.76 Ma without any obvious pattern related to sample depth or lithology (Fig. 2.4C). The $1/P_{aq}$ ratio varies from 2.6 to 3.9 (Fig. 2.4D).

The four Site U1353 samples are from the middle Miocene (Table 2.2). The 13.13 and 13.59 Ma samples contain high amounts of the C_{16}, C_{18}, and C_{20} mid-chain *n*-alkanes, whereas the 12.03 and 13.81 Ma samples contain more of the long-chain *n*-alkanes with an odd carbon number predominance (Fig. 2.4B). The $CPI_{(22-32)}$ varies from 1.0–1.5 with increasing values with depth, the $1/P_{aq}$ ratio has a similar trend (2.4–3.1), whereas there is an opposite trend for the TAR (45–16) (Fig. 2.4B-D).

The early Oligocene samples (1904–1874 mbsf) from the U1352 Site have no significant predominance of any *n*-alkane groups (Table 2.2) and are characterised by a strong even-over-odd carbon number predominance, low $CPI_{(22-32)}$ values (0.12–0.94) and a very low TAR (0.2–3.51) (Fig. 2.4B,C). A similar pattern of *n*-alkanes is present in most of the early Miocene samples from 18.87 to 16.85 Ma (Fig. 2.4B; Table 2.2). The 19.06 Ma sample is an exception as it has a strong predominance of long chain *n*-alkanes without obvious even or odd predominance. The 16.85 Ma sample has a very strong predominance of *n*-C_{29} and *n*-C_{31} *n*-alkanes and a high $CPI_{(22-32)}$ of 4.7, whereas the 16.62 Ma sample has predominant *n*-alkane chain lengths at C_{24}, C_{26}, and C_{28} and thus a rather low $CPI_{(22-32)}$ of 0.53. The TAR is mainly <2, with three samples having extremely high values of 91, 58, and 17 at 19.06, 17.23,

and 16.85 Ma , respectively (Fig. 2.4C; Table 2.2). The $1/P_{aq}$ values mostly range from 1.0 to 3.5 with the 16.85 Ma sample having a high ratio of 13.3 (Fig. 2.4D).

In general, the middle, late Miocene, and early Pliocene samples in U1352 Site have a more diverse distribution of *n*-alkanes (Table 2.2). The samples mainly have C_{14}, C_{16}, and C_{18}

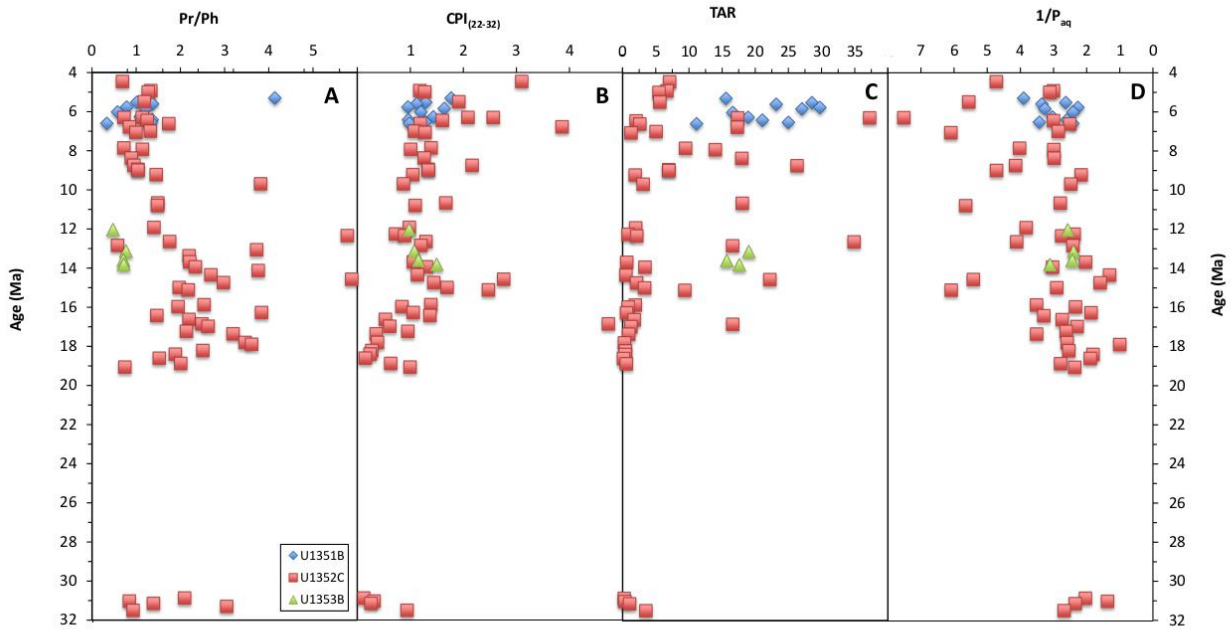

Figure 2.4: n-Alkane and isoprenoid ratios calculated for three drilled sites versus the interpreted age from the biostratigraphy. **A** – Pristane/Phytane (Pr/Ph) ratio; **B** – Carbon preference index ($CPI_{(22-32)}$) for the C_{22}-C_{32} n-alkanes; **C**- terrigenous/aquatic ratio (TAR); **D** – submerged/floating aquatic macrophyte input relative to the terrigenous input ($1/P_{aq}$). Ratios are defined in Table 2.2.

predominance, and/or C_{27}, C_{29}, and C_{31} predominance. No obvious correlations between changes in the *n*-alkane distribution and age or lithology could be identified. The $CPI_{(22-32)}$ for this period varies from 0.8 to 2.8 (Fig. 2.4B) without correlation to sample depth. However the TAR has more significant variations during the middle Miocene from 55 at 16.43 Ma to 0.6 at 13.68 Ma. While most TAR values are below 9.4, three other samples at 14.57, 12.84, and 12.64 Ma also have high values (Table 2.2; Fig. 2.4C). The $1/P_{aq}$ ratio varies from 1.3 to 6.1 with the highest value at 15.11 Ma and the lowest at 14.34 Ma (Fig. 2.4D).

The pristane/phytane (Pr/Ph) ratios in the Site U1353 samples are low (0.47-0.77; Fig. 2.4A; Table 2.2). The Site U1351 samples have a more complicated Pr/Ph variation, with a low value of 0.33 at 6.60 Ma, and higher values to 1.37 at 5.60 Ma. One sample at 5.30 Ma has a much higher Pr/Ph of 4.1. The early Oligocene samples from the U1352 Site have Pr/Ph values between 0.85 and 3.05 (Fig. 2.4A; Table 2.2). The early Miocene samples from 19.06 to 14.12 Ma have widely variable Pr/Ph ratios from 0.74 to 5.9, and then the middle Miocene mostly have lower Pr/Ph ratios, with a very low value of 0.58 for the sample at 12.84 Ma (Fig. 2.4A). The samples younger than 8.37 Ma have Pr/Ph ratios from 0.7–1.7 (Fig. 2.4A; Table 2.2).

The Pr/n-C_{17} values from the U1353 and U1351 shelf sites do not exceed 1.5, except for two samples at 5.52 and 5.84 Ma in Site U1351 that have much higher values (Table 2.2). The Ph/n-C_{18} ratios for these sites are all <1.0 (Table 2.2). The U1352 Site samples from the Oligocene and Eocene are characterised by Pr/n-C_{17} from 0.24–1.87 and Ph/n-C_{18} ratios from 0.08–0.43 (Table 2.2). Pr/n-C_{17} ratio in the early to middle Miocene sediments varies from 0.3 to 17, with the majority of the samples with values <3.2 (Table 2.2). The Ph/n-C_{18} ratio in the early Miocene sediments varies from 0.04 to 5.2 without specific correlation to sample depth and/or lithology. Late Miocene and early Pliocene samples are characterised by Pr/n-C_{17} values between 1.0 and 4.8 and Ph/n-C_{18} values between 0.3 and 1.9 (Table. 2), also without correlation to sample depth and/or lithology.

2.3.4. Hopanes

Hopanes and tricyclic pentanes were identified in samples from all three sites. The results are presented using various ratios and summarised in Table 2.3 and Fig. 2.5. Of the analysed samples from Site U1352, 22 did not contain detectable hopanes or tricyclic terpanes (Table 2.3).

The late Miocene samples from the Site U1351 have widely varying relative abundances of C_{27} 17α-trisnorhopane (Tm) and C_{27} 18α-trisnorneohopane (Ts) compounds. The Ts/(Ts+Tm) ratio varies between 0.12 to 0.62 without correlation to sample depth or lithology (Table 2.3; Fig. 2.5A). The distribution of the C_{30} hopanes αβ/(αβ+βα) hopane ratio varies from 0.30 to 0.43, except for two samples at 6.60 and 5.76 Ma with values of 0.66 and 0.71, respectively. The C_{31} αβ hopane 22S/(22S+22R) ratio varies between 0.07 and 0.14, with high values of 0.38 and 0.26 at 6.60 Ma and 5.76 Ma, respectively. Only low amount of oleanane (oleanane/C_{30} αβ hopane = 0.02 and 0.10) are present in the late Miocene samples.

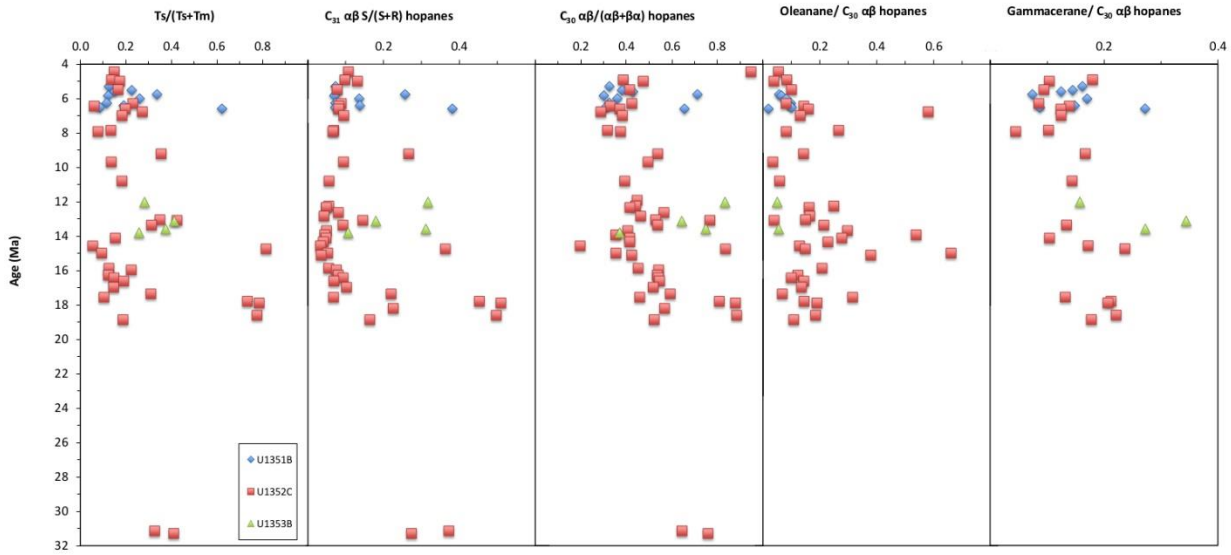

Figure 2.5: Distribution of the hopane data for the U1351 (blue), U1352 (red), and U1353 (green) sites. **A** – C_{27} 17α-22,29,30-trisnorhopane (Tm) and C_{27} 18α-22,29,30-trisnorneohopane (Ts) abundance represented by Ts/(Ts+Tm), **B** – C_{31} αβ 22S and 22R hopane abundance, **C** – C_{30} 17β,21α(H) moretanes and C_{30} 17α,21β(H) hopane abundance, **D** – Oleanane abundance relative to C30 αβ hopane, **E** – Gammacerane abundance relative to C30 αβ hopane. Ratios are defined in Table 2.3.

The gammacerane/C_{30} αβ hopane ratio varies from 0.07–0.17, with high value of 0.27 at 6.60 Ma. The C_{29} αβ hopane and C_{31} αβ hopane abundances are presented relative to C_{30} αβ hopane (Table 2.3; Fig. 2.5B, C). The C_{29}/C_{30} αβ hopane ratio varies significantly through the late Miocene between 0.07 and 1.00, without correlation to sample depth or lithology. The

C_{31}/C_{30} αβ hopane ratio has a wide distribution range from 1.28 at 6.60 Ma to 12.58 at 5.84 Ma (Table 2.3).

C_{21} and C_{23} tricyclic terpanes and C_{24} tetracyclic terpanes were identified in most of the Site U1351 samples (Table 2.3). The C_{23}/C_{21} tricyclic terpane ratio varies between 0.33 to 2.20, with the highest value at 5.60 Ma. No specific correlation to samples depth or lithology was detected. The C_{24} tetracyclic terpanes/C_{23} tricyclic terpane ratio varies between 0.53 and 1.08, with the exception of 6.60 Ma sample which has a value of 0.31.

The identified hopanes and terpanes in middle Miocene Site U1353 samples are presented in Table 2.3 and Fig. 2.5. The Ts/(Ts+Tm) ratio varies between 0.26 and 0.41 with the highest value at 13.13 Ma. The C_{30} hopanes αβ/(αβ+βα) ratio increases from 0.37 to 0.83 during the middle Miocene. The C_{31} αβ hopanes 22S/(22S+22R) ratio varies in the range of 0.11–0.32 without a specific pattern. Only very low amounts of oleanane were detected in two samples. The gammacerane/C_{30} αβ hopane ratio varies from 0.34 to 0.16, with the lowest value at 12.03 Ma. The C_{29}/C_{30} αβ hopane ratio increases from 0.90 at 13.81 Ma to 1.10 at 12.03 Ma with the highest value of 1.13 at 13.13 Ma. The abundance of the C_{31}/C_{30} αβ hopane ratio decreases from 12.7 (13.81 Ma) to 1.9 (12.03 Ma). The C_{23}/C_{21} tricyclic terpanes ratio varies from 1.3 to 2.6. No C_{24} tetracyclic terpane were detected in samples from this site.

The oleanane/C_{30} αβ hopane and gammacerane/C_{30} αβ hopane ratios are presented in Table 2.3 and Fig. 2.5D,E. Oleanane and gammacerane were not detected in the Oligocene samples. The early Miocene samples have oleanane/C_{30} αβ hopane ratio values of 0.07–0.32 and gammacerane/C_{30} αβ hopane ratios <0.22 (Table 3; Fig. 2.5E). The middle Miocene samples from Site U1352 have higher oleanane/C_{30} αβ hopane ratios between 0.21–0.66, with a low ratio of 0.04 at 13.09 Ma (Fig. 2.5D). Gammacerane/C_{30} αβ hopane ratios for the middle Miocene samples are <0.24 (Table 2.3).

The late Miocene samples from Site U1352 have high variability in the oleanane/C_{30} αβ hopane ratio from 0.03 to 0.58 (Table 2.3; Fig. 2.5D). The gammacerane/C_{30} αβ hopane ratio for the late Miocene is <0.17 (Table 3). No oleanane was recorded in the early Pliocene. The gammacerane/C_{30} αβ hopane ratio was only calculated for two early Pliocene samples (0.10 and 0.18).

The early Miocene samples have C_{29} αβ/C_{30} αβ hopane ratios between 0.43–0.89 (Table 2.3), and middle Miocene ratios are <0.75. Three samples at 15.11, 13.93, and 12.64 Ma have high ratios (>0.90), and one sample at 14.57 Ma has a ratio of 1.93. The late Miocene samples have C_{29} αβ/C_{30} αβ hopane ratios of 0.21–1.30. The early Pliocene samples have values between 0.30 and 0.85 (Table 2.3).

The C_{31} αβ hopane 22S/(22S+22R) ratios for all U1352 Site samples are low (<0.4) (Table 2.3). Only three samples at 18.60 Ma, 17.89 Ma, and 17.80 Ma samples have higher values (> 0.45) (Table 2.3).

The C_{31} αβ hopane abundance for the U1352 site samples is presented relative to C_{30} αβ hopane (Table 2.3). The ratio varies significantly between 0.9 to 16.3 through all U1352 Site samples. The middle Miocene period between 15.87–13.69 Ma is characterised by very high values (>10), except for the 14.74 Ma sample with a ratio of 1.4.

The C_{23}/C_{21} tricyclic terpane ratio was only calculated for 17 samples at the U1352 site (Table 2.3). Ratios vary, with most values > 1.0, and only four samples at 18.21, 15.87, 5.49, and 4.45 Ma having values <1.0 (Table 2.3). The C_{24} tetracyclic/C_{23} tricyclic terpane ratio was calculated for some samples for the U1352 Site samples (Table 2.3). The values vary between 0.17 and 1.49, with the lowest value in the early Miocene and the highest in the early Pliocene.

2.3.5. Steranes and diasteranes

The distribution of the C_{27}, C_{28}, and C_{29} ααα 20R steranes for the three sites is plotted on a ternary diagram (Fig. 2.6). The diagram is divided into six areas (I–VI) that define the main sources of OM based on the sterane types and abundance (Huang and Meinschein, 1979). No sterenes were detected in the samples.

The ten U1351 Site samples have sterane distributions that indicate mixed OM sources, including open marine, shallow water and terrigenous environments. The sterane distribution for the U1353 Site samples suggest a mix of terrigenous and shallow marine OM input. Steranes were not identified in 30 of the 67 samples from the continental shelf U1352 Site, but the samples that do contain steranes mostly plot in the open marine environment (Fig. 2.6).

The C_{30} sterane index shows the relative abundance of 24-*n*-propylcholestane to the C_{27}-C_{30} steranes (Table 2.4; Fig. 2.7C). The U1351 Site samples have a C_{30} sterane index from 3.4 to 8.9, without correlation to depth or lithology. Only one samples from the U1351 Site (13.51 Ma) contains C_{30} steranes, and it has a C_{30} sterane index of 5.3. Two early Oligocene samples from the U1352 Site have a C_{30} sterane index of 3.4 and 5.9. The early and middle Miocene samples have high variability in the C_{30} sterane index, with values between 2.9 and 11.4. The late Miocene samples have C_{30} sterane index values between 2.9 and 6.7, without correlation to depth or lithology (Table 2.4; Fig. 2.7C). The Pliocene samples have values <4.6 for the C_{30} sterane index.

The C_{29} ααα 20S/(20S+20R) sterane ratio was calculated for 33 samples from the three sites (Table 2.4; Fig. 2.7B). The late Miocene samples from the U1351 site have values between 0.08 and 0.37. The middle Miocene U1353 site samples have limited ratio variation (0.13–0.21). The early and middle Miocene samples from the U1352 site have C_{29} ααα 20S/(20S+20R) sterane ratios >0.2, except for the sample at 18.87 Ma with a value of 0.14.

The ratios for the late Miocene samples ranges between 0.29 and 0.06. One Pliocene sample has a C_{29} ααα 20S/(20S+20R) sterane ratio of 0.13 (Table 2.4).

Vitrinite reflectance equivalent (VRE) was calculated using the Sofer et al. (1993) equation for 34 samples from the three sites (Table 2.4) The late Miocene samples from the U1351 site have values between 0.33 and 0.68. The middle Miocene U1353 site samples have limited ratio variation (0.40–0.47). The early and middle Miocene samples from the U1352 site have values between 0.41 and 0.68. The ratios for the late Miocene samples have values between 0.33 and 0.53. One Pliocene sample has a VRE value of 0.40 (Table 2.4).

The C_{27}/C_{29} and C_{28}/C_{29} ααα 20R sterane ratios are presented in Table 4. The U1351 site samples have C_{27}/C_{29} αααR from 0.30–0.93 and C_{28}/C_{29} ααα 20R sterane ratios from 0.38–1.07, with the highest values at 6.52 Ma and the lowest at 5.60 Ma for both ratios (Table 2.4). The middle Miocene samples in Site U1353 have C_{27}/C_{29} ααα 20R ratios between 0.31 and 0.42, without correlation with depth or lithology. The U1353 site C_{28}/C_{29} ααα 20R ratio varies from 0.35 at 13.81 Ma to 0.66 at 12.01 Ma.

The C_{27}/C_{29} αααR sterane ratio varies from 0.43 to 1.58 in the U1352 site samples (Table 2.4). The values <0.6 are concentrated in the early and middle Miocene samples. The highest ratio (1.58) is from the early Pliocene (4.92 Ma). The C_{28}/C_{29} αααR sterane ratio for the U1352 site samples varies between 0.34 and 1.81 (Table 2.4). The highest value is from the early Oligocene (31.14 Ma) and the lowest in the middle Miocene (14.57 Ma) (Table 2.4).

The C_{27} αβ diasterane/C_{27} ααα sterane ratio could only be calculated for a few samples due to poor diasterane preservation (Table 2.4, Fig. 2.7A). The late Miocene samples from the U1351 Site have C_{27} αβ diasterane/C_{27} ααα sterane ratios of 0.02 to 0.37. The U1353 samples have values of 0.30–0.56, without correlation to depth or lithology. The U1352 site samples have values between 0.02–0.57 (Table 2.4, Fig. 2.7A). The lowest values are dated to the early Miocene (16.98 Ma), and the highest to the middle Miocene (15.97 Ma).

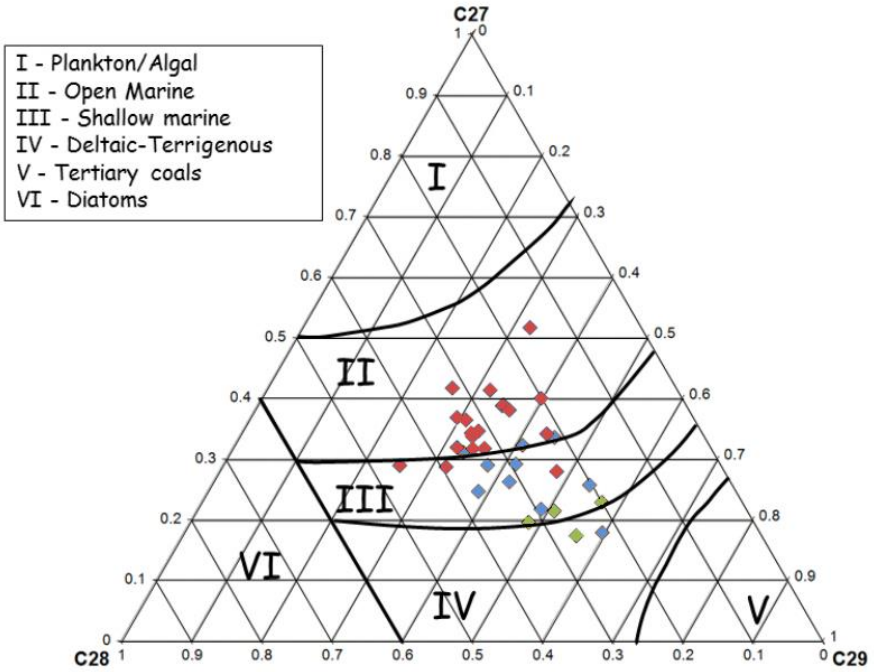

Figure 2.6: C_{27}, C_{28}, and C_{29} ααα 20R sterane distributions for all three sites for the U1351 (orange), U1352 (blue), and U1353 (red) sites. Fields are divided after Huang and Meinschein, 1979.

2.3.6. Aromatic fraction

Some aromatic hydrocarbons were identified only in the U1351 and U1352 Site samples (Table 2.4, Fig. 2.7D), including phenanthrene, methylphenanthrenes and retene. The relative abundance of phenanthrene and four methylphenanthrene isomers (1-methylphenanthrene, 2-methylphenanthrene, 3-methylphenanthrene, and 9-methylphenanthrene) was used to calculate the methylphenanthrene index (MPI) and calculated reflectance (Rc) using the Radke et al. (1986) equation. An approximation of the maximum sediment temperature (max*T)* was calculated based on the Wang et al. (2005) equation, using Rc.

Seven U1351 late Miocene samples have MPI values between 0.31–0.55, with the lowest value at 6.41 Ma (Table 2.4). The VRE values for these samples (0.37–0.62) are consistently

lower than calculated R_c (0.59–0.73). The max*T* parameter suggests maximum sediment temperatures between 100ºC and 118 ºC. The U1351 samples are characterised by high retene/phenanthrene ratios (11.3–41.3), with the highest value at 5.84 Ma.

Phenanthrene and the methylphenanthrenes were identified in 20 U1352 Site samples. The MPI index varies from 0.11 to 0.73 (Table 2.4; Fig. 2.7D). Based on the biomarker preservation the VRE and R_c values couldn't be calculated for the same samples. The highest and lowest values are from the middle Miocene (15.87 and 13.68 Ma, respectively). The max*T* values suggest maximum sediment temperatures between 82ºC and 129ºC (Fig. 2.7E). Retene/phenanthrene values vary for the U1352 Site samples in the range of 0.5–1.5, except for two samples at 16.43 Ma (5.1), and 4.45 Ma (8.4).

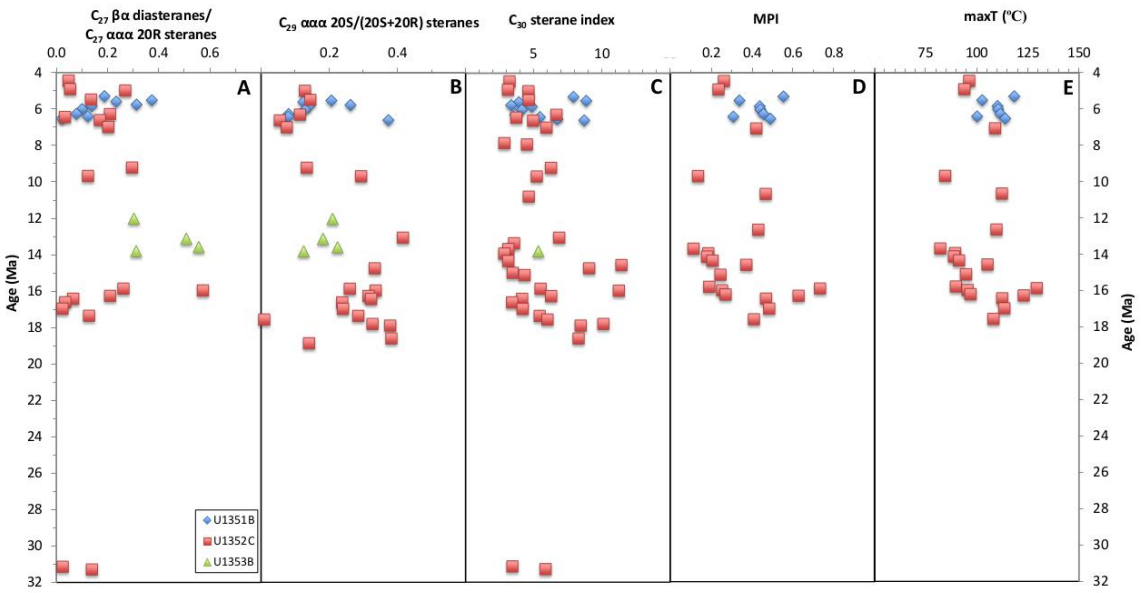

Figure 2.7: Distribution of the sterane data for the U1351 (blue), U1352 (red), and U1353 (green) sites. **A** – C_{27} βα diasterane abundance relative to C_{27} ααα sterane, **B** – C_{29} ααα 20S and 20R Sterane abundance, **C** – C_{30} sterane abundance relative to C_{27}-C_{30} steranes, **D** – Methylphenanthrene index, and **E** – calculated maximum sediment temperature (max*T)* based on Rc. Ratios are defined in Table 2.4.

Phenanthrene and the methylphenanthrenes were only identified in 22 samples from Site U1352. The early Oligocene and earliest Miocene (23.03–20.44 Ma) samples do not have

good preservation of aromatic compounds. Only the early Miocene samples dated between 17.56–16.20 Ma have good preservation of the alkylphenanthrenes. The MPI values for these samples vary significantly (0.27–0.73). The results show increasing MPI values up to 17.23 Ma and gradual decrease afterwards (Table 2.4; Fig. 2.7D). Calculated Max*T* for the early Miocene is between 97ºC and 123ºC. Retene/phenanthrene ratio was calculated only identified in three early Miocene samples at 16.43 Ma, 16.20 Ma, and 15.97 with values of 5.1, 0.8, and 1.1, respectively (Table 2.4).

The middle Miocene Site U1352 samples have good preservation of aromatic compounds. The MPI values vary from 0.11–0.73 without correlation to lithology. However, the highest MPI is at the beginning of the period (15.87 Ma), followed by a significant drop in MPI later. The reconstructed Max*T* varies from 82–129ºC (Table 2.4, Fig. 2.7E). Retene/phenanthrene values mostly vary from 1.5 to 0.5 during the middle Miocene.

Phenanthrene and the methylphenanthrenes are only present in three late Miocene samples (Table 2.4). The MPI values are 0.47, 0.14, and 0.42 in samples from 10.66, 9.69, and 7.07 Ma, respectively. The calculated Max*T* for these samples is from 85–112ºC (Table 2.4; Fig. 2.7E). Retene/phenanthrene is present only in two samples in the late Miocene (10.80 and 9.69 Ma), and the retene/phenanthrene ratios are 0.5 and 0.3, respectively (Table 2.4).

Aromatic compounds are well preserved in two Pliocene samples from Site U1352. The MPI values are 0.24 and 0.26 in samples dated to 4.92 and 4.45 Ma. The reconstructed Max*T* for these samples are 94ºC and 97ºC. The retene/phenanthrene ratios are 0.6 in the 4.92 Ma sample and 8.4 in the 4.45 Ma sample.

2.4. Discussion

TOC/TN data can be divided into three main categories: predominantly marine organic input (TOC/TN < 8), predominantly terrigenous organic input (TOC/TN > 12), and mixed input (8<TOC/TN<12) (Müller and Mathesius, 1999). However, this simple model of the factors influencing TOC/TN ratios is not always applicable. For example, high TOC/TN ratios atypical for algal source organic matter have been measured in organic-rich Mediterranean sapropel layers, upper Neogene sediment from the Benguela upwelling region, Eocene horizons from the Arctic Ocean, and Cenomanian–Turonian black shales (Meyers, 1990; Twichell et al., 2002; Stein and Macdonald, 2004; Stein et al., 2004). It has been suggested that in organic-rich marine sediments these high TOC/TN ratios can be explained by (1) algae that are able to synthesise lipid-rich organic carbon during times of abundant nutrient supply, and/or (2) during sinking, partial degradation of algal organic carbon may selectively diminish nitrogen-rich proteinaceous components and thus the TOC/TN ratio (Meyers, 1997).

The Miocene samples from Site U1351 are interpreted to contain predominantly terrigenous or degraded marine organic matter, based on the low hydrogen indices (most samples = <70 mg S_2/g TOC). A modified van Krevelen diagram of hydrogen index versus oxygen index (Fig.3A) shows that the sediments dominantly contain Type IV organic matter (no oil or gas-generative potential; dominated by inertinitic macerals), typical of poorly preserved terrigenous organic matter. These results are consistent with data from smear slides, which indicate that little marine organic matter is present and that the visible kerogen comprises mainly of plant cells and poorly preserved pollen (Fulthorpe et al., 2011b).

The unit III limestones contain the highest amounts of carbonate and the lowest TN at Site U1352. Organic matter in units II and III is more diagenetically stabilised as protokerogen, as shown in the lower part of Unit II (Fig. 3; Fulthorpe et al., 2011b).

The overall low hydrogen indices (Fig. 2.2C and 2.3) show that the organic matter is largely terrigenous or degraded marine in origin (Fulthorpe et al., 2011b). This finding contrasts with deeper Pukeiwitahi Formation coals (Sykes, 2004), which have higher hydrogen indices. The lack of correlation between sample depth and the $CPI_{(22-32)}$ suggests little influence of thermal maturity on the samples.

For Site U1353 low OM contents probably represent active biological oxidation and roughly correlates with intervals of increased alkalinity and decreased sulfate (Fulthorpe et al., 2011b). Pyrolysis results suggest a largely terrigenous plant origin for organic matter, but TOC/TN values suggest some marine influence.

The Rock-eval data can be used to measure the kerogen type (Espitalie et al., 1977) and the thermal maturity of the organic matter (Katz, 1983), but should be used with caution. Hydrocarbons generated during pyrolysis can be associated with heavy fractions of OM, and this might influence the HI index (Katz, 1983). Moreover, studies showed influence of mineralogy on OI (Katz, 1983) as well as an influence of humic acids on the OI in immature samples (Tissot and Welte, 1978). The Site U1353 middle Miocene samples contain high levels of C_{16},C_{18}, and C_{20} *n*-alkanes (Table 2.2) which suggest zooplankton (Saliot, 1981) and algae (Youngblood and Blumer, 1973) to be a main source of the OM. This type of *n*-alkane distribution was reported in coastal sediments (Nishimura and Baker, 1986; Mille et al., 2007) and derive from direct bacterial input into marine sediments. The C_{27}, C_{29}, and C_{31} *n*-alkanes that are indicative of the land-plant epicuticular waxes input to the sediments (Eglinton and Hamilton, 1967; Barnes and Barnes, 1978) are not abundant in middle Miocene samples.

The observation is supported by $CPI_{(22-32)}$ values close to 1 suggesting low terrigenous OM input. In general, $CPI_{(22-32)}$ index below 1.0 is associated with marine and aquatic environments when CPI higher than 1.0 is associated with terrigenous organic matter input.

Terrigenous/aquatic ratio (TAR) lower than 1 indicative of strong algal input and higher values indicate terrigenous OM input predominance (Silliman et al., 2000). The Silliman et al., 2000). The Site U1353 samples have high TAR, indicating high terrigenous OM input during the ~12–14 Ma period (Fig. 2.4C). The TAR ratio might over represent the absolute amount of terrigenous sources, assuming much higher *n*-alkane production by land plants (Cranwell et al., 1987; Meyers and Ishiwatari, 1993a). It should be noted that bimodal even *n*-alkane distributions can be part of the petrogenic contamination as well (Ekpo et al., 2005; Aloulou et al., 2010).

The Site U1353 samples have low $1/P_{aq}$ ratios (Table 2.2) because of the high abundance of submerged/floating aquatic macrophyte vegetation. The ratio was proposed by Ficken et al., (2000) for the detection of submerged/floating environments based on distribution of C_{21}, C_{23}, and C_{25} *n*-alkanes (Barnes and Barnes, 1978; Cranwell, 1984; Viso et al., 1993). It was used in the Haukari Gulf, New Zealand (Sikes et al., 2009) and in East China Sea shelf (Xing et al., 2011) to detect terrigenous OM input into continental shelf sediments. The study proposed correlation between levels of the P_{aq} and the distance from the continent. The $1/P_{aq}$ >10 was observed near the continent with high terrigenous OM input. The ratio decreased significantly in the continental slope area in both (Sikes et al., 2009; Xing et al., 2011). Therefore, deeper ocean levels close to the South island of New Zealand shore for the ~12-14 Ma period or further distance of the drilled site from the shore line can be suggested.

During the late Miocene period samples from the Site U1351 show unimodal *n*-alkane distribution with high C_{29}, C_{31} *n*-alkane signals, indicative of land-plant epicuticular waxes (Eglinton and Hamilton, 1967; Barnes and Barnes, 1978; Cranwell, 1984). The $CPI_{(22\text{-}32)}$ values above 1 in most samples support dominant terrigenous OM input (Peters et al., 2005). The TAR for the late Miocene samples is above 10, suggesting terrigenous OM input (Bourbonniere and Meyers, 1996). Based on high level of bioturbation of the sediments partial biodegradation of the OM can be suggested (Bourbonniere and Meyers, 1996; Meyers,

1997). The $1/P_{aq}$ ratios show a mix of aquatic and terrigenous environments as a main vegetation source (Ficken et al., 2000).

The early Oligocene samples from the Site U1352 (Table2; Fig. 2.4) have a strong predominance of even-to-odd *n*-alkanes (Fig. 2.4B) with $CPI_{(22-32)}$ <1. This type of distribution is indicative of marine OM input dominated by diatoms and phytoplankton (Albaigés et al., 1984; Saliot et al., 1998). Low TAR and $1/P_{aq}$ ratios suggest strong aquatic plant input with low terrigenous vegetation imprint (Fig. 2.4). Some studies suggest that bacterial input from river sediments can produce similar *n*-alkane distributions (Nishimura and Baker, 1986; Grimalt and Albaigés, 1987). Even-to-odd predominance in high molecular weight *n*-alkanes (>C_{24}) can be associated with early diagenetic alterations of *n*-alkonols originated in terrigenous plants as well (Simoneit, 1977).

Very similar distributions of *n*-alkanes and odd-to-even predominance was recorded in early Miocene samples (Fig. 2.4B). Very low $CPI_{(22-32)}$ index from ~19 and 17 Ma suggest strong marine OM input followed by increase in long chain *n*-alkane abundance with high $CPI_{(22-32)}$. The change is indicative to terrigenous OM input (Eglinton and Hamilton, 1967) during the second part of the early Miocene. Low TAR and $1/P_{aq}$ values up to ~16 Ma suggest high marine OM input with low terrigenous OM interference, similar to the early Oligocene period. Two samples have extremely high TAR values of 58.3 and 55.3 at 17.23 Ma and 16.43 Ma (Table 2.2) suggesting high spikes of terrigenous OM input.

The middle Miocene *n*-alkanes in the Site U1352 samples have bimodal distributions, similar to the Site U1353 samples. High levels of C_{16} and C_{18} *n*-alkanes can be derived from input of zooplankton (Saliot, 1981) and algae (Youngblood and Blumer, 1973). The C_{15} and C_{17} *n*-alkanes are usually derived from the algal/planktonic origins (Cranwell, 1984; Meyers and Ishiwatari, 1993b). The middle Miocene samples have increasing $CPI_{(22-32)}$ indicating increase in terrestrial OM input (Fig. 2.4B). The decrease of $CPI_{(22-32)}$ around 12 Ma suggest a

decrease in terrigenous OM input. The TAR and $1/P_{aq}$ indices show marine OM input during the same time with significant increase in terrigenous OM input around 15 Ma (Fig. 2.4 C,D).

Late Miocene samples show an increase in marine OM input with high C_{14}, C_{16}, and C_{18} values for several samples (Table 2.2). A significant increase in terrigenous OM between 6.5 Ma and 5.4 Ma can be observed through increase in $CPI_{(22-32)}$. The TAR and $1/P_{aq}$ for the late Miocene samples show increase in $1/P_{aq}$, suggesting an increase in terrigenous OM input up to ~6 Ma followed by its partial decrease (Fig. 2.4C,D). TAR data suggest at least three strong terrigenous OM input events at 10.8 Ma, 8Ma, and 6 Ma (Fig. 2.4C).

The early Pliocene data show C_{16}, C_{18}, and C_{20} *n*-alkane predominance from strong zooplankton (Saliot, 1981) and algae (Youngblood and Blumer, 1973) inputs. Similar distribution of even *n*-alkanes in the range of C_{12}-C_{20} was reported in some coastal sediments (Nishimura and Baker, 1986; Mille et al., 2007) assuming possible bacterial input. The $CPI_{(22-32)}$ values during the early Pliocene are around 1 (Fig. 2.4B) suggesting mixed input source (Bray and Evans, 1961).

Important to note, even *n*-alkane distribution can be attributed to petrogenic contamination of the samples (Ekpo et al., 2005; Aloulou et al., 2010). The *n*-alkane indices can be partially alternated by thermal maturation of the samples as well as by biodegradation (Bourbonniere and Meyers, 1996; Meyers, 1997).

To discuss the relative abundances of pristane (2,6,10,14-tetramethylpentadecane; Pr) and phytane (2,6,10,14-tetramethylhexadecane; Ph) in marine sediments the Pr/Ph, Pr/*n*-C_{17} and Ph/*n*-C_{18} ratios are used. The Pr/*n*-C_{17} and Ph/*n*-C_{18} (Fig. 2.3) ratios are indicative of the type of OM, its thermal maturation, and the oxidation levels of the depositional environment. The results suggest low thermal maturity for all the samples. Type III and mix of type III and II are the dominant kerogen types in the samples. High Pr/*n*-C_{17} ratio values at 5.84 and 5.52 Ma

(8.43 and 9.25, respectively; Table 2.2) could be due either to some biodegradation in the U1351 Site samples, or a highly oxic depositional environment.

The Pr/Ph ratio is indicative of oxicity of the depositional environment and show levels of thermal maturation and biodegradation of the samples (Volkman and Maxwell, 1986). The main source of Pr and Ph is a phytyl side chain of chlorophyll in phototrophic organisms and bacteriophyll from purple sulphur bacteria (Powell and McKirdy, 1973). Some marine organisms such as calanoid copepods have been suggested to be one of the biological sources as well (Blumer et al., 1964). In addition, Pr could be derived from anaerobic bacterial degradation (Rontani et al., 2010), thermal degradation (Lao et al., 1989) and clay catalysed degradation of the chlorophyll phytyl chain (Lao et al., 1989; Rontani et al., 2010). Ph can also be produced through anaerobic biodegradation (Grossi et al., 1998) and clay catalysed thermal hydrogenation of the isoprenoid alkenes (Gelin et al., 1995) as well as thermal maturation of methanogenic bacteria (Rowland, 1990). In general, Pr/Ph <0.8 indicates anoxic depositional environment, whereas Pr/Ph >3 indicates terrigenous organic matter input deposited under oxic conditions (Peters et al., 2005). Although, the ratio is widely used in environmental interpretations, the multiple input sources of both compounds and the influence of the post depositional environment means that conclusions should be supported with other biomarker ratios. The Pr/*n*-C_{17} and Ph/*n*-C_{18} ratios characterise the biodegradation levels in sediments (Peters and Moldowan, 1993). Ratios increase with increasing biodegradation levels and thermal maturation of the sediment (Tissot et al., 1971).

The Pr/Ph ratio for the Site U1353 samples suggest an anoxic depositional environment (Fig. 2.4A). This suggestion is consistent with low $CPI_{(22\text{-}32)}$ index assuming high marine OM deposition. The data are also consistent with TOC/TN and $1/P_{aq}$ interpretation. However, it is not consistent with *n*-alkane distribution and TAR ratio which show a relatively high terrigenous OM input (Fig. 2.4C).

Samples from Site U1351 show an increase in Pr/Ph values to 1.6 (Fig.5A), except for the 5.3 Ma sample suggesting oxic depositional environment. In general, the increasing oxicity of the depositional environment can be observed. This data is consistent with $CPI_{(22-32)}$, TAR and $1/P_{aq}$ values that show increase of the terrigenous OM input with time.

Early Oligocene samples do not show any consistent pattern of Pr/Ph and suggest sub-oxic to oxic depositional environment. (Fig.5A). The early Miocene samples show increasing oxicity pattern all the way to the middle Miocene. This pattern is consistent with $CPI_{(22-32)}$, $1/P_{aq}$, and TOC/TN results suggesting gradual increase of terrigenous OM input during the recorded period. The changes in accumulation of OM during the early Oligocene and early Miocene can be attributed to global sea level fluctuations, up to 30 m (Fig. 2.8D) (Van Sickel et al., 2004). The reconstructed tectonic activity of New Zealand for these periods (Fig. 2.8E) does not suggest any major activity in the area (Winkworth et al., 2002).

The middle Miocene samples have Pr/Ph ratios that suggest a suboxic depositional environment, except for the 15–12 Ma period when a strong oxic pattern is present (Fig. 2.4A). Samples with high Pr/ Ph values also have high TOC/TN (above 20) suggesting high terrigenous OM input. The same samples have very high sedimentation rates of 52.4–47 cm/ky (Table 2.1).

From 11 Ma, the Pr/Ph ratios decrease towards sub-oxic to oxic conditions. This observation is supported by increasing TAR, $CPI_{(22-32)}$, $1/P_{aq}$, and TOC/TN values. During the same period the sedimentation rates decreased to 32 cm/ky (Fulthorpe et al., 2011b).

The fluctuations in oxicity of the depositional environment are consistent with global sea levels fluctuations during the middle Miocene (Van Sickel et al., 2004). Increasing terrigenous input between 14–12 Ma together with high sedimentation rates at the same time can be attributed to significant land mass build up in the south island of New Zealand (Fig. 2.8 E) related to an increase in the convergence rate from ~20 Ma (Lu et al., 2005). The slow

uplift of the western part of the south island and an increase in the sloping gradient of the Canterbury region created an anoxic environment in the continental margin area and increased the rate of sedimentary input to the continental slope area. Slow, continuous uplift of the Southern Alps (Lu et al., 2005), an increase in vegetation cover, together with a decrease in global temperatures from ~15 Ma (Zachos et al., 2001) can be proposed as reasons for low terrigenous input of the material up to 11 Ma. The cooling event was followed by the late Miocene constant increase in terrigenous OM input. The event could correlate to another increase in the land mass (Lu et al., 2005). The highest input of terrigenous OM was recorded around 6 Ma, based on TOC/TN data and other ratios organic ratios. This spike can be attributed to an increase in the convergence rate between the Pacific and Australian plates to >7 mm/yr around 6 Ma (Lu et al., 2005; Wood and Stagpoole, 2007). This increase spiked an increase in the Southern Alps elevation, and is possibly related to higher Angiosperm vegetation cover of the island.

Oleanane, produced by angiosperms, originates in betulin or other pentacyclic triterpenoids (e.g. Whithead, 1973; Ekweozor and Udo, 1988). The oleanane/ hopane (oleanane index) show the relative abundance of angiosperm vegetation (Murray et al., 1994). An increasing oleanane index was interpreted as due to an increase in terrigenous OM input (Murray et al., 1997). The oleanane index values for the 15–13 Ma interval and around 7 Ma (Fig. 2.5D) show an increase in angiosperm input for the U1352 and U1353 sites. This increase is consistent with an increase in the $CPI_{(22\text{-}32)}$ and the TAR as discussed above, and can be attributed to increase in land mass during these periods.

The presence of gammacerane in sediments is related to water-column stratification (Sinninghe Damsté et al., 1995). Levels of gammacerane increase in hypersaline environments. The origin of this biomarker is not known, but one of its precursors, tetrahymanol, is a membrane lipid in some protozoa (Caspi et al., 1968; Ourisson et al., 1987). High values of the gammacerane/hopane ratio are indicative of marine carbonates, and

the virtual absence of gammacerane is typical of deltaic shales (Peters et al., 2005). Our data suggest relatively low gammacerane/hopane values and higher water salinity levels during the early Miocene (Fig. 2.5E) and around 13 Ma, suggesting lower sea levels in the region.

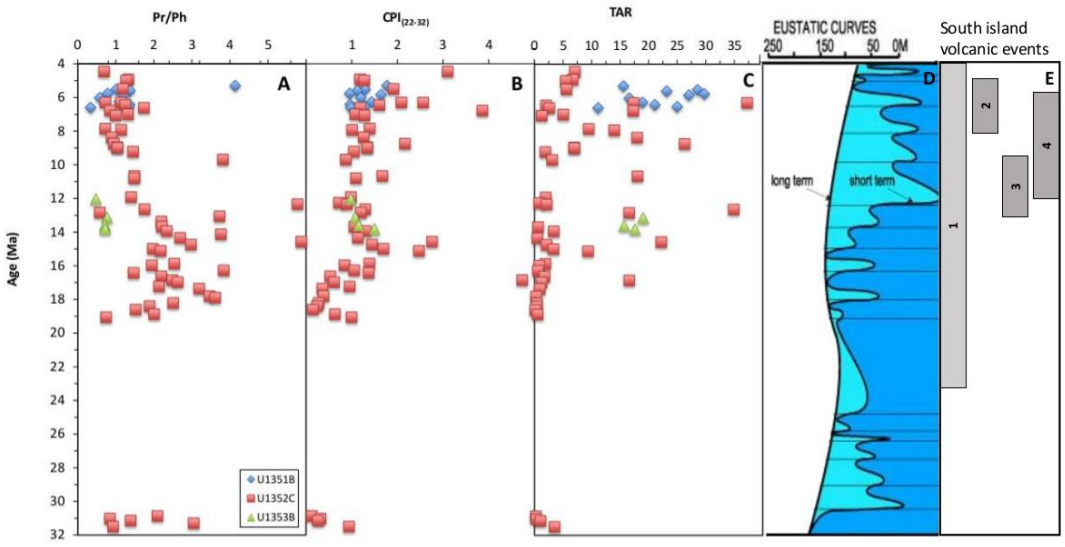

Figure 2.8: Summary of the isoprenoids (**A**) (this study) and *n*-alkane results (**B,C**) (this study) against eustatic curves (**D**) after Haq et al. (1987) and Miller et al. (2005) and South island seismic events, volcanism (**E**), where **1** – Dextral strike-slip motion along Alpine Fault since 23 Ma (Kamp, 1987), **2** – Initiation of uplift of Southern Alps 8-5 Ma (Tippett and Kamp, 1993), **3** – Otago volcanic activity 12.9–9.6 Ma (Coombs et al., 1986), and **4** – Banks volcanic activity 12–5.8 Ma (Watters, 1978).

High C_{24} tetracyclic/C_{23} tricyclic terpane ratios (>0.6) are indicative of marine sediments. The lower ratios can usually be seen in carbonates and marls (Peters et al., 2005). High C_{23}/C_{21} tricyclic terpanes ratio together with low C_{24} tetracyclic terpane abundance is indicative of marine OM input to the sediment.

The Oligocene samples do not contain enough terpanes to determine the OM input. The early Miocene samples have tricyclic terpane distributions that suggest carbonates.

The Site U1351 samples show high marine OM input through the late Miocene, with only two samples at 6.60 Ma and 5.60 Ma with C_{24} tetracyclic/C_{23} tricyclic terpane ratios <0.6, that

indicate high terrigenous input. Same samples show high C_{23}/C_{21} tricyclic terpanes values that supports the terrigenous OM input suggestion.

The middle Miocene Site U1353 samples do not have a C_{24} tetracyclic terpane record. The C_{23}/C_{21} tricyclic terpanes ratio for this period suggest higher terrigenous OM input.

Steranes are source specific compounds that contain between 27 and 29 carbons in the structure. The C_{27} steranes are derived from zooplankton, whereas C_{29} steranes are typically derived from higher plants (Huang and Meinschein, 1979). The source for C_{28} steranes is not fully identified, but some studies suggest that diatoms are rich in C_{28} steranes (Peters et al., 2005). The C_{27}-C_{28}-C_{29} ternary plot diagram was used to determine the source of organic matter (Moldowan et al., 1985). In addition, the diagram was successfully used in oil-source correlations (Grantham and Wakefield, 1988). A significant difference in sterane percentages for deltaic and continental shelf sediments has been reported (Meyers, 1997).

The data summarised in Fig. 2.6 suggest correlation between the site location and the type of OM based on sterane inputs. The majority of the Site U1353 samples, located in the inner shelf area, have a deltaic-terrigenous sterane input. The samples from Site U1351 on the outer continental shelf have a mixed OM input from deltaic-terrigenous and shallow marine sources, based on steranes. The Site U1352 samples have steranes derived from shallow or open marine OM organisms. Our data thus place steranes as indicators of the site location relative to the shore line. The closer to the land mass the location is, the higher the deltaic-terrigenous signal in the sterane record will be. In general, an open water sterane signal is present only in the outer continental shelf and continental slope sites. No open water sterane signal is present in the inner continental shelf samples. In contrast, the deltaic-terrigenous steranes signal is not present in the continental slope samples.

The detailed comparison between *n*-alkane and sterane OM inputs during the different epochs in the Site U1352 samples can be made. The early Oligocene and early Miocene *n*-alkane data

suggest strong marine OM source inputs. The sterane data for the same samples suggest open marine environment as the main OM input source (Table 2.3). The middle Miocene samples show a shallow marine environment input for the steranes, and closer proximity of the shore line can be suggested for the ~16–14 Ma interval. The n-alkane data for the same interval show an increasing input of terrigenous OM, arguably suggesting a shorter distance to the shoreline as well. This conclusion can also be supported by the high sedimentation rate during the same time. The sterane data for the 12–10 Ma period show a higher input of open marine OM. The $CPI_{(22\text{-}32)}$ and the $1/P_{aq}$ data also show an increase in marine OM input. The late Miocene was previously characterised by increasing terrestrial OM input to the continental slope, and transition of the sterane source from open to shallow marine OM supports this reconstruction. Despite the fact that steranes do not have well identified sources (Moldowan et al., 1985), their presence in the samples can help with determination of the OM source input.

The C_{30} sterane index is an index of 24-*n*-propylcholestanes relative to the other C_{27}-C_{30} identified steranes and is very specific for marine organic matter input as well (Seifert and Moldowan, 1978; Peters et al., 2005, for review). High C_{30} sterane index values are indicative of marine OM input. The early Oligocene data suggest high marine OM input (Table 2.4). The marine OM input stays low through the early Miocene period and increases at the beginning of the middle Miocene. Another strong input of marine OM is recorded in the C_{30} sterane index at 14.57 Ma, followed by a significant decrease until the Pliocene (Table 2.4). These data are quite consistent with previously suggested source interpretations.

Most hopanes in the rocks are derived from bacteria (Ourisson et al., 1984). Despite the fact that some hopanes have a very specific source, they are also often used as indicators of thermal maturity (e.g. Seifert and Moldowan, 1978, 1980; Moldowan et al., 1986; Peters et al., 2005).

C_{27} 17α-22,29,30-trisnorhopane (Tm) and C_{27} 18α-22,29,30-trisnorneohopane (Ts) are commonly used as biomarkers for thermal maturity evaluation (Seifert and Moldowan, 1978; Stephens and Carroll, 1999; Nuzzo et al., 2012). Tm is less stable than Ts and their relative abundance is usually measured by the Ts/(Ts+Tm) ratio. However, the sedimentation processes, early diagenesis, or the source of OM can significantly alter this ratio (Ourisson et al., 1984).

Most analysed samples have Ts/(Ts+Tm) ratios lower than 0.4, suggesting low thermal maturities up to the 2 km maximum core depth (Table 2.4). The 6.5 Ma sample from Site U1351 has a high Ts/(Ts+Tm) ratio, probably based of variations in the source of the OM. The 18 Ma and 15 Ma samples from the Site U1352 have high Ts/(Ts+Tm) ratios, suggesting low levels of thermal maturation.

The 22S/(22S+22R) hopane epimer ratios vary between 0 to 0.62 and reach equilibrium between 0.57-0.62 for the oil generation level (Seifert and Moldowan, 1980; Moldowan et al., 1986). The C_{31} pseudo homologs consistently show lower epimer ratios because they comprise a significant contribution of the indigenous 22R epimer (typical immature signature). The C_{31} αβ 22S/(22S+22R) hopanes ratios suggest low thermal maturity for the samples (Table 2.4).

The moretane/hopane ratio is also used as a thermal maturity indicator. The C_{30} 17β,21α(H)–moretanes are less thermally stable than the C_{30} 17α,21β(H)-hopanes, so the moretane concentration in sediment decreases with increasing thermal maturity (Mackenzie et al., 1980; Seifert and Moldowan, 1980). Our data suggest low C_{30} αβ/(αβ+βα) hopane ratio values, indicative of low thermal maturity.

Although all hopanes can be influenced by the source of the OM, all the ratios together show a low thermal maturity of the analysed sediments, with some increase in maturation with

depth. Some levels of biodegradation (Howell and Ellender, 1984; Peters and Moldowan, 1991) based on low 25-norhopanes values can be suggested.

Maturity-related parameters can also be obtained from the isomerisation ratio of C_{29} 5α,14α,17α(H) 20S/(20S+20R) steranes, which equilibrates at 0.52-0.55 (Seifert and Moldowan, 1986). The ratio of C_{27} diasteranes to steranes increases with increasing thermal maturity (Rubinstein et al., 1975; Peters et al., 2005). Our data suggest low maturity levels based on sterane and diasterane data. However, lithology and redox potential of the depositional environment can alter these data as well. Diasterane levels in sediments can be increased through the oxidation processes or during clay catalysed reactions (Kirk and Shaw, 1975; Seifert and Moldowan, 1986).

The maturity-related parameters were obtained from the aromatic data, MPI index, that show a thermal maturity related distribution of methylphenanthrenes (Radke et al., 1986). The max*T* calculated based on the MPI index does not show correlation to sample depth. Its highest and lowest values dated to middle Miocene (15.87 and 13.68 Ma, respectively). The results show low thermal maturity levels for the all three sites. This is consistent with the previously discussed maturity parameters. However, variations in the lithology or type of the OM (Cassani et al., 1988) as well as its migration (Radke et al., 1986) can alternate the MPI index. Moreover, not all methylphenanthrenes preserved well under the same conditions. 1-methyl and 3-methyl phenanthrenes are more stable than 2-methyl and 9-methyl phenanthrenes (Radke et al., 1986). This can significantly alternate the MPI ratio.

The C29ααα 20S/20R sterane ratio was used to calculate VRE (Table 2.4) based on the Sofer et al., (1993) equation. The values of these maturity parameters for all three sites are very far from equilibrium values and showing that the OM of all samples is immature. This is consistent with the previously discussed maturity parameters. This calculated vitrinite reflectance is consistently lower than the previously discussed one based on the MPI ratio.

2.5. Conclusion

Samples from IODP Expedition 317 provide a unique opportunity to look into OM accumulated during the second part of the Cenozoic epoch. A low thermal maturity is indicated by bulk geochemistry (HI and OI indices), diversity in *n*-alkane chain lengths, the CPI, isoprenoids (Pr/*n*-C_{17} and Ph/*n*-C_{18} ratios), as well as various hopane (e.g., Ts/(Ts+Tm), C_{30} hopanes αβ/(αβ+βα) and sterane ratios (C_{29} 5α,14α,17α(H) 20S/(20S+20R)) suggest low thermal alteration of the OM accumulation and relatively high reliability of the interpretations.

Bulk geochemistry results show low levels of OM present in the samples. In addition, based on the bulk geochemistry data type IV organic matter is dominant, which somewhat contradicts the Pr/*n*-C_{17} and Ph/*n*-C_{18} results. Based on the organic compound data (*n*-alkanes, isoprenoids, and steranes), local tectonic activity had a rapid, but significant influence on the accumulation of OM in the Canterbury Basin marine sediments. This can be seen due to rapid increases in terrigenous OM input in short time periods, that can be attributed to major tectonic activity in New Zealand (Fig. 2.8). Moreover, the tectonic influence can be identified for the 14-12 Ma and ~6 MA periods. These periods partially overlap with the time of the Otago volcanic activity (12.9–9.6 Ma) and uplift of the Southern Alps (8–5 Ma). The influence of sea level changes and global temperature variations are suggested for before 14 Ma, between 12 and 7 Ma and after 6 Ma, based on distributions of *n*-alkanes, isoprenoids, steranes, and hopanes. The results are consistent with increasing sea levels during these periods causing an increase in marine OM productivity and better preservation of the terrigenous OM.

Differences in the carbon number distribution of steranes in the samples allow estimation of the relative distance of the samples from the shoreline through time. Sterane data can also help in determination the input of terrigenous material. An increase in land mass and an

increase in the continental slope angle can be suggested for the ~14-12 Ma and ~11 Ma periods, respectively.

2.6. Acknowledgements

This work was supported by post-cruise funding from the Australia-New Zealand IODP Consortium (ANZIC), and by Macquarie University who provided a PhD scholarship and research funding

2.7. References

Albaigés, J., Grimalt, J., Bayona, J., Risebrough, R., De Lappe, B., Walker, W., 1984. Dissolved, particulate and sedimentary hydrocarbons in a deltaic environment. *Organic Geochemistry* 6, 237-248.

Aloulou, F., Kallel, M., Dammak, M., Elleuch, B., Saliot, A., 2010. Even-numbered n-alkanes/n-alkenes predominance in surface sediments of Gabes Gulf in Tunisia. *Environmental Earth Sciences* 61, 1-10.

Barnes, M., Barnes, W., 1978. Organic compounds in lake sediments, Lakes. Springer, pp. 127-152.
Beu, A.G., Griffin, M., Maxwell, P., 1997. Opening of Drake Passage gateway and Late Miocene to Pleistocene cooling reflected in Southern Ocean molluscan dispersal: evidence from New Zealand and Argentina. *Tectonophysics* 281, 83-97.

Blumer, M., Mullin, M.M., Thomas, D.W., 1964. Pristane in the marine environment. *Helgoländer Wissenschaftliche Meeresuntersuchungen* 10, 187-201.

Bourbonniere, R., Meyers, P., 1996. Anthropogenic influences on hydrocarbon contents of sediments deposited in eastern Lake Ontario since 1800. *Environmental Geology* 28, 22-28.

Bray, E., Evans, E., 1961. Distribution of n-paraffins as a clue to recognition of source beds. *Geochimica et Cosmochimica Acta* 22, 2-15.

Caspi, E., Zander, J.M., Greig, J.B., Mallory, F.B., Conner, R.L., Landrey, J.R., 1968. Evidence for a nonoxidative cyclization of squalene in the biosynthesis of tetrahymanol. *Journal of the American Chemical Society* 90, 3563-3564.

Cassani, F., Gallango, O., Talukdar, S., Vallejos, C., Ehrmann, U., 1988. Methylphenanthrene maturity index of marine source rock extracts and crude oils from the Maracaibo Basin. *Organic Geochemistry* 13, 73-80.

Chaproniere, G.C., 1984. Oligocene and Miocene larger foraminiferida from Australia and New Zealand. *Unknown* 1.

Coombs, D.S., Cas, R., Kawachi, Y., Landis, C., McDonough, W., Reay, A., 1986. Cenozoic volcanism in north, east and central Otago. *Royal Society of New Zealand Bulletin* 23, 278-312.

Cranwell, P., 1984. Lipid geochemistry of sediments from Upton Broad, a small productive lake. *Organic Geochemistry* 7, 25-37.

Cranwell, P., Eglinton, G., Robinson, N., 1987. Lipids of aquatic organisms as potential contributors to lacustrine sediments—II. *Organic Geochemistry* 11, 513-527.

Eglinton, G., Hamilton, R.J., 1967. Leaf epicuticular waxes. *Science* 156, 1322-1335.

Ekpo, B., Oyo-Ita, O., Wehner, H., 2005. Even-n-alkane/alkene predominances in surface sediments from the Calabar River, SE Niger Delta, Nigeria. *Naturwissenschaften* 92, 341-346.

Ekweozor, C., Udo, O.T., 1988. The oleananes: Origin, maturation and limits of occurence in southern Nigeria sedimentary basins. *Organic Geochemistry* 13, 131-140.

Espitalié, J., 1986. Use of Tmax as a maturation index for different types of organic matter. Comparison with vitrinite reflectance, Thermal modelling in sedimentary basins. Editions Technip Paris, pp. 475-496.

Espitalie, J., Madec, M., Tissot, B., Mennig, J., Leplat, P., 1977. Source rock characterization method for petroleum exploration, Offshore Technology Conference. Offshore Technology Conference.
Ficken, K.J., Li, B., Swain, D., Eglinton, G., 2000. An n-alkane proxy for the sedimentary input of submerged/floating freshwater aquatic macrophytes. *Organic Geochemistry* 31, 745-749.

Fulthorpe, C.S., Hoyanagi, K., Blum, P., Scientists, a.t.E., 2011a. *Proc*. IODP, 317: Tokyo (Integrated Ocean Drilling Program Management International, Inc.).
Fulthorpe, C.S., Hoyanagi, K., Crundwell, M.P., Dinarès-Turell, J., Ding, X., George, S.C., Hepp, D.A., Jaeger, J., Kawagata, S., Kemp, D.B., 2011b. Expedition 317 summary.

Gelin, F., Damsté, J.S.S., Harrison, W.N., Maxwell, J.R., De Leeuw, J.W., 1995. Molecular indicators for palaeoenvironmental change in a Messinian evaporitic sequence (Vena del Gesso, Italy): III. Stratigraphic changes in the molecular structure of kerogen in a single marl bed as revealed by flash pyrolysis. *Organic Geochemistry* 23, 555-566.

Grantham, P.J., Wakefield, L.L., 1988. Variations in the sterane carbon number distributions of marine source rock derived crude oils through geological time. *Organic Geochemistry* 12, 61-73.

Grimalt, J., Albaigés, J., 1987. Sources and occurrence of C 12□ C 22 n-alkane distributions with even carbon-number preference in sedimentary environments. *Geochimica et Cosmochimica Acta* 51, 1379-1384.

Grossi, V., Hirschler, A., Raphel, D., Rontani, J.-F., De Leeuw, J., Bertrand, J.-C., 1998. Biotransformation pathways of phytol in recent anoxic sediments. *Organic Geochemistry* 29, 845-861.

Haq, B.U., Hardenbol, J., Vail, P.R., 1987. Chronology of fluctuating sea levels since the Triassic. *Science* 235, 1156-1167.

Hedges, J., Keil, R., Benner, R., 1997. What happens to terrestrial organic matter in the ocean? *Organic Geochemistry* 27, 195-212.

Hedges, J.I., Keil, R.G., 1995. Sedimentary organic matter preservation: an assessment and speculative synthesis. *Marine Chemistry* 49, 81-115.

Howell, F.G., Ellender, R., 1984. Observations on growth and diet of Argiope aurantia Lucas (Araneidae) in a successional habitat. *Journal of Arachnology*, 29-36.

Huang, W.-Y., Meinschein, W.G., 1979. Sterols as ecological indicators. *Geochimica et Cosmochimica Acta* 43, 739-745.

Jenkins, D.G., 1965. Planktonic foraminiferal zones and new taxa from the Danian to Lower Miocene of New Zealand. *New Zealand Journal of Geology and Geophysics* 8, 1088-1126.

Kamp, P., 1987. Age and origin of the New Zealand orocline in relation to Alpine Fault movement. *Journal of the Geological Society* 144, 641-652.

Katz, B.J., 1983. Limitations of 'Rock-Eval'pyrolysis for typing organic matter. *Organic Geochemistry* 4, 195-199.

Keigwin, L., Keller, G., 1984. Middle Oligocene cooling from equatorial Pacific DSDP site 77B. *Geology* 12, 16-19.

King, P.R., 2000. Tectonic reconstructions of New Zealand: 40 Ma to the present. *New Zealand Journal of Geology and Geophysics* 43, 611-638.

Kirk, D.N., Shaw, P.M., 1975. Backbone rearrangements of steroidal 5-enes. *Journal of the Chemical Society, Perkin Transactions 1*, 2284-2294.

Kominz, M.A., Miller, K.G., Browning, J.V., 1998. Long-term and short-term global Cenozoic sea-level estimates. *Geology* 26, 311-314.

Lao, Y., Korth, J., Ellis, J., Crisp, P., 1989. Heterogeneous reactions of 1-pristene catalysed by clays under simulated geological conditions. *Organic Geochemistry* 14, 375-379.

Lawver, L.A., Gahagan, L.M., Coffin, M.F., 1992. The development of paleoseaways around Antarctica. *The Antarctic Paleoenvironment: A Perspective on Global Change: Part One*, 7-30.

Lu, H., Fulthorpe, C.S., Mann, P., Kominz, M.A., 2005. Miocene–Recent tectonic and climatic controls on sediment supply and sequence stratigraphy: Canterbury basin, New Zealand. *Basin Research* 17, 311-328.

MacDonald, G.J., 1990. Role of methane clathrates in past and future climates. *Climatic Change* 16, 247-281.

Mackenzie, A., Patience, R., Maxwell, J., Vandenbroucke, M., Durand, B., 1980. Molecular parameters of maturation in the Toarcian shales, Paris Basin, France—I. Changes in the configurations of acyclic isoprenoid alkanes, steranes and triterpanes. *Geochimica et Cosmochimica Acta* 44, 1709-1721.

Meyers, P.A., 1990. Impacts of late Quaternary fluctuations in water level on the accumulation of sedimentary organic matter in Walker Lake, Nevada. *Palaeogeography, Palaeoclimatology, Palaeoecology* 78, 229-240.

Meyers, P.A., 1997. Organic geochemical proxies of paleoceanographic, paleolimnologic, and paleoclimatic processes. *Organic Geochemistry* 27, 213-250.

Meyers, P.A., Ishiwatari, R., 1993a. The Early Diagenesis of Organic Matter in Lacustrine Sediments, in: Engel, M., Macko, S. (Eds.), Organic Geochemistry. Springer US, pp. 185-209.
Meyers, P.A., Ishiwatari, R., 1993b. Lacustrine organic geochemistry—an overview of indicators of organic matter sources and diagenesis in lake sediments. *Organic Geochemistry* 20, 867-900.

Middelburg, J.J., 1989. A simple rate model for organic matter decomposition in marine sediments. *Geochimica et Cosmochimica Acta* 53, 1577-1581.

Mille, G., Asia, L., Guiliano, M., Malleret, L., Doumenq, P., 2007. Hydrocarbons in coastal sediments from the Mediterranean sea (Gulf of Fos area, France). *Marine Pollution Bulletin* 54, 566-575.

Miller, K.G., Kominz, M.A., Browning, J.V., Wright, J.D., Mountain, G.S., Katz, M.E., Sugarman, P.J., Cramer, B.S., Christie-Blick, N., Pekar, S.F., 2005. The Phanerozoic record of global sea-level change. *Science* 310, 1293-1298.

Miller, K.G., Mountain, G.S., Browning, J.V., Kominz, M., Sugarman, P.J., Christie-Blick, N., Katz, M.E., Wright, J.D., 1998. Cenozoic global sea level, sequences, and the New Jersey transect: results from coastal plain and continental slope drilling. *Reviews of Geophysics* 36, 569-601.

Miller, K.G., Sugarman, P.J., Browning, J.V., Kominz, M.A., Hernández, J.C., Olsson, R.K., Wright, J.D., Feigenson, M.D., Van Sickel, W., 2003. Late Cretaceous chronology of large, rapid sea-level changes: Glacioeustasy during the greenhouse world. *Geology* 31, 585-588.

Miller, K.G., Wright, J.D., Fairbanks, R.G., 1991. Unlocking the ice house: Oligocene-Miocene oxygen isotopes, eustasy, and margin erosion. *Journal of Geophysical Research: Solid Earth* 96, 6829-6848.

Moldowan, J.M., Seifert, W.K., Gallegos, E.J., 1985. Relationship between petroleum composition and depositional environment of petroleum source rocks. *AAPG bulletin* 69, 1255-1268.

Moldowan, J.M., Sundararaman, P., Schoell, M., 1986. Sensitivity of biomarker properties to depositional environment and/or source input in the Lower Toarcian of SW-Germany. *Organic Geochemistry* 10, 915-926.

Müller, A., Mathesius, U., 1999. The palaeoenvironments of coastal lagoons in the southern Baltic Sea, I. The application of sedimentary C org/N ratios as source indicators of organic matter. *Palaeogeography, Palaeoclimatology, Palaeoecology* 145, 1-16.

Murray, A.P., Sosrowidjojo, I.B., Alexander, R., Kagi, R.I., Norgate, C.M., Summons, R.E., 1997. Oleananes in oils and sediments: Evidence of marine influence during early diagenesis? *Geochimica et Cosmochimica Acta* 61, 1261-1276.

Murray, A.P., Summons, R.E., Boreham, C.J., Dowling, L.M., 1994. Biomarker and n-alkane isotope profiles for Tertiary oils: relationship to source rock depositional setting. *Organic Geochemistry* 22, 521IN525-542IN526.

Nelson, C.S., Cooke, P.J., 2001. History of oceanic front development in the New Zealand sector of the Southern Ocean during the Cenozoic—a synthesis. *New Zealand Journal of Geology and Geophysics* 44, 535-553.

Nishimura, M., Baker, E.W., 1986. Possible origin of n-alkanes with a remarkable even-to-odd predominance in recent marine sediments. *Geochimica et Cosmochimica Acta* 50, 299-305.

Nuzzo, M., Elvert, M., Schmidt, M., Scholz, F., Reitz, A., Hinrichs, K.-U., Hensen, C., 2012. Impact of hot fluid advection on hydrocarbon gas production and seepage in mud volcano sediments of thick Cenozoic deltas. *Earth and Planetary Science Letters* 341, 139-157.

Ourisson, G., Albrecht, P., Rohmer, M., 1984. Microbial origin of fossil fuels. *Sci. Am.;(United States)* 251.

Ourisson, G., Rohmer, M., Poralla, K., 1987. Microbial lipids betrayed by their fossils. *Microbiological sciences* 4, 52-57.

Peters, K., Moldowan, J., 1991. Effects of source, thermal maturity, and biodegradation on the distribution and isomerization of homohopanes in petroleum. *Organic Geochemistry* 17, 47-61.

Peters, K.E., Moldowan, J.M., 1993. The biomarker guide : interpreting molecular fossils in petroleum and ancient sediments. Prentice Hall, Englewood Cliffs, N.J.
Peters, K.E., Walters, C.C., Moldowan, J.M., 2005. The biomarker guide, 2nd ed. Cambridge University Press, Cambridge, UK ; New York.
Pitman, W., Golovchenko, X., 1991. The effect of sea level changes on the morphology of mountain belts. *Journal of Geophysical Research: Solid Earth* 96, 6879-6891.

Posamentier, H., 1988. Eustatic controls on clastic deposition II—sequence and systems tract models.

Powell, T., McKirdy, D., 1973. Relationship between ratio of pristane to phytane, crude oil composition and geological environment in Australia. *Nature* 243, 37-39.

Radke, M., Welte, D., Willsch, H., 1986. Maturity parameters based on aromatic hydrocarbons: influence of the organic matter type. *Organic Geochemistry* 10, 51-63.

Rontani, J.-F., Nassiry, M., Michotey, V., Guasco, S., Bonin, P., 2010. Formation of pristane from α-tocopherol under simulated anoxic sedimentary conditions: A combination of biotic and abiotic degradative processes. *Geochimica et Cosmochimica Acta* 74, 252-263.

Rowland, S., 1990. Production of acyclic isoprenoid hydrocarbons by laboratory maturation of methanogenic bacteria. *Organic Geochemistry* 15, 9-16.

Royer, D.L., 2006. CO 2-forced climate thresholds during the Phanerozoic. *Geochimica et Cosmochimica Acta* 70, 5665-5675.

Rubinstein, I., Sieskind, O., Albrecht, P., 1975. Rearranged sterenes in a shale: occurrence and simulated formation. *Journal of the Chemical Society, Perkin Transactions 1*, 1833-1836.

Sahagian, D., Pinous, O., Olferiev, A., Zakharov, V., 1996. Eustatic Curve for the Middle Jurassic--Cretaceous Based on Russian Platform and Siberian Stratigraphy: Zonal Resolution. *AAPG bulletin* 80, 1433-1458.

Saliot, A., 1981. Natural Hydrocarbons in Sea Water Alain Saliot. *Elsevier Oceanography Series* 31, 327-374.

Saliot, A., Denant, V., Bigot, M., 1998. Organic matter in large Chinese rivers and their estuaries: the Changjiang River and the Huanghe River. *Land-Sea Interaction in Chinese Coastal Zones. Ocean Press, Beijing*, 176-191.

Seifert, W., Moldowan, J., 1986. Use of biological markers in petroleum exploration. *Methods in geochemistry and geophysics* 24, 261-290.

Seifert, W.K., Moldowan, J.M., 1978. Applications of steranes, terpanes and monoaromatics to the maturation, migration and source of crude oils. *Geochimica et Cosmochimica Acta* 42, 77-95.

Seifert, W.K., Moldowan, J.M., 1980. The effect of thermal stress on source-rock quality as measured by hopane stereochemistry. *Physics and Chemistry of the Earth* 12, 229-237.

Shackleton, N.J., Kennett, J.P., 1975. Paleotemperature history of the Cenozoic and the initiation of Antarctic glaciation: oxygen and carbon isotope analyses in DSDP Sites 277, 279, and 281. *Initial reports of the deep sea drilling project* 29, 743-755.

Shackleton, N.J., Pisias, N., 1985. Atmospheric carbon dioxide, orbital forcing, and climate. *The Carbon Cycle and Atmospheric CO: Natural variations Archean to Present*, 303-317.

Sikes, E.L., Uhle, M.E., Nodder, S.D., Howard, M.E., 2009. Sources of organic matter in a coastal marine environment: evidence from n-alkanes and their δ 13 C distributions in the Hauraki Gulf, New Zealand. *Marine Chemistry* 113, 149-163.

Silliman, J., Meyers, P., Ostrom, P., Ostrom, N., Eadie, B., 2000. Insights into the origin of perylene from isotopic analyses of sediments from Saanich Inlet, British Columbia. *Organic Geochemistry* 31, 1133-1142.

Simoneit, B.R., 1977. Diterpenoid compounds and other lipids in deep-sea sediments and their geochemical significance. *Geochimica et Cosmochimica Acta* 41, 463-476.

Sinninghe Damsté, J.S., Kenig, F., Koopmans, M.P., Köster, J., Schouten, S., Hayes, J., de Leeuw, J.W., 1995. Evidence for gammacerane as an indicator of water column stratification. *Geochimica et Cosmochimica Acta* 59, 1895-1900.

Sofer, Z., Regan, D., Muller, D., 1993. Sterane isomerization ratios of oils as maturity indicators and their use as an exploration tool, Neuquen basin, Argentina, XII Congreso de Geológico Argentino y II Congreso de Exploración de Hidrocarburos Actas, pp. 407-411.
Stein, R., Macdonald, R., 2004. Organic carbon budget: Arctic Ocean vs. global ocean, The organic carbon cycle in the Arctic Ocean. Springer, pp. 315-322.
Stein, R., Macdonald, R.W., Stein, R., MacDonald, R.W., 2004. The organic carbon cycle in the Arctic Ocean.

Stephens, N.P., Carroll, A.R., 1999. Salinity stratification in the Permian Phosphoria sea; a proposed paleoceanographic model. *Geology* 27, 899-902.

Sykes, R., 2004. Peat biomass and early diagenetic controls on the paraffinic oil potential of humic coals, Canterbury Basin, New Zealand. *Petroleum Geoscience* 10, 283-303.

Tippett, J.M., Kamp, P.J., 1993. The role of faulting in rock uplift in the Southern Alps, New Zealand. *New Zealand Journal of Geology and Geophysics* 36, 497-504.

Tissot, B., Califet-Debyser, Y., Deroo, G., Oudin, J., 1971. Origin and evolution of hydrocarbons in early Toarcian shales, Paris Basin, France. *AAPG bulletin* 55, 2177-2193.

Tissot, B., Welte, D., 1978. Petroleum Formation and Occurance: A New Approach to Oil and Gas Exploration. Springer.
Tomczak, M., Godfrey, J.S., 2013. Regional oceanography: an introduction. Elsevier.
Twichell, S.C., Meyers, P.A., Diester-Haass, L., 2002. Significance of high C/N ratios in organic-carbon-rich Neogene sediments under the Benguela Current upwelling system. *Organic Geochemistry* 33, 715-722.

Van Sickel, W.A., Kominz, M.A., Miller, K.G., Browning, J.V., 2004. Late Cretaceous and Cenozoic sea-level estimates: backstripping analysis of borehole data, onshore New Jersey. *Basin Research* 16, 451-465.

Viso, A.-C., Pesando, D., Bernard, P., Marty, J.-C., 1993. Lipid components of the Mediterranean seagrass Posidonia oceanica. *Phytochemistry* 34, 381-387.

Volkman, J.K., Maxwell, J.R., 1986. Acyclic isoprenoids as biological markers. *Methods in geochemistry and geophysics* 24, 1-42.

Wang, W., Zhou, Z.Y., Yu, P., 2005. Relations Between Vitrinite Reflectance, Peek Temperature and its Neighboring Temperature Variation Rate: A Comparison of Methods. *Chinese Journal of Geophysics* 48, 1443-1453.

Watters, W., 1978. Tertiary volcanism–Miocene. *The Geology of New Zealand: Wellington (New Zealand Govt. Printer)* 2, 637-644.

Whithead, J.M., 1973. The structure of petroleum pentacyclanes, in: Tissot, B.a., Bienner, F. (Eds.), Advances in Organic Geochemistry. Editions Technip, Paris, pp. 225-243.
Winkworth, R.C., Wagstaff, S.J., Glenny, D., Lockhart, P.J., 2002. Plant dispersal news from New Zealand. *Trends in Ecology & Evolution* 17, 514-520.

Wood, R., Stagpoole, V., 2007. Validation of tectonic reconstructions by crustal volume balance: New Zealand through the Cenozoic. *Geological Society of America Bulletin* 119, 933-943.

Xing, L., Zhang, H., Yuan, Z., Sun, Y., Zhao, M., 2011. Terrestrial and marine biomarker estimates of organic matter sources and distributions in surface sediments from the East China Sea shelf. *Continental Shelf Research* 31, 1106-1115.

Youngblood, W., Blumer, M., 1973. Alkanes and alkenes in marine benthic algae. *Marine Biology* 21, 163-172.

Zachos, J., Pagani, M., Sloan, L., Thomas, E., Billups, K., 2001. Trends, rhythms, and aberrations in global climate 65 Ma to present. *Science* 292, 686-693.

Zachos, J.C., Dickens, G.R., Zeebe, R.E., 2008. An early Cenozoic perspective on greenhouse warming and carbon-cycle dynamics. *Nature* 451, 279-283.

2.8. Appendix: Tables

Table 2.1: On-board bulk geochemistry data (Fulthorpe et al., 2011) for the analysed IODP Expedition 317 samples including sample depth (mbsf), main lithology, lithological unit, and age (Ma).

Core ans section number	Sample depth (mbsf)	Main lithology	Lithological unit	Age (Ma)	$CaCO_3$ (wt%)	TOC[1] (wt%)	TN[2] (wt%)	TOC/TN	HI[3] (mg HC/g TOC)	OI[4] (mg CO_2/g TOC)	*T*max[5] (°C)	Production index[6]
U1351B_94X4	817.82	Greenish-grey very fine sandy mud	II	5.06	12.4	0.47	-	-	44	32	423	13
U1351B_95XCC	822.40	Greenish-grey very fine sandy mud	II	5.10	10.8	0.36	-	-	37	36	427	15
U1351B_97X1	842.36	Greenish-grey very fine sandy mud	II	5.27	11.8	0.21	-	-	43	36	425	12
U1351B_97X4	845.72	Greenish-grey very fine sandy mud	II	5.30	4.6	0.96	-	-	43	36	416	16
U1351B_98X1	851.23	Greenish-grey very fine sandy mud	II	5.35	7.2	0.30	-	-	27	29	424	30
U1351B_99X1	860.85	Greenish-grey very fine sandy mud	II	5.43	5.9	0.28	-	-	29	32	419	22
U1351B_100X1	871.62	Greenish-grey very fine sandy mud	II	5.52	5.7	0.25	-	-	32	41	403	27
U1351B_101X1	880.93	Greenish-grey very fine sandy mud	II	5.60	5.0	0.10	-	-	26	45	409	59
U1351B_103X1	900.04	Greenish-grey very fine sandy mud	II	5.76	8.7	0.21	-	-	22	29	416	21
U1351B_104X1	908.97	Greenish-grey very fine sandy mud	II	5.84	8.2	0.36	-	-	40	69	413	18
U1351B_104X3	911.92	Greenish-grey very fine sandy mud	II	5.86	7.5	0.29	-	-	-	-	-	-
U1351B_106X1	929.41	Greenish-grey very fine sandy mud	II	6.01	8.4	0.28	-	-	41	42	400	18
U1351B_106X3	931.40	Greenish-grey very fine sandy mud	II	6.03	14.4	0.22	-	-	51	45	410	15
U1351B_107X1	937.70	Greenish-grey very fine sandy mud	II	6.08	7.9	0.31	-	-	31	49	418	22
U1351B_107X1	937.73	Greenish-grey very fine sandy mud	II	6.08	7.8	0.27	-	-	31	36	417	27
U1351B_109X2	959.05	Greenish-grey very fine sandy mud	II	6.27	4.9	0.33	-	-	47	58	410	23
U1351B_109X3	961.04	Greenish-grey very fine sandy mud	II	6.28	14.2	0.15	-	-	31	28	418	28
U1351B_111X1	976.21	Greenish-grey very fine sandy mud	II	6.41	12.5	0.34	-	-	39	34	419	15
U1351B_111X1	976.25	Greenish-grey very fine sandy mud	II	6.41	12.9	0.28	-	-	26	44	417	18
U1351B_112X3	989.18	Greenish-grey very fine sandy mud	II	6.52	11.7	0.31	-	-	35	32	403	18
U1351B_113X2	997.74	Greenish-grey very fine sandy mud	II	6.60	11.6	0.28	-	-	32	25	418	18
U1351B_115XCC	1014.33	Greenish-grey very fine sandy mud	II	6.74	11.5	0.32	-	-	38	32	417	21
U1352C_70R1	1247.82	Sandy marlstone	IIB	4.39	43.28	0.56	0.026	22	57	57	424	7
U1352C_71R1	1257.15	Sandy marlstone	IIB	4.70	41.76	0.48	0.018	26	47	67	424	8
U1352C_72R1	1266.06	Sandy marlstone	IIB	5.00	37.60	0.65	0.016	40	31	62	420	9

Core and section number	Sample depth (mbsf)	Main lithology	Lithological unit	Age (Ma)	$CaCO_3$ (wt%)	TOC[1] (wt%)	TN[2] (wt%)	TOC/TN	HI[3] (mg HC/g TOC)	OI[4] (mg CO_2/g TOC)	*T*max[5] (°C)	Production index[6]
U1352C_73R5	1281.69	Sandy marlstone	IIB	5.52	22.21	0.41	0.024	17	47	6	415	11
U1352C_77R1	1309.00	Sandy marlstone	IIB	6.43	33.35	0.39	0.023	17	42	58	425	9
U1352C_78R3	1317.20	Sandy marlstone	IIB	6.70	32.72	0.47	0.014	34	30	32	407	10
U1352C_79R1	1318.10	Sandy marlstone	IIB	6.73	34.63	0.61	0.018	34	36	5	417	8
U1352C_80R1	1323.69	Sandy marlstone	IIB	6.92	25.94	0.42	0.019	22	29	47	412	10
U1352C_81R1	1328.31	Sandy marlstone	IIB	7.07	21.37	0.50	0.026	19	52	42	408	8
U1352C_82R1	1332.75	Sandy marlstone	IIB	7.22	26.40	0.51	0.016	32	40	9	418	9
U1352C_85R2	1349.21	Sandy marlstone	IIB	7.77	35.99	0.41	0.020	20	32	41	421	9
U1352C_85R4	1351.41	Sandy marlstone	IIB	7.85	12.96	0.16	0.026	6	29	21	407	13
U1352C_86R2	1353.29	Sandy marlstone	IIB	7.91	47.02	0.41	0.017	24	53	74	426	8
U1352C_87R1	1362.75	Sandy marlstone	IIB	8.23	38.06	0.28	0.011	25	21	50	421	11
U1352C_88R2	1373.07	Sandy marlstone	IIB	8.57	6.14	0.49	0.025	20	21	28	416	13
U1352C_88R5	1378.29	Sandy marlstone	IIB	8.74	4.02	0.21	0.024	9	39	-	-	15
U1352C_89R3	1384.35	Sandy marlstone	IIB	8.95	6.53	0.44	0.022	20	70	70	423	11
U1352C_89R4	1385.04	Sandy marlstone	IIB	8.97	10.75	0.50	0.030	17	75	33	419	9
U1352C_89R4	1385.71	Sandy marlstone	IIB	8.99	13.69	0.69	0.041	17	59	37	421	8
U1352C_90R1	1390.52	Sandy marlstone	IIB	9.15	3.42	0.32	0.024	13	45	-	415	15
U1352C_90R3	1393.40	Sandy marlstone	IIB	9.25	28.62	0.99	0.056	18	22	49	429	13
U1352C_91R1	1401.06	Sandy marlstone	IIB	9.50	56.31	0.70	0.019	37	58	89	419	6
U1352C_94R1	1428.92	Sandy marlstone	IIB	10.44	43.31	0.45	0.020	23	33	41	427	6
U1352C_94R6	1436.59	Sandy marlstone	IIB	10.69	20.82	0.60	0.031	19	50	64	432	8
U1352C_95R2	1440.21	Sandy marlstone	IIB	10.79	36.27	0.43	0.022	19	26	31	426	9
U1352C_99R1	1477.64	Sandy marlstone	IIB	11.54	50.18	0.67	0.016	42	19	44	417	10
U1352C_102Rcc	1496.47	Sandy marlstone	IIB	11.92	30.92	0.48	0.017	28	21	18	421	12
U1352C_103R1	1506.70	Sandy marlstone	IIB	12.12	39.31	0.53	0.018	30	20	23	422	10
U1352C_103R2	1508.23	Sandy marlstone	IIB	12.15	37.37	0.45	0.021	22	27	30	431	8
U1352C_103R5	1513.24	Sandy marlstone	IIB	12.25	17.07	0.34	0.025	14	20	43	414	11
U1352C_104R1	1516.55	Sandy marlstone	IIB	12.32	35.34	0.38	0.011	34	25	23	425	8

U1352C_105R1	1526.17	Sandy marlstone	IIB	12.51	38.50	0.47	0.022	21	29	39	433	6
U1352C_105R1	1526.20	Sandy marlstone	IIB	12.52	45.32	0.67	0.018	38	27	44	431	11
U1352C_106R4	1540.15	Sandy marlstone	IIB	12.80	37.44	0.62	0.018	35	24	-	436	12
U1352C_106R6	1542.35	Sandy marlstone	IIB	12.84	17.26	0.42	0.017	25	23	21	428	9
U1352C_107R2	1546.48	Sandy marlstone	IIB	12.92	44.77	0.69	0.019	37	23	-	431	9
U1352C_107R3	1549.21	Sandy marlstone	IIB	12.98	52.93	0.52	0.017	30	35	19	431	7
U1352C_108R4	1558.94	Sandy marlstone	IIB	13.17	23.07	0.49	0.020	24	24	-	431	9
U1352C_109R1	1565.29	Sandy marlstone	IIB	13.30	46.18	0.50	0.022	22	66	16	428	5
U1352C_109R3	1568.05	Sandy marlstone	IIB	13.36	25.18	0.64	0.018	36	120	27	429	4
U1352C_110R2	1575.83	Sandy marlstone	IIB	13.51	13.12	1.02	0.038	26	120	27	429	4
U1352C_110R3	1577.08	Sandy marlstone	IIB	13.54	19.90	0.75	0.028	26	46	19	429	5
U1352C_111R1	1584.74	Sandy marlstone	IIB	13.69	8.41	0.52	0.027	20	33	-	415	9
U1352C_111R4	1588.45	Sandy marlstone	IIB	13.77	67.65	0.31	0.005	65	8	14		30
U1352C_112R1	1594.11	Sandy marlstone	IIB	13.88	63.14	0.28	0.006	44	41	-	432	7
U1352C_112R3	1596.68	Sandy marlstone	IIB	13.93	23.50	0.73	0.029	25	70	12	429	4
U1352C_113R2	1605.23	Sandy marlstone	IIB	14.11	54.49	0.98	0.012	82	47	7	432	6
U1352C_113R4	1608.81	Sandy marlstone	IIB	14.18	53.87	0.33	0.018	19	33	12	425	6
U1352C_114R3	1617.03	Sandy marlstone	IIB	14.34	40.30	0.40	0.016	26	73	-	428	4
U1352C_114R4	1618.03	Sandy marlstone	IIB	14.36	65.35	0.03	0.004	6	11	2	-	13
U1352C_115R6	1630.35	Sandy marlstone	IIB	14.61	19.18	1.37	0.037	37	67	8	427	6
U1352C_115R6	1631.02	Sandy marlstone	IIB	14.62	68.14	0.42	0.007	59	17	7	431	10
U1352C_116R2	1634.30	Sandy marlstone	IIB	14.69	67.37	0.27	0.007	39	10	16	441	18
U1352C_116R3	1635.67	Sandy marlstone	IIB	14.72	55.55	0.44	0.018	25	121	27	432	4

Core ans section number	Sample depth (mbsf)	Main lithology	Lithological unit	Age (Ma)	$CaCO_3$ (wt%)	TOC[1] (wt%)	TN[2] (wt%)	TOC/TN	HI[3] (mg HC/g TOC)	OI[4] (mg CO_2/g TOC)	*Tmax*[5] (°C)	Production index[6]
U1352C_117R6	1649.06	Sandy marlstone	IIB	14.99	64.23	0.07	0.007	10	14	11	436	10
U1352C_118R3	1654.38	Sandy marlstone	IIB	15.09	44.64	0.29	0.015	19	17	9	428	10
U1352C_118R3	1654.85	Sandy marlstone	IIB	15.10	39.68	0.45	0.017	26	57	-	429	6
U1352C_119R4	1666.45	Sandy marlstone	IIB	15.34	9.78	0.71	0.036	20	54	11	434	6
U1352C_119R4	1666.68	Sandy marlstone	IIB	15.34	57.51	0.39	0.010	39	12	23	417	13
U1352C_120RCC	1668.90	Sandy marlstone	IIB	15.39	30.97	0.70	0.022	32	40	25	425	6
U1352C_120RCC	1669.24	Sandy marlstone	IIB	15.39	50.52	0.32	0.013	24	15	11	418	12
U1352C_122R1	1688.87	Sandy marlstone	IIB	15.79	41.44	0.53	0.019	27	19	-	430	7
U1352C_122R2	1690.26	Sandy marlstone	IIB	15.82	71.56	0.35	0.010	35	18	17	425	8
U1352C_123R1	1693.23	Sandy marlstone	IIB	15.88	29.39	0.70	0.019	36	36	-	414	8
U1352C_123R2	1694.65	Sandy marlstone	IIB	15.90	76.59	0.01	0.005	3	13	16	418	11
U1352C_124R6	1705.96	Glauconitic sandstone interspersed with sandy marlstone	IIC	16.13	56.91	0.32	0.010	31	12	14	429	14
U1352C_125R2	1709.41	Glauconitic sandstone interspersed with sandy marlstone	IIC	16.20	30.86	0.36	0.024	15	29	41	426	5
U1352C_125R5	1714.16	Glauconitic sandstone interspersed with sandy marlstone	IIC	16.30	55.25	0.22	0.006	36	30	37	431	7
U1352C_126R3	1720.51	Glauconitic sandstone interspersed with sandy marlstone	IIC	16.43	78.36	0.24	0.011	21	30	37	431	7
U1352C_126R6	1724.31	Glauconitic sandstone interspersed with sandy marlstone	IIC	16.50	78.14	0.24	0.005	46	20	22	426	18
U1352C_127R2	1728.06	Glauconitic sandstone interspersed with sandy marlstone	IIC	16.58	77.95	0.13	0.005	26	11	15	-	13
U1352C_127R3	1730.22	Glauconitic sandstone interspersed with sandy marlstone	IIC	16.62	40.39	0.51	0.018	29	34	25	434	5
U1352C_128R1	1736.38	Glauconitic sandstone interspersed with sandy marlstone	IIC	16.74	85.58	0.13	-	-	15	19	425	11
U1352C_128R5	1741.69	Glauconitic sandstone interspersed with sandy marlstone	IIC	16.85	6.87	0.73	0.056	13	78	21	427	4
U1352C_129R1	1745.44	Glauconitic sandstone interspersed with sandy marlstone	IIC	16.93	80.16	0.24	0.002	115	-	-	-	-
U1352C_129R2	1747.88	Glauconitic sandstone interspersed with sandy marlstone	IIC	16.98	76.06	0.10	0.004	24	21	54	428	17

Core ans section number	Sample depth (mbsf)	Main lithology	Lithological unit	Age (Ma)	$CaCO_3$ (wt%)	TOC[1] (wt%)	TN[2] (wt%)	TOC/TN	HI[3] (mg HC/g TOC)	OI[4] (mg CO_2/g TOC)	*T*max[5] (°C)	Production index[6]
U1352C_129R2	1747.88	Glauconitic sandstone interspersed with sandy marlstone	IIC	16.98	36.77	0.29	0.020	14	42	44	431	8
U1352C_130R2	1757.20	Glauconitic sandstone interspersed with sandy marlstone	IIC	17.16	83.45	0.06	0.000	140	12	40	415	17
U1352C_130R3	1758.63	Glauconitic sandstone interspersed with sandy marlstone	IIC	17.19	29.39	0.33	0.021	16	27	33	425	6
U1352C_130R4	1760.44	Glauconitic sandstone interspersed with sandy marlstone	IIC	17.23	83.65	0.12	0.003	35	18	73	427	20
U1352C_130R4	1760.44	Glauconitic sandstone interspersed with sandy marlstone	IIC	17.23	31.36	0.24	0.012	20	27	44	421	7
U1352C_131R2	1766.98	Glauconitic sandstone interspersed with sandy marlstone	IIC	17.36	88.71	0.05	0.003	17	26	39	434	25
U1352C_131R2	1766.98	Glauconitic sandstone interspersed with sandy marlstone	IIC	17.36	29.25	0.16	0.016	10	23	37	422	9
U1352C_131R2	1767.13	Glauconitic sandstone interspersed with sandy marlstone	IIC	17.36	87.52	0.30	0.002	174	15	42	429	14
U1352C_132R3	1776.86	Glauconitic sandstone interspersed with sandy marlstone	IIC	17.56	67.38	0.22	0.007	33	15	44	426	6
U1352C_132R3	1777.38	Glauconitic sandstone interspersed with sandy marlstone	IIC	17.57	36.04	0.05	0.011	5	25	75	432	14
U1352C_133R2	1786.74	Glauconitic sandstone interspersed with sandy marlstone	IIC	17.76	28.83	0.18	0.023	8	38	40	433	5
U1352C_134R1	1794.18	Glauconitic sandstone interspersed with sandy marlstone	IIC	17.91	20.11	0.17	0.023	7	17	31	424	9
U1352C_134R3	1796.58	Glauconitic sandstone interspersed with sandy marlstone	IIC	17.96	85.31	0.04	0.001	41	13	21	-	17
U1352C_135R1	1803.84	Glauconitic sandstone interspersed with sandy marlstone	IIC	18.10	86.60	0.17	0.001	343	13	28	-	17
U1352C_135R4	1807.91	Glauconitic sandstone interspersed with sandy marlstone	IIC	18.18	23.47	0.11	0.018	6	26	26	434	7
U1352C_136R3	1816.86	Glauconitic sandstone interspersed with sandy marlstone	IIC	18.36	22.32	0.28	0.021	13	28	20	429	5
U1352C_136R4	1818.50	Glauconitic sandstone interspersed with sandy marlstone	IIC	18.40	29.98	0.17	0.016	10	21	11	429	20
U1352C_136R5	1818.86	Glauconitic sandstone interspersed with sandy marlstone	IIC	18.40	89.59	0.18	0.000	747	11	18	-	17
U1352C_137R4	1827.88	Glauconitic sandstone interspersed with sandy marlstone	IIC	18.59	90.82	0.14	0.001	220	-	-	-	-
U1352C_137R5	1828.82	Glauconitic sandstone interspersed with sandy marlstone	IIC	18.60	49.17	0.06	0.007	8	17	17	436	20
U1352C_138R1	1832.84	Glauconitic sandstone interspersed with sandy marlstone	IIC	18.69	83.92	0.23	-	-	8	18	433	20

Core and section number	Sample depth (mbsf)	Main lithology	Lithological unit	Age (Ma)	$CaCO_3$ (wt%)	TOC[1] (wt%)	TN[2] (wt%)	TOC/TN	HI[3] (mg HC/g TOC)	OI[4] (mg CO_2/g TOC)	*T*max[5] (°C)	Production index[6]
U1352C_138R4	1836.52	Glauconitic sandstone interspersed with sandy marlstone	IIC	18.76	89.15	0.52	0.001	877	11	3	-	20
U1352C_138R4	1837.73	Glauconitic sandstone interspersed with sandy marlstone	IIC	18.78	27.44	0.33	0.023	14	18	8	433	14
U1352C_139R1	1842.10	Glauconitic sandstone interspersed with sandy marlstone	IIC	18.87	25.64	0.12	0.016	7	12	10	422	20
U1352C_139R1	1842.36	Glauconitic sandstone interspersed with sandy marlstone	IIC	18.88	87.66	0.23	-	-	11	25	-	17
U1352C_140R1	1851.26	Glauconitic sandstone interspersed with sandy marlstone	IIC	19.06	87.79	0.40	0.001	499	27	41	422	18
U1352C_140R1	1851.45	Glauconitic sandstone interspersed with sandy marlstone	IIC	19.06	78.44	1.46	0.001	1514	11	2	-	25
U1352C_140R2	1852.69	Glauconitic sandstone interspersed with sandy marlstone	IIC	19.08	96.44	0.77	0.092	8	29	0	-	22
U1352C_141R1	1861.69	Glauconitic sandstone interspersed with sandy marlstone	IIC	19.27	95.88	0.09	-	-	12	33	-	20
U1352C_143R2	1877.20	White, cemented, fine-grained limestone	III	30.90	96.16	0.12	-	-	13	43	-	20
U1352C_144R4	1884.24	White, cemented, fine-grained limestone	III	31.02	96.08	0.19	-	-	14	31	-	20
U1352C_145R3	1892.90	White, cemented, fine-grained limestone	III	31.16	93.30	0.26	-	-	13	58	424	25
U1352C_146R3	1902.47	White, cemented, fine-grained limestone	III	31.32	91.68	-	-	-	12	26	-	17
U1352C_147R3	1911.56	White, cemented, fine-grained limestone	III	31.47	90.12	0.09	-	-	14	29	-	17
U1352C_147R4	1913.23	White, cemented, fine-grained limestone	III	31.50	37.89	0.54	0.013	40	17	20	427	12
U1352C_147R6	1916.31	White, cemented, fine-grained limestone	III	31.55	44.67	0.33	0.013	26	29	19	426	9
U1352C_148R3	1921.41	White, cemented, fine-grained limestone	III	31.63	51.59	0.50	0.011	45	26	27	424	11
U1352C_148R5	1924.03	White, cemented, fine-grained limestone	III	31.67	89.41	0.13	-	-	9	13	-	14
U1353B_88X1	510.09	Dark greenish-grey, very fine sandy mud; and dark greenish-grey mud	II	12.03	0.54	0.11	0.013	8	25	-	408	30
U1353B_90XCC	528.66	Dark greenish-grey, very fine sandy mud; and dark greenish-grey mud	II	12.47	1.13	0.12	0.014	9	31	-	406	31
U1353B_91XCC	537.63	Dark greenish-grey, very fine sandy mud; and dark greenish-grey mud	II	12.68	4.15	0.08	0.011	7	24	-	401	27
U1353B_92XCC	547.10	Dark greenish-grey, very fine sandy mud; and dark greenish-grey mud	II	12.90	39.49	0.21	0.008	27	40	-	422	20
U1353B_93X1	556.82	Dark greenish-grey, very fine sandy mud; and dark greenish-grey mud	II	13.13	0.51	0.16	0.022	7	30	-	404	25

Core ans section number	Sample depth (mbsf)	Main lithology	Lithological unit	Age (Ma)	$CaCO_3$ (wt%)	TOC[1] (wt%)	TN[2] (wt%)	TOC/TN	HI[3] (mg HC/g TOC)	OI[4] (mg CO_2/g TOC)	*T*max[5] (°C)	Production index[6]
U1353B_94XCC	566.37	Dark greenish-grey, very fine sandy mud; and dark greenish-grey mud	II	13.36	0.41	0.06	0.012	5	20	-	370	33
U1353B_95X1	576.28	Dark greenish-grey, very fine sandy mud; and dark greenish-grey mud	II	13.59	0.61	0.16	0.015	11	37	-	398	33
U1353B_96X1	585.57	Dark greenish-grey, very fine sandy mud; and dark greenish-grey mud	II	13.81	0.56	0.10	0.013	8	42	-	397	33
U1353B_97XCC	595.13	Dark greenish-grey, very fine sandy mud; and dark greenish-grey mud	II	14.04	0.83	0.11	0.013	9	32	-	397	29

[1]Total organic carbon = total carbon (TC)-inorganic carbon; TC = ($CaCO_3$/8.33); after Fulthorpe et al., 2011

[2]TN = total nitrogen

[3]Hydrogen Index = 100*S_2/TOC; after Espitalié et al., 1977

[4]Oxygen Index = 100*S_3/TOC; after Espitalié et al., 1977

[5]*T*max is the pyrolysis temperature at which the evolution rate of S_2 is at a maximum; after Espitalié et al., 1986

[6]Production Index = S_1/(S_1+S_2)*100; after Espitalié et al., 1986

Table 2.2: Extractability of the organic matter (mg OM/g sediment) for the analysed IODP Expedition 317 samples, n-alkane and isoprenoid ratios, and n-alkanes distribution.

U1351B_112	U1351B_111	U1351B_109	U1351B_106	U1351B_104	U1351B_103	U1351B_101	U1351B_100	U1351B_97X	**Core and section number**
sq.c.	c.s.	sq.c.	sq.c.	sq.c.	c.s.	c.s.	sq.c.	sq.c.	**Sample type[1]**
989.18	976.25	959.05	929.41	908.97	900.04	880.93	871.62	845.75	**Sample depth (mbsf)**
6.52	6.41	6.27	6.01	5.84	5.76	5.60	5.52	5.30	**Age (Ma)**
50.2	9.3	49.2	50.5	49.0	9.9	10.5	49.9	51.0	**Extracted sediment (g)**
0.12	0.15	0.07	0.15	0.17	0.14	0.28	0.10	0.08	**Extractability (mg OM/g**
1.28	0.96	1.44	1.20	1.64	0.95	1.12	1.29	1.77	**$CPI_{(22-32)}$[2]**
3.4	2.6	3.0	2.4	3.3	2.3	3.4	2.6	3.9	**$1/P_{aq}$[3]**
25.0	21.1	18.9	16.6	27.0	29.7	23.2	28.6	15.6	**TAR[4]**
1.34	1.36	1.09	0.58	1.22	0.78	1.37	1.01	4.14	**Pr/Ph**
1.29	1.12	1.34	0.91	8.43	0.63	1.47	9.25	0.78	**Pr/n-C_{17}**
0.67	0.33	0.80	0.65	0.49	0.44	0.38	0.59	0.14	**Ph/n-C_{18}**
-	-	-	-	-	-	-	-	-	**10**
-	-	1.6	0.4	0.4	-	-	3.3	-	**11**
0.4	2.0	1.2	0.3	0.2	-	-	1.1	-	**12**
1.4	3.0	2.8	0.3	0.9	-	-	2.9	2.0	**13**
1.2	7.4	8.9	1.1	1.3	1.5	8.8	1.5	2.3	**14**
1.4	6.3	3.6	1.3	1.4	1.0	3.9	0.0	2.2	**15**
9.0	4.6	12.7	5.3	7.5	2.9	21.0	7.4	6.2	**16**
5.0	2.3	4.4	5.1	0.6	3.4	4.0	0.7	8.2	**17**
7.2	5.8	6.8	12.4	7.8	6.1	11.3	11.0	11.3	**18**
4.9	3.7	5.0	9.8	6.8	3.8	3.7	8.1	2.5	**19**
10.4	10.8	11.3	24.0	12.1	14.4	12.7	18.9	11.0	**20**
10.1	8.6	10.0	21.1	12.0	10.8	6.4	22.0	11.8	**21**
19.4	25.4	24.8	45.3	21.3	36.0	20.6	43.2	17.4	**22**
24.9	32.6	31.1	51.0	28.7	40.9	24.4	50.3	24.4	**23**
44.2	65.6	51.5	81.9	44.0	75.1	51.9	61.6	40.1	**24**
56.7	73.5	57.1	81.5	50.3	80.7	57.4	63.1	32.4	**25**
69.1	100	59.6	86.9	49.5	100	79.0	66.9	30.9	**26**
83.2	90.0	66.5	81.3	58.9	89.1	77.1	67.4	36.6	**27**
72.9	88.9	52.0	68.9	42.5	87.3	75.4	59.3	29.6	**28**
98.2	84.5	78.9	87.2	78.6	82.0	92.6	85.2	64.7	**29**
67.3	83.9	44.0	56.7	35.6	77.9	73.3	55.4	26.8	**30**
100	85.2	100	100	100	71.7	100	100	100	**31**
39.7	56.0	25.5	35.1	21.8	46.9	47.7	37.7	19.5	**32**
38.9	37.1	32.3	39.7	35.7	32.7	41.5	39.2	41.8	**33**
16.6	20.2	9.3	15.7	7.5	18.5	20.0	17.2	9.0	**34**
10.2	12.6	8.9	13.2	9.8	12.9	15.0	14.9	13.0	**35**
5.0	6.8	3.9	4.9	2.5	9.5	8.2	6.7	4.1	**36**
-	-	-	-	-	6.3	-	-	-	**37**
-	-	-	-	-	-	-	-	-	**38**

U1352C_81R	U1352C_80R	U1352C_79R	U1352C_78R	U1352C_77R	U1352C_76R	U1352C_76R	U1352C_73R	U1352C_72R	U1352C_71R	U1352C_70R	U1351B_113
c.s.	c.s.	c.s.	c.s.	c.s.	c.s.	sq.c.	c.s.	c.s.	c.s.	c.s.	c.s.
1328.03	1326.05	1319.47	1314.52	1309.64	1305.04	1305.02	1280.91	1265.98	1263.81	1249.85	997.74
7.07	7.00	6.78	6.61	6.45	6.30	6.30	5.49	4.99	4.92	4.45	6.60
10.9	11.3	12.1	11.4	13.1	13.2	50.2	13.7	13.2	13.0	13.5	10.3
0.16	0.07	0.16	0.06	0.25	0.05	0.14	0.07	0.16	0.18	0.30	0.09
1.28	1.08	3.86	1.19	1.60	2.56	2.09	1.92	1.27	1.18	3.10	0.99
6.1	2.9	8.6	2.5	3.0	7.5	8.1	5.6	3.1	3.0	4.7	2.4
1.3	5.0	17.3	2.6	2.0	37.3	17.3	5.6	5.5	6.7	7.1	11.1
0.99	1.32	0.85	1.74	1.25	0.72	1.14	1.18	1.27	1.33	0.69	0.33
1.14	1.35	1.85	1.56	3.59	3.00	1.37	2.02	4.20	3.49	4.77	0.54
0.63	0.68	1.57	0.50	1.38	1.88	0.86	0.90	2.00	1.23	0.71	0.58
4.3	6.4	1.8	5.0	90.0	-	3.9	3.2	2.4	2.8	1.4	-
16.9	18.2	3.5	12.4	69.3	-	14.8	10.7	7.8	9.0	4.3	-
15.6	14.4	3.7	11.5	14.9	0.3	15.0	13.5	8.1	10.3	6.0	-
16.4	19.8	4.6	15.7	21.2	0.6	11.3	17.4	14.7	16.1	9.5	-
93.2	100	25.2	100	100	0.7	30.2	100	92.0	100	60.8	7.7
27.8	22.2	6.0	29.0	23.1	0.4	4.6	21.0	34.1	23.4	16.1	7.0
100	52.8	17.3	78.9	50.4	1.2	14.1	50.2	75.9	80.5	100	11.9
30.0	10.0	3.7	10.3	6.7	1.7	6.2	10.9	13.6	11.2	8.1	4.1
54.4	15.1	5.2	18.2	13.9	3.2	8.7	20.6	22.5	23.7	79.6	11.4
16.3	4.9	1.7	3.7	2.7	1.8	0.9	2.2	3.6	5.2	4.5	10.6
42.9	9.9	1.9	5.2	3.6	3.5	8.7	11.4	5.9	8.2	26.8	14.0
14.5	4.4	2.1	3.1	3.6	4.0	1.3	3.0	4.4	8.5	5.4	13.0
30.2	7.8	2.6	6.7	5.4	7.9	9.7	12.6	8.0	12.7	8.9	28.4
9.2	11.9	4.9	9.2	7.5	10.9	4.8	8.0	16.4	20.8	9.8	34.5
20.6	28.6	7.9	20.6	11.8	12.4	17.1	22.3	37.8	39.3	12.8	67.8
6.9	49.6	17.1	34.2	15.7	14.2	19.0	25.2	69.5	65.3	31.1	77.3
17.7	74.1	16.3	46.4	18.2	10.7	30.2	36.1	91.3	86.1	21.5	100
10.9	73.3	32.9	45.7	19.8	20.2	35.2	40.0	100	93.2	50.9	83.7
15.8	68.2	16.2	36.8	13.4	8.8	28.7	29.4	82.9	84.8	19.6	88.5
30.1	67.7	66.1	38.7	22.1	63.8	68.5	66.5	98.1	94.9	67.5	91.8
13.7	47.4	13.4	20.8	8.0	10.5	23.4	19.7	61.3	66.6	16.5	69.5
52.0	46.3	100	26.9	24.1	100	100	84.8	83.3	77.6	84.9	66.6
5.2	17.4	4.5	5.3	3.0	4.7	9.5	6.9	22.4	30.4	7.8	38.6
11.2	9.7	16.7	2.3	0.1	15.8	21.5	13.7	23.3	23.0	20.2	26.1
1.5	3.7	-	-	-	1.4	1.2	0.7	4.2	6.3	-	18.0
-	0.4	-	-	-	2.7	0.9	0.2	3.6	4.2	-	-
-	1.0	-	-	-	0.2	-	-	-	-	-	-
-	-	-	-	-	-	-	-	-	-	-	-
-	-	-	-	-	-	-	-	-	-	-	-

U1352C_103	U1352C_102	U1352C_95R	U1352C_94R	U1352C_91R	U1352C_90R	U1352C_89R	U1352C_89R	U1352C_88R	U1352C_87R	U1352C_86R	U1352C_85R
c.s.	c.c.	c.s.	sq.c.	c.s.	c.s.	sq.c.	c.s.	c.s.	sq.c.	c.s.	c.s.
1513.25	1496.43	1440.76	1435.75	1406.54	1392.51	1385.71	1384.35	1378.31	1367.05	1353.80	1351.57
12.25	11.92	10.80	10.66	9.69	9.22	8.99	8.95	8.74	8.37	7.93	7.85
9.5	9.0	10.2	50.0	12.8	10.4	76.0	15.2	9.0	50.1	11.1	13.0
-	-	0.09	0.08	0.10	0.09	0.31	0.07	0.14	0.09	0.04	0.05
0.72	0.98	1.09	1.67	0.87	1.05	1.34	1.34	2.17	1.26	1.01	1.39
2.4	3.8	5.6	2.8	2.5	2.2	4.7	-	4.1	3.0	3.0	4.0
0.8	2.0	41.9	18.1	3.1	1.9	7.0	7.0	26.3	18.0	14.0	9.5
13.17	1.40	1.48	1.49	3.82	1.45	1.04	1.04	0.95	0.89	1.14	0.72
1.72	0.57	1.67	2.56	4.29	1.38	1.04	1.04	0.96	3.10	2.03	1.30
0.04	2.60	0.46	0.86	0.59	0.54	0.46	0.46	0.33	1.67	0.89	0.61
4.3	11.6	0.3	-	3.3	7.8	3.1	-	1.1	-	2.4	1.7
10.0	22.4	0.9	-	11.2	21.8	10.8	-	3.9	0.6	7.2	4.4
11.4	29.0	0.6	-	9.0	13.6	12.4	-	3.9	0.8	6.0	3.5
12.7	28.1	0.6	-	10.9	15.4	16.4	-	3.5	1.2	5.9	3.9
78.0	100	6.1	-	86.2	100	86.6	-	19.8	9.9	29.5	28.5
19.3	24.9	2.1	-	28.1	25.2	19.7	-	4.5	0.5	8.4	11.7
100	55.3	12.6	5.2	100	81.4	65.8	-	21.0	4.8	27.6	47.5
12.3	30.7	2.6	4.3	17.1	12.5	13.1	-	4.1	5.9	7.0	10.0
40.2	4.8	6.4	8.6	32.6	22.2	28.5	-	12.7	11.9	14.1	29.4
1.7	9.2	1.0	8.6	7.7	2.3	4.0	-	2.3	7.3	2.9	5.8
17.4	25.6	5.1	14.6	17.3	5.6	14.0	-	5.3	14.7	12.1	17.3
1.2	5.0	2.0	18.9	6.1	2.9	2.9	-	2.2	13.0	4.2	6.1
9.3	23.9	7.0	35.7	45.4	6.2	14.0	-	5.8	27.9	13.1	13.3
3.1	11.2	8.1	47.8	15.1	7.5	9.7	-	9.9	32.3	14.3	14.8
11.9	30.4	20.4	55.3	39.9	17.2	29.2	-	24.5	60.0	42.6	31.5
9.0	22.6	31.7	51.8	50.6	26.9	40.2	-	53.2	65.8	65.3	48.1
15.7	42.9	48.9	45.6	76.8	37.1	62.4	-	64.5	86.5	100	63.1
10.8	32.6	56.4	54.6	66.5	35.7	70.3	-	87.6	92.8	97.4	70.4
13.1	39.3	65.0	37.2	67.4	28.7	64.6	-	61.0	70.0	94.7	63.2
11.0	55.2	84.8	78.7	57.7	26.2	85.6	-	100	100	87.9	90.3
8.1	32.7	84.2	33.6	47.6	16.7	52.1	-	1.1	50.5	72.5	54.4
5.8	40.2	100	100	39.3	13.9	100	-	98.5	94.6	70.7	100
3.5	15.0	70.3	19.8	18.2	4.8	26.4	-	14.6	22.5	34.2	26.8
-	-	57.4	35.3	7.5	1.8	27.4	-	15.1	24.9	19.2	27.1
-	-	35.3	9.0	2.6	0.8	6.7	-	1.6	6.8	6.4	6.1
-	-	21.0	7.9	1.4	0.0	4.8	-	0.3	6.7	3.2	-
-	-	12.3	3.9	-	-	3.3	-	-	2.9	1.6	-
-	-	-	-	-	-	1.7	-	-	-	-	-
-	-	-	-	-	-	-	-	-	-	-	-

U1352C_116	U1352C_115	U1352C_114	U1352C_113	U1352C_112	U1352C_111	U1352C_109	U1352C_108	U1352C_107	U1352C_106	U1352C_105	U1352C_104
c.s.	c.s.	c.s.	c.s.	c.s.	c.s.	c.s.	c.s.	c.s.	c.s.	sq.c.	c.s.
1636.89	1628.21	1617.04	1605.98	1596.68	1584.24	1568.52	1554.61	1553.19	1542.31	1532.33	1517.31
14.74	14.57	14.34	14.12	13.93	13.68	13.37	13.09	13.06	12.84	12.64	12.34
9.3	10.8	12.5	10.5	8.3	6.2	8.6	10.0	7.7	11.0	50.1	12.2
0.06	0.26	0.08	0.12	0.11	0.34	-	-	0.03	0.07	0.05	0.08
1.44	2.76	1.13	-	1.30	1.06	-	-	-	1.20	1.29	0.89
1.6	5.4	1.3	-	3.0	2.0	-	-	-	2.4	4.1	2.8
2.1	22.2	0.5	-	3.4	0.6	-	-	-	16.6	34.9	2.1
2.97	5.88	2.69	3.76	2.34	2.21	2.20	14.37	3.73	0.58	1.76	5.78
6.12	6.92	10.00	9.65	5.58	4.69	3.94	2.02	2.70	0.91	2.00	1.39
0.93	1.13	2.93	3.25	1.60	1.00	1.01	0.22	0.59	0.65	0.39	1.56
29.6	-	-	-	10.8	4.9	-	-	-	-	-	11.4
27.0	-	-	-	17.4	8.1	-	-	-	0.4	-	31.2
45.9	-	-	-	26.0	12.6	-	-	-	0.3	-	34.8
53.9	1.3	-	-	32.8	18.0	-	-	-	0.3	0.3	29.8
100	4.5	-	-	100	100	-	-	-	1.1	2.7	100
20.3	2.0	-	-	26.6	29.9	-	-	-	1.3	0.6	18.2
24.1	3.4	-	-	53.7	51.6	-	-	-	5.3	6.1	59.1
6.5	3.0	-	-	13.3	7.1	-	-	-	5.1	2.0	23.1
14.3	3.1	-	-	19.9	15.0	-	-	-	12.4	4.7	3.6
-	3.6	-	-	4.7	1.3	-	-	-	9.8	2.5	3.4
-	4.2	-	-	8.2	2.6	-	-	-	24.0	6.1	26.1
-	6.2	-	-	6.5	-	-	-	-	21.1	6.3	1.9
-	7.5	-	-	12.8	5.5	-	-	-	45.3	13.4	28.0
19.1	12.8	-	-	14.3	3.9	-	-	-	51.0	17.0	12.1
16.8	15.3	-	-	28.9	6.9	-	-	-	81.9	29.2	32.1
38.6	22.5	-	-	37.5	9.7	-	-	-	81.5	35.9	24.7
38.1	21.1	-	-	48.9	10.0	-	-	-	86.9	45.9	40.7
22.4	35.1	-	-	44.9	10.1	-	-	-	81.3	60.6	31.2
19.8	22.5	-	-	36.7	8.7	-	-	-	68.9	49.4	34.6
19.3	100.0	-	-	66.6	8.3	-	-	-	87.2	100	40.2
4.5	17.9	-	-	27.7	7.1	-	-	-	56.7	43.0	23.6
14.9	55.9	-	-	38.5	5.7	-	-	-	100	64.5	24.4
-	2.9	-	-	12.6	-	-	-	-	35.1	23.8	6.7
-	5.7	-	-	3.8	-	-	-	-	39.7	21.3	-
-	-	-	-	-	-	-	-	-	15.7	8.7	-
-	-	-	-	-	-	-	-	-	13.2	7.6	-
-	-	-	-	-	-	-	-	-	4.9	4.2	-
-	-	-	-	-	-	-	-	-	-	-	-
-	-	-	-	-	-	-	-	-	-	-	-

U1352C_133	U1352C_131	U1352C_130	U1352C_129	U1352C_128	U1352C_127	U1352C_126	U1352C_125	U1352C_124	U1352C_123	U1352C_118	U1352C_117
c.s.	c.s.	c.s.	c.s.	c.s.	c.s.	c.s.	c.s.	c.s.	c.s.	c.s.	c.s.
1788.83	1766.99	1760.44	1747.88	1741.71	1730.24	1720.51	1712.88	1697.95	1692.95	1655.27	1649.18
17.80	17.36	17.23	16.98	16.85	16.62	16.43	16.27	15.97	15.87	15.11	14.99
6.0	11.6	1.6	9.1	10.4	6.0	7.5	15.2	4.0	12.7	8.0	8.0
0.07	0.02	0.25	0.08	0.34	0.13	0.09	0.07	0.20	0.05	0.18	0.21
0.38	0.36	0.95	0.61	4.73	0.53	1.37	1.06	0.84	1.39	2.47	1.69
2.6	3.5	2.6	2.3	13.3	2.7	3.3	1.9	2.3	3.5	6.1	2.9
0.3	0.9	58.3	1.2	16.6	1.8	55.3	0.6	0.8	1.9	9.4	3.3
3.46	3.19	2.14	2.63	2.49	2.19	1.47	3.84	1.95	2.54	2.18	1.97
1.62	0.91	-	3.18	12.99	2.36	2.30	2.72	1.65	3.55	15.27	17.17
0.28	0.19	-	0.78	3.73	0.70	0.97	0.59	0.67	0.93	5.24	4.88
6.0	24.9	-	7.5	0.6	19.3	0.3	192.4	639.0	118.0	23.0	15.7
19.3	56.3	-	25.6	1.3	46.1	0.6	31.6	133.7	25.4	7.1	5.0
18.4	57.2	-	21.8	2.7	41.3	1.0	29.6	95.2	22.8	11.7	37.4
20.8	37.7	-	21.6	5.0	26.9	1.3	27.9	100	26.2	14.2	54.2
100	100	-	100	20.9	100	4.4	100	332.3	100	39.0	100
25.2	12.8	-	29.4	5.9	19.2	1.6	20.7	66.5	35.2	10.5	22.4
61.9	60.7	-	64.6	10.4	64.1	2.5	32.7	92.3	49.6	14.7	31.6
18.3	32.0	-	27.0	4.0	37.1	1.7	8.6	18.1	11.1	6.3	10.9
30.4	47.8	-	42.1	5.6	56.9	2.7	10.3	22.9	16.6	8.5	19.4
4.8	3.1	-	6.5	2.8	8.6	2.0	-	-	3.2	5.6	5.6
20.9	40.9	-	35.7	4.3	56.2	4.1	-	10.2	5.3	5.7	9.1
3.8	2.8	-	7.9	3.3	8.9	4.4	2.5	-	3.5	4.7	4.7
20.8	40.0	-	36.0	4.7	60.5	11.7	0.0	13.0	6.6	6.5	10.1
2.7	5.0	-	11.7	4.5	14.8	19.9	3.1	0.0	7.1	8.0	19.3
13.3	37.6	-	41.5	6.4	67.0	38.6	7.5	24.7	13.5	14.6	21.4
3.4	8.4	-	25.1	10.2	31.0	63.1	8.3	28.5	18.9	24.6	28.6
9.9	35.1	-	48.9	8.2	73.9	84.5	7.8	36.1	25.0	26.7	36.2
3.2	10.3	-	31.1	29.5	34.2	98.1	7.4	33.1	29.0	45.6	38.3
7.1	32.5	-	42.5	13.4	65.3	100	7.0	31.2	24.7	28.4	25.3
4.5	18.6	-	28.1	100	47.8	99.9	5.8	21.8	41.4	100.0	57.8
7.1	28.2	-	30.6	14.6	52.0	0.9	5.0	19.8	17.3	23.8	16.8
5.2	15.0	-	19.2	81.3	31.7	90.4	4.1	16.2	24.2	65.5	33.5
4.2	14.3	-	12.6	5.4	24.8	82.0	-	-	6.4	3.3	-
-	7.6	-	5.4	12.7	1.0	71.1	-	-	4.3	7.4	-
-	-	-	-	-	-	55.3	-	-	-	-	-
-	-	-	-	-	-	46.6	-	-	-	-	-
-	-	-	-	-	-	33.2	-	-	-	-	-
-	-	-	-	-	-	29.4	-	-	-	-	-
-	-	-	-	-	-	21.1	-	-	-	-	-

U1353B_88X	U1352C_147	U1352C_146	U1352C_145	U1352C_144	U1352C_143	U1352C_140	U1352C_139	U1352C_137	U1352C_136	U1352C_135	U1352C_134
c.s.	c.s.	c.s.	c.s.	c.s.	c.s.	c.s.	c.s.	c.s.	c.s.	c.s.	c.s.
510.09	1913.24	1900.92	1891.76	1884.51	1875.04	1851.46	1842.11	1828.83	1818.51	1809.40	1793.51
12.03	31.50	31.29	31.14	31.02	30.87	19.06	18.87	18.60	18.40	18.21	17.89
8.0	14.5	10.2	8.2	9.6	4.0	15.4	12.0	8.0	6.2	6.0	8.1
0.33	0.01	0.01	0.09	0.04	0.03	0.03	0.09	0.04	0.05	0.07	0.07
0.98	0.94	-	0.26	0.32	0.12	1.00	0.63	0.15	0.24	0.27	-
2.6	2.7	-	2.3	1.4	2.0	2.4	2.8	1.9	1.8	2.5	1.0
44.9	3.5	-	1.1	0.3	0.2	90.5	0.6	0.1	0.4	0.4	-
0.47	0.93	3.05	1.39	0.85	2.10	0.74	2.01	1.52	1.89	2.51	3.61
0.75	1.87	0.38	0.50	0.97	0.24	2.69	1.24	0.82	0.47	0.77	0.25
0.35	0.42	0.09	0.21	0.43	0.08	0.79	0.41	0.30	0.08	0.17	-
-	-	-	82.1	22.0	33.8	6.2	6.2	15.7	5.9	10.4	-
-	-	-	92.0	77.0	100	1.1	23.6	45.8	18.0	39.9	-
-	-	-	78.9	61.8	65.2	-	28.4	39.1	11.1	32.7	-
-	-	3.9	51.1	33.8	27.4	-	27.7	21.9	7.0	26.5	-
3.1	-	50.5	68.2	9.6	70.5	0.8	100	100	49.8	100	-
1.7	-	15.0	9.9	18.6	7.7	-	20.2	25.7	12.5	21.4	-
17.6	-	100	82.6	85.4	74.5	2.0	46.1	96.2	100	71.1	-
2.0	-	11.7	43.5	37.7	53.1	2.4	14.6	34.0	28.3	26.9	-
9.4	-	56.0	74.6	100.0	77.8	11.0	22.1	61.1	86.3	47.8	-
1.9	-	11.4	7.4	17.8	5.7	-	4.8	5.1	6.1	5.2	-
9.3	-	25.6	88.0	88.1	79.1	5.0	14.0	46.7	56.9	46.1	-
5.5	-	15.9	7.0	22.4	6.0	5.1	4.0	4.6	5.8	6.1	-
25.3	-	21.3	100	94.5	81.6	8.0	15.8	49.2	46.9	43.0	-
30.5	-	18.2	9.5	27.2	6.4	15.7	4.4	2.9	6.6	6.0	-
59.3	-	27.9	94.4	63.9	67.7	38.0	12.2	32.7	33.9	33.0	-
67.0	-	33.0	19.6	13.6	4.8	70.0	5.0	4.0	5.5	5.1	-
95.8	-	48.0	86.7	39.6	48.9	96.9	10.9	23.1	27.9	28.8	-
100.0	-	47.9	25.2	9.4	3.8	100	5.6	3.0	7.6	6.6	-
96.3	-	54.3	68.7	32.4	36.2	95.0	9.0	15.7	20.0	23.3	-
90.9	-	50.8	25.0	11.4	6.4	77.3	9.6	3.6	6.2	9.0	-
73.0	-	42.4	50.0	20.1	21.9	58.1	8.5	8.7	13.1	15.8	-
62.1	-	35.1	14.0	3.7	5.3	39.3	7.2	2.5	3.5	7.9	-
42.8	-	27.8	24.0	7.5	5.3	23.6	4.0	2.2	6.5	8.4	-
25.4	-	14.0	3.2	-	-	11.8	2.6	-	-	2.0	-
15.4	-	10.0	-	-	-	6.7	-	-	-	-	-
10.2	-	-	-	-	-	3.6	-	-	-	-	-
-	-	-	-	-	-	2.4	-	-	-	-	-
-	-	-	-	-	-	-	-	-	-	-	-
-	-	-	-	-	-	-	-	-	-	-	-

U1353C_96X	U1353B_95X	U1353B_93X
sq.c.	c.s.	c.s.
585.57	576.28	556.82
13.81	13.59	13.13
50.5	9.9	9.8
0.02	0.10	0.18
1.50	1.15	1.07
3.1	2.4	2.4
17.6	15.7	19.0
0.72	0.71	0.77
0.55	0.91	1.00
0.19	0.12	0.15
-	-	-
-	-	-
-	-	-
-	10.7	-
-	15.6	3.1
-	5.9	2.1
0.8	66.9	38.1
4.7	7.8	7.5
25.2	82.3	62.9
8.7	4.8	3.7
26.3	36.9	30.4
33.6	10.6	10.2
52.2	37.9	27.6
42.3	42.1	34.6
42.4	79.4	67.8
45.6	91.9	81.2
43.6	100.0	100.0
59.3	98.5	91.9
40.0	84.5	83.2
85.1	98.4	87.0
35.9	65.9	61.4
100.0	94.0	74.3
24.1	40.5	35.4
32.8	34.9	29.2
9.6	14.7	14.0
3.7	10.2	9.7
3.8	-	-
-	-	-
-	-	-

[1] sq.c. = squeeze cake; c.s. = cut sample

[2]Carbon Preference Index ($CPI_{(22-32)}$) = $C_{23}+C_{25}+C_{27}+C_{29}+C_{31}/(C_{22}+2*(C_{24}+C_{26}+C_{28}+C_{30})+C_{32}$); after Bray and Evans, 1961

[3]$1/P_{aq}= (C_{23}+C_{25}+C_{27}+C_{29}+C_{31})/(C_{23}+C_{25})$; after Ficken et al., 2000; Sickes et al., 2009

[4] Terrigenous/aquatic ratio (TAR) = $(C_{27}+C_{29}+C_{31})/(C_{15}+C_{17}+C_{19})$; after Bourbonniere and Meyers, 1996

10-38 = carbon numbers in *n*-alkane chain

Table 2.3: Hopane, tricyclic terpane, and tetracyclic terpane data for the analysed IODP Expedition 317 samples.

Core and section number	Sample depth (mbsf)	Age (Ma)	Ts/(Ts+Tm)	C_{30} hopanes αβ/(αβ+βα)	C_{31} αβ hopanes 22S/(22S+22R)	Oleanane/C_{30}αβ hopane	Gammacerane/C_{30} αβ hopane	C_{29} αβ /C_{30} αβ hopane	C_{31} αβ hopane/ C_{30} αβ hopane	C_{23}/C_{21} tricyclic terpanes	C_{24} tetracyclic/ C_{23} tricyclic terpanes
U1351B_97X2	845.75	5.30	0.13	0.33	0.07	-	0.16	0.64	8.91	0.69	0.91
U1351B_100X3	871.62	5.52	0.23	0.38	0.08	-	0.15	0.67	10.88	0.80	0.79
U1351B_101X1	880.93	5.60	0.15	0.43	0.08	-	0.12	0.98	11.94	2.20	0.53
U1351B_103X1	900.04	5.76	0.34	0.71	0.26	0.06	0.07	1.00	2.21	2.03	-
U1351B_104X2	908.97	5.84	0.12	0.30	0.07	0.07	-	0.39	12.58	0.33	1.08
U1351B_106X2	929.41	6.01	0.26	0.36	0.14	0.08	0.17	0.07	3.95	1.06	0.92
U1351B_109X1	959.05	6.27	0.12	0.33	0.07	0.10	-	0.09	8.88	0.76	-
U1351B_111X1	976.25	6.41	0.19	0.32	0.14	0.10	0.15	0.60	2.86	1.75	0.91
U1351B_112X3	989.18	6.52	0.09	0.31	0.07	0.10	0.09	0.33	3.68	0.56	0.84
U1351B_113X2	997.74	6.60	0.62	0.66	0.38	0.02	0.27	0.55	1.28	1.62	0.31
U1352C_70R3	1249.85	4.45	0.15	0.95	0.11	0.05	-	0.85	2.19	0.65	-
U1352C_71R6	1263.81	4.92	0.14	0.39	0.10	0.08	0.18	0.52	3.40	1.83	0.39
U1352C_72R1	1265.98	4.99	0.17	0.47	0.13	0.04	0.10	0.30	2.33	-	1.49
U1352C_73R4	1280.91	5.49	0.17	0.42	0.08	0.10	0.09	0.48	6.15	0.92	1.12
U1352C_76R1	1305.02	6.30	0.23	0.43	0.09	0.08	0.09	0.34	3.45	1.08	-
U1352C_77R1	1309.64	6.45	0.06	0.33	0.08	0.14	0.14	0.77	2.90	-	1.10
U1352C_78R1	1314.52	6.61	0.20	0.37	0.08	0.16	0.12	0.40	3.12	1.35	-
U1352C_79R2	1319.47	6.78	0.27	0.29	-	0.58	-	0.66	7.97	1.35	-
U1352C_80R3	1326.05	7.00	0.18	0.38	0.10	0.13	0.13	1.30	2.55	1.67	0.90
U1352C_85R4	1351.57	7.85	0.13	0.32	0.07	0.27	0.10	0.35	4.92	-	0.42
U1352C_86R2	1353.80	7.93	0.08	0.38	0.07	0.08	0.05	0.21	2.10	-	0.50
U1352C_90R2	1392.51	9.22	0.36	0.54	0.27	0.14	0.17	0.70	1.35	2.46	0.48
U1352C_91R5	1406.54	9.69	0.14	0.50	0.10	0.03	-	0.38	2.02	1.57	-
U1352C_95R2	1440.76	10.80	0.18	0.39	0.06	0.06	0.14	0.44	7.00	-	-
U1352C_102R	1496.43	11.92	-	0.45	-	-	-	0.40	-	-	-
U1352C_103R5	1513.25	12.25	-	0.44	0.06	0.25	-	0.10	6.45	-	-
U1352C_104R2	1517.31	12.34	-	0.42	0.05	0.16	-	0.11	8.71	-	-

Core and section number	Sample depth (mbsf)	Age (Ma)	Ts/(Ts+Tm)	C_{30} hopanes αβ/(αβ+βα)	C_{31} αβ hopanes 22S/(22S+22R)	Oleanane/C_{30}αβ hopane	Gammacerane/C_{30} αβ hopane	C_{29} αβ /C_{30} αβ hopane	C_{31} αβ hopane/ C_{30} αβ hopane	C_{23}/C_{21} tricyclic terpanes	C_{24} tetracyclic/ C_{23} tricyclic terpanes
U1352C_105R5	1532.33	12.64	-	0.57	0.08	-	-	0.94	7.08	-	-
U1352C_106R6	1542.31	12.84	-	0.46	0.04	0.16	-	0.36	8.23	-	-
U1352C_107R6	1553.19	13.06	0.35	0.53	-	0.15	-	0.64	-	-	-
U1352C_108R1	1554.61	13.09	0.43	0.77	0.15	0.04	-	0.52	2.92	-	-
U1352C_109R3	1568.52	13.37	0.31	0.54	0.09	0.21	0.13	0.55	5.35	-	-
U1352C_111R1	1584.24	13.68	-	0.41	0.05	0.30	-	0.40	11.66	-	-
U1352C_112R3	1596.68	13.93	-	0.35	0.05	0.54	-	0.92	16.34	-	-
U1352C_113R2	1605.98	14.12	0.15	0.42	0.05	0.28	0.10	0.43	11.40	-	-
U1352C_114R3	1617.04	14.34	-	0.42	0.04	0.23	-	0.49	13.78	-	-
U1352C_115R4	1628.21	14.57	0.06	0.20	0.03	0.13	0.17	1.93	13.93	-	-
U1352C_116R3	1636.89	14.74	0.82	0.84	0.36	0.15	0.24	0.75	1.36	-	0.31
U1352C_117R6	1649.18	14.99	0.09	0.35	0.05	0.66	-	-	13.49	-	-
U1352C_118R4	1655.27	15.11	-	0.42	0.04	0.38	-	0.93	13.86	-	-
U1352C_123R1	1692.95	15.87	0.13	0.45	0.06	0.21	-	0.49	11.48	0.25	-
U1352C_124R1	1697.95	15.97	0.22	0.54	0.08	0.00	-	0.43	6.37	-	-
U1352C_125R4	1712.88	16.27	0.12	0.54	0.08	0.12	-	0.46	5.75	1.32	
U1352C_126R3	1720.51	16.43	0.15	0.54	0.09	0.10	-	0.50	4.71	1.61	0.58
U1352C_127R3	1730.24	16.62	0.19	0.55	0.07	0.14	-	0.72	5.32	1.07	-
U1352C_129R2	1747.88	16.98	0.15	0.52	0.10	0.14	-	0.61	3.93	1.01	1.07
U1352C_131R2	1766.99	17.36	0.31	0.59	0.22	0.07	-	0.48	1.76	1.43	-
U1352C_132R3	1776.88	17.56	0.10	0.46	0.07	0.32	0.13	0.89	6.62	-	-
U1352C_133R4	1788.83	17.80	0.73	0.81	0.45	0.15	0.21	0.76	1.04	-	0.17
U1352C_134R1	1793.51	17.89	0.79	0.88	0.51	0.19	0.21	0.82	0.96	-	0.24
U1352C_135R5	1809.40	18.21	-	0.57	0.23	-	-	0.58	1.77	0.63	-
U1352C_137R5	1828.83	18.60	0.78	0.89	0.50	0.19	0.22	0.79	0.96	-	0.17
U1352C_139R1	1842.11	18.87	0.19	0.52	0.16	0.11	0.18	0.60	1.92	-	-
U1352C_145R2	1891.76	31.14	0.33	0.65	0.37	-	-	0.50	0.93	-	-
U1352C_146R2	1900.92	31.29	0.41	0.76	0.27	-	-	0.82	1.40	2.04	-
U1353B_88X1	510.09	12.03	0.28	0.83	0.32	0.05	0.16	1.10	1.86	2.55	-

Core and section number	Sample depth (mbsf)	Age (Ma)	Ts/(Ts+Tm)	C_{30} hopanes αβ/(αβ+βα)	C_{31} αβ hopanes 22S/(22S+22R)	Oleanane/C_{30}αβ hopane	Gammacerane/C_{30} αβ hopane	C_{29} αβ /C_{30} αβ hopane	C_{31} αβ hopane/ C_{30} αβ hopane	C_{23}/C_{21} tricyclic terpanes	C_{24} tetracyclic/ C_{23} tricyclic terpanes
U1353B_93X1	556.82	13.13	0.41	0.64	0.18	-	0.34	1.13	3.29	1.48	-
U1353B_95X1	576.28	13.59	0.37	0.75	0.31	0.06	0.27	0.84	1.71	2.14	-
U1353C_96X1	585.57	13.81	0.26	0.37	0.11	-	-	0.90	12.68	1.30	-

Ts: C_{27} 18α-trisnorneohopane

Tm: C_{27} 17α-trisnorhopane

C_{30} αβ hopane: 17α,21β(H)-hopane

C_{30} βα hopane: 17β,21α(H)-hopane

C_{31} αβ hopane 22S: 17α,21β(H)-22S homohopane

C_{31} αβ hopane 22R: 17α,21β(H)-22R homohopane

C_{29} αβ hopane - 17α,21β(H)-30-norhopane

Table 2.4: Sterane, diasterane, and aromatic hydrocarbon data for the analysed IODP Expedition 317 samples.

Core and section number	Sample depth (mbsf)	Age (Ma)	C_{27} ααα R sterane %	C_{28} ααα R sterane %	C_{29} ααα R sterane %	C_{30} sterane index	C_{27}/C_{29} ααα R steranes	C_{28}/C_{29} ααα R steranes	C_{29} ααα S/(S+R) steranes	C_{29} ααα S/R steranes	C_{27} βα diasteranes / C_{27} ααα steranes	Retene/Phenanthrene	VRE	MPI	Rc (0.6xMPI)+0.4	MaxT= (LnRc+1.78)/ 0.0124
U1351B_97X2	845.75	5.30	34	21	45	7.9	0.74	0.47	0.14	0.16	0.19	32.0	0.41	0.55	0.73	118
U1351B_100X3	871.62	5.52	26	20	54	8.9	0.48	0.38	0.21	0.26	0.37	14.7	0.46	0.34	0.60	103
U1351B_101X1	880.93	5.60	18	22	60	3.9	0.30	0.38	0.12	0.14	0.23	-	0.40	-	-	-
U1351B_103X1	900.04	5.76	22	29	49	3.4	0.44	0.60	0.26	0.36	0.31	-	0.50	-	-	-
U1351B_104X2	908.97	5.84	32	27	41	4.9	0.78	0.65	0.14	0.16	0.14	41.3	0.41	0.44	0.66	110
U1351B_106X2	929.41	6.01	29	29	42	4.2	0.70	0.70	0.13	0.15	0.10	11.3	0.40	0.44	0.66	111
U1351B_109X1	959.05	6.27	29	33	38	3.7	0.77	0.88	0.08	0.09	0.08	-	0.37	0.46	0.67	112
U1351B_111X1	976.25	6.41	26	32	42	5.5	0.62	0.75	0.08	0.09	0.12	20.9	0.37	0.31	0.59	100
U1351B_112X3	989.18	6.52	31	36	33	6.7	0.93	1.07	-	-	0.02	-	-	0.49	0.69	114
U1351B_113X2	997.74	6.60	25	37	39	8.7	0.64	0.95	0.37	0.60	-	-	0.62	-	-	-
U1352C_70R3	1249.85	4.45	29	39	32	3.2	0.90	1.23	-	-	0.05	8.4	-	0.26	0.56	97
U1352C_71R6	1263.81	4.92	42	32	26	3.1	1.58	1.21	-	-	0.05	0.6	-	0.24	0.54	94
U1352C_72R1	1265.98	4.99	34	33	33	4.6	1.04	1.00	0.13	0.15	0.27	-	0.40	-	-	-
U1352C_73R4	1280.91	5.49	39	26	35	4.6	1.11	0.75	0.14	0.17	0.14	-	0.41	-	-	-
U1352C_76R1	1305.02	6.30	39	26	35	6.7	1.11	0.74	0.11	0.13	0.21	-	0.39	-	-	-
U1352C_76R1	1305.04	6.30	-	-	-	-	-	-	-	-	-	-	-	-	-	-
U1352C_77R1	1309.64	6.45	36	33	31	3.7	1.17	1.05	-	-	0.03	-	-	-	-	-
U1352C_78R1	1314.52	6.61	32	32	36	5.0	0.88	0.90	0.06	0.06	0.17	-	0.36	-	-	-
U1352C_79R2	1319.47	6.78	-	-	-	-	-	-	-	-	-	-	-	-	-	-
U1352C_80R3	1326.05	7.00	35	32	34	5.9	1.03	0.94	0.08	0.08	0.20	-	0.37	-	-	-
U1352C_81R1	1328.03	7.07	-	-	-	-	-	-	-	-	-	-	-	0.42	0.65	109
U1352C_85R4	1351.57	7.85	33	28	38	2.9	0.87	0.74	-	-	-	-	-	-	-	-
U1352C_86R2	1353.80	7.93	35	28	37	4.5	0.95	0.74	-	-	-	-	-	-	-	-
U1352C_87R4	1367.05	8.37	-	-	-	-	-	-	-	-	-	-	-	-	-	-
U1352C_88R5	1378.31	8.74	-	-	-	-	-	-	-	-	-	-	-	-	-	-
U1352C_89R3	1384.35	8.95	-	-	-	-	-	-	-	-	-	-	-	-	-	-
U1352C_89R4	1385.71	8.99	-	-	-	-	-	-	-	-	-	-	-	-	-	-
U1352C_90R2	1392.51	9.22	32	36	32	6.3	1.00	1.13	0.13	0.16	0.30	-	0.41	-	-	-
U1352C_91R5	1406.54	9.69	41	27	32	5.2	1.30	0.84	0.29	0.42	0.12	0.3	0.53	0.14	0.48	85

Core and section number	Sample depth (mbsf)	Age (Ma)	C_{27} *ααα* R sterane %	C_{28} *ααα* R sterane %	C_{29} *ααα* R sterane %	C_{30} sterane index	C_{27}/C_{29} *ααα* R steranes	C_{28}/C_{29} *ααα* R steranes	C_{29} *ααα* S/(S+R) steranes	C_{29} *ααα* S/R steranes	C_{27} *βα* diasteranes / C_{27} *ααα* steranes	Retene/Phenanthrene	VRE	MPI	Rc (0.6xMPI)+0.4	Max*T*= (LnRc+1.78)/ 0.0124
U1352C_94R5	1435.75	10.66	-	-	-	-	-	-	-	-	-	-	-	0.47	0.68	112
U1352C_95R2	1440.76	10.80	40	23	37	4.6	1.08	0.63	-	-	-	0.5	-	-	-	-
U1352C_102R	1496.43	11.92	-	-	-	-	-	-	-	-	-	-	-	-	-	-
U1352C_103R5	1513.25	12.25	-	-	-	-	-	-	-	-	-	-	-	-	-	-
U1352C_104R2	1517.31	12.34	-	-	-	-	-	-	-	-	-	-	-	-	-	-
U1352C_105R5	1532.33	12.64	-	-	-	-	-	-	-	-	-	0.8	-	0.43	0.66	110
U1352C_106R6	1542.31	12.84	-	-	-	-	-	-	-	-	-	-	-	-	-	-
U1352C_107R6	1553.19	13.06	39	-	61	6.9	0.63	-	0.42	0.71	-	-	0.68	-	-	-
U1352C_107R6	1553.57	13.07	-	-	-	-	-	-	-	-	-	-	-	-	-	-
U1352C_108R1	1554.61	13.09	26	26	47	-	0.56	0.56	-	-	-	-	-	-	-	-
U1352C_109R3	1568.52	13.37	31	35	35	3.6	0.88	1.01	-	-	-	0.6	-	-	-	-
U1352C_110R2	1575.84	13.51	-	-	-	-	-	-	-	-	-	-	-	-	-	-
U1352C_111R1	1584.24	13.68	29	33	38	3.2	0.77	0.88	-	-	-	0.5	-	0.11	0.47	82
U1352C_112R3	1596.68	13.93	31	32	37	2.8	0.84	0.87	-	-	-	0.7	-	0.19	0.51	90
U1352C_113R2	1605.98	14.12	-	-	-	-	-	-	-	-	-	0.9	-	0.18	0.51	89
U1352C_114R3	1617.04	14.34	29	33	38	3.2	0.77	0.88	-	-	-	1.0	-	0.21	0.52	92
U1352C_115R4	1628.21	14.57	-	26	74	11.4	-	0.34	-	-	-	1.5	-	0.37	0.62	105
U1352C_116R3	1636.89	14.74	22	26	52	9.1	0.43	0.50	0.33	0.50	-	-	0.58	-	-	-
U1352C_117R6	1649.18	14.99	29	37	34	3.5	0.86	1.08	-	-	-	0.5	-	-	-	-
U1352C_118R4	1655.27	15.11	28	39	33	4.3	0.85	1.20	-	-	-	0.6	-	0.25	0.55	95
U1352C_122R1	1688.35	15.78	-	-	-	-	-	-	-	-	-	0.6	-	0.19	0.51	90
U1352C_123R1	1692.95	15.87	28	24	48	5.5	0.58	0.50	0.26	0.35	0.26	-	0.50	0.73	0.84	129
U1352C_124R1	1697.95	15.97	28	24	48	11.3	0.57	0.51	0.34	0.51	0.57	1.1	0.58	0.25	0.55	96
U1352C_125R2	1709.42	16.20	-	-	-	-	-	-	-	-	-	0.8	-	0.27	0.56	97
U1352C_125R4	1712.88	16.27	40	20	40	6.3	1.00	0.50	0.32	0.46	0.21	-	0.56	0.63	0.78	123
U1352C_126R3	1720.51	16.43	52	16	33	4.2	1.59	0.49	0.32	0.48	0.07	5.1	0.56	0.47	0.68	113
U1352C_127R3	1730.24	16.62	37	34	30	3.4	1.25	1.14	0.24	0.31	0.03	-	0.48	-	-	-
U1352C_128R5	1741.71	16.85	-	-	-	-	-	-	-	-	-	-	-	-	-	-
U1352C_129R2	1747.88	16.98	34	33	33	4.2	1.01	0.99	0.24	0.32	0.02	-	0.49	0.48	0.69	114
U1352C_130R4	1760.44	17.23	-	-	-	-	-	-	-	-	-	-	-	-	-	-
U1352C_131R2	1766.99	17.36	38	26	36	5.4	1.05	0.70	0.29	0.40	0.13	-	0.53	-	-	-

Core and section number	Sample depth (mbsf)	Age (Ma)	C_{27} ααα R sterane %	C_{28} ααα R sterane %	C_{29} ααα R sterane %	C_{30} sterane index	C_{27}/C_{29} ααα R steranes	C_{28}/C_{29} ααα R steranes	C_{29} ααα S/(S+R) steranes	C_{29} ααα S/R steranes	C_{27} βα diasteranes / C_{27} ααα steranes	Retene/Phenanthrene	VRE	MPI	Rc (0.6xMPI)+0.4	Max*T*= (LnRc+1.78)/ 0.0124
U1352C_132R3	1776.88	17.56	-	56	44	6.0	-	1.27	-	-	-	-	-	0.41	0.65	108
U1352C_133R3	1786.76	17.76	-	-	-	-	-	-	-	-	-	-	-	-	-	-
U1352C_133R4	1788.83	17.80	26	26	48	10.1	0.54	0.53	0.33	0.49	-	-	0.57	-	-	-
U1352C_134R1	1793.51	17.89	21	32	47	8.5	0.46	0.69	0.38	0.61	-	-	0.63	-	-	-
U1352C_135R5	1809.40	18.21	-	-	-	-	-	-	-	-	-	-	-	-	-	-
U1352C_136R4	1818.51	18.40	-	-	-	-	-	-	-	-	-	-	-	-	-	-
U1352C_136R5	1818.59	18.40	-	-	-	-	-	-	-	-	-	-	-	-	-	-
U1352C_137R5	1828.83	18.60	24	28	48	8.3	0.51	0.57	0.38	0.62	-	-	0.63	-	-	-
U1352C_138R4	1837.74	18.78	-	-	-	-	-	-	-	-	-	-	-	-	-	-
U1352C_139R1	1842.11	18.87	34	20	46	-	0.73	0.45	0.14	0.16	-	-	0.41	-	-	-
U1352C_140R1	1851.46	19.06	-	-	-	-	-	-	-	-	-	-	-	-	-	-
U1352C_143R1	1875.04	30.87	-	-	-	-	-	-	-	-	-	-	-	-	-	-
U1352C_144R4	1884.51	31.02	-	-	-	-	-	-	-	-	-	-	-	-	-	-
U1352C_145R2	1891.76	31.14	29	46	25	3.4	1.14	1.81	-	-	0.03	-	-	-	-	-
U1352C_146R2	1900.92	31.29	32	34	34	5.9	0.92	0.99	-	-	0.14	-	-	-	-	-
U1352C_147R4	1913.24	31.50	-	-	-	-	-	-	-	-	-	-	-	-	-	-
U1352C_148R5	1917.90	31.57	-	-	-	-	-	-	-	-	-	-	-	-	-	-
U1353B_88X1	510.09	12.03	20	32	48	-	0.40	0.66	0.21	0.27	0.30	-	0.46	-	-	-
U1353B_93X1	556.82	13.13	21	28	51	-	0.42	0.54	0.18	0.22	0.51	-	0.44	-	-	-
U1353B_95X1	576.28	13.59	17	26	56	-	0.31	0.47	0.22	0.29	0.56	-	0.47	-	-	-
U1353C_96X1	585.57	13.81	23	20	57	5.3	0.40	0.35	0.13	0.14	0.31	-	0.40	-	-	-

$C_{27,}$ C_{28} and C_{29} ααα R sterane: 5α,14α,17α(H)-20R steranes

C_{30} sterane index = C_{30}/(C_{27}+C_{28}+C_{29}+C_{30}) αααR steranes

MPI = Methylphenanthrene Index: (1.5*(3-MP+2-MP)/(P+9-MP+1-MP)

MP: Methylphenanthrene

P: Phenanthrene

R_c: Calculated reflectance, based on Radke et al., 1986

VRE: Calculated vertinite reflectance, based on Sofer et al., 1993:

(0.49x(C29 ααα 20S/20R steranes))+0.33)

Max*T*: maximum temperature, based on Wang et al. (2005)

3. From tropical to temperate climate: decreasing sea surface temperatures in the Canterbury Basin, New Zealand, based on lipid analyses of drilled sediments from IODP Expedition 317

Sophia Aharonovich[1], Julius S. Lipp[2], Simon C. George[1]

[1] Department of Earth and Planetary Sciences and Macquarie University Marine Research Centre, Macquarie University, Sydney, NSW 2109, Australia.

[2] Organic Geochemistry Group, MARUM Center for Marine Environmental Sciences & Department of Geosciences, University of Bremen, 28359 Bremen, Germany.

Statement of authors' contribution

This Chapter is an article to be submitted to *Palaeogeography, Palaeoclimatology, Palaeoecology*. This paper has been formatted to conform to the font and referencing style adopted in this thesis. Section, Figures, and Tables included within the text are prefixed with the chapter number.

I am the primary author (70% of the effort). I extracted the organic material from the samples. I analysed the organic data and created the proposed climate reconstructions. I wrote and designed the structure of the paper. The co-authors provided analytical feedback, carefully reviewed and provided feedback and valuable refinements on this version of the manuscript (30%). Neither this manuscript nor one with similar content under our authorship has been published or is being considered for publication elsewhere, except as described above.

Abstract

The climate during the Cenozoic was influenced by major tectonic and eustatic changes. The New Zealand region was surrounded by tropical and subtropical seas until the Miocene. The planktonic foraminifera and $\delta^{18}O$ records suggest warm SSTs at the Oligocene/Miocene boundary for the region. The Southern Hemisphere experienced rapid climate change especially during the Neogene, becoming cooler much faster than the Northern Hemisphere.

The main purpose of the International Ocean Discovery Program Expedition 317 in the Canterbury Basin, New Zealand was to compare the relative influence of local tectonics and global sea level changes on sediments accumulated on the continental shelf and slope off the east coast of the South Island. The recovered cored sediments dated from the early Oligocene to the Holocene, and there was a particular focus on the sequence stratigraphy of the last 19 Ma. The interpretation of global eustatic and climatic transformations suggest that cooler Neogene seawater conditions were coupled with a decrease in global sea levels. In this work Cenozoic biomarker records were used to reconstruct sea surface temperature (SST) variations along with varying terrestrial organic matter inputs so as to distinguish climatic variations in the area. These organic records were compared to fossil and palynological investigations in the region, and may hold the key to understanding the mechanism for climatic variations in the Southern Hemisphere.

Interpretation of glycerol dialkyl glycerol tetraether lipids (GDGTs) suggests a warm SST of 29.8ºC at the Oligocene/Miocene boundary in the Canterbury Basin. A slow SST decrease is recorded from the early Miocene as cooler subtropical palaeo-currents and later on intrusions of cold sub-Antarctic currents started to influence ocean temperatures, especially around the east coast of New Zealand. This influence is increased from the middle Miocene, ~ 15 Ma. These reconstructions are supported by land fossil records from New Zealand, which show warm environments for the first part of the Neogene.

3.1. Introduction

The Cenozoic era represents the last 66 million years and is characterised by significant climate variations (e.g., Zachos et al., 2001; Zachos et al., 2008). Distinguishing between local tectonic and global climatic triggers in Cenozoic is a challenging task (Zachos et al., 2008). Global sea-level changes (eustasy) are influenced by high tectonic activity (Haq et al., 1987; Van Sickel et al., 2004) and quasi-periodic oscillations in Earth's orbital parameters (eccentricity, obliquity, and precession), currently considered to be the main source of these variations (Miller et al., 2005; Zachos et al., 2008). On the other hand, local or regional tectonic activity also had very significant impacts on the distribution of sediments and life on the continental margins (Van Sickel et al., 2004).

Climate variations during the Cenozoic were influenced by major tectonic and eustatic deviations (Haq et al., 1987; Head and Nelson, 1994; Abreu and Anderson, 1998; Hardenbol et al., 1998; Zachos et al., 2001; Van Sickel et al., 2004). During the Cenozoic the Southern Hemisphere experienced rapid climate change (Kennett et al., 1974; Moss and McGowran, 1993; Exon et al., 2004), influenced by ice accumulation in Antarctica as well as plate tectonic movements (Barker et al., 2007; DeConto et al., 2007; Cristini et al., 2012). The climate in the Southern Hemisphere became cooler much faster than in the Northern Hemisphere, with glaciation over Antarctica (Barker et al., 2007). Of the possible glaciation that have triggered the development of the Antarctic Circumpolar Current (Kennett et al., 1974; Kennett, 1977), a decrease in atmospheric carbon dioxide (pCO_2) levels (Zachos et al., 2001; DeConto and Pollard, 2003), global tectonic activity, land uplift (e.g., Raymo and Ruddiman, 1992), and variations in ocean circulation (Lawver and Gahagan, 2003) have been suggested to be the probably causes.

Cenozoic sea surface temperatures (SST) and changes in global ice volume levels are usually reconstructed based on the $\delta^{18}O$ and Mg/Ca ratios from foraminiferal records (Keigwin and Keller, 1984; Shackleton and Pisias, 1985; Miller et al., 1991). These records suggest a global SST decrease during the last 50 Ma (from the early Eocene) (Zachos et al., 2001; Zachos et

al., 2008). In addition, during the Cenozoic the global climatic optima that are related to high temperature levels, warm poles and no ice cover are associated with high pCO_2 (Zachos et al., 2001). The CO_2 levels have been calculated using various proxy data sets, such as boron, alkenones, and nahcolites from marine and lacustrine environments (Royer, 2006). Other greenhouse gases such as methane show quite similar trends related to the palaeoclimate reconstructions of the Cenozoic (MacDonald, 1990).

Global accumulation and melting of ice cover is strongly related to eustatic sea-level changes. Both processes are also related to the temperature variations (Haq et al., 1987; Van Sickel et al., 2004). The signal of eustatic variations can be found in regional sedimentary records on continental margins (Posamentier, 1988; Kominz et al., 1998; Van Sickel et al., 2004). The sequence modelling described by Haq et al. (1987) is widely used nowadays. New eustatic models based on the Siberian Platform (Sahagian et al., 1996) and the New Jersey Margin (Van Sickel et al., 2004) sediments show some variation to the classical study. Strong disagreements in eustatic reconstructions can be observed the first half of the Neogene (to 11 Ma). Studies also suggest that Cenozoic sea level changes are influenced by large continental ice sheet accumulation, which can be responsible for large (>100 m) sea-level fluctuations (Haq et al., 1987; Pitman and Golovchenko, 1991). Correlation between global ice cover and sea level fluctuations for the late Cenozoic were shown by John et al. (2004) and Miller et al. (2005). However, fluctuations of up to 25 m in sea level can be related to relatively modest climate changes and ice volume fluctuations (Miller et al., 1998; Miller et al., 2003; Van Sickel et al., 2004).

Mg/Ca ratios and alkenones (Müller et al., 1998) have been used to reconstruct the SST to have been above 29ºC around 13.8 Ma in the eastern southern Atlantic, with a significant decrease of about 4ºC around 13 Ma (Badger et al., 2008; Badger et al., 2013). During the same time the Antarctic ice sheet expansion occurred, represented by large fluctuations in marine carbonate $\delta^{13}C$ and $\delta^{18}O$ (Zachos et al., 2001). The increase in marine carbonate $\delta^{13}C$

was correlated to the increase in organic carbon followed by a decrease in atmospheric pCO_2 (Flower and Kennett, 1993a; Flower and Kennett, 1993b, 1994). The decrease in pCO_2 is commonly interpreted to be related to a global temperature decrease (Miller et al., 1991; Flower and Kennett, 1994). An alternative correlation between benthic foraminifera $\delta^{13}C$ and ice sheet expansion has been proposed as well (Pagani et al., 1999; Lear et al., 2004). In this interpretation, the accumulation of the ice sheet was the main cause of the decrease in silicate basement surface in the region that was responsible for the pCO_2 sinking.

A relatively high pCO_2 has been reported throughout the Miocene (Kürschner et al., 2008; Foster et al., 2012). These studies report a decrease in pCO_2 from ~16 Ma to 13 Ma. Changes in pCO_2 were determined based on $\delta^{11}B$-CO_2 and $\delta^{13}C$-CO_2 measurements and have also been correlated to the rise and fall of sea level (Foster and Rohling, 2013). Values between ~200 and ~300 ppm CO_2 were associated with -10 to +20 m sea level variations, with an error range of ±10 m, for the Miocene to the Pleistocene. The earlier Oligocene and Eocene periods were characterised by much higher CO_2 levels (>650 ppm) with significantly higher sea levels during this period (to +70 m) (Foster and Rohling, 2013).

Correlations between global atmospheric pCO_2, ice sheet build up, and sea level changes during the Cenozoic have been suggested (Foster and Rohling, 2013). It was noted that 20-30 m higher sea levels during the Pliocene and Miocene were correlated to CO_2 levels between 400 and 280 ppm, and overlap with a decrease of Greenland ice cover and western Antarctic ice accumulation (Miller et al., 2003; Miller et al., 2005).

Global cooling was recorded by the $\delta^{18}O$ of benthic foraminifera from the late Miocene until the Quaternary (Atkins, 2001; Zachos et al., 2001; Molnar, 2004). Major ice formation in the east and west Antarctic regions lead to a decrease in sea levels by 45-70 m during the middle Miocene. This caused increase in sedimentary input from rivers to the continental palaeo-shelf due to lowering of the base level, migration of the shoreline towards the ocean, and

creation of additional river channels in the exposed sediment (Molnar, 2004; Miller et al., 2005).

Simulations of global late Miocene terrestrial temperatures between 11.6-5.3 Ma show warmer conditions than the modern climate, with mean annual air temperatures (MAAT) 3.8ºC higher than preindustrial ones (Lunt et al., 2008), while New Zealand MAAT was about 3ºC higher. Steppuhn et al. (2006) used a simulation to calculate that the late Miocene MAAT for the Australasian region was between 15.6 ºC and 26.6 ºC.

The modern New Zealand (NZ) subcontinent lies at the interface between the southwest Pacific Ocean and the Southern Ocean (Nelson and Cooke, 2001; Tomczak and Godfrey, 2013). Tectonic reconstructions show significant movement of the New Zealand land mass to the north for the last 40 million years (King, 2000). These models also suggest the presence of some New Zealand land mass from the Oligocene (King, 2000) for the South Island, and the first appearance of the Southern Alps as early as the middle Miocene (~11 Ma) (Wood and Stagpoole, 2007). Rapid uplift of the Southern Alps with an associated significant increase of the land mass is proposed from 7-6 Ma (Nelson and Cooke, 2001).

The Eastern New Zealand Oceanic Sedimentary System (ENZOSS) is another model that integrates climatic, geological, and oceanographic factors controlling sediment accumulation in the Pacific Ocean during the Cenozoic (Carter et al., 2004). The results of ODP Leg 189 (Exon et al., 2001) added additional information regarding the palaeo-circulation off shore New Zealand and Tasmania, and allowed the ENZOSS model to be updated (Carter et al., 2004).

Until the Oligocene, New Zealand was surrounded by tropical and subtropical seas. For example, planktonic foraminifera (Jenkins, 1965) and $\delta^{18}O$ (Shackleton and Kennett, 1975) records suggest warm SSTs at the Oligocene/Miocene boundary for the New Zealand region.

During the late Oligocene to early Miocene the terrigenous input from the New Zealand landmass was low, because of the long lasting, major land flooding that started ~80 Ma, and was controlled by variations in the sea level (Carter and Norris, 1976; Fulthorpe et al., 1996; King, 2000).

During the Neogene the Antarctic oceanic front developed (Lawver et al., 1992; Nelson and Cooke, 2001). This caused a decrease in the SST around New Zealand from the early Miocene, as cooler subtropical palaeo-currents and later on the cold intrusions of the sub-Antarctic currents started to influence the ocean temperature, especially around the east coast of New Zealand (Nelson and Cooke, 2001). Other studies suggest that less pronounced erosional phases, with brief hiatuses happening at ~17 Ma and 14.5 Ma (Carter and Wilkin, 1999; Hall et al., 2003), were related to the cold periods linked to episodes of East Antarctic ice sheet expansion (Barrett et al., 1987; Miller et al., 1991; Flower and Kennett, 1995). These influences increased from the middle Miocene, ~ 15 Ma. These reconstructions are supported by land fossil records from New Zealand, which show warm-water environments for the first part of the Neogene (Chaproniere, 1984; Beu et al., 1997). During the late Miocene the terrigenous supply from New Zealand increased due to rapid uplift and erosion of the Southern Alps (Walcott, 1998; Carter et al., 2004).

The modern New Zealand mass land is a part of the New Zealand Plateau that rifted from Antarctica ~80 Ma (Molnar and Tapponnier, 1975). The South Island of New Zealand is part of the continent-continent convergence between the Australian and Pacific plates (Norris et al., 1990). This tectonic activity started between 8 and 6 Ma and caused the uplift of the Southern Alps. Multiple studies have dated the beginning of the Southern Alps uplift (Mason, 1961; Adams, 1981; Adams and Gabites, 1985; Tippett and Kamp, 1993; Batt et al., 2000).The latest K-Ar dating of biotite and muscovite puts the beginning of movement on the Alpine Fault by at least 8 Ma (Batt et al., 2004).

Botanical investigations on the South and North islands show a relatively young biota dating from the Oligocene (Pole, 1994). Further botanical studies suggest that the main land mass was submerged during the late Oligocene (Landis et al., 2008) and reappeared above sea level after 30 Ma (Waters and Craw, 2006; Landis et al., 2008). Recent plant fossil and charcoal discoveries show that the South Island of New Zealand was not fully submerged for least 30 Ma (Lee et al., 2012). Research on cicada adaptation to temperature change in New Zealand (Fleming, 1975) suggested subtropical to tropical conditions during the middle Miocene.

Warm sea surface temperatures (SSTs) in the New Zealand area are possibly correlating to closure of the Indonesian gateway in the middle Miocene (Nelson and Cooke, 2001), and presumably meant warmer land temperatures and higher precipitation levels (Folland and Salinger, 1995; White and Cherry, 1999). Lu et al. (2005) suggests, after Hornibrook (1992), that there is a warm tropical climate in New Zealand during most of the Miocene, and that this is changing in the end of the late Miocene to cooler, less stable temperatures, influenced by the glacial cycles that became dominant in the Pliocene. A decrease in New Zealand temperatures coincides with a decrease in global sea levels (Haq et al., 1987). The results suggest that sub-Antarctic SSTs dominated the New Zealand area from the Pliocene, thus cooling the water in the Canterbury Basin to the modern 13ºC (World Sea Temperature, 2017). These changes coincide with the expansion of the West Antarctic ice-sheet during the last part of the late Miocene, that is followed by an increase in ice cover in the Northern Hemisphere (Zachos et al., 2001). Global $\delta^{18}O$ records show a similar trend for reconstructions of the New Zealand area, with a constant temperature decrease from the middle Miocene climatic optimum (Nelson and Cooke, 2001; Zachos et al., 2001).

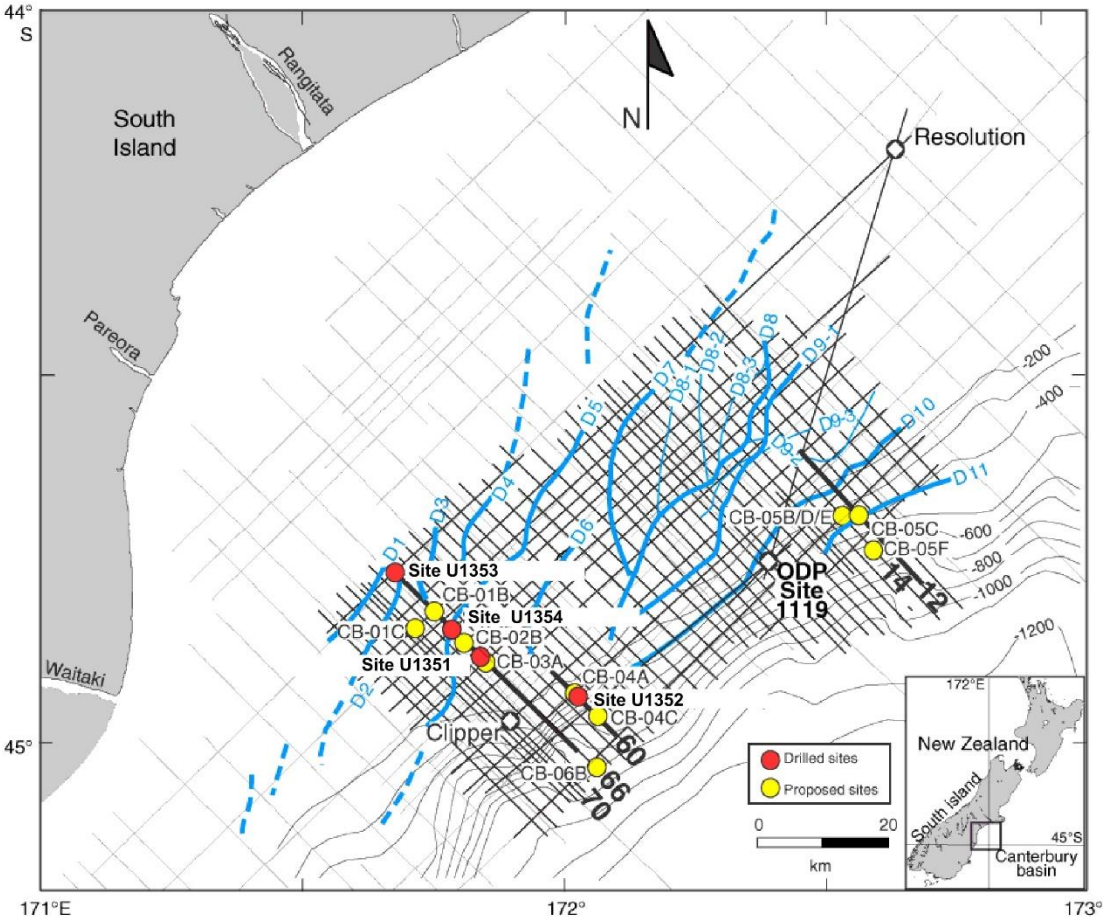

Figure 3.1 Drilled and proposed Expedition 317 sites, with multichannel seismic (MCS) commercial low-resolution grid. Blue curved lines show the distribution of seismically resolvable sediment drifts (Fulthorpe et al., 2011).

The main purpose of the International Ocean Discovery Program (IODP) Expedition 317, which occurred from November 2009 to January 2010 in the Canterbury Basin, New Zealand (Fig. 3.1), was to compare the relative influence of local tectonics and global sea level changes on sediments accumulated on the continental shelf and slope off the east coast of the South Island. The recovered cored sediments dated from the early Oligocene to the Holocene, and there was a particular focus on the sequence stratigraphy of the last 19 million years, when global sea level changes were dominated by glacioeustasy (Fulthorpe et al., 2011). Sedimentary sequences (Fig. 3.1) were drilled in a transect of three sites on the continental shelf (landward to basinward, Sites U1353, U1354, and U1351) and one on the continental slope (Site U1352) (Fulthorpe et al., 2011). The Canterbury Basin sedimentary record

provides a unique opportunity for examining the accumulated biomarker signal in the region. A global climatic optimum and temperature increase at the early/middle Miocene boundary, together with the increasing land mass of the sub-continent based on an increase in sedimentation rates since the middle Miocene (Lu et al., 2005), shows a gradual intensification in the amount of land vegetation. Interpretation of global eustatic and climatic transformations suggest that cooler Neogene seawater conditions were coupled with a decrease in global sea levels (Zachos et al., 2001; Van Sickel et al., 2004). Moreover, Cramer et al. (2011) suggested a linear correlation between increase in ice sheet cover and $\delta^{18}O$, showing a temperature influence on global climate. Therefore, the influence of this climate shift on the accumulation and preservation of organic matter in the marine sediments is expected.

This study aims to examine the organic geochemistry of the Cenozoic marine sediments recovered during Expedition 317 to reconstruct variations in SST and terrigenous organic matter inputs, and to distinguish climate variations in the area. The organic geochemical data are compared with investigations of fossils and palynology, which together hold the key to understanding the dramatic climatic variations in the Southern Hemisphere that influenced global flora and fauna dramatically (Fleming, 1975; Warny et al., 2009; Lee et al., 2012). The study aims to examine the transition from tropical and subtropical environments to subantarctic environments in New Zealand during the second part of the Cenozoic.

3.2. Material and Methods

3.2.1. Age model, lithology and sampling

This study is based on a set of sedimentary samples from three drilling sites: U1351, U1352, and U1353 (Fig. 3.1). The age model for each site is based on the shipboard study of calcareous nannofossils, diatoms, and planktonic and benthic foraminiferas (Fulthorpe et al.,

2011). Overall, hydrocarbon and biomarker contents were determined for 108 samples. The lithological unit definitions for each of the sites were based on the observed variation in lithology in the cores (Fig. 3.2) (Fulthorpe et al., 2011; Marsaglia et al., 2017). In general, Unit I is heterogeneous, containing a wide variety of facies including interbedded terrigenous lithologies and green marls, and calcareous beds with sharp (or bioturbated) bases. Unit II is divided into three sub-units A-C and dominated by mud or muddy sand, with lower percentages of carbonate components, and less frequent greenish calcareous beds in Sites U1351 and U1353. A homogeneous sandy marlstone is part of Unit II in Site U1352. Unit III (Oligocene–Eocene) in U1352 is composed of limestones, deposited in truly oceanic environments, with little to no terrigenous sediment input.

The U1353 Site is the most onshore of the shelf sites from Expedition 317 (Fig. 3.1). Hole B at the U1353 Site is characterised by dark greenish-grey, micaceous very fine sandy-mud and mud (Fulthorpe et al., 2011). The Miocene/Pliocene boundary was not detected from the biostratigraphical data (Fig. 3.2). However, stratigraphic correlation suggests that the 510.52–518.66 meters below sea floor (mbsf) interval could be dated to 12.03 Ma. In addition, the deepest sample from this site has a biostratigraphical assemblage dated to middle to early Miocene. Based on that, the four samples that were analysed from this site are from the middle to late Miocene (Fulthorpe et al., 2011).

Site U1351 was located on the outer continental shelf (Fig. 3.1). Lower Pliocene–late Miocene sediments are characterised by low levels of erosion (Fulthorpe et al., 2011). The Miocene section of the site was mainly dated using planktonic foraminifers, which showed a major depositional hiatus of ~3.4 million years between 7.07 Ma and 10.50 Ma (Fig. 3.2). The bottom of Hole B at the U1351 Site was dated as late Miocene (10.60–10.91 Ma). All eight analysed samples are from lithological Unit II, dated to the late Miocene (Table 3.1). Unit II is composed of dark greenish grey to greenish black sandy mud, muddy sand and shell hash.

The mineralogy suggests a dominant provenance from the southerly Otago Schist (Fulthorpe et al., 2011).

Site U1352 was located on the upper slope within the Canterbury Basin and is the most basinward site in this study (Fig. 3.1). Lipid contents were determined for 96 samples from three lithological units. Unit I was dated between the Holocene and mid-Pliocene. This unit contains predominantly mud-rich sediments, mainly calcareous sandy muds (Fulthorpe et al., 2011; Marsaglia et al., 2017). Forty six samples were analysed from this unit. Lithological Unit II consists of homogenous calcareous mud and sandy marlstone, which was dated by foraminifera and nannofossil proxies (Table 3.1) which show that the late Miocene/early Pliocene boundary is between 1266 and 1284 mbsf (Fig. 3.2). The unit is divided into three subunits: IIA (711–1189 mbsf) is defined as homogenous marl and bioturbated marlstone; IIB (1189–1694 mbsf) is defined as dark-coloured mudstone beds which increase in frequency toward the base

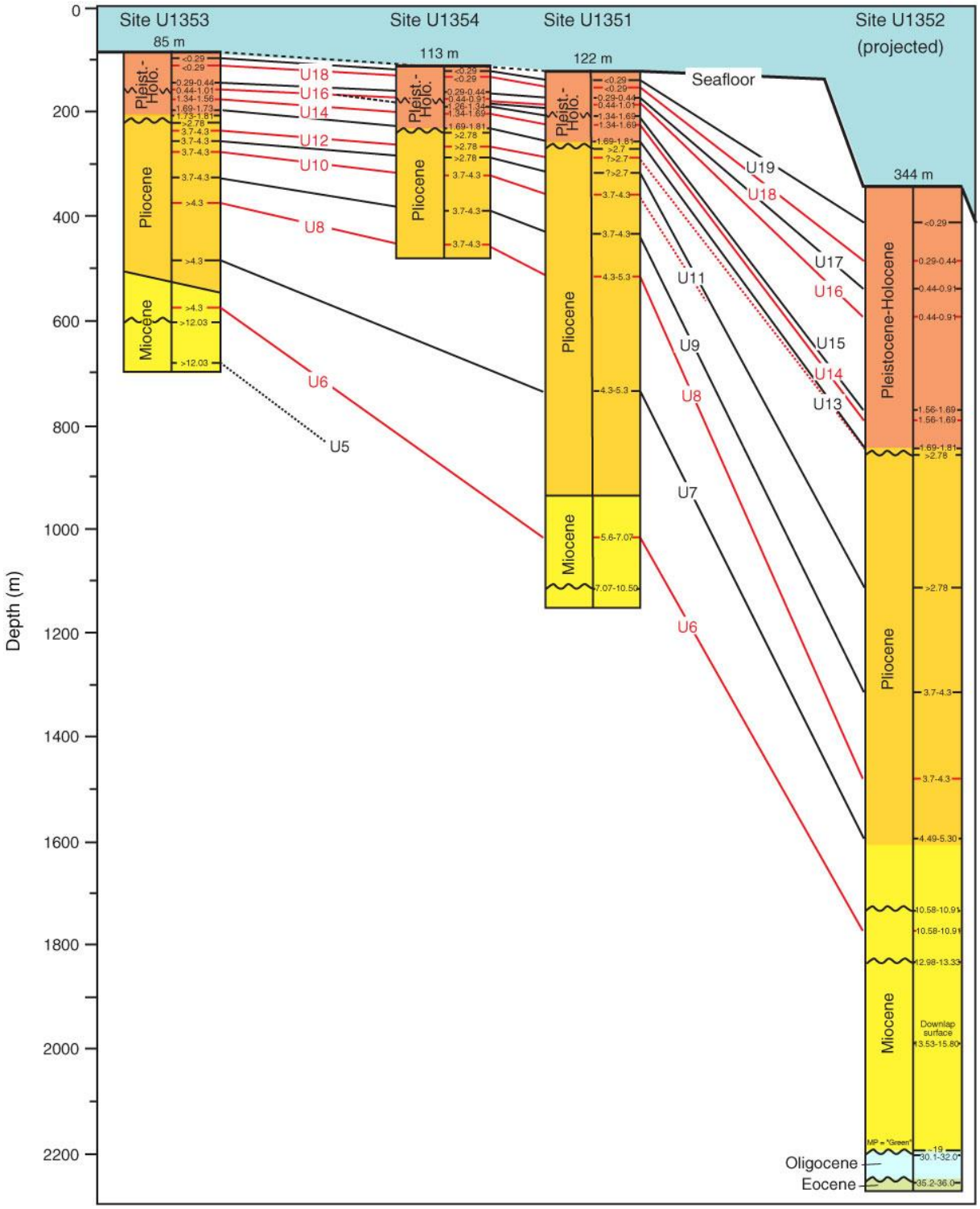

Figure 3.2: Chronostratigraphic framework and biostratigraphic ages of predicted seismic sequence boundary units across the Expedition 317 drilling transect. Pleistocene ages are derived from calcareous nannofossils (Fulthorpe et al, 2011).

of the subunit; IIC (1694–1853 mbsf) contains a gradual progression from marlstone to limestone. Forty two samples were analysed from lithological Unit II, which are characterised by hemipelagic and pelagic sedimentation in Hole C (1275–1851 mbsf). The Miocene part of

Unit II consists of a low frequency of dark-coloured mudstone beds. There are also hiatuses in deposition between 1394 and 1410 mbsf, where at least 5 million years are missing, and between 1487 and 1497 mbsf, where 1.3 million years are missing. The lower part of Unit II consists of a gradual progression from marlstone to limestone with frequent glauconitic laminae and beds. There is a large unconformity of 11-12 million years between 1851 and 1875 mbsf (Fulthorpe et al., 2011).

The early Oligocene to Eocene sediments with hemipelagic to pelagic foraminifer-bearing nannofosil limestones and minor amounts of quartz and clay were identified as lithological Unit III (Fulthorpe et al., 2011). This unit is correlative to the onshore Amuri Limestone (Marsaglia et al., 2017). One long unconformity from 19–30.1 Ma (1903 –1917 mbsf) is present in Unit III, and the bottom part of Hole C was dated to 35.2–36.0 Ma in the Eocene (Fulthorpe et al., 2011). Eight samples representing Unit III, below 1875 mbsf, were analysed.

3.2.2. Solvent extraction and fractionation of lipids

The lipid analyses for glycerol dialkyl glycerol tetraether lipids (GDGTs) and alkenones were performed on sediment samples taken on-board ship in the organic geochemistry laboratory at MARUM, Bremen.

Two different solvent extraction methods were used. The sixty-four samples from Site U1352 from 1.05 to 1183.7 mbsf were extracted using a modified Bligh and Dyer protocol as described previously (Sturt et al., 2004). Total lipids were extracted with a dichloromethane (DCM)/methanol/buffer [1:2:0.8; v/v] solvent mixture in a ratio of 4 mL solvent per gram of sediment. Extraction was in four stages, with the first two stages using a phosphate buffer (pH 7.4), and the final two stages using a trichloroacetic acid buffer (pH 2). Every extraction stage involved 10 min. ultrasonication, and then 10 min. centrifuging at 800 rpm to enable separation of the sediment and solvent phases. The four solvent extracts were combined,

washed with water, and evaporated to dryness with a nitrogen stream at 40ºC. The total lipid extract (TLE) was then analysed by high-performance liquid chromatography (HPLC).

The rest of the samples from the U1352 Site and from the U1351 and U1353 Sites (Table 3.2) were hand crushed using a ceramic pestle and mortar and sieved through a 125 μm sieve. Samples were mixed ~50:50 with pre-extracted and baked sand (3 hours at 450°C) so as to increase solvent extraction efficiency and were extracted using a Dionex Accelerated Solvent Extractor (ASE300) using 9:1 DCM:methanol. Two extraction runs were used, each of which consisted of three cycles of 5 min. preheating, 5 min. static at 1500 bar pressure and 100°C, and 3 min. solvent purging to the collection bottle. Sulphur was removed from the extractable organic matter (EOM) of all samples by refluxing at 40°C with acid-activated copper turnings. The EOM was separated using a short silica column into three fractions using organic solvent solutions: aliphatic hydrocarbons (*n*-hexane), aromatic hydrocarbons (n-hexane:DCM, 4:1), and polar compounds (DCM:methanol, 1:1). The polar fraction was analysed using HPLC-MS.

3.2.3. Instrumentation for high-performance liquid chromatography (HPLC)-MS

Separation of the polar fractions for isoprenoidal GDGTs (iGDGTs), branched GDGTs (brGDGTs) and long chain alkenone analysis was carried out according to Becker et al. (2013), using a Dionex Ultimate 3000RS UHPLC instrument coupled to a Bruker maXis ultra-high resolution quadrupole time-of-flight mass spectrometer (qToF-MS), equipped with an Atmospheric Pressure Chemical Ionisation (APCI II) ion source for the samples extracted by ultrasonication (Fig. 3.3 and Fig. 3.4). The ASE300 extracted samples was analysed using the same instruments. See Appendix 7.1 for the structures of these lipids. Aliquots of the polar fractions (typically 10 μl) in *n*-hexane:propan-2-ol (99.5:0.5, v:v) were injected onto two

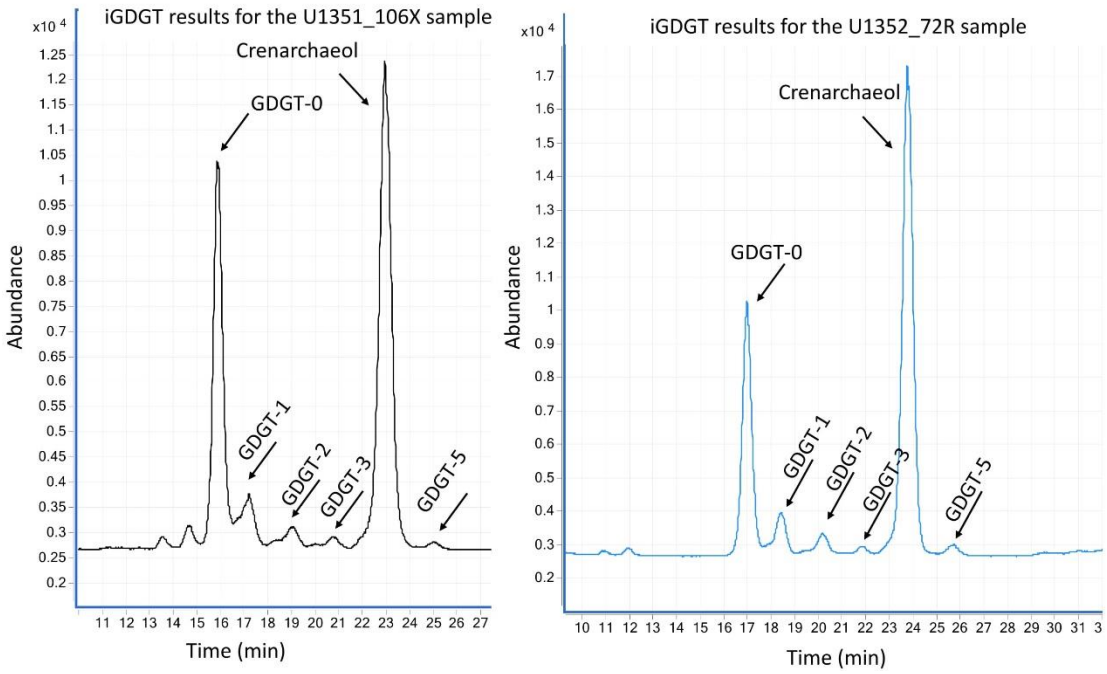

Figure 3.3: Partial m/z 1300, 1298, 1296, 1294, and 1292 HPLC-MS chromatograms for samples 106X from Site U1351 and sample 72R from Site U1352, showing the identification of the iGDGTs.

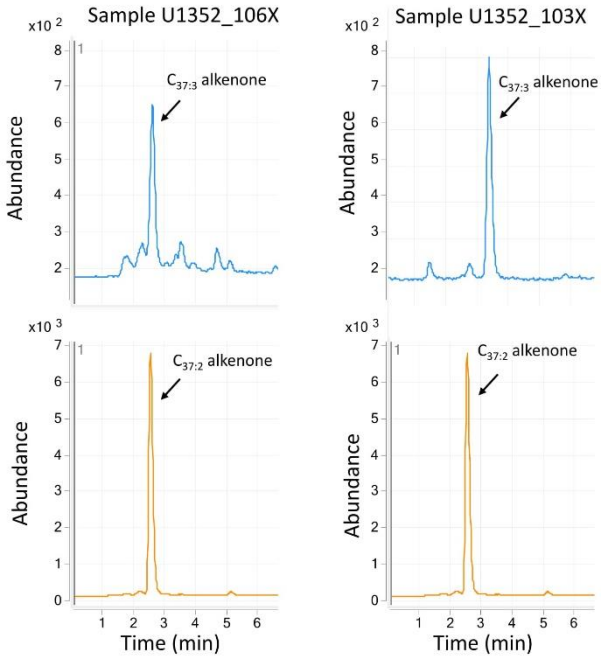

Figure 3.4: Partial HPLC-MS chromatograms for the C37:2 (m/z 531.5) and C37:3 (m/z 529.5) alkenones identified in samples 106X and 103X from U1352 Site.

coupled Acquity BEH amide columns (each 2.1 x 150 mm, 1.7 mm; Waters, Eschborn, Germany) kept at 50 °C. Lipids were eluted using the following gradient and eluent A (*n*-hexane) and eluent B (*n*-hexane:propan-2-ol (90:10, v:v)) with a constant flow of 0.5 ml/min: 3% B to 5% B in 2 min, to 10% B in 8 min, to 20% B in 10 min, to 50% B in 15 min and to 100% B in 10 min. Columns were washed with 100% B for 6 min and equilibrated with 3% B for 9 min between injections. GDGTs were detected using positive ion APCI and a scanning range from m/z 150 to 2000. The source parameters were as follows: corona current = 3500 nA, nebulizer gas = 5 bar, drying gas = 8 L/min drying gas 160ºC, and vaporiser 400ºC with a scan rate of 2 Hz. The advantages of improved separation chromatography have been widely discussed in the literature (Liu et al., 2011; Becker et al., 2013; Hopmans et al., 2016). This method provides a good separation for the iGDGTs, brGDGTs, and alkenone isomers that are essential for SST reconstructions (Becker et al., 2013; Becker et al., 2015). Typical mass chromatograms are presented in Figs 3.2 and 3.3.

3.2.4. GDGT and alkenone calculations

3.2.4.1. iGDGTs

The TEX_{86}^{H} for subtropical and greenhouse periods, when temperatures were higher than today, was calculated from the distribution of iGDGTs using the definition of Kim et al. (2010) for the 10°C to 40°C temperature range:

Eq. 1 $$TEX_{86}^{H} = \frac{[GDGT-2]+[GDGT-3]+[Cren']}{[GDGT-1]+[GDGT-2]+[GDGT-3]+[Cren']}$$

where numbers refer to the number of rings in the GDGT, and Cren' refers to the crenarchaeol regio isomer. TEX_{86}^{H} was converted to SST using the correlation for the 10°C - 40°C temperature range with a proposed residual standard error of ±2.5°C (Kim et al., 2008; Kim et al., 2010):

Eq. 2 $$SST = 68.4 \times TEX_{86}^{H} + 38.6 \quad (r^2 = 0.87, n = 255, p < 0.0001)$$

GDGT cyclisation was calculated to evaluate the ring index (Pearson et al., 2004):

Eq. 3 $$Ring\ index = \frac{[GDGT-1]+2\times[GDGT-2]+3\times[GDGT-3]+4\times[GDGT-4]+5\times[Cren+Cren']}{[GDGT-0]+[GDGT-1]+[GDGT-2]+[GDGT-3]+[GDGT-4]+[Cren+Cren']}$$

3.2.4.2. brGDGTs

To calculate the relative fluvial input of terrigenous organic matter in the marine environment the branched isoprenoid tetraether (BIT) index was calculated from the brGDGTs (Hopmans et al., 2004):

Eq. 4 $$BIT\ index = \frac{[GDGT-Ia]+[GDGT-IIa]+[GDGT-IIIa]}{[GDGT-Ia]+[GDGT-IIa]+[GDGT-IIIa]+[Cren]}$$

The methylation index of branched isoprenoid tetraethers (MBT) and the cyclisation index of branched isoprenoid tetraethers (CBT) were calculated from the brGDGTs as proxies for marine environment palaeo-reconstructions (Weijers et al., 2007):

Eq. 5 $$MBT = \frac{[GDGT-I]}{\sum[GDGT-I]+\sum[GDGT-II]+\sum[GDGT-III]}$$

Eq. 6 $$CBT = -\log(\frac{[GDGT-Ib]+[GDGT-IIb]}{[GDGT-Ia]+[GDGT-IIa]})$$

MAAT was calculated from MBT based on various continental soils, and soil pH was calculated from CBT (Weijers et al., 2007):

Eq. 7 $$MBT = 0.122 + 0.187 \times CBT + 0.020 \times MAAT \ \ (r^2 = 0.77, n = 134)$$

Eq. 8 $$CBT = 3.33 - 0.38 \times pH \ \ (r^2 = 0.70, n = 134)$$

The error ranges for pH and MAAT are relatively high, at 0.7 and 4.8°C, respectively. Therefore, the absolute values for these measurements should be used with great caution. Moreover, the relative abundance of the brGDGTs in the samples could be influenced by type of vegetation cover, soil temperature, precipitation levels (Peterse et al., 2012).

3.2.4.3. Alkenones and the $U_{37}^{K'}$ ratio calculations

The relative distribution of long chain unsaturated ketones can be presented as the $U_{37}^{K'}$ ratio and calculated according to (Prahl and Wakeham, 1987):

Eq. 9 $$U_{37}^{K'} = \frac{C_{37:2}}{C_{37:3}+C_{37:2}}$$

The $U_{37}^{K'}$ values were subsequently converted into SSTs using a global calibration and by applying the core top transfer function with a water temperature range of -1°C to +30°C and an estimated error of ±1.2°C (Conte et al., 2006):

Eq. 10 $$SST(°C) = 29.876\ (U_{37}^{K'}) - 1.334 \qquad n = 592;\ r^2 = 0.97$$

3.3. Results and discussion

3.3.1. SST reconstructions

3.3.1.1. Alkenone data

Alkenones were only detected in the late Miocene samples in the U1351 and U1352 sites, and in the middle Miocene samples in Site U1353 (Fig. 3.5). Concentrations are presented as ng per g sediment in Appendix 3.1. The concentration of alkenones in the analysed samples varies from 0.003 ng/g to 2.98 ng/g sediment for the U1351 Site, 0.03 ng/g to 0.91 ng/g sediment for the U1352 Site, and 0.41 ng/g to 1.9 ng/g sediment for the U1353 Site. The highest concentration of alkenones in Site U1351 is from the 5.30 Ma sample (Appendix 3.1).

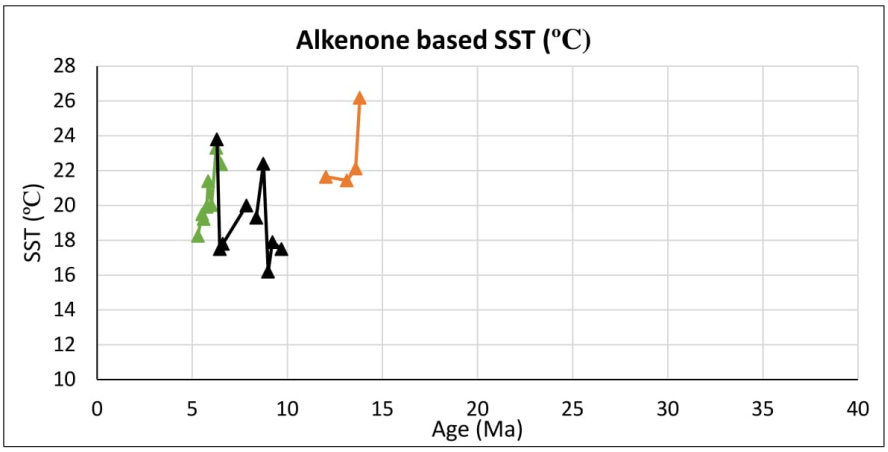

Figure 3.5: Reconstructed sea surface temperature based on Uk`37 index from the outer continental shelf core (U1351, green), the continental slope core (U1352, black) and the inner continental shelf core (U1353, orange).

3.3.1.2. iGDGT and brGDGT data

iGDGTs, crenarchaeol and brGDGTs were identified for all periods in the samples from the U1351, U1352, and U1353 sites. Relative abundances of different isomers are presented as BIT index TEX_{86}^{H} , methylation index of branched isoprenoid tetraethers (MBT) and the cyclisation index of branched isoprenoid tetraethers (CBT) (Table 3.1).

3.3.1.3. The branched isoprenoid tetraether (BIT) index

The BIT index is used as an indicator of the amount of terrestrial OM input into marine sediments (Hopmans et al., 2004), and as a result of that the quality of the reconstructed SST based on TEX_{86} data (Weijers et al., 2006). The BIT index for Site U1352 samples varies from 0.03 to 0.51 (Fig. 3.6; Table 3.2). The Eocene-Oligocene samples have a BIT index between 0.05 and 0.24, suggesting very low terrestrial OM input into the sediment. The three early Miocene samples have a BIT index below 0.1 (Fig. 3.6; Table 3.2) indicating low terrestrial OM input from the early Miocene period. The middle Miocene samples have higher variability in the BIT indices (0.068 – 0.162), which are also consistent with mainly marine OM input into sediment. The late Miocene samples have more variability in the BIT index, with a high value of 0.32 at 8.74 Ma suggesting an increase in terrestrial OM input. The BIT

indices from 10.49–8.74 Ma and 8.37–7.85 Ma is below 0.185 and indicative of high marine input to the samples. The Pleistocene-Pliocene samples have a significant increase in terrestrial OM input, with recorded BIT indices mostly >0.2. The 4.5–3 Ma period has only a short period of dominant marine OM in the samples (up to 4.34 Ma), followed by a significant increase in terrestrial input, with just one sample at 3.65 Ma having a BIT Index <0.2. Between 3.0 and 0.5 Ma there is high variability of the BIT index, with values varying in the range of 0.12 to 0.40. After 0.5 Ma there was an increasing terrestrial OM input with BIT values >0.2, with the majority of the samples having values from 0.3–0.6. Only the youngest sample (0.002 Ma) has a BIT index <0.2.

The samples from the U1351 Site have BIT indices in the range 0.21–0.74, with a peak of terrestrial input at 5.84 Ma (BIT index = 0.74). The samples at 6.52, 5.76, and 5.30 Ma have the lowest terrestrial interference in the marine sediments, with BIT indices of 0.21, 0.23, and 0.22, respectively (Table 3.2). The BIT indices calculated for the U1353 Site samples are consistently high (≥0.5), suggesting significant terrestrial OM input into the marine sediment and thus biased SST (TEX^{H}_{86}) reconstructions.

The sources of brGDGTs can vary. High BIT indices have been attributed to lacustrine or terrigenous sediments, and low BIT indices have been detected in coastal areas with low terrigenous sediment flux (Hopmans et al., 2004). Although the BIT index cannot be used as a quantitative measure of the terrigenous input in marine sediments, it has been suggested that values >0.8 likely correspond to strong fluvial flux into sediments, while values <0.2 are attributed to mainly marine OM input. It has been noted that high terrigenous OM input can influence the relative abundance of iGDGTs and trigger an error in the SST estimation for samples with a BIT index >0.5 (Schouten et al., 2004). Therefore, for SST reconstructions the samples with a BIT index >0.5 were excluded from being used for SST reconstruction.

3.3.1.4. Proxy based SST reconstructions

The alkenone-based SST reconstructions from the U1351 Site decrease from 22.4 ºC to 18.3 ºC during the 6.52 to 5.30 Ma time period (Fig. 3.5). The alkenone based SST for the U1353 Site show a significant temperature decrease from 26.2ºC at 13.81 Ma to 21.6ºC at 12.03 Ma. The alkenone data for the U1352 Site was only recovered for the late Miocene 9.69 to 6.30 Ma time period. The highest SST for this period (23.8 ºC) was at 6.30 Ma and the lowest of 16.2 ºC was at 8.99 Ma (Fig. 3.5; Table 3.1).

The reconstructed SSTs based on the iGDGT proxy data are presented in Fig. 3.6 and Table 3.1. The U1351 Site samples record SST(TEX^{H}_{86}) between 17.2ºC and 14.6 ºC for the 6.52–5.52 Ma time period, with the lowest value recorded at 5.60 Ma. The SST(TEX^{H}_{86}) for the U1352 Site samples vary between 1.0ºC and 29.8ºC, with the lowest value at 2.76 Ma and the highest at 35.28 Ma in the Eocene. 1.0ºC is an extremely cold temperature to record and can be attributed to the SST calculation error range, and/or the calibration used. Importantly, low SSTs were reconstructed for the Pliocene, so this period is interpreted to have been the cooler part of the Neogene. Two Oligocene samples have SST(TEX^{H}_{86}) values of 21.5ºC and 22.1ºC at 31.14 Ma and 31.01 Ma, respectively. Early Miocene samples show a SST(TEX^{H}_{86}) decrease from 26.0ºC at 18.87 Ma to 22.1ºC at 16.83 Ma. The middle Miocene samples have decreasing SST(TEX^{H}_{86}) values from 24.7ºC at 15.42 Ma to 18.9ºC at 13.72. The late Miocene samples from the U1352 Site have SST(TEX^{H}_{86}) values between 9.3ºC and 20.4ºC (Fig. 3.6; Table 3.1), with the lowest value at 8.39 Ma. There is a warmer period with temperature ~19.5°C in the late Miocene from 8.37 Ma to 7.93 Ma, but the temperatures decrease steeply afterwards to 12.8ºC at 6.30 Ma. The last 4.45 million years are well represented by 64 samples from the three holes. SST(TEX^{H}_{86}) during the Pliocene varies between 1.0ºC and 12.3ºC, with most samples having values <10ºC, but there are three samples with higher temperatures (3.65 Ma, 10.7ºC; 3.31 Ma, 10.5ºC; 1.11 Ma, 11.8ºC). The

end of the Pliocene has a very cool reconstructed temperature of 1.0ºC at 2.76 Ma. The Pleistocene SST(TEX^{H}_{86}) record has more variations in temperature from 1.1 ºC to 12.3ºC.

The Eocene and Oligocene samples from the U1352 Site have high SST temperatures >21°C. Early Oligocene samples from ODP site 511 (South Atlantic Ocean, Falkland Plateau) have low (<17°C) reconstructed SSTs from GDGT and alkenone proxies (Miller et al., 2008). Reconstructed SSTs for samples from DSDP Leg 26, Sites 250-252 (South Africa) have warm temperatures during the beginning of the Oligocene (Miller et al., 2008; Liu et al., 2009), which correlates well with the U1352 Site data at 31 Ma. Temperature reconstructions for Antarctica in the early and middle Eocene suggest a warm tropical environment on the continent (Pross et al., 2012). Warm SST temperatures at the Eocene/Oligocene boundary were also recorded in global oxygen isotope records (Zachos et al., 2001; Zachos et al., 2008), and these also show a global decrease in temperature from the Eocene to the Oligocene, which was also recorded in the Canterbury Basin SSTs. The early Miocene in the Canterbury Basin started warmer than the Oligocene, but then SST decrease through to a minimum in the middle Miocene, based on both TEX^{H}_{86} and the $U^{K`}_{37}$ index.

The differences in the reconstructed SSTs from the different proxies can be attributed to biases influencing the presence of the lipids in the sediment. Several factors influence the alkenone distribution in coastal samples, including lateral transportation in shallow environments (Benthien and Müller, 2000), species variation (Volkman et al., 1995), and probably most importantly mixed layers of different productivity levels (Prahl et al., 2001; Prahl et al., 2005).

Prahl et al. (1989) and Goni et al. (2004) have shown that early diagenesis of alkenones can lead to the preferential degradation of the $C_{37:3}$ alkenone (Kim et al., 2010; Prahl et al., 2010). The reduction of the $C_{37:3}$ alkenone isomer allow the SST reconstructions only to the 28-29°C range (Conte et al., 2006). Also, the degree of unsaturation of alkenones can be influenced by

various factors such as the main producer, nutrient levels, low abundance, and the post depositional mix of alkenones in a sediment (Epstein et al., 1998; Yamamoto et al., 2008). The calculated SST can be influenced by regional distribution differences of alkenones, and is dependent on strong currents and productivity gradients (Conte et al., 2006).

iGDGT preservation in sediments can be due to seasonal growth of *Thaumarchaeolata* (Huguet et al., 2011), but it may undergo its major growth in deeper and cooler waters, thus influencing the accumulation of iGDGTs above the mixed layer (Huguet et al., 2007; Kim et al., 2012; Seki et al., 2012). Moreover, the regional effect of each proxy must be considered during the reconstruction (Tierney and Tingley, 2014, 2015). In addition, different amounts of biotic and abiotic selective degradation could cause variations in the reconstructed SST by up to 5.9°C (Rontani et al., 2006; Rontani et al., 2013).

The SST data from the Canterbury Basin show a constant temperature decrease from the early Miocene. This contradicts the global $\delta^{18}O$ reconstructions for the 17–15 Ma period (the mid-Miocene Climatic Optimum) (Zachos et al., 2001 and references within) and suggests a cooling trend. However, during the Neogene the Antarctic oceanic front developed (Lawver et al., 1992; Nelson and Cooke, 2001). This caused a decrease in the SST around New Zealand from the early Miocene as cooler subtropical paleo-currents and later on the cold intrusions of the sub-Antarctic currents started to influence the ocean temperature, especially around the east coast of New Zealand (Nelson and Cooke, 2001). This influence increased from the Middle Miocene, ~ 15 Ma. These cooling trend was also supported by land fossil records from New Zealand, which show warm-water environments for the first part of the Neogene (Beu et al., 1997; Chaproniere, 1984).

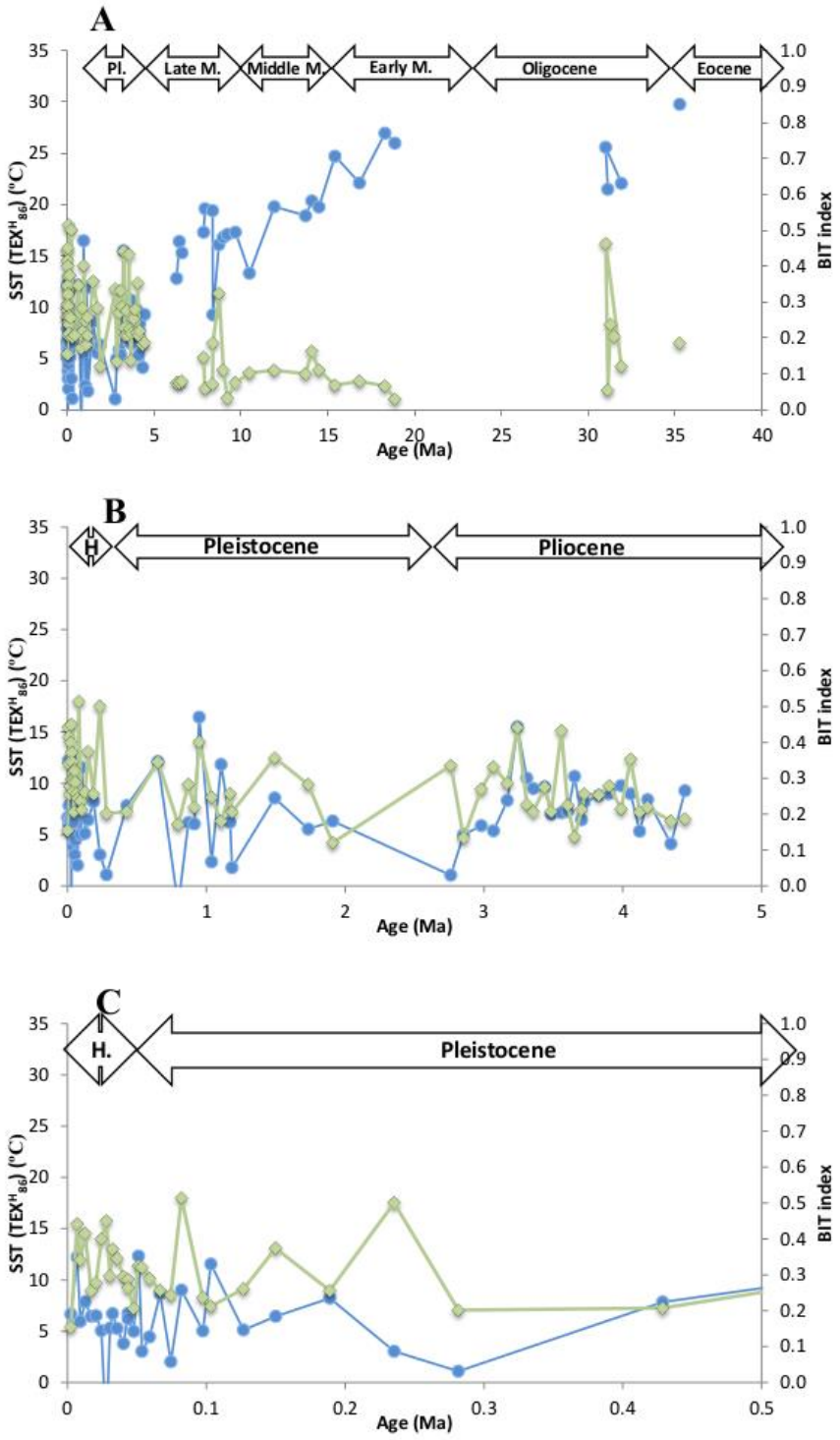

Figure 3.6: Reconstructed sea surface temperature based on TEX^H_{86} (blue) and the branched isoprenoid tetraether (BIT) index (green) for the U1352 Site samples, where Pl. – Pliocene, M. – Miocene, and H. – Holocene. Three different time scales are used: back to 35 Ma (**A**), back to 5 Ma (**B**), and back to 0.5 Ma (**C**).

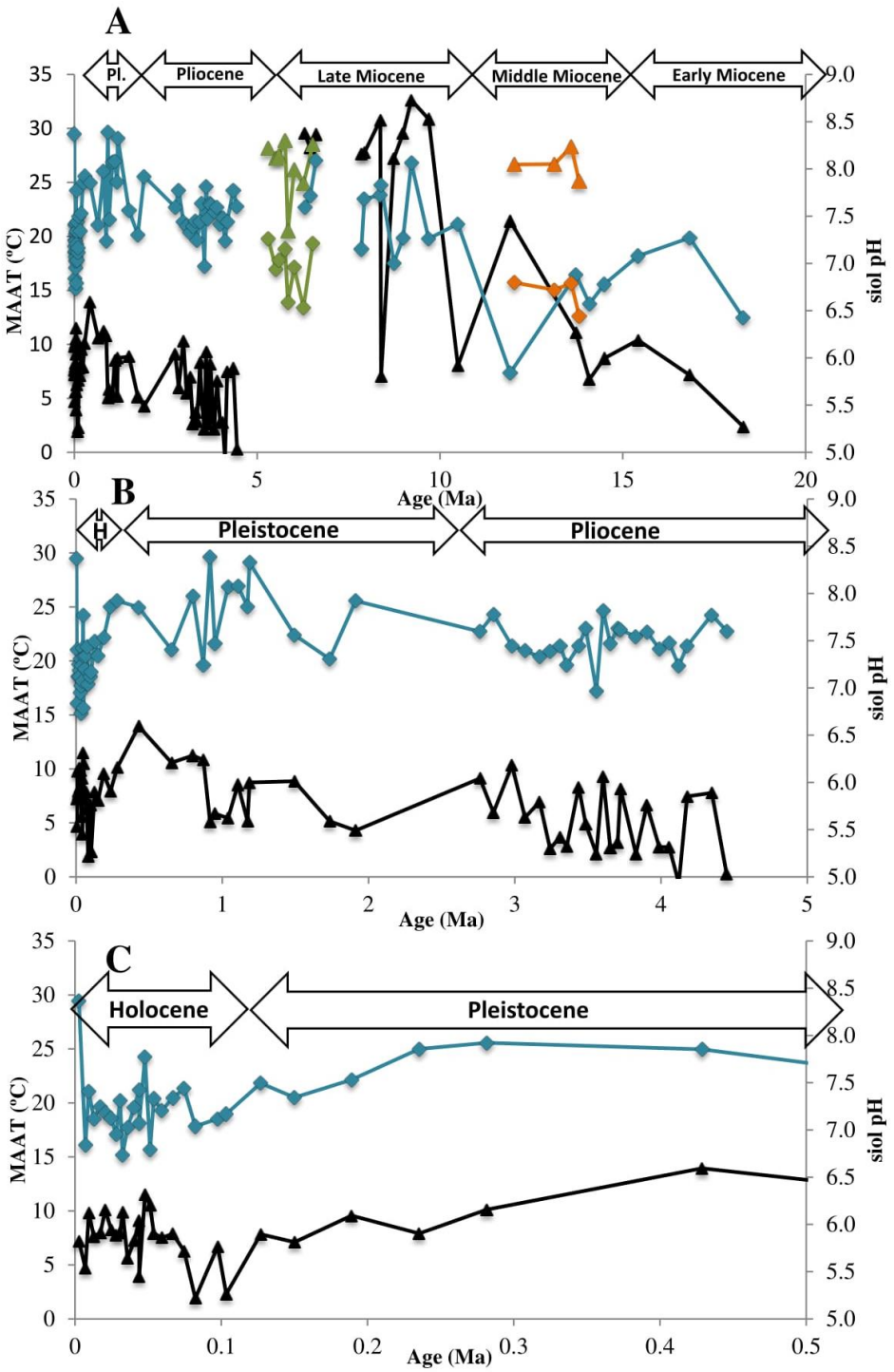

Figure 3.7: Reconstructed mean annual air temperatures (MAAT, triangles) and soil pH (diamonds) for the analysed samples from the outer continental shelf core (U1351, green), the continental slope core (U1352, black for MAAT, blue for soil pH), and the inner continental shelf core (U1353, orange). Three different time scales are used: back to 20 Ma (**A**), back to 5 Ma (**B**), and back to 0.5 Ma (**C**).

A similar SST decrease during the mid-Miocene Climatic Optimum was recorded in DSDP Site 593, southern Tasman Sea (Cooke et al., 2008). From the start of the late Miocene (10 Ma) to the Holocene the SST(TEX^{H}_{86}) from the Canterbury Basin (Fig. 3.6) correlates well

with the global temperature decrease reconstructed from $\delta^{18}O$ (Zachos et al., 2001). The late Miocene has a warmer, subtropical temperature (to 20ºC) at 7.93 Ma, which was also recorded at the ODP site 590 (south western Pacific) using the alkenone proxy (Karas et al., 2011a), and ODP site 763 (north eastern Indian Ocean) using Mg/Ca ratio (Karas et al., 2011b). Variations between the reconstructed temperatures can be attributed to the different proxies used in the studies. However, a similar warm trend around 8 Ma was recorded at all three sites, suggesting a global warming trend in the oceans before a significant temperature drop.

In addition, a decrease in SST was recorded in multiple locations around the globe during the Miocene (Herbert et al., 2016). This study showed a significant temperature drop in both the northern and southern hemispheres, based on various drilling site samples. For example, DSDP 594, located in the Southern Pacific region (Herbert et al., 2016), shows a similar temperature decrease after 8 Ma as samples from this study. The late Miocene SST decrease can be correlated to an increase in ice sheet cover in southeast Greenland (Larsen et al., 1994), South America (Mercer and Sutter, 1982), and possible formation of ice sheets in Western Antarctica (Kennett, 1990).

3.3.2. Reconstructed MAAT

Samples from the U1351 Site show warm MAAT for the South Island of New Zealand for the 6.52–5.3 Ma period (Table 3.1). The temperature reaches 28.9ºC at 5.76 Ma and does not drop below 20ºC for all analysed samples. The coolest MAAT (20.5ºC) is at 5.84 Ma. MAAT was only recorded back to the early Miocene for the U1352 Site (Fig. 3.7A). There is a significant increase in MAAT from 18.3 Ma to 6.3 Ma. Most early and middle Miocene samples have a MAAT not exceeding 11ºC, except for one middle Miocene samples at 11.9 Ma with 21.4ºC. The samples from 9.69–6.30 Ma mostly have a MAAT of 27–32.6ºC, with only one rather cool sample at 7.1ºC (8.40 Ma, late Miocene). The Pliocene-Pleistocene

samples have much lower MAATs, varying from 0.3ºC at 4.1 Ma to 14.0ºC at 0.43 Ma. High temperature variability is present during the last 4.5 million years, with temperatures below 10ºC until 1 Ma (Fig. 3.7B). From 1 Ma the MAAT increase slightly to a maximum of 14.0ºC at 0.43 Ma, before decreasing again to the Holocene (Fig. 3.7C). The U1353 Site also records warm MAAT (25.1–28.3ºC) during the middle Miocene. The lowest MAAT is recorded at 13.81 Ma and the highest at 13.59 Ma.

A relatively large calibration error for Eq. 8 (±5ºC) introduces large uncertainty for the MAAT estimates (Weijers et al., 2007; Schouten et al., 2013). Although, the introduced temperature error is significant, it produces a better temperature evaluation than pollen or leaf based analysis, where the potential biases are harder to evaluate (Schouten et al., 2013). Because of the high analytical error, the exact MAAT evaluation is problematic and only general temperature trends can be discussed from the data.

Our data show a warming MAAT trend in New Zealand that correlates well with the established mid-Miocene Climatic Optimum reconstruction (Zachos et al., 2001). The MAAT in the New Zealand samples continues to rise through the second part of the middle Miocene and the late Miocene, with only two major cooling events 10.49 and 8.39 Ma. The MAAT warming after 14 Ma in New Zealand is supported by fossil studies of New Zealand vegetation (Mildenhall, 2003).

The warm MAAT during the late Miocene period contradicts the proposed global late Neogene cooling (Herbert et al., 2016). However, the global cooling trend was not constant everywhere. Some studies show partial warming in the Arctic and Antarctic regions during the end of the late Miocene and Pliocene (Kennett, 1990; Thiede et al., 1998). The temperature fluctuations probably correlate to the pCO_2 changes in the late Miocene related to the orbital scale shifts forcing climatic and ecosystem changes (Herbert et al., 2016). The data from the Canterbury Basin suggests a time delay between cooling of the ocean, as reflected in

the SST, and any cooling effect on the New Zealand MAAT temperature. The new results show a SST decrease during the late Miocene that only influenced the MAAT during the Pliocene. Rapid cooling in New Zealand coincides with a significant increase in ice sheet cover in Antarctica (Ross Sea), dated between 3.3 and 2.5 Ma (McKay et al., 2012).

3.3.3. Soil pH

Soil pH was calculated for all sites from the early Miocene. There is a gradual increase in soil pH levels through the time (Fig. 3.7A). The late Miocene samples from the U1351 Site (6.52 – 5.3 Ma) have soil pH values between 6.5 and 7.3, with the lowest value in the first half of this period. The middle Miocene samples from the U1353 Site have soil pH values between 6.4 at 13.81 Ma and 6.8 at 12.03 Ma. The early Miocene samples from the U1352 Site have soil pH values between 6.4 – 7.3. The middle Miocene samples have soil pH decreasing from 7.1 at 15.4 Ma to an outlier of 5.8 at 11.9 Ma, which is also the lowest pH of all the samples. The late Miocene samples generally have higher soil pH (7.0–8.1) after 10.4 Ma. The Pliocene samples from the U1352 Site have stable soil pH, mostly in the range 7.2–7.6 (23 samples; Fig. 3.7B). Three samples from 4.35 Ma, 3.60 Ma, and 2.85 Ma have a slightly higher soil pH (7.8), and the 3.56 Ma sample has a slightly lower soil pH (7.0). The Pleistocene and Holocene soil pH record can be divided into two major parts, 2-0.2 Ma, and 0.2 Ma to recent (Fig. 3.7B,C). The first interval has soil pH values between 7.2 and 8.4 with the highest at 0.92 Ma and the lowest at 0.87 Ma. The second interval shows a generally decreasing soil pH trend in the range of 7.5 to 6.7, except for the most recent sample (0.003 Ma) which has an anomalously high value of 8.4. Three spikes of low soil pH can be distinguished at 0.051, 0.033, and 0.007 Ma, with values of 6.8, 6.7, and 6.8, respectively. Each of these spikes are followed by significant increases in soil pH to 7.8, 7.3, and 8.4 at 0.048, 0.031, and 0.003 Ma, respectively.

Changing precipitation alters the acidity of soil. Higher precipitation washes away Ca and Mg ions from the system, leaving the soil more acidic. Based on the MBT/CBT ratio and the resultant soil pH parameter it is not possible to calibrate the exact amount of regional rainfall, but it is possible to evaluate the duration of precipitation changes. The reconstructed soil pH for the New Zealand region suggest a general trend of decreasing precipitation for the last 19 Ma (Fig. 3.7). Some intervals with higher inferred precipitation in New Zealand can be identified by drops in soil pH, for example at 13.72 Ma, 11.92 Ma, 3.60 Ma and 3.56 Ma. Another significant drop in soil pH is recorded from 0.235 to 0.003 Ma when soil pH dropped from 7.9 to 6.7. The increase in soil pH to 7.8 at 0.048 Ma divides this period into two high precipitation periods, with a short drier period in between. The significant jump in soil alkalinity at 0.003 Ma to 8.4 suggests a rapid decrease in precipitation.

Palynological evidence supported by moisture availability and the spread of fire in the New Zealand area suggests a warm temperate climate for the early Miocene (Mildenhall et al., 2003; Pole, 2003). This model contradicts the previously suggested cool early Miocene climate (Pockhall, 1989). Miocene cooling in New Zealand regions arguably started from 14 Ma (Molnar and Pole, 1997; Pole et al., 2003). However, these climate reconstructions are commonly based on plant fossil evidence (e.g., Utescher et. al., 2000) as well as on structural fossil leaf analyses (e.g. Fricke and Wing, 2004; Wing et al., 2005), and can be problematic due to poor plant preservation in the geological record and the difficulty of finding the fossils for all geological intervals.

Reconstructed mean annual precipitation (MAP) levels in East Antarctica for the early Miocene period show a large increase in MAP from 20 Ma to 15 Ma (Passchier et al., 2013), from 500 mm to about 790 mm. The new data correlate well with these reconstructions, suggesting a gradual increase in precipitation levels from 16.83 Ma until the end of the middle Miocene. Huang et al. (2007) argued in favour of C4 plant expansion in the Himalaya foreland and Arabian Peninsula regions from ~10 Ma to 5.5 Ma. This expansion would be

consistent with a decrease in global precipitation levels and development of the savanna vegetation in the North Africa and Arabian Peninsula.

The Canterbury Basin data show a decrease in precipitation from the late Miocene to the beginning of the Pliocene over the same time, suggesting that this event also affected New Zealand. The BIT index is <0.15 for most Canterbury Basin samples during the late Miocene, supporting low terrestrial OM runoff into the ocean (Fig. 3.6). At the same time the MAAT data show a high temperature spike during the late Miocene, up to 32.6ºC. Such a temperature increase correlates well with the inferred decrease in precipitation in New Zealand and partial aridification. This dry period was recorded in previous studies based on radiometrically-dated fossil pollen records preserved in speleothems from semiarid southern Australia (Sniderman et al., 2016) and atmospheric carbon dioxide fluctuations (Pagani et al., 1999).

3.4. Conclusions

Until the Oligocene New Zealand was surrounded by tropical and subtropical seas. For example, planktonic foraminifera (Jenkins, 1965) and $\delta^{18}O$ (Shackleton and Kennett, 1975) records suggest a warm SST at the Oligocene/Miocene boundary in the New Zealand region. Reconstructed SSTs from the Canterbury Basin show a high (29.8ºC) temperature for the Eocene. The SST in the New Zealand region decreased during the Neogene, following the development of the Antarctic oceanic front (Lawver et al., 1992; Nelson and Cooke, 2001). The early Miocene in the Canterbury Basin started warmer than the Oligocene, but then the SST decreased through to a minimum in the middle Miocene, based on both TEX^{H}_{86} and the $U^{K`}_{37}$ index.

The new data show a warming MAAT trend in New Zealand that correlates well with the established mid-Miocene Climatic Optimum reconstruction (Zachos et al., 2001). The MAAT in the New Zealand region continued to rise through the second part of the middle Miocene and the late Miocene. The warm MAAT during the late Miocene period is consistent with partial warming in the Arctic and Antarctic regions during the end of the late Miocene and Pliocene (Kennett, 1990; Thiede et al., 1998). In addition, the new data are suggestive of a delay in the influence of the late Miocene SST cooling effect on the New Zealand MAAT. Rapid MAAT cooling in New Zealand can be attributed to an increase in ice sheet cover in Antarctica (Ross Sea) during the Pliocene. The reconstructed soil pH for the New Zealand region shows a general trend of decreasing precipitation for the last 19 Ma, consistent with a general increase in global aridification.

3.5. Acknowledgments

This work was supported by post-cruise funding from the Australia-New Zealand IODP Consortium (ANZIC), and by Macquarie University who provided a PhD scholarship and research funding.

3.6. References

Abreu, V.S., Anderson, J.B., 1998. Glacial eustasy during the Cenozoic: sequence stratigraphic implications. *AAPG Bulletin* 82, 1385-1400.

Adams, C., 1981. Uplift rates and thermal structure in the Alpine fault zone and Alpine schists, Southern Alps, New Zealand. *Geological Society, London, Special Publications* 9, 211-222.

Adams, C., Gabites, J., 1985. Age of metamorphism and uplift in the Haast Schist Group at Haast Pass, Lake Wanaka and Lake Hawea, South Island, New Zealand. *New Zealand Journal of Geology and Geophysics* 28, 85-96.

Atkins, C., 2001. Glacial influence from clast features in Oligocene and Miocene stata cored in CRP-2/2A and CRP-3, Victoria Land Basin, Antarctica. *Terra Antartica* 8, 263-274.

Badger, M., Lear, C., Pancost, R., Bailey, T., Leng, M., Abels, H., 2008. Atmospheric Carbon Dioxide and Climate Following the Middle Miocene Expansion of the East Antarctic Ice Sheet, AGU Fall Meeting Abstracts.
Badger, M.P., Lear, C.H., Pancost, R.D., Foster, G.L., Bailey, T.R., Leng, M.J., Abels, H.A., 2013. CO2 drawdown following the middle Miocene expansion of the Antarctic Ice Sheet. *Paleoceanography* 28, 42-53.

Barker, P.F., Diekmann, B., Escutia, C., 2007. Onset of Cenozoic Antarctic glaciation. *Deep Sea Research Part II: Topical Studies in Oceanography* 54, 2293-2307.

Barrett, P., Elston, D., Harwood, D., McKelvey, B., Webb, P.-N., 1987. Mid-Cenozoic record of glaciation and sea-level change on the margin of the Victoria Land basin, Antarctica. *Geology* 15, 634-637.

Batt, G.E., Baldwin, S.L., Cottam, M.A., Fitzgerald, P.G., Brandon, M.T., Spell, T.L., 2004. Cenozoic plate boundary evolution in the South Island of New Zealand: New thermochronological constraints. *Tectonics* 23.

Batt, G.E., Braun, J., Kohn, B.P., McDougall, I., 2000. Thermochronological analysis of the dynamics of the Southern Alps, New Zealand. *Geological Society of America Bulletin* 112, 250-266.

Becker, K.W., Lipp, J.S., Versteegh, G.J., Wörmer, L., Hinrichs, K.-U., 2015. Rapid and simultaneous analysis of three molecular sea surface temperature proxies and application to sediments from the Sea of Marmara. *Organic Geochemistry* 85, 42-53.

Becker, K.W., Lipp, J.S., Zhu, C., Liu, X.-L., Hinrichs, K.-U., 2013. An improved method for the analysis of archaeal and bacterial ether core lipids. *Organic Geochemistry* 61, 34-44.

Benthien, A., Müller, P.J., 2000. Anomalously low alkenone temperatures caused by lateral particle and sediment transport in the Malvinas Current region, western Argentine Basin. *Deep Sea Research Part I: Oceanographic Research Papers* 47, 2369-2393.

Beu, A.G., Griffin, M., Maxwell, P., 1997. Opening of Drake Passage gateway and Late Miocene to Pleistocene cooling reflected in Southern Ocean molluscan dispersal: evidence from New Zealand and Argentina. *Tectonophysics* 281, 83-97.

Carter, L., Carter, R., McCave, I., 2004. Evolution of the sedimentary system beneath the deep Pacific inflow off eastern New Zealand. *Marine Geology* 205, 9-27.

Carter, L., Wilkin, J., 1999. Abyssal circulation around New Zealand—A comparison between observations and a global circulation model. *Marine Geology* 159, 221-239.

Carter, R.t., Norris, R., 1976. Cainozoic history of southern New Zealand: an accord between geological observations and plate-tectonic predictions. *Earth and Planetary Science Letters* 31, 85-94.

Chaproniere, G.C., 1984. Oligocene and Miocene larger foraminiferida from Australia and New Zealand. *Unknown* 1.

Conte, M.H., Sicre, M.A., Rühlemann, C., Weber, J.C., Schulte, S., Schulz-Bull, D., Blanz, T., 2006. Global temperature calibration of the alkenone unsaturation index (UK′ 37) in surface waters and comparison with surface sediments. *Geochemistry, Geophysics, Geosystems* 7.

Cooke, P.J., Nelson, C.S., Crundwell, M.P., 2008. Miocene isotope zones, paleotemperatures, and carbon maxima events at intermediate water-depth, Site 593, Southwest Pacific. *New Zealand Journal of Geology and Geophysics* 51, 1-22.

Cramer, B., Miller, K., Barrett, P., Wright, J., 2011. Late Cretaceous–Neogene trends in deep ocean temperature and continental ice volume: Reconciling records of benthic foraminiferal geochemistry (δ18O and Mg/Ca) with sea level history. *Journal of Geophysical Research: Oceans* 116.

Cristini, L., Grosfeld, K., Butzin, M., Lohmann, G., 2012. Influence of the opening of the Drake Passage on the Cenozoic Antarctic Ice Sheet: a modeling approach. *Palaeogeography, Palaeoclimatology, Palaeoecology* 339, 66-73.

DeConto, R., Pollard, D., Harwood, D., 2007. Sea ice feedback and Cenozoic evolution of Antarctic climate and ice sheets. *Paleoceanography* 22.

DeConto, R.M., Pollard, D., 2003. Rapid Cenozoic glaciation of Antarctica induced by declining atmospheric CO2. *Nature* 421, 245-249.

Epstein, B.L., D'Hondt, S., Quinn, J.G., Zhang, J., Hargraves, P.E., 1998. An effect of dissolved nutrient concentrations on alkenone-based temperature estimates. *Paleoceanography* 13, 122-126.

Exon, N., Kennett, J., Malone, M., 2001. the Leg 189 Shipboard Scientific Party (2001), Proc. ODP, Initial Reports, pp. 77845-79547.
Exon, N.F., Kennett, J.P., Malone, M.J., 2004. Leg 189 synthesis: Cretaceous–Holocene history of the Tasmanian gateway, Proceedings of the ocean drilling program, scientific results, pp. 1-37.
Fleming, C.A., 1975. The geological history of New Zealand and its biota, Biogeography and ecology in New Zealand. Springer, pp. 1-86.
Flower, B., Kennett, J., 1993a. Middle Miocene ocean-climate transition: High-resolution oxygen and carbon isotopic records from Deep Sea Drilling Project Site 588A, southwest Pacific. *Paleoceanography* 8, 811-843.

Flower, B.P., Kennett, J.P., 1993b. Relations between Monterey Formation deposition and middle Miocene global cooling: Naples Beach section, California. *Geology* 21, 877-880.

Flower, B.P., Kennett, J.P., 1994. The middle Miocene climatic transition: East Antarctic ice sheet development, deep ocean circulation and global carbon cycling. *Palaeogeography, Palaeoclimatology, Palaeoecology* 108, 537-555.

Flower, B.P., Kennett, J.P., 1995. Middle Miocene deepwater paleoceanography in the southwest Pacific: relations with East Antarctic Ice Sheet development. *Paleoceanography* 10, 1095-1112.

Folland, C.K., Salinger, M.J., 1995. Surface temperature trends and variations in New Zealand and the surrounding ocean, 1871–1993. *International Journal of Climatology* 15, 1195-1218.

Foster, G.L., Lear, C.H., Rae, J.W., 2012. The evolution of pCO 2, ice volume and climate during the middle Miocene. *Earth and Planetary Science Letters* 341, 243-254.

Foster, G.L., Rohling, E.J., 2013. Relationship between sea level and climate forcing by CO2 on geological timescales. *Proceedings of the National Academy of Sciences* 110, 1209-1214.

Fulthorpe, C.S., Carter, R.M., Miller, K.G., Wilson, J., 1996. Marshall Paraconformity: a mid-Oligocene record of inception of the Antarctic Circumpolar Current and coeval glacio-eustatic lowstand? *Marine and petroleum geology* 13, 61-77.

Fulthorpe, C.S., Hoyanagi, K., Crundwell, M.P., Dinarès-Turell, J., Ding, X., George, S.C., Hepp, D.A., Jaeger, J., Kawagata, S., Kemp, D.B., 2011. Expedition 317 summary.

Goni, M.A., Woodworth, M.P., Aceves, H.L., Thunell, R.C., Tappa, E., Black, D., Müller-Karger, F., Astor, Y., Varela, R., 2004. Generation, transport, and preservation of the alkenone-based U37K′ sea surface temperature index in the water column and sediments of the Cariaco Basin (Venezuela). *Global Biogeochemical Cycles* 18.

Hall, I.R., McCave, I.N., Zahn, R., Carter, L., Knutz, P.C., Weedon, G.P., 2003. Paleocurrent reconstruction of the deep Pacific inflow during the middle Miocene: Reflections of East Antarctic Ice Sheet growth. *Paleoceanography* 18.

Haq, B.U., Hardenbol, J., Vail, P.R., 1987. Chronology of fluctuating sea levels since the Triassic. *Science* 235, 1156-1167.

Hardenbol, J., Thierry, J., Farley, M.B., Jacquin, T., De Graciansky, P.-C., Vail, P.R., 1998. Mesozoic and Cenozoic sequence chronostratigraphic framework of European basins.

Head, P., Nelson, C., 1994. A high-resolution oxygen isotope record for the past 6.4 million years at DSDP Site 593, Challenger Plateau, southern Tasman Sea. *Evolution of the Tasman Sea Basin. Rotterdam, AA Balkema*, 159-179.

Herbert, T.D., Lawrence, K.T., Tzanova, A., Peterson, L.C., Caballero-Gill, R., Kelly, C.S., 2016. Late Miocene global cooling and the rise of modern ecosystems. *Nature Geosci* 9, 843-847.

Hopmans, E.C., Schouten, S., Damsté, J.S.S., 2016. The effect of improved chromatography on GDGT-based palaeoproxies. *Organic Geochemistry* 93, 1-6.

Hopmans, E.C., Weijers, J.W., Schefuß, E., Herfort, L., Damsté, J.S.S., Schouten, S., 2004. A novel proxy for terrestrial organic matter in sediments based on branched and isoprenoid tetraether lipids. *Earth and Planetary Science Letters* 224, 107-116.

Hornibrook, N.d.B., 1992. New Zealand Cenozoic marine paleoclimates: a review based on the distribution of some shallow water and terrestrial biota. *Pacific Neogene: environment, evolution, and events. University of Tokyo Press, Tokyo*, 83-106.

Huang, Y., Clemens, S.C., Liu, W., Wang, Y., Prell, W.L., 2007. Large-scale hydrological change drove the late Miocene C4 plant expansion in the Himalayan foreland and Arabian Peninsula. *Geology* 35, 531-534.

Huguet, C., Fietz, S., Stockhecke, M., Sturm, M., Anselmetti, F., Rosell-Mele, A., 2011. Biomarker seasonality study in lake van, Turkey. *Organic Geochemistry* 42, 1289-1298.

Huguet, C., Schimmelmann, A., Thunell, R., Lourens, L.J., Sinninghe Damsté, J.S., Schouten, S., 2007. A study of the TEX86 paleothermometer in the water column and sediments of the Santa Barbara Basin, California. *Paleoceanography* 22.

Ishida, S., 1970. The Noroshi Flora of Note Peninsula, Central Japan.

Jenkins, D.G., 1965. Planktonic foraminiferal zones and new taxa from the Danian to Lower Miocene of New Zealand. *New Zealand Journal of Geology and Geophysics* 8, 1088-1126.

John, C.M., Karner, G.D., Mutti, M., 2004. δ18O and Marion Plateau backstripping: combining two approaches to constrain late middle Miocene eustatic amplitude. *Geology* 32, 829-832.

Karas, C., Nürnberg, D., Tiedemann, R., Garbe-Schönberg, D., 2011a. Pliocene climate change of the Southwest Pacific and the impact of ocean gateways. *Earth and Planetary Science Letters* 301, 117-124.

Karas, C., Nürnberg, D., Tiedemann, R., Garbe-Schönberg, D., 2011b. Pliocene Indonesian throughflow and Leeuwin current dynamics: implications for Indian Ocean polar heat flux. *Paleoceanography* 26.

Keigwin, L., Keller, G., 1984. Middle Oligocene cooling from equatorial Pacific DSDP site 77B. *Geology* 12, 16-19.

Kennett, J., Houtz, R., Andrews, P., Edwards, A., Gostin, V., Hajos, M., Hampton, M., Jenkins, D., Margolis, S., Ovenshine, A., 1974. Development of the circum-Antarctic current. *Science* 186, 144-147.

Kennett, J.P., 1977. Cenozoic evolution of Antarctic glaciation, the circum-Antarctic Ocean, and their impact on global paleoceanography. *Journal of geophysical research* 82, 3843-3860.

Kennett, J.P., 1990. Latest Cretaceous to Cenozoic climate and oceanographic developments in the Weddell Sea, Antarcitca: An ocean-Drilling perspective, Proc. ODP, Sci. Results, pp. 937-960.
Kennett, J.P., Barker, P.F., 1990. Latest Cretaceous to Cenozoic climate and oceanographic developments in the Weddell Sea, Antarctica: an ocean-drilling perspective, Proceedings of the Ocean Drilling Program, Scientific Results. Ocean Drilling Program College Station, TX, pp. 937-960.
Kim, J.-H., Romero, O.E., Lohmann, G., Donner, B., Laepple, T., Haam, E., Damste, J.S.S., 2012. Pronounced subsurface cooling of North Atlantic waters off Northwest Africa during Dansgaard–Oeschger interstadials. *Earth and Planetary Science Letters* 339, 95-102.

Kim, J.-H., Schouten, S., Hopmans, E.C., Donner, B., Sinninghe Damsté, J.S., 2008. Global sediment core-top calibration of the TEX86 paleothermometer in the ocean. *Geochimica et Cosmochimica Acta* 72, 1154-1173.

Kim, J.-H., Van der Meer, J., Schouten, S., Helmke, P., Willmott, V., Sangiorgi, F., Koç, N., Hopmans, E.C., Damsté, J.S.S., 2010. New indices and calibrations derived from the distribution of crenarchaeal isoprenoid tetraether lipids: Implications for past sea surface temperature reconstructions. *Geochimica et Cosmochimica Acta* 74, 4639-4654.

King, P.R., 2000. Tectonic reconstructions of New Zealand: 40 Ma to the present. *New Zealand Journal of Geology and Geophysics* 43, 611-638.

Kominz, M.A., Miller, K.G., Browning, J.V., 1998. Long-term and short-term global Cenozoic sea-level estimates. *Geology* 26, 311-314.

Kürschner, W.M., Kvaček, Z., Dilcher, D.L., 2008. The impact of Miocene atmospheric carbon dioxide fluctuations on climate and the evolution of terrestrial ecosystems. *Proceedings of the National Academy of Sciences* 105, 449-453.

Landis, C., Campbell, H., Begg, J., Mildenhall, D., Paterson, A.M., Trewick, S., 2008. The Waipounamu Erosion Surface: questioning the antiquity of the New Zealand land surface and terrestrial fauna and flora. *Geological Magazine* 145, 173-197.

Larsen, H., Saunders, A., Clift, P., Beget, J., Wei, W., Spezzaferri, S., Ali, J., Cambray, H., Demant, A., Fitton, G., 1994. Seven million years of glaciation in Greenland. *Science-AAAS-Weekly Paper Edition-including Guide to Scientific Information* 264, 952-954.

Lawver, L.A., Gahagan, L.M., 2003. Evolution of Cenozoic seaways in the circum-Antarctic region. *Palaeogeography, Palaeoclimatology, Palaeoecology* 198, 11-37.

Lawver, L.A., Gahagan, L.M., Coffin, M.F., 1992. The development of paleoseaways around Antarctica. *The Antarctic Paleoenvironment: A Perspective on Global Change: Part One*, 7-30.

Lear, C.H., Rosenthal, Y., Coxall, H.K., Wilson, P., 2004. Late Eocene to early Miocene ice sheet dynamics and the global carbon cycle. *Paleoceanography* 19.

Lee, D.E., Conran, J.G., Lindqvist, J.K., Bannister, J.M., Mildenhall, D.C., 2012. New Zealand Eocene, Oligocene and Miocene macrofossil and pollen records and modern plant distributions in the Southern Hemisphere. *The Botanical Review* 78, 235-260.

Liu, X., Lipp, J.S., Hinrichs, K.-U., 2011. Distribution of intact and core GDGTs in marine sediments. *Organic Geochemistry* 42, 368-375.

Liu, Z., Pagani, M., Zinniker, D., DeConto, R., Huber, M., Brinkhuis, H., Shah, S.R., Leckie, R.M., Pearson, A., 2009. Global cooling during the Eocene-Oligocene climate transition. *Science* 323, 1187-1190.

Lu, H., Fulthorpe, C.S., Mann, P., Kominz, M.A., 2005. Miocene–Recent tectonic and climatic controls on sediment supply and sequence stratigraphy: Canterbury basin, New Zealand. *Basin Research* 17, 311-328.

Lunt, D.J., Flecker, R., Valdes, P.J., Salzmann, U., Gladstone, R., Haywood, A.M., 2008. A methodology for targeting palaeo proxy data acquisition: A case study for the terrestrial late Miocene. *Earth and Planetary Science Letters* 271, 53-62.

MacDonald, G.J., 1990. Role of methane clathrates in past and future climates. *Climatic Change* 16, 247-281.

Marsaglia, K.M., Browne, G.H., George, S.C., Kemp, D.B., Jaeger, J.M., Carson, D., Richaud, M., Expedition, I., 2017. The Transformation of Sediment Into Rock: Insights From IODP Site U1352, Canterbury Basin, New Zealand. *Journal of Sedimentary Research* 87, 272-287.

Mason, B., 1961. Potassium-argon ages of metamorphic rocks and granites from Westland, New Zealand. *New Zealand Journal of Geology and Geophysics* 4, 352-356.

McKay, R., Naish, T., Carter, L., Riesselman, C., Dunbar, R., Sjunneskog, C., Winter, D., Sangiorgi, F., Warren, C., Pagani, M., 2012. Antarctic and Southern Ocean influences on Late Pliocene global cooling. *Proceedings of the National Academy of Sciences* 109, 6423-6428.

Mercer, J.H., Sutter, J.F., 1982. Late Miocene—earliest Pliocene glaciation in southern Argentina: implications for global ice-sheet history. *Palaeogeography, Palaeoclimatology, Palaeoecology* 38, 185-206.

Mildenhall, D., 2003. Deep-sea record of Pliocene and Pleistocene terrestrial palynomorphs from offshore eastern New Zealand (ODP Site 1123, Leg 181). *New Zealand Journal of Geology and Geophysics* 46, 343-361.

Miller, K.G., Browning, J.V., Aubry, M.-P., Wade, B.S., Katz, M.E., Kulpecz, A.A., Wright, J.D., 2008. Eocene–Oligocene global climate and sea-level changes: St. Stephens Quarry, Alabama. *Geological Society of America Bulletin* 120, 34-53.

Miller, K.G., Kominz, M.A., Browning, J.V., Wright, J.D., Mountain, G.S., Katz, M.E., Sugarman, P.J., Cramer, B.S., Christie-Blick, N., Pekar, S.F., 2005. The phanerozoic record of global sea-level change. *Science* 310, 1293-1298.

Miller, K.G., Mountain, G.S., Browning, J.V., Kominz, M., Sugarman, P.J., Christie-Blick, N., Katz, M.E., Wright, J.D., 1998. Cenozoic global sea level, sequences, and the New Jersey transect: results from coastal plain and continental slope drilling. *Reviews of Geophysics* 36, 569-601.

Miller, K.G., Sugarman, P.J., Browning, J.V., Kominz, M.A., Hernández, J.C., Olsson, R.K., Wright, J.D., Feigenson, M.D., Van Sickel, W., 2003. Late Cretaceous chronology of large, rapid sea-level changes: Glacioeustasy during the greenhouse world. *Geology* 31, 585-588.

Miller, K.G., Wright, J.D., Fairbanks, R.G., 1991. Unlocking the ice house: Oligocene-Miocene oxygen isotopes, eustasy, and margin erosion. *Journal of Geophysical Research: Solid Earth* 96, 6829-6848.

Molnar, P., 2004. Late Cenozoic increase in accumulation rates of terrestrial sediment: How might climate change have affected erosion rates? *Annu. Rev. Earth Planet. Sci.* 32, 67-89.

Molnar, P., Tapponnier, P., 1975. Cenozoic tectonics of Asia: effects of a continental collision. *Science* 189, 419-426.

Moss, G., McGowran, B., 1993. Foraminiferal turnover in neritic environments: the end-Eocene and mid-Oligocene events in southern Australia. *Memoir of the Association of Australasian Palaeontologists* 15, 407-416.

Müller, P.J., Kirst, G., Ruhland, G., Von Storch, I., Rosell-Melé, A., 1998. Calibration of the alkenone paleotemperature index U 37 K′ based on core-tops from the eastern South Atlantic and the global ocean (60 N-60 S). *Geochimica et Cosmochimica Acta* 62, 1757-1772.

Nelson, C.S., Cooke, P.J., 2001. History of oceanic front development in the New Zealand sector of the Southern Ocean during the Cenozoic - a synthesis. *New Zealand Journal of Geology and Geophysics* 44, 535-553.

Norris, R., Koons, P., Cooper, A., 1990. The obliquely-convergent plate boundary in the South Island of New Zealand: implications for ancient collision zones. *Journal of structural geology* 12, 715-725.

Ozaki, K., 1974. Miocene Floras of the Pacific Side of Central Japan (I) Inkyoyama Flora. 21, 1-21f.

Pagani, M., Arthur, M.A., Freeman, K.H., 1999. Miocene evolution of atmospheric carbon dioxide. *Paleoceanography* 14, 273-292.

Pancost, R.D., Steart, D.S., Handley, L., Collinson, M.E., Hooker, J.J., Scott, A.C., Grassineau, N.V., Glasspool, I.J., 2007. Increased terrestrial methane cycling at the Palaeocene–Eocene thermal maximum. *Nature* 449, 332-335.

Passchier, S., Bohaty, S., Jiménez-Espejo, F., Pross, J., Röhl, U., Flierdt, T., Escutia, C., Brinkhuis, H., 2013. Early Eocene to middle Miocene cooling and aridification of East Antarctica. *Geochemistry, Geophysics, Geosystems* 14, 1399-1410.

Pearson, A., Huang, Z., Ingalls, A., Romanek, C., Wiegel, J., Freeman, K., Smittenberg, R., Zhang, C., 2004. Nonmarine crenarchaeol in Nevada hot springs. *Applied and Environmental Microbiology* 70, 5229-5237.

Peterse, F., van der Meer, J., Schouten, S., Weijers, J.W.H., Fierer, N., Jackson, R.B., Kim, J.-H., Sinninghe Damsté, J.S., 2012. Revised calibration of the MBT–CBT paleotemperature proxy based on branched tetraether membrane lipids in surface soils. *Geochimica et Cosmochimica Acta* 96, 215-229.

Pitman, W., Golovchenko, X., 1991. The effect of sea level changes on the morphology of mountain belts. *Journal of Geophysical Research: Solid Earth* 96, 6879-6891.

Pole, M., 1994. The New Zealand flora-entirely long-distance dispersal? *Journal of Biogeography*, 625-635.

Posamentier, H., 1988. Eustatic controls on clastic deposition II—sequence and systems tract models.

Prahl, F., De Lange, G., Lyle, M., Sparrow, M., 1989. Post-depositional stability of long-chain alkenones under contrasting redox conditions. *Nature* 341, 434-437.

Prahl, F., Pilskaln, C., Sparrow, M., 2001. Seasonal record for alkenones in sedimentary particles from the Gulf of Maine. *Deep Sea Research Part I: Oceanographic Research Papers* 48, 515-528.

Prahl, F., Rontani, J.-F., Zabeti, N., Walinsky, S., Sparrow, M., 2010. Systematic pattern in–Temperature residuals for surface sediments from high latitude and other oceanographic settings. *Geochimica et Cosmochimica Acta* 74, 131-143.

Prahl, F., Wakeham, S., 1987. Calibration of unsaturation patterns in long-chain ketone compositions for palaeotemperature assessment. *Nature* 330, 367-369.

Prahl, F.G., Popp, B.N., Karl, D.M., Sparrow, M.A., 2005. Ecology and biogeochemistry of alkenone production at Station ALOHA. *Deep Sea Research Part I: Oceanographic Research Papers* 52, 699-719.

Pross, J., Contreras, L., Bijl, P.K., Greenwood, D.R., Bohaty, S.M., Schouten, S., Bendle, J.A., Röhl, U., Tauxe, L., Raine, J.I., 2012. Persistent near-tropical warmth on the Antarctic continent during the early Eocene epoch. *Nature* 488, 73-77.

Raymo, M., Ruddiman, W.F., 1992. Tectonic forcing of late Cenozoic climate. *Nature* 359, 117-122.

Rontani, J.-F., Volkman, J.K., Prahl, F., Wakeham, S.G., 2013. Biotic and abiotic degradation of alkenones and implications for paleoproxy applications: a review. *Organic Geochemistry* 59, 95-113.

Rontani, J.F., Prahl, F.G., Volkman, J.K., 2006. Re-examinationof the double bond positions in alkenonesand derivatives: biosynthetic implications. *Journal of phycology* 42, 800-813.

Royer, D.L., 2006. CO 2-forced climate thresholds during the Phanerozoic. *Geochimica et Cosmochimica Acta* 70, 5665-5675.

Sahagian, D., Pinous, O., Olferiev, A., Zakharov, V., 1996. Eustatic Curve for the Middle Jurassic--Cretaceous Based on Russian Platform and Siberian Stratigraphy: Zonal Resolution. *AAPG bulletin* 80, 1433-1458.

Schouten, S., Hopmans, E.C., Damsté, J.S.S., 2004. The effect of maturity and depositional redox conditions on archaeal tetraether lipid palaeothermometry. *Organic Geochemistry* 35, 567-571.

Schouten, S., Hopmans, E.C., Damsté, J.S.S., 2013. The organic geochemistry of glycerol dialkyl glycerol tetraether lipids: a review. *Organic Geochemistry* 54, 19-61.

Seki, O., Schmidt, D.N., Schouten, S., Hopmans, E.C., Sinninghe Damsté, J.S., Pancost, R.D., 2012. Paleoceanographic changes in the Eastern Equatorial Pacific over the last 10 Myr. *Paleoceanography* 27.

Shackleton, N.J., Kennett, J.P., 1975. Paleotemperature history of the Cenozoic and the initiation of Antarctic glaciation: oxygen and carbon isotope analyses in DSDP Sites 277, 279, and 281. *Initial reports of the deep sea drilling project* 29, 743-755.

Shackleton, N.J., Pisias, N., 1985. Atmospheric carbon dioxide, orbital forcing, and climate. *The Carbon Cycle and Atmospheric CO: Natural variations Archean to Present*, 303-317.

Sniderman, J.K., Woodhead, J.D., Hellstrom, J., Jordan, G.J., Drysdale, R.N., Tyler, J.J., Porch, N., 2016. Pliocene reversal of late Neogene aridification. *Proceedings of the National Academy of Sciences* 113, 1999-2004.

Steppuhn, A., Micheels, A., Geiger, G., Mosbrugger, V., 2006. Reconstructing the Late Miocene climate and oceanic heat flux using the AGCM ECHAM4 coupled to a mixed-layer ocean model with adjusted flux correction. *Palaeogeography, Palaeoclimatology, Palaeoecology* 238, 399-423.

Sturt, H.F., Summons, R.E., Smith, K., Elvert, M., Hinrichs, K.U., 2004. Intact polar membrane lipids in prokaryotes and sediments deciphered by high-performance liquid chromatography/electrospray ionization multistage mass spectrometry—new biomarkers for biogeochemistry and microbial ecology. *Rapid Communications in Mass Spectrometry* 18, 617-628.

Thiede, J., Winkler, A., Wolf-Welling, T., Eldholm, O., Myhre, A.M., Baumann, K.-H., Henrich, R., Stein, R., 1998. Late Cenozoic history of the polar North Atlantic: results from ocean drilling. *Quaternary Science Reviews* 17, 185-208.

Tierney, J.E., Tingley, M.P., 2014. A Bayesian, spatially-varying calibration model for the TEX 86 proxy. *Geochimica et Cosmochimica Acta* 127, 83-106.

Tierney, J.E., Tingley, M.P., 2015. A TEX86 surface sediment database and extended Bayesian calibration. *Scientific data* 2.

Tippett, J.M., Kamp, P.J., 1993. Fission track analysis of the late Cenozoic vertical kinematics of continental Pacific crust, South Island, New Zealand. *Journal of Geophysical Research: Solid Earth* 98, 16119-16148.

Tomczak, M., Godfrey, J.S., 2013. Regional oceanography: an introduction. Elsevier.
Van Sickel, W.A., Kominz, M.A., Miller, K.G., Browning, J.V., 2004. Late Cretaceous and Cenozoic sea-level estimates: backstripping analysis of borehole data, onshore New Jersey. *Basin Research* 16, 451-465.

Volkman, J.K., Barrerr, S.M., Blackburn, S.I., Sikes, E.L., 1995. Alkenones in Gephyrocapsa oceanica: Implications for studies of paleoclimate. *Geochimica et Cosmochimica Acta* 59, 513-520.

Walcott, R., 1998. Modes of oblique compression: Late Cenozoic tectonics of the South Island of New Zealand. *Reviews of Geophysics* 36, 1-26.

Wan, S., Kürschner, W.M., Clift, P.D., Li, A., Li, T., 2009. Extreme weathering/erosion during the Miocene Climatic Optimum: evidence from sediment record in the South China Sea. *Geophysical Research Letters* 36.

Warny, S., Askin, R.A., Hannah, M.J., Mohr, B.A., Raine, J.I., Harwood, D.M., Florindo, F., 2009. Palynomorphs from a sediment core reveal a sudden remarkably warm Antarctica during the middle Miocene. *Geology* 37, 955-958.

Waters, J.M., Craw, D., 2006. Goodbye Gondwana? New Zealand biogeography, geology, and the problem of circularity. *Systematic Biology* 55, 351-356.

Weijers, J.W., Schouten, S., Spaargaren, O.C., Damsté, J.S.S., 2006. Occurrence and distribution of tetraether membrane lipids in soils: implications for the use of the TEX 86 proxy and the BIT index. *Organic Geochemistry* 37, 1680-1693.

Weijers, J.W.H., Schouten, S., Sluijs, A., Brinkhuis, H., Sinninghe Damsté, J.S., 2007. Warm arctic continents during the Palaeocene–Eocene thermal maximum. *Earth and Planetary Science Letters* 261, 230-238.

White, W.B., Cherry, N.J., 1999. Influence of the Antarctic circumpolar wave upon New Zealand temperature and precipitation during autumn–winter. *Journal of Climate* 12, 960-976.

Wolfe, J.A., Tanai, T., 1980. The Miocene Seldovia point flora from the Kenai group, Alaska. US Government Printing Office.
Wood, R., Stagpoole, V., 2007. Validation of tectonic reconstructions by crustal volume balance: New Zealand through the Cenozoic. *Geological Society of America Bulletin* 119, 933-943.

World Sea Temperature, 2017. https://www.seatemperature.org/australia-pacific/new-zealand/canterbury/.
Yamamoto, M., Okino, T., Sugisaki, S., Sakamoto, T., 2008. Late Pleistocene changes in terrestrial biomarkers in sediments from the central Arctic Ocean. *Organic Geochemistry* 39, 754-763.

Zachos, J., Pagani, M., Sloan, L., Thomas, E., Billups, K., 2001. Trends, rhythms, and aberrations in global climate 65 Ma to present. *Science* 292, 686-693.

Zachos, J.C., Dickens, G.R., Zeebe, R.E., 2008. An early Cenozoic perspective on greenhouse warming and carbon-cycle dynamics. *Nature* 451, 279-283.

3.7. Supplementary: Tables

Table 3.1: Calculated lipid indices and reconstructed SST, MAAT, and soil pH for the samples from IODP Expedition 317

Site and Hole number	Sample number	Sample type[1]	Sample depth (mbsf[2])	Age (Ma)	BIT index	SST (TEX^H_{86}) (°C)	BIT altered SST (TEX^H_{86}) (°C)	$U^{K'}_{37}$ SST(°C)	CBT	MBT	pH	MAAT (°C)
U1351B	97X	c.s.	845.75	5.30	0.45	16.6	-	18.3	0.53	0.31	7.3	28.1
U1351B	100X	c.s.	871.62	5.52	0.34	15.4	15.4	19.5	0.69	0.36	6.9	27.3
U1351B	101X	c.s.	880.93	5.60	0.39	14.6	14.6	19.2	0.68	0.36	7.0	27.5
U1351B	103X	c.s.	900.04	5.76	0.31	17.0	17.0	19.9	0.64	0.33	7.2	28.9
U1351B	104X	c.s.	908.97	5.84	0.74	17.2	-	21.4	0.83	0.52	6.6	20.5
U1351B	106X	c.s.	929.41	6.01	0.56	15.3	-	20.0	0.66	0.37	7.0	26.2
U1351B	109X	c.s.	959.05	6.27	0.53	15.7	-	23.3	0.83	0.42	6.5	24.9
U1351B	112X	c.s.	989.18	6.52	0.31	17.2	17.2	22.4	0.62	0.33	7.2	28.5
U1352A	1H1	c.s.	1.05	0.00256	0.15	6.7	6.7	-	-	-	8.4	7.2
U1352A	1H2	sq.c	2.9	0.00706	0.44	12.2	-	-	-	-	6.8	4.7
U1352A	1H3	sq.c	3.86	0.00940	0.34	5.9	5.9	-	-	-	7.4	9.8
U1352A	2H1	c.s.	5.25	0.01279	0.41	7.8	-	-	-	-	7.1	7.7
U1352A	2H2	sq.c	7.1	0.01730	0.26	6.4	6.4	-	-	-	7.2	8.0
U1352A	2H3	sq.c	8.5	0.02071	0.28	6.5	6.5	-	-	-	7.2	10.1
U1352A	2H4	sq.c	10.1	0.02460	0.40	5.0	-	-	-	-	7.1	8.3
U1352A	2H5	c.s.	11.55	0.02814	0.45	-5.2	-	-	-	-	7.0	7.7
U1352A	2H6	sq.c	12.6	0.03069	0.30	5.3	5.3	-	-	-	7.3	7.9
U1352A	2H7	sq.c	13.35	0.03252	0.37	6.7	6.7	-	-	-	6.7	9.9
U1352A	3H1	c.s.	14.75	0.03593	0.35	5.3	5.3	-	-	-	7.0	5.6
U1352A	3H2	sq.c	16.6	0.04044	0.29	3.8	3.8	-	-	-	7.2	7.2
U1352A	3H3	c.s.	17.95	0.04373	0.29	6.7	6.7	-	-	-	7.4	9.1
U1352A	3H3	sq.c	18	0.04385	0.26	6.2	6.2	-	-	-	7.1	3.9
U1352A	3H4	sq.c	19.6	0.04775	0.21	5.0	5.0	-	-	-	7.8	11.5
U1352A	3H5	c.s.	21.05	0.05128	0.32	12.3	12.3	-	-	-	6.8	10.5
U1352A	3H6	sq.c	22.1	0.05384	0.32	3.0	3.0	-	-	-	7.3	7.9
U1352A	4H1	sq.c	24.3	0.05920	0.29	4.4	4.4	-	-	-	7.2	7.5
U1352A	4H3	c.s.	27.45	0.06687	0.26	8.6	8.6	-	-	-	7.3	7.9
U1352A	4H5	sq.c	30.6	0.07454	0.24	2.0	2.0	-	-	-	7.4	6.3
U1352A	5H1	c.s.	33.75	0.08222	0.51	9.0	-	-	-	-	7.0	1.9
U1352A	5H5	c.s.	40.05	0.09756	0.24	5.0	5.0	-	-	-	7.1	6.7
U1352A	5H7	sq.c	42.43	0.10336	0.21	11.5	11.5	-	-	-	7.2	2.3
U1352B	6H4	sq.c	52.1	0.12692	0.26	5.1	5.1	-	-	-	7.5	7.8
U1352B	7H4	sq.c	61.6	0.15006	0.37	6.4	6.4	-	-	-	7.3	7.1
U1352B	9H2	sq.c	77.6	0.18904	0.26	8.2	8.2	-	-	-	7.5	9.6
U1352B	11H2	sq.c	96.6	0.23532	0.50	3.0	-	-	-	-	7.9	7.9

Site and Hole number	Sample number	Sample type[1]	Sample depth (mbsf[2])	Age (Ma)	BIT index	SST (TEX^H_{86}) (°C)	BIT altered SST (TEX^H_{86}) (°C)	$U^{K'}_{37}$ SST(°C)	CBT	MBT	pH	MAAT (°C)
U1352B	13H2	sq.c	115.58	0.28156	0.20	1.1	1.1	-	-	-	7.9	10.1
U1352B	15H4	c.s.	137.27	0.42873	0.21	7.8	7.8	-	-	-	7.9	14.0
U1352B	19H2	sq.c	168.6	0.65317	0.35	12.1	12.1	-	-	-	7.4	10.6
U1352B	23H3	sq.c	203.1	0.79888	0.17	-1.9	-	-	-	-	8.0	11.2
U1352B	26H3	c.s.	231.37	0.87098	0.28	6.2	6.2	-	-	-	7.2	10.8
U1352B	28H2	sq.c	249.03	0.91602	0.22	6.0	6.0	-	-	-	8.4	5.1
U1352B	30H3	sq.c	262.1	0.94935	0.40	16.5	-	-	-	-	7.5	5.9
U1352B	32H3	sq.c	276.6	1.03943	0.25	2.3	2.3	-	-	-	8.1	5.4
U1352B	33H4	sq.c	286.04	1.10685	0.18	11.8	11.8	-	-	-	8.1	8.5
U1352B	37X1	c.s.	298.25	1.17210	0.26	6.2	6.2	-	-	-	7.9	5.2
U1352B	41X3	sq.c	335.9	1.18648	0.21	1.8	1.8	-	-	-	8.3	8.8
U1352B	48X3	c.s.	402.95	1.49304	0.36	8.6	8.6	-	-	-	7.6	8.9
U1352B	52X3	sq.c	441.5	1.73457	0.28	5.5	5.5	-	-	-	7.3	5.2
U1352B	56X3	sq.c	479.9	1.91166	0.12	6.3	6.3	-	-	-	7.9	4.3
U1352B	61X1	c.s.	524.25	2.76188	0.34	1.0	1.0	-	-	-	7.6	9.1
U1352B	68X1	sq.c	582.4	2.85396	0.13	5.0	5.0	-	-	-	7.8	6.0
U1352B	73X3	c.s.	633.35	2.98107	0.27	5.9	5.9	-	-	-	7.4	10.3
U1352B	77X1	sq.c	668.95	3.06988	0.33	5.4	5.4	-	-	-	7.4	5.5
U1352B	81X2	c.s.	708.8	3.16930	0.29	8.3	8.3	-	-	-	7.3	7.0
U1352B	85X2	sq.c	737.75	3.24152	0.44	15.5	-	-	-	-	7.4	2.6
U1352B	88X1	sq.c	764.85	3.30913	0.23	10.5	10.5	-	-	-	7.4	3.7
U1352B	90X1	sq.c	783.46	3.35556	0.21	9.5	9.5	-	-	-	7.2	2.9
U1352C	22R1	c.s.	816.27	3.43742	0.28	9.7	9.7	-	-	-	7.4	8.3
U1352C	24R1	sq.c	835.48	3.48534	0.21	7.0	7.0	-	-	-	7.6	4.9
U1352C	27R2	sq.c	864.61	3.55801	0.43	7.1	-	-	-	-	7.0	2.1
U1352C	29R1	c.s.	882.93	3.60372	0.22	7.3	7.3	-	-	-	7.8	9.3
U1352C	31R1 SC	sq.c	902.56	3.65269	0.14	10.7	10.7	-	-	-	7.5	2.7
U1352C	33R2 SC	sq.c	923.05	3.70381	0.21	6.4	6.4	-	-	-	7.6	3.2
U1352C	34R1	c.s.	930.84	3.72324	0.26	8.2	8.2	-	-	-	7.6	8.2
U1352C	38R3	sq.c	972.85	3.82805	0.25	8.8	8.8	-	-	-	7.5	2.1
U1352C	41R4	c.s.	1002.98	3.90322	0.28	9.0	9.0	-	-	-	7.6	6.6
U1352C	45R1	sq.c	1036.91	3.98787	0.21	9.8	9.8	-	-	-	7.4	2.8
U1352C	48R1	sq.c	1064.4	4.05645	0.35	9.0	9.0	-	-	-	7.5	2.8
U1352C	50R5	sq.c	1090.6	4.12181	0.21	5.3	5.3	-	-	-	7.2	-
U1352C	53R1	c.s.	1113.39	4.17867	0.22	8.4	8.4	-	-	-	7.4	7.5
U1352C	58R4	c.s.	1164.22	4.34678	0.18	4.1	4.1	-	-	-	7.8	7.8
U1352C	60R3	sq.c	1183.7	4.44890	0.19	9.3	9.3	-	-	-	7.6	0.3
U1352C	76R1	c.s.	1305.02	6.30000	0.07	12.8	12.8	23.8	0.45	0.27	7.6	29.5
U1352C	77R	c.s.	1309.64	6.45000	0.07	16.4	16.4	17.5	0.40	0.28	7.7	28.2
U1352C	78R	c.s.	1314.52	6.61000	0.08	15.3	15.3	17.8	0.25	0.27	8.1	29.4

Site and Hole number	Sample number	Sample type[1]	Sample depth (mbsf[2])	Age (Ma)	BIT index	SST (TEX^H_{86}) (°C)	BIT altered SST (TEX^H_{86}) (°C)	$U^{K`}_{37}$ SST(°C)	CBT	MBT	pH	MAAT (°C)
U1352C	79R	c.s.	1319.47	6.78000	-	-	-	-	-	-	-	-
U1352C	80R	c.s.	1326.05	7.00000	-	-	-	-	-	-	-	-
U1352C	81R	c.s.	1328.03	7.07000	-	-	-	-	-	-	-	-
U1352C	85R	c.s.	1351.57	7.85000	0.15	17.3	17.3	20	0.59	0.35	7.2	27.6
U1352C	86R	c.s.	1353.8	7.93000	0.06	19.6	19.6	-	0.41	0.32	7.7	27.8
U1352C	87R	c.s.	1367.05	8.37000	0.07	19.4	19.4	19.3	0.39	0.29	7.7	30.8
U1352C	87R4	c.s.	1370.02	8.38818	0.19	9.3	9.3	-	-	-	7.8	7.1
U1352C	88R	c.s.	1378.31	8.74000	0.32	16.1	16.1	22.4	0.67	0.36	7.0	27.2
U1352C	89R	c.s.	1385.71	8.99000	0.11	16.8	16.8	16.2	0.57	0.30	7.3	29.5
U1352C	90R	c.s.	1392.51	9.22000	0.03	17.1	17.1	17.9	0.27	0.21	8.1	32.6
U1352C	91R	c.s.	1406.54	9.69000	0.07	17.3	17.3	17.5	0.57	0.27	7.3	30.9
U1352C	94R5	c.s.	1435.7	10.49260	0.10	13.3	13.3	-	-	-	7.4	8.0
U1352C	102R	c.s.	1496.43	11.92000	0.11	19.8	19.8		1.11	0.52	5.8	21.4
U1352C	105R5	c.s.	1532.28	13.72090	0.10	18.9	18.9	-	-	-	6.9	11.1
U1352C	107R6	sq.c.	1553.57	14.09052	0.16	20.4	20.4	-	-	-	6.6	6.8
U1352C	110R2	c.s.	1576.94	14.49624	0.11	19.8	19.8	-	-	-	6.8	8.7
U1352C	115R5	c.s.	1630.05	15.41828	0.07	24.7	24.7	-	-	-	7.1	10.4
U1352C	125R3	c.s.	1711.3	16.82886	0.08	22.1	22.1	-	-	-	7.3	7.2
U1352C	134R2	c.s.	1795.78	18.29552	0.07	27.0	27.0	-	-	-	6.4	2.4
U1352C	139R	c.s.	1842.11	18.87000	0.03	26.0	26.0	-	-	0.59	-	-
U1352C	140R	c.s.	1851.46	19.06000	-	-	-	-	-	-	-	-
U1352C	143R	c.s.	1875.04	30.87000	-	-	-	-	-	-	-	-
U1352C	144R3	c.s.	1883.97	31.01736	0.12	22.1	22.1	-	-	-	-	-
U1352C	144R	c.s.	1884.51	31.02000	0.46	25.6	-	-	-	0.22	-	-
U1352C	145R	c.s.	1891.76	31.14000	0.05	21.5	21.5	-	-	0.47	-	-
U1352C	146R	c.s.	1900.92	31.29000	0.24	-	-	-	-	0.31	-	-
U1352C	147R	c.s.	1913.24	31.50000	0.20	-	-	-	-	0.73	-	-
U1352C	148R	c.s.	1917.9	31.57000	-	-	-	-	-	-	-	-
U1352C	148R3	c.s.	1922.2	35.28397	0.19	29.8	29.8	-	-	-	-	-
U1353B	88X	c.s.	510.09	12.03	0.50	17.5	-	21.6	0.75	0.39	6.8	26.7
U1353B	93X	c.s.	556.82	13.13	0.53	22.6	-	21.4	0.80	0.39	6.7	26.7
U1353B	95X	c.s.	576.28	13.59	0.53	16.0	-	22.1	0.78	0.35	6.8	28.3
U1353B	96X	c.s.	585.57	13.81	0.69	14.5	-	26.2	0.91	0.44	6.4	25.1

[1] sq.c. = squeeze cake; c.s. = cut sample

[2] mbsf = meters below sea floor

Appendix 3.1: Calculated weight of the alkenone isotopes $C_{37:2}$ and $C_{37:3}$ in analysed samples

Site and Hole number	Sample number	Lithological unit	Sample type[1]	Sample depth (mbsf[2])	Age (Ma)	Extraction type	$C_{37:2}$ (ng/g sediment)	$C_{37:3}$ (ng/g sediment)	$U^{K'}_{37}$ SST (°C)
U1351B	97X	II	c.s.	845.75	5.30	ASE	2.98	1.56	18.3
U1351B	100X	II	c.s.	871.62	5.52	ASE	0.01	0.003	19.5
U1351B	101X	II	c.s.	880.93	5.60	ASE	0.75	0.34	19.2
U1351B	103X	II	c.s.	900.04	5.76	ASE	0.57	0.23	19.9
U1351B	104X	II	c.s.	908.97	5.84	ASE	0.01	0.003	21.4
U1351B	106X	II	c.s.	929.41	6.01	ASE	0.35	0.14	20.0
U1351B	109X	II	c.s.	959.05	6.27	ASE	0.07	0.02	23.3
U1351B	112X	II	c.s.	989.18	6.52	ASE	0.03	0.01	22.4
U1352C	76R1	IIB	c.s.	1305.02	6.30	ASE	0.50	0.09	23.8
U1352C	77R	IIB	c.s.	1309.64	6.45	ASE	0.22	0.13	17.5
U1352C	78R	IIB	c.s.	1314.52	6.61	ASE	0.07	0.04	17.8
U1352C	85R	IIB	c.s.	1351.57	7.85	ASE	0.40	0.16	20.0
U1352C	86R	IIB	c.s.	1353.8	7.93	ASE	0.18	-	-
U1352C	87R	IIB	c.s.	1367.05	8.37	ASE	0.13	0.06	19.3
U1352C	88R	IIB	c.s.	1378.31	8.74	ASE	0.91	0.23	22.4
U1352C	89R	IIB	c.s.	1385.71	8.99	ASE	0.04	0.03	16.2
U1352C	90R	IIB	c.s.	1392.51	9.22	ASE	0.06	0.03	17.9
U1352C	91R	IIB	c.s.	1406.54	9.69	ASE	0.08	0.05	17.5
U1353B	88X	II	c.s.	510.09	12.03	ASE	0.61	0.46	21.6
U1353B	93X	II	c.s.	556.82	13.13	ASE	1.91	0.57	21.4
U1353B	95X	II	c.s.	576.28	13.59	ASE	1.43	0.41	22.1
U1353B	96X	II	c.s.	585.57	13.81	ASE	1.55	0.16	26.2

[1] c.s. = cut sample

[2] mbsf = meters below sea floor

4. Global climate trends during the Miocene examined through an organic geochemistry prism: comparison of the biomarker data from cored sedimentary rocks from IODP Expeditions 317 (Canterbury Basin, New Zealand) and 313 (New Jersey continental shelf)

Sophia Aharonovich[1*] and Simon C. George[1]

[1] Department of Earth and Planetary Sciences and Macquarie Marine Research Centre, Macquarie University, NSW, Australia

* corresponding author (e-mail: sophia.aharonovich@mq.edu.au)

Statement of authors' contribution

This Chapter is an article to be submitted to *Paleoceanography, Paleoclimatology, Paleoecology*. This paper has been formatted to conform to the font and referencing style adopted in this thesis. Section, Figures, and Tables included within the text are prefixed with the chapter number.

I am the primary author (90% of the effort). I extracted the organic material from the samples. I analysed the organic data and created the proposed climate reconstructions. I wrote and designed the structure of the paper. The co-author carefully reviewed and provided feedback and valuable refinements on this version of the manuscript (10%). Neither this manuscript nor one with similar content under our authorship has been published or is being considered for publication elsewhere, except as described above.

Abstract

Significant climate changes during the Cenozoic (the last 66 million years) have been recorded by multiple proxies from around the world. A general cooling pattern can be seen through the Cenozoic, but the Miocene is characterised as globally warm. An overall increase in aridity related to mountain building caused grassland expansion and was recorded around the globe during the middle and late Miocene. At the same time, continental isolation of Antarctica and formation of the Antarctic Circumpolar Current caused significant changes in global oceanic and atmospheric circulations. These processes reduced the mixing of warm, tropical ocean water and cold, polar water, which caused the build-up of the Antarctic polar ice cap, the global ocean and land temperatures to decrease, followed by development of seasonality and aridity in various regions.

To investigate the relative importance of eustatic and local influences on climate in the Miocene, two Integrated Ocean Discovery Program (IODP) expedition locations were studied. The main purpose of IODP Expedition 313 on the New Jersey continental shelf, was to estimate the corresponding amplitudes, rates, and mechanism of sea-level changes through dating of the Late Paleogene–Neogene deposits, and by comparing these to the sea level lowering proposed by interpretation of the $\delta^{18}O$ glacio-eustatic proxy. The recovered sediments were dated from the late Eocene to the early Miocene, and provide a nearly continuous composite of sea level cycles between 22 and 12 Ma. The purpose of IODP Expedition 317 in the Canterbury Basin, New Zealand was to compare the relative influence of local tectonics and global sea level changes on sediments accumulated on the continental shelf and slope off the east coast of the South Island. The recovered cored sediments dated from the early Oligocene to the Holocene, and there was a particular focus on the sequence stratigraphy of the last 19 million years, when global sea level changes were dominated by glacioeustasy. This paper provides the first cross-correlation of the organic geochemical

record of early Oligocene to late Miocene sediments from three IODP drilling sites from these two expeditions: M0027A, M0028A, and U1352.

The continental slope site from New Zealand has much lower total organic carbon (TOC) values than the two continental shelf sites from the New Jersey region. Based on *n*-alkanes, isoprenoids, GDGTs and TOC data, the late-early Miocene and early-middle Miocene periods are interpreted to have been strongly influenced by global sea level decreases. Variations in interpreted sea surface temperatures at both locations show a general decrease in water temperature from the early Oligocene to the late Miocene, with a temporary increase around the early/middle Miocene boundary for the New Jersey region. Soil pH data derived from brGDGT data for the New Zealand samples suggest a decrease in precipitation levels during the Miocene, but the New Jersey samples show a different soil pH pattern during the Miocene, suggesting a regional increase in precipitation. The New Jersey samples show a strong dependence on eustasy around the mid-Miocene Climatic Optimum and afterwards, but the New Zealand samples show a much stronger dependence on local tectonic activity and creation of the land mass during the same period.

4.1. Introduction

Significant climate changes during the Cenozoic (the last 66 million years) have been recorded by multiple proxies from around the world (e.g. Zachos et al., 2001; Zachos et al., 2008). A general cooling pattern can be seen through the Cenozoic, but the Miocene can be characterised as globally warm. An overall increase in aridity has been suggested to be related to mountain building caused grassland expansion (Pagani et al., 1999; Zhisheng et al., 2001; Keeley and Rundel, 2005). In North America, the build-up of the Sierra Nevada and Cascade Mountain ranges created a drier climate, with a decrease in rainfall during the middle and late Miocene (Poage and Chamberlain, 2002; Retallack, 2004). In Australia, a mixture of wet and dry periods occurred during the Miocene (Flower and Kennett, 1994; Martin, 2006). By the late Miocene the rainforests in Australia began to decrease and were replaced by dry forests and woodlands. Eurasia also experienced increasing aridification during the Miocene. These climatic changes were related to significant tectonic rearrangements – the closing of the Tethys connection between the Mediterranean and the Indian Ocean (Heine et al., 2004; Metcalfe, 2013), and the Himalaya mountain and Tibetan plateau uplift (Zhisheng et al., 2001; Clift et al., 2008). This uplift was associated with rifting in East Africa and the union of the African-Arabian and Indian plates with Eurasia. These tectonic processes were related to development of the Asian Monsoon (Zhisheng et al., 2001) and creation of a rain shadow effect between wet Central-West Africa and dry East Africa (Bonnefille, 2010). Moreover, Antarctica became isolated from the other continents in the Miocene, leading to the formation of the Antarctic Circumpolar Current which caused significant changes in global ocean and atmospheric circulations during the Miocene (e.g., Tynan, 1998; Lawver and Gahagan, 2003; Passchier et al., 2013). These changes reduced the mixing of warm, tropical ocean water and cold, polar water, causing the build-up of the Antarctic polar ice cap which caused global cooling and accelerated the development of global seasonality and aridity.

Global paleoclimate reconstructions during the Cenozoic mostly rely on $\delta^{18}O$ and Mg/Ca ratios from foraminiferal records (Zachos et al., 2008). These data provide information regarding the sea surface temperatures (SST) and changes in global ice volume levels (Keigwin and Keller, 1984; Shackleton and Pisias, 1985; Miller et al., 1991). The oxygen isotope record suggests global SST decreased from the early Eocene all the way through the Neogene (Zachos et al., 2001; Zachos et al., 2008), with a warm period called the "mid-Miocene Climatic Optimum" (Flower and Kennett, 1994; Böhme 2003). One of the challenges in Cenozoic climate reconstructions is to separate the regional and global triggers that prompted these changes (Zachos et al., 2008). One option is to analyse sediments accumulated under similar conditions in different geographical areas. This enables global sea-level changes (eustasy) influenced by high tectonic activity (Haq et al., 1987; Van Sickel et al., 2004) and quasi-periodic oscillations in Earth's orbital parameters (eccentricity, obliquity, and precession) (Miller et al., 2005) to be distinguished from local or regional tectonic activity that controls sedimentary distribution on the continental margins (Van Sickel et al., 2004).

To investigate the relative importance of eustatic and local influences on climate in the Miocene, two Integrated Ocean Discovery Program (IODP) expedition locations were studied. The main purpose of IODP Expedition 313, which occurred from April to July 2009 on the New Jersey continental shelf (Fig. 4.1B) off the east coast of the United States of America. The purpose of the expedition was to estimate the corresponding amplitudes, rates, and mechanism of sea-level changes through dating of the Late Paleogene–Neogene deposits, by comparing these to the sea level lowering proposed by interpretation of the $\delta^{18}O$ glacio-eustatic proxy (Mountain et al., 2010). The sedimentary sequences were drilled in a transect of three sites (Fig. 4.1B) on the continental shelf (landward to basinward: Sites M0027A, M0028A, and M0029A) (Mountain et al., 2010). The recovered sediments from the three sites were dated from the late Eocene to the early Miocene, and provide a nearly continuous

composite of sea level cycles between 22 and 12 Ma (Mountain et al., 2010). The New Jersey sediments enable the study of the influence of eustasy versus local tectonic activity on the formation and preservation of these long geological sequences.

The main purpose of IODP Expedition 317, which occurred from November 2009 to January 2010 in the Canterbury Basin, New Zealand (Fig. 4.1A), was to compare the relative influence of local tectonics and global sea level changes on sediments accumulated on the continental shelf and slope off the east coast of the South Island. The recovered cored sediments dated from the early Oligocene to the Holocene, and there was a particular focus on the sequence stratigraphy of the last 19 million years, when global sea level changes were dominated by glacioeustasy (Fulthorpe et al., 2011c). Sedimentary sequences (Fig. 4.1A) were drilled in a transect of three sites on the continental shelf (landward to basinward, Sites U1353, U1354, and U1351) and one on the continental slope (Site U1352) (Fulthorpe et al., 2011c). The Canterbury Basin sedimentary record enables the examination of the accumulated biomarker signal in the region. A global climatic optimum at the early/middle Miocene boundary (Nelson and Cooke, 2001a) was accompanied by the growing land mass of the sub-continent, based on an increase in sedimentation rates since the middle Miocene (King, 2000; Lu et al., 2005). This observation suggests gradual intensification in the amount of land vegetation. Interpretation of global eustatic and climatic transformations suggest that cooler Neogene seawater conditions were coupled with a decrease in global sea levels (Zachos et al., 2001; Van Sickel et al., 2004). Therefore, the influence of this climate shift on the accumulation and preservation of organic matter in the marine sediments is expected.

Correlations between increasing CO_2 concentrations and increases in global SST have been proposed (Zachos et al., 2008). During the Cenozoic the global climatic optima that are related to high temperature levels, warm poles and no ice cover are associated with high pCO_2 (Zachos et al., 2001). The CO_2 levels were calculated using various proxy data sets such as boron, alkenones, and nahcolites from marine and lacustrine environments (Royer, 2006).

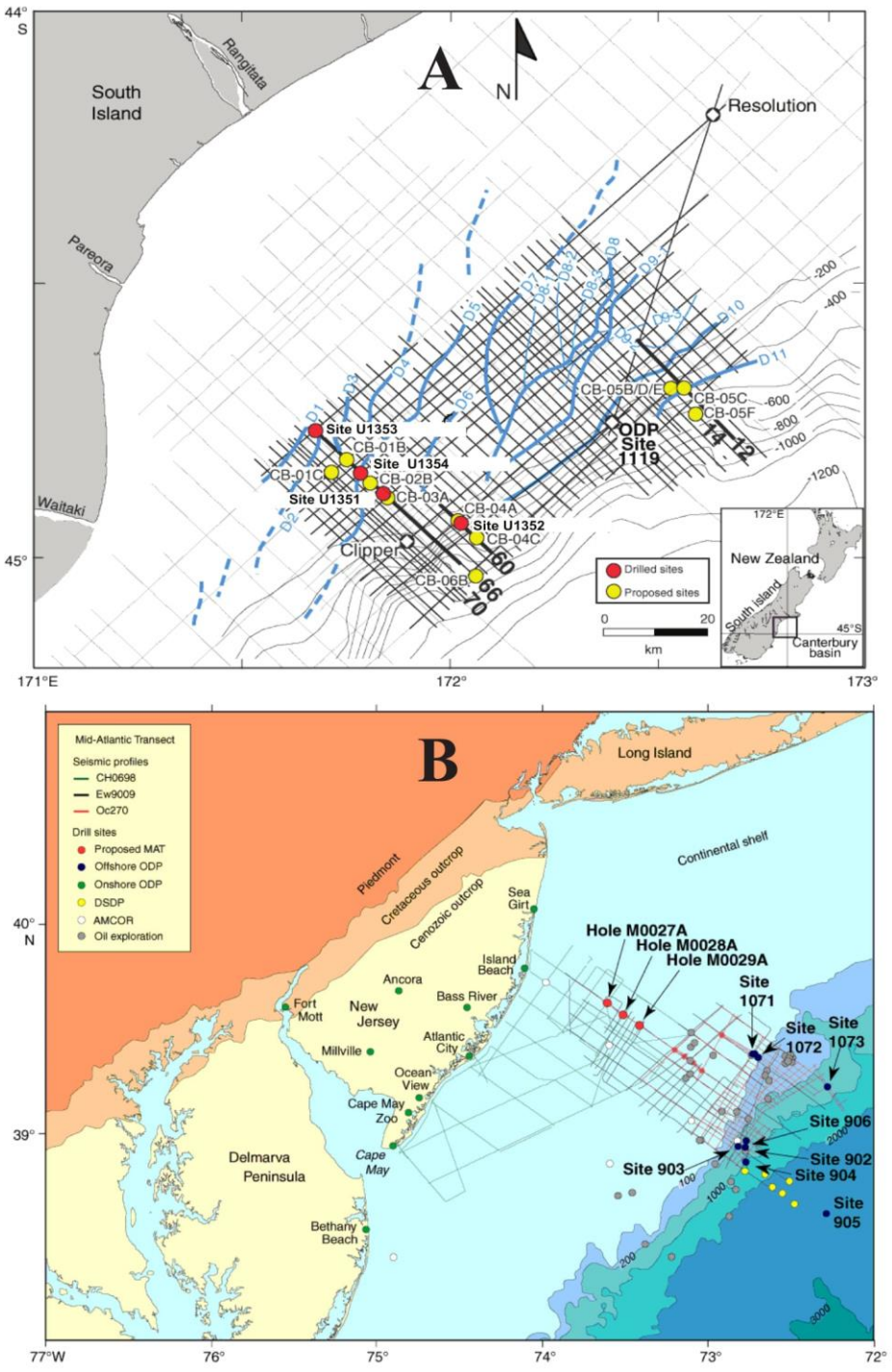

Figure 4.1: Drilled and proposed Expedition 317 (Fulthorpe et al., 2011c) (**A**) and Expedition 313 (Mountain et al., 2010) (**B**) sites, with the multichannel seismic (MCS) commercial low-resolution grids. Blue curved lines show the distribution of seismically-resolvable sediment drifts

Eustatic sea-level changes are influenced by variations in the ice sheet volumes around the globe, mainly in Antarctica and Greenland. These variations are strongly related to

temperature variations (Haq et al., 1987; Van Sickel et al., 2004; Miller et al., 2005). The imprint of Cenozoic sea level changes can be seen in sediments and sedimentary rocks on continental margins (Posamentier, 1988; Kominz et al., 1998; Van Sickel et al., 2004). While accumulation and melting of large continental ice sheets is proposed to be responsible for large (>100 m) sea-level fluctuations (Haq et al., 1987; Pitman and Golovchenko, 1991), smaller changes, up to 25 m, can be related to modest climatic changes and ice volume fluctuations (Miller et al., 1998; Miller et al., 2003; Van Sickel et al., 2004). The sequence stratigraphic modelling described by Haq et al. (1987) is still widely used. Later stratigraphic modelling based on the accumulation of sediments on the Siberian Platform (Sahagian et al., 1996) and the New Jersey Margin (Van Sickel et al., 2004) suggest slightly different global sea level fluctuations. The global eustatic sequence was updated lately based on the new accumulated data (Miller et al., 2005). High levels of disagreement between all sea-level models for the Cenozoic are observed for the first half of the Neogene (to 11 Ma).

The modern New Zealand subcontinent lies at the interface between the southwest Pacific Ocean and the Southern Ocean (Nelson and Cooke, 2001a; Tomczak and Godfrey, 2013). Tectonic reconstructions show significant movement of the New Zealand land mass to the north for the last 40 Ma (King, 2000; Nelson and Cooke, 2001a). These models also suggest the presence of some New Zealand land mass from the Oligocene (King, 2000) for the South Island, and the first appearance of the Southern Alps as early as the middle Miocene (~11 Ma) (Wood and Stagpoole, 2007). Rapid uplift of the Southern Alps with an associated significant increase of the land mass is proposed from 7-6 Ma (Nelson and Cooke, 2001a).

Tropical and subtopical ocean temperatures have been proposed for the New Zealand region at the Oligocene/Miocene boundary, based on planktonic foraminifera (Jenkins, 1965) and $\delta^{18}O$ (Shackleton and Kennett, 1975). The development of multiple Antarctic fronts during the Neogene caused a decrease in the SST around New Zealand (Lawver et al., 1992; Nelson and Cooke, 2001a). From the early Miocene the recorded SSTs are strongly influenced by

cold intrusions of the sub-Antarctic currents, especially around the east coast of New Zealand (Nelson and Cooke, 2001). This influence increased from the middle Miocene, ~ 15 Ma. These reconstructions are supported by land fossil records from New Zealand, which show warm-water environments for the first part of the Neogene (Chaproniere, 1984; Beu et al., 1997).

Simulations of global late Miocene terrestrial temperatures between 11.6-5.3 Ma show warmer conditions than the modern climate, with mean annual air temperatures (MAAT) 3.8ºC higher than preindustrial ones (Lunt et al., 2008). Steppuhn et al. (2006) proposed a simulation that calculated the late Miocene MAAT for the Australasian region to be between 15.6 ºC and 26.6 ºC. However, the reconstructed values should be used carefully due to a large calculation error (±5ºC) in the MAAT estimation (Weijers et al., 2007).

Palynological evidence supported by moisture availability and the spread of fire in the New Zealand area suggests a warm temperate climate for the early Miocene (Mildenhall et al., 2003; Pole, 2003). This model contradicts the previously suggested cool early Miocene climate (Pockhall, 1989). Miocene cooling in New Zealand regions arguably started from 14 Ma (Molnar and Pole, 1997; Pole et al., 2003). However, these climate reconstructions are commonly based on plant fossil evidence (e.g., Utescher et. al., 2000) and on structural fossil leaf analyses (e.g. Fricke and Wing, 2004; Wing et al., 2005). These can be problematic due to poor plant preservation in the geological record and the difficulty of finding the fossils for all geological intervals.

This paper provides the first cross examination of the organic geochemical record from three IODP drilling sites (Tables 4.1-4.3). IODP Expedition 313 is represented by 18 samples from the M0027A Site, dated from late Oligocene to middle Miocene, and by 25 samples from the M0028A Site dated from early to late Miocene. IODP Expedition 317 is represented by 55 samples from the continental slope site (U1352), dated from early Oligocene to late Miocene.

The hydrocarbon and biomarker data sets show the differences between local tectonic and eustatic influences on the organic reservoirs in the Canterbury Basin and New Jersey sediments. The main aim of this research is to find evidence of global climatic transformations in hydrocarbon and biomarker data in both sites through the Miocene, and distinguish these from local tectonic activity influences.

4.2. Materials and methods

4.2.1. Lithology, age/depth models and sample collection

The 55 analysed samples from Site U1352 (Fig. 4.1A) are from the late Oligocene and the early, middle and late Miocene, and are dated from 31.50 to 5.49 Ma (Tables 4.1 and 4.2). The samples represent geological units II and III (Fulthorpe et al., 2011c; Marsaglia et al., 2017). The age model is presented in Fig. 4.2. The age-depth model shows four hiatuses in the recovered sequence.

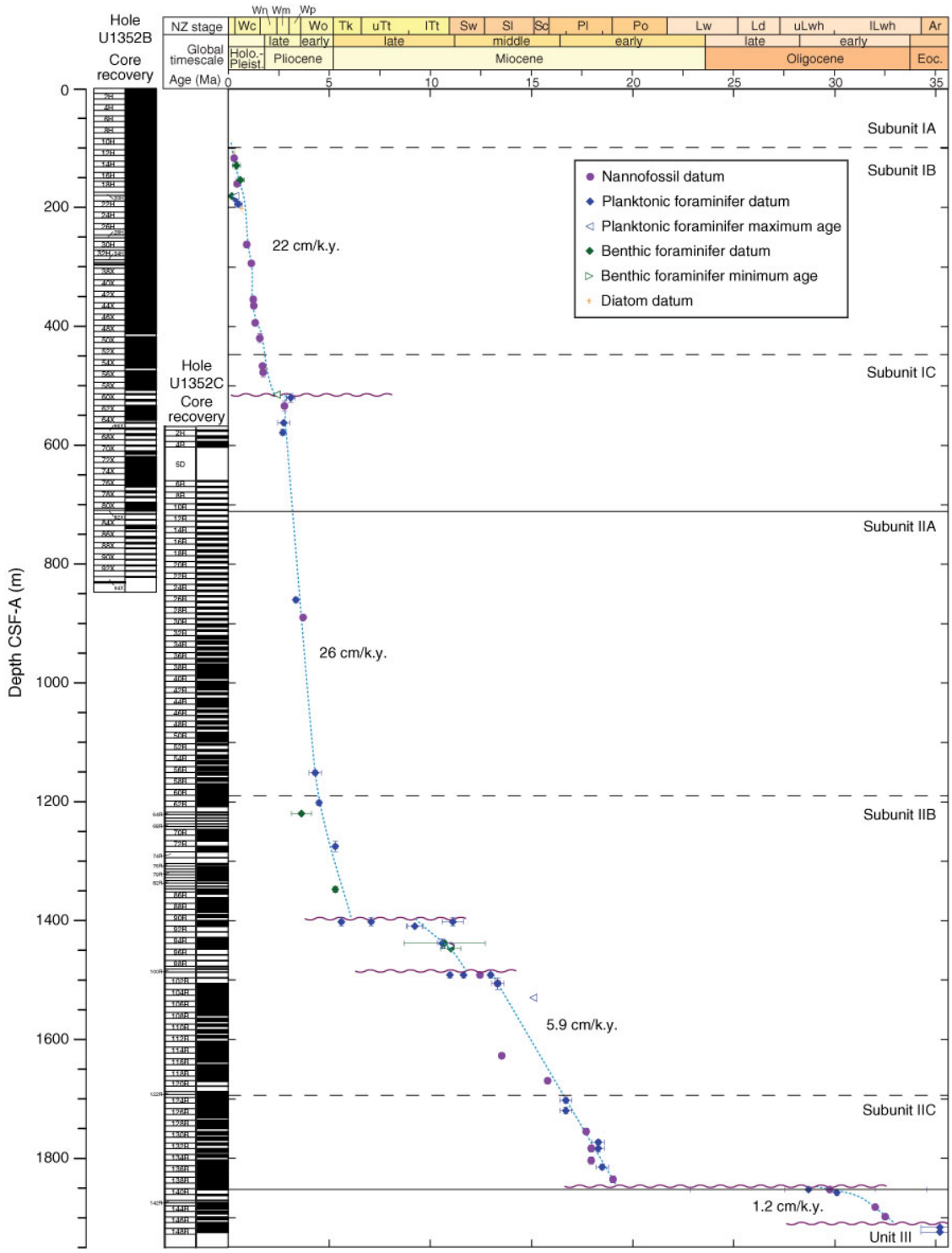

Figure 4.2: Age-depth plot for Holes U1352B and U1352C. Sedimentation rates are tentative and based on visual correlation of data. Hiatuses are marked as purple waves (Fulthorpe et al., 2011c).

The 18 samples from Site M0027 and the 25 samples from Site M0028 are from the early–late

Miocene, dated from ~ 28.37 to 5.85 Ma and representing geological units VIII to III

(Mountain et al., 2010). The age model is presented in Fig. 4.3. The age-depth model shows several hiatuses in the recovered sequence.

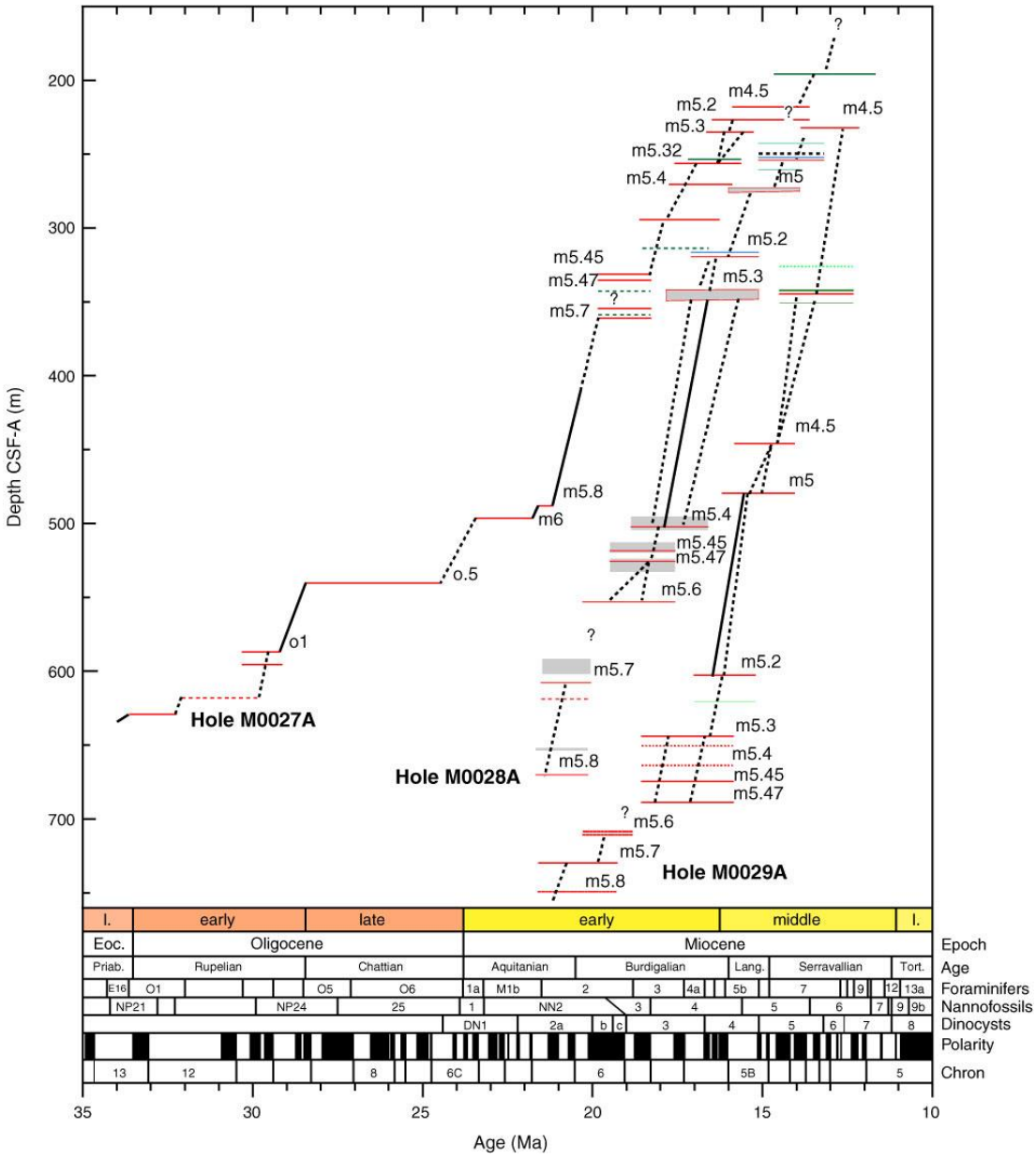

Figure 4.3: Expedition 313 chronology for the uppermost Eocene to Pleistocene section, based on integrating biostratigraphy and Sr isotopic ages obtained in Holes M0027A–M0029A (Mountain et al., 2010).

4.2.1.1. IODP 317

The eastern margin of the South Island of New Zealand is part of a continental fragment, the New Zealand Plateau, that started rifted from Antarctica at ~80 Ma. The rifting continued to be active until ~55 Ma. This rifting linked the Indian and Pacific Oceans through the southern Tasman Sea in the late Eocene (Molnar et al., 1975).

The Canterbury Basin lies at the landward edge of the rifted continental fragment and underlies the present-day onshore Canterbury Plains and offshore continental shelf (Field and Browne, 1989). Basin sediments thin toward the Bank and Otago peninsulas. The basin formed part of a simple passive margin from the Late Cretaceous to the late Eocene.

The Alpine Fault formed during the earliest Miocene (~23 Ma) (Kamp, 1987; King, 2000) and was recorded by the deposition of a widespread shelf siltstone (the Bluecliffs Formation), starting in the latest Oligocene or earliest Miocene. The uplift of the Southern Alps accelerated at ~8–5 Ma (Tippett and Kamp, 1993; Batt et al., 2000) or at ~10–8 Ma (Carter and Norris, 1976; Adams, 1981; Norris et al., 1990), leading to an increase in the rate of sediment supply to the offshore Canterbury Basin (Lu et al., 2005). Large sediment drifts within the basin suggest that similar currents existed throughout much of the Neogene (Fulthorpe and Carter, 1991; Carter et al., 2004).

This study is based on a set of sedimentary samples from Site U1352 located on the upper slope within the Canterbury Basin, New Zealand (Fig. 4.1A). Hydrocarbon and biomarker contents were determined for 55 samples from lithological units II and III, dated from the late Oligocene to the late Miocene, with one sample dated to the late Eocene (Table 4.2; 4.3). Lithological units were defined based on the observed variation in lithology in the cores (Fulthorpe et al., 2011c). The age model for the site is based on the shipboard study of calcareous nannofossils, diatoms, and planktonic and benthic foraminifera (Fulthorpe et al., 2011c). The bottom part of Hole C is dated to 36.0 – 35.2 Ma in the Eocene (Fulthorpe et al., 2011c), which is followed by the Eocene to early Oligocene (Unit III) hemipelagic to pelagic foraminifer-bearing nannofosil limestones with minor amounts of quartz and clay sediments (Fulthorpe et al., 2011c). This unit is correlative to the onshore Amuri Limestone and is followed by a long unconformity from 19–30.1 Ma (1916.63 – 1903.29 mbsf). Six samples representing the early Oligocene from unit III, below 1875 mbsf, were analysed.

The lower part of Unit II is dated to the early to middle Miocene and consists of a gradual progression from marlstone to limestone with frequent glauconitic laminae and beds (Marsaglia et al., 2017). There is a large unconformity of 12–11 million years between 1875.46 and 1851.46 mbsf (Fulthorpe et al., 2011c). Good sediment recovery led to an excellent record of the Miocene. The Miocene part of unit II, represented by 55 samples, consists of a low frequency of dark-coloured mudstone beds. There are also hiatuses in deposition between 1496.91 and 1486.78 mbsf, where 1.3 million years are missing, and between 1409.66 and 1394.62 mbsf, where at least 5 million years are missing (Fulthorpe et al., 2011c). The Miocene part of the lithological unit IIB is characterised by hemipelagic and pelagic sedimentation in Hole C (1851–1275 mbsf) (Marsaglia et al., 2017). The late Miocene/early Pliocene boundary is between 1284 and 1266 mbsf.

4.2.1.2. IODP 313

The New Jersey–Delaware–Maryland middle Atlantic margin is a classic passive margin initiated in the late Triassic (~230 Ma) with sea floor spreading from the middle Jurassic (Sheridan and Grow, 1988; Withjack et al., 1998). The sediment accumulation rates were generally low during the late Cretaceous to Paleogene, which are characterised by siliciclastic and carbonate deposition (Poag, 1985). A major switch from carbonate ramp deposition to starved siliciclastic sedimentation occurred in the late middle Eocene onshore to earliest Oligocene on the slope in response to global and regional cooling (Miller et al., 1998). Sedimentation rates increased dramatically in the late Oligocene to Miocene (Poag, 1985; Miller et al., 1998), which could be related to tectonics in the hinterland. Also, some greenhouse sequences during the Cretaceous and the Eocene that are related to eustasy were recognised (Miller et al., 1991, 1998, 2003).

This study is based on a set of sedimentary samples from Sites M0027 and M0028 located on the shallow New Jersey Shelf off the east coast of the United States of America (Fig. 4.1B). Hydrocarbon and biomarker contents were analysed in 43 samples from lithological units II – VII dating from the early Oligocene to late Miocene (Tables 4.2 and 4.3). The lithological units were defined based on the observed variation in lithology of the cores (Mountain et al., 2010). The age model for the sites is based on the shipboard analysis of calcareous nannofossils, diatoms, and planktonic and benthic foraminiferas (Mountain et al., 2010). Of the analysed samples from Expedition 313, only 26 had a strong *n*-alkane signal (Table 4.2). Of these samples, two are from the early Oligocene, fifteen are from the early Miocene, and nine are from the middle Miocene.

The M0028 Site was drilled on the shallow New Jersey continental shelf, but further offshore than Site M0027 (Fig. 4.1B). The M0027 Site sediments are dated from the late Eocene to the Pleistocene, without the Pliocene. The M0028 Site sediments are dated from early to late Miocene (Mountain et al., 2010). Of the analysed samples from Site M0027, eleven have *n*-alkanes suitable for analysis (Table 4.2), and eighteen samples have high lipid contents (Table 4.3). Fifteen samples were analysed from the M0028 Site (Tables 4.2 and 4.3).

The recovered sediment is divided into eight lithostratigraphic units and only units II – VII were sampled for this study (Mountain et al., 2010). Unit VII is dated to the early Oligocene–early Miocene for the M0027 Site and to early Miocene for the M0028 Site. Unit VII at Site M0027 consists of silt, very fine sand and poorly sorted glauconite-rich coarse sand with some signs of bioturbation. Unit VII at the M0028 Site comprises dark brown siltstone with thin-walled articulated shells deposited in a deep offshore environment.

Unit VI for both sites is dated to the early Miocene and consist of a pale brown clayey silt with intercalated fine sand beds. The overlying unit V at the M0027 Site is dated to the late-

early Miocene and shows an abrupt change to poorly sorted glauconite-rich sand. Unit V at the M0027 Site (middle-early Miocene) consist of turbidites with poorly sorted coarse sediments.

Unit IV is dated to the late-early Miocene for both sites and comprises a transition from a shoreface to an offshore facies. Unit II at the M0027 Site is dated to the middle Miocene and consists of shoreface to an offshore facies, with clay-rich layers in the upper part of the unit. Unit II at the M0028 Site (middle Miocene) consists of poorly sorted, coarse grained sediments, followed by transgressive and shore face to offshore and regressive offshore to shoreface sedimentary cycles.

In general, Units VII and VI consist of sediments deposited in a river dominated offshore environment, followed by Unit V turbidites deposited during river flood events in an offshore environment. Unit IV is defined as multiple river flood events in an offshore environment, and Unit III consist of storm dominated and river-influenced deltaic sediments. Unit II is defined as a series of transgressive shore face to offshore and regressive offshore to shore face sedimentary cycles influenced by eustatic changes (Mountain et al., 2010).

An erosional surface separates unit IV and III (295.01–236.16 mbsf; middle Miocene), which comprises deepening- and shallowing-upward packages of silt with periodic major storm influences, and is followed by sediments defined as unit IV (525.52–512.29 mbsf).

Unit II (236.16–167.74 mbsf) is dated to the middle Miocene and consists of a series of deepening-upward sedimentary cycles deposited in environments evolving from a shoreface to an offshore facies, with clay-rich layers in the upper part of the unit. Unit II (335.37–223.33 mbsf; middle Miocene) consists of poorly sorted, coarse grained sediments, followed by transgressive and shore face to offshore and regressive offshore to shoreface sedimentary cycles.

4.2.2. IODP 313 and IODP 317 total organic carbon measurements

For the IODP 313 samples (Methods in Mountain et al., 2010) the total organic carbon (TOC) measurements were analysed at the University of Bremen straight after the expedition. Five cm^3 of sediment was freeze dried and finely ground by hand in an agate mortar. Sediment samples were analysed for contents of organic carbon and carbonate using a LECO CS-125 carbon-sulphur analyser. About 50 mg of dried, ground sample were analysed for the CO_2 and SO_2 content using a nondispersive infrared detector. A second aliquot of ~90 mg was weighed in a ceramic cup, reacted with 12.5% HCl twice, washed with deionised water twice, and reanalysed as above. The CO_2 measured in the second run was assumed to come from organic carbon. The analytical precision was about ±0.02% absolute. Sample data are summarised in Table 4.1.

For the IODP 317 samples TOC and total nitrogen (TN) analyses were performed on board (Methods in Fulthorpe et al., 2011b). Nominally 10 cm^3 wet volume (about 3 g dry mass) of sediment was selected based on the changes in lithology, with organic-rich lithologies identified based on visual differences. Dried samples were crushed and homogenised to a fine powder. The inorganic carbon (IC) content was determined by a UIC 5011 CO_2 coulometer. About 10 mg of the sample was reacted with 1N HCl. Total carbon (TC) and the TN content of the sediment samples were determined using a ThermoElectron FlashEA 1112 elemental analyser equipped with a ThermoElectron packed column (CHNS/NCS) and a thermal conductivity detector (TCD). Between 8-12 mg of each sample was mixed with one small spatula of vanadium pentoxide catalyst and the sample was combusted in a stream of oxygen at 900°C. The TOC content was calculated as the difference between TC and IC from coulometry (Table 4.1).

4.2.3. Solvent extraction and fractionation of the soluble organic matter

The IODP 317 samples were sampled on board the JOIDES Resolution during the expedition. The IODP 313 samples were sampled at the MARUM core repository at the University of Bremen about 4 years after the end of the expedition. All samples were hand crushed using a ceramic pestle and mortar and sieved through a 125 μm sieve. Samples were mixed ~50:50 with pre-extracted and baked sand (3 hours at 450°C) so as to increase solvent extraction efficiency and were extracted using a Dionex Accelerated Solvent Extractor (ASE 300) using 9:1 dichloromethane (DCM): methanol. Two extraction runs were used, each of which consisted of three cycles of 5 min. preheating, 5 min. static at 1500 bar pressure and 100°C, and 3 min. solvent purging to the collection bottle. Sulphur was removed from the extractable organic matter (EOM) of all samples by refluxing at 40°C with acid-activated copper turnings. The volume of the EOM was reduced to 10 mL using a rotary evaporator (Buchii R-210), and 1 mL was dried in order to obtain the weight of the EOM recovered. The extractability was calculated relative to the weight of sediment used (mg EOM/g sediment) (Table 4.1).

The rest of the EOM was separated using a short silica column into three fractions using organic solvent solutions: aliphatic hydrocarbons (*n*-hexane), aromatic hydrocarbons (*n*-hexane:DCM, 4:1), and polar compounds (DCM:methanol, 1:1). The polar fraction was dried, weighed and redissolved in *n*-hexane:propan-2-ol (99.5:0.5, v:v) before analysis for glycerol dialkyl glycerol tetraether lipids (GDGTs). The hydrocarbon fractions were spiked with a mixture of internal standards (IS) of known concentration (terphenyl d14, anthracene d10, and tetracosane d50) before analysis.

4.2.4. Gas chromatography-mass spectrometry (GC-MS)

The two hydrocarbon fractions were analysed by gas chromatography-mass spectrometry (GC-MS), using an Agilent GC (6890N) coupled to an Agilent Mass Selective Detector (5975B). 1 μL of solution was injected onto a Programmable Temperature Vaporizing (PTV) inlet at 35°C, followed by a temperature increase at 700°C/min. to 310°C. Separation was performed on a J&W DB5MS UI column (60 m x 250 μm x 0.25 μm), with helium carrier gas at 1.5 mL/min. constant flow rate and 155 KPa starting pressure. The MS was operated in full-scan mode (50–550 amu) for all samples and fractions. In addition, some of the samples were analysed using two selective ion monitoring (SIM) mode programmes. For the aliphatic fraction the targeting ion masses were: m/z 123.1, 177.2, 191.2, 205.2, 217.2, 218.2, 231.2, 253.2, and 259.2. For the aromatic fraction the targeting ion masses were: m/z 91.1, 106.1, 120.1, 128.1, 134.1, 142.1, 152.2, 154.2, 156.1, 164.2, 166.1, 168.1, 170.1, 178.1, 180.1, 182.1, 192.1, 197.1, 202.1, 206.1, 212.1, 216.1, 220.1, 230.1, 234.1, and 241.1. In addition, SIM ion masses m/z 66.1, 183.2, and 188.1 were added to each programme for IS identification. The target compounds are identified using retention times relative to known standards, and mass spectral comparison to NIST and WILEY library data.

4.2.5. High performance liquid chromatography-mass spectrometry (HPLC-MS)

Separation was carried out for isoprenoidal GDGTs (iGDGTs), branched GDGTs (brGDGTs) after (Becker et al., 2013) using a 1260 Infinity liquid chromatograph coupled to a 6120 quadrupole mass spectrometer. Aliquots of the polar fraction (typically 10 μl) in *n*-hexane:propan-2-ol (99.5:0.5, v:v) were injected onto two coupled Acquity BEH amide columns (each 2.1 x 150 mm, 1.7 lm; Waters, Eschborn, Germany) at 50 °C. Lipids were eluted using the following gradient with eluent A (*n*-hexane) and eluent B (*n*-hexane:propan-2-ol (90:10, v:v), using a constant flow of 0.5 ml/min: 3% B to 5% B in 2 min, to 10% B in 8 min, to 20% B in 10 min, to 50% B in 15 min an d to 100% B in 10 min. The columns were

washed with 100% B for 6 min and equilibrated with 3% B for 9 min between injections. GDGTs were identified using positive ion atmospheric pressure chemical ionisation with the targeted ion masses of m/z 1018, 1020, 1022, 1032, 1034, 1036, 1046, 1048, 1050, 1292, 1294, 1296, 1298, and 1300. The source parameters were as follows: corona current 3500 nA, nebulizer gas 5 bar, drying gas 8 litre/min, drying gas 160ºC, vaporiser 400ºC, and a MS scan rate of 2 Hz. The advantages of improved separation chromatography during HPLC-MS have been widely discussed in the literature (Liu et al., 2011; Becker et al., 2013; Hopmans et al., 2016). This method provides good separations of the iGDGT, brGDGT, and alkenone isomers that are essential for the SST reconstructions (Becker et al., 2013; Becker et al., 2015).

4.2.6. Ratios and temperature reconstructions

4.2.6.1. iGDGTs

The TEX_{86}^{H} was calculated from the distribution of iGDGTs using the definition of Kim et al. (2010) for the 10°C to 40°C temperature range:

Eq. 11 $$TEX_{86}^{H} = \frac{[GDGT-2]+[GDGT-3]+[Cren']}{[GDGT-1]+[GDGT-2]+[GDGT-3]+[Cren']}$$

where numbers refer to the number of rings in the GDGT, and Cren' refers to the crenarchaeol regio isomer. TEX_{86}^{H} was converted to SST using the correlation for the 10°C to 40°C temperature range with a proposed residual standard error of ±2.5°C (Kim et al., 2008; Kim et al., 2010):

Eq. 12 $$SST = 68.4 \times TEX_{86}^{H} + 38.6 \ (r^2 = 0.87, n = 255, p < 0.0001)$$

GDGT cyclisation was calculated to evaluate the ring index (Pearson et al., 2004):

Eq. 13 $$Ring\ index = \frac{[GDGT-1]+2\times[GDGT-2]+3\times[GDGT-3]+4\times[GDGT-4]+5\times[Cren+Cren']}{[GDGT-0]+[GDGT-1]+[GDGT-2]+[GDGT-3]+[GDGT-4]+[Cren+Cren']}$$

4.2.6.2. brGDGTs

To estimate the relative fluvial input of terrigenous organic matter in the marine environment the branched isoprenoid tetraether (BIT) index was calculated from the brGDGTs (Hopmans et al., 2004):

Eq. 14 $$BIT\ index = \frac{[GDGT-Ia]+[GDGT-IIa]+[GDGT-IIIa]}{[GDGT-Ia]+[GDGT-IIa]+[GDGT-IIIa]+[Cren]}$$

The methylation index of branched isoprenoid tetraethers (MBT) and the cyclisation index of branched isoprenoid tetraethers (CBT) were calculated from the brGDGTs as proxies for marine environment palaeo-reconstructions (Weijers et al., 2007):

Eq. 15 $$MBT = \frac{[GDGT-I]}{\sum[GDGT-I]+\sum[GDGT-II]+\sum[GDGT-III]}$$

Eq. 16 $$CBT = -\log(\frac{[GDGT-Ib]+[GDGT-IIb]}{[GDGT-Ia]+[GDGT-IIa]})$$

Mean annual air temperature (MAAT) was calculated from MBT based on various continental soils, and soil pH was calculated from CBT (Weijers et al., 2007):

Eq. 17 $$MAAT = \frac{0.122+0.187\times CBT}{0.020} \quad (r^2 = 0.77, n = 134)$$

Eq. 18 $$CBT = 3.33 - 0.38 \times pH\ (r^2 = 0.70, n = 134)$$

The error ranges for pH and MAAT are relatively high, 0.7 and 4.8°C , respectively. Therefore, the absolute values for this measurements should be used with a great level of caution. Moreover, the relative abundance of the brGDGTs in the samples could be influenced by type of vegetation cover, soil temperature, and precipitation levels (Peterse et al., 2012).

4.3. Results

4.3.1. Expedition 313 and 317 TOC data

For the U1352 Site Miocene and early Oligocene samples the TOC varies from 0.03 to 1.5 wt%, with most values <0.5 wt% and an average of ~0.42 wt% (Table 4.1; Fig. 4.4A). The highest TOC values are between 18.7 Ma and 19.3 Ma (reaching 1.5 wt%) and between 13.5 Ma and 14.6 Ma with values as high as 1.0 wt%. TN values for the U1352 Site are scattered in the range of <0.001–0.04 wt%, with very low or undetectable levels of TN in the range of 31.67 – 11.92 Ma, and some higher values of 0.09 and 0.06 wt% at 19.07 and 17.39 Ma, respectively (Table 4.1).

For the Site M0027 middle Miocene and Oligocene samples the TOC varies from 0.11 to 7.45 wt%, with most values <2.0 wt% (Table 4.1; Fig. 4.4A). The highest TOC values are between 22.1 and 20.8 Ma (reaching 4.4 wt%) and one sample in the middle Miocene with a TOC of 7.45 wt%. For the M0028A Site the early to middle Miocene samples have TOC values from 0.13 to 2.9 wt% , with most values <2.0 wt% (Table 4.1; Fig. 4.4A). The highest TOC values are in the early Miocene between 17.8 and 17.1 Ma reaching 2.9 wt%, and one sample in the middle Miocene at 12.65 Ma with a value of 2.1 wt%. TN values were not measured for these sites.

4.3.2. Expedition 313 and 317 solvent extractability

The solvent extractability of the analysed samples vary between 0.01 and 8.15 mg EOM/g sediment. There is no correlation between the amount of sample extracted and the extractability (Table 4.2; Fig. 4.4B). Overall, the samples from the U1352 Site have lower extractability than the samples from the M0027 and M0028 Sites.

The Site U1352 sediments have low extractabilities that do not exceed 0.5 mg EOM/g sediment (Table 4.2). Two depth ranges with higher than average extractability can be

identified in Site U1352 between 1750–1580 mbsf and 1390–1245 mbsf. These depths are characterised by darker grey layers of fine sandy mudstone alternating with greenish grey very fine sandy marlstones for the deeper section, and brownish very fine sandy mudstones for the upper section. There is no obvious correlation between extractability and TOC in the Site U1352 sediments. Lithological subunit IIC in U1352C is characterised by many samples with low extractabilities (<0.1 mg/g), which correlates with recovered sandstone layers (Fulthorpe et al., 2011). The foraminifera limestone lithology of unit III in U1352C is also characterised by similarly low extractability levels.

The Site M0027 samples have high and quite variable extractabilities, in the range between 0.35 and 8.15 mg EOM/g sediment (Table 4.2; Fig. 4.4B). The lowest extractabilities correlate with lithological Units VI and IV from the early Miocene. The sample with the highest extractability is part of lithological Unit III which is characterised by silt with a major storm influence (Mountain et al., 2010a).

The Site M0028 samples have extractabilities that vary between 0.21 and 4.0 mg EOM/g sediment (Table 4.2; Fig. 4.4B). While most samples have extractabilities < 2.0 mg EOM/g sediment, two samples at 603 mbsf (early Miocene) and 300 mbsf (late-early Miocene) have extractabilities of 4.0 and 3.29 mg EOM/g sediment, respectively. These samples are from lithological unit VII, composed of silt and very fine sand, and unit IV, composed of transitions from red clay to very fine sand. In both IODP 313 sites the highest extractability samples are dated to the late-early Miocene.

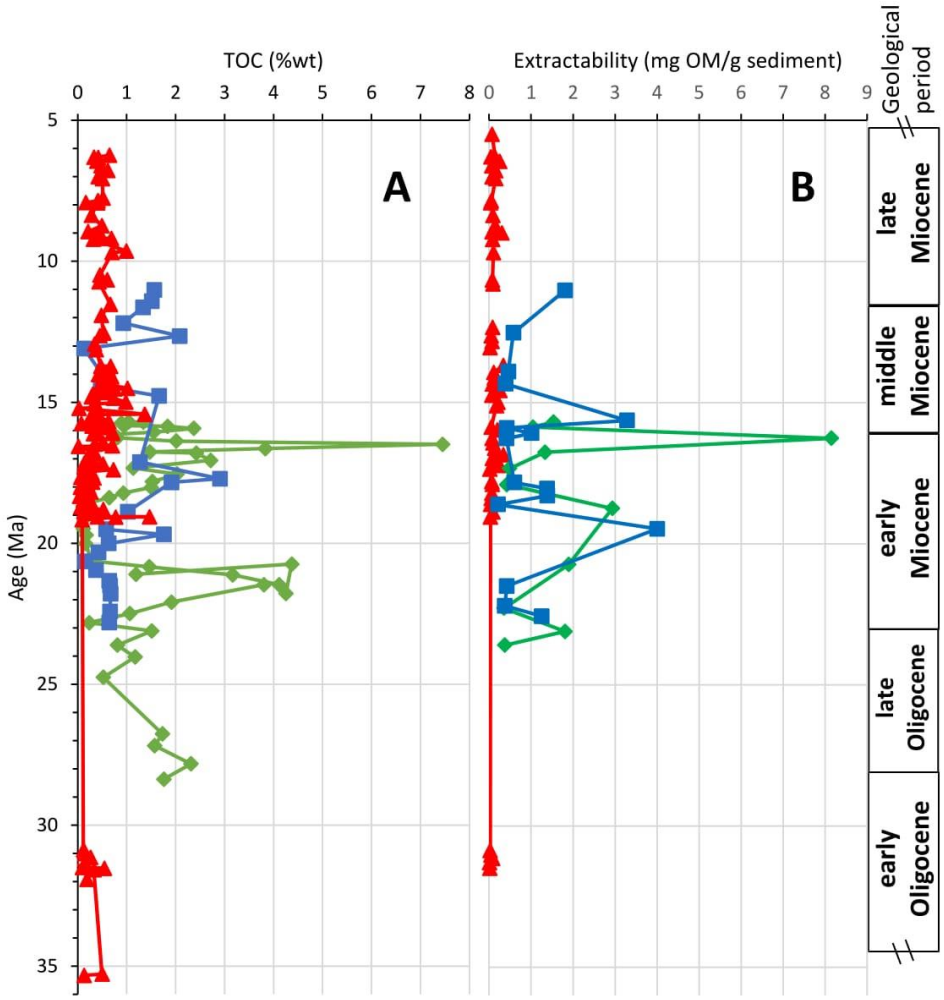

Figure 4.4: On-board acquired bulk geochemistry data for the IODP Expedition 317 continental slope site (U1352, red; Fulthorpe et al., 2011), and the IODP Expedition 313 continental shelf sites (M0027A, green; and M0028A, blue; Mountain et al., 2010). Parameters are plotted against interpreted age from the biostratigraphy (Table 4.1). TOC is total organic carbon.

4.3.3. Expedition 313 and 317 *n*-alkanes and isoprenoids

The early Oligocene samples (1904–1874 mbsf) from the U1352 Site are characterised by a strong even-over-odd carbon number predominance, a low carbon preference index for the C_{22}-C_{32} *n*-alkanes ($CPI_{(22\text{-}32)}$; 0.12–0.94) and a very low terrigenous/aquatic ratio (TAR; 0.2–3.51) (Fig. 4.5A; Fig. 4.6A,B; Table 4.2). A similar pattern of *n*-alkanes is present in most of the early Miocene samples from 18.9 to 16.9 Ma (Table 4.2; Fig. 4.5B). Samples from 18.40– and 17.36 Ma have a high predominance of even-over-odd short-chain n-alkanes (Fig. 4.5B).

The 19.06 Ma sample is an exception as it has a strong predominance of long chain *n*-alkanes without obvious even or odd predominance. The 16.85 Ma sample has a very strong predominance of C_{29} and C_{31} *n*-alkanes and a high $CPI_{(22-32)}$ of 4.7 reflecting this odd predominance, whereas the 16.62 Ma sample has predominant *n*-alkane chain lengths at C_{24}, C_{26}, and C_{28} and thus a rather low $CPI_{(22-32)}$ of 0.53 (Fig. 4.5B; Fig. 4.6A). The TAR is mainly <2, with three samples having extremely high values of 91, 58, and 17 at 19.06, 17.23, and 16.85 Ma, respectively (Fig. 4.6B; Fig. 4.5C; Table 4.2).

In general, the middle and late Miocene samples in U1352 Site have a more diverse distribution of *n*-alkanes (Table 4.2). The samples mainly have C_{14}, C_{16}, and C_{18} predominance, and/or C_{27}, C_{29}, and C_{31} predominance (Fig. 4.5C,D). No obvious correlations between changes in the *n*-alkane distribution and age or lithology could be identified. The $CPI_{(22-32)}$ for this period varies from 0.8 to 2.8 (Fig. 4.6A) without correlation to sample depth. However the TAR has more significant variations during the middle Miocene from 55 at 16.43 Ma to 0.6 at 13.68 Ma (Fig. 4.6B). While most TAR values are below 9.4, three other samples at 14.57, 12.84, and 12.64 Ma also have high values (Fig. 4.6B).

Two late Oligocene samples (505-498 mbsf) from the M0027A inner continental shelf Site have a high predominance of long chain *n*-alkanes (Table 4.2; Fig. 4.5E) and are characterised by a strong odd-over-even carbon number predominance, high $CPI_{(22-32)}$ values (>3.0) and a very high TAR (>30) (Fig. 4.6A,B). The earliest part of the early Miocene (the Aquitanian Stage (23.03 – 20.44 Ma)) is represented by two samples at 22.28 and 20.74 Ma (Table 4.2). The 22.28 Ma sample has a bimodal distribution of short and long chain *n*-alkanes, together with a high abundance of *n*-C_{17}, a $CPI_{(22-32)}$ of 2.7 and a relatively low TAR of 3.5 (Fig. 4.6A,B). The 20.74 Ma sample contains only *n*-C_{21} to *n*-C_{33}. The following Burdigalian Stage (20.44–15.97 Ma) – late-early Miocene, is represented by seven samples with a strong predominance of long chain *n*-alkanes with strong odd-over-even predominance ($CPI_{(22-32)}$ >5.0) for most samples (Table 4.2). The exception is the 17.9 Ma sample which has

very high relative abundances of *n*-C_{24}, *n*-C_{26}, and *n*-C_{28} and thus a $CPI_{(22\text{-}32)}$ of 0.24. The TAR values for all seven samples are >10.0 (Fig. 4.6A,B).

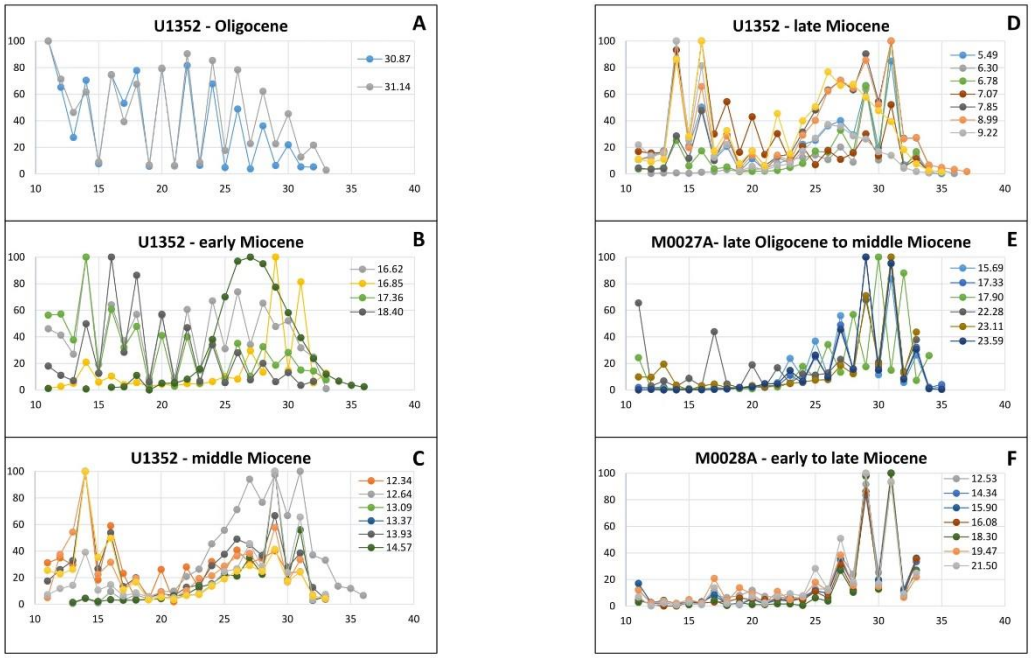

Figure 4.5: Representative n-alkane distributions for the IODP Expedition 317 continental slope Site U1352 (**A**–**D**), and the IODP Expedition 313 continental shelf sites M0027A (**E**), and M0028A (**F**).

The three Aquitanian Stage (23.03–20.44 Ma) samples (673–620 mbsf) from the M0028A middle continental shelf Site have a bimodal *n*-alkane distribution with short and long chain *n*-alkane predominance for two samples, and only long chain *n*-alkane predominance for the 673 mbsf sample. The $CPI_{(22\text{-}32)}$ values are >4.0 and TAR values are >11 (Fig. 4.6A,B). The Burdigalian Stage (20.44–15.97 Ma) (603–439 mbsf) is represented by seven samples with varying *n*-alkane distributions. The 18.61 and 16.08 Ma samples have a bimodal *n*-alkane distribution, whereas the other five samples have a unimodal distribution with long chain *n*-alkane predominance. The $CPI_{(22\text{-}32)}$ for the Burdigalian Stage samples is mostly in the range 1.9–4.1, but the 18.30 Ma sample has an exceptionally high value of 7.3 (Fig. 4.5F; Fig. 4.6A; Table 4.2). The TAR for these samples varies from 2.89 and 28.61 with the highest value in the 18.30 Ma sample (Fig. 4.6B). The middle Miocene in the M0028A Site (322–220 mbsf) is

represented by six samples. The 14.34–12.53 Ma samples have highly abundant long chain *n*-alkanes, except for the 13.90 Ma sample. The other three middle Miocene samples have a unimodal distribution with long chain *n*-alkanes predominating (Table 4.2). The $CPI_{(22\text{-}32)}$ varies in the range 1.1–5.1, with the lowest value dated to 13.90 Ma (Fig. 4.6A). The TAR values vary significantly between 12.86 and 69.29, with the lowest value dated to 12.53 Ma (Fig. 4.6B).

The pristane/phytane (Pr/Ph) ratios in the Site U1352 vary with geological period (Table 4.2; Fig. 4.6C). The early Oligocene samples have Pr/Ph values between 0.85 and 3.05. The early Miocene samples from 19.06 to 14.12 Ma have widely variable Pr/Ph ratios from 0.74 to 5.9, and then the middle Miocene samples mostly have lower Pr/Ph ratios, with a very low value of 0.58 for the sample at 12.84 Ma (Fig. 4.6C). The samples younger than 8.37 Ma have Pr/Ph ratios from 0.7–1.7 (Table 4.2; Fig. 4.6C). The M0027A Site samples have highly variable Pr/Ph ratios (0.38–5.5; Table 4.2; Fig. 4.6C). Only two samples at 22.28 and 15.69 Ma have Pr/Ph values <0.8. The very high value of 5.5 is from the sample at 17.90 Ma. The M0028A Site samples have Pr/Ph values in the range 0.47–15.6 (Table 4.2; Fig. 4.6C). The three Aquitanian Stage samples have Pr/Ph values <0.5. The younger 19.47 Ma sample has an extremely high Pr/Ph value of 15.6, and the following samples have ratios > 1.0 from 18.16 to 15.63 Ma. The samples between 15.63 and 11.02 Ma mostly have Pr/Ph values <0.8, with one sample at 14.34 Ma having a value of 2.6.

The U1352 Site samples from the Oligocene and the Eocene are characterised by Pr/*n*-C_{17} ratios from 0.24–1.9 and Ph/*n*-C_{18} ratios from 0.08–0.43 (Table 4.2; Fig. 4.6D). Pr/*n*-C_{17} ratios in the early to middle Miocene sediments vary from 0.3 to 17, with the majority of the samples having values <3.2 (Table 4.2; Fig. 4.6D). The Ph/*n*-C_{18} ratio in the early Miocene sediments varies from 0.04 to 5.2 without specific correlation to sample depth and/or lithology. Late Miocene and early Pliocene samples are characterised by Pr/*n*-C_{17} values

between 1.0 and 4.8 and Ph/n-C_{18} values between 0.3 and 1.9 (Table. 4.2; Fig. 4.6D), also without correlation to sample depth and/or lithology.

The M0027A Site samples have Pr/*n*-C_{17} ratios in the range of 0.11–0.53 with only one exception (17.90 Ma, 5.2; Table 4.2; Fig. 4.6E). The Ph/*n*-C_{18} ratios vary between 0.37 and 1.56 (Table 4.2; Fig 4.3E). The M0028A sSite samples are characterised by Pr/*n*-C_{17} ratios in the range of 0.05–1.24 and Ph/n-C_{18} ratios between 0.09 and 1.96 (Table 4.2; Fig. 4.6F).

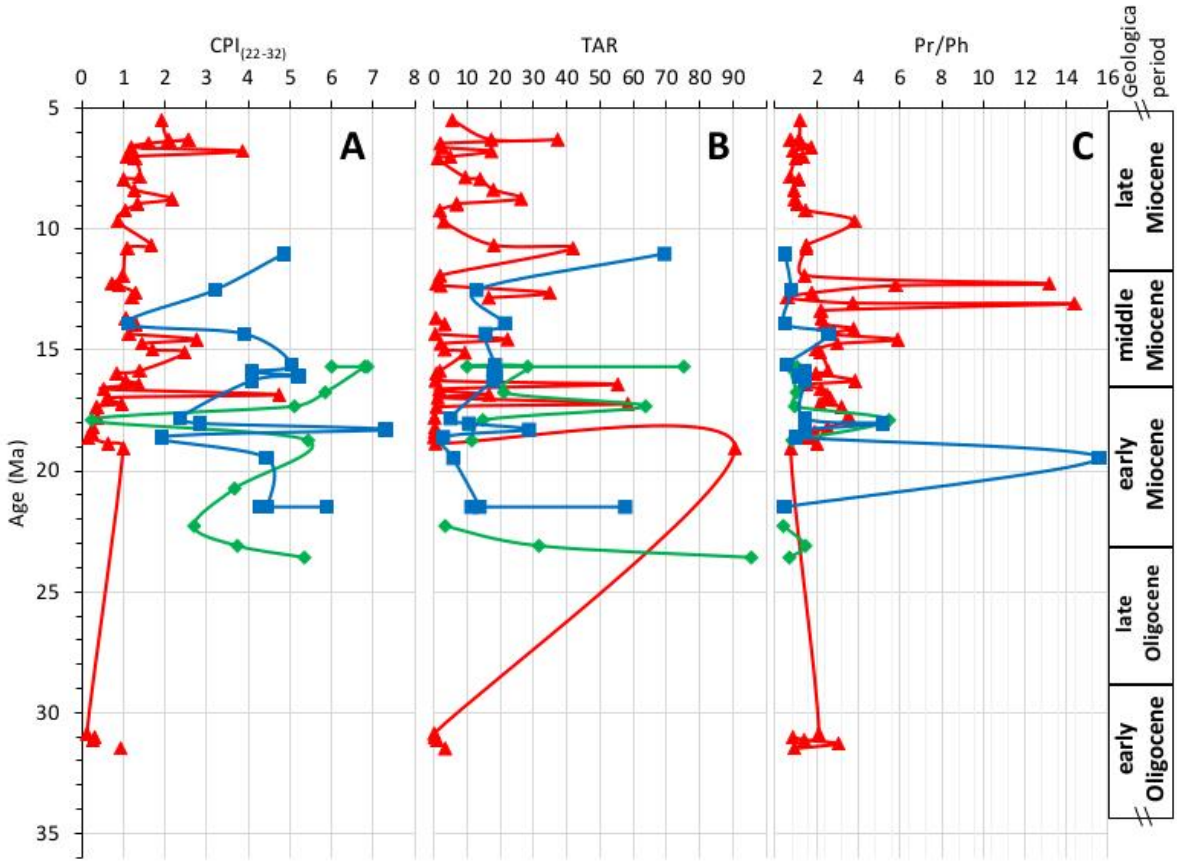

Figure 4.6: *n*-Alkane and isoprenoid ratios calculated for the IODP Expedition 317 continental slope site (U1352, red), and the IODP Expedition 313 continental shelf sites (M0027A, green and M0028A, blue) versus the interpreted age from the biostratigraphy. **A** – Carbon preference index ($CPI_{(22-32)}$) for the C_{22}-C_{32} *n*-alkanes; **B**- terrigenous/aquatic ratio (TAR); **C** – Pristane/Phytane (Pr/Ph) ratio; **D** – Pr/n-C_{17} and Ph/*n*-C_{18} ratios for the Site U1352; **E** – Pr/n-C_{17} and Ph/n-C_{18} ratios for the Site M0027A; **F** – Pr/*n*-C_{17} and Ph/n-C_{18} ratios for the Site M0028A.

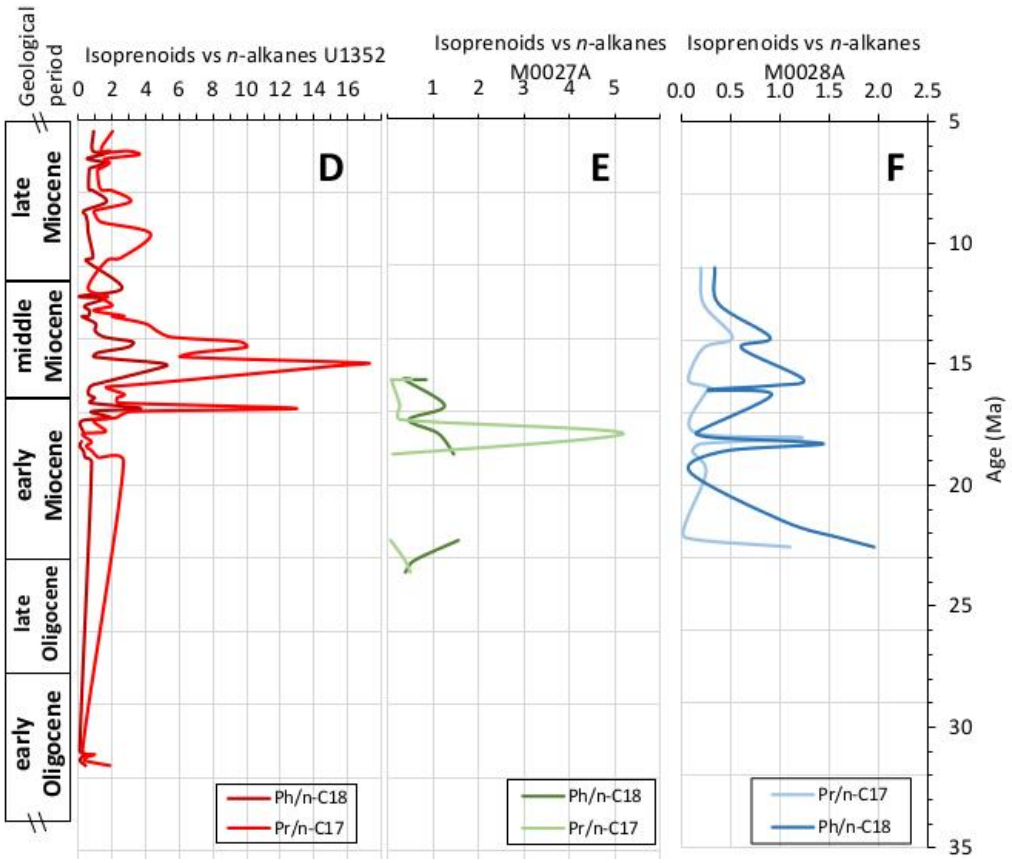

Figure 4.6 (continued): *n*-Alkane and isoprenoid ratios calculated for the IODP Expedition 317 continental slope site (U1352, red), and the IODP Expedition 313 continental shelf sites (M0027A, green and M0028A, blue) versus the interpreted age from the biostratigraphy. **A** – Carbon preference index ($CPI_{(22-32)}$) for the C_{22}-C_{32} *n*-alkanes; **B**- terrigenous/aquatic ratio (TAR); **C** – Pristane/Phytane (Pr/Ph) ratio; **D** – Pr/*n*-C_{17} and Ph/*n*-C_{18} ratios for the Site U1352; **E** – Pr/*n*-C_{17} and Ph/*n*-C_{18} ratios for the Site M0027A; **F** – Pr/*n*-C_{17} and Ph/*n*-C_{18} ratios for the Site M0028A.

4.3.4. Expedition 313 and 317 branched isoprenoid tetraether (BIT) index

The BIT index is used as an indicator of terrestrial organic matter (OM) input into marine sediments (Hopmans et al., 2004). It is also used to qualify the reliability of the reconstructed SST based on TEX_{86} data (Weijers et al., 2006; Damsté et al., 2010). The calculated BIT index for the Site U1352 samples varies from 0.03 to 0.46 (Fig. 4.7A; Table 4.3). The Eocene-Oligocene samples have a BIT index between 0.05 and 0.24 suggesting low terrestrial OM input into the sediment, except for the 31.02 Ma sample. The three early Miocene samples have BIT values <0.1 (Fig. 4.7A), suggesting less terrestrial OM input compared to

the Oligocene. The middle Miocene samples have higher variability in BIT index values (0.068–0.162), but still indicate mainly marine OM input into the sediments. The late Miocene samples have higher variability in the BIT index, with the 0.32 value at 8.74 Ma suggesting an increase in terrestrial OM input. The BIT index from 10.49–8.99 Ma and 8.37–7.85 Ma stays below 0.19 and is indicative of dominant marine OM input into these samples.

The BIT index for the M0027A Site samples generally higher than for Site U1352 (0.24–0.66; Table 4.3; Fig. 4.7A). The late Oligocene samples are characterised by a high BIT index (>0.5) indicating high terrigenous OM input. The earliest Miocene (Aquitanian Stage) samples have a lower BIT index (0.26–0.34), indicative of more marine OM input into the sediments. The samples from the Burdigalian Stage at the M0027A Site have a BIT index between 0.24 and 0.62 with no correlation with sample age. The 18.75, 16.76, and 15.69 Ma samples have recorded values >0.5 indicating very strong terrigenous OM input.

The Site M0028A samples have highly variable BIT index values between 0.21 and 0.79 (Table 4.3), which are similar to those of Site M0027A (Fig. 4.7A). The Aquitanian Stage samples have BIT values between 0.29 and 0.48 with higher values in the deeper samples (Table 4.3; Fig. 4.7A). The overlying Burdigalian Stage samples have highly variable BIT index values between 0.17 at 18.30 Ma and 0.79 at 19.28 Ma. The data suggest a decrease in the BIT index from 0.76 to 0.22 between 19.47 Ma and 18.05 Ma, indicating a decrease in terrigenous OM input, but without any specific depth trend. The 18.61 to 18.05 Ma period has the lowest BIT values for this site (Fig. 4.7A). The middle Miocene samples have BIT index values between 0.32 and 0.61, suggesting a mixture of marine and terrigenous OM input. Somewhat higher terrigenous OM input is suggested at 12.53 Ma.

4.3.5. Expedition 313 and 317 sea surface temperature (SST) based on TEX^{H}_{86}

The reconstructed SST based on TEX^{H}_{86} is presented in Fig. 4.7B. Only samples with BIT indices <0.5 were considered as reliable for SST reconstruction (Fig. 4.7B; Table 4.3), as a high BIT index is associated with an increase in the error of the reconstructed SST (Hopmans et al., 2004). A separate column is provided in Table 4.3 for the filtered data.

The U1352 Site samples show reconstructed SST between 9.3ºC and 29.8ºC for the period from 35 to 6 Ma (Table 4.3). The highest value was recorded at 35.28 Ma and the lowest at 8.39 Ma. The Eocene-Oligocene is represented by four samples which show a decreasing temperature from 29.8ºC at 35.3 Ma to 21.5ºC at 31.1 Ma (Fig. 4.7B). The early and middle Miocene are represented by nine samples and show a consistent SST decrease through time from 27.0ºC at 18.3 Ma to 18.9ºC at 13.7 Ma. All reconstructed temperatures for the late Miocene period do not exceed 20ºC (Fig. 4.7B). The early-late Miocene samples follow the same decreasing SST trend to 13.3ºC at 10.5 Ma. The shallower late Miocene samples are generally consistent with a warming period, with a SST increase to 19.6ºC at 7.9 Ma, although these is more variability between samples in this interval (Fig. 4.7B). This warm period is reversing after 7.3 Ma, with a low SST value of 12.8ºC reached at 6.3 Ma.

Of the analysed samples from the M0027A Site only nine have a BIT index <0.5 and thus can be interpreted. The results show SST variation between 13.8ºC and 23.0ºC (Table 4.3; Fig. 4.7B). The early Miocene samples have SST varying from 18.4ºC and 23.0ºC with the highest temperature at 19.74 Ma. The younger samples show a decreasing SST to 13.8 ºC at 16.2 Ma, following by an increase to 17.2ºC at 15.69 Ma (Table 4.3; Fig. 4.7B). The Miocene samples from the M0028A Site show SST variation between 24.1ºC at 22.20 Ma and 15.5°C at 16.3 Ma, representing an overall decrease, albeit with substantial variation (Table 4.3; Fig. 4.7B). The youngest sample (from 11Ma) has a slightly higher SST (20.2°C).

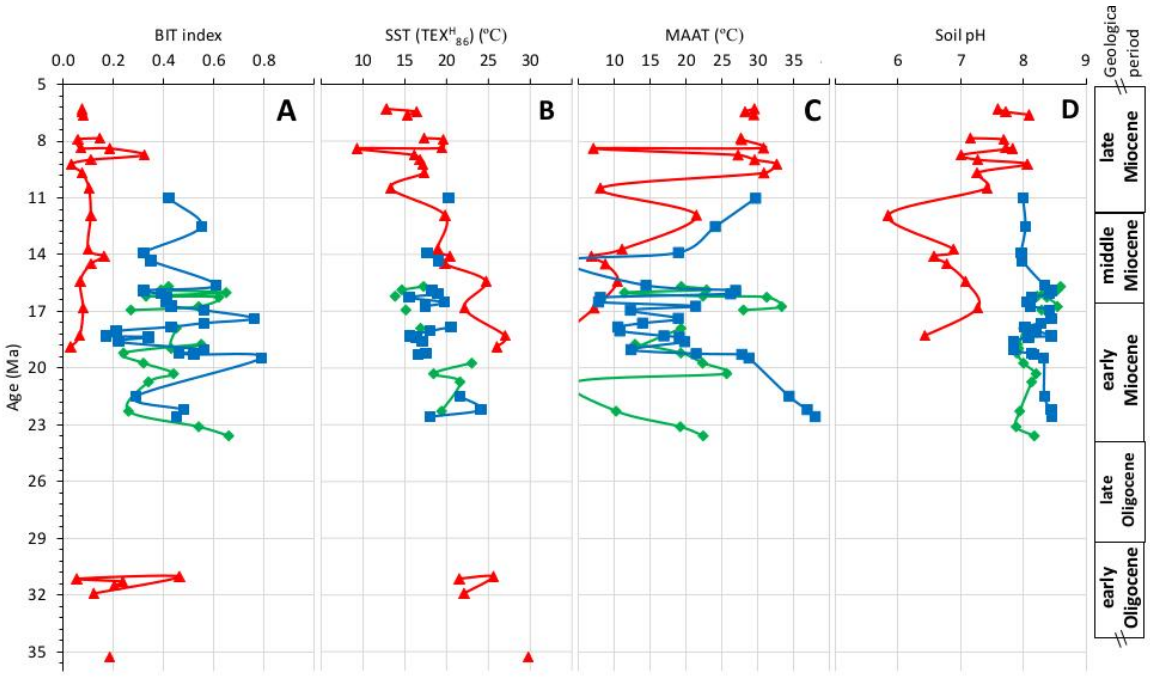

Figure 4.7: Lipid ratios, temperature and soil pH reconstructions for the IODP Expedition 317 continental slope site (U1352, red), and the IODP Expedition 313 continental shelf sites (M0027A, green and M0028A, blue) versus the interpreted age from the biostratigraphy. **A** – BIT index; **B**- Sea surface temperature (SST (TEX^{H}_{86}) (ºC)); **C** – Mean annual air temperature (MAAT (ºC)); **D** – soil pH. Samples with BIT index >0.5 were excluded from the SST (TEX^{H}_{86}) plot.

4.3.6. Expedition 313 and 317 mean annual air temperatures (MAAT)

MAAT (ºC) was only recorded from the early Miocene for the U1352 Site (Fig. 4.7C). MAAT significant increases from 18.30 Ma (6.4°C) to 6.30 Ma (29.5°C). Early and middle Miocene samples have MAAT values that do not exceed 10ºC, except for the 11.9 Ma sample (21.4ºC), whereas samples younger than 10 Ma have much higher values (27.2ºC to 32.6ºC).

The Site M0027A samples have large MAAT variability from 4.5ºC to 33.3ºC. The late Oligocene samples have a MAAT of 22.4 ºC and 19.2ºC (Table 4.3; Fig. 4.7C). The Aquitanian Stage samples show a significant temperature drop to 4.5ºC at 20.74 Ma, but then a much higher value of 25.7ºC at 20.30 Ma, following by a temperature decrease to 12.5ºC at 18.96 Ma. From 17.90 Ma to 15.69 Ma the MAAT increases significantly to >30ºC, before reducing to 19.3ºC in the shallowest sample (Table 4.3).

The Site M0028A samples show big MAAT variations from 3.1ºC to 38.0ºC (Table 4.3; Fig 4.4C). The three oldest samples (21.50–22.57 MA) have the highest recorded values >34ºC, which are following by a consistent temperature decrease to 12.3ºC at 19.03 Ma. The MAAT then vary between 26.2ºC and 7.8ºC, with no obvious pattern, with the lowest MAAT reached at 16.52 Ma, shortly followed by a much higher MAAT at 16.08 Ma (26.2°C). The middle Miocene samples then show a rapid MAAT decrease to 3.1ºC at 14.34 Ma, followed by warmer values in the shallower samples (Table 4.3).

4.3.7. Expedition 313 and 317 soil pH

The soil pH could only be calculated for the U1352 Site samples from the early Miocene (Table 4.3). Soil pH has an overall increase through time (Fig. 4.7), with early Miocene samples having interpreted soil pH in the range 6.4–7.3. The middle Miocene samples have soil pH data that decrease from 7.1 at 15.4 Ma to 5.8 at 11.9 Ma. The late Miocene and Pliocene samples have higher values between 7.0 and 8.1.

The Site M0027A samples have near neutral soil pH that vary between 7.9 and 8.6 for all samples, and in the early Miocene are significantly higher than those seen in Site U1352 samples. The deeper samples have slightly lower values, and there is a slight increase in soil pH from 7.9 at 19.21 Ma to a maximum of 8.6 at 15.69 Ma (Fig. 4.7D; Table 4.3).

The Site M0028A samples have a similar soil pH range (7.8–8.4) as for Site M0027A. The Aquitanian Stage samples have slightly higher soil pH values between 8.5 and 8.3 (Fig. 4.7D; Table 4.3), and there is a slight tendency for these to decrease during the Burdigalian Stage and reach a minimum of 7.8 at 19.03 Ma. The soil pH values increase upwards through the middle Miocene period to 8.4 around 15.90 Ma, followed by a decrease to 8.0 at 14.34, above which they remain constant until the shallowest (11.02 Ma) sample (Table 4.3).

4.4. Discussion

High levels of OM burial in marine sediments are known from around the world (Berner, 1982; Walsh, 1988). The TOC of marine sediments consists of material derived from the land (terrigenous OM) and from the ocean (marine OM). Estimated calculations suggest about 180×10^{12}g TOC/year are exported to marine sediments via rivers (Meybeck, 1982). TOC levels generally decrease with distance from the shore (Prahl et al., 1994). Bioturbation also influences TOC levels in continental shelf areas by decreasing the original organic input and mixing up TOC from different sediment layers. The bioturbation influence is higher closer to the shore, and might decrease the relative abundance of TOC in the sample (Prahl et al., 1994; Dickens et al., 2004). Moreover, the way that organic carbon is transported and distributed in marine sediments, and bottom water oxicity, can significantly alter the TOC content (Berner, 1990; Cowie and Hedges, 1992; Hedges and Keil, 1995). Deltaic sediments are responsible for ~45% total TOC input into ocean (Berner, 1989). Anoxic bottom water can support preservation of the TOC in coastal environments (Cowie and Hedges, 1992).

Our data (Table 4.1; Fig. 4.4A) supports previous observations. The continental slope site in the Canterbury Basin (~82 km offshore now) has much lower TOC values than the two continental shelf sites from New Jersey. Distance to shore is also a control on the TOC values of the M0027A and M0028A Sites. The M0027 Site is closer to the shore (~45 km offshore now) and has samples with very high TOC levels (> 3 wt% for the 21.47–20.33 Ma period in the early Miocene, with an exception at 21.10 Ma, and 7.5 wt% for a sample in the middle Miocene (Fig. 4.4A). These high TOC values are possibly due to the proximity of the drilling site to the shore in the Miocene (Prahl and Coble, 1994). The M0028 Site is further offshore (~56 km offshore now; Fig. 4.1B) and samples have much lower TOC values than for the M0027 Site (up to 2.9 wt%). At the M0028 Site the early to middle Miocene samples from the 18.88 – 14.78 Ma interval have TOC values from 1.02 to 2.9 wt%. This could possibly

indicate a temporal change in the proximity of the shoreline to the site, and possibly a decrease in the global sea level.

Clear indication of coastal onlap associated with a major downward shift was recorded in New Jersey area from middle Oligocene bringing nearshore marine and coastal-plain depositional environments during late Oligocene and early-early Miocene – Aquatanian (Greenlee and Moore, 1988). Low global sea levels during the early Miocene were recorded by Haq et al. (1987), who estimated a decrease just after 21 Ma. In addition, a major downward shift is noted in New Jersey area ~21 Ma (Greenlee and Moore, 1988). Abreu and Anderson (1998) also show a global sea level decrease, with minimal sea levels during the early Miocene around 21 Ma and slightly after 20 Ma (Abreu and Anderson, 1998). Moreover, the sea level reconstruction for the New Jersey region by Van Sickel et al. (2004) does show low sea levels around 21 Ma with global sea level decrease from 21.5 Ma to ~18 Ma.

Most of the U1352 Site samples have very low TOC contents, with the majority <1 wt% and only three samples at 19.06, 15.42, and 14.50 Ma with TOC values > 1 wt% (Fig. 4.4A). A slight increase in TOC is apparent for the Site U1352 samples from 17 and 14 Ma, which correlates with the proposed lower sea level for the New Jersey region over this time (Miller et al., 2005).

In general, a $CPI_{(22\text{-}32)}$ <1 is associated with marine and aquatic environments, whereas a $CPI_{(22\text{-}32)}$ >1.0 is associated with terrigenous OM input (Bray and Evans, 1961). Low $CPI_{(22\text{-}32)}$ <1 values for the early Oligocene samples are Fig. 4.6indicative of marine OM input dominated by diatoms and phytoplankton (Albaigés et al., 1984; Saliot et al., 1998), and is consistent with high sea levels during this period.

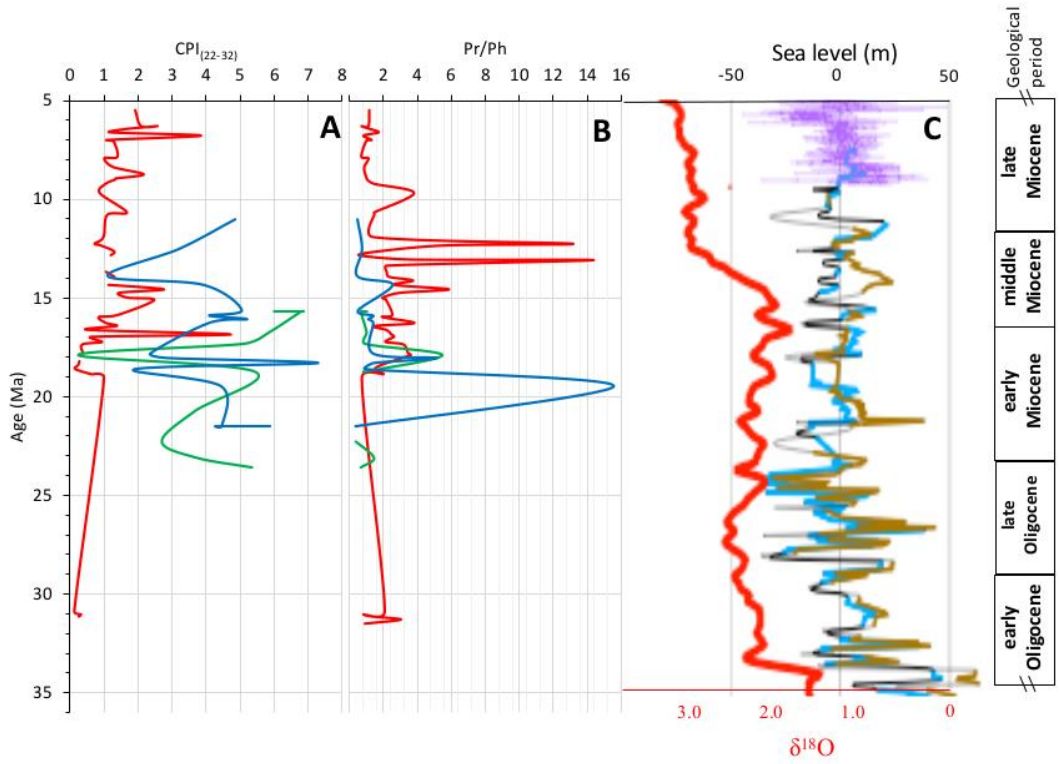

Figure 4.8: *n*-Alkane and isoprenoid ratios calculated for the IODP Expedition 317 continental slope site (U1352, red), and the IODP Expedition 313 continental shelf sites (M0027A, green and M0028A, blue) versus the changes in global $\delta^{18}O$ (**C**, red) (Cramer et al., 2011) and global sea level fluctuations (C, blue and black; Miller et al., 2005 and green;Kominz et al., 2008).

A similar distribution of even *n*-alkanes in the range of C_{12}-C_{20} in the early Oligocene samples from the Site U1352 has been reported in some coastal sediments from Gulf of Fos, Mediterranean sea (Mille et al., 2007) and Gulf of Mexico (Nishimura and Baker, 1986), but were suggested to be due to possible bacterial input. Importantly, an even *n*-alkane distribution can also be attributed to petrogenic contamination of the samples (Ekpo et al., 2005; Aloulou et al., 2010). A TAR < 1 is indicative of strong algal input, whereas higher values indicate a predominance of terrigenous OM input (Silliman et al., 2000). Therefore, the low TAR values for the early Oligocene period in the U1352Site are interpreted to suggest a strong aquatic plant input, with low terrigenous vegetation imprint (Fig. 4.6B).

The two late Oligocene samples from the M0027A Site have high $CPI_{(22\text{-}32)}$ indices and a high TAR (Fig. 4.6A,B) that indicate high terrigenous OM input. Both ratios significantly decrease at the beginning of Aquitanian Stage which indicates an increase in marine OM input. Another rapid decrease in $CPI_{(22\text{-}32)}$ to 0.24 is recorded for the 17.90 Ma sample, suggesting dominant marine OM input, but the TAR suggest the reverse and may be misleading (Cranwell et al., 1987; Meyers and Ishiwatari, 1993a). The samples from the second part of the Burdigalian Stage and the beginning of the middle Miocene have a high $CPI_{(22\text{-}32)}$ and TAR, indicating high terrigenous OM input.

Very similar distributions of *n*-alkanes and a low $CPI_{(22\text{-}32)}$ values are recorded in early Miocene samples from the Site U1352 (Fig. 4.6A) which suggest strong marine OM input. The late-early Miocene is characterised by an increase in long chain *n*-alkane abundance and high $CPI_{(22\text{-}32)}$ values at 16.85 Ma. This change is indicative of greater terrigenous OM input during the second part of early Miocene (Eglinton and Hamilton, 1967). Low TAR values before ~16 Ma also indicate high marine OM input. Two early Miocene samples with high TAR values of 58.3 and 55.3 at 17.23 Ma and 16.43 Ma (Table 4.2) show high terrigenous OM input for the New Zealand region at these times. Importantly to note, the TAR might over-represent the absolute amount of terrigenous sources in marine sediments, due to much higher *n*-alkane production by land plants (Cranwell et al., 1987; Meyers and Ishiwatari, 1993a).

The samples from the Aquitanian Stage in the M0028A Site have a high $CPI_{(22\text{-}32)}$ and TAR, with some variations between the samples, indicating high terrigenous OM input (Fig. 4.6A,B). The samples from the Burdigalian Stage are characterised by $CPI_{(22\text{-}32)}$ >1.9 indicating high terrigenous OM input. The TAR for these samples indicates a decrease in terrigenous OM input until 18.61 Ma, following by an increase in terrigenous OM input to 18.05 Ma. The short term increase in marine OM input around 17.83 Ma is followed by an increase in TAR through the last part of Burdigalian Stage and into the middle Miocene

samples. The increase in marine OM input at 18.61 and 17.83 Ma was recorded in both of the New Jersey sites (Fig 4.4A,B).

The middle Miocene Site U1352 samples from around 15 Ma have high $CPI_{(22-32)}$ values, indicating an increase in terrestrial OM input (Fig. 4.6A). The decrease of $CPI_{(22-32)}$ around 12 Ma suggests a decrease in terrigenous OM input, as is also indicated by a low TAR index showing dominant marine OM input (Fig. 4.6B). Some late Miocene Site U1352 samples also contain significant marine OM input, with high *n*-C_{14}, *n*-C_{16}, and *n*-C_{18} abundances for several samples (Table 4.2). A significant increase in terrigenous OM between 6.5 Ma and 5.4 Ma can be observed through an increase in $CPI_{(22-32)}$. TAR data suggest at least three strong terrigenous OM input events at 10.8 Ma, 8 Ma, and 6 Ma (Fig. 4.6A,B). These data suggest a strong influence of the Southern Alps uplift on input of terrestrial OM.

The $CPI_{(22-32)}$ and TAR data for the early Miocene do not completely correlate with the TOC data for the same period. This can be attributed to local factors such as river runoffs and local marine productivity that have a strong influence on biomarker signals.

.

The main source of pristane (2,6,10,14-tetramethylpentadecane; Pr) and phytane (2,6,10,14-tetramethylhexadecane; Ph) is the phytol side chain of chlorophyll in phototrophic organisms and bacteriophyl from purple sulphur bacteria (Powell and McKirdy, 1973). Some marine organisms such as calanoid copepods have been suggested to be an additional biological sources (Blumer et al., 1964). In addition, Pr could be derived from anaerobic bacterial degradation (Rontani et al., 2010), thermal degradation (Lao et al., 1989) or clay-catalysed degradation of the chlorophyll phytyl chain (Lao et al., 1989; Rontani et al., 2010). Ph can also be produced through anaerobic biodegradation (Grossi et al., 1998), clay-catalysed thermal hydrogenation of the isoprenoid alkenes (Gelin et al., 1995), and by thermal maturation of methanogenic bacteria (Rowland, 1990). In general, Pr/Ph <0.8 indicates an

anoxic depositional environment, and >3 indicates terrigenous organic matter input deposited under oxic conditions. (Peters et al., 2005). Although the ratio is widely used in environmental interpretations, the multiple possible sources of both compounds and the influence of the post depositional environment means that conclusions should be supported with other biomarker ratios. The Pr/*n*-C_{17} and Ph/*n*-C_{18} ratios are sensitive to the biodegradation levels of sediments (the ratios increase with increasing biodegradation) and to thermal maturity (the ratios decrease) (Peters and Moldowan, 1993) (Tissot et al., 1971).

The early Oligocene Site U1352 samples do not show any consistent pattern of Pr/Ph, and suggest a sub-oxic to oxic depositional environment (Fig. 4.6C). Pr/Ph increases from the early Miocene samples to the middle Miocene in the Site U1352, indicating an increasing oxicity trend that is consistent with $CPI_{(22\text{-}32)}$ and TAR results that showed a gradual increase of terrigenous OM input over that period. The changes in accumulation of OM in the Canterbury Basin during the early Oligocene and early Miocene can be attributed to a decrease in global sea level (up to 30 m) (Haq et al., 1987; Van Sickel et al., 2004; Miller et al., 2005). The reconstructed tectonic activity of New Zealand for these periods doesn't suggest any major activity in the area (Winkworth et al., 2002).

The middle Miocene Site U1352 samples have Pr/Ph ratios that suggest a suboxic depositional environment, except for the 15 – 12 Ma period where a strongly oxic pattern is sometimes present (Fig. 4.6C). From 11 Ma the Pr/Ph ratios decrease to values that suggest mainly sub-oxic conditions. During the same time there is an increase TAR and $CPI_{(22\text{-}32)}$ values indicating increase in terrigenous sediment input. The fluctuations in oxicity of the depositional environment in the Canterbury Basin are consistent with global sea levels fluctuations during the middle Miocene (Fig. 2.8) (Van Sickel et al., 2004; Miller et al., 2005; Fulthorpe et al., 2011a)(Haq et al., 1987; Van Sickel et al., 2004; Miller et al., 2005; Fulthorpe et al., 2011a). The increase in sea level would contribute to increased erosion of previously exposed shore line regions that, in turn, would increase the input of terrigenous

OM into the marine sediments. This deposition would not occur under oxic conditions (e.g., with a high Pr/Ph ratio), but under a new, sub-oxic environment. Increased terrigenous input from 14–12 Ma, together with high sedimentation rates at the same time, can be attributed to significant land mass build up on the South Island related to increase in convergence rate from ~20 Ma (Lu et al., 2005). The slow uplift of the western part of the South Island, and the resulting increase in the erosional gradient of the Canterbury Basin created an sub-oxic environment in the continental margin area, and fast sedimentary input to the continental slope area.

The relatively high sea levels during the Middle Miocene climatic optimum, including an increase in global temperatures and a decrease in ice sheet cover (Zachos et al., 2001; Miller et al., 2005; Zachos et al., 2008), can be proposed as a reason for low terrigenous OM input before 11 Ma. Cooling during the late Miocene and stable uplift of the Southern Alps (Lu et al., 2005) at the same time lead to an increase in vegetation cover and led to an increase in terrigenous OM input. This event could correlate to another increase in the land mass of the South Island of New Zealand (Lu et al., 2005). The highest input of terrigenous OM was recorded around 6 Ma, based on TOC data, $CPI_{(22\text{-}32)}$ and TAR indices. This spike can be attributed to an increase in convergence rate between the Pacific and Australian plates to >7 mm/year around 6 Ma (Lu et al., 2005; Wood and Stagpoole, 2007). The higher amount of terrigenous OM is consistent with the increase in the elevation of the Southern Alps, and may possibly be related to expanding angiosperm vegetation cover of the South Island.

The middle Miocene increase in oxicity of the depositional environment recorded in Site U1352 samples is correlating with the Haq et al., (1987) and Abreau et al., (1998) reconstructions, but oppose the Van Sickel et al. (2004) sea level fluctuations. This variations in the oxicity could be influenced more by the local tectonic activity and uplift of the New

Zealand Southern Island rather than global climate change events. This also correlates well with $CPI_{(22\text{-}32)}$ and TAR data sets for this period.

Most M0027A Site samples have Pr/Ph ratios close to or below 0.8 (Fig. 4.6C), indicative of an anoxic depositional environment. One late Oligocene sample (23.11 Ma) has a higher Pr/Ph ratio (1.46), suggesting a transient suboxic depositional environment. Another sample dated to 17.90 Ma has a Pr/Ph of 5.5, indicative of a transient oxic depositional environment in the early Miocene. These data are consistent with TOC variations that indicate low sea levels during this period (Table 4.2). More generally, the mainly anoxic depositional environment at the M0027A Site on the New Jersey continental shelf explains the good preservation of OM and higher TOC contents, compared to the more oxic Canterbury Basin.

However, the M0028A Site samples show a different picture of the depositional environment. While all three Aquitanian Stage samples have very low Pr/Ph ratios (<0.5), consistent with an anoxic depositional environment similar to that seen at the M0027A Site, the 19.47 Ma sample from the M0028A Site has a very high Pr/Ph ratio (15.6), consistent with a strongly oxic depositional environment which is consistent with the recovered thin coaly layer at this depth (Mountain et al., 2010). The second part of the Burdigalian Stage samples from the M0028A Site have Pr/Ph ratios consistent with a suboxic depositional environment, with the exception of an oxic spike at 18.05 Ma (Pr/Ph = 5.2), which is at the same time as when a Site M0027A sample also indicated an oxic depositional environment in the early Miocene. The middle Miocene at the M0028A Site is characterised by interpreted anoxic depositional environments, the only exception being one sample at 14.34 Ma with a Pr/Ph ratio value of 2.6.

The New Jersey samples show a close correlation between global sea level fluctuations and the oxicity of the depositional environment (Fig. 2.8). The 18 Ma oxicity spike recorded at both sites occurred at the same time as a global sea level decrease (Van Sickel et al., 2004;

Miller et al., 2005). The 18 Ma increase in oxicity of the depositional environment is also recorded in the U1352 Site samples, supporting the idea of an influence by a global eustatic event. However, the 19.47 Ma spike in oxicity of the depositional environment seen only in Site M0028A is not correlated to a global sea level decrease, and could be due to an increase of terrigenous input as a part of a storm deposit, high river input, or localised development of a coal.

Isoprenoid data have a good correlation to TOC variation in all three locations. The proposed decrease in global sea level based on TOC correlates with an increase in the Pr/Ph ratio. There is some delay in the Pr/Ph ratio increase for the M0028 Site, which can be attributed to the distance of the site from the shore line and the later influence of sea level change on deeper marine sites.

The Pr/*n*-C_{17} and Ph/*n*-C_{18} ratios show the degree of thermal maturation and biodegradation of the samples (Volkman and Maxwell, 1986), and are relatively low for all the samples (Table 4.2; Fig. 4.6D-F).

The samples from the U1352 Site (Fig. 4.6D) have low Pr/*n*-C_{17} and Ph/*n*-C_{18} ratios, consistent with low levels of biodegradation and thermal maturity of the samples. Both ratios increase during the early and middle Miocene, around 16.85 Ma and between 13.5–15.5 Ma. The same samples have poor preservation of *n*-alkanes (Table 4.2), which may have affected the calculated ratios.

Additional biomarkers were analysed to determine the thermal maturity of the U1352 Site samples. A detailed discussion regarding the low thermal maturity is summarised in Chapter 2. In short, the C_{27} 17α-22,29,30-trisnorhopane (Tm) and C_{27} 18α-22,29,30-trisnorneohopane (Ts) relative abundance (Ts/(Ts+Tm)) indicates a low thermal maturity for the samples from the Eocene to the late Miocene (Table 2.4). However, the sedimentation processes, early diagenesis, or source of OM can significantly alter this ratio (Ourisson et al., 1984). The C_{31}

αβ 22S/(22S+22R) hopane ratio suggests a low thermal maturity for the samples (Table 2.4). The hopane/mortane ratio is also used as a thermal maturity indicator. The low C_{30} αβ/(αβ+βα) ratios are indicative of a low thermal maturity (Mackenzie et al., 1980; Seifert and Moldowan, 1980). Maturity-related parameters can also be obtained from the isomerisation ratio of 20S/(20S+20R) C_{29} 5α,14α,17α(H) steranes (Seifert and Moldowan, 1986). Based on this ratio, the sample set has a low maturity as well.

Although individually, hopanes can be influenced by the source of the OM, the combination of all these ratios shows a low thermal maturity for the analysed sediments, with some increase in maturation with depth. Diasterane levels in sediments can be increased through the oxidation processes or during clay catalysed reactions.(Kirk and Shaw, 1975; Seifert and Moldowan, 1986).

The Site M0027A samples (Fig. 4.6E) have stable Ph/*n*-C_{18} ratios < 2.0 during all periods. The Pr/*n*-C_{17} are also low (< 1), except for one sample at 17.90 Ma with a Pr/*n*-C_{17} ratio of 5.9, which could be due to some increase in biodegradation. The M0028A Site samples (Fig. 4.6F) have very low Pr/*n*-C_{17} and Ph/*n*-C_{18} ratios, similar to the M0027A Site. The Pr/*n*-C_{17} ratios stay < 1.5, when Ph/*n*-C_{18} does not exceed 2.0. These data indicated low levels of biodegradation for this site as well. Data from both sites suggest a low thermal maturity influence on the OM.

The only Eocene sample from Site U1352 has a reconstructed SST of 29.8 ºC. The Oligocene samples (Fig. 4.7B) have a SST between 21.5ºC and 25.6ºC. No Eocene or Oligocene SST data were recorded for the IODP 313 samples. These Canterbury Basin data are consistent with a proposed tropical environment for all southern regions. The early Oligocene records recovered from ODP site 511 (South Atlantic Ocean, Falkland Plateau) have relatively low SSTs (between 16ºC and 19ºC) reconstructed from GDGT and alkenone proxies (Liu et al., 2009).

The BIT index is used as indicator of the amount of terrigenous OM input into marine sediments (Hopmans et al. 2004). The data collected at both locations shows a correlation between distance of the drilling site from the shore and the BIT index (Table 4.3; Fig. 4.7A). The U1352 Site is a continental slope site and has the lowest BIT indices (mostly <0.2, with three samples in the range of 0.2–0.4; Fig. 4.7A). In contrast, the M0027A and M0028A Sites have BIT indices between 0.2 and 0.8, with only one sample <0.2. These sites are located on the continental shelf and have a higher influence from terrigenous sediment flux.

Very high BIT indices (>0.5) mean that SST reconstructions can't be based on the calculated TEX^{H}_{86} index. For the M0027A and M0028A Sites the samples the discussed SSTs have BIT indices <0.5 (Table 4.3; Fig. 4.7B). All SSTs calculated for the U1352 Site samples can be considered in the discussion, based on their low BIT indices. However, the exact calculated SST value should be used with caution, due to reconstruction errors (Hopmans 2004; Hopmans et al., 2013).

Reconstructed SST from the DSDP Leg 26, sites 250-252 (South Africa) show warm temperatures (> 20ºC) for the beginning of the Oligocene (Müller et al., 2008), which correlates well with the reconstructed SST for 31 Ma in the Canterbury Basin. Moreover, temperature reconstructions in the Antarctic region for the early and middle Eocene suggest warm tropical environments on the continent (Pross et al., 2012). Warm SST at the Eocene/Oligocene boundary (~6ºC warmer than today) were also recorded by global oxygen isotope records (Zachos et al., 2001, 2008). The same records also showed a global decrease in temperature from the Eocene to the Oligocene, which is also apparent in the Canterbury Basin SST data (Fig. 4.7B).

The reconstructed temperature data from the Canterbury basin and New Jersey Shelf show a decreasing SST trend from the early Miocene to the middle Miocene (Fig. 4.7). A global climatic optimum and temperature increase occurred at the early/middle Miocene boundary

based on the $\delta^{18}O$ and $\delta^{13}C$ composition of calcareous microfossil shells (Shackleton and Kennett, 1975; Rohling and Cooke, 1999). Nelson and Cooke (2001a), together with the increasing land mass of the New Zealand sub-continent as inferred by an increase in terrigenous sedimentation rates since the middle Miocene (Lu et al., 2005), suggest gradual intensification in the amount of land vegetation in southern island of New Zealand. Interpretation of global eustatic sea level changes and climatic transformations such as accumulation of Antarctic ice cover suggest that cooler Neogene seawater conditions were coupled with a decrease in global sea levels (Zachos et al., 2001; Van Sickel et al., 2004).

The middle Miocene climatic optimum recorded in the $\delta^{18}O$ data (Barker et al., 1999) suggested some SST increase between 16 Ma and 14 Ma. These SST spikes can be seen in the New Jersey Shelf data, but not in the New Zealand data. This can be attributed to a high local influence in the New Zealand depositional setting, and a higher eustatic influence on SST in the New Jersey region. Important climate trends in the southern hemisphere such as the Western and Eastern Antarctica ice sheet accumulation (Miller et al., 1991) and development of cold Antarctic currents (Belkin and Gordon, 1996; Nelson and Cooke, 2001b) are likely to be the main factors influencing the SST around New Zealand (Nelson and Cooke, 2001b), rather than global climate and eustasy fluctuations.

The Site U1352 samples from the late Miocene show a decrease in SST from 19ºC at 11.92 Ma to about 13ºC at 6.3 Ma, with plenty of scatter. The only data point from the late Miocene from the New Jersey Shelf fits within this trend (Fig. 4.7B). These data indicate an increasing influence of the Eastern Antarctic ice cover accumulation and development of the ACC (Vincent et al., 1985; Flower and Kennett, 1994).

The mid-Miocene Climatic Optimum is a very well-studied event in the Miocene (e.g., Itoigawa and Yamanoi, 1990; Mcgowran et al., 1997; Schwarz, 1997). Warm palaeotemperatures around 16 Ma were followed by a rapid decrease in global temperatures

by 15 Ma (Graham, 1999). In the eastern coast of North America there is fossil evidence for tropical plants from ~16 Ma (Graham, 1999), and mammal fossils suggest the presence of tropical- and savanna-adapted animals (Janis et al., 1998). This North American warm period was also recorded by palaeosols, with reconstructed MAAT for the 16 Ma samples of ~16ºC. The temperature decreased afterwards to ~9ºC around 15.65 Ma (Sheldon, 2006). Since the existing MAAT calibration has a relatively large error (±5ºC), only the general temperature trends can be interpreted. However, the MAAT produces a better temperature evaluation than pollen or leaf-based analyses where the potential biases are hard to evaluate (Weijers et al., 2007; Schouten et al., 2013).

Warmer high latitude areas were proposed in North America (Wolfe, 1994b; Graham, 1999) and in the Beringia area between Canada and Russia (Wolfe, 1994a) for the mid-Miocene Climatic Optimum. Warm temperatures for polar regions were also proposed (Bruch et al., 2006). General cooling through the Miocene from mid-Miocene Climatic Optimum was recorded in global $\delta^{18}O$ records from ~15Ma (Zachos et al., 2001). The new Canterbury Basin data show some MAAT in New Zealand that correlates well to the established cool climate reconstructions during the middle Miocene (Fig. 4.7C), with temperatures below 15ºC.

The increase in MAAT during the mid-Miocene Climatic Optimum is recorded for the New Jersey samples between 17 and 15 Ma supporting previously proposed reconstructions (Zachos et al., 2001; Sheldon, 2006). A second warming after the mid-Miocene Climatic Optimum is recorded in the M0028A and Site U1352 data sets from 14.34 Ma until 6.3 Ma (Fig. 4.7C). This interpreted warming is unexpected given the established global cooling inferred from the $\delta^{18}O$ record (Zachos et al., 2001) and the reconstructed SST.

The MAAT for the New Zealand region shows relatively high reconstructed values for the late Miocene period (Fig. 4.7C), with only two samples showing a temperature decrease at 10.49 and 8.39 Ma. Continuing warming through the late Miocene in New Zealand was

proposed by fossil studies of New Zealand vegetation (Mildenhall, 2003). A tropical climate, a temperature increase, a decrease in precipitation levels and a high fire signal were proposed for the New Zealand region during the late Miocene (Pole, 2003).The study suggested slow movement of subtropical pressure over New Zealand, causing warm subtropical temperatures on land. The proposed model contradicts the previously suggested cool climate (Pocknall, 1989). The warm subtropical late Miocene climate also contradicts the development of the oceanic currents proposed by Nelson and Cooke (2001b), which suggested cooling of the region from the mid-Miocene Climatic Optimum caused by development of the Antarctic Circumpolar Current. The new data from the Canterbury Basin in New Zealand supports a local subtropical climate for New Zealand during the late Miocene period (Nelson and Cooke, 2001a).

The reconstructed early-middle Eocene latitudinal temperature gradients calculated for North America and Australia show that MAAT decreases poleward in the Southern Hemisphere in an almost linear manner. The MAAT gradient along the North American east coast also shows an almost linear MAAT gradient poleward (Greenwood and Wing, 1995). The reconstructions show Northern Hemisphere temperatures for New Jersey were around 20ºC and for New Zealand around 10ºC during the Eocene. The MAAT reconstructed in this study is dated only to the Neogene. However, Fig. 4.7 shows that the MAAT from New Jersey for the early Miocene is higher than the MAAT in New Zealand. This supports the general latitudinal temperature gradients differences discussed earlier.

Soil pH can be estimated from relative abundances of terrigenous lipids in samples (Weijers et al., 2006). Increasing precipitation increases soil acidity by washing out Ca and Mg ions from the system. The biomarker signal is not sensitive enough to calibrate the exact precipitation levels, but it is possible to evaluate the duration of the precipitation change based on the calculated pH (Weijers et al., 2006; Schouten et al., 2013). The Site U1352 samples show a broad trend of decreasing acidity based on soil pH in New Zealand (Table

4.3; Fig. 4.7D). These data are consistent with decreasing precipitation levels in New Zealand during the Miocene. Some pH fluctuations can be seen in the general pattern, including slowly increasing soil acidity between 16.73 and 14.09 Ma (Fig. 4.7D), perhaps suggesting a partial increase in precipitation.

The New Zealand samples show a decrease in soil acidity during the late Miocene (Fig. 4.7D). This decrease in precipitation can be attributed to a general decrease in precipitation around the globe and an increase in C4 plant vegetation distribution (Cerling et al., 1993; Pagani et al., 1999). In addition, there is a strong correlation between a decrease in precipitation and initiation of the uplift of the Southern Alps (Tippett and Kamp, 1993).

The New Jersey samples show a different soil pH pattern through the Miocene (Table 4.3; Fig. 4.7D). In general, higher soil pH values are proposed for all the New Jersey samples (7.8–8.6), in comparison to those from New Zealand. These data suggest no significant temporal variations in precipitation patterns in the New Jersey region.

The higher early and middle Miocene soil pH values for New Jersey compared to New Zealand might indicate differences in the type of terrigenous material eroded at the two places. The New Zealand soil pH values fluctuate by 1.5 pH values, indicating significant variations in rainfall patterns during the early and middle Miocene. In contrast, the New Jersey data for the same time show a small variability of 0.6 pH values for these periods. The New Zealand samples show some soil pH decrease that starts at ~17 Ma and continues up to 11.92 Ma (Fig. 4.5D). The New Jersey samples do not show a significant soil pH decrease. Site M0028A samples from ~14 Ma until ~11 Ma have soil pH values close to 8, which are consistently lower than for the period before (Fig. 4.7D). These values are slightly lower between 15.69 and 14.34 Ma than for the New Zealand samples. It is important to note that in the New Zealand samples the slow decrease in soil pH is also recorded between 16.83 and 12 Ma.

Significant variation in precipitation pattern in New Zealand must have been influenced by local variations in evaporation patterns (Kennett et al., 1974; Pocknall, 1989). Wetter conditions during the mid-Miocene Climatic Optimum have been widely discussed in the literature (e.g., Retallack, 2009; Wan et al., 2009; You et al., 2009; Bruch et al., 2011). The Serravallian Stage (13.82 – 11.62 Ma) in Europe was characterised by a decrease in precipitation caused by global cooling events (Shevenell et al., 2004). However, later studies based on physiological structure of herpetological assemblages did not find any significant precipitation decrease in Europe related to this cooling (Böhme et al., 2011). The New Jersey data in this study supports the later study and show no change to higher precipitation for this period. The New Zealand data for the same Serravallian Stage does show an increase in precipitation, as is also supported by flora proxy data collected in southern New Zealand (Reichgelt et al., 2015).

Reconstructed mean annual precipitation (MAP) levels in East Antarctica for the early Miocene show a large increase from 20 Ma to 15 Ma (Passchier et al., 2013), from 500 mm to about 790 mm. Our data correlates well with these reconstructions, suggesting a gradual increase in precipitation levels from 16.83 Ma until the end of the middle Miocene. Huang et al. (2007) argued in favour of C4 plant expansion in the Himalaya foreland and Arabian Peninsula regions from ~10 Ma to 5.5 Ma. This expansion would be consistent with a decrease in global precipitation levels and development of the savanna vegetation in the North Africa and Arabian Peninsula. The data from New Zealand show a persistent interpreted decrease in precipitation from 11.92 Ma to 6.3 Ma.

In addition, the low BIT index (< 0.15) for most Canterbury Basin samples during the late Miocene supports low terrestrial OM runoff into the Pacific Ocean (Fig. 4.7A). At the same time the MAAT data show a high temperature spike during the late Miocene, up to 32.6ºC for the New Zealand region (Fig. 4.7A). Such a temperature increase correlates well with a decrease of precipitation in the New Zealand region and partial aridification. This dry period

was recorded through global atmospheric carbon dioxide evolution (Pagani et al., 1999), compound specific *n*-alkane records of $\delta^{13}C$ and δD in northern Japan (Seki et al., 2010), and pollen records preserved in speleothems from semiarid southern Australia (Sniderman et al., 2016).

The relatively good preservation of brGDGTs in marine and continental sediments provides a good alternative to the sometimes poorly preserved floral proxies such as leaf structure or pollen grains. However, further studies to create a numerical correlation between soil pH and amount of precipitation must be carried out.

4.5. Conclusions

This paper provides a unique opportunity for hydrocarbon and biomarker data set comparison from two IODP drilling expeditions that were part of the continental shelf drilling project. One site was drilled in New Jersey on the continental shelf area, and the other one in the Canterbury Basin, New Zealand. Despite the differences in the locations, similar variations are observed in the biomarker data. These enable discussion of the influence of global climate changes on organic accumulation in both regions.

The continental slope Site U1352 has much lower TOC values than the two continental shelf sites from the New Jersey region, supporting the previous observations (Prahl et al., 1994) that TOC decreases with distance from the shore line. The alteration of the shore line during the Miocene can be suggested through comparison of the M0027A and M0028A site samples, assuming alterations in global sea levels. Low sea levels can be proposed for the early Miocene period dated between 21 and 18 Ma (Haq et al., 1987; Prahl et al., 1994; Van Sickel et al., 2004).

TOC and isoprenoid data show a good correlation in all three locations. The proposed decrease in global sea level based on TOC correlates with an increase in Pr/Ph ratios. The delay in the Pr/Ph increase for the M0028 site can be attributed to the distance of the site from the shore line, and thus a delay in the influence of the sea level change for the deeper marine sites.

A low thermal maturity is indicated by the *n*-alkane assemblages and the Pr/*n*-C_{17} and Ph/*n*-C_{18} ratios, suggesting low thermal alteration of the OM and relatively high reliability of the interpretations.

The $CPI_{(22\text{-}32)}$ and the TAR data are well correlated with each other in all three sites. A low $CPI_{(22\text{-}32)}$ in the early Miocene samples from New Zealand is correlated to low land mass in the area during this time, and an increase in global sea level. The New Jersey samples also

show high marine OM input during the early Miocene. This supports the suggested influence of high global sea levels. High spikes in the TAR in New Zealand around 16 and 17 Ma arguably can be related to the land mass creation during the uplift of the south island of New Zealand (Tippett and Kamp, 1993). An increase in marine OM input at both locations suggests an increase in global sea levels around 17–18 Ma. The $CPI_{(22\text{-}32)}$ and TAR data for the early Miocene do not completely correlate with the TOC data for the same period. This can be attributed to local factors such as river runoffs and local marine productivity that have strong influences on biomarker signals.

The first part of the middle Miocene period shows high terrigenous OM input in all three sites, suggesting a strong influence of global sea level decrease (Haq et al., 1987; Van Sickel et al., 2004). The second part of the middle Miocene shows some variability in the data. While the New Jersey samples show strong dependence on eustasy around the mid-Miocene Climatic Optimum and afterwards, the New Zealand samples show much stronger dependence on local tectonic activity and creation of the land mass during the same period. The BIT index supports the *n*-alkane based observations.

The reconstructed SST for the Site U1352 shows high values of 26.0ºC and 27.0ºC at 18 Ma. The SST decreases to 22.1ºC at 16.83 Ma. The early Miocene samples from the IODP 313 Sites show generally lower temperatures that the IODP 317 Site samples. The samples show high variation in SST between 24.1ºC and 18.4ºC, with the lowest temperature dated to 20.30 Ma. The reconstructed data suggest a decreasing SST trend from the early Miocene until the middle Miocene. A global climatic optimum and temperature increase at the early/middle Miocene boundary (Nelson and Cooke, 2001a), together with the increasing land mass of the sub-continent based on an increase in sedimentation rates since the middle Miocene (Lu et al., 2005), suggests gradual intensification in the amount of land vegetation.

High SST variations in the New Jersey data are attributed to the influence of local tectonic activity. These SST variations are not recorded in the New Zealand data. This is attributed to the low local tectonic influence on the New Zealand samples and thus a higher eustasy influence on SSTs. Southern Hemisphere influenced trends such as Western Antarctica ice sheet accumulation (Miller et al., 1991) and development of colder Antarctic currents (Belkin and Gordon, 1996; Nelson and Cooke, 2001b) can be proposed as the main factors influencing the SST around New Zealand (Nelson and Cooke, 2001b), rather than global climate and eustasy fluctuations.

The data show a warming MAAT trend in New Zealand that correlates well to the established mid-Miocene Climatic Optimum reconstruction. The MAAT in the New Zealand samples continues to rise through the second part of middle Miocene and during the late Miocene, with only two major cooling events at 10.49 and 8.39 Ma. Some variation of MAAT increase after the mid-Miocene Climatic Optimum is recorded in the Site M0028A record. In addition, the MAAT for the New Jersey region shows an increasing trend to 29.7ºC at 11.02 Ma. The increase in MAAT during the mid-Miocene Climatic Optimum is recorded for all three sites between 17 Ma and 15 Ma. The MAAT warming after 14 Ma in New Zealand is supported by fossil studies of the New Zealand vegetation (Mildenhall, 2003).

Soil pH from New Zealand samples shows a decrease in precipitation levels during the Miocene. The New Jersey samples show no change in precipitation pattern.

4.6. Acknowledgements

This work was supported by the post-cruise funding by the Australia-New Zealand IODP Consortium (ANZIC) and by a Macquarie University High Degree Excellence Scholarship.

4.7. References

Abreu, V.S., Anderson, J.B., 1998. Glacial eustasy during the Cenozoic: sequence stratigraphic implications. *AAPG Bulletin* 82, 1385-1400.

Adams, C., 1981. Uplift rates and thermal structure in the Alpine fault zone and Alpine schists, Southern Alps, New Zealand. *Geological Society, London, Special Publications* 9, 211-222.

Albaigés, J., Grimalt, J., Bayona, J., Risebrough, R., De Lappe, B., Walker, W., 1984. Dissolved, particulate and sedimentary hydrocarbons in a deltaic environment. *Organic Geochemistry* 6, 237-248.

Aloulou, F., Kallel, M., Dammak, M., Elleuch, B., Saliot, A., 2010. Even-numbered n-alkanes/n-alkenes predominance in surface sediments of Gabes Gulf in Tunisia. *Environmental Earth Sciences* 61, 1-10.

Barker, P.F., Barrett, P.J., Cooper, A.K., Huybrechts, P., 1999. Antarctic glacial history from numerical models and continental margin sediments. *Palaeogeography, Palaeoclimatology, Palaeoecology* 150, 247-267.

Batt, G.E., Braun, J., Kohn, B.P., McDougall, I., 2000. Thermochronological analysis of the dynamics of the Southern Alps, New Zealand. *GSA Bulletin* 112, 250-266.

Becker, K.W., Lipp, J.S., Versteegh, G.J., Wörmer, L., Hinrichs, K.-U., 2015. Rapid and simultaneous analysis of three molecular sea surface temperature proxies and application to sediments from the Sea of Marmara. *Organic Geochemistry* 85, 42-53.

Becker, K.W., Lipp, J.S., Zhu, C., Liu, X.-L., Hinrichs, K.-U., 2013. An improved method for the analysis of archaeal and bacterial ether core lipids. *Organic Geochemistry* 61, 34-44.

Belkin, I.M., Gordon, A.L., 1996. Southern Ocean fronts from the Greenwich meridian to Tasmania. *Journal of Geophysical Research: Oceans* 101, 3675-3696.

Berner, R., 1990. Atmospheric carbon dioxide levels over Phanerozoic time. *Science* 249, 1382-1386.

Berner, R.A., 1989. Biogeochemical cycles of carbon and sulfur and their effect on atmospheric oxygen over Phanerozoic time. *Palaeogeography, Palaeoclimatology, Palaeoecology* 75, 97-122.

Beu, A.G., Griffin, M., Maxwell, P., 1997. Opening of Drake Passage gateway and Late Miocene to Pleistocene cooling reflected in Southern Ocean molluscan dispersal: evidence from New Zealand and Argentina. *Tectonophysics* 281, 83-97.

Blumer, M., Mullin, M.M., Thomas, D.W., 1964. Pristane in the marine environment. *Helgoländer Wissenschaftliche Meeresuntersuchungen* 10, 187-201.

Böhme, M., Winklhofer, M., Ilg, A., 2011. Miocene precipitation in Europe: temporal trends and spatial gradients. *Palaeogeography, Palaeoclimatology, Palaeoecology* 304, 212-218.

Bonnefille, R., 2010. Cenozoic vegetation, climate changes and hominid evolution in tropical Africa. *Global and Planetary Change* 72, 390-411.

Bourbonniere, R., Meyers, P., 1996. Anthropogenic influences on hydrocarbon contents of sediments deposited in eastern Lake Ontario since 1800. *Environmental Geology* 28, 22-28.

Bruch, A., Utescher, T., Mosbrugger, V., Gabrielyan, I., Ivanov, D., 2006. Late Miocene climate in the circum-Alpine realm—a quantitative analysis of terrestrial palaeofloras. *Palaeogeography, Palaeoclimatology, Palaeoecology* 238, 270-280.

Bruch, A.A., Utescher, T., Mosbrugger, V., 2011. Precipitation patterns in the Miocene of Central Europe and the development of continentality. *Palaeogeography, Palaeoclimatology, Palaeoecology* 304, 202-211.

Carter, L., Carter, R., McCave, I., 2004. Evolution of the sedimentary system beneath the deep Pacific inflow off eastern New Zealand. *Marine Geology* 205, 9-27.

Carter, R.t., Norris, R., 1976. Cainozoic history of southern New Zealand: an accord between geological observations and plate-tectonic predictions. *Earth and Planetary Science Letters* 31, 85-94.

Cerling, T.E., Wang, Y., Quade, J., 1993. Expansion of C4 ecosystems as an indicator of global ecological change in the late Miocene. *Nature* 361, 344-345.

Chaproniere, G.C., 1984. Oligocene and Miocene larger foraminiferida from Australia and New Zealand. 1.

Clift, P., Hodges, K., Heslop, D., Hannigan, R., Hoang, L., Calves, G., 2008. Greater Himalayan exhumation triggered by Early Miocene monsoon intensification. *Nature Geoscience* 1, 875-880.

Cowie, G., Hedges, J., 1992. The role of anoxia in organic matter preservation in coastal sediments: relative stabilities of the major biochemicals under oxic and anoxic depositional conditions. *Organic Geochemistry* 19, 229-234.

Cramer, B., Miller, K., Barrett, P., Wright, J., 2011. Late Cretaceous–Neogene trends in deep ocean temperature and continental ice volume: Reconciling records of benthic foraminiferal geochemistry (δ18O and Mg/Ca) with sea level history. *Journal of Geophysical Research: Oceans* 116.

Cranwell, P., 1984. Lipid geochemistry of sediments from Upton Broad, a small productive lake. *Organic Geochemistry* 7, 25-37.

Cranwell, P., Eglinton, G., Robinson, N., 1987. Lipids of aquatic organisms as potential contributors to lacustrine sediments—II. *Organic Geochemistry* 11, 513-527.

Damsté, J.S.S., van Bentum, E.C., Reichart, G.-J., Pross, J., Schouten, S., 2010. A CO 2 decrease-driven cooling and increased latitudinal temperature gradient during the mid-Cretaceous Oceanic Anoxic Event 2. *Earth and Planetary Science Letters* 293, 97-103.

Dickens, A.F., Gélinas, Y., Masiello, C.A., Wakeham, S., Hedges, J.I., 2004. Reburial of fossil organic carbon in marine sediments. *Nature* 427, 336-339.

Eglinton, G., Hamilton, R.J., 1967. Leaf epicuticular waxes. *Science* 156, 1322-1335.

Ekpo, B., Oyo-Ita, O., Wehner, H., 2005. Even-n-alkane/alkene predominances in surface sediments from the Calabar River, SE Niger Delta, Nigeria. *Nature* 92, 341-346.

Flower, B.P., Kennett, J.P., 1994. The middle Miocene climatic transition: East Antarctic ice sheet development, deep ocean circulation and global carbon cycling. *Palaeogeography, Palaeoclimatology, Palaeoecology* 108, 537-555.

Fulthorpe, C.S., Carter, R.M., 1991. Continental-shelf progradation by sediment-drift accretion. *Geological Society of America Bulletin* 103, 300-309.

Fulthorpe, C.S., Hoyanagi, K., Blum, P., Expedition, I., 2011a. IODP Expedition 317: Exploring the Record of Sea-Level Change Off New Zealand. *Scientific Drilling* 12, 4-14.

Fulthorpe, C.S., Hoyanagi, K., Blum, P., Scientists, a.t.E., 2011b. *Proc*. IODP, 317: Tokyo (Integrated Ocean Drilling Program Management International, Inc.).
Fulthorpe, C.S., Hoyanagi, K., Crundwell, M.P., Dinarès-Turell, J., Ding, X., George, S.C., Hepp, D.A., Jaeger, J., Kawagata, S., Kemp, D.B., 2011c. Expedition 317 summary.

Gelin, F., Damsté, J.S.S., Harrison, W.N., Maxwell, J.R., De Leeuw, J.W., 1995. Molecular indicators for palaeoenvironmental change in a Messinian evaporitic sequence (Vena del Gesso, Italy): III. Stratigraphic changes in the molecular structure of kerogen in a single marl bed as revealed by flash pyrolysis. *Organic Geochemistry* 23, 555-566.

Graham, A., 1999. Late Cretaceous and Cenozoic history of North American vegetation: north of Mexico. Oxford University Press on Demand.
Greenlee, S.M., Moore, T.C., 1988. Recognition and interpretation of depositional sequences and calculation of sea-level changes from stratigraphic data—offshore New Jersey and Alabama Tertiary.

Greenwood, D.R., Wing, S.L., 1995. Eocene continental climates and latitudinal temperature gradients. *Geology* 23, 1044-1048.

Grimalt, J., Albaigés, J., 1987. Sources and occurrence of C 12 C 22 n-alkane distributions with even carbon-number preference in sedimentary environments. *Geochimica et Cosmochimica Acta* 51, 1379-1384.

Grossi, V., Hirschler, A., Raphel, D., Rontani, J.-F., De Leeuw, J., Bertrand, J.-C., 1998. Biotransformation pathways of phytol in recent anoxic sediments. *Organic Geochemistry* 29, 845-861.

Haq, B.U., Hardenbol, J., Vail, P.R., 1987. Chronology of fluctuating sea levels since the Triassic. *Science* 235, 1156-1167.

Hedges, J.I., Keil, R.G., 1995. Sedimentary organic matter preservation: an assessment and speculative synthesis. *Marine Chemistry* 49, 81-115.

Heine, C., Müller, R.D., Gaina, C., 2004. Reconstructing the lost eastern Tethys ocean basin: convergence history of the SE Asian margin and marine gateways. *Continent-Ocean Interactions within East Asian Marginal Seas*, 37-54.

Hopmans, E.C., Schouten, S., Damsté, J.S.S., 2016. The effect of improved chromatography on GDGT-based palaeoproxies. *Organic Geochemistry* 93, 1-6.

Hopmans, E.C., Weijers, J.W., Schefuß, E., Herfort, L., Damsté, J.S.S., Schouten, S., 2004. A novel proxy for terrestrial organic matter in sediments based on branched and isoprenoid tetraether lipids. *Earth and Planetary Science Letters* 224, 107-116.

Huang, Y., Clemens, S.C., Liu, W., Wang, Y., Prell, W.L., 2007. Large-scale hydrological change drove the late Miocene C4 plant expansion in the Himalayan foreland and Arabian Peninsula. *Geology* 35, 531-534.

Itoigawa, J., Yamanoi, T., 1990. Climatic optimum in the Mid-Neogene of the Japanese Islands. In, Pacific Neogene events, their timing, nature and interrelationship. Univ. Tokyo Press.

Janis, C.M., Scott, K.M., Jacobs, L.L., 1998. Evolution of Tertiary mammals of North America: Volume 1, terrestrial carnivores, ungulates, and ungulate like mammals. Cambridge University Press.
Jenkins, D.G., 1965. Planktonic foraminiferal zones and new taxa from the Danian to Lower Miocene of New Zealand. *New Zealand Journal of Geology and Geophysics* 8, 1088-1126.

Kamp, P., 1987. Age and origin of the New Zealand orocline in relation to Alpine Fault movement. *Journal of the Geological Society* 144, 641-652.

Keeley, J.E., Rundel, P.W., 2005. Fire and the Miocene expansion of C4 grasslands. *Ecology Letters* 8, 683-690.

Keigwin, L., Keller, G., 1984. Middle Oligocene cooling from equatorial Pacific DSDP site 77B. *Geology* 12, 16-19.

Kennett, J., Houtz, R., Andrews, P., Edwards, A., Gostin, V., Hajos, M., Hampton, M., Jenkins, D., Margolis, S., Ovenshine, A., 1974. Development of the circum-Antarctic current. *Science* 186, 144-147.

Kim, J.-H., Schouten, S., Hopmans, E.C., Donner, B., Sinninghe Damsté, J.S., 2008. Global sediment core-top calibration of the TEX86 paleothermometer in the ocean. *Geochimica et Cosmochimica Acta* 72, 1154-1173.

Kim, J.-H., Van der Meer, J., Schouten, S., Helmke, P., Willmott, V., Sangiorgi, F., Koç, N., Hopmans, E.C., Damsté, J.S.S., 2010. New indices and calibrations derived from the distribution of crenarchaeal isoprenoid tetraether lipids: Implications for past sea surface temperature reconstructions. *Geochimica et Cosmochimica Acta* 74, 4639-4654.

King, P.R., 2000. Tectonic reconstructions of New Zealand: 40 Ma to the present. *New Zealand Journal of Geology and Geophysics* 43, 611-638.

Kirk, D.N., Shaw, P.M., 1975. Backbone rearrangements of steroidal 5-enes. *Journal of the Chemical Society, Perkin Transactions 1*, 2284-2294.

Kominz, M.A., Browning, J., Miller, K., Sugarman, P., Mizintseva, S., Scotese, C., 2008. Late Cretaceous to Miocene sea-level estimates from the New Jersey and Delaware coastal plain coreholes: An error analysis. *Basin Research* 20, 211-226.

Kominz, M.A., Miller, K.G., Browning, J.V., 1998. Long-term and short-term global Cenozoic sea-level estimates. *Geology* 26, 311-314.

Lao, Y., Korth, J., Ellis, J., Crisp, P., 1989. Heterogeneous reactions of 1-pristene catalysed by clays under simulated geological conditions. *Organic Geochemistry* 14, 375-379.

Lawver, L.A., Gahagan, L.M., 2003. Evolution of Cenozoic seaways in the circum-Antarctic region. *Palaeogeography, Palaeoclimatology, Palaeoecology* 198, 11-37.

Lawver, L.A., Gahagan, L.M., Coffin, M.F., 1992. The development of paleoseaways around Antarctica. *The Antarctic Paleoenvironment: A Perspective on Global Change: Part One*, 7-30.

Liu, X., Lipp, J.S., Hinrichs, K.-U., 2011. Distribution of intact and core GDGTs in marine sediments. *Organic Geochemistry* 42, 368-375.

Liu, Z., Pagani, M., Zinniker, D., DeConto, R., Huber, M., Brinkhuis, H., Shah, S.R., Leckie, R.M., Pearson, A., 2009. Global cooling during the Eocene-Oligocene climate transition. *Science* 323, 1187-1190.

Lu, H., Fulthorpe, C.S., Mann, P., Kominz, M.A., 2005. Miocene–Recent tectonic and climatic controls on sediment supply and sequence stratigraphy: Canterbury basin, New Zealand. *Basin Research* 17, 311-328.

Lunt, D.J., Flecker, R., Valdes, P.J., Salzmann, U., Gladstone, R., Haywood, A.M., 2008. A methodology for targeting palaeo proxy data acquisition: A case study for the terrestrial late Miocene. *Earth and Planetary Science Letters* 271, 53-62.

Mackenzie, A., Patience, R., Maxwell, J., Vandenbroucke, M., Durand, B., 1980. Molecular parameters of maturation in the Toarcian shales, Paris Basin, France—I. Changes in the configurations of acyclic isoprenoid alkanes, steranes and triterpanes. *Geochimica et Cosmochimica Acta* 44, 1709-1721.

Marsaglia, K.M., Browne, G.H., George, S.C., Kemp, D.B., Jaeger, J.M., Carson, D., Richaud, M., Expedition, I., 2017. The Transformation of Sediment Into Rock: Insights From IODP Site U1352, Canterbury Basin, New Zealand. *Journal of Sedimentary Research* 87, 272-287.

Martin, H., 2006. Cenozoic climatic change and the development of the arid vegetation in Australia. *Journal of Arid Environments* 66, 533-563.

Mcgowran, B., Li, Q., Moss, G., 1997. The Cenozoic neritic record in southern Australia: the biogeohistorical framework.

Metcalfe, I., 2013. Gondwana dispersion and Asian accretion: tectonic and palaeogeographic evolution of eastern Tethys. *Journal of Asian Earth Sciences* 66, 1-33.

Meybeck, M., 1982. Carbon, nitrogen, and phosphorus transport by world rivers. *American Journal of Science* 282, 401-450.

Meyers, P.A., 1997. Organic geochemical proxies of paleoceanographic, paleolimnologic, and paleoclimatic processes. *Organic Geochemistry* 27, 213-250.

Meyers, P.A., Ishiwatari, R., 1993a. The Early Diagenesis of Organic Matter in Lacustrine Sediments, in: Engel, M., Macko, S. (Eds.), Organic Geochemistry. Springer US, pp. 185-209.
Meyers, P.A., Ishiwatari, R., 1993b. Lacustrine organic geochemistry—an overview of indicators of organic matter sources and diagenesis in lake sediments. *Organic Geochemistry* 20, 867-900.

Mildenhall, D., 2003. Deep-sea record of Pliocene and Pleistocene terrestrial palynomorphs from offshore eastern New Zealand (ODP Site 1123, Leg 181). *New Zealand Journal of Geology and Geophysics* 46, 343-361.

Mille, G., Asia, L., Guiliano, M., Malleret, L., Doumenq, P., 2007. Hydrocarbons in coastal sediments from the Mediterranean sea (Gulf of Fos area, France). *Marine Pollution Bulletin* 54, 566-575.

Miller, K.G., Kominz, M.A., Browning, J.V., Wright, J.D., Mountain, G.S., Katz, M.E., Sugarman, P.J., Cramer, B.S., Christie-Blick, N., Pekar, S.F., 2005. The Phanerozoic record of global sea-level change. *Science* 310, 1293-1298.

Miller, K.G., Mountain, G.S., Browning, J.V., Kominz, M., Sugarman, P.J., Christie-Blick, N., Katz, M.E., Wright, J.D., 1998. Cenozoic global sea level, sequences, and the New Jersey transect: results from coastal plain and continental slope drilling. *Reviews of Geophysics* 36, 569-601.

Miller, K.G., Sugarman, P.J., Browning, J.V., Kominz, M.A., Hernández, J.C., Olsson, R.K., Wright, J.D., Feigenson, M.D., Van Sickel, W., 2003. Late Cretaceous chronology of large, rapid sea-level changes: Glacioeustasy during the greenhouse world. *Geology* 31, 585-588.

Miller, K.G., Wright, J.D., Fairbanks, R.G., 1991. Unlocking the ice house: Oligocene-Miocene oxygen isotopes, eustasy, and margin erosion. *Journal of Geophysical Research: Solid Earth* 96, 6829-6848.

Molnar, P., Atwater, T., Mammerickx, J., Smith, S.M., 1975. Magnetic anomalies, bathymetry and the tectonic evolution of the South Pacific since the Late Cretaceous. *Geophysical Journal International* 40, 383-420.

Mountain, G., Proust, J., McInroy, D., Cotterill, C., 2010. the Expedition 313 Scientists, 2010, Proceedings of the Integrated Ocean Drilling Program.
Müller, R.D., Sdrolias, M., Gaina, C., Steinberger, B., Heine, C., 2008. Long-term sea-level fluctuations driven by ocean basin dynamics. *Science* 319, 1357-1362.

Nelson, C.S., Cooke, P.J., 2001a. History of oceanic front development in the New Zealand sector of the Southern Ocean during the Cenozoic—a synthesis. *New Zealand Journal of Geology and Geophysics* 44, 535-553.

Nelson, C.S., Cooke, P.J., 2001b. History of oceanic front development in the New Zealand sector of the Southern Ocean during the Cenozoic - a synthesis. *New Zealand Journal of Geology and Geophysics* 44, 535-553.

Nishimura, M., Baker, E.W., 1986. Possible origin of n-alkanes with a remarkable even-to-odd predominance in recent marine sediments. *Geochimica et Cosmochimica Acta* 50, 299-305.

Norris, R., Koons, P., Cooper, A., 1990. The obliquely-convergent plate boundary in the South Island of New Zealand: implications for ancient collision zones. *Journal of structural geology* 12, 715-725.

Ourisson, G., Albrecht, P., Rohmer, M., 1984. Microbial origin of fossil fuels. *Sci. Am.;(United States)* 251.

Pagani, M., Arthur, M.A., Freeman, K.H., 1999. Miocene evolution of atmospheric carbon dioxide. *Paleoceanography* 14, 273-292.

Pancost, R.D., Steart, D.S., Handley, L., Collinson, M.E., Hooker, J.J., Scott, A.C., Grassineau, N.V., Glasspool, I.J., 2007. Increased terrestrial methane cycling at the Palaeocene–Eocene thermal maximum. *Nature* 449, 332-335.

Passchier, S., Bohaty, S., Jiménez-Espejo, F., Pross, J., Röhl, U., Flierdt, T., Escutia, C., Brinkhuis, H., 2013. Early Eocene to middle Miocene cooling and aridification of East Antarctica. *Geochemistry, Geophysics, Geosystems* 14, 1399-1410.

Pearson, A., Huang, Z., Ingalls, A., Romanek, C., Wiegel, J., Freeman, K., Smittenberg, R., Zhang, C., 2004. Nonmarine crenarchaeol in Nevada hot springs. *Applied and Environmental Microbiology* 70, 5229-5237.

Peters, K.E., Moldowan, J.M., 1993. The biomarker guide : interpreting molecular fossils in petroleum and ancient sediments. Prentice Hall, Englewood Cliffs, N.J.
Peters, K.E., Walters, C.C., Moldowan, J.M., 2005. The biomarker guide, 2nd ed. Cambridge University Press, Cambridge, UK ; New York.
Peterse, F., van der Meer, J., Schouten, S., Weijers, J.W.H., Fierer, N., Jackson, R.B., Kim, J.-H., Sinninghe Damsté, J.S., 2012. Revised calibration of the MBT–CBT paleotemperature proxy based on branched tetraether membrane lipids in surface soils. *Geochimica et Cosmochimica Acta* 96, 215-229.

Pitman, W., Golovchenko, X., 1991. The effect of sea level changes on the morphology of mountain belts. *Journal of Geophysical Research: Solid Earth* 96, 6879-6891.

Poag, C., 1985. Cenozoic and Upper Cretaceous sedimentary facies and depositional systems of the New Jersey slope and rise. *Geological Evolution of the United States Atlantic Margin: New York (Van Nostrand Reinhold)*, 343-365.

Poage, M., Chamberlain, C., 2002. Stable isotopic evidence for a pre-Middle Miocene rain shadow in the western Basin and Range: Implications for the paleotopography of the Sierra Nevada. *Tectonics* 21.

Pocknall, D.T., 1989. Late Eocene to Early Miocene vegetation and climate history of New Zealand. *Journal of the Royal Society of New Zealand* 19, 1-18.

Pole, M., 2003. New Zealand climate in the Neogene and implications for global atmospheric circulation. *Palaeogeography, Palaeoclimatology, Palaeoecology* 193, 269-284.

Posamentier, H., 1988. Eustatic controls on clastic deposition II—sequence and systems tract models.

Powell, T., McKirdy, D., 1973. Relationship between ratio of pristane to phytane, crude oil composition and geological environment in Australia. *Nature* 243, 37-39.

Prahl, F.G., Coble, P.G., 1994. Input and behavior of dissolved organic carbon in the Columbia River Estuary. *Changes in Fluxes in Estuaries: Implications from Science to Management*, 451-457.

Prahl, F.G., Ertel, J.R., Goni, M.A., Sparrow, M.A., Eversmeyer, B., 1994. Terrestrial Organic-Carbon Contributions to Sediments on the Washington Margin. *Geochimica et Cosmochimica Acta* 58, 3035-3048.

Reichgelt, T., Kennedy, E.M., Conran, J.G., Mildenhall, D.C., Lee, D.E., 2015. The early Miocene paleolake Manuherikia: vegetation heterogeneity and warm-temperate to subtropical climate in southern New Zealand. *Journal of Paleolimnology* 53, 349-365.

Retallack, G.J., 2004. Late Miocene climate and life on land in Oregon within a context of Neogene global change. *Palaeogeography, Palaeoclimatology, Palaeoecology* 214, 97-123.

Retallack, G.J., 2009. Refining a pedogenic-carbonate CO 2 paleobarometer to quantify a middle Miocene greenhouse spike. *Palaeogeography, Palaeoclimatology, Palaeoecology* 281, 57-65.

Rohling, E.J., Cooke, S., 1999. Stable oxygen and carbon isotopes in foraminiferal carbonate shells, Modern foraminifera. Springer, pp. 239-258.

Rontani, J.-F., Nassiry, M., Michotey, V., Guasco, S., Bonin, P., 2010. Formation of pristane from α-tocopherol under simulated anoxic sedimentary conditions: A combination of biotic and abiotic degradative processes. *Geochimica et Cosmochimica Acta* 74, 252-263.

Rowland, S., 1990. Production of acyclic isoprenoid hydrocarbons by laboratory maturation of methanogenic bacteria. *Organic Geochemistry* 15, 9-16.

Royer, D.L., 2006. CO 2-forced climate thresholds during the Phanerozoic. *Geochimica et Cosmochimica Acta* 70, 5665-5675.

Sahagian, D., Pinous, O., Olferiev, A., Zakharov, V., 1996. Eustatic Curve for the Middle Jurassic--Cretaceous Based on Russian Platform and Siberian Stratigraphy: Zonal Resolution. *AAPG bulletin* 80, 1433-1458.

Saliot, A., 1981. Natural Hydrocarbons in Sea Water Alain Saliot. *Elsevier Oceanography Series* 31, 327-374.

Saliot, A., Denant, V., Bigot, M., 1998. Organic matter in large Chinese rivers and their estuaries: the Changjiang River and the Huanghe River. *Land-Sea Interaction in Chinese Coastal Zones. Ocean Press, Beijing*, 176-191.

Schouten, S., Hopmans, E.C., Damsté, J.S.S., 2013. The organic geochemistry of glycerol dialkyl glycerol tetraether lipids: a review. *Organic Geochemistry* 54, 19-61.

Schwarz, T., 1997. Lateritic bauxite in central Germany and implications for Miocene palaeoclimate. *Palaeogeography, Palaeoclimatology, Palaeoecology* 129, 37-50.

Seifert, W., Moldowan, J., 1986. Use of biological markers in petroleum exploration. *Methods in geochemistry and geophysics* 24, 261-290.

Seifert, W.K., Moldowan, J.M., 1980. The effect of thermal stress on source-rock quality as measured by hopane stereochemistry. *Physics and Chemistry of the Earth* 12, 229-237.

Seki, O., Nakatsuka, T., Shibata, H., Kawamura, K., 2010. A compound-specific n-alkane δ13C and δD approach for assessing source and delivery processes of terrestrial organic matter within a forested watershed in northern Japan. *Geochimica et Cosmochimica Acta* 74, 599-613.

Shackleton, N.J., Kennett, J.P., 1975. Paleotemperature history of the Cenozoic and the initiation of Antarctic glaciation: oxygen and carbon isotope analyses in DSDP Sites 277, 279, and 281. *Initial reports of the deep sea drilling project* 29, 743-755.

Shackleton, N.J., Pisias, N., 1985. Atmospheric carbon dioxide, orbital forcing, and climate. *The Carbon Cycle and Atmospheric CO: Natural variations Archean to Present*, 303-317.

Sheldon, N.D., 2006. Using paleosols of the Picture Gorge Basalt to reconstruct the middle Miocene climatic optimum. *PaleoBios* 26, 27-36.

Sheridan, R.E., Grow, J.A., 1988. The Atlantic continental margin: US. Geological Society of America, Boulder, CO (USA).
Shevenell, A.E., Kennett, J.P., Lea, D.W., 2004. Middle Miocene southern ocean cooling and Antarctic cryosphere expansion. *Science* 305, 1766-1770.

Silliman, J., Meyers, P., Ostrom, P., Ostrom, N., Eadie, B., 2000. Insights into the origin of perylene from isotopic analyses of sediments from Saanich Inlet, British Columbia. *Organic Geochemistry* 31, 1133-1142.

Simoneit, B.R., 1977. Diterpenoid compounds and other lipids in deep-sea sediments and their geochemical significance. *Geochimica et Cosmochimica Acta* 41, 463-476.

Sniderman, J.K., Woodhead, J.D., Hellstrom, J., Jordan, G.J., Drysdale, R.N., Tyler, J.J., Porch, N., 2016. Pliocene reversal of late Neogene aridification. *Proceedings of the National Academy of Sciences* 113, 1999-2004.

Steppuhn, A., Micheels, A., Geiger, G., Mosbrugger, V., 2006. Reconstructing the Late Miocene climate and oceanic heat flux using the AGCM ECHAM4 coupled to a mixed-layer ocean model with adjusted flux correction. *Palaeogeography, Palaeoclimatology, Palaeoecology* 238, 399-423.

Tippett, J.M., Kamp, P.J., 1993. The role of faulting in rock uplift in the Southern Alps, New Zealand. *New Zealand Journal of Geology and Geophysics* 36, 497-504.

Tissot, B., Califet-Debyser, Y., Deroo, G., Oudin, J., 1971. Origin and evolution of hydrocarbons in early Toarcian shales, Paris Basin, France. *AAPG bulletin* 55, 2177-2193.

Tomczak, M., Godfrey, J.S., 2013. Regional oceanography: an introduction. Elsevier.
Tynan, C.T., 1998. Ecological importance of the southern boundary of the Antarctic Circumpolar Current. *Nature* 392, 708.

Van Sickel, W.A., Kominz, M.A., Miller, K.G., Browning, J.V., 2004. Late Cretaceous and Cenozoic sea-level estimates: backstripping analysis of borehole data, onshore New Jersey. *Basin Research* 16, 451-465.

Vincent, E., Killingley, J.S., Berger, W.H., 1985. Miocene oxygen and carbon isotope stratigraphy of the tropical Indian Ocean. *Geological Society of America Memoirs* 163, 103-130.

Volkman, J.K., Maxwell, J.R., 1986. Acyclic isoprenoids as biological markers. *Methods in geochemistry and geophysics* 24, 1-42.

Wan, S., Kürschner, W.M., Clift, P.D., Li, A., Li, T., 2009. Extreme weathering/erosion during the Miocene Climatic Optimum: evidence from sediment record in the South China Sea. *Geophysical Research Letters* 36.

Weijers, J.W., Schouten, S., Spaargaren, O.C., Damsté, J.S.S., 2006. Occurrence and distribution of tetraether membrane lipids in soils: implications for the use of the TEX 86 proxy and the BIT index. *Organic Geochemistry* 37, 1680-1693.

Weijers, J.W.H., Schouten, S., Sluijs, A., Brinkhuis, H., Sinninghe Damsté, J.S., 2007. Warm arctic continents during the Palaeocene–Eocene thermal maximum. *Earth and Planetary Science Letters* 261, 230-238.

Winkworth, R.C., Wagstaff, S.J., Glenny, D., Lockhart, P.J., 2002. Plant dispersal news from New Zealand. *Trends in Ecology & Evolution* 17, 514-520.

Withjack, M.O., Schlische, R.W., Olsen, P.E., 1998. Diachronous rifting, drifting, and inversion on the passive margin of central eastern North America: an analog for other passive margins. *AAPG bulletin* 82, 817-835.

Wolfe, J.A., 1994a. An analysis of Neogene climates in Beringia. *Palaeogeography, Palaeoclimatology, Palaeoecology* 108, 207-216.

Wolfe, J.A., 1994b. Tertiary climatic changes at middle latitudes of western North America. *Palaeogeography, Palaeoclimatology, Palaeoecology* 108, 195-205.

Wood, R., Stagpoole, V., 2007. Validation of tectonic reconstructions by crustal volume balance: New Zealand through the Cenozoic. *Geological Society of America Bulletin* 119, 933-943.

You, Y., Huber, M., Müller, R., Poulsen, C., Ribbe, J., 2009. Simulation of the middle Miocene climate optimum. *Geophysical Research Letters* 36.

Youngblood, W., Blumer, M., 1973. Alkanes and alkenes in marine benthic algae. *Marine Biology* 21, 163-172.

Zachos, J., Pagani, M., Sloan, L., Thomas, E., Billups, K., 2001. Trends, rhythms, and aberrations in global climate 65 Ma to present. *Science* 292, 686-693.

Zachos, J.C., Dickens, G.R., Zeebe, R.E., 2008. An early Cenozoic perspective on greenhouse warming and carbon-cycle dynamics. *Nature* 451, 279-283.

Zhisheng, A., Kutzbach, J.E., Prell, W.L., Porter, S.C., 2001. Evolution of Asian monsoons and phased uplift of the Himalaya–Tibetan plateau since Late Miocene times. *Nature* 411, 62-66.

4.8. Appendix: Tables

Table 4.1: On-board bulk geochemistry data (Fulthorpe et al., 2011) for the analysed geological periods for Site U1352 (Fulthorpe et al., 2011), M0027A (Mountain et al., 2010), and M0028A (Mountain et al., 2010).

IODP Expedition	Site and Hole number	Sample number	Age (Ma)	Sample depth (mbsf)	IC[1] (wt%)	$CaCO_3$[2] (wt%)	TC[3] (wt%)	TOC[4] (wt%)
317	U1352C	72R1	6.24	1266.06	4.51	37.60	5.16	0.65
317	U1352C	73R4	6.31	1280.3	0.96	7.99	1.29	0.33
317	U1352C	73R5	6.32	1281.69	2.67	22.21	3.08	0.41
317	U1352C	77R1	6.45	1309	4.00	33.35	4.39	0.39
317	U1352C	78R3	6.61	1317.2	3.93	32.72	4.40	0.47
317	U1352C	79R1	6.78	1318.1	4.16	34.63	4.77	0.61
317	U1352C	80R1	7.00	1323.69	3.11	25.94	3.53	0.42
317	U1352C	81R1	7.07	1328.31	2.57	21.37	3.07	0.50
317	U1352C	82R1	7.75	1332.75	3.17	26.40	3.68	0.51
317	U1352C	85R2	7.85	1349.21	4.32	35.99	4.73	0.41
317	U1352C	85R4	7.92	1351.41	1.56	12.96	1.72	0.16
317	U1352C	86R2	7.93	1353.29	5.64	47.02	6.05	0.41
317	U1352C	87R1	8.37	1362.75	4.57	38.06	4.85	0.28
317	U1352C	88R2	8.74	1373.07	0.74	6.14	1.23	0.49
317	U1352C	88R5	8.95	1378.29	0.48	4.02	0.69	0.21
317	U1352C	89R3	8.99	1384.35	0.78	6.53	1.22	0.44
317	U1352C	89R4	9.18	1385.04	1.29	10.75	1.79	0.50
317	U1352C	89R4	9.19	1385.71	1.64	13.69	2.33	0.69
317	U1352C	90R1	9.22	1390.52	0.41	3.42	0.73	0.32
317	U1352C	90R3	9.64	1393.4	3.44	28.62	4.43	0.99
317	U1352C	91R1	9.69	1401.06	6.76	56.31	7.46	0.70
317	U1352C	94R1	10.49	1428.92	5.20	43.31	5.65	0.45
317	U1352C	94R6	10.65	1436.59	2.50	20.82	3.10	0.60
317	U1352C	95R2	10.73	1440.21	4.35	36.27	4.79	0.43
317	U1352C	99R1	11.52	1477.64	6.02	50.18	6.69	0.67
317	U1352C	102RCC	11.92	1496.47	3.71	30.92	4.19	0.48
317	U1352C	103R1	12.54	1506.7	4.72	39.31	5.25	0.53
317	U1352C	103R2	12.63	1508.23	4.49	37.37	4.94	0.45
317	U1352C	103R5	12.94	1513.24	2.05	17.07	2.39	0.34

IODP Expedition	Site and Hole number	Sample number	Age (Ma)	Sample depth (mbsf)	IC[1] (wt%)	$CaCO_3$[2] (wt%)	TC[3] (wt%)	TOC[4] (wt%)
317	U1352C	104R1	13.14	1516.55	4.24	35.34	4.62	0.38
317	U1352C	105R1	13.72	1526.17	4.62	38.50	5.09	0.47
317	U1352C	105R1	13.72	1526.2	5.44	45.32	6.11	0.67
317	U1352C	106R4	13.97	1540.15	4.49	37.44	5.11	0.62
317	U1352C	106R6	14.01	1542.35	2.07	17.26	2.50	0.42
317	U1352C	107R2	14.09	1546.48	5.38	44.77	6.07	0.69
317	U1352C	107R3	14.13	1549.21	6.35	52.93	6.87	0.52
317	U1352C	108R4	14.26	1558.94	2.77	23.07	3.26	0.49
317	U1352C	109R1	14.35	1565.29	5.54	46.18	6.04	0.50
317	U1352C	109R3	14.39	1568.05	3.02	25.18	3.66	0.64
317	U1352C	110R2	14.50	1575.83	1.57	13.12	2.59	1.02
317	U1352C	110R3	14.52	1577.08	2.39	19.90	3.14	0.75
317	U1352C	111R1	14.65	1584.74	1.01	8.41	1.53	0.52
317	U1352C	111R4	14.71	1588.45	8.12	67.65	8.43	0.31
317	U1352C	112R1	14.81	1594.11	7.58	63.14	7.86	0.28
317	U1352C	112R3	14.85	1596.68	2.82	23.50	3.55	0.73
317	U1352C	113R2	15.00	1605.23	6.54	54.49	7.52	0.98
317	U1352C	113R4	15.06	1608.81	6.47	53.87	6.80	0.33
317	U1352C	114R3	15.20	1617.03	4.84	40.30	5.24	0.40
317	U1352C	114R4	15.21	1618.03	7.84	65.35	7.87	0.03
317	U1352C	115R6	15.42	1630.35	2.30	19.18	3.67	1.37
317	U1352C	115R6	15.43	1631.02	8.18	68.14	8.60	0.42
317	U1352C	116R2	15.49	1634.3	8.09	67.37	8.36	0.27
317	U1352C	116R3	15.51	1635.67	6.67	55.55	7.11	0.44
317	U1352C	117R3	15.68	1644.79	3.56	29.68	4.19	0.63
317	U1352C	117R6	15.75	1649.06	7.71	64.23	7.78	0.07
317	U1352C	118R3	15.85	1654.38	5.36	44.64	5.65	0.29
317	U1352C	118R3	15.86	1654.85	4.76	39.68	5.21	0.45
317	U1352C	119R4	16.06	1666.45	1.17	9.78	1.88	0.71
317	U1352C	119R4	16.07	1666.68	6.90	57.51	7.29	0.39
317	U1352C	120RCC	16.11	1668.9	3.72	30.97	4.42	0.70
317	U1352C	120RCC	16.11	1669.24	6.06	50.52	6.38	0.32
317	U1352C	122R1	16.46	1688.87	4.97	41.44	5.50	0.53

IODP Expedition	Site and Hole number	Sample number	Age (Ma)	Sample depth (mbsf)	IC[1] (wt%)	$CaCO_3$[2] (wt%)	TC[3] (wt%)	TOC[4] (wt%)
317	U1352C	122R2	16.49	1690.26	8.59	71.56	8.94	0.35
317	U1352C	123R1	16.54	1693.23	3.53	29.39	4.23	0.70
317	U1352C	123R2	16.57	1694.65	9.20	76.59	9.21	0.01
317	U1352C	124R6	16.77	1705.96	6.83	56.91	7.15	0.32
317	U1352C	125R2	16.83	1709.41	3.70	30.86	4.06	0.36
317	U1352C	125R5	16.91	1714.16	6.63	55.25	6.85	0.22
317	U1352C	126R3	17.02	1720.51	9.41	78.36	9.65	0.24
317	U1352C	126R6	17.09	1724.31	9.38	78.14	9.62	0.24
317	U1352C	127R2	17.15	1728.06	9.36	77.95	9.49	0.13
317	U1352C	127R3	17.19	1730.22	4.85	40.39	5.36	0.51
317	U1352C	128R1	17.30	1736.38	10.27	85.58	10.40	0.13
317	U1352C	128R5	17.39	1741.69	0.82	6.87	1.55	0.73
317	U1352C	129R1	17.45	1745.44	9.62	80.16	9.86	0.24
317	U1352C	129R2	17.50	1747.88	4.41	36.77	4.70	0.29
317	U1352C	130R2	17.66	1757.2	10.02	83.45	10.08	0.06
317	U1352C	130R3	17.68	1758.63	3.53	29.39	3.86	0.33
317	U1352C	130R4	17.71	1760.44	3.77	31.36	4.01	0.24
317	U1352C	131R2	17.83	1766.98	3.51	29.25	3.67	0.16
317	U1352C	131R2	17.83	1767.13	10.51	87.52	10.81	0.30
317	U1352C	132R3	18.00	1776.86	8.09	67.38	8.31	0.22
317	U1352C	132R3	18.01	1777.38	4.33	36.04	4.38	0.05
317	U1352C	133R2	18.17	1786.74	3.46	28.83	3.64	0.18
317	U1352C	133R3	18.18	1787.37	10.38	86.49	10.65	0.27
317	U1352C	134R1	18.30	1794.18	2.41	20.11	2.58	0.17
317	U1352C	134R3	18.33	1796.58	10.24	85.31	10.28	0.04
317	U1352C	135R1	18.41	1803.84	10.40	86.60	10.57	0.17
317	U1352C	135R4	18.46	1807.91	2.82	23.47	2.93	0.11
317	U1352C	136R3	18.57	1816.86	2.68	22.32	2.96	0.28
317	U1352C	136R4	18.59	1818.5	3.60	29.98	3.77	0.17
317	U1352C	136R5	18.59	1818.86	10.75	89.59	10.93	0.18
317	U1352C	137R4	18.70	1827.88	10.90	90.82	11.04	0.14
317	U1352C	137R5	18.71	1828.82	5.90	49.17	5.96	0.06
317	U1352C	138R1	18.76	1832.84	10.07	83.92	10.30	0.23

IODP Expedition	Site and Hole number	Sample number	Age (Ma)	Sample depth (mbsf)	IC[1] (wt%)	$CaCO_3$[2] (wt%)	TC[3] (wt%)	TOC[4] (wt%)
317	U1352C	138R4	18.80	1836.52	10.70	89.15	11.22	0.52
317	U1352C	138R4	18.82	1837.73	3.29	27.44	3.62	0.33
317	U1352C	139R1	18.87	1842.1	3.08	25.64	3.20	0.12
317	U1352C	139R1	18.87	1842.36	10.52	87.66	10.75	0.23
317	U1352C	140R1	19.06	1851.26	10.54	87.79	10.94	0.40
317	U1352C	140R1	19.06	1851.45	9.42	78.44	10.88	1.46
317	U1352C	140R2	19.07	1852.69	11.58	96.44	12.35	0.77
317	U1352C	141R1	19.17	1861.69	11.51	95.88	11.60	0.09
317	U1352C	143R2	30.87	1877.2	11.54	96.16	11.66	0.12
317	U1352C	144R4	31.92	1884.24	11.53	96.08	11.72	0.19
317	U1352C	145R3	31.14	1892.9	11.20	93.30	11.46	0.26
317	U1352C	146R3	31.29	1902.47	11.01	91.68	10.88	-0.13
317	U1352C	147R3	31.50	1911.56	10.82	90.12	10.91	0.09
317	U1352C	147R4	31.53	1913.23	4.55	37.89	5.09	0.54
317	U1352C	147R6	31.58	1916.31	5.36	44.67	5.69	0.33
317	U1352C	148R3	35.28	1921.41	6.19	51.59	6.69	0.50
317	U1352C	148R5	35.33	1924.03	10.73	89.41	10.86	0.13
313	M0027A	67X2	15.69	198.68	0.77	-	1.81	1.04
313	M0027A	67X3	15.69	200.06	0.85	-	2.19	1.34
313	M0027A	68X1	15.69	202.26	0.71	0.002	1.6	0.89
313	M0027A	70X2	15.69	209.22	0.39	0.013	1.33	0.94
313	M0027A	72H1	15.69	210.7	0.4	0.030	2.23	1.83
313	M0027A	75X1	15.69	216.67	0.21	0.039	2.58	2.37
313	M0027A	80R1	15.69	226.24	0.65	0.012	2.2	1.55
313	M0027A	82R2	15.69	232.36	0.06	-	0.8	0.74
313	M0027A	85R1	15.69	241.35	0.02	-	0.83	0.81
313	M0027A	88R1	15.69	250.38	1.33	0.061	3.34	2.01
313	M0027A	91R1	15.69	259.03	0.96	0.043	8.41	7.45
313	M0027A	94R2	15.69	270.28	0.24	0.028	4.06	3.83
313	M0027A	97R2	16.76	279.33	0.07	0.003	1.53	1.47
313	M0027A	98R1	16.80	280.86	0.25	0.027	2.67	2.42
313	M0027A	101R1	17.06	290.3	0.31	0.017	3.02	2.71
313	M0027A	104R1	17.33	299.24	0.19	-	1.33	1.13

IODP Expedition	Site and Hole number	Sample number	Age (Ma)	Sample depth (mbsf)	IC[1] (wt%)	$CaCO_3$[2] (wt%)	TC[3] (wt%)	TOC[4] (wt%)
313	M0027A	107R1	17.55	308.23	0.31	0.033	2.34	2.03
313	M0027A	110R2	17.81	318.76	0.39	0.042	1.9	1.52
313	M0027A	113R1	18.02	326.81	0.27	0.011	1.77	1.5
313	M0027A	115R2	18.22	334.36	0.11	0.004	1.04	0.93
313	M0027A	119R1	18.38	340.08	0.02	0.007	0.65	0.64
313	M0027A	122R1	18.61	347.96	0.06	0.002	0.21	0.16
313	M0027A	123R1	18.69	350.95	0.57	0.003	0.79	0.21
313	M0027A	129R1	19.14	365.96	0.04	0.001	0.17	0.13
313	M0027A	133R2	19.48	376.81	0.09	0.001	0.2	0.11
313	M0027A	136R1	19.71	383.96	0.02	0.001	0.18	0.17
313	M0027A	138R2	20.01	392.83	0.04	0.002	0.2	0.16
313	M0027A	144R1	20.63	409.75	0.02	0.001	0.3	0.28
313	M0027A	146R1	20.83	415.18	0.13	0.007	1.59	1.46
313	M0027A	148R2	21.12	422.73	0.27	0.024	3.43	3.16
313	M0027A	151R2	21.47	431.86	0.23	0.015	4.34	4.11
313	M0027A	153R2	21.78	438.06	0.11	0.014	4.36	4.25
313	M0027A	154R1	20.74	439.77	0.21	0.014	4.58	4.37
313	M0027A	157R1	21.10	448.67	0.16	0.008	1.35	1.19
313	M0027A	158R1	21.21	451.37	-	0.001	-	-
313	M0027A	160R1	21.47	457.72	0.61	0.049	4.41	3.8
313	M0027A	165R1	22.09	473.1	0.12	0.015	2.04	1.91
313	M0027A	168R1	22.49	483	0.69	0.014	1.74	1.06
313	M0027A	171R2	22.82	491.1	0.47	0.009	0.71	0.23
313	M0027A	175R1	23.11	498.2	0.25	0.008	1.76	1.51
313	M0027A	179R2	23.62	509.1	1.46	0.139	2.27	0.81
313	M0027A	183R2	24.03	518.1	0.85	0.073	2.02	1.17
313	M0027A	190R1	24.75	533.63	3.24	0.002	3.76	0.52
313	M0027A	206R1	26.76	576.96	0.3	0.035	2.02	1.73
313	M0027A	209R1	27.18	585.86	0.18	0.013	1.75	1.57
313	M0027A	213R2	27.82	599.78	0.73	0.070	3.04	2.31
313	M0027A	217R2	28.37	611.56	0.42	0.012	2.18	1.76
313	M0028A	2R1	11.02	223.33	0.54	0.007	2.1	1.56
313	M0028A	3R2	11.42	228.4	0.21	0.010	1.73	1.51

IODP Expedition	Site and Hole number	Sample number	Age (Ma)	Sample depth (mbsf)	IC[1] (wt%)	$CaCO_3$[2] (wt%)	TC[3] (wt%)	TOC[4] (wt%)
313	M0028A	4R2	11.63	231.46	0.77	0.011	2.1	1.33
313	M0028A	7R2	12.19	240.46	0.17	0.006	1.11	0.93
313	M0028A	10R2	12.65	250.64	0.23	0.010	2.31	2.08
313	M0028A	14R1	13.10	257.96	0.09	0.001	0.23	0.13
313	M0028A	19R1	14.28	268.82	0.46	0.008	1.07	0.61
313	M0028A	21R2	14.42	276.46	0.4	0.005	0.87	0.47
313	M0028A	29R	14.78	297.37	0.34	0.036	2	1.66
313	M0028A	81R1	17.12	422.61	0.2	0.012	1.47	1.27
313	M0028A	97R1	17.71	470.98	0.26	0.025	3.16	2.9
313	M0028A	100R2	17.84	481.42	0.31	0.027	2.21	1.91
313	M0028A	113R2	18.88	520.86	0.18	0.016	1.2	1.02
313	M0028A	127R2	19.51	548.87	0.05	0.044	0.63	0.58
313	M0028A	130R2	19.69	557.87	0.03	0.001	1.79	1.76
313	M0028A	133R2	20.00	566.87	0.11	0.002	0.74	0.63
313	M0028A	136R2	20.32	575.87	0.03	0.002	0.45	0.42
313	M0028A	141R2	20.64	584.87	0.09	0.001	0.25	0.15
313	M0028A	145R3	20.96	593.87	0.03	0.001	0.4	0.37
313	M0028A	149R1	21.33	604.42	0.09	0.001	0.74	0.64
313	M0028A	152R1	21.50	611.86	0.42	-	1.08	0.66
313	M0028A	155R1	21.50	620.14	0.31	0.003	0.98	0.67
313	M0028A	161R1	21.50	638.14	0.73	-	1.39	0.66
313	M0028A	164R2	21.50	649.13	0.37	-	1.01	0.64

[1]IC = inorganic carbon

[2]$CaCO_3$ = calcium carbonate

[3]TC = total carbon

[4]Total organic carbon = total carbon (TC)-inorganic carbon; TC = ($CaCO_3$/8.33); after Fulthorpe et al., 2011

Table 4.2: Extractability of the organic matter (mg OM/g sediment), n-alkane and isoprenoid ratios, and n-alkane distributions for the analysed IODP Expedition 317 (U1352) and IODP Expedition 313 (M0027A and M0028A) samples.

Core and section number	Sample depth (mbsf)	Age (Ma)	Extracted sediment (g)	Extractability (mg OM/g sediment)	$CPI_{(22-32)}$[1]	TAR[2]	Pr^3/Ph^4	$Pr/n\text{-}C_{17}$	$Ph/n\text{-}C_{18}$	11	12	13	14	15
U1352C_73R4	1281	5.49	13.7	0.07	1.92	5.6	1.18	2.02	0.90	10.7	13.5	17.4	100	21.0
U1352C_76R1	1305	6.30	50.2	0.14	2.09	17.3	1.14	1.37	0.86	14.8	15.0	11.3	30.2	4.6
U1352C_76R1	1305	6.30	13.2	0.05	2.56	37.3	0.72	3.00	1.88	-	0.3	0.6	0.7	0.4
U1352C_77R1	1310	6.45	13.1	0.25	1.60	2.0	1.25	3.59	1.38	69.3	14.9	21.2	100	23.1
U1352C_78R1	1315	6.61	11.4	0.06	1.19	2.6	1.74	1.56	0.50	12.4	11.5	15.7	100	29.0
U1352C_79R2	1319	6.78	12.1	0.16	3.86	17.3	0.85	1.85	1.57	3.5	3.7	4.6	25.2	6.0
U1352C_80R3	1326	7.00	11.3	0.07	1.08	5.0	1.32	1.35	0.68	18.2	14.4	19.8	100	22.2
U1352C_81R1	1328	7.07	10.9	0.16	1.28	1.3	0.99	1.14	0.63	16.9	15.6	16.4	93.2	27.8
U1352C_85R4	1352	7.85	13.0	0.05	1.39	9.5	0.72	1.30	0.61	4.4	3.5	3.9	28.5	11.7
U1352C_86R2	1354	7.93	11.1	0.04	1.01	14.0	1.14	2.03	0.89	7.2	6.0	5.9	29.5	8.4
U1352C_87R4	1367	8.37	50.1	0.09	1.26	18.0	0.89	3.10	1.67	0.6	0.8	1.2	9.9	0.5
U1352C_88R5	1378	8.74	9.0	0.14	2.17	26.3	0.95	0.96	0.33	3.9	3.9	3.5	19.8	4.5
U1352C_89R3	1384	8.95	15.2	0.07	1.34	7.0	1.04	1.04	0.46	-	-	-	-	-
U1352C_89R4	1386	8.99	76.0	0.31	1.34	7.0	1.04	1.04	0.46	10.8	12.4	16.4	86.6	19.7
U1352C_90R2	1393	9.22	10.4	0.09	1.05	1.9	1.45	1.38	0.54	21.8	13.6	15.4	100	25.2
U1352C_91R5	1407	9.69	12.8	0.10	0.87	3.1	3.82	4.29	0.59	11.2	9.0	10.9	86.2	28.1
U1352C_94R5	1436	10.66	50.0	0.08	1.67	18.1	1.49	2.56	0.86	-	-	-	-	-
U1352C_95R2	1441	10.80	10.2	0.09	1.09	41.9	1.48	1.67	0.46	0.9	0.6	0.6	6.1	2.1
U1352C_102R	1496	11.92	9.0	-	0.98	2.0	1.40	0.57	2.60	22.4	29.0	28.1	100	24.9
U1352C_103R5	1513	12.25	9.5	-	0.72	0.8	13.17	1.72	0.04	10.0	11.4	12.7	78.0	19.3
U1352C_104R2	1517	12.34	12.2	0.08	0.89	2.1	5.78	1.39	1.56	31.2	34.8	29.8	100	18.2
U1352C_105R5	1532	12.64	50.1	0.05	1.29	34.9	1.76	2.00	0.39	-	-	0.3	2.7	0.6
U1352C_106R6	1542	12.84	11.0	0.07	1.20	16.6	0.58	0.91	0.65	0.4	0.3	0.3	1.1	1.3
U1352C_107R6	1553	13.06	7.7	0.03	-	-	3.73	2.70	0.59	-	-	-	-	-
U1352C_108R1	1555	13.09	10.0	-	-	-	14.37	2.02	0.22	-	-	-	-	-
U1352C_109R3	1569	13.37	8.6	-	-	-	2.20	3.94	1.01	-	-	-	-	-
U1352C_111R1	1584	13.68	6.2	0.34	1.06	0.6	2.21	4.69	1.00	8.1	12.6	18.0	100	29.9
U1352C_112R3	1597	13.93	8.3	0.11	1.30	3.4	2.34	5.58	1.60	17.4	26.0	32.8	100	26.6
U1352C_113R2	1606	14.12	10.5	0.12	-	-	3.76	9.65	3.25	-	-	-	-	-
U1352C_114R3	1617	14.34	12.5	0.08	1.13	0.5	2.69	10.00	2.93	-	-	-	-	-
U1352C_115R4	1628	14.57	10.8	0.26	2.76	22.2	5.88	6.92	1.13	-	-	1.3	4.5	2.0
U1352C_116R3	1637	14.74	9.3	0.06	1.44	2.1	2.97	6.12	0.93	27.0	45.9	53.9	100	20.3
U1352C_117R6	1649	14.99	8.0	0.21	1.69	3.3	1.97	17.17	4.88	5.0	37.4	54.2	100	22.4

Core and section number	Sample depth (mbsf)	Age (Ma)	Extracted sediment (g)	Extractability (mg OM/g sediment)	$CPI_{(22-32)}$[1]	TAR[2]	Pr^3/Ph^4	$Pr/n\text{-}C_{17}$	$Ph/n\text{-}C_{18}$	11	12	13	14	15
U1352C_118R4	1655	15.11	8.0	0.18	2.47	9.4	2.18	15.27	5.24	7.1	11.7	14.2	39.0	10.5
U1352C_123R1	1693	15.87	12.7	0.05	1.39	1.9	2.54	3.55	0.93	25.4	22.8	26.2	100	35.2
U1352C_124R1	1698	15.97	4.0	0.20	0.84	0.8	1.95	1.65	0.67	40.2	28.7	30.1	100	20.0
U1352C_125R4	1713	16.27	15.2	0.07	1.06	0.6	3.84	2.72	0.59	31.6	29.6	27.9	100	20.7
U1352C_126R3	1721	16.43	7.5	0.09	1.37	55.3	1.47	2.30	0.97	0.6	1.0	1.3	4.4	1.6
U1352C_127R3	1730	16.62	6.0	0.13	0.53	1.8	2.19	2.36	0.70	46.1	41.3	26.9	100	19.2
U1352C_128R5	1742	16.85	10.4	0.34	4.73	16.6	2.49	12.99	3.73	1.3	2.7	5.0	20.9	5.9
U1352C_129R2	1748	16.98	9.1	0.08	0.61	1.2	2.63	3.18	0.78	25.6	21.8	21.6	100	29.4
U1352C_130R4	1760	17.23	1.6	0.25	0.95	58.3	2.14	2.27	1.90	-	-	-	-	-
U1352C_131R2	1767	17.36	11.6	0.02	0.36	0.9	3.19	0.91	0.19	56.3	57.2	37.7	100	12.8
U1352C_133R4	1789	17.80	6.0	0.07	0.38	0.3	3.46	1.62	0.28	19.3	18.4	20.8	100	25.2
U1352C_134R1	1794	17.89	8.1	0.07	-	-	3.61	0.25	-	-	-	-	-	-
U1352C_135R5	1809	18.21	6.0	0.07	0.27	0.4	2.51	0.77	0.17	39.9	32.7	26.5	100	21.4
U1352C_136R4	1819	18.40	6.2	0.05	0.24	0.4	1.89	0.47	0.08	18.0	11.1	7.0	49.8	12.5
U1352C_137R5	1829	18.60	8.0	0.04	0.15	0.1	1.52	0.82	0.30	45.8	39.1	21.9	100	25.7
U1352C_139R1	1842	18.87	12.0	0.09	0.63	0.6	2.01	1.24	0.41	23.6	28.4	27.7	100	20.2
U1352C_140R1	1851	19.06	15.4	0.03	1.00	90.5	0.74	2.69	0.79	1.1	-	-	0.8	-
U1352C_143R1	1875	30.87	4.0	0.03	0.12	0.2	2.10	0.24	0.08	100	65.2	27.4	70.5	7.7
U1352C_144R4	1885	31.02	9.6	0.04	0.32	0.3	0.85	0.97	0.43	77.0	61.8	33.8	9.6	18.6
U1352C_145R2	1892	31.14	8.2	0.09	0.26	1.1	1.39	0.50	0.21	100	71.3	46.2	61.7	9.0
U1352C_146R2	1901	31.29	10.2	0.01	-	-	3.05	0.38	0.09	-	-	3.9	50.5	15.0
U1352C_147R4	1913	31.50	14.5	0.01	0.94	3.5	0.93	1.87	0.42	-	-	-	-	-
M0027A_67X	195	15.69	15	1.53	6.00	75.14	1.03	0.53	0.84	1.2	2.1	0.7	0.2	0.4
M0027A_70X	209	15.87	9.9	1.04	6.87	10.05	0.87	0.12	0.58	5.7	0.6	1.8	0.3	2.1
M0027A_84X	240	16.26	10	8.15	6.80	28.23	0.68	0.08	0.37	-	0.8	2.1	0.5	1.0
M0027A_97R	279	16.76	10.2	1.33	5.85	21.08	1.02	0.27	1.25	11.1	-	-	-	-
M0027A_104R	300	17.33	10	0.49	5.11	63.67	0.94	0.28	0.46	1.9	1.5	2.2	0.3	0.3
M0027A_111R	321	17.90	10.2	0.42	0.24	14.81	5.47	5.20	1.12	24.3	0.9	0.8	1.2	1.1
M0027A_127R	361	18.75	10.4	2.93	5.44	11.41	0.82	0.11	1.45	-	-	2.8	-	2.0
M0027A_154R	439	20.74	10.5	1.90	3.67		-	-	-	-	-	-	-	-
M0027A_167R	479	22.28	11	0.35	2.70	3.51	0.38	0.06	1.56	65.5	3.0	6.8	2.6	8.7
M0027A_175R	498	23.11	9.9	1.81	3.74	31.63	1.46	0.38	0.59	9.8	9.5	19.4	3.6	0.0
M0027A_177R	505	23.59	12	0.37	5.35	95.42	0.68	0.49	0.39	0	0.4	0.0	0.1	0.2
M0028A_2R	220	11.02	9.8	1.81	4.85	69.29	0.48	0.20	0.34	0.7	3.8	1.0	0.1	0.6
M0028A_9R	243	12.53	10.0	0.58	3.20	12.86	0.75	0.23	0.38	12.4	2.3	-	-	1.9

Core and section number	Sample depth (mbsf)	Age (Ma)	Extracted sediment (g)	Extractability (mg OM/g sediment)	$CPI_{(22-32)}$[1]	TAR[2]	Pr^3/Ph^4	$Pr/n\text{-}C_{17}$	$Ph/n\text{-}C_{18}$	11	12	13	14	15
M0028A_15R	260	13.90	12.0	0.46	1.11	21.47	0.47	0.52	0.90	7.2	1.0	0.8	0.3	0.3
M0028A_22R	280	14.34	9.9	0.39	3.91	15.53	2.55	0.23	0.61	4.0	1.9	2.4	1.0	2.1
M0028A_31R	300	15.63	7.0	3.29	5.05	18.46	0.52	0.08	1.24	3.7	1.1	4.0	1.3	2.1
M0028A_38R	322	15.90	10.0	0.42	4.09	17.91	1.41	0.24	0.92	17.0	2.6	4.2	1.9	2.8
M0028A_45R	337	16.08	10.0	1.01	5.21	18.68	1.12	0.33	0.27	5.1	1.1	0	0	2.7
M0028A_54R	439	16.27	12.3	0.41	4.09	17.91	1.41	0.24	0.92	17.0	2.6	4.2	1.9	2.8
M0028A_98R	481	17.83	10.0	0.60	2.35	5.11	1.42	0.14	0.16	-	2.6	0.6	0.7	3.3
M0028A_104R	499	18.05	9.8	1.38	2.83	10.62	5.16	1.24	0.33	-	-	-	-	11.9
M0028A_111R	520	18.30	7.3	1.38	7.29	28.61	1.41	0.21	1.44	2.8	-	-	-	0.9
M0028A_121R	542	18.61	10.0	0.21	1.91	2.89	0.96	0.12	0.43	82.2	74.4	63.0	11.3	6.7
M0028A_153R	603	19.47	10.5	4.00	4.43	5.89	15.56	0.25	0.09	11.8	2.2	3.8	1.9	4.8
M0028A_160R	620	21.50	10.2	0.42	4.46	13.81	0.37	0.05	1.04	6.8	0.0	2.2	0.8	2.7
M0028A_167R	662	22.20	9.9	0.37	4.28	11.33	0.39	0.06	1.62	18.1	1.1	0	1.3	3.6
M0028A_171R	673	22.57	7.10	1.25	5.88	57.51	0.49	1.10	1.96	-	1.6	1.3	1.0	1.1

Table 4.2 (continued): Extractability of the organic matter (mg OM/g sediment), n-alkane and isoprenoid ratios, and n-alkane distributions for the analysed IODP Expedition 317 (U1352) and IODP Expedition 313 (M0027A and M0028A) samples.

Core and section number	16	17	18	19	20	21	22	23	24	25	26	27	28	29	30	31
U1352C_73R4	50.2	10.9	20.6	2.2	11.4	3.0	12.6	8.0	22.3	25.2	36.1	40.0	29.4	66.5	19.7	84.8
U1352C_76R1	14.1	6.2	8.7	0.9	8.7	1.3	9.7	4.8	17.1	19.0	30.2	35.2	28.7	68.5	23.4	100
U1352C_76R1	1.2	1.7	3.2	1.8	3.5	4.0	7.9	10.9	12.4	14.2	10.7	20.2	8.8	63.8	10.5	100
U1352C_77R1	50.4	6.7	13.9	2.7	3.6	3.6	5.4	7.5	11.8	15.7	18.2	19.8	13.4	22.1	8.0	24.1
U1352C_78R1	78.9	10.3	18.2	3.7	5.2	3.1	6.7	9.2	20.6	34.2	46.4	45.7	36.8	38.7	20.8	26.9
U1352C_79R2	17.3	3.7	5.2	1.7	1.9	2.1	2.6	4.9	7.9	17.1	16.3	32.9	16.2	66.1	13.4	100
U1352C_80R3	52.8	10.0	15.1	4.9	9.9	4.4	7.8	11.9	28.6	49.6	74.1	73.3	68.2	67.7	47.4	46.3
U1352C_81R1	100	30.0	54.4	16.3	42.9	14.5	30.2	9.2	20.6	6.9	17.7	10.9	15.8	30.1	13.7	52.0
U1352C_85R4	47.5	10.0	29.4	5.8	17.3	6.1	13.3	14.8	31.5	48.1	63.1	70.4	63.2	90.3	54.4	100
U1352C_86R2	27.6	7.0	14.1	2.9	12.1	4.2	13.1	14.3	42.6	65.3	100.0	97.4	94.7	87.9	72.5	70.7
U1352C_87R4	4.8	5.9	11.9	7.3	14.7	13.0	27.9	32.3	60.0	65.8	86.5	92.8	70.0	100	50.5	94.6
U1352C_88R5	21.0	4.1	12.7	2.3	5.3	2.2	5.8	9.9	24.5	53.2	64.5	87.6	61.0	100	1.1	98.5
U1352C_89R3	-	-	-	-	-	-	-	-	-	-	-	-	-	-	-	-
U1352C_89R4	65.8	13.1	28.5	4.0	14.0	2.9	14.0	9.7	29.2	40.2	62.4	70.3	64.6	85.6	52.1	100
U1352C_90R2	81.4	12.5	22.2	2.3	5.6	2.9	6.2	7.5	17.2	26.9	37.1	35.7	28.7	26.2	16.7	13.9
U1352C_91R5	100	17.1	32.6	7.7	17.3	6.1	45.4	15.1	39.9	50.6	76.8	66.5	67.4	57.7	47.6	39.3
U1352C_94R5	5.2	4.3	8.6	8.6	14.6	18.9	35.7	47.8	55.3	51.8	45.6	54.6	37.2	78.7	33.6	100
U1352C_95R2	12.6	2.6	6.4	1.0	5.1	2.0	7.0	8.1	20.4	31.7	48.9	56.4	65.0	84.8	84.2	100
U1352C_102R	55.3	30.7	4.8	9.2	25.6	5.0	23.9	11.2	30.4	22.6	42.9	32.6	39.3	55.2	32.7	40.2
U1352C_103R5	100	12.3	40.2	1.7	17.4	1.2	9.3	3.1	11.9	9.0	15.7	10.8	13.1	11.0	8.1	5.8
U1352C_104R2	59.1	23.1	3.6	3.4	26.1	1.9	28.0	12.1	32.1	24.7	40.7	31.2	34.6	40.2	23.6	24.4
U1352C_105R5	6.1	2.0	4.7	2.5	6.1	6.3	13.4	17.0	29.2	35.9	45.9	60.6	49.4	100.0	43.0	64
U1352C_106R6	5.3	5.1	12.4	9.8	24.0	21.1	45.3	51.0	81.9	81.5	86.9	81.3	68.9	87.2	56.7	100
U1352C_107R6	-	-	-	-	-	-	-	-	-	-	-	-	-	-	-	-
U1352C_108R1	-	-	-	-	-	-	-	-	-	-	-	-	-	-	-	-
U1352C_109R3	-	-	-	-	-	-	-	-	-	-	-	-	-	-	-	-
U1352C_111R1	51.6	7.1	15.0	1.3	2.6	0.0	5.5	3.9	6.9	9.7	10.0	10.1	8.7	8.3	7.1	5.7
U1352C_112R3	53.7	13.3	19.9	4.7	8.2	6.5	12.8	14.3	28.9	37.5	48.9	44.9	36.7	66.6	27.7	38.5
U1352C_113R2	-	-	-	-	-	-	-	-	-	-	-	-	-	-	-	-
U1352C_114R3	-	-	-	-	-	-	-	-	-	-	-	-	-	-	-	-

Core and section number	16	17	18	19	20	21	22	23	24	25	26	27	28	29	30	31
U1352C_115R4	3.4	3.0	3.1	3.6	4.2	6.2	7.5	12.8	15.3	22.5	21.1	35.1	22.5	100	17.9	55.9
U1352C_116R3	24.1	6.5	14.3	-	-	-	-	19.1	16.8	38.6	38.1	22.4	19.8	19.3	4.5	14.9
U1352C_117R6	31.6	10.9	19.4	5.6	9.1	4.7	10.1	19.3	21.4	28.6	36.2	38.3	25.3	57.8	16.8	33.5
U1352C_118R4	14.7	6.3	8.5	5.6	5.7	4.7	6.5	8.0	14.6	24.6	26.7	45.6	28.4	100	23.8	65.5
U1352C_123R1	49.6	11.1	16.6	3.2	5.3	3.5	6.6	7.1	13.5	18.9	25.0	29.0	24.7	41.4	17.3	24.2
U1352C_124R1	27.8	5.5	6.9	-	3.1	-	3.9	-	7.4	8.6	10.9	10.0	9.4	6.6	6.0	4.9
U1352C_125R4	32.7	8.6	10.3	-	-	2.5	-	3.1	7.5	8.3	7.8	7.4	7.0	5.8	5.0	4.1
U1352C_126R3	2.5	1.7	2.7	2.0	4.1	4.4	11.7	19.9	38.6	63.1	84.5	98.1	100	99.9	0.9	90.4
U1352C_127R3	64.1	37.1	56.9	8.6	56.2	8.9	60.5	14.8	67.0	31.0	73.9	34.2	65.3	47.8	52.0	31.7
U1352C_128R5	10.4	4.0	5.6	2.8	4.3	3.3	4.7	4.5	6.4	10.2	8.2	29.5	13.4	100	14.6	81.3
U1352C_129R2	64.6	27.0	42.1	6.5	35.7	7.9	36.0	11.7	41.5	25.1	48.9	31.1	42.5	28.1	30.6	19.2
U1352C_130R4	-	-	-	-	-	-	-	-	-	-	-	-	-	-	-	-
U1352C_131R2	60.7	32.0	47.8	3.1	40.9	2.8	40.0	5.0	37.6	8.4	35.1	10.3	32.5	18.6	28.2	15.0
U1352C_133R4	61.9	18.3	30.4	4.8	20.9	3.8	20.8	2.7	13.3	3.4	9.9	3.2	7.1	4.5	7.1	5.2
U1352C_134R1	-	-	-	-	-	-	-	-	-	-	-	-	-	-	-	-
U1352C_135R5	71.1	26.9	47.8	5.2	46.1	6.1	43.0	6.0	33.0	5.1	28.8	6.6	23.3	9.0	15.8	7.9
U1352C_136R4	100	28.3	86.3	6.1	56.9	5.8	46.9	6.6	33.9	5.5	27.9	7.6	20.0	6.2	13.1	3.5
U1352C_137R5	96.2	34.0	61.1	5.1	46.7	4.6	49.2	2.9	32.7	4.0	23.1	3.0	15.7	3.6	8.7	2.5
U1352C_139R1	46.1	14.6	22.1	4.8	14.0	4.0	15.8	4.4	12.2	5.0	10.9	5.6	9.0	9.6	8.5	7.2
U1352C_140R1	2.0	2.4	11.0	0.0	5.0	5.1	8.0	15.7	38.0	70.0	96.9	100	95.0	77.3	58.1	39.3
U1352C_143R1	74.5	53.1	77.8	5.7	79.1	6.0	81.6	6.4	67.7	4.8	48.9	3.8	36.2	6.4	21.9	5.3
U1352C_144R4	85.4	37.7	100	17.8	88.1	22.4	94.5	27.2	63.9	13.6	39.6	9.4	32.4	11.4	20.1	3.7
U1352C_145R2	74.7	39.3	67.5	6.7	79.6	6.3	90.4	8.6	85.4	17.7	78.4	22.8	62.2	22.6	45.3	12.7
U1352C_146R2	100	11.7	56.0	11.4	25.6	15.9	21.3	18.2	27.9	33.0	48.0	47.9	54.3	50.8	42.4	35.1
U1352C_147R4	-	-	-	-	-	-	-	-	-	-	-	-	-	-	-	-
M0027A_67X	0.5	1.6	0.9	1.2	2.1	4.3	5.4	23.7	9.3	36.7	10.7	55.9	13.1	100	11.4	83.5
M0027A_70X	1.3	14.9	3.5	4.4	9.5	4.0	6.1	0.0	3.1	6.3	3.8	29.5	9.4	100	10.6	84.3
M0027A_84X	1.0	5.8	1.7	1.1	3.2	1.0	2.8	1.7	2.3	7.6	4.8	32.0	10.8	100	11.9	89.9
M0027A_97R	-	6.1	1.3	4.7	3.1	1.0	3.4	5.1	3.5	18.8	8.9	43.9	13.3	100	12.3	82.8
M0027A_104R	0.7	1.9	1.2	1.6	2.1	2.1	3.1	11.0	5.7	25.0	9.8	48.9	15.9	100	17.5	95.0
M0027A_111R	1.2	1.1	0.9	1.0	0.9	4.0	2.3	5.2	17.7	9.3	34.1	13.3	56.7	17.5	100	14.8
M0027A_127R	1.0	16.8	1.5	1.4	6.4	1.5	7.2	4.7	5.0	14.6	7.4	42.4	13.5	100	13.0	88.3
M0027A_154R	-	-	-	-	-	2.4	4.4	30.1	19.2	48.8	24.0	71.4	21.1	100	17.6	72.6
M0027A_167R	2.8	43.9	4.5	1.8	18.9	1.9	16.7	5.0	12.0	11.1	12.8	23.0	15.8	67.8	20.8	100

Core and section number	16	17	18	19	20	21	22	23	24	25	26	27	28	29	30	31
M0027A_175R	3.2	4.4	2.0	1.6	3.3	2.7	3.8	4.8	6.2	7.4	7.8	18.4	12.1	71.0	19.4	100
M0027A_177R	0.1	0.4	0.8	1.9	2.2	4.7	4.5	14.6	6.5	26.2	9.4	45.4	15.5	100	15.0	95.4
M0028A_2R	0.8	1.2	1.5	1.6	1.3	2.4	3.5	24.2	8.7	35.4	12.8	53.6	17.9	100	15.6	82.8
M0028A_9R	3.1	8.0	6.4	7.9	11.8	7.2	6.7	6.6	6.0	12.9	12.8	38.3	23.9	91.6	25.3	100
M0028A_15R	0.8	1.1	1.4	1.9	2.7	1.4	1.2	1.3	1.6	2.9	7.1	14.1	20.8	29.6	29.7	28.5
M0028A_22R	1.2	10.8	1.6	1.1	5.3	1.3	6.3	3.9	7.2	11.6	9.6	34.1	15.9	83.4	18.7	100
M0028A_31R	0.9	9.6	1.1	1.4	4.8	1.5	4.5	8.4	5.6	23.5	10.4	48.2	17.5	100	14.9	93.7
M0028A_38R	3.2	8.2	1.5	2.1	5.3	1.8	4.6	3.7	6.0	11.0	10.2	35.5	16.8	98.8	19.7	100
M0028A_45R	2.4	3.0	3.3	5.9	5.2	4.8	4.7	6.1	4.5	11.0	6.1	30.8	11.9	86.2	15.9	100
M0028A_54R	3.2	8.2	1.5	2.1	5.3	1.8	4.6	3.7	6.0	11.0	10.2	35.5	16.8	98.8	19.7	100
M0028A_98R	4.8	17.3	10.5	20.8	16.9	22.0	18.1	29.2	18.0	23.4	17.8	34.0	23.1	77.4	33.3	100
M0028A_104R	8.7	4.6	6.6	15.8	22.1	94.8	38.0	100	38.1	66.1	22.3	72.1	21.4	38	0.0	0.0
M0028A_111R	-	4.3	0.4	2.6	1.2	1.1	1.7	1.6	0.5	6.1	3.7	26.8	10.3	97.7	12.7	100
M0028A_121R	7.3	50.2	14.2	9.2	29.5	9.3	26.3	11.8	18.7	19.5	22.6	39.0	26.9	76.4	27.8	75.9
M0028A_153R	2.4	20.8	3.7	13.7	9.1	2.0	11.0	4.9	6.8	17.8	11.5	38.2	15.5	100	14.8	93.1
M0028A_160R	1.0	13.6	1.9	1.3	7.0	2.3	7.2	9.3	7.7	28.2	12.6	50.8	17.9	100	16.8	93.6
M0028A_167R	1.2	17.1	1.7	0.8	9.4	1.5	8.3	12.1	11.1	30.0	12.9	46.7	17.6	97.3	17.1	100
M0028A_171R	0.7	1.1	1.2	1.9	1.9	2.6	2.1	5.4	4.7	20.5	8.7	56.5	14.0	100	13.8	80.7

Table 4.2 (continued): Extractability of the organic matter (mg OM/g sediment), n-alkane and isoprenoid ratios, and n-alkane distributions for the analysed IODP Expedition 317 (U1352) and IODP Expedition 313 (M0027A and M0028A) samples.

Core and section number	32	33	34	35	36	37	38	Pr	Ph
U1352C_73R4	6.9	13.7	0.7	0.2	-	-	-	22.1	18.6
U1352C_76R1	9.5	21.5	1.2	0.9	-	-	-	8.5	7.5
U1352C_76R1	4.7	15.8	1.4	2.7	0.2	-	-	5.1	6.1
U1352C_77R1	3.0	0.1	-	-	-	-	-	24.0	19.2
U1352C_78R1	5.3	2.3	-	-	-	-	-	16.0	9.2
U1352C_79R2	4.5	16.7	-	-	-	-	-	6.9	8.1
U1352C_80R3	17.4	9.7	3.7	0.4	1.0	-	-	13.5	10.2
U1352C_81R1	5.2	11.2	1.5	-	-	-	-	34.3	34.5
U1352C_85R4	26.8	27.1	6.1	-	-	-	-	13.0	18.0
U1352C_86R2	34.2	19.2	6.4	3.2	1.6	-	-	14.3	12.5
U1352C_87R4	22.5	24.9	6.8	6.7	2.9	-	-	18.4	20.0
U1352C_88R5	14.6	15.1	1.6	0.3	-	-	-	3.9	4.1
U1352C_89R3	-	-	-	-	-	-	-	-	-
U1352C_89R4	26.4	27.4	6.7	4.8	3.3	1.7	-	13.6	13.1
U1352C_90R2	4.8	1.8	0.8	-	-	-	-	17.3	11.9
U1352C_91R5	18.2	7.5	2.6	1.4	-	-	-	73.2	19.2
U1352C_94R5	19.8	35.3	9.0	7.9	3.9	-	-	11.1	7.4
U1352C_95R2	70.3	57.4	35.3	21.0	12.3	-	-	4.3	2.9
U1352C_102R	15.0	-	-	-	-	-	-	17.5	12.5
U1352C_103R5	3.5	-	-	-	-	-	-	21.2	1.6
U1352C_104R2	6.7	-	-	-	-	-	-	32.1	5.6
U1352C_105R5	23.8	21.3	8.7	7.6	4.2	-	-	3.9	1.8
U1352C_106R6	35.1	39.7	15.7	13.2	4.9	-	-	4.7	8.0
U1352C_107R6	-	-	-	-	-	-	-	-	-
U1352C_108R1	-	-	-	-	-	-	-	-	-
U1352C_109R3	-	-	-	-	-	-	-	-	-
U1352C_111R1	-	-	-	-	-	-	-	33.1	15.0
U1352C_112R3	12.6	3.8	-	-	-	-	-	74.3	31.8

Core and section number	32	33	34	35	36	37	38	Pr	Ph
U1352C_113R2	-	-	-	-	-	-	-	-	-
U1352C_114R3	-	-	-	-	-	-	-	-	-
U1352C_115R4	2.9	5.7	-	-	-	-	-	20.7	3.5
U1352C_116R3	-	-	-	-	-	-	-	39.6	13.3
U1352C_117R6	-	-	-	-	-	-	-	186.9	94.7
U1352C_118R4	3.3	7.4	-	-	-	-	-	96.9	44.5
U1352C_123R1	6.4	4.3	-	-	-	-	-	39.2	15.5
U1352C_124R1	-	-	-	-	-	-	-	9.0	4.6
U1352C_125R4	-	-	-	-	-	-	-	23.4	6.1
U1352C_126R3	82.0	71.1	55.3	46.6	33.2	29.4	21.1	3.9	2.6
U1352C_127R3	24.8	1.0	-	-	-	-	-	87.4	39.8
U1352C_128R5	5.4	12.7	-	-	-	-	-	51.7	20.8
U1352C_129R2	12.6	5.4	-	-	-	-	-	85.9	32.7
U1352C_130R4	-	-	-	-	-	-	-	-	-
U1352C_131R2	14.3	7.6	-	-	-	-	-	29.3	9.2
U1352C_133R4	4.2	-	-	-	-	-	-	29.6	8.6
U1352C_134R1	-	-	-	-	-	-	-	-	-
U1352C_135R5	8.4	2.0	-	-	-	-	-	20.9	8.3
U1352C_136R4	6.5	-	-	-	-	-	-	13.2	7.0
U1352C_137R5	2.2	-	-	-	-	-	-	27.8	18.3
U1352C_139R1	4.0	2.6	-	-	-	-	-	18.1	9.0
U1352C_140R1	23.6	11.8	6.7	3.6	2.4	-	-	6.4	8.6
U1352C_143R1	5.3	-	-	-	-	-	-	12.8	6.1
U1352C_144R4	7.5	-	-	-	-	-	-	36.6	43.3
U1352C_145R2	21.7	2.9	-	-	-	-	-	19.6	14.1
U1352C_146R2	27.8	14.0	10.0	-	-	-	-	4.4	5.3
U1352C_147R4	-	-	-	-	-	-	-	-	-
M0027A_67X	5.7	26.3	1.1	2.4	-	-	-	0.8	0.8
M0027A_70X	4.4	18.1	-	-	-	-	-	1.8	2.0
M0027A_84X	5.6	21.4	0.8	1.8	-	-	-	0.4	0.6

Core and section number	32	33	34	35	36	37	38	Pr	Ph
M0027A_97R	6.2	21.3	-	-	-	-	-	1.6	1.6
M0027A_104R	8.8	32.1	2.0	4.0	-	-	-	0.5	0.6
M0027A_111R	88.0	7.2	25.8	-	-	-	-	5.5	1.0
M0027A_127R	6.8	21.6	-	-	-	-	-	1.8	2.2
M0027A_154R	8.0	13.3	-	-	-	-	-	-	-
M0027A_167R	13.8	37.8	-	-	-	-	-	2.7	7.0
M0027A_175R	13.0	43.5	-	-	-	-	-	1.7	1.2
M0027A_177R	8.0	30.5	0.9	0.4	-	-	-	0.2	0.3
M0028A_2R	8.6	28.9	-	-	-	-	-	0.2	0.5
M0028A_9R	13.1	36.1	-	-	-	-	-	1.8	2.4
M0028A_15R	18.3	12.2	7.6	4.3	-	-	-	0.6	1.2
M0028A_22R	10.3	33.4	-	-	-	-	-	2.5	1.0
M0028A_31R	7.1	28.2	-	-	-	-	-	0.7	1.4
M0028A_38R	11.9	35.9	-	-	-	-	-	1.9	1.4
M0028A_45R	8.5	35.5	-	-	-	-	-	1.0	0.9
M0028A_54R	11.9	35.9	-	-	-	-	-	1.9	1.4
M0028A_98R	21.7	57.6	7.0	10.2	-	-	-	2.4	1.7
M0028A_104R	-	-	-	-	-	-	-	20.5	4.0
M0028A_111R	7.5	26.9	-	-	-	-	-	0.9	0.6
M0028A_121R	15.2	31.6	4.4	5.5	-	-	-	5.9	6.1
M0028A_153R	6.5	21.8	-	-	-	-	-	5.3	0.3
M0028A_160R	9.1	24.8	-	-	-	-	-	0.7	2.0
M0028A_167R	8.1	25.9	13.8	-	-	-	-	1.1	2.8
M0028A_171R	5.0	18.1	-	-	-	-	-	1.2	2.4

[1]Carbon Preference Index ($CPI_{(22-32)}$) = $C_{23}+C_{25}+C_{27}+C_{29}+C_{31}/(C_{22}+2*(C_{24}+C_{26}+C_{28}+C_{30})+C_{32}$); after Bray and Evans, 1961

[2]Terrigenous/aquatic ratio (TAR) = $(C_{27}+C_{29}+C_{31})/(C_{15}+C_{17}+C_{19})$; after Bourbonniere and Meyers, 1996

[3]Pristane

[4]Phytane

Table 4.3: Summary of the lipid analysis data for isoprenoidal GDGTs and branched GDGTs for the analysed IODP Expedition 317 (U1352) and IODP Expedition 313 (M0027A and M0028A) samples. All calculations are defined in the "Materials and Methods" section.

Site and Hole number	Sample number	Sample depth (mbsf)	Age (Ma)	BIT index[1]	SST (TEX^{H}_{86})[2] (°C)	SST (TEX^{H}_{86}) (°C) with BIT < 0.5	CBT[3]	MBT[4]	soil pH	MAAT[5] (°C)
U1352C	76R1	1305.02	6.30	0.07	12.8	12.8	0.45	0.27	7.6	29.5
U1352C	77R	1309.64	6.45	0.07	16.4	16.4	0.40	0.28	7.7	28.2
U1352C	78R	1314.52	6.61	0.08	15.3	15.3	0.25	0.27	8.1	29.4
U1352C	79R	1319.47	6.78	-	-	-	-	-	-	-
U1352C	80R	1326.05	7.00	-	-	-	-	-	-	-
U1352C	81R	1328.03	7.07	-	-	-	-	-	-	-
U1352C	85R	1351.57	7.85	0.15	17.3	17.3	0.59	0.35	7.2	27.6
U1352C	86R	1353.8	7.93	0.06	19.6	19.6	0.41	0.32	7.7	27.8
U1352C	87R	1367.05	8.37	0.07	19.4	19.4	0.39	0.29	7.7	30.8
U1352C	87R4	1370.02	8.39	0.19	9.3	9.3	-	-	7.8	7.1
U1352C	88R	1378.31	8.74	0.32	16.1	16.1	0.67	0.36	7.0	27.2
U1352C	89R	1385.71	8.99	0.11	16.8	16.8	0.57	0.30	7.3	29.5
U1352C	90R	1392.51	9.22	0.03	17.1	17.1	0.27	0.21	8.1	32.6
U1352C	91R	1406.54	9.69	0.07	17.3	17.3	0.57	0.27	7.3	30.9
U1352C	94R5	1435.7	10.49	0.10	13.3	13.3	-	-	7.4	8.0
U1352C	102R	1496.43	11.92	0.11	19.8	19.8	1.11	0.52	5.8	21.4
U1352C	105R5	1532.28	13.72	0.10	18.9	18.9	-	-	6.9	11.1
U1352C	107R6	1553.57	14.09	0.16	20.4	20.4	-	-	6.6	6.8
U1352C	110R2	1576.94	14.50	0.11	19.8	19.8	-	-	6.8	8.7
U1352C	115R5	1630.05	15.42	0.07	24.7	24.7	-	-	7.1	10.4
U1352C	125R3	1711.3	16.83	0.08	22.1	22.1	-	-	7.3	7.2
U1352C	134R2	1795.78	18.30	0.07	27.0	27.0	-	-	6.4	2.4
U1352C	139R	1842.11	18.87	0.03	26.0	26.0	-	0.59	-	-
U1352C	140R	1851.46	19.06	-	-	-	-	-	-	-

Site and Hole number	Sample number	Sample depth (mbsf)	Age (Ma)	BIT index[1]	SST (TEX^{H}_{86})[2] (°C)	SST (TEX^{H}_{86}) (°C) with BIT < 0.5	CBT[3]	MBT[4]	soil pH	MAAT[5] (°C)
U1352C	143R	1875.04	30.87	-	-	-	-	-	-	-
U1352C	144R3	1883.97	31.92	0.12	22.1	22.1	-	-	-	-
U1352C	144R	1884.51	31.02	0.46	25.6	25.6	-	0.22	-	-
U1352C	145R	1891.76	31.14	0.05	21.5	21.5	-	0.47	-	-
U1352C	146R	1900.92	31.29	0.24	-	-	-	0.31	-	-
U1352C	147R	1913.24	31.50	0.20	-	-	-	0.73	-	-
U1352C	148R	1917.9	31.57	-	-	-	-	-	-	-
U1352C	148R3	1922.2	35.28	0.19	29.8	29.8	-	-	-	-
M0027A	67X2	195	15.69	0.42	17.2	17.2	0.17	0.54	8.6	19.3
M0027A	70X2	209	15.87	0.39	14.6	14.6	0.22	0.62	8.5	22.8
M0027A	76X2	221	16.02	0.65	14.9	-	0.43	0.43	8.3	11.4
M0027A	83X2	236	16.21	0.33	13.8	13.8	0.54	0.67	8.2	22.4
M0027A	84X2	240	16.26	0.62	8.5	-	0.39	0.82	8.4	31.3
M0027A	97X1	279	16.76	0.54	15.8	-	0.22	0.83	8.5	33.3
M0027A	98X1	282	16.94	0.27	15.1	15.1	0.47	0.77	8.3	28.0
M0027A	104R1	300	17.33	-	15.8		-	-	-	-
M0027A	111R1	321	17.90	0.45	16.9	16.9	0.76	0.65	8.0	19.3
M0027A	119R	340	18.96	0.43	-	-	0.84	0.53	7.9	12.5
M0027A	127R1	361	18.75	0.55	-	-	0.86	0.54	7.9	12.9
M0027A	134R1	379	19.21	0.24	-	-	0.87	0.67	7.9	19.3
M0027A	141R1	400	19.74	0.32	23.0	23.0	0.76	0.71	8.0	22.3
M0027A	148R1	422	20.30	0.44	18.4	18.4	0.56	0.74	8.2	25.7
M0027A	154R1	439	20.74	0.34	21.6	21.6	0.63	0.33	8.1	4.5
M0027A	167R1	479	22.28	0.26	19.4	19.4	0.82	0.48	7.9	10.2
M0027A	175R1	498	23.11	0.54	20.9	-	0.88	0.67	7.9	19.2
M0027A	177R1	505	23.59	0.66	17.8	-	0.59	0.68	8.2	22.4

Site and Hole number	Sample number	Sample depth (mbsf)	Age (Ma)	BIT index[1]	SST (TEX^{H}_{86})[2] (°C)	SST (TEX^{H}_{86}) (°C) with BIT < 0.5	CBT[3]	MBT[4]	soil pH	MAAT[5] (°C)
M0028A	2R1	220	11.02	0.42	20.2	20.2	0.77	0.86	8.0	29.7
M0028A	9R1	243	12.53	0.55	12.0	-	0.73	0.74	8.0	24.1
M0028A	15R1	260	13.90	0.32	17.6	17.6	0.80	0.65	8.0	18.9
M0028A	22R1	280	14.34	0.35	19.0	19.0	0.78	0.33	8.0	3.1
M0028A	31R1	300	15.63	0.61	19.3	-	0.43	0.49	8.3	14.4
M0028A	38R1	322	15.90	0.32	18.2	18.2	0.32	0.72	8.4	26.9
M0028A	45R1	337	16.08	0.39	18.9	18.9	0.34	0.71	8.4	26.2
M0028A	54R1	360	16.27	0.41	15.5	15.5	0.63	0.40	8.1	8.0
M0028A	61R1	382	16.52	0.41	19.7	19.7	0.71	0.41	8.1	7.8
M0028A	67R1	401	16.73	0.43	17.4	17.4	0.65	0.67	8.1	21.3
M0028A	79R1	420	16.94	0.56	13.1	-	0.34	0.43	8.4	12.2
M0028A	92R1	459	17.38	0.76	19.0	-	0.32	0.56	8.4	18.9
M0028A	98R1	481	17.63	0.56	19.1	-	0.48	0.49	8.3	13.9
M0028A	104R1	499	17.83	0.43	20.5	20.5	0.74	0.47	8.0	10.5
M0028A	111R1	520	18.05	0.21	18.0	18.0	0.55	0.44	8.2	10.8
M0028A	115R1	530	18.30	0.17	15.6	15.6	0.32	0.52	8.4	16.9
M0028A	117R1	532	18.37	0.34	16.4	16.4	0.68	0.63	8.1	19.0
M0028A	121R1	542	18.61	0.22	17.1	17.1	0.92	0.69	7.8	19.8
M0028A	136R1	580	19.03	0.56	17.9	-	0.92	0.54	7.8	12.3
M0028A	145R1	599	19.24	0.46	17.5	17.5	0.64	0.67	8.1	21.4
M0028A	146R1	603	19.28	0.52	16.6	16.6	0.60	0.79	8.2	27.8
M0028A	153R1	620	19.47	0.79	-	-	0.44	0.78	8.3	28.8
M0028A	160R1	641	21.50	0.29	21.6	21.6	0.43	0.89	8.3	34.4
M0028A	167R1	662	22.20	0.48	24.1	24.1	0.32	0.92	8.4	36.9
M0028A	171R1	673	22.57	0.45	18.0	18.0	0.31	0.94	8.5	38.0

[1]branched isoprenoid tetraether index

[2]sea surface temperature based on the tetraether index (TEX_{86}) of GDGTs consisting of 86 carbons

[3]cyclisation of branched tetraethers ratio

[4]methylation of branched tetraethers ratio

[5]mean annual air temperature

5. Multi-proxy geochemical analyses of Indus Submarine Fan sediments from IODP Expedition 355: implications for sediment provenance and palaeoclimate reconstructions.

Sophia Aharonovich[1], Simon C. George[1], James Bendle[2], Hannah Liddy[3], Sarah J. Feakins[3], Peter D. Clift[4], Dhananjai K. Pandey[5], Denise K. Kulhanek[6], Sergio Andò[7], Manish Tiwari[5], Boo-Keun Khim[8], Elizabeth Griffith[9], Stephan Steinke[10], Kenta Suzuki[11], Jongmin Lee[8], Kate Newton[2], Shubham Tripathi[5], and the Expedition 355 Scientific Party

[1] Department of Earth and Planetary Sciences and Macquarie University Marine Research Centre, Macquarie University, North Ryde, Sydney, NSW, Australia;

[2]University of Birmingham, Edgbaston, United Kingdom;

[3]University of Southern California, Los Angeles, CA, USA;

[4]Louisiana State University, Baton Rouge, LA, USA;

[5]National Centre for Antarctic and Ocean Research, Vasco da Gama, Goa, India;

[6]Texas A&M University, College Station, TX, USA;

[7]University of Milano Bicocca, Milan, Italy;

[8]Pusan National University, Busan, Republic of Korea;

[9]University of Texas at Arlington, Arlington, TX, USA;

[10]MARUM, University of Bremen, Bremen, Germany;

[11]Hokkaido University, Sapporo, Japan

Statement of authors' contribution

This Chapter is an article to be submitted to *Earth and Planetary Sciences*. This paper has been formatted to conform to the font and referencing style adopted in this thesis. Section, Figures, and Tables included within the text are prefixed with the chapter number.

I am the primary author (80% of the effort). I extracted the organic material from the samples. I analysed the organic data and created the proposed climate reconstructions. I wrote and designed the structure of the paper. The co-authors reviewed and provided feedback and refinements on this version of the manuscript (20%). Neither this manuscript nor one with similar content under our authorship has been published or is being considered for publication elsewhere, except as described above.

Abstract

The interplay between uplift of the Himalayas and the Tibetan Plateau and the development of the Asian monsoon during the Cenozoic era has been widely debated as an example of climate-tectonic coupling. It is hard to draw links between climate and tectonics is impossible without a better understanding of the major phases in mountain uplift, erosion and sedimentation, and when and how the monsoon developed. There has been significant progress in understanding the link between insolation-driven changes in the Asian monsoon and 10^4 to 10^5 year scale perturbations in the Earth's orbit, but the role of tectonics in driving long-term (>10^6 years) climate change is more complex, and is still currently limited by a lack of Cenozoic geological records from the core monsoon region. Multi-proxy provenance and biomarker analyses of samples from the Indus Submarine Fan recovered during IODP Expedition 355 enable changes in the source of the marine sediments and inferred on-land precipitation to be inferred for the period from ~8.5–5.5 Ma. These data suggest intensification of monsoon precipitation during the last 3 million years, which had a significant influence on vegetation patterns including changes in C_4 grassland vegetation cover. The results also reveal a correlation between variations in Asian monsoon amplification and the beginning of the drier and warmer Pliocene.

5.1.Introduction

Climate variations during the Cenozoic are a source of wide debate in the scientific community (Haq et al., 1987; Raymo and Ruddiman, 1992; Zachos et al., 2001). Variations in global sea level (eustasy) as well as continental tectonic movements and mountain uplift are among the major factors influencing climate shifts for the last 65 million years (Myr) (e.g., Vail and Mitchum Jr, 1979; Haq et al., 1987; Raymo and Ruddiman, 1992). In particular positioning of the Antarctic continent near the southern pole (Kennett, 1977), and the beginning of massive ice accumulation on the eastern part of the continent from the early Eocene to the middle Miocene (Miller et al., 1991; Zachos et al., 1992). Development of the Antarctic Circumpolar Current (ACC) around Antarctica caused local cooling and further ice accumulation, and was also an influence on global climate (Kennett, 1977). Low southern ocean temperatures on the other hand influenced the global sea surface temperature (SST) by circulating cold water towards the Pacific, Atlantic, and Indian oceans.

Uplift of the Himalayas and the Tibetan Plateau and its influence on the Asian summer monsoons is one of the most significant examples of climate-tectonic coupling, influencing about 70% of the current global population (Webster et al., 1998). Although, the evolution of the influence and its mechanisms are strongly debated, the correlation between present day regional precipitation and the physical land barrier is obvious. The modern Tibetan Plateau is elevated to ~ 5,000 m and is about 2,000 km wide (Kutzbach et al., 1989), creating a physical barrier and influencing air circulation, and inducing monsoonal precipitation (Molnar et al., 1993).

In general, the uplift of the Tibetan Plateau and the Andes Mountains, which both started during the middle Miocene, arguably triggered global cooling in the polar regions and the beginning of ice accumulation, which, in turn, could have influenced monsoonal intensity (Ruddiman and Kutzbach, 1991; Ruddiman, 2010). Global long term and slow cooling

through the Cenozoic has been recorded using $\delta^{18}O$ isotope levels in $CaCO_3$ of marine shells (e.g. Shackleton and Kennett, 1975; Raymo and Ruddiman, 1992; Miller et al., 1998). Palaeotemperature records show three major cooling events during the early Oligocene (Barrett, 1989), the middle Miocene, and the early Pliocene (Shackleton and Kennett, 1975; Miller et al., 1998). The first two probably were triggered by the appearance and growth of Antarctic ice, while the third correlates to the appearance of ice cover in the Northern Hemisphere. In addition, Raymo et al. (1988) and Berner (1990) suggested correlation between decreasing pCO_2 levels and global Cenozoic cooling. Further climate modelling (Knorr et al., 2011) showed an even stronger influence of vegetation distribution on Miocene climate (Knorr et al., 2011). By reconstructing the type of local vegetation in the western Himalaya region, we can better understand climate variations in the area, and reconstruct changes in precipitation patterns. The sediments in the Laxmi Basin, eastern Arabian Sea, were sourced from the Indus River over the last 8–10 Myr, providing a unique opportunity to study changes in organic inputs during this period.

One of the main sources of sediment into the eastern Arabian Sea are the Indus River and the Indian passive margin (Clift et al., 2001). The Indus River flows from Tibet to the Arabian Sea mostly through arid lands, with the summer monsoon being the main source of rainfall (Fig. 5.1). Eroded sediment is mainly derived from the Upper Himalaya and Karakoram regions (Garzanti et al., 2005). An increase in the altitude of the Himalaya region likely began around 55-45 Ma with collision of the Indian and Asian plates (Rowley, 1996) The uplift of southern Tibet arguably started from ~25 Ma, but gained significance during the beginning of the late Miocene (Miller et al., 1998). The $\delta^{18}O$ of meteoric water can be used as an altitude proxy, and suggests that the Tibetan Plateau reached modern levels by ~11 Ma (Garzione et al., 2000).

There is an ongoing discussion in the literature about the uplift of the Tibetan Plateau that created the precipitation barrier (e.g. Kutzbach et al., 1989; Molnar et al., 1993; Zhisheng et

al., 2001; Spicer et al., 2003). While some palaeobotanical studies suggest the Tibetan Plateau reached elevation levels of over 4000 m around 15 Ma, by which time they would have started to influence the intensity of the monsoon (Spicer et al., 2003), other studies suggest that only the 10 Ma expansion of the Tibetan Plateau (Harrison and Copeland, 1992; Zhisheng et al., 2001) triggered an atmospheric response on a regional geological scale (Ramstein et al., 1997). Gupta et al. (2004) suggested that significant uplift and expansion happened even later, ~8 Ma.

Sediment erosion can significantly influence local and global climate through changes in water chemistry caused by fluvial deposition (Richter et al., 1992). Continental erosion is influenced by multiple factors such as increase in elevation, climate variation and precipitation changes (Peizhen et al., 2001; Burbank et al., 2003; Molnar, 2004). Burbank et al. (2003) showed a decrease in glacial erosion of the sediments in the Himalayas during the middle Miocene temperature optima. The study suggested intensification in monsoon activity after 9 Ma. This observation was supported by the increased strontium flux into the Arabian Sea that was recorded in the Murray and Owen ridges from 9 to 6 Ma (Rea, 1993) (Fig. 5.1). Later studies have shown that the increasingly high gradient between the Himalayas and the Indian Plateau forced lateral and vertical transport of the rocks, more than changes in the climate (Burbank et al., 2003).

A study performed by Rea (1993) recorded two increases in terrigenous sediment input to the Arabian Sea between 9 – 6 Ma and during 4 – 2 Ma. Further studies of the sedimentation pattern in the Indus River area (Fig. 5.1) suggested an increase in sediment flux to the Arabian Sea during the middle Miocene, and a decrease from the late Miocene until modern times that is related to tectonic uplift in the Himalayas and the Karakoram region (Clift et al., 2002). However, these authors could not see a correlation between the increase in sediment flux and monsoon intensification at 8.5 Ma.

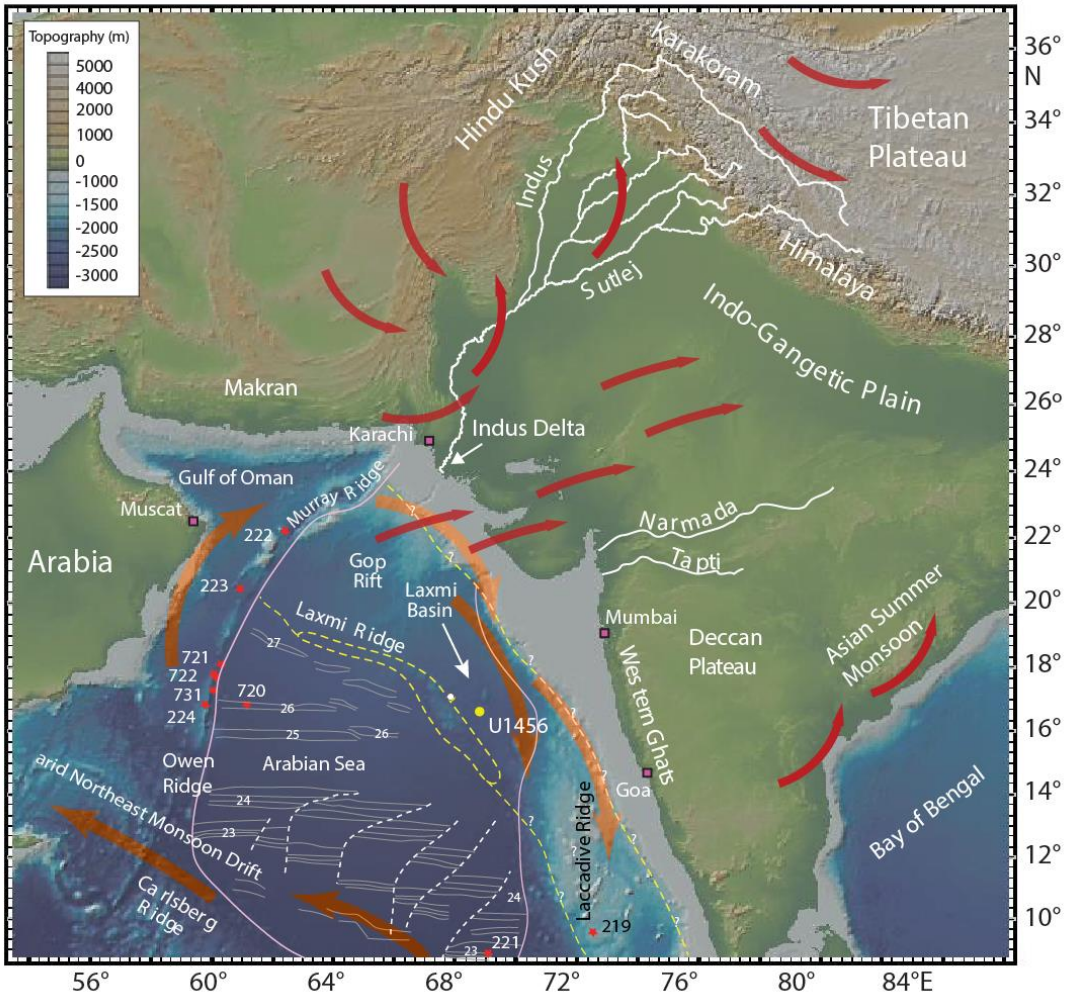

Figure 5.1: Location of the International Ocean Discovery Project U1456 drilling Site (modified after Pandey et al., 2016) in the Laxmi Basin, Arabian Sea, including major western Himalayan river systems (white lines), summer monsoon wind directions (red arrows) and Arabian Sea current directions (orange arrows).

Various atmospheric general circulation models have been used to examine the correlation between the uplift of mountain ranges and regional or global climate variations (e.g. Ruddiman and Kutzbach, 1989; Prell and Kutzbach, 1992; Kutzbach et al., 1993). From the Oligocene to the middle Miocene the models show cooling by 10ºC in central Asia during the winter, with 4ºC warming and a rapid decrease in precipitation during the summer (Ramstein et al., 1997). In addition, a correlation between regional uplift and climate change around 10 Ma has been suggested (Ramstein et al., 1997). Moreover, climate modelling that compared the regional climate at 30 Ma and 10 Ma suggested a strong correlation between shrinkage of

the Paratethys Ocean and an increase in seasonal precipitation that triggered a regional cooling effect (Ramstein et al., 1997). Latter simulations (Zhongshi et al., 2007a; Zhongshi et al., 2007b) showed a strong correlation between development of monsoon precipitation patterns in eastern Asia, shrinkage of the Parathethys Ocean, uplift of the Tibetan Plateau, and expansion of the South China Sea.

Changes in haematite and goethite abundance in marine sediments have been recognised as reliable precipitation proxies in drilled sediments (Bassinot et al., 1994). The analysis of these minerals in marine sediments from the South China Sea shows a strong correlation between an increase in monsoon intensity at ~0.5 Ma and an increase in fresh water input into the Indian Ocean (Bassinot et al., 1994). This observation is consistent with the presence of sapropels in the eastern Mediterranean region (Rossignol-Strick et al., 1998). Moreover, benthic foraminifera show heavier $\delta^{13}C$ signal at ~0.5 Ma was interpreted to be related to the increase in Monsoon intensity as well (Wang et al., 2005). High variations in SST in the South China Sea were also observed during interpreted periods of increased Asian monsoon intensity (Juneng and Tangang, 2005).

Some attempts have been made to correlate the development of the western Pacific warm pool and monsoon intensity (Li and Wang, 2005). A rapid SST decrease by 6ºC in the tropical Pacific area after the middle Miocene climate optimum ~14 Ma was measured by $\delta^{18}O$ and the Mg/Ca ratio of foraminiferal calcite (Mashiotta et al., 1999; Lea et al., 2000; Shevenell et al., 2004). While the accumulation of Antarctic ice was proposed to be a reason for global water temperature cooling (e.g. Shackleton and Pisias, 1985; Zachos et al., 2001; Miller et al., 2005), based on $\delta^{18}O$ marine data, the middle Miocene temperature decrease was probably triggered by astronomic forcing (Holbourn et al., 2004). Other studies have suggested a warming SST trend during the end of the middle Miocene and the beginning of the late Miocene (Haq et al., 1987; Li and Wang, 2005). However, this warming trend was only partially supported by western Pacific foraminiferal data (Kennett et al., 1985; Savin et al.,

1985). It was suggested that closing of the Indonesian seaway at the beginning of the late Miocene may have been a major influence on the decrease of SST, because the closure possibly triggered a decrease in Asian monsoon intensity in the South China Sea region (Li and Wang, 2005). Chemical weathering records from the South China Sea suggest a decreasing monsoon intensification pattern from the middle Miocene to the early Pliocene (Huntington et al., 2006). Despite the general decrease of the monsoon, Clemens et al. (1991) suggested intensification of precipitation cyclicity for this period. The study showed very strong deviation between low winter and high summer precipitation patterns. The intensity of the monsoon started increasing about 4 Ma ago (Huntington et al., 2006).

The abundance of wind-driven upwelling-related planktonic foraminifera (Prell et al., 1993) in the western Arabian Sea is consistent with monsoon strengthening from ~9–8 Ma ago and a decrease of the monsoon intensity in the eastern Asia region at ~8–6 Ma ago (Steinke et al., 2010), coupled with significant C_4 grassland expansion worldwide (Cerling et al., 1993). The movement of the Indian plate northwards, in conjunction with an increased monsoon intensity in eastern Asia, brought a more contrasting climate to central Asia and eastern Africa (Traverse, 1982), with an increased population of C4 plants in western India and Pakistan around 7-8 Ma (Prell and Kutzbach, 1992). Moreover, soil carbonate oxygen isotope compositions indicate a change from C_3 vegetation to C_4 in the Tibetan Plateau (Zhisheng et al., 2001) after ~8.5 Ma, followed by the same switch in Pakistan from ~8 Ma (Kroon et al., 1991), typically indicative of drier summer conditions.

Here we reconstruct the evolving provenance of deep sea sediments in the Laxmi Basin using heavy mineral and bulk isotopic data (Fig. 5.2), coupled with bulk and molecular geochemistry, including biomarker analyses (Fig. 5.3) of sediments drilled during the International Ocean Discovery Project (IODP) Expedition 355 at Site U1456 (Fig. 5.1). The provenance of the sediments and the main source inputs were reconstructed based on single grain heavy mineral counting techniques together with strontium (Sr) and neodymium (Nd)

isotopic compositions. The molecular compositions including the carbon preference index (CPI), average chain length (ACL), terrestrial/aquatic ratio (TAR), branched isoprenoid tetraether (BIT) index and compound specific $\delta^{13}C$ and δD isotopic compositions enable us to infer changes in organic matter provenance and preservation. We show palaeothermometry of the last 10 Myr based on glycerol dialkyl glycerol tetraethers (GDGTs) and long chain unsaturated alkenones. These data allow us to reconstruct environmental conditions from marine sediments containing terrigenous organic matter that can be combined with palaeoclimate changes and related to intensification of the Asian monsoon. The new age-model is based on calcareous nannofossils and planktonic foraminifer biostratigraphy, supported by magnetostratigraphy. Based on the age model, the analysed sediments represent the last 10.15 Myr, with three major hiatuses of ~0.45 Myr during the early Pleistocene, ~2 Myr at the Pliocene/Miocene boundary, and ~0.5 Myr between 8–9 Ma. Erosional and biogeochemical data independently suggest significant intensification of precipitation at ~8–6 Ma and ~3–0.03 Ma. The intensity of the Asian monsoon, as well as global climate variations since 10 Ma, could be influenced by significant uplift of the Himalayas as recorded in the Laxmi Basin sediments (France-Lanord et al., 1993; Pagani et al., 1999; Berger, 2007; Ivanova, 2009).

5.2. Sampling and Methods

All data are listed in Supplementary 1 (Supplementary 1, Tables 1, 2, 3, 4, 5 and 6).

5.2.1. Organic carbon and nitrogen measurements geochemistry

5.2.1.1. Sample preparation

Core sediment samples were collected for shipboard analysis from the interstitial water (IW) squeeze cakes, core catcher samples, and from the representative lithology moisture and density (MAD) analysis residues. Samples were freeze-dried for at least 24 h and then about 5

g of the samples were carefully homogenised to a fine powder using an agate mortar and pestle in preparation for elemental analyses (Pandey et al., 2016).

5.2.1.2. Instrumentation

Total carbon (TC) and total nitrogen (TN) of the samples (Fig. 5.4) were determined with a ThermoElectron Corporation FlashEA 1112 CHNS elemental analyser equipped with a ThermoElectron packed column CHNS/NCS gas chromatograph and a thermal conductivity detector (TCD). Approximately 15 mg of sediments were weighed into a tin cup and then combusted at 950°C in a stream of oxygen. The inorganic carbon (IC) content of the samples was determined using a UIC 5011 CO_2 coulometer, where 10 mg of freeze-dried, ground sediments were reacted with 1N HCl. The liberated CO_2 was back-titrated to a colorimetric end-point (Pandey et al., 2016). All measurements were calibrated to a Soil CNS Reference Material PDWR [PN 3472541] (carbon = 3.496 wt%, nitrogen = 0.365 wt%, and sulphur = 0.063 wt%) that was reanalysed every 8 samples. Analyses were only continued if standard data varied by <5% for C and < 8.5% for N.

The weight percentage of calcium carbonate was calculated from the IC content using:

$$\text{Eq. 17} \qquad CaCO_3(wt\%) = IC(wt\%) \times 8.33$$

Standard $CaCO_3$ (standard reference material) was used to confirm accuracy. The total organic carbon (TOC) content was calculated as the difference between total and inorganic carbon:

$$\text{Eq. 18} \qquad TOC = TC - IC$$

5.2.2. Sample lab measurements of bulk organic data

Sediment residues from IW squeeze cakes and core catcher samples were split for on-shore bulk geochemistry, organic geochemistry, heavy minerals, and bulk isotope analyses. The analytical methodologies are presented below.

5.2.2.1. Sample preparation and analysis for bulk organic data

Between 10-20 g of freeze-dried samples were finely ground and homogenised with a solvent cleaned mortar and pestle (2N-HCl and Milli-Q water). Homogeneous samples were divided into two batches for further analyses- (i) 2N HCl treatment for TOC and $\delta^{13}C$ measurements, and (ii) untreated samples split for the determination of TN content and $\delta^{15}N$ values. 20 mL of 2N HCl solution was added to 5–10 g of finely ground sediment. The mixture was mechanically mixed and left overnight. The samples were then washed with ultrapure distilled water three times to remove possible inorganic carbon and acid residues. About 25 mg of treated sample was used for TOC and $\delta^{13}C$ analyses and 40 mg was used for TN and $\delta^{15}N$ measurements.

An ISOPRIME-isotope ratio mass spectrometer coupled with a vario EL cube element analyser was used for the $\delta^{15}N$ and $\delta^{13}C$ bulk sediment data for half of the samples (Supplementary 1, Table 3). The rest of the samples were analysed by an isotope ratio mass spectrometer (20-20, Europa Scientific) coupled with an element analyser (ANCA-SL, Europa Scientific). Ammonium sulfate (IAEA-N-1, IA-R045, IA-R046), cellulose (IAEA-CH-3), beet sugar (IA-R005), and cane sugar (IA-R006) were used as analytical standards. The analytical precision for $\delta^{15}N$ and $\delta^{13}C$ were ±0.05‰ and ±0.03‰, respectively, while for TN and TOC analytical precision was ±0.17% and ±0.35%, respectively.

5.2.2.2. Interpretation of bulk organic data

The TOC/TN ratios are used as indicators for the type of organic matter (OM) input, and can be divided into three main categories: predominantly marine (TOC/TN < 8), predominantly terrigenous (TOC/TN > 12), and mixed input (8<TOC/TN<12) (Müller and Mathesius, 1999). However, a simple model of the factors influencing TOC/TN ratios is not always applicable. High TOC/TN ratios atypical for algal source organic matter have been measured in organic-rich Mediterranean sapropel layers, upper Neogene sediment from the Benguela upwelling region, Eocene horizons from the Arctic Ocean, and Cenomanian–Turonian black shales (Meyers, 1997; Twichell et al., 2002; Stein and Macdonald, 2004; Stein et al., 2004). Meyers (1997) suggests that in organic-rich marine sediments these high TOC/TN ratios can be explained by either (1) algae that are able to synthesise lipid-rich organic carbon during times of abundant nutrient supply, and/or (2) that during sinking, partial degradation of algal organic carbon may selectively diminish nitrogen-rich proteinaceous components, and thus the TOC/TN ratio.

Stable isotopes of TOC and TN are widely used as proxies for depositional and post depositional biogeochemical processes, but can be influenced by dilution effects of detrital material and/or the preservation patterns of sediments (Hedges and Keil, 1995). However, selective degradation of organic compounds and isotope fractionation might significantly alter the isotopic signal (Hedges and Prahl, 1993). Marine OM, carbohydrates and amino acids are usually enriched in ^{15}N and ^{13}C isotopes relative to terrigenous OM (De Lange et al., 1994), so generally heavier isotopic compositions are expected with higher marine OM input. However, bacterial metabolism can significantly decrease ^{15}N isotope concentration in marine sediments (Meyers, 1997).

5.2.3. Organic geochemistry analyses

5.2.3.1. Lipid extraction

The samples were freeze-dried in a Virtis 2k unit and homogenised with a mortar and pestle. Dry, powdered sediment samples (17.1–31.8 g) were extracted with an Accelerated Solvent Extraction system (ASE 350®, DIONEX) at University of Southern California, using dichloromethane (DCM):methanol (MeOH) (9:1 v/v) at 100°C and 1500 psi for two 15-minute cycles. Total lipid extracts (TLE) were shipped to the University of Birmingham for separation. About 20% of the sample volume was taken prior to separation for GDGT analyses and shipped to Macquarie University.

At the University of Birmingham, TLEs were separated over a silica gel column where the total neutral fraction was eluted with 4 mL of 1:1 DCM:isopropanol, and the total acid fractions were eluted with 4% acetic acid in ethyl-ether solution. The total neutral fraction was transferred onto a new silica gel column and further separated with 4 mL of *n*-hexane, 2 mL of 2:1 *n*-hexane/DCM, 4 mL DCM, and 5 mL MeOH to obtain the aliphatic hydrocarbon, aromatic hydrocarbon, aldehyde and ketone (F3), and alcohol fractions, respectively. The total acid fraction was methylated with MeOH of known isotopic composition using 95:5 MeOH:hydrochloric acid at 70°C for 12 hours. Methylated products were recovered using liquid-liquid extraction with 1 mL milli-Q water and hexane. The hexane extract was passed through an anhydrous sodium sulphate column and then further purified over a silica gel column (5 cm x 40 mm Pasteur pipette, 5% water-deactivated silica gel, 100–200 mesh) eluted with *n*-hexane and DCM, resulting in non-polar and fatty acid methyl ester fractions, respectively.

5.2.3.2. n-Alkanes, Isoprenoids, n-Alkanoic acids, Hopanes, and Steranes

5.2.3.2.1. Gas chromatography-mass spectrometry (GC-MS) for n-alkane, isoprenoid, hopane and sterane identification

Aliphatic hydrocarbon fractions were dissolved in 50 μL of DCM and analysed using an Agilent gas chromatograph (6890N) coupled to an Agilent Mass Selective Detector (5975B). The GC conditions were as followed: injection of 1μL into a programmable temperature vaporisation (PTV) inlet at 35°C, with a temperature increase of 700°C/min to 310°C. Separation was performed on a J&W DB5MS UI (60 m × 0.25 mm, film thickness 0.25 μm) column with 1.5 mL/min constant flow rate and helium as the carrier gas. The initial GC oven temperature of 35°C was held for 4 minutes followed by a sample run to 310°C, held for an additional 40 minutes. The MS was operated in full-scan mode (50–550 amu) and selected ion monitoring (SIM) mode for the target compounds as well as the 0.1 mL of internal standards mix of terphenyl d-14, anthracene d-10, and tetracosane d-50 added prior the SIM mode run , using m/z 66.1, 123.1, 177.2, 183.2, 188.1 191.1, 205.2, 217.2, 218.2, 231.2, 253.2, and 259.2. The compounds were identified using MSD ChemStation F.01.00.1903, using relative retention times and the NIST MS library, and comparison with laboratory standards.

5.2.3.2.2. Leaf wax quantification

The fatty acid methyl ester fractions were identified and quantified using gas chromatography coupled with both a mass-selective detector and flame ionisation detection (GC-MSD/FID Agilent) at the University of Southern California. 1/100 uL of the sample was analysed by gas chromatography with injection via a split/splitless inlet in splitless mode, to a capillary column (Rxi-5MS 30 m × 0.25 mm, film thickness 0.25 μm) with a constant He flow rate of 1 mL/min. The initial GC oven temperature of 50°C was held for 3.5 minutes followed by a temperature ramp of 20°C min^{-1} to 300°C, held for an additional 10 minutes. Quantification was achieved using an in-house standard comprising a mixture of four *n*-alkanes and three *n*-

alkanoic acids of varied and known concentrations, with the calibrations determined separately for the two compound classes. The *n*-alkanoic acid concentrations are reported relative to the mass of dry sediment extracted (µg/g).

After quantification of the individual peak areas, the CPI_f was calculated for the C_{22}-C_{30} *n*-alkanoic acids to quantify the abundance of even over odd *n*-alkanoic acids:

$$\text{Eq. 19} \qquad CPI_f = \frac{1}{2}\frac{\sum[C_{22-30\ even}]}{\sum[C_{21-29\ odd}]} + \frac{\sum[C_{22-30\ even}]}{\sum[C_{23-31\ odd}]}$$

The C_{31} *n*-alkanoic acid was assumed to be 0 when below the detection limit.

To determine changes in the average chain length (ACL_f) of land plants, we calculated the ACL_f of the concentration-weighted abundances of long-chain homologues using the following equation for *n*-alkanoic acids:

$$\text{Eq. 20} \qquad ACL_f = \frac{24\times[C_{24}]+26\times[C_{26}]+28\times[C_{28}]+30\times[C_{30}]}{\Sigma C_{24-30}}$$

5.2.3.2.3. *n*-Alkanoic acids $\delta^{13}C$ compound specific identification and quantification

The stable carbon isotope ratio ($\delta^{13}C$) of fatty acids was analysed using Agilent HP6890 gas chromatograph with Agilent CPSIL-8CB capillary column (30 m × 0.32 mm i.d., film thickness 0.25 µm) coupled to a Finnigan Delta Plus IRMS. The GC oven temperature was programed from 50–120 °C at 30°C /min, from 120–310 °C at 6 °C /min and remained at 310 °C for 30 min. The C_{13} *n*-alkane (-27.24 ‰) was used as an internal standard for calculation of the $\delta^{13}C$ of the fatty acids. The $\delta^{13}C$ values are expressed in ppm relative to Pee Dee Belemnite (PDB). In this study, the $\delta^{13}C$ of fatty acids ranging from 16 to 30 carbons were measured in replicate. Standard deviations for the $\delta^{13}C$ of fatty acids were found to be within 0.5‰ error range.

5.2.3.2.4. *n*-Alkane and isoprenoid abundance, CPI, P_{aq}, ACL, and Pr/Ph

C_{16}-C_{40} *n*-alkane abundance was calculated relative to the anthracene d-10 internal standard and are reported relative to the mass of dry sediment extracted (ng/g). The relative odd-over-even carbon number preference for the *n*-alkanes is given by $CPI_{22–32}$:

$$\text{Eq. 21} \qquad CPI_{(22-32)} = \frac{[C_{23}]+[C_{25}]+[C_{27}]+[C_{29}]+[C_{31}]}{[C_{22}]+2*\sum[C_{24-30\ even}]+[C_{32}]}$$

The presence of long chain odd carbon numbered *n*-alkanes (C_{27}, C_{29}, and C_{31}) has been attributed to land-plant epicuticular waxes input to sediments (Eglinton and Hamilton, 1967; Barnes and Barnes, 1978), whereas the presence of the C_{15}, and C_{17} *n*-alkanes can be attributed to an algal/planktonic origin (Cranwell, 1984; Meyers and Ishiwatari, 1993). Studies of plants from submerged and floating ecosystems show high C_{21}, C_{23}, C_{25} *n*-alkanes (Barnes and Barnes, 1978; Cranwell, 1984; Viso et al., 1993). The terrigenous/aquatic ratio (TAR) based on n-alkane carbon number distribution has been applied to lacustrine (Bourbonniere and Meyers, 1996) and marine environments (Silliman et al., 2000). TARs < 1 indicate strong algal input, whereas higher values indicate a terrigenous OM predominance (Bourbonniere and Meyers, 1996):

$$\text{Eq. 22} \qquad TAR = \frac{C_{27}+C_{29}+C_{31}}{C_{15}+C_{17}+C_{19}}$$

The TAR might over-represent the absolute amount of terrigenous sources, assuming much higher *n*-alkane production by land plants (Cranwell et al., 1987; Meyers and Ishiwatari, 1993). The relative abundance of submerged/floating aquatic macrophyte input relative to the terrigenous input was calculated using the $1/P_{aq}$ ratio, where P_{aq} is defined as:

$$\text{Eq. 23} \qquad P_{aq} = \frac{(C_{23}+C_{25})}{(C_{23}+C_{25}+C_{29}+C_{31})}$$

The average chain length (ACL) of *n*-alkanes was calculated after (Gagosian and Peltzer, 1986):

$$\text{Eq. 24} \qquad ACL_{27-33} = \frac{27[C_{27}]+29[C_{29}]+31[C_{31}]+33[C_{33}]}{[C_{27}]+[C_{29}]+[C_{31}]+[C_{33}]}$$

The abundance of n-alkanes can also be influenced by thermal maturation (Bray and Evans, 1961) as well as by post-depositional biodegradation processes (Wenger and Isaksen, 2002).

The relative abundance of pristane (2,6,10,14-tetramethylpentadecane; Pr) and phytane (2,6,10,14-tetramethylhexadecane; Ph) is related to the oxicity of the depositional environment (Didyk, 1978). The phytyl side chain of chlorophyll in phototrophic organisms and bacteriochlorophyll from purple sulphur bacteria have been suggested to be the main source for Pr and Ph (Powell and McKirdy, 1973). Anaerobic bacterial degradation (Rontani et al., 2010), thermal degradation (Lao et al., 1989; Rowland, 1990) and clays can catalyse the degradation of the chlorophyll phytyl chain (Rontani et al., 2010), leading to Pr in sediments. Ph is known to be derived from methanogens and thermoacidophilic archaea (Tornabene et al., 1979), as well as by anaerobic biodegradation (Grossi et al., 1998), clay catalysed thermal hydrogenation of isoprenoid alkenes (Gelin et al., 1995).

5.2.3.2.5. Sterane abundance – ternary diagram

Steranes are source-specific compounds deriving mainly from zooplankton (C_{27} steranes) (Huang and Meinschein, 1979), diatoms (C_{28} steranes) (Moldowan et al., 1985), and high plants (C_{29} steranes) (Huang and Meinschein, 1979), although there are many other sources that complicate this pattern (Gagosian, 1976; Volkman, 1986, 2005; Kodner et al., 2008). Steranes were identified by SIM using *m/z* 217 (Supplementary 1, Table 6) as the indicative ion and plotted in a ternary diagram (Huang and Meinschein, 1979). The diagram was divided into six areas (I – VI) that define the main source of OM based on the sterane types and abundances (after (Huang and Meinschein, 1979).

The C_{30} sterane index is an index of 24-*n*-propylcholestanes relative to the other C_{27}-C_{30} identified steranes (Supplementary 1, Table 6) and is very specific for marine organic matter input as well (Seifert and Moldowan, 1978; Peters et al., 2005, for review). High C_{30} sterane index values are indicative of marine OM input.

Maturity-related parameters can be obtained from the isomerisation ratio of 20S/(20S+20R) C_{29} 5α,14α,17α(H) steranes (Supplementary 1, Table 6), which equilibrates at 0.52-0.55 (Seifert and Moldowan, 1986).

5.2.3.2.6. Hopane abundance

Most hopanes in rocks are derived from bacteria (Ourisson et al., 1984), although some have more specific sources. Hopanes can also be used as indicators of thermal maturity (e.g. Seifert and Moldowan, 1978, 1980; Moldowan et al., 1986; Peters et al., 2005). For example, C_{27} 17α-22,29,30-trisnorhopane (Tm) is less stable than C_{27} 18α-22,29,30-trisnorneohopane (Ts) and Ts/(Ts+Tm) ratio is thermal maturity dependent (Seifert and Moldowan, 1978; Stephens and Carroll, 1999; Nuzzo et al., 2012) (Supplementary 1, Table 6). However, the sedimentation processes, early diagenesis, and varying sources of OM can significantly alter this ratio (Ourisson et al., 1984). The 22S/(22S+22R) hopane epimer ratio varies between 0 to 0.62 in response to the thermal maturation of sediments, and reaches equilibrium between 0.57-0.62 during the early oil window (Seifert and Moldowan, 1980; Moldowan et al., 1986). The C_{31} αβ pseudo homologs consistently show lower epimer ratios because they comprise a significant contribution of the indigenous 22R epimer (a typical immaturity signature).

Oleanane (Supplementary 1, Table 6) is produced by angiosperms and originates in betulin or other pentacyclic triterpenoids (e.g. Whithead, 1973; Ekweozor and Udo, 1988). The oleanane/ hopane ratio (the oleanane index) can be used to show the relative abundance of angiosperms (Murray et al., 1994). More generally, a high oleanane index can also be

interpreted as reflecting an increase in terrigenous OM input (Murray et al., 1997). Some diagenetic influence can be expected during the contact of the oleanane with sea water during the deposition (Murray et al., 1997).

5.2.3.3. Glycerol dialkyl glycerol tetraethers (GDGTs)

5.2.3.3.1. Instrumentation for analysis of GDGTs

GDGTs in 18 samples were separated and identified using a method modified from Becker et al. (2013). In short, 20% of a TLE was re-dissolved in *n*-hexane:propan-2-ol (99:1 v/v) and filtered through Merck 0.45 micrometer PTFE syringe filters (4 mm diameter). The samples were then dried and re-dissolved in 20 or 50 µl *n*-hexane:propan-2-ol (99.5:0.5 v/v) before high performance liquid chromatography-MS (HPLC-MS) analysis. 10 µl of the sample was injected onto coupled Acquity BEH amide columns (each 2.1 x 150 mm, 1.7 m; Waters, Eschborn, Germany) kept at 50 °C on an Agilent 1260 Infinity LC coupled to an Agilent 6120 Quadrupole MS. Compounds were eluted using eluent A (*n*-hexane) and eluent B (*n*-hexane:propan-2-ol, 90:10 v:v) and a constant flow of 0.5 mL/min. The flow regime was initially 3% B, to 5% B at 2 min, to 10% B at 8 min, to 20% B at 10 min, to 50% B at 15 min, and to 100% B at 10 min. The columns were washed with 100% B for 6 min and equilibrated with 3% B for 9 min before the next injection. The MS conditions were as follows: atmospheric-pressure chemical ionisation positive mode, nebulizer pressure 60 psi, gas temperature 400°C, drying gas (N_2) flow 6 mL/min, and drying gas temperature 200°C, with a capillary voltage of 3 kV and a corona current of 5.0 µA. The detector was set for SIM mode with $[M+H]^+$ parameters of *m/z* 1018, 1020, 1022, 1032, 1034, 1036, 1046, 1048, 1050, 1292, 1294, 1296, 1298, 1300, and 1302; the fragmentor voltage was 70 kV). Collected data was analysed by Mass Hunter Workstation B.06.00.

5.2.3.3.2. Isoprenoidal GDGTs – TEX^{H}_{86} and sea surface temperature (SST) calculations

The TEX^{H}_{86} for subtropical and greenhouse periods, when temperatures were higher than today, was calculated from the distribution of iGDGTs using the definition of Kim et al. (2010) for the 10°C to 40°C temperature range:

$$\text{Eq. 25} \qquad TEX^{H}_{86} = \frac{[GDGT-2]+[GDGT-3]+[Cren']}{[GDGT-1]+[GDGT-2]+[GDGT-3]+[Cren']}$$

where numbers refer to the number of rings in the GDGT, and Cren' refers to the crenarchaeol regio isomer. TEX^{H}_{86} was converted to SST using the correlation for the10°C - 40°C temperature range with a proposed residual standard error of ±2.5°C (Kim et al., 2008; Kim et al., 2010):

$$\text{Eq. 26} \qquad SST = 68.4 \times TEX^{H}_{86} + 38.6 \quad (r^2 = 0.87, n = 255, p < 0.0001)$$

GDGT cyclisation was calculated to evaluate the ring index (Pearson et al., 2004):

$$\text{Eq. 27} \qquad Ring\ index = \frac{[GDGT-1]+2\times[GDGT-2]+3\times[GDGT-3]+4\times[GDGT-4]+5\times[Cren+Cren']}{[GDGT-0]+[GDGT-1]+[GDGT-2]+[GDGT-3]+[GDGT-4]+[Cren+Cren']}$$

5.2.3.3.3. Branched GDGTs – BIT, MBT, CBT, pH, and MAAT

To calculate the relative fluvial input of terrigenous organic matter in the marine environment the branched isoprenoid tetraether BIT index was calculated from the brGDGTs (Hopmans et al., 2004):

$$\text{Eq. 28} \qquad BIT\ index = \frac{[GDGT-Ia]+[GDGT-IIa]+[GDGT-IIIa]}{[GDGT-Ia]+[GDGT-IIa]+[GDGT-IIIa]+[Cren]}$$

The methylation index of branched isoprenoid tetraethers (MBT) and the cyclisation index of branched isoprenoid tetraethers (CBT) were calculated from the brGDGTs as proxies for marine environment palaeo-reconstructions (Weijers et al., 2007):

Eq. 29 $$MBT = \frac{[GDGT-I]}{\sum[GDGT-I]+\sum[GDGT-II]+\sum[GDGT-III]}$$

Eq. 30 $$CBT = -\log(\frac{[GDGT-Ib]+[GDGT-IIb]}{[GDGT-Ia]+[GDGT-IIa]})$$

Mean annual air temperature (MAAT) was calculated from MBT based on various continental soils, and soil pH was calculated from CBT (Weijers et al., 2007):

Eq. 31 $$MBT = 0.122 + 0.187 \times CBT + 0.020 \times MAAT \ \ (r^2 = 0.77, n = 134)$$

Eq. 32 $$CBT = 3.33 - 0.38 \times pH \ \ (r^2 = 0.70, n = 134)$$

5.2.3.4. Alkenones

5.2.3.4.1. Instrumentation for analysis of alkenones

An Agilent 7890B GC with an FID was used for quantitative analysis of the alkenones within the N3 fraction. Compound separation was achieved using a 60 m BP1 column (SGE) (i.d. = 0.32 mm, film thickness = 0.25 μm), with hydrogen as the carrier gas, set at a constant flow of 3 mL/min. The GC oven programme was set at: 70°C (1 min), 150°C (rate: 30°C/min), 340°C (rate: 3°C/min; held for 10 min). Alkenone identification was achieved using an Agilent 7890B GC coupled to an Agilent 5977A MSD, using the same GC column and method as above, except using helium as the carrier gas set at a constant flow of 2.4 mL/min. The MS was run in scan mode with a scan width of 50 to 800 amu. External standards containing mostly *n*-alkanes were regularly analysed on both the GC and GC-MS to check instrument precision.

5.2.3.4.2. $U^{K'}_{37}$ and SST

SSTs were reconstructed using the alkenone unsaturation index ($U^{k'}_{37}$) for 14 samples. The relative abundances of $C_{37:2}$ and $C_{37:3}$ alkenones were used to obtain $U^{k'}_{37}$ values:

$$\text{Eq. 33} \qquad U_{37}^{K'} = \frac{C_{37:2}}{C_{37:2}+C_{37:3}}$$

where $C_{37:2}$ and $C_{37:2}$ is the response of the $C_{37:2}$ and $C_{37:3}$ alkenones.

The Uk'37 values were subsequently converted into SSTs using an Indian Ocean calibration by (Sonzogni et al., 1997; Eq. (19)) and a global calibration described by (Conte et al., 2006; Eq. (20)):

$$\text{Eq. 34} \qquad SST(℃) = \frac{U_{37}^{K'} - (0.013 \pm 0.063)}{0.023 \pm 0.004}$$

$$n = 54;\ r^2 = 0.936;\quad Temperature\ range\ (℃) = 5 - 30$$

$$\text{Eq. 35} \qquad SST(℃) = 29.876\ (U_{37}^{K'}) - 1.334$$

$$n = 592;\ r^2 = 0.97;\quad Temperature\ range\ (℃) = -1 - 29$$

Duplicate GC analyses of alkenone samples indicate the analytical error (±1ºC) to be less than 0.4°C.

5.2.4. Heavy mineral analysis

5.2.4.1. Sample preparation for heavy mineral analysis

Thirteen samples were analysed by separating heavy minerals from silt to sand grain sizes using methods described by Andò et al. (2012) . Between 4-16 g of sediments were sieved with a standard 500 μm steel sieve coupled with handmade special tissue net sieves of 15 and 5 μm. The >500 μm and <5 μm fractions were dried and weighed for a quantitative estimation of each grain-size fraction. Heavy minerals were separated by centrifuging the 5-15 and 15-

500 μm grain-size fractions in sodium polytungstate (ρ=2.90 g/cm^3) and were recovered by partial freezing with liquid nitrogen. Heavy minerals were weighed in every grain-size fraction.

5.2.4.2. Instrumentation and counting for heavy mineral analysis

The heavy minerals were mounted with Canada balsam, and 200 to 250 transparent heavy-mineral grains were point-counted at suitable regular spacing (100 μm) using a polarising microscope with 10×, 20× and 63× magnifying lenses to obtain volume percentages (Carver, 1971). The surface textures of detrital grains were studied by polarising microscope to estimate the extent of chemical dissolution. Stages of progressive weathering were recognised for diverse detrital minerals, so as to quantify any possible compositional bias from the original suite of heavy minerals (Andò et al., 2012). Dubious heavy mineral grains and minerals smaller than 15 μm were checked and properly identified by an inVia Renishaw Raman spectrometer equipped with a green laser (532 nm) and a 50× long working distance (LWD) objective (Andò et al., 2014). The Raman spectrometer was used in the lower spectral range (144-1900 cm^{-1}; OH^- region) for identification of hydrated minerals, amphiboles, epidotes, and phyllosilicates (Andò et al., 2014). Unknown Raman spectra were recognised by comparison with a laboratory database using known standard minerals and samples collected in the Indus River modern sands (Garzanti et al., 2005; Clift et al., 2010).

The heavy mineral concentration was calculated as the weight percentage of total heavy minerals index (HMC) and of transparent heavy minerals (tHMC) index.

5.3. Results and discussion

The compositional variability of cored sediments together with the relative contributions of different sources to the turbiditic deposits of the Laxmi Basin were assessed by heavy-

minerals, as well as by bulk sample Sr and Nd isotopic composition (Supplementary 2 for additional lithology) (Garzanti et al., 2005; Clift et al., 2008b) (Fig. 5.2). Heavy mineral concentrations in sediments depend primarily on the chemistry and tectonostratigraphic level of eroded rocks within continental-block, arc, or orogenic source terranes (Garzanti and Andò, 2007). However, the concentration of heavy mineral grains in sandy sediments may fluctuate considerably because of several factors, including provenance, hydrodynamic processes during transport, and post-depositional dissolution (Garzanti and Andò, 2007; Garzanti et al., 2011).

Nd isotope compositions can be compared with source rock compositions to constrain the origin of the bulk sediment, although if more than two sources are involved this analysis by itself may not be unique (France-Lanord et al., 1993; DePaolo, 2012). There are relatively high ε_{Nd} values (-5 to -10) for the late Miocene samples (Fig. 5.2), which suggest that the Karakoram (Fig. 5.1) was a dominant source of sediment supply until ~6 Ma ago (Clift et al., 2002). The ε_{Nd} values are lower (-8 to -12) during the late Pliocene, with a further decrease to -14 in the early Pleistocene, and then an increase to -11 from the middle Pleistocene to the present day. These variations in ε_{Nd} values through time require variability in sediment source (Clift et al., 2002). A possible increase in sediment flux from the more radiogenic Greater Himalayas and especially the Lesser Himalayas, relative to less radiogenic sources such as the Karakoram, may be inferred towards the end of the late Miocene and during the Pleistocene. The range of Pliocene-Pleistocene ε_{Nd} values is similar to that seen in the last 15 ka in the Indus River Delta (Clift et al., 2010). Older samples with more positive ε_{Nd} values arguably point towards greater sediment flux from the Transhimalaya mountain range in China and/or Karakoram during the Late Miocene (Clift et al., 2002).

The Sr isotope composition of marine sediments is influenced by chemical weathering and sediment transportation, as well as by provenance (Edmond, 1992; Derry and France-Lanord,

1996; Clift et al., 2008b) (Fig. 5.2). $^{87}Sr/^{86}Sr$ values vary coherently with ε_{Nd} variations through time, with a constant decrease from 0.718 to 0.715 in the late Miocene. The rapid changes in sedimentary $^{87}Sr/^{86}Sr$ after ~6.29 Ma (Fig. 5.2 and Supplementary 1, Table 5) correlate with similar changes in sediments of the Bengal Fan, suggesting an increase of the intensity of chemical weathering across the area, as well as similar changes in the focus of bedrock erosion (Derry and France-Lanord, 1996). $^{87}Sr/^{86}Sr$ values declined after ~1.6 Ma and increased again from ~1.2 Ma to reach modern levels around 30 ka. The data suggest increased erosion at ~8.27–6.29 Ma in the High Himalaya and Transhimalayan regions, suggesting stronger precipitation in the summer monsoon (Ramstein et al., 1997; Clift et al., 2008b).

By integrating the heavy mineral assemblages with the bulk sediment assemblage, and the single groups of minerals (e.g., amphibole, epidote, garnet, spinel) we can reconstruct the routing of minerals between the deep Indian Ocean and the source area to the Himalaya or along the Western Indian Passive Margin (Garzanti et al., 2005; Garzanti and Andò, 2007). In the analysed samples the volume percentage of heavy minerals (the HMC index) ranges from low ($0.5 \leq HMC < 1$) to rich ($5 \leq HMC < 12$) (Fig. 5.2). Heavy mineral assemblages in the silt to sand-sized fractions are well preserved and only weakly affected by diagenesis and intrastratal dissolution. The proportion of heavy minerals (Supplementary 1, Table 4) could be controlled by the grain size distribution (Garzanti and Andò, 2007), because the coarser sediments contain more abundant and more variable heavy mineral suites.

The heavy mineral assemblage of the youngest sample, dated to ~30 kyr ago, was characterised by dominant green augite derived from the erosion of the Indian Passive margin (Deccan Trap basalt), with common amphibole and epidote, and with rare garnet, titanite, and tourmaline; this conclusion is also supported by Nd isotope compositions (Supplementary 1, Table 5; Fig. 5.2).

In older samples the heavy mineral assemblage is similar to the composition of the modern Indus River, indicating an orogenic provenance within the Himalayas. The suite of heavy minerals from the Indus River is rich in hornblende and epidote, with common garnet, titanite, and clinopyroxenes (Garzanti et al., 2005). The composition remains the same throughout the entire section at IODP Site U1456 (Supplementary 1, Table 5). The 15–500 μm size fraction represents 80% of the bulk sample at ~1.15 Ma, which overlaps with the composition of the modern Indus River mouth. In samples from ~1.26 Ma and 2.69 Ma there is an abrupt enrichment in platy minerals with very abundant phyllosilicates and hornblende concentrated due to suspension sorting. All samples from the upper Miocene (hole U1456D) show a tendency to be enriched in epidote and depleted in amphibole; this systematic trend could be related to a bias introduced by diagenesis. The total assemblage and the presence of unstable minerals with rare corrosion features allow us to argue that the provenance remained essentially the same at least as far back as ~8.09 Ma. The increase in monsoon precipitation levels after 6.29 Ma, recorded in the Nd/Sr data, cannot be seen in the heavy mineral results (Fig. 5.2).

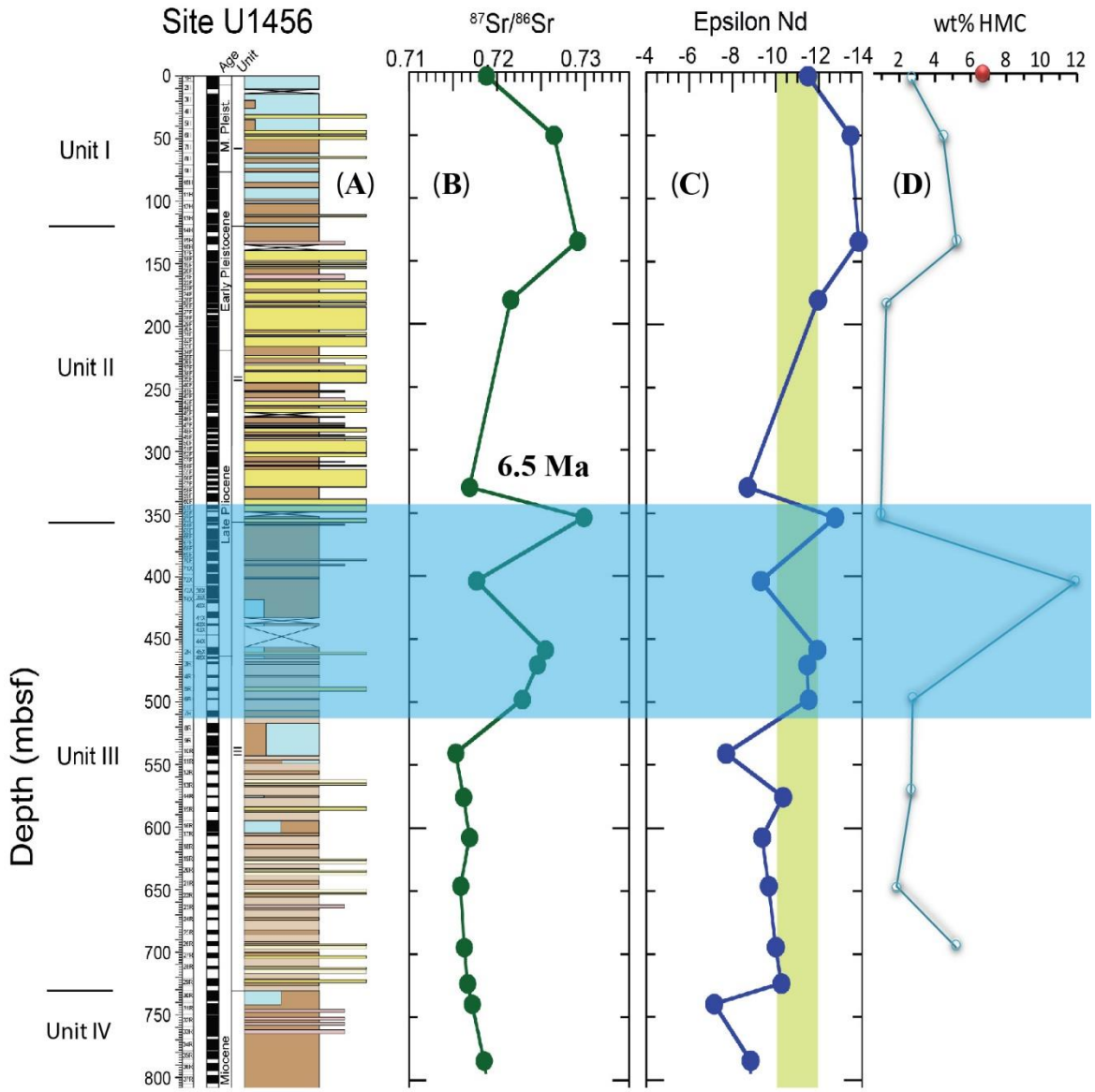

Figure 5.2: Heavy mineral data and isotope analyses of the IODP U1456 drilling site sediments. (A) drilled sediment age and lithology, with blue as nannofossil ooze, brown as clay grain-size sediment, pink as silt grain-size sediment, and yellow as sand-size sediment (Supplementary 2) (Pandey et al., 2016); (B) bulk sediment strontium isotope data; (C) bulk sediment epsilon neodymium isotope data, with the green shading indicating modern regional Nd levels; (D) weight percentage of total heavy minerals (wt% HMC) present in the samples (blue) and modern Indus river heavy mineral representation (red) (after Garzanti et al., 2005). The blue shaded area indicates the depth range when there were significant changes in Sr and Nd isotopes.

Bulk sediment TOC and TOC/TN values are usually used, with some caution (Meyers, 2003), to define the main OM input into marine sediments (Meyers, 2003; Blair and Aller, 2012).

The TOC data from U1456 Site (Fig. 5.4A) are mostly low (≤1.1 wt %), except for a

maximum value of 1.7 wt % at 1.07 Ma. TOC/TN values are ≤10 from the middle Miocene, indicating high marine OM input to the sediment (Fig. 5.4A). Three samples from the Pliocene and Pleistocene (2.78, 1.07, and 0.03 Ma) are characterised by a ratio greater than 12, reflecting relative increases in terrigenous input. The $\delta^{15}N$ values fluctuate between 2.4‰ and 8.2‰, with an average value of 5.3‰ (Fig. 5.4B), and can be divided into two periods: 10.15–5.86 Ma ago with 4.0 to 6.4‰, and 3.09–0.03 Ma ago with 5.5–8.2‰. The more positive $\delta^{15}N$ values indicate enhanced denitrification from the Pliocene onwards (Tesdal et al., 2013). Low $\delta^{15}N$ values of 4‰ around 8 Ma suggest mixing of marine OM with strong terrigenous source input, which is typically indicated where $\delta^{15}N$ clusters around 0‰ (Knapp et al., 2010). The $\delta^{13}C$ bulk values vary between -18.2‰ and -24.5‰, with the ~8 Ma interval having the lightest values consistent with a significant increase in terrigenous material input (Farquhar et al., 1989).

Concentrations of the individual C_{16}-C_{35} *n*-alkanes vary between 394 and 762,909 ng/g (dry weight) (Supplementary 1, Table 2). The *n*-alkanes have a unimodal distribution pattern dominated by high molecular weight *n*-alkanes and maximising at C_{31} (Fig. 5.5), suggesting high terrigenous OM input (Bray and Evans, 1961) (Supplementary 1, Table 2). This interpretation is supported by high $CPI_{(22\text{-}32)}$ (Bray and Evans, 1961) (>3) and TAR (Bourbonniere and Meyers, 1996) (>30) values for most samples (Fig. 5.3). There is an increase in $CPI_{(22\text{-}32)}$ and TAR during the 8 to 6 Ma period, suggest an increase in terrigenous OM input. This result is consistent with $\delta^{13}C$ bulk values for the same period. The $ACL_{(27\text{-}33)}$ varies between 28.9 and 30.1 (Fig. 5.3). Higher $ACL_{(27\text{-}33)}$ values predominantly indicate a warmer climate similar to that of southern China (Simoneit et al., 1991). The data suggest input of terrigenous OM dominated by vegetation from warm regions during the last 10 Myr. Samples around 7.4 and 0.5 Ma show high input of terrigenous OM dominating by vegetation from cooler climates. The Pr/Ph ratio is mostly <0.8, suggesting an anoxic depositional

environment, except for a period around 8 Ma when ratios are higher (1.5-2.0), suggestive of a more oxidising depositional environment (Fig. 5.3) (Powell and McKirdy, 1973).

Total C_{16}-C_{34} *n*-alkanoic acid concentrations range from 412.1 to 1415.7 ng/g dry weight and have a bimodal distribution dominated by C_{16} and C_{18} for homologues <C_{22}, and C_{24} and C_{26} in the higher molecular range (Supplementary 1, Table 2). *n*-Alkanoic acid distributions have an even-over-odd preference, with $CPI_{(22\text{-}30)}$ ranging between 3.3 and 6.6 indicative of a terrigenous OM input (Kvenvolden, 1966). The *n*-alkanoic acid ACL values vary between 25.8 and 27.6, with lower values (<26.4) between ~10.15 and 8.27 Ma, and an increase to 27.4 at 7.79 Ma. The *n*-alkanoic acid ACL_f values remain high until 5.86 Ma ago, then decrease to average values of 25.9 between 2.78 and 1 Ma ago.

The hydrogen isotopic composition of the mid to long chain length *n*-alkanoic acids (C_{24}-C_{28}) displays a similar isotopic changes in different acids, suggesting a common source of higher land plants. The weighted average (δD_{WM}) of the δD of the C_{24}-C_{30} *n*-alkanoic acids varies

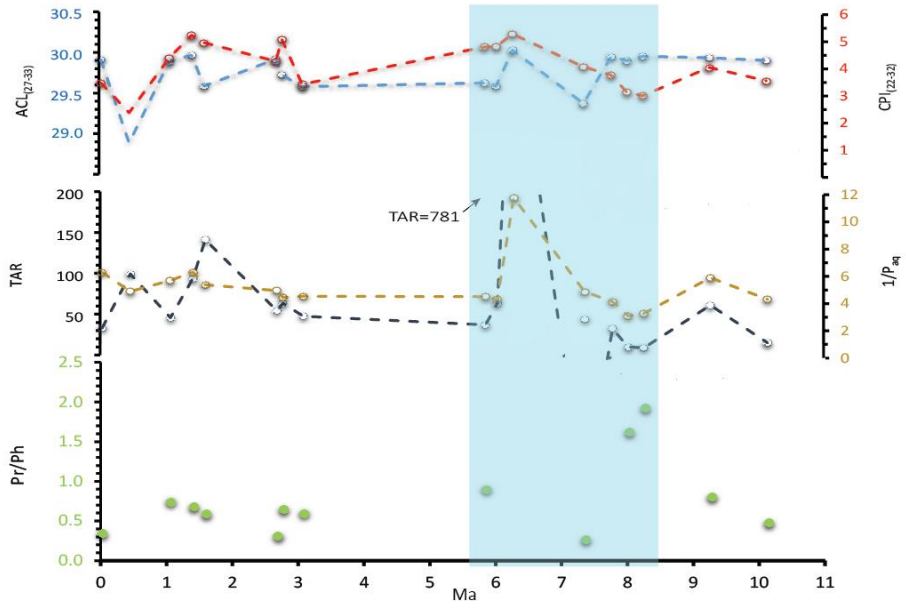

Figure 5.3: n-Alkane and isoprenoid data presented as average chain length ($ACL_{(27\text{-}33)}$; blue), carbon preference index ($CPI_{(22\text{-}32)}$; red), terrigenous/aquatic ratio (TAR; black), relative abundance of submerged/floating aquatic macrophyte input relative to the terrigenous input ($1/P_{aq}$; brown), and pristane/phytane (Pr/Ph) ratio (green). The blue shaded area indicates a period with interpreted increase in precipitation.

between -116.5 and -207.3‰ (Fig. 5.4C). From ~10.15 to 9.28 Ma δD_{WM} averages -142‰, but there are significantly more negative values in the late Miocene from 8.27 to 6.29 Ma (-206‰ to -195‰). In the Pliocene and Pleistocene, δD_{WM} shifts back to more positive values (~ -122‰) with the most positive value (-117‰) occurring at 1.07 Ma.

In general, δD values of *n*-alkanoic acids are generally similar for higher plants within different photosynthetic pathways. The soil becomes heavier in D through soil evaporation and respiration (Liu and Huang, 2005; Sachse et al., 2006), and bio-isotopic fractionation of the compounds during photosynthesis (e.g. Schimmelmann et al., 2006; Sessions, 2006a, b). Compound specific δD values vary relative to precipitation and evaporation levels of specific organisms or environments (Schefuß et al., 2005; Pagani et al., 2006; Sachse et al., 2006). The results suggest a significant increase in precipitation between 8 – 6 Ma. The precipitation levels decrease after this period and stay low to present. Because of the low sample resolution the influence of glacial/interglacial cycles on precipitation levels cannot be analysed.

The compound specific carbon isotope ($\delta^{13}C$) values for C_{24}-C_{28} *n*-alkanoic acids range from -21.6 ‰ to -31.8 ‰ (Fig. 5.4D). Most values are around 24 ‰, consistent with a high abundance of C_3 vegetation, but values are significantly more negative (-28.1‰ to -31.8‰) from 8.5-7.5 Ma ago, suggesting an increased input of C_4 vegetation (Collister et al., 1994).

Isoprenoid and branched GDGTs (iGDGTs and brGDGTs , respectively) were identified in eighteen samples. The data are presented as calculated indices and ratios (see Methods section; Supplementary 1). The brGDGT based BIT index (Hopmans et al., 2004; Weijers et al., 2006) indicates the level of terrigenous versus marine OM input, with values below 0.4 indicating a low terrigenous contribution. The BIT index is ≥0.5 for two late Miocene time intervals, 8.27–7.79 Ma and 6.04–5.86 Ma, suggesting high terrigenous sediment input (Fig. 5.4G). Bulk $\delta^{13}C$ values for these two intervals vary from -23.0 to -24.5 ‰ and -20.3 to -21.2‰, respectively (Fig. 5.4D). The isotopically light values between 8.27–7.79 Ma are

perhaps indicative of C_3 plant input (Dickens et al., 2004). An additional isolated BIT index spike of 0.51in the Pliocene (2.69 Ma; Fig 4G) has a bulk $\delta^{13}C$ of -20.6 ‰ (Fig. 5.4D). The rest of the samples have BIT indices ≤0.2, and rather high variation in bulk $\delta^{13}C$ (-18.2 to -22.6 ‰). The bulk $\delta^{13}C$ values since 6.04 Ma are indicative of marine plankton rather than terrigenous material (Dickens et al., 2004).

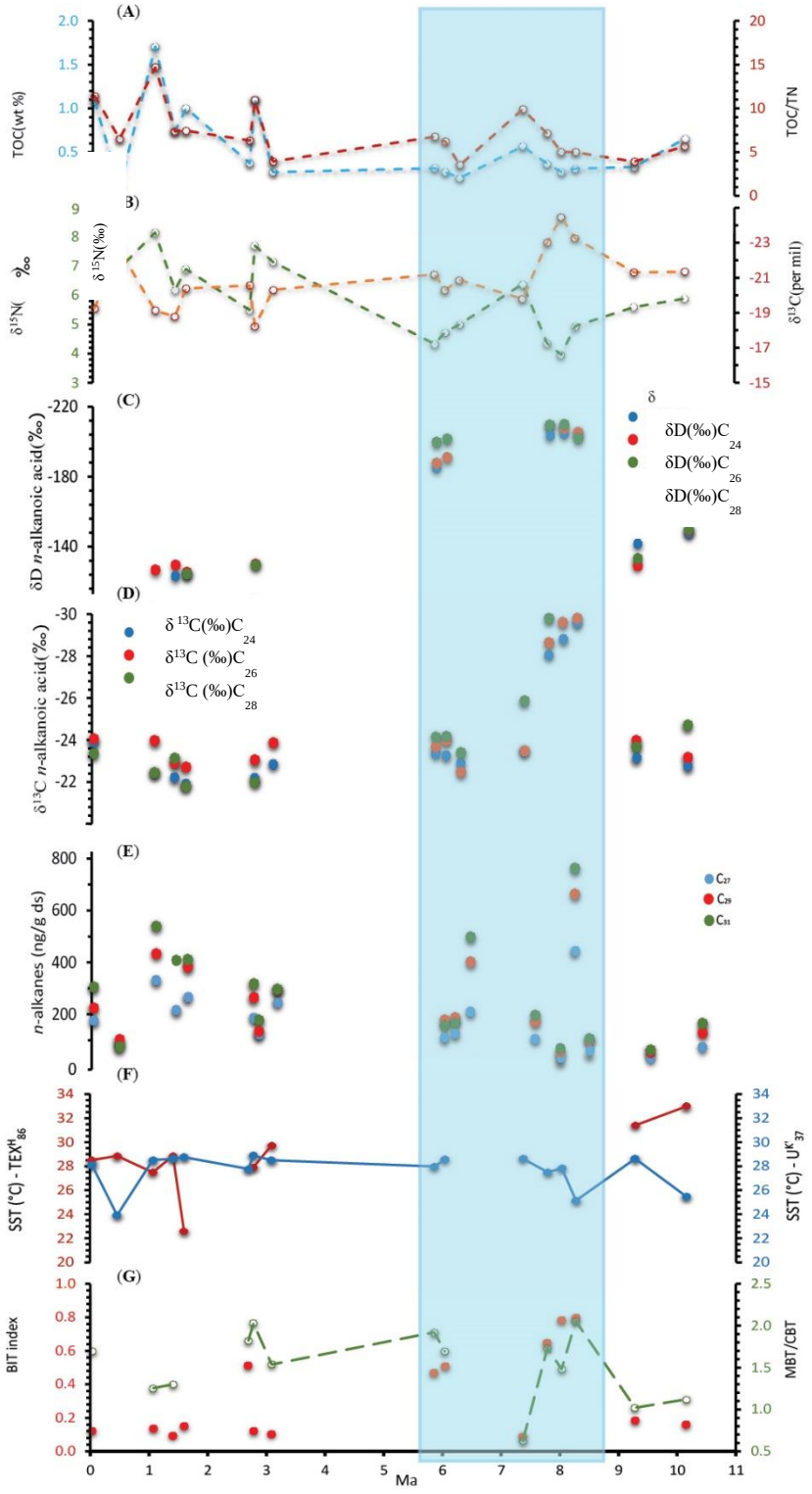

Figure 5.4: Isotopic composition, organic data, and lipid analysis results. (**A**) total organic carbon (TOC; blue) and TOC/TN ratio (red); (**B**) bulk sediment $\delta^{13}C$ (orange) and $\delta^{15}N$ (green) isotope data; (**C**) hydrogen isotope data (δD) for C_{24}, C_{26}, and C_{28} n-alkanoic acids; (**D**) carbon isotope data ($\delta^{13}C$) for C_{24}, C_{26}, and C_{28} n-alkanoic acids; (**E**) quantitative amounts of the C_{27}, C_{29}, and C_{31} n-alkanes (ng/g dry sediment); (**F**) Sea surface temperature (SST) based on the TEX^{H}_{86} (red) and $U^{K'}_{37}$ (blue) proxies; (**G**) BIT index (red) and the MBT/CBT ratio (green). The blue shaded area indicates a period with interpreted increase in precipitation.

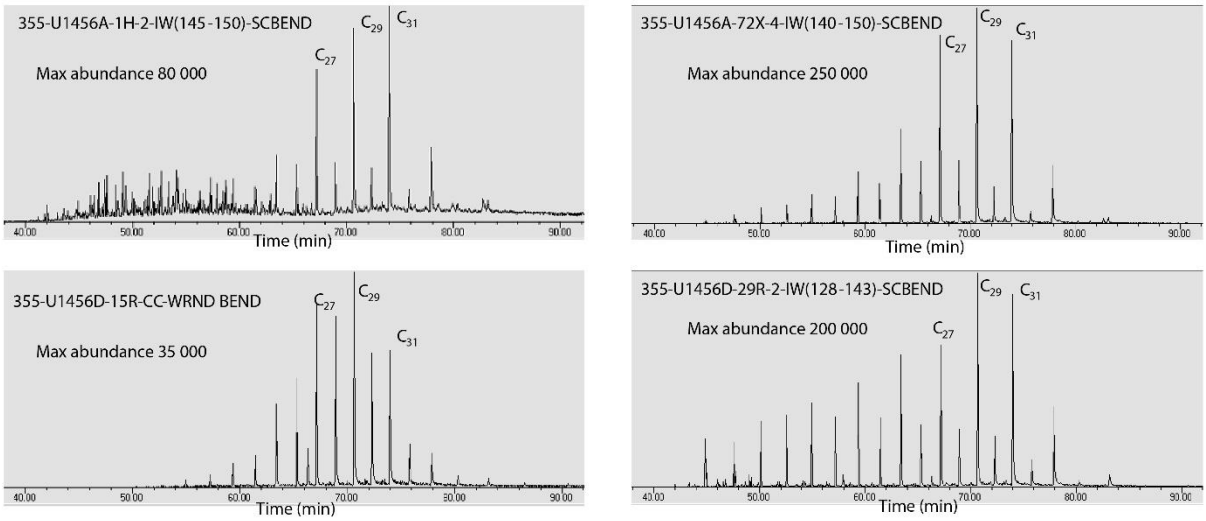

Figure 5.5: Representative m/z 57 chromatograms for four samples, showing unimodal n-alkane distribution patterns.

SSTs were reconstructed based on (1) the relative abundance of iGDGTs using the TEX^{H}_{86} index (Hopmans et al., 2000), and (2) the alkenone data using the $U^{k'}_{37}$ parameter (Prahl and Wakeham, 1987) (Fig. 5.4F). The TEX^{H}_{86} data may be strongly influenced by high terrigenous input, because of additional land derived sources of iGDGTs (Weijers et al., 2006). Therefore, only samples with a BIT index <0.4 were considered for the SST reconstruction. The TEX^{H}_{86} results indicate a slight decreasing temperature trend of 33.0°C to 30.5°C from 10.15 Ma until 7.73 Ma. After 3 Ma the TEX^{H}_{86} SST is mostly stable around 28.6°C, with one significant temperature drop to 22.6°C at 1.60 Ma. The alkenone based SST ($U^{k'}_{37}$) show a temperature decrease from 28°C at 10.15 Ma to 25°C at 7.37 Ma , and a relatively stable SST from 6.04 to 1.07 Ma ago averaging 28.6°C, similar to the TEX^{H}_{86} reconstruction (Fig. 5.4F). However, the SST based on $U^{k'}_{37}$ decreases significantly to 23.9°C at 0.46 Ma ago in contrast to the TEX^{H}_{86} reconstruction for this sample which is 28.9°C (Fig. 5.4F). No significant temperature drop was recorded by the alkenone proxy at 1.6 Ma ago, in contrast to the TEX^{H}_{86} data. The $U^{k'}_{37}$ record generally gives lower SST estimates than TEX_{86}, which can be partly explained by the upper limit of the $U^{k'}_{37}$ calibration of 29°C (Sonzogni et

al., 1997). The two SST proxies also vary based on seasonal and depth interval variations (Kim et al., 2010; Leider et al., 2010).

C_{27} –C_{29} ααα 20R steranes were identified in 14 samples and their molecular weight distribution is presented in Fig. 5.6 (Supplementary 1, Table 6), which shows variation in OM input. The sterane distribution changes in the late Miocene from 8.27–6.29 Ma and is characterised by spasmodically enhanced terrigenous sediment contributions into the marine environment. This observation is supported by the high amounts of long chain *n*-alkanes and the high oleanane index indicative of angiosperm OM input (Whithead, 1973; Ekweozor and Udo, 1988; Murray et al., 1994; Murray et al., 1997) during the same period (Fig. 5.4E; Supplementary 1, Table 6), and is consistent with strong energy pulses from the Indus River region. The sediments deposited at other times have a sterane signature characteristic of a mixed shallow marine environment, which can be explained by slow movement of sediment from the main deltaic source of the Indus River towards the Laxmi Basin. This observation is supported by the C_{30} sterane index, which is specific for marine organic matter (Seifert and Moldowan, 1978; Peters et al., 2005), and which increases from 6.29 to 3.04 Ma (Supplementary 1, Table 6).

Thermal maturity evaluation of the sedimentary sequence was achieved using commonly used biomarker ratios. A generally low Ts/(Ts+Tm) ratio for the Site U1456 samples (<0.25) is indicative of low thermal maturities (Seifert and Moldowan, 1978; Stephens and Carroll, 1999; Nuzzo et al., 2012). A higher thermal maturity is suggested for the two deepest samples (10.15 Ma and 13.53–17.71 Ma), with Ts/(Ts+Tm) ratio values >0.4 (Supplementary 1, Table 6). Most 22S/(22S+22R) C_{31} αβ hopane epimer ratios ((Seifert and Moldowan, 1980; Moldowan et al., 1986) are also consistent with a low thermal maturity for the samples (Supplementary 1, Table 6). Three samples at 7.79, 8.27, and 13.53-17.71 Ma have higher 22S/(22S+22R) ratios, possibly showing high thermal maturity. A low thermal maturity is also supported by low (<0.5) 20S/(20S+20R) C_{29} 5α,14α,17α(H) sterane ratios (Moldowan et

al., 1986) (Supplementary 1, Table 6), with the exception for the 7.79 Ma sample (0.61). Some of these hopane and sterane ratios may be influenced by source variations, but overall most show a low thermal maturity for the analysed sediments, with a slight increase in maturation in the deeper samples.

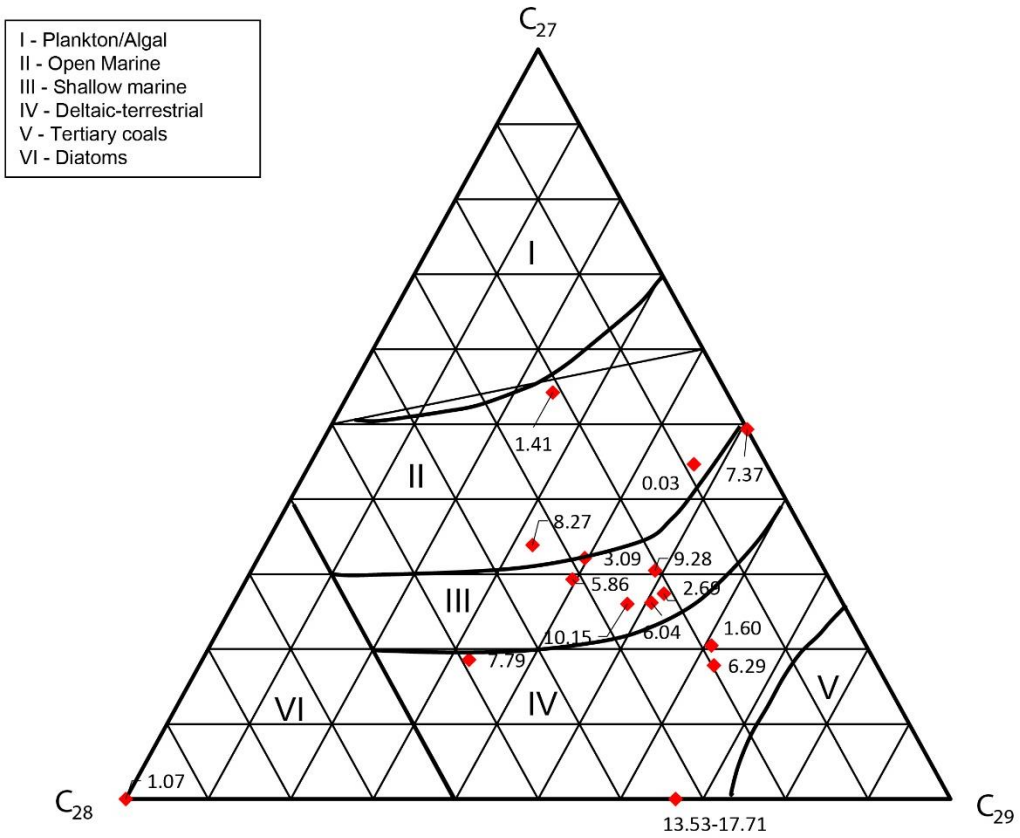

Figure 5.6: Ternary diagram showing the C_{27}, C_{28}, and C_{29} ααα 20R sterane distributions. The areas are defined after Huang and Meinschein (1979): I – plankton/algal OM source; II – open marine OM source; III – shallow marine OM source; IV – deltaic or terrigenous OM source; V – OM source in Tertiary coal; and VI – diatom OM source.

5.4. Synthesis

One of the major factors in precipitation development is the sea-land thermal gradient (Webster et al., 1998). The SST reconstructions suggest a decreasing but still warm SST during the late Miocene (>30°C based on iGDGTs and averaging ~27°C for the alkenone proxy). These results are consistent with data from the northern South China Sea and global SST reconstructions based on $\delta^{18}O$ and Mg/Ca proxies. Temperature changes and increases in upwelling in the Indian Ocean during the late Miocene have been attributed to accumulation of Antarctic ice cover (Norris et al., 2013). Other studies have proposed that the modest sized permanent ice sheets in the Northern Hemisphere and the distribution of solar radiation are the main causes for the intensification of the monsoon in the late Miocene (Clemens et al., 1991). However, ice-temperature change models do not support such a correlation at that time (Cramer et al., 2011).

Debate continues about the nature of monsoon change in the late Miocene, and whether it strengthened or weakened. Some studies predict monsoon weakening between 10.15 and 3.09 Ma (Clift et al., 2008b), and after 8.27 Ma for the southern Asia area, while others argue for increasing summer rains over the same interval. Regardless of the direction of change, the closure of the Tethys Ocean together with the uplift of the Himalayas and Tibetan Plateau have been linked to major alternations in monsoon strength. Climate models suggest that coastal upwelling in the western Arabian Sea is consistent with an increase in southwest winds between ~10.15 and 8.27 Ma, as supported by recent scientific drilling in the Maldives (Prell et al., 1993; Betzler et al., 2016). However, such studies are primary indicators of wind strength and not precipitation. Indeed, our observations suggest no significant increase in precipitation between 10.15 and 8.26 Ma. This period was followed by an increase in summer monsoon levels together with a possible increase of the Indus River run-off for the eastern Arabian Sea region in the late Miocene (8.27 – 6.29 Ma), as recorded in the *n*-alkane (e.g., TAR and $1/P_{aq}$) and sterane data. This observation is supported by $\delta^{13}C$ record. The increase

in precipitation levels recorded by δD during the 8.27 to 6.29 Ma period supports a stronger Indus River runoff as well.

Variations in SST since 3 Ma are consistent with existing reconstructions of tropical ocean temperatures, which argue for a significant control by glacial-interglacial cyclicity over precipitation patterns, with changing glaciation in the northern hemisphere (Beu et al., 1997; Zhisheng et al., 2001). These cycles mainly developed because of the major changes in thermohaline circulation that followed closure of the Isthmus of Panama and onset of Northern Hemisphere Glaciation with a decrease in atmospheric CO_2 content. Variations in magnetic sustainability suggest a strong influence of orbital forcing on Asian monsoon intensification, together with an increase in central Asian aridity levels (Clemens et al., 1991; Prell and Kutzbach, 1992; Zhisheng et al., 2001). All these line of evidence support the strong influence of glacial cyclicity on the Asian monsoon over the last 3 Myr.

The TOC/TN data and Pr/Ph also suggest strong but short-lived inputs of terrigenous OM around ~8.3 Ma. High precipitation levels in the period from ~2.6 to ~1.6 Ma are also clearly recorded by increasing terrigenous OM inputs, based on *n*-alkanes, steranes, and the BIT index (Fig. 5.4G; Supplementary 1, Table 2). Falls in eustatic sea level may have increased terrigenous material input into the basin. Nonetheless, variations in climate between the glacial-interglacial cycles are also well-recognised as factors intensifying continental erosion and would also help increase terrigenous flux after ~3 Ma ago.

The development of the Asian monsoonal circulation may have occurred as early as the Eocene (Licht et al., 2014), but other studies argue for an intense phase beginning at the start of the Neogene (Clift et al., 2014). Some of these reconstructions have been informed by changes in eastern Asian vegetation patterns, as well as by chemical weathering proxies. Chemical weathering data from ODP Site 1146 in the South China Sea indicate a pattern of decreasing humidity from the middle Miocene to the early Pliocene and a decrease in

monsoon intensity (Steinke et al., 2010). The decline in chemical weathering intensity parallels a decrease of sedimentation rates on the Indus Fan, as well as a decline in chemical weathering and sedimentation rates at ODP Site 718 on the Bengal Fan (Cochran and Stow, 1987; Clift et al., 2008a; Clift et al., 2008b). In light of the regional character of these changes across the Himalayas and the Tibetan Plateau, it seems likely they may reflect a common climatic driver. The vegetation signal since 10.15 Ma at IODP Site U1456 is derived mainly from the continental source for the last 10 Ma. The studies of Pakistan climate suggest a development of strong aridity and changes in precipitation patterns from 9 Ma (Quade et al., 1989). Sediment from the western Arabian Sea (ODP Site 722 drilling site) also showed an increase in terrigenous sediment input from 8–6 Ma, although an increase in primary marine production was not detected because of poor carbonate preservation (Prell and Kutzbach, 1992; Zhisheng et al., 2001).

Moreover, the data indicate an increase in relative C_4 vegetation abundance for the western Himalaya region from ~10.15 until ~8.27 Ma, suggesting a regional decrease in precipitation. A strong increase in relative C_3 vegetation abundance from 8.27–7.5 Ma may be indicative of an increase in precipitation, consistent with an increase in Asian monsoon intensity. The aridity of the region increasing again after 7.5 Ma Ma, with higher relative C_4 vegetation abundance in the sediments based on $\delta^{13}C$ data (Fig. 5.4D). However, our δD results together with the high terrigenous OM input suggest an increase in precipitation from ~8.3 to ~6.3 Ma, followed by high precipitation with an increase in C_4 vegetation input until ~5.9 Ma. A decrease in C_4 intensity was recorded only after ~3.1 Ma.

Data collected from the Eastern Arabian Sea area was integrated into the general regional climate history since the late Miocene, showing the strong control of regional climate change on temperatures and precipitation in the area. The Indus River is the main source of sediments into the Laxmi Basin, so that sediment can be used to reconstruct precipitation, vegetation and erosion patterns in the western Himalayan region and adjacent floodplains. The recorded

geochemical data together with detailed heavy mineral analysis of the Laxmi Basin sediment allows better reconstruction of organic variability in relationship to precipitation shifts. The data show a correlation between uplift in the western Himalaya region and an increase in precipitation around 8 Ma. This could be an indicator of an increase in the Asian monsoon intensity. The various analytical approaches for determining sedimentary provenance and paleoclimate organic signals in marine sediments provide tremendous potential for building a full regional paleogeographic picture.

5.5. Conclusions

The research show the Indus River is the main source of sediments into the Laxmi Basin. A possible increase in sediment flux from the Greater Himalayas and especially the Lesser Himalayas relative to the Karakoram region may be inferred towards the end of the late Miocene and during the Pleistocene. The data suggest increased erosion at ~8.27–6.29 Ma in the High Himalaya and Transhimalayan regions and possibly pointing towards stronger precipitation as part of the development of the summer monsoon.

The organic geochemical data indicate low thermal maturity of the organic matter. The *n*-alkane data for the 8 to 6 Ma period indicate an increase in terrigenous OM input with possibly a warmer climate. The data also show the input of terrigenous OM mostly dominated by vegetation from warm regions during the last 10 Myr. Samples around 7.4 and 0.5 Ma show high input of terrigenous OM dominating by vegetation from cooler climates. In addition, the BIT index is ≥0.5 for two late Miocene time intervals, 8.27–7.79 Ma and 6.04–5.86 Ma, suggesting high terrigenous sediment input.

The isoprenoid data indicate a mainly anoxic depositional environment, except for a period around 8 Ma with more oxic depositional environment. The compound specific δD results suggest a significant increase in precipitation from 8–7 Ma. Precipitation decreased after this

period, and has stayed low to the present. Because of the low sample resolution the influence of glacial/interglacial cycles on precipitation levels cannot be analysed.

The SST (TEX^{H}_{86}) results indicate a slight decreasing temperature trend of 33.0°C to 30.5°C from 10.15 Ma until 7.73 Ma. After 3 Ma the TEX^{H}_{86} SST is mostly stable around 28.6°C. The alkenone based SST ($U^{k'}_{37}$) show a temperature decrease from 28°C at 10.15 Ma to 25°C at 7.37 Ma, and a relatively stable SST from 6.04 to 1.07 Ma ago, averaging 28.6°C, similar to the SST (TEX^{H}_{86}) reconstruction. However, the SST based on $U^{k'}_{37}$ decreases significantly to 23.9°C at 0.46 Ma ago.

The sterane distribution changes in the late Miocene from 8.27–6.29 Ma, and is characterised by spasmodically enhanced terrigenous sediment contributions into the marine environment. The sediments deposited at other times have a sterane signature characteristic of a mixed shallow marine environment, which can be explained by the slow movement of sediment from the main deltaic source of the Indus River towards the Laxmi Basin.

The data show a correlation between uplift in the western Himalaya region and an increase in precipitation around 8 Ma. This could be an indicator of an increase in the Asian monsoon intensity.

5.6. Acknowledgements

We thank the crew of the RV *JOIDES Resolution* for professional seamanship, excellent drilling, and the scientific support on board. This work was supported by post-cruise funding by the Australia-New Zealand IODP Consortium (ANZIC) that was awarded to S.A. and S.C.G.. Macquarie University is thanked for a PhD scholarship awarded to S.A.

5.7. References

Andò, S., Garzanti, E., Padoan, M., Limonta, M., 2012. Corrosion of heavy minerals during weathering and diagenesis: A catalog for optical analysis. *Sedimentary Geology* 280, 165-178.

Andò, S., Morton, A., Garzanti, E., 2014. Metamorphic grade of source rocks revealed by chemical fingerprints of detrital amphibole and garnet. *Geological Society, London, Special Publications* 386, 351-371.

Barnes, M., Barnes, W., 1978. Organic compounds in lake sediments, Lakes. Springer, pp. 127-152.
Barrett, P.J., 1989. Antarctic Cenozoic history from the CIROS-1 drillhole, McMurdo Sound. DRIS Publishing.
Bassinot, F.C., Labeyrie, L.D., Vincent, E., Quidelleur, X., Shackleton, N.J., Lancelot, Y., 1994. The astronomical theory of climate and the age of the Brunhes-Matuyama magnetic reversal. *Earth and Planetary Science Letters* 126, 91-108.

Becker, K.W., Lipp, J.S., Zhu, C., Liu, X.-L., Hinrichs, K.-U., 2013. An improved method for the analysis of archaeal and bacterial ether core lipids. *Organic Geochemistry* 61, 34-44.

Berger, W., 2007. Cenozoic cooling, Antarctic nutrient pump, and the evolution of whales. *Deep Sea Research Part II: Topical Studies in Oceanography* 54, 2399-2421.

Berner, R., 1990. Atmospheric carbon dioxide levels over Phanerozoic time. *Science* 249, 1382-1386.

Betzler, C., Eberli, G.P., Kroon, D., Wright, J.D., Swart, P.K., Nath, B.N., Alvarez-Zarikian, C.A., Alonso-García, M., Bialik, O.M., Blättler, C.L., 2016. The abrupt onset of the modern South Asian Monsoon winds. *Scientific Reports* 6.

Beu, A.G., Griffin, M., Maxwell, P., 1997. Opening of Drake Passage gateway and Late Miocene to Pleistocene cooling reflected in Southern Ocean molluscan dispersal: evidence from New Zealand and Argentina. *Tectonophysics* 281, 83-97.

Blair, N.E., Aller, R.C., 2012. The fate of terrestrial organic carbon in the marine environment. *Annual Review of Marine Science* 4, 401-423.

Bourbonniere, R., Meyers, P., 1996. Anthropogenic influences on hydrocarbon contents of sediments deposited in eastern Lake Ontario since 1800. *Environmental Geology* 28, 22-28.

Bray, E., Evans, E., 1961. Distribution of n-paraffins as a clue to recognition of source beds. *Geochimica et Cosmochimica Acta* 22, 2-15.

Burbank, D., Blythe, A., Putkonen, J., Pratt-Sitaula, B., 2003. Decoupling of erosion and precipitation in the Himalayas. *Nature* 426, 652.

Carver, R.E., 1971. Procedures in sedimentary petrology. Wiley-Interscience New York.
Cerling, T.E., Wang, Y., Quade, J., 1993. Expansion of C4 ecosystems as an indicator of global ecological change in the late Miocene. *Nature* 361, 344-345.

Clemens, S., Prell, W., Murray, D., Shimmield, G., Weedon, G., 1991. Forcing mechanisms of the Indian Ocean monsoon. *Nature* 353, 720-725.

Clift, P., Hodges, K., Heslop, D., Hannigan, R., Hoang, L., Calves, G., 2008a. Greater Himalayan exhumation triggered by Early Miocene monsoon intensification. *Nat Geosci* 1, 875-880.

Clift, P., Shimizu, N., Layne, G., Blusztajn, J., Gaedicke, C., Schlüter, H.-U., Clark, M., Amjad, S., 2001. Development of the Indus Fan and its significance for the erosional history of the Western Himalaya and Karakoram. *Geological Society of America Bulletin* 113, 1039-1051.

Clift, P.D., Giosan, L., Carter, A., Garzanti, E., Galy, V., Tabrez, A.R., Pringle, M., Campbell, I.H., France-Lanord, C., Blusztajn, J., 2010. Monsoon control over erosion patterns in the western Himalaya: possible feed-back into the tectonic evolution. *Geological Society, London, Special Publications* 342, 185-218.

Clift, P.D., Hodges, K.V., Heslop, D., Hannigan, R., Van Long, H., Calves, G., 2008b. Correlation of Himalayan exhumation rates and Asian monsoon intensity. *Nature Geosci* 1, 875-880.

Clift, P.D., Lee, J.I., Hildebrand, P., Shimizu, N., Layne, G.D., Blusztajn, J., Blum, J.D., Garzanti, E., Khan, A.A., 2002. Nd and Pb isotope variability in the Indus River System: implications for sediment provenance and crustal heterogeneity in the Western Himalaya. *Earth and Planetary Science Letters* 200, 91-106.

Clift, P.D., Wan, S., Blusztajn, J., 2014. Reconstructing chemical weathering, physical erosion and monsoon intensity since 25Ma in the northern South China Sea: A review of competing proxies. *Earth-Science Reviews* 130, 86-102.

Cochran, J., Stow, D., 1987. 32. HIMALAYAN UPLIFT, SEA LEVEL, AND THE RECORD OF BENGAL FAN SEDIMENTATION AT THE ODP LEG 116 SITES1, Proceedings of the Ocean Drilling Program: Scientific results. The Program, p. 397.
Collister, J.W., Rieley, G., Stern, B., Eglinton, G., Fry, B., 1994. Compound-specific δ 13C analyses of leaf lipids from plants with differing carbon dioxide metabolisms. *Organic geochemistry* 21, 619-627.

Conte, M.H., Sicre, M.A., Rühlemann, C., Weber, J.C., Schulte, S., Schulz-Bull, D., Blanz, T., 2006. Global temperature calibration of the alkenone unsaturation index (UK′ 37) in surface waters and comparison with surface sediments. *Geochemistry, Geophysics, Geosystems* 7.

Cramer, B., Miller, K., Barrett, P., Wright, J., 2011. Late Cretaceous–Neogene trends in deep ocean temperature and continental ice volume: Reconciling records of benthic foraminiferal geochemistry (δ18O and Mg/Ca) with sea level history. *Journal of Geophysical Research: Oceans* 116.

Cranwell, P., 1984. Lipid geochemistry of sediments from Upton Broad, a small productive lake. *Organic Geochemistry* 7, 25-37.

Cranwell, P., Eglinton, G., Robinson, N., 1987. Lipids of aquatic organisms as potential contributors to lacustrine sediments—II. *Organic Geochemistry* 11, 513-527.

De Lange, G.J., Van Os, B., Pruysers, P.A., Middelburg, J.J., Castradori, D., Van Santvoort, P., Müller, P.J., Eggenkamp, H., Prahl, F.G., 1994. Possible early diagenetic alteration of palaeo proxies, Carbon Cycling in the Glacial Ocean: Constraints on the Ocean's Role in Global Change. Springer, pp. 225-258.
DePaolo, D.J., 2012. Neodymium isotope geochemistry: an introduction. Springer Science & Business Media.
Derry, L.A., France-Lanord, C., 1996. Neogene Himalayan weathering history and river87Sr86Sr: impact on the marine Sr record. *Earth and Planetary Science Letters* 142, 59-74.

Dickens, A.F., Gélinas, Y., Masiello, C.A., Wakeham, S., Hedges, J.I., 2004. Reburial of fossil organic carbon in marine sediments. *Nature* 427, 336-339.

Didyk, B., 1978. Organic geochemical indicators of palaeoenvnonmental conditions of sedimentation. *Nature* 272, 216-222.

Edmond, J., 1992. Himalayan tectonics, weathering processes, and the strontium isotope record in marine limestones. *SCIENCE-NEW YORK THEN WASHINGTON*- 258, 1594-1594.

Eglinton, G., Hamilton, R.J., 1967. Leaf epicuticular waxes. *Science* 156, 1322-1335.

Ekweozor, C., Udo, O.T., 1988. The oleananes: Origin, maturation and limits of occurence in southern Nigeria sedimentary basins. *Organic Geochemistry* 13, 131-140.

Farquhar, G.D., Ehleringer, J.R., Hubick, K.T., 1989. Carbon isotope discrimination and photosynthesis. *Annual review of plant biology* 40, 503-537.

France-Lanord, C., Derry, L., Michard, A., 1993. Evolution of the Himalaya since Miocene time: isotopic and sedimentological evidence from the Bengal Fan. *Geological Society, London, Special Publications* 74, 603-621.

Gagosian, R.B., 1976. A detailed vertical profile of sterols in the Sargasso Sea. *Limnol. Oceanogr* 21, 702-710.

Gagosian, R.B., Peltzer, E.T., 1986. The importance of atmospheric input of terrestrial organic material to deep sea sediments. *Organic Geochemistry* 10, 661-669.

Garzanti, E., Andò, S., 2007. Chapter 20 Heavy Mineral Concentration in Modern Sands: Implications for Provenance Interpretation, in: Maria, A.M., David, T.W. (Eds.), Developments in Sedimentology. Elsevier, pp. 517-545.
Garzanti, E., Andó, S., France-Lanord, C., Censi, P., Vignola, P., Galy, V., Lupker, M., 2011. Mineralogical and chemical variability of fluvial sediments 2. Suspended-load silt (Ganga–Brahmaputra, Bangladesh). *Earth and Planetary Science Letters* 302, 107-120.

Garzanti, E., Vezzoli, G., Ando, S., Paparella, P., Clift, P.D., 2005. Petrology of Indus River sands: a key to interpret erosion history of the Western Himalayan Syntaxis. *Earth and Planetary Science Letters* 229, 287-302.

Garzione, C.N., Quade, J., DeCelles, P.G., English, N.B., 2000. Predicting paleoelevation of Tibet and the Himalaya from δ 18 O vs. altitude gradients in meteoric water across the Nepal Himalaya. *Earth and Planetary Science Letters* 183, 215-229.

Gelin, F., Damsté, J.S.S., Harrison, W.N., Maxwell, J.R., De Leeuw, J.W., 1995. Molecular indicators for palaeoenvironmental change in a Messinian evaporitic sequence (Vena del Gesso, Italy): III. Stratigraphic changes in the molecular structure of kerogen in a single marl bed as revealed by flash pyrolysis. *Organic Geochemistry* 23, 555-566.

Grossi, V., Hirschler, A., Raphel, D., Rontani, J.-F., De Leeuw, J., Bertrand, J.-C., 1998. Biotransformation pathways of phytol in recent anoxic sediments. *Organic Geochemistry* 29, 845-861.

Gupta, A.K., Singh, R.K., Joseph, S., Thomas, E., 2004. Indian Ocean high-productivity event (10-8 Ma): Linked to global cooling or to the initiation of the Indian monsoons? *Geology* 32, 753-756.

Haq, B.U., Hardenbol, J., Vail, P.R., 1987. Chronology of fluctuating sea levels since the Triassic. *Science* 235, 1156-1167.

Harrison, T.M., Copeland, P., 1992. Raising tibet. *Science* 255, 1663.

Hedges, J.I., Keil, R.G., 1995. Sedimentary organic matter preservation: an assessment and speculative synthesis. *Marine Chemistry* 49, 81-115.

Hedges, J.I., Prahl, F.G., 1993. Early diagenesis: consequences for applications of molecular biomarkers, Organic Geochemistry. Springer, pp. 237-253.
Holbourn, A., Kuhnt, W., Simo, J.T., Li, Q., 2004. Middle Miocene isotope stratigraphy and paleoceanographic evolution of the northwest and southwest Australian margins (Wombat Plateau and Great Australian Bight). *Palaeogeography, Palaeoclimatology, Palaeoecology* 208, 1-22.

Hopmans, E.C., Schouten, S., Pancost, R.D., van der Meer, M.T., Sinninghe Damsté, J.S., 2000. Analysis of intact tetraether lipids in archaeal cell material and sediments by high performance liquid chromatography/atmospheric pressure chemical ionization mass spectrometry. *Rapid Communications in Mass Spectrometry* 14, 585-589.

Hopmans, E.C., Weijers, J.W., Schefuß, E., Herfort, L., Damsté, J.S.S., Schouten, S., 2004. A novel proxy for terrestrial organic matter in sediments based on branched and isoprenoid tetraether lipids. *Earth and Planetary Science Letters* 224, 107-116.

Huang, W.-Y., Meinschein, W.G., 1979. Sterols as ecological indicators. *Geochimica et Cosmochimica Acta* 43, 739-745.

Huntington, K.W., Blythe, A.E., Hodges, K.V., 2006. Climate change and Late Pliocene acceleration of erosion in the Himalaya. *Earth and Planetary Science Letters* 252, 107-118.

Ivanova, E., 2009. The global thermohaline paleocirculation. Springer Science & Business Media.
Juneng, L., Tangang, F.T., 2005. Evolution of ENSO-related rainfall anomalies in Southeast Asia region and its relationship with atmosphere–ocean variations in Indo-Pacific sector. *Climate Dynamics* 25, 337-350.

Kennett, J.P., 1977. Cenozoic evolution of Antarctic glaciation, the circum-Antarctic Ocean, and their impact on global paleoceanography. *Journal of geophysical research* 82, 3843-3860.

Kennett, J.P., Keller, G., Srinivasan, M., 1985. Miocene planktonic foraminiferal biogeography and paleoceanographic development of the Indo-Pacific region. *Geological Society of America Memoirs* 163, 197-236.

Kim, J.-H., Schouten, S., Hopmans, E.C., Donner, B., Sinninghe Damsté, J.S., 2008. Global sediment core-top calibration of the TEX86 paleothermometer in the ocean. *Geochimica et Cosmochimica Acta* 72, 1154-1173.

Kim, J.-H., Van der Meer, J., Schouten, S., Helmke, P., Willmott, V., Sangiorgi, F., Koç, N., Hopmans, E.C., Damsté, J.S.S., 2010. New indices and calibrations derived from the distribution of crenarchaeal isoprenoid tetraether lipids: Implications for past sea surface temperature reconstructions. *Geochimica et Cosmochimica Acta* 74, 4639-4654.

Knapp, A.N., Hastings, M.G., Sigman, D.M., Lipschultz, F., Galloway, J.N., 2010. The flux and isotopic composition of reduced and total nitrogen in Bermuda rain. *Marine Chemistry* 120, 83-89.

Knorr, G., Butzin, M., Micheels, A., Lohmann, G., 2011. A warm Miocene climate at low atmospheric CO2 levels. *Geophysical Research Letters* 38.

Kodner, R.B., Pearson, A., Summons, R.E., Knoll, A.H., 2008. Sterols in red and green algae: quantification, phylogeny, and relevance for the interpretation of geologic steranes. *Geobiology* 6, 411-420.

Kroon, D., Steens, T., Troelstra, S.R., 13. ONSET OF MONSOONAL RELATED UPWELLING IN THE WESTERN ARABIAN SEA AS REVEALED BY PLANKTONIC FORAMINIFERS1.

Kroon, D., Steens, T., Troelstra, S.R., 1991. 13. Onset of monsoonal related upwelling in the Western Araibian sea as revealed by planctonic foraminiders.

Kutzbach, J., Guetter, P., Ruddiman, W., Prell, W., 1989. Sensitivity of climate to late Cenozoic uplift in Southern Asia and the American West: Numerical experiments. *Journal of Geophysical Research: Atmospheres* 94, 18393-18407.

Kutzbach, J., Prell, W., Ruddiman, W.F., 1993. Sensitivity of Eurasian climate to surface uplift of the Tibetan Plateau. *The Journal of Geology* 101, 177-190.

Kvenvolden, K.A., 1966. Molecular Distributions of Normal Fatty Acids and Paraffins in Some Lower Cretaceous Sediments. *Nature* 209, 573-577.

Lao, Y., Korth, J., Ellis, J., Crisp, P., 1989. Heterogeneous reactions of 1-pristene catalysed by clays under simulated geological conditions. *Organic Geochemistry* 14, 375-379.

Lea, D.W., Pak, D.K., Spero, H.J., 2000. Climate impact of late Quaternary equatorial Pacific sea surface temperature variations. *Science* 289, 1719-1724.

Leider, A., Hinrichs, K.-U., Mollenhauer, G., Versteegh, G.J., 2010. Core-top calibration of the lipid-based and TEX 86 temperature proxies on the southern Italian shelf (SW Adriatic Sea, Gulf of Taranto). *Earth and Planetary Science Letters* 300, 112-124.

Li, T., Wang, B., 2005. A review on the western North Pacific monsoon: Synoptic-to-interannual variabilities. *Terr Atmos Ocean Sci* 16, 285-314.

Licht, A., Van Cappelle, M., Abels, H., Ladant, J.-B., Trabucho-Alexandre, J., France-Lanord, C., Donnadieu, Y., Vandenberghe, J., Rigaudier, T., Lécuyer, C., 2014. Asian monsoons in a late Eocene greenhouse world. *Nature* 513, 501-506.

Liu, W., Huang, Y., 2005. Compound specific D/H ratios and molecular distributions of higher plant leaf waxes as novel paleoenvironmental indicators in the Chinese Loess Plateau. *Organic Geochemistry* 36, 851-860.

Mashiotta, T.A., Lea, D.W., Spero, H.J., 1999. Glacial–interglacial changes in Subantarctic sea surface temperature and δ 18 O-water using foraminiferal Mg. *Earth and Planetary Science Letters* 170, 417-432.

Meyers, P.A., 1997. Organic geochemical proxies of paleoceanographic, paleolimnologic, and paleoclimatic processes. *Organic Geochemistry* 27, 213-250.

Meyers, P.A., 2003. Applications of organic geochemistry to paleolimnological reconstructions: a summary of examples from the Laurentian Great Lakes. *Organic Geochemistry* 34, 261-289.

Meyers, P.A., Ishiwatari, R., 1993. Lacustrine organic geochemistry—an overview of indicators of organic matter sources and diagenesis in lake sediments. *Organic Geochemistry* 20, 867-900.

Miller, K.G., Barrera, E., Olsson, R.K., Sugarman, P.J., Savin, S.M., 1999. Does ice drive early Maastrichtian eustasy? *Geology* 27, 783-786.

Miller, K.G., Kominz, M.A., Browning, J.V., Wright, J.D., Mountain, G.S., Katz, M.E., Sugarman, P.J., Cramer, B.S., Christie-Blick, N., Pekar, S.F., 2005. The phanerozoic record of global sea-level change. *Science* 310, 1293-1298.

Miller, K.G., Mountain, G.S., Browning, J.V., Kominz, M., Sugarman, P.J., Christie-Blick, N., Katz, M.E., Wright, J.D., 1998. Cenozoic global sea level, sequences, and the New Jersey transect: results from coastal plain and continental slope drilling. *Reviews of Geophysics* 36, 569-601.

Miller, K.G., Wright, J.D., Fairbanks, R.G., 1991. Unlocking the ice house: Oligocene-Miocene oxygen isotopes, eustasy, and margin erosion. *Journal of Geophysical Research: Solid Earth* 96, 6829-6848.

Moldowan, J.M., Seifert, W.K., Gallegos, E.J., 1985. Relationship between petroleum composition and depositional environment of petroleum source rocks. *AAPG bulletin* 69, 1255-1268.

Moldowan, J.M., Sundararaman, P., Schoell, M., 1986. Sensitivity of biomarker properties to depositional environment and/or source input in the Lower Toarcian of SW-Germany. *Organic Geochemistry* 10, 915-926.

Molnar, P., 2004. Late Cenozoic increase in accumulation rates of terrestrial sediment: How might climate change have affected erosion rates? *Annu. Rev. Earth Planet. Sci.* 32, 67-89.

Molnar, P., England, P., Martinod, J., 1993. Mantle dynamics, uplift of the Tibetan Plateau, and the Indian monsoon. *Reviews of Geophysics* 31, 357-396.

Müller, A., Mathesius, U., 1999. The palaeoenvironments of coastal lagoons in the southern Baltic Sea, I. The application of sedimentary C org/N ratios as source indicators of organic matter. *Palaeogeography, Palaeoclimatology, Palaeoecology* 145, 1-16.

Murray, A.P., Sosrowidjojo, I.B., Alexander, R., Kagi, R.I., Norgate, C.M., Summons, R.E., 1997. Oleananes in oils and sediments: Evidence of marine influence during early diagenesis? *Geochimica et Cosmochimica Acta* 61, 1261-1276.

Murray, A.P., Summons, R.E., Boreham, C.J., Dowling, L.M., 1994. Biomarker and n-alkane isotope profiles for Tertiary oils: relationship to source rock depositional setting. *Organic Geochemistry* 22, 521IN525-542IN526.

Norris, R., Turner, S.K., Hull, P., Ridgwell, A., 2013. Marine ecosystem responses to Cenozoic global change. *Science* 341, 492-498.

Nuzzo, M., Elvert, M., Schmidt, M., Scholz, F., Reitz, A., Hinrichs, K.-U., Hensen, C., 2012. Impact of hot fluid advection on hydrocarbon gas production and seepage in mud volcano sediments of thick Cenozoic deltas. *Earth and Planetary Science Letters* 341, 139-157.

Ourisson, G., Albrecht, P., Rohmer, M., 1984. Microbial origin of fossil fuels. *Sci. Am.;(United States)* 251.

Pagani, M., Arthur, M.A., Freeman, K.H., 1999. Miocene evolution of atmospheric carbon dioxide. *Paleoceanography* 14, 273-292.

Pagani, M., Pedentchouk, N., Huber, M., Sluijs, A., Schouten, S., Brinkhuis, H., Damsté, J.S.S., Dickens, G.R., Backman, J., Clemens, S., 2006. Arctic hydrology during global warming at the Palaeocene/Eocene thermal maximum. *Nature* 442, 671-675.

Pandey, D., Clift, P., Kulhanek, D., Andò, S., Bendle, J., Bratenkov, S., Griffith, E., Gurumurthy, G., Hahn, A., Iwai, M., 2016. Expedition 355 summary. *Pandey, DK, Clift, PD, Kulhanek, DK, and the Expedition* 355.

Pearson, A., Huang, Z., Ingalls, A., Romanek, C., Wiegel, J., Freeman, K., Smittenberg, R., Zhang, C., 2004. Nonmarine crenarchaeol in Nevada hot springs. *Applied and Environmental Microbiology* 70, 5229-5237.

Peizhen, Z., Molnar, P., Downs, W.R., 2001. Increased sedimentation rates and grain sizes 2–4 Myr ago due to the influence of climate change on erosion rates. *Nature* 410, 891-897.

Peters, K.E., Walters, C.C., Moldowan, J.M., 2005. The biomarker guide, 2nd ed. Cambridge University Press, Cambridge, UK ; New York.
Powell, T., McKirdy, D., 1973. Relationship between ratio of pristane to phytane, crude oil composition and geological environment in Australia. *Nature* 243, 37-39.

Prahl, F., Wakeham, S., 1987. Calibration of unsaturation patterns in long-chain ketone compositions for palaeotemperature assessment.

Prell, W., Kutzbach, J.E., 1992. Sensitivity of the Indian monsoon to forcing parameters and implications for 'its evolution. *Nature* 360, 17.

Prell, W.L., Murray, D.W., Clemens, S.C., Anderson, D.M., 1993. Evolution and variability of the Indian Ocean summer monsoon: Evidence from the western Arabian Sea drilling program. *Synthesis of Results from Scientific Drilling in the Indian Ocean*, 447-469.

Quade, J., Cerling, T.E., Bowman, J.R., 1989. Development of Asian monsoon revealed by marked ecological shift during the latest Miocene in northern Pakistan. *Nature* 342, 163-166.

Ramstein, G., Fluteau, F., Besse, J., Joussaume, S., 1997. Effect of orogeny, plate motion and land-sea distribution on Eurasian climate change over the past 30 million years. *Nature* 386, 788-795.

Raymo, M., Ruddiman, W.F., 1992. Tectonic forcing of late Cenozoic climate. *Nature* 359, 117-122.

Raymo, M.E., Ruddiman, W.F., Froelich, P.N., 1988. Influence of late Cenozoic mountain building on ocean geochemical cycles. *Geology* 16, 649-653.

Rea, D.K., 1993. Delivery of Himalayan sediment to the northern Indian Ocean and its relation to global climate, sea level, uplift, and seawater strontium. *Synthesis of results from scientific drilling in the Indian Ocean*, 387-402.

Richter, F.M., Rowley, D.B., DePaolo, D.J., 1992. Sr isotope evolution of seawater: the role of tectonics. *Earth and Planetary Science Letters* 109, 11-23.

Rontani, J.-F., Nassiry, M., Michotey, V., Guasco, S., Bonin, P., 2010. Formation of pristane from α-tocopherol under simulated anoxic sedimentary conditions: A combination of biotic and abiotic degradative processes. *Geochimica et Cosmochimica Acta* 74, 252-263.

Rossignol-Strick, M., Paterne, M., Bassinot, F., Emeis, K.-C., De Lange, G., 1998. An unusual mid-Pleistocene monsoon period over Africa and Asia. *Nature* 392, 269-272.

Rowland, S., 1990. Production of acyclic isoprenoid hydrocarbons by laboratory maturation of methanogenic bacteria. *Organic Geochemistry* 15, 9-16.

Rowley, D.B., 1996. Age of initiation of collision between India and Asia: A review of stratigraphic data. *Earth and Planetary Science Letters* 145, 1-13.

Ruddiman, W., Kutzbach, J., 1989. Forcing of late Cenozoic northern hemisphere climate by plateau uplift in southern Asia and the American West. *Journal of Geophysical Research: Atmospheres* 94, 18409-18427.

Ruddiman, W.F., 2010. Plows, plagues, and petroleum: how humans took control of climate. Princeton University Press.
Ruddiman, W.F., Kutzbach, J.E., 1991. Plateau uplift and climatic change. *Scientific American;(United States)* 264.

Sachse, D., Radke, J., Gleixner, G., 2006. δD values of individual n-alkanes from terrestrial plants along a climatic gradient–Implications for the sedimentary biomarker record. *Organic Geochemistry* 37, 469-483.

Savin, S.M., Abel, L., Barrera, E., Hodell, D., Kennett, J.P., Murphy, M., Keller, G., Killingley, J., Vincent, E., 1985. The evolution of Miocene surface and near-surface marine temperatures: oxygen isotopic evidence. *Geological Society of America Memoirs* 163, 49-82.

Schefuß, E., Schouten, S., Schneider, R.R., 2005. Climatic controls on central African hydrology during the past 20,000 years. *Nature* 437, 1003-1006.

Schimmelmann, A., Sessions, A.L., Mastalerz, M., 2006. Hydrogen isotopic (D/H) composition of organic matter during diagenesis and thermal maturation. *Annu. Rev. Earth Planet. Sci.* 34, 501-533.

Seifert, W., Moldowan, J., 1986. Use of biological markers in petroleum exploration. *Methods in geochemistry and geophysics* 24, 261-290.

Seifert, W.K., Moldowan, J.M., 1978. Applications of steranes, terpanes and monoaromatics to the maturation, migration and source of crude oils. *Geochimica et Cosmochimica Acta* 42, 77-95.

Seifert, W.K., Moldowan, J.M., 1980. The effect of thermal stress on source-rock quality as measured by hopane stereochemistry. *Physics and Chemistry of the Earth* 12, 229-237.

Sessions, A.L., 2006a. Isotope-ratio detection for gas chromatography. *Journal of separation science* 29, 1946-1961.

Sessions, A.L., 2006b. Seasonal changes in D/H fractionation accompanying lipid biosynthesis in Spartina alterniflora. *Geochimica et Cosmochimica Acta* 70, 2153-2162.

Shackleton, N.J., Kennett, J.P., 1975. Paleotemperature history of the Cenozoic and the initiation of Antarctic glaciation: oxygen and carbon isotope analyses in DSDP Sites 277, 279, and 281. *Initial reports of the deep sea drilling project* 29, 743-755.

Shackleton, N.J., Pisias, N., 1985. Atmospheric carbon dioxide, orbital forcing, and climate. *The Carbon Cycle and Atmospheric CO: Natural variations Archean to Present*, 303-317.

Shevenell, A.E., Kennett, J.P., Lea, D.W., 2004. Middle Miocene southern ocean cooling and Antarctic cryosphere expansion. *Science* 305, 1766-1770.

Silliman, J., Meyers, P., Ostrom, P., Ostrom, N., Eadie, B., 2000. Insights into the origin of perylene from isotopic analyses of sediments from Saanich Inlet, British Columbia. *Organic Geochemistry* 31, 1133-1142.

Simoneit, B.R., Sheng, G., Chen, X., Fu, J., Zhang, J., Xu, Y., 1991. Molecular marker study of extractable organic matter in aerosols from urban areas of China. *Atmospheric Environment. Part A. General Topics* 25, 2111-2129.

Sonzogni, C., Bard, E., Rostek, F., Dollfus, D., Rosell-Melé, A., Eglinton, G., 1997. Temperature and salinity effects on alkenone ratios measured in surface sediments from the Indian Ocean. *Quaternary Research* 47, 344-355.

Spicer, R.A., Harris, N.B., Widdowson, M., Herman, A.B., Guo, S., Valdes, P.J., Wolfe, J.A., Kelley, S.P., 2003. Constant elevation of southern Tibet over the past 15 million years. *Nature* 421, 622-624.

Stein, R., Macdonald, R., 2004. Organic carbon budget: Arctic Ocean vs. global ocean, The organic carbon cycle in the Arctic Ocean. Springer, pp. 315-322.
Stein, R., Macdonald, R.W., Stein, R., MacDonald, R.W., 2004. The organic carbon cycle in the Arctic Ocean.

Steinke, S., Groeneveld, J., Johnstone, H., Rendle-Bühring, R., 2010. East Asian summer monsoon weakening after 7.5 Ma: Evidence from combined planktonic foraminifera Mg/Ca and δ 18 O (ODP Site 1146; northern South China Sea). *Palaeogeography, Palaeoclimatology, Palaeoecology* 289, 33-43.

Stephens, N.P., Carroll, A.R., 1999. Salinity stratification in the Permian Phosphoria sea; a proposed paleoceanographic model. *Geology* 27, 899-902.

Tesdal, J.-E., Galbraith, E., Kienast, M., 2013. Nitrogen isotopes in bulk marine sediment: linking seafloor observations with subseafloor records. *Biogeosciences* 10, 101.

Tornabene, T., Langworthy, T., Holzer, G., Oro, J., 1979. Squalenes, phytanes and other isoprenoids as major neutral lipids of methanogenic and thermoacidophilic "archaebacteria". *Journal of Molecular Evolution* 13, 73-83.

Traverse, A., 1982. Response of world vegetation to Neogene tectonic and climatic events. *Alcheringa* 6, 197-209.

Twichell, S.C., Meyers, P.A., Diester-Haass, L., 2002. Significance of high C/N ratios in organic-carbon-rich Neogene sediments under the Benguela Current upwelling system. *Organic Geochemistry* 33, 715-722.

Vail, P., Mitchum Jr, R., 1979. Global cycles of relative changes of sea level from seismic stratigraphy: resources, comparative structure, and eustatic changes in sea level.

Viso, A.-C., Pesando, D., Bernard, P., Marty, J.-C., 1993. Lipid components of the Mediterranean seagrass Posidonia oceanica. *Phytochemistry* 34, 381-387.

Volkman, J.K., 1986. A review of sterol markers for marine and terrigenous organic matter. *Organic Geochemistry* 9, 83-99.

Volkman, J.K., 2005. Sterols and other triterpenoids: source specificity and evolution of biosynthetic pathways. *Organic Geochemistry* 36, 139-159.

Wang, W., Zhou, Z.Y., Yu, P., 2005. Relations Between Vitrinite Reflectance, Peek Temperature and its Neighboring Temperature Variation Rate: A Comparison of Methods. *Chinese Journal of Geophysics* 48, 1443-1453.

Webster, P.J., Magana, V.O., Palmer, T., Shukla, J., Tomas, R., Yanai, M., Yasunari, T., 1998. Monsoons: Processes, predictability, and the prospects for prediction. *Journal of Geophysical Research: Oceans* 103, 14451-14510.

Weijers, J.W., Schouten, S., Spaargaren, O.C., Damsté, J.S.S., 2006. Occurrence and distribution of tetraether membrane lipids in soils: implications for the use of the TEX 86 proxy and the BIT index. *Organic Geochemistry* 37, 1680-1693.

Weijers, J.W.H., Schouten, S., Sluijs, A., Brinkhuis, H., Sinninghe Damsté, J.S., 2007. Warm arctic continents during the Palaeocene–Eocene thermal maximum. *Earth and Planetary Science Letters* 261, 230-238.

Wenger, L.M., Isaksen, G.H., 2002. Control of hydrocarbon seepage intensity on level of biodegradation in sea bottom sediments. *Organic Geochemistry* 33, 1277-1292.

Whithead, J.M., 1973. The structure of petroleum pentacyclanes, in: Tissot, B.a., Bienner, F. (Eds.), Advances in Organic Geochemistry. Editions Technip, Paris, pp. 225-243.
Zachos, J., Pagani, M., Sloan, L., Thomas, E., Billups, K., 2001. Trends, rhythms, and aberrations in global climate 65 Ma to present. *Science* 292, 686-693.

Zachos, J.C., Breza, J.R., Wise, S.W., 1992. Early Oligocene ice-sheet expansion on Antarctica: Stable isotope and sedimentological evidence from Kerguelen Plateau, southern Indian Ocean. *Geology* 20, 569-573.

Zhisheng, A., Kutzbach, J.E., Prell, W.L., Porter, S.C., 2001. Evolution of Asian monsoons and phased uplift of the Himalaya-Tibetan plateau since Late Miocene times. *Nature* 411, 62-66.

Zhongshi, Z., Huijun, W., Zhengtang, G., Dabang, J., 2007a. Impacts of tectonic changes on the reorganization of the Cenozoic paleoclimatic patterns in China. *Earth and Planetary Science Letters* 257, 622-634.

Zhongshi, Z., Wang, H., Guo, Z., Jiang, D., 2007b. What triggers the transition of palaeoenvironmental patterns in China, the Tibetan Plateau uplift or the Paratethys Sea retreat? *Palaeogeography, Palaeoclimatology, Palaeoecology* 245, 317-331.

5.8. Supplementary 1: Data Tables

Supplementary Table 5.1: General sample information

Sample number	Depth (mbsf)	Age (Ma)	Geological epoch	Lithological Unit	Lithology
355-U1456A-1H-2-IW(145-150)-SCBEND	2.95	0.03	Pleistocene	I	carbonate ooze/stone
355-U1456A-6H-5-IW(145-150)-SCBEND	49.95	0.46	Pleistocene	I	clay/claystone
355-U1456A-13H-5-IW(145-150)-SCBEND	116.42	1.07	Pleistocene	I	carbonate ooze/stone
355-U1456A-15H5-IW(145-150)-SCBEND	134.12	1.15	Pleistocene	I	clay/claystone
355-U1456A-25F-3-IW-SCBEND	180.56	1.26	Pleistocene	I	clay/claystone
355-U1456A-40F-2-IW-SCBEND	247.55	1.41	Pleistocene	I	sand/sandstone
355-U1456A-58F-1-IW(89-99)-SCBEND	329.29	1.60	Pleistocene	I	sand/sandstone
355-U1456A-63F-1-IW(140-150)-SCBE	353.30	2.57	Pleistocene	I	sand/sandstone
355-U1456A-65F-2-IW(140-150)-SCBEND	364.20	2.69	Pliocene	II	clay/claystone
355-U1456A-67F-2-IW(140-150)-SCBE	373.60	2.78	Pliocene	II	clay/claystone
355-U1456A-72X-4-IW(140-150)-SCBE	403.70	3.09	Pliocene	II	clay/claystone
355-U1456C-45X-2-IW(111-121)-SCBE	458.41	3.65	Pliocene	II	clay/claystone
355-U1456D-3R-CC-WRND BEND	470.21	5.40	Late Miocene	III	clay/claystone
355-U1456D-6R-CC-WRND BEND	497.81	5.86	Late Miocene	III	clay/claystone
355-U1456D-7R-1-IW(84-94)-SCBEND	508.14	6.04	Late Miocene	III	clay/claystone
355-U1456D-8R-5-IW(140-150)-SCBEND	523.49	6.29	Late Miocene	III	clay/claystone
355-U1456D-10R-3-IW(135-145)-SCBEND	540.55	6.58	Late Miocene	III	clay/claystone
355-U1456D-14R-CC-WRND BEND	575.30	7.16	Late Miocene	III	clay/claystone
355-U1456D-15R-CC-WRND BEND	587.82	7.37	Late Miocene	III	clay/claystone
355-U1456D-17R-CC-WRND BEND	607.40	7.55	Late Miocene	III	clay/claystone
355-U1456D-21R-2-IW(115-130)-SCBE	645.75	7.79	Late Miocene	III	clay/claystone
355-U1456D-25R-2-IW(135-150)-SCBE	684.75	8.03	Late Miocene	III	clay/claystone
355-U1456D-26R-CC-WRND BEND	694.46	8.09	Late Miocene	III	clay/claystone
355-U1456D-29R-2-IW(128-143)-SCBE	723.18	8.27	Late Miocene	III	sand/sandstone
355-U1456D-30R-CC-BEND	739.59	9.28	Late Miocene	III	clay and carbonate ooze
355-U1456D-35R-4-IW(107-122)-SCBE	775.10	10.15	Late Miocene	III	clay/claystone
355-U1456E-19R-CC-WRND BEND	1104.42	13.53-17.71	Middle Miocene	IV	sand/sandstone

Supplementary Table 5.2: Organic geochemistry data

			Weight of identified *n*-alkanes, pristane and phytane (ng/gdw)																						
	Age (Ma)	**weight (g)**	**16**	**17**	**18**	**19**	**20**	**21**	**22**	**23**	**24**	**25**	**26**	**27**	**28**	**29**	**30**	**31**	**32**	**33**	**34**	**35**	**36**	**37**	**38**	**Pr**	**Ph**
355-U1456A-1H-2-IW(145-150)-SCBEND	0.03	17.11	14630	19264	57205	19332	28342	25231	22050	40321	28333	59778	57493	176254	56273	225299	61477	304658	32528	134941	5206	18220	-	-	-	4819	14158
355-U1456A-6H-5-IW(145-150)-SCBEND	0.46	21.24	-	2945	4189	2604	10403	3886	8385	12914	14598	33252	32828	88397	38731	104099	35239	75469	12116	1363	4838	-	-	-	-	-	1536
355-U1456A-13H-5-IW(145-150)-SCBEND	1.07	29.44	12428	15577	14537	26403	25760	56275	38271	56275	49028	150803	80914	332354	100451	434528	78962	540285	30025	257899	3949	29867	-	-	-	21306	28812
355-U1456A-40F-2-IW-SCBEND	1.41	27.12	-	2055	4092	9522	10918	23352	18638	45283	28746	88681	48453	216529	59577	301464	46499	409864	19507	181073	4403	23774	-	-	-	2185	3205
355-U1456A-58F-1-IW(89-99)-SCBEND	1.60	27.34	-	830	2897	7319	9814	42106	24981	66801	39784	114352	65052	266056	72377	382978	51988	411600	16524	109198	-	-	-	-	-	1912	3234
355-U1456A-65F-2-IW(140-150)-SCBEND	2.69	26.86	-	3110	10725	13332	7738	18814	26941	56408	32122	91362	48258	186260	57558	265240	48811	318384	28006	154202	6485	35466	-	-	-	1518	4901
355-U1456A-67F-2-IW(140-150)-SCBEND	2.78	31.29	-	1307	2756	6492	6235	15251	10347	29420	18139	60993	27738	122146	24551	134620	22500	177891	9961	67676	5256	6588	-	-	-	2352	3642
355-U1456A-72X-4-IW(140-150)-SCBEND	3.09	30.35	-	4089	9119	16300	19577	30460	29424	56580	49320	110142	79518	245092	86040	295187	53816	295520	17664	122081	3717	10139	-	-	-	3322	5569
355-U1456D-6R-CC-WRND BEND	5.86	31.81	-	1392	4563	10981	13221	19632	18515	35506	19606	60440	25002	110817	30926	179221	22970	157344	10192	60802	394	7338	-	-	-	2816	3138
355-U1456D-7R-1-IW(84-94)-SCBEND	6.04	30.05	-	-	2412	7159	11200	18534	16775	37216	20378	69389	24188	126424	32210	187228	29464	166455	14364	64772	2617	5547	-	-	-	-	2076

355-U1456E-19R-CC-WRND BEND	355-U1456D-35R-4-IW(107-122)-SCBEND	355-U1456D-30R-CC-BEND	355-U1456D-29R-2-IW(128-143)-SCBEND	355-U1456D-25R-2-IW(135-150)-SCBEND	355-U1456D-21R-2-IW(115-130)-SCBEND	355-U1456D-15R-CC-WRND BEND	355-U1456D-8R-5-IW(140-150)-SCBEND
13.53-	10.15	9.28	8.27	8.03	7.79	7.37	6.29
24.38	31.81	30.24	30.14	31.35	30.21	30.38	30.55
-	7479	2628		19980	-	7192	-
-	8313	2208	15836	112031	2686	8499	-
-	14415	4506	14835	117099	1789	15727	-
-	19728	2230	21322	137716	4422	9973	1422
-	13378	3563	23834	151110	6200	15922	2725
2776	20441	4627	28802	194552	9582	21776	6946
3565	13504	3661	24742	163803	8869	17471	7734
9270	39554	8845	38235	286277	15198	36237	20530
24176	21605	6436	25797	183173	10146	25511	19369
43753	49627	14416	51927	395300	24809	58905	63047
66873	28695	10486	26096	184799	11531	38023	49756
100182	73740	30083	61476	444226	33220	105914	209994
152493	31712	11550	24202	166722	11927	33237	76015
214481	130087	51989	98944	663029	57793	172491	402580
286816	32615	8749	22118	142345	11404	27984	61256
295331	165458	61990	107317	762909	68268	195695	498667
280081	14659	4423	16728	106217	6724	12030	31114
203823	53216	25158	57412	363059	28785	3954	206183
147836	-	918	3086	20074	-	-	6039
78792	-	3462	7742	56557	4299	5522	23062
44408	-	-	-	-	-	-	-
10377	-	-	-	-	-	-	-
2893	-	-	-	-	-	-	-
-	8844	774	14070	85332	-	4756	-
-	18635	967	7323	52566	1371	17890	-

Supplementary Table 5.3: Organic geochemistry data (continued)

	***n*-alkane and isoprenoids ratios**									**Mean values of compound specific values for various *n*-alkanoic acids**							
	Pr/Ph	**Pr/*n*-C_{17}**	**Ph/*n*-C_{18}**	**CPI (22-32)**	**TAR**	**OEP**	**Paq**	**ACL**	**1/Paq**	**δD (‰) C_{22}**	**δD (‰) C_{24}**	**δD (‰) C_{26}**	**δD (‰) C_{28}**	**$\delta^{13}C$ (‰) C_{22}**	**$\delta^{13}C$ (‰) C_{24}**	**$\delta^{13}C$ (‰) C_{26}**	**$\delta^{13}C$ (‰) C_{28}**
355-U1456A-1H-2-IW(145-150)-SCBEND	0.34	0.25	0.25	3.5	36.5	4.6	0.16	29.95	6.3	-	-	-	-	-23.8	-23.9	-24.1	-23.4
355-U1456A-6H-5-IW(145-150)-SCBEND	-	-	0.37	2.4	102.9	2.7	0.20	28.92	4.9	-	-	-	-	-	-	-	-
355-U1456A-13H-5-IW(145-150)-SCBEND	0.74	1.37	1.98	4.4	49.5	6.5	0.18	29.92	5.7	-	-104	-127	-	-23.7	-22.4	-24.0	-22.5
355-U1456A-40F-2-IW-SCBEND	0.68	1.06	0.78	5.2	97.4	7.9	0.16	30.00	6.3	-123	-123	-129	-	-23.0	-22.2	-22.9	-23.1
355-U1456A-58F-1-IW(89-99)-SCBEND	0.59	2.30	1.12	5.0	144.9	7.9	0.19	29.62	5.4	-123	-125	-125	-124	-21.6	-21.9	-22.7	-21.8
355-U1456A-65F-2-IW(140-150)-SCBEND	0.31	0.49	0.46	4.3	57.7	6.2	0.20	29.95	4.9	-	-	-	-	-	-	-	-
355-U1456A-67F-2-IW(140-150)-SCBEND	0.65	1.80	1.32	5.1	67.0	7.4	0.22	29.76	4.5	-	-109	-130	-130	-	-22.2	-23.1	-22.0
355-U1456A-72X-4-IW(140-150)-SCBEND	0.60	0.81	0.61	3.4	51.3	5.5	0.22	29.62	4.5	-	-	-	-	-24.4	-22.8	-23.9	-
355-U1456D-6R-CC-WRND BEND	0.90	2.02	0.69	4.8	40.7	7.5	0.22	29.66	4.5	-	-185	-188	-200	-23.4	-23.4	-23.7	-24.2

355-U1456D-7R-1-IW(84-94)-SCBEND	-	-	0.86	4.8	67.1	6.3	0.23	29.62	4.3	-	-	-191	-201	-33.2	-23.3	-24.0	-24.2
355-U1456D-8R-5-IW(140-150)-SCBEND	-	-	-	5.3	781.5	7.6	0.08	30.06	11.8	-	-	-	-	-24.9	-22.9	-22.5	-23.4
355-U1456D-15R-CC-WRND BEND	0.27	0.56	1.14	4.1	47.5	6.9	0.21	29.41	4.9	-	-	-	-	-26.1	-23.5	-23.5	-25.9
355-U1456D-21R-2-IW(115-130)-SCBEND	-		0.77	3.8	36.0	5.8	0.24	29.98	4.2	-	-203	-209	-209	-29.4	-28.1	-28.6	-29.8
355-U1456D-25R-2-IW(135-150)-SCBEND	1.62	0.76	0.45	3.1	13.6	5.1	0.32	29.94	3.1	-	-205	-208	-210	-26.3	-28.8	-29.6	-30.5
355-U1456D-29R-2-IW(128-143)-SCBEND	1.92	0.89	0.49	3.0	12.6	4.8	0.30	29.99	3.3	-205	-205	-205	-202	-29.7	-29.6	-29.8	-31.8
355-U1456D-30R-CC-BEND	0.80	0.35	0.21	4.1	64.6	6.7	0.17	29.97	5.9	-	-142	-129	-133	-29.1	-23.1	-24.0	-23.7
355-U1456D-35R-4-IW(107-122)-SCBEND	0.47	1.06	1.29	3.6	18.7	4.9	0.23	29.94	4.3	-155	-148	-149	-150	-23.8	-22.8	-23.2	-24.7
355-U1456E-19R-CC-WRND BEND	-	-	-	0.99	-	0.95	0.09	30.48	10.6	-	-	-	-	-	-	-	-

Supplementary Table 5.3: Organic geochemistry data (continued)

	TEX^{H}_{86}	BIT	CBT	pH	MBT	MAT	MBT/CBT	SST (TEX^{H}_{86})	$U^{K'}_{37}$	SST $(U^{K'}_{37})^1$	SST $(U^{K'}_{37})^2$
355-U1456A-1H-2-IW(145-150)-SCBEND	-0.15	0.12	0.3	8.0	0.5	15.4	1.69	28.5	0.97	28.12	27.61
355-U1456A-6H-5-IW(145-150)-SCBEND	-0.14	-	0.3	8.0	-	-	-	28.9	0.83	23.92	23.35
355-U1456A-13H-5-IW(145-150)-SCBEND	-0.16	0.14	0.3	8.0	0.4	10.3	1.25	27.5	0.98	28.53	28.03
355-U1456A-40F-2-IW-SCBEND	-0.14	0.10	0.2	8.1	0.3	7.1	1.30	28.9	0.99	28.61	28.11
355-U1456A-58F-1-IW(89-99)-SCBEND	-0.23	0.15	-0.1	8.9	0.2	4.2	-3.11	22.6	0.99	28.75	28.26
355-U1456A-65F-2-IW(140-150)-SCBEND	-0.17	0.51	0.3	8.0	0.6	18.7	1.82	-	0.96	27.79	27.28
355-U1456A-67F-2-IW(140-150)-SCBEND	-0.16	0.12	0.2	8.2	0.4	12.5	2.03	27.9	1.00	28.89	28.40
355-U1456A-72X-4-IW(140-150)-SCBEND	-0.13	0.10	0.3	8.0	0.4	12.3	1.54	29.7	0.98	28.50	28.00
355-U1456D-6R-CC-WRND BEND	-0.15	0.47	0.3	7.9	0.6	21.4	1.92	-	0.96	27.98	27.48
355-U1456D-7R-1-IW(84-94)-SCBEND	-0.14	0.51	0.4	7.7	0.7	23.4	1.69	-	0.98	28.55	28.06
355-U1456D-8R-5-IW(140-150)-SCBEND	-	-	-	-	-	-	-	-	-	-	-
355-U1456D-15R-CC-WRND BEND	-0.12	0.09	0.4	7.8	0.2	2.3	0.63	30.5	0.99	28.62	28.12
355-U1456D-21R-2-IW(115-130)-SCBEND	-0.12	0.65	0.3	7.8	0.6	20.9	1.73	-	0.95	27.51	26.99
355-U1456D-25R-2-IW(135-150)-SCBEND	-0.11	0.78	0.5	7.5	0.7	25.2	1.48	-	0.96	27.83	27.32
355-U1456D-29R-2-IW(128-143)-SCBEND	-0.11	0.80	0.3	8.0	0.6	22.7	2.06	-	0.87	25.14	24.59
355-U1456D-30R-CC-BEND	-0.11	0.18	0.5	7.5	0.5	13.1	1.02	31.4	0.99	28.64	28.14
355-U1456D-35R-4-IW(107-122)-SCBEND	-0.08	0.16	0.5	7.4	0.6	18.4	1.12	33.0	0.88	25.48	24.93
355-U1456E-19R-CC-WRND BEND	-	-	-	-	-	-	-	-	0.89	25.90	25.36

SST $(U^{K'}_{37})^1$ -sea surface temperature reconstruction after Sonzogni et al., 1997

SST $(U^{K'}_{37})^2$ -sea surface temperature reconstruction after Conte et al., 2006

Supplementary Table 5.4: Bulk sediment geochemistry data

	Age (Ma)	TOC (wt%)	TN (wt%)	TOC/TN	$\delta^{15}N$ (‰)	$\delta^{13}C$ (‰)
355-U1456A-1H-2-IW(145-150)-SCBEND	0.03	1.08	0.09	11.4	0.12	-19.3
355-U1456A-6H-5-IW(145-150)-SCBEND	0.46	0.11	0.02	6.5	-	-22.6
355-U1456A-13H-5-IW(145-150)-SCBEND	1.07	1.71	0.12	14.7	0.14	-19.1
355-U1456A-40F-2-IW-SCBEND	1.41	0.74	0.10	7.4	0.10	-18.8
355-U1456A-58F-1-IW(89-99)-SCBEND	1.60	1.00	0.13	7.4	0.15	-20.4
355-U1456A-65F-2-IW(140-150)-SCBEND	2.69	0.37	0.06	6.3	0.51	-20.6
355-U1456A-67F-2-IW(140-150)-SCBEND	2.78	1.10	0.10	10.9	0.12	-18.2
355-U1456A-72X-4-IW(140-150)-SCBEND	3.09	0.27	0.07	3.9	0.10	-20.3
355-U1456D-6R-CC-WRND BEND	5.86	0.31	0.05	6.8	0.47	-21.2
355-U1456D-7R-1-IW(84-94)-SCBEND	6.04	0.27	0.04	6.2	0.51	-20.3
355-U1456D-8R-5-IW(140-150)-SCBEND	-	0.20	0.06	3.5	-	-20.9
355-U1456D-15R-CC-WRND BEND	7.37	0.57	0.06	9.9	0.09	-19.8
355-U1456D-21R-2-IW(115-130)-SCBEND	7.79	0.37	0.05	7.1	0.65	-23.0
355-U1456D-25R-2-IW(135-150)-SCBEND	8.03	0.27	0.05	5.0	0.78	-24.5
355-U1456D-29R-2-IW(128-143)-SCBEND	8.27	0.31	0.06	5.0	0.80	-23.3
355-U1456D-30R-CC-BEND	9.28	0.33	0.08	3.9	0.18	-21.3
355-U1456D-35R-4-IW(107-122)-SCBEND	10.15	0.65	0.12	5.7	0.16	-21.3
355-U1456E-19R-CC-WRND BEND	13.53-17.71	0.08	0.02	4.7	3.1	-22.9

TOC - total organic carbon; TN - total nitrogen

Supplementary Table 5.5: Bulk heavy minerals data

3.09	2.69	1.26	1.15	0.46	0.03	0.00	**Age (Ma)**	**Heavy minerals indices**
12	1	1	5	4	3	7	**HMC**	
2.76	2.65	2.65	2.68	2.68	2.67	2.70	**SRD**	
5.5	0.5	1.3	5.0	4.2	2.3	5.1	**tHMC**	
1	0	0	1	0	0	0	**zircon**	
2	2	1	1	1	1	2	**Tourmali**	
0	1	0	0	0	0	1	**rutile**	
1	1	3	4	0	0	0	**apatite**	**Heavy minerals total counts**
2	2	3	3	2	2	2	**titanite**	
1	0	0	0	0	0	0	**others**	
28	21	20	25	23	21	25	**epidote**	
5	1	2	7	2	2	12	**garnet**	
1	2	3	2	2	0	0	**chloritoid**	
0	0	1	0	0	0	1	**staurolite**	
0	0	0	0	0	0	0	**Andalusit**	
0	0	1	1	0	0	1	**kyanite**	
0	0	1	4	0	0	1	**sillimanite**	
51	68	67	50	62	25	50	**amphibole**	
10	0	2	3	5	47	3	**Clinopyro**	
0	0	0	0	1	0	1	**hypersthe**	
2	0	0	0	0	0	0	**spinel**	
100	100	100	100	100	100	100	**Total**	
26%	8%	11%	66%	55%	53%	-		**Percentage of total counts in the heavy mineral fraction**
19%	1%	0%	2%	1%	6%	-	**opaque**	
9%	1%	0%	0%	1%	1%	-	**Fe oxide**	
2%	0%	0%	1%	2%	2%	-	**Ti oxide**	
0%	4%	0%	0%	0%	0%	-		
0%	1%	0%	1%	0%	0%	-	**RF**	
1%	0%	0%	0%	0%	1%	-	**soils &**	
20%	26%	11%	7%	10%	5%	-	**chlorite**	
17%	51%	78%	22%	29%	13%	-	**biotite**	
5%	3%	0%	1%	2%	17%	-		
3%	4%	0%	1%	1%	2%	-	**light**	
100%	100%	100%	100%	100%	100%	-	**Total**	
0.034	0.526	1.200	5.532	3.430	1.585	-	**Initial**	
0.020	0.409	1.008	5.068	3.104	1.419	-	**Light**	
0.007	0.034	0.133	0.421	0.266	0.069	-	**Dense**	

8.09	7.79	7.16	**Age (Ma)**	5.86
5	2	3	**HMC**	3
2.69	2.66	2.66	**SRD**	2.67
4.8	1.6	2.4	**tHMC**	2.0
0	0	0	**zircon**	0
0	0	0	**Tourmali**	1
0	0	0	**rutile**	1
1	1	0	**apatite**	1
2	1	2	**titanite**	3
0	0	1	**others**	0
39	30	32	**epidote**	28
5	1	1	**garnet**	6
0	3	1	**chloritoid**	0
1	0	0	**staurolite**	1
1	0	0	**Andalusit**	0
0	0	0	**kyanite**	0
0	0	0	**sillimanite**	0
49	60	60	**amphibole**	50
1	3	1	**clinopyro**	5
0	0	0	**hypersthe**	0
0	0	0	**spinel**	0
100	100	100	**Total**	100
77%	33%	38%	**transpare**	43%
4%	1%	2%	**opaque**	5%
0%	1%	2%	**Fe oxide**	2%
3%	2%	1%	**Ti oxide**	0%
0%	0%	0%	**weathered**	8%
5%	1%	1%	**RF**	7%
1%	0%	1%	**soils &**	0%
3%	21%	16%	**chlorite**	8%
5%	36%	37%	**biotite**	18%
1%	3%	2%	**carbonate**	2%
1%	2%	2%	**light**	7%
100%	100%	100%	**Total**	100%
1.228	1.510	0.929	**Initial**	0.047
1.121	1.378	0.830	**Light**	0.026
0.076	0.076	0.057	**Dense**	0.002

HM = heavy mineral; HMC = total heavy minerals index; SRD = Source Rock Density index; tHMC = transparent heavy minerals index; RF = rock fragments;

Supplementary Table 5.6: Bulk isotope analyses

Sample Number	Age (Ma)	Depth (mbsf)	$^{87}Sr/^{86}Sr$	$^{143}Nd/^{144}Nd$
355-U1456A-1H-2-IW(145-150)-SCBEND	0.03	3.0	0.71878	0.51205
355-U1456A-6H-5-IW(145-150)-SCBEND	0.46	50.0	0.72649	0.51195
355-U1456A-15H-5-IW(129-134)-SCBEND	1.15	134.1	0.72918	0.51193
355-U1456A-25F-3-IW(145-150)-SCBEND	1.26	180.6	0.72154	0.51203
355-U1456A-58F-1-IW(89-99)-SCBEND	1.60	329.3	0.71689	0.51219
355-U1456A-63F-1-IW(140-150)-SCBEND	2.57	353.4	0.72988	0.51198
355-U1456A-72X-4-IW(140-150)-SCBEND	3.09	403.8	0.71764	0.51216
355-U1456C-45X-2-IW(111-121)-SCBEND	3.65	458.5	0.72550	0.51203
355-U1456D-3R-CC-WRND BEND	5.40	470.2	0.72461	0.51205
355-U1456D-6R-CC-WRND BEND	5.86	497.8	0.72290	0.51205
355-U1456D-10R-3-IW(135-145)-SCBEND	6.58	540.6	0.71529	0.51224
355-U1456D-14R-CC-WRND BEND	7.16	575.3	0.71619	0.51211
355-U1456D-17R-CC-WRND BEND	7.55	607.4	0.71689	0.51216
355-U1456D-21R-2-IW(115-130)-SCBEND	7.79	645.8	0.71587	0.51214
355-U1456D-26R-CC-WRND BEND	8.09	694.5	0.71629	0.51213
355-U1456D-29R-2-IW(128-143)-SCBEND	8.27	723.3	0.71664	0.51211
355-U1456D-30R-CC-BEND	9.28	739.6	0.71717	0.51227
355-U1456D-35R-4-IW(107-122)-SCBEND	10.15	784.5	0.71855	0.51219
355-U1456E-19R-CC-WRND BEND	13.53-17.71	1104.4	0.72551	0.51219

Supplementary Table 5.7: Sterane and hopane data

Sample number	Age (Ma)	C_{27} ααα*R* %	C_{28} ααα*R* %	C_{29} ααα*R* %	Ternary group*	Oleanane/C_{30} αβ hopane	C_{30} sterane index	Ts/(Ts+Tm)	C_{31} αβ 22S/(22S+22R)	C_{29} ααα 20S/(20S+20R)
355-U1456A-1H-2-IW(145-150)-SCBEND	0.03	44.65	8.78	46.57	II	0.09	0.09	0.17	0.45	0.36
355-U1456A-6H-5-IW(145-150)-SCBEND	0.46	-	-	-	-	-	-	0.19	0.38	-
355-U1456A-13H-5-IW(145-150)-SCBEND	1.07	-	-	-	VI	0.24	-	0.17	0.27	-
355-U1456A-40F-2-IW-SCBEND	1.41	54.21	21.12	24.67	II	0.02	-	0.14	0.19	0.12
355-U1456A-58F-1-IW(89-99)-SCBEND	1.60	20.47	18.75	60.78	IV	-	0.20	0.11	0.10	-
355-U1456A-65F-2-IW(140-150)-SCBEND	2.69	27.38	21.05	51.56	III	0.07	0.11	0.14	0.16	0.21
355-U1456A-67F-2-IW(140-150)-SCBEND	2.78	-	-	-	-	0.09	-	0.17	0.29	-
355-U1456A-72X-4-IW(140-150)-SCBEND	3.09	32.12	28.28	39.60	III	-	0.28	0.25	0.25	0.08
355-U1456D-6R-CC-WRND BEND	5.86	29.28	31.19	39.53	III	0.09	0.16	0.14	0.14	-
355-U1456D-7R-1-IW(84-94)-SCBEND	6.04	26.18	23.17	50.65	III	0.15	0.17	0.15	0.16	0.16
355-U1456D-8R-5-IW(140-150)-SCBEND	6.29	17.82	19.77	62.40	IV	-	0.07	0.21	0.31	0.28
355-U1456D-15R-CC-WRND BEND	7.37	49.30	-	50.70	II	0.03	-	0.18	0.18	-
355-U1456D-21R-2-IW(115-130)-SCBEND	7.79	18.56	49.10	32.34	IV	0.10	0.13	0.15	0.56	0.61
355-U1456D-25R-2-IW(135-150)-SCBEND	8.03	-	-	-	-	-	-	-	-	-
355-U1456D-29R-2-IW(128-143)-SCBEND	8.27	33.86	33.74	32.40	II	0.17	0.12	0.17	0.55	0.48
355-U1456D-30R-CC-BEND	9.28	30.48	20.57	48.95	III	0.03	0.20	0.20	0.26	0.34
355-U1456D-35R-4-IW(107-122)-SCBEND	10.15	26.01	26.18	47.81	III	0.07	-	0.42	0.28	0.24
355-U1456E-19R-CC-WRND BEND	13.53-17.71	-	33.33	66.67	IV	0.04	-	0.54	0.57	0.17

5.9. Supplementary 2: Site U1456 Lithology and biostratigraphy

The cored section at Site U1456 (Pandey et al., 2016) is divided into four lithological units based on a compilation of Holes U1456A through U1456E (Fig. 5.7). The age model for the Site U1456 is based on subtropical to tropical assemblages of calcareous and siliceous nannofossils and foraminifera, together with magnetostratigraphy. The recovered sediment was dated back to the late to middle Miocene, and is punctuated by two hiatuses between ~8 and 9 Ma, and a ~2 million year gap encompassing the Miocene/Pliocene boundary.

Lithological Unit I consists of a ~121 m thick sequence of Pleistocene light brown to light greenish nannofossil ooze and foraminifer-rich nannofossil ooze interbedded with clay, silt, and sand. The sandy layers are considered to be distal basin plain turbidites with sharp, erosive bases. Low abundances of heavy minerals such as hornblende, kyanite, tourmaline, augitic clinopyroxene, apatite, and glauconite are present throughout Unit I.

Lithological Unit II is ~240 m thick and is dated to the late Pliocene to early Pleistocene. The unit consists mainly of massive dark greyish to blackish sand and silt, suggested by sharp erosive bases to be turbidites interbedded with thinly-bedded nannofossil-rich clay. Heavy minerals, similar to those in Unit I, are in high abundance in Unit II. The presence of diagnostic high-pressure sodic amphiboles (glaucophane) and pink-green hypersthene is distinctive of Unit II, and are indicative of erosion from the Indus Suture Zone.

Lithological Unit III is ~370 m thick and is dated to the late Miocene to late Pliocene. It mainly consists of semi-indurated to indurated light brown to dark green clay/claystone, light brown to dark grey sand/sandstone, light greenish nannofossil chalk, and light to dark greenish grey nannofossil-rich claystone. Clay/claystone and sand/sandstone cycles of sedimentation are separated by intervals dominated by nannofossil chalk and nannofossil-rich claystone. The mineral assemblage of the silt fraction observed under the microscope is similar to that of Unit II, and is typical of the Greater Himalaya erosional fingerprint (Garzanti et al., 2005).

Lithological Unit IV is ~380 m thick and consists of a mixture of interbedded lithologies dominated by dark grey massive claystone, light greenish massive calcarenite and calcilutite, and conglomerate/breccia, with minor amounts of limestone, especially toward the base of the unit. Unit IV appears to have been rapidly deposited during the late Miocene, based on the presence of nannofossils within two short hemipelagic intervals within the transported unit.

The bottom of Unit IV is dated to extend into the middle Miocene (between 13.53 and 17.71 Ma) based on the nannofossil assemblages.

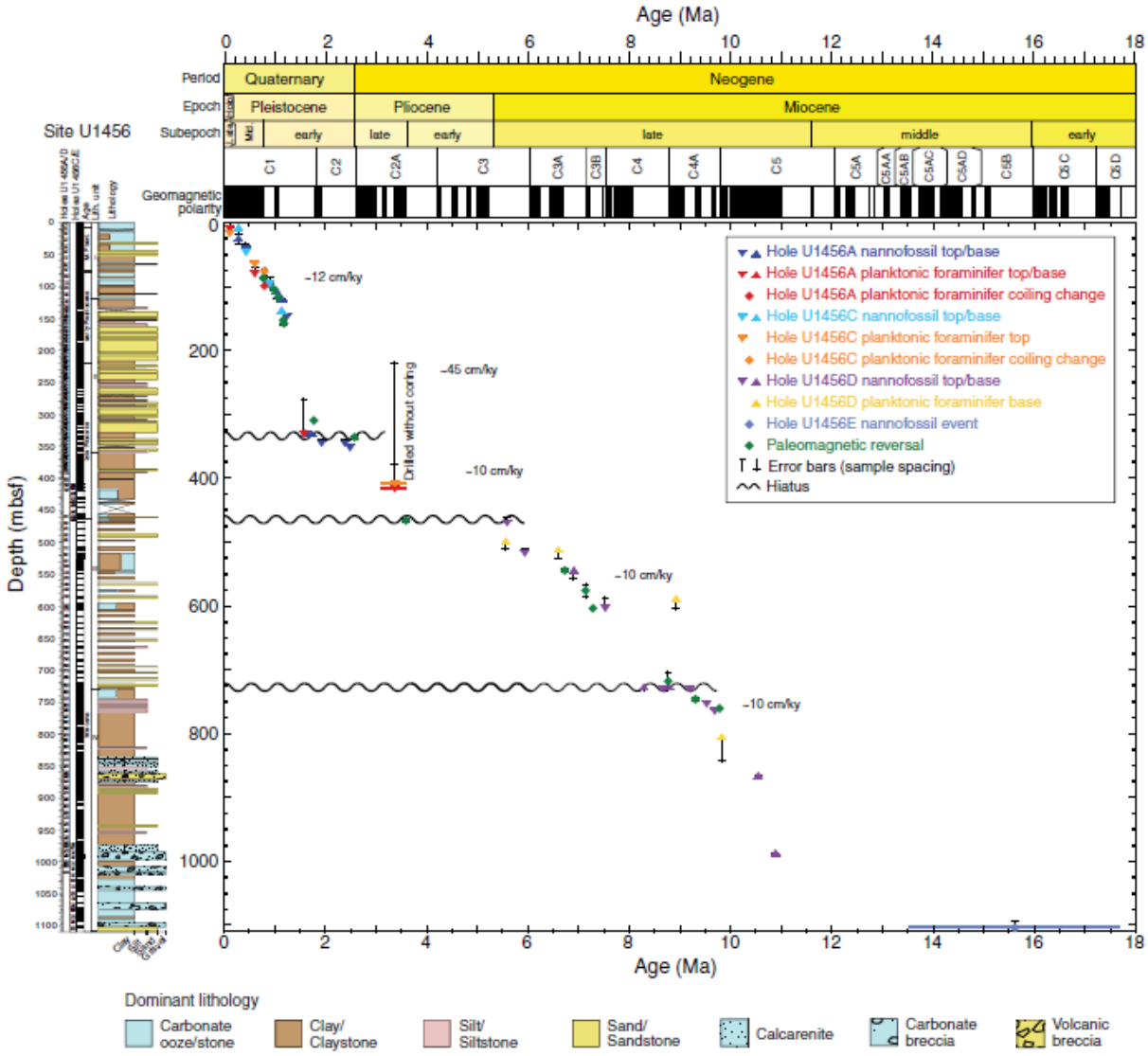

Figure 5.7: Depth-age plot for the U1356 Site (Pandey et al., 2016).

6. Summary

Below is a summary of the biogeochemical analysis from the three IODP Expeditions discussed in this thesis. The analysed sediments are from:

1. IODP Expedition 317, Canterbury Basin, New Zealand, southern Pacific Ocean, represented by Sites U1351, U1352, and U1353.

2. IODP Expedition 313, from the New Jersey continental margin of the northern Atlantic Ocean, represented by Sites M0027A and M0028A.

3. IODP Expedition 355, Arabian Sea Monsoon, the northern Indian Ocean, represented by Site U1456.

6.1. Total organic carbon (TOC), total nitrogen (TN) and the source of organic matter (OM)

The TOC consists of material derived from the shore (terrigenous OM) and from the ocean (marine OM). Global estimated calculations suggest that about $180x10^{12}$ g TOC/year arrives to the marine environment by rivers (Meybeck, 1982). Organic carbon levels generally decrease with distance from the shore (Prahl et al., 1994). Bioturbation is a strong influence on organic carbon in the continental shelf areas. Bioturbation increases closer to the shore because of the higher TOC levels (Prahl et al., 1994; Dickens et al., 2004). Moreover, the way that organic carbon is transported into the depositional environment and distributed throughout the sediment can significantly alter the signal (Berner, 1990; Hedges and Keil, 1995). Therefore, bulk sediment TOC and TOC/TN values should be used with some caution (Meyers, 2003; Blair and Aller, 2012).

In the Canterbury Basin, the TOC data from the Miocene samples from the U1351 Site contain predominantly terrigenous or degraded marine organic matter, and dominantly contain Type IV organic matter (no oil or gas-generative potential), typical of poorly

preserved terrigenous organic matter. The limestones from the U1352 Site contain the highest amounts of carbonate and the lowest TN at the U1352 Site. Low hydrogen indices show that the organic matter is largely terrigenous or degraded marine in origin (Fulthorpe et al., 2011). This finding contrasts with the deeper Pukeiwitahi Formation coals (Sykes, 2004), which have higher hydrogen indices. Samples from the U1353 Site have low OM contents, representing active biological oxidation that correlates with intervals of increased alkalinity and decreased sulphate (Fulthorpe et al., 2011). Pyrolysis results suggest a largely terrigenous plant origin for the organic matter, but TOC/TN values suggest some marine influence.

On the New Jersey continental margin the M0027 Site is closer to the shoreline than the Canterbury Basin sites, and has samples with very high TOC levels. The samples from the beginning of the middle Miocene have high organic carbon contents that possibly indicate low global sea levels (Prahl and Coble, 1994). The M0028 Site samples have much lower TOC levels which fluctuate during the 18.88–14.78 Ma period, possibly indicating a temporal change in the proximity of the shoreline to the site, and a decrease in the global sea level.

The northern Indian Ocean samples from the U1456 Site have low TOC values. Three samples from the Pliocene and Pleistocene (2.78, 1.07, and 0.03 Ma) are characterised by a TOC/TN ratio greater than 12, reflecting relative increases in terrigenous input. The bulk $\delta^{15}N$ data can be divided into two periods: 10.15–5.86 Ma ago with 4.0 to 6.4‰, and 3.09–0.03 Ma ago with 5.5–8.2‰, respectively. The more positive $\delta^{15}N$ values indicate enhanced denitrification from the Pliocene onwards (Tesdal et al., 2013). Low $\delta^{15}N$ values around 8 Ma suggest mixing of marine OM with a strong terrigenous source input (Knapp et al., 2010). The $\delta^{13}C$ bulk values vary between -18.2‰ and -24.5‰, with the ~8 Ma interval having the lightest values, consistent with a significant increase in terrigenous organic matter input (Farquhar et al., 1989).

6.2. *n*-Alkane distributions, BIT index and the source of OM

The *n*-alkane distribution of a sediment is indicative of the organic matter source (Eglinton and Hamilton, 1967; Barnes and Barnes, 1978; Cranwell, 1984). The relative fluvial input of terrigenous OM can be calculated using the BIT index. High BIT indices can be attributed to lacustrine or terrigenous sediments, whereas low BIT indices are seen in coastal areas with low terrigenous sediment fluxes and in deeper marine sediments with low terrigenous input (Hopmans et al., 2004). Although the BIT index cannot be used as a quantitative measure of the terrigenous input into marine sediments, it was suggested that values >0.8 correspond to strong fluvial flux into the marine environment, while values <0.2 were attributed predominantly to marine OM input. High terrigenous OM input can also influence the relative abundance of iGDGTs and trigger an error in the SST estimation when the BIT index values are >0.5 (Schouten et al., 2004).

The late Miocene samples from the U1351 Site have unimodal *n*-alkane distributions with high amounts of C_{29} and C_{31} *n*-alkanes, indicative of land-plant epicuticular waxes (Eglinton and Hamilton, 1967; Barnes and Barnes, 1978; Cranwell, 1984). The $CPI_{(22\text{-}32)}$ values are >1 in most samples and support a dominant terrigenous OM input (Peters et al., 2005). The TAR for the late Miocene samples are >10, suggesting terrigenous OM input (Bourbonniere and Meyers, 1996). Based on the high level of biotурbation of the sediments, partial biodegradation of the OM is inferred (Bourbonniere and Meyers, 1996; Meyers, 1997). The $1/P_{aq}$ ratios of the samples show a mix of aquatic and terrigenous environments as the main vegetation source (Ficken et al., 2000).

The BIT index for the Site U1351 samples varies significantly between 0.31 and 0.74 (Fig. 3.5), with an inferred increase in terrigenous OM input from 6.52 to 5.84 Ma. High terrigenous OM input in this interval was also recorded by the $CPI_{(22\text{-}32)}$ index and TAR ratio. At 5.74 Ma the BIT index drops to 0.31, indicating a significant decrease in terrigenous input, followed by a gradual increase in the BIT index to 0.45 at 5.30 Ma.

However, two Pliocene samples (3.56 and 3.24 Ma) have BIT indices of 0.42 and 0.44, respectively, indicating strong terrigenous sediment flux towards the continental slope region. The Pleistocene samples (younger than 2.98 Ma) show high variation in the BIT index between 0.13 and 0.51, with four samples (at 0.235, 0.082, 0.028, and 0.013 Ma) having recorded values >0.4.

The early Oligocene samples from the U1352 Site have a strong predominance of even-to-odd *n*-alkanes with a $CPI_{(22\text{-}32)}$ <1. The Eocene-Oligocene samples from the U1352 Site are mainly characterised by BIT indices <0.4, with just one sample at 31.02 Ma with a value of 0.46. This type of distribution is indicative of marine OM input dominated by diatoms and phytoplankton (Albaigés et al., 1984; Saliot et al., 1998). Low TAR and $1/P_{aq}$ ratios suggest a strong algal and phytoplankton input with low terrigenous vegetation input (Fig. 2.4). Some earlier studies suggested that bacterial input from river sediments could produce similar *n*-alkane distributions (Nishimura and Baker, 1986; Grimalt and Albaigés, 1987). Even-to-odd predominance in high *n*-alkanes (>C_{24}) can also be associated with early diagenetic alteration of *n*-alkonols originated in terrigenous plants (Simoneit, 1977).

A very similar distribution of *n*-alkanes was recorded in Early Miocene U1352 Site samples, with very low $CPI_{(22\text{-}32)}$ from ~19 and 17 Ma, indicative of strong marine OM input, followed by an increase in long chain *n*-alkane abundance with a high $CPI_{(22\text{-}32)}$. The increase in long chain *n*-alkane abundance parallel to the high $CPI_{(22\text{-}32)}$ is indicative of terrigenous OM input (Eglinton and Hamilton, 1967) during the second part of the early Miocene. Low TAR and $1/P_{aq}$ values to ~16 Ma suggest high marine OM input with low terrigenous OM input, similar to the early Oligocene period. Most of the early Miocene samples from the U1352 Site also have very low BIT indices in the range, indicating very low terrigenous and high marine OM input during this period.

The middle Miocene *n*-alkanes in the U1352 Site samples have a bimodal distribution, similar to the U1353 Site samples. High levels of C_{16} and C_{18} *n*-alkanes can be derived from input of zooplankton (Saliot, 1981) and algae (Youngblood and Blumer, 1973). The C_{15} and C_{17} *n*-alkanes originate from algal/planktonic origins as well (Cranwell, 1984; Meyers and Ishiwatari, 1993b). The middle Miocene samples have a low BIT index, indicating mainly marine OM input. The middle Miocene samples have a higher $CPI_{(22\text{-}32)}$ than the older samples, indicating an increase in terrigenous OM input. The decrease of $CPI_{(22\text{-}32)}$ around 12 Ma suggests a decrease in terrigenous OM input. The TAR and $1/P_{aq}$ indices show marine OM input during the same time, with a significant increase in terrigenous OM input around 15 Ma.

The late Miocene U1352 Site samples are interpreted to contain more marine OM input, with high C_{14}, C_{16}, and C_{18} n-alkanes for several samples. This observation is supported by low BIT indices between 0.03 and 0.16. Only two samples at 8.74 and 8.39 Ma have higher (0.32 and 0.19), indicating small increase in terrigenous OM input. A significant increase in terrigenous OM between 6.5 Ma and 5.4 Ma is observed through an increase in $CPI_{(22\text{-}32)}$. The TAR and $1/P_{aq}$ for the late Miocene samples is also higher than in the middle Miocene, suggesting an increase in terrigenous OM input up to ~6 Ma. TAR data suggests at least three strong terrigenous OM input events at 10.8 Ma, 8Ma, and 6 Ma, respectively.

The early Pliocene U1352 Site samples have C_{16}, C_{18}, and C_{20} *n*-alkane dominance, interpreted to be due to strong zooplankton (Saliot, 1981) and algal (Youngblood and Blumer, 1973) inputs. A similar distribution of even *n*-alkanes in the range C_{12}-C_{20} has been reported in some coastal sediments (Nishimura and Baker, 1986; Mille et al., 2007) and was attributed to possible bacterial input. The $CPI_{(22\text{-}32)}$ values during the Early Pliocene are around 1, suggest a mixed source input (Bray and Evans, 1961). The Pliocene samples (4.45–2.98 Ma) mostly have BIT indices from 0.12–0.35, indicate some minor increase in terrigenous OM input compared to the Miocene.

The Site U1353 middle Miocene samples have a bimodal *n*-alkane distribution with high levels of C_{16}, C_{18}, and C_{20} *n*-alkanes, which as for the early Pliocene U1352 Site samples suggests zooplankton and algae inputs. The C_{27}, C_{29}, and C_{31} *n*-alkanes, which are indicative of land-plant epicuticular wax input to the sediments (Eglinton and Hamilton, 1967; Barnes and Barnes, 1978), are not abundant in these samples. The BIT indices for the Site U1353 samples are all >0.5, indicating high terrigenous OM input into the system. Higher BIT indices for this site are to be expected due to its closer location to the shoreline compared to the other Canterbury Basin sites.

The late Oligocene samples from the M0027A Site have a high $CPI_{(22\text{-}32)}$ and a high TAR ratio that indicate high terrigenous OM input. Both ratios decrease significantly at the beginning of Aquitanian Stage, indicating an increase in marine OM input. Another rapid decrease in $CPI_{(22\text{-}32)}$ is recorded for the 17.90 Ma sample, indicative of a very strong marine OM input. Although the TAR ratio for the same sample shows an increase in terrigenous OM input, this ratio might be over representing the absolute amount of the terrigenous sources, as a result of the much higher *n*-alkane production by land plants (Cranwell et al., 1987; Meyers and Ishiwatari, 1993a). Very low TAR values were recorded for the 22.28 Ma and 18.75 Ma samples, indicating low terrigenous OM input during the Aquitanian Stage. The second part of the Burdigalian and the beginning of the middle Miocene samples have a high $CPI_{(22\text{-}32)}$ and TAR ratio indicating high terrigenous OM input.

The Aquitanian Stage in the M0028A Site has high $CPI_{(22\text{-}32)}$ and TAR values with some variation between the samples, overall indicating high terrigenous OM input. The Burdigalian Stage is characterised by $CPI_{(22\text{-}32)}$ >1.9, indicating high terrigenous OM input. The TAR ratio show some terrigenous OM input decrease until 18.61 Ma, following by an increase in the terrigenous OM input until 18.05 Ma. The short term increase in marine OM input around 17.83 Ma is followed by an increase in TAR ratio through the last part of Burdigalian Stage

and the middle Miocene samples. The increase in marine OM input at 18.61 and 17.83 Ma was recorded in both data sets.

The M0027A and M0028A New Jersey Sites have BIT indices between 0.2 and 0.8 with only one sample <0.2. These sites are located on the continental shelf and thus have a high influence from terrigenous sediment flux.

The *n*-alkanes from the U1456 Site have a unimodal distribution pattern dominated by a high molecular weight *n*-alkanes, achieving a maximum at C_{31}, suggesting a high terrigenous OM input (Bray and Evans, 1961). This is supported by a high $CPI_{(22\text{-}32)}$ (Bray and Evans, 1961) (>3) and TAR (Bourbonniere and Meyers, 1996) (>30) values for most samples. There is an increase in $CPI_{(22\text{-}32)}$ and TAR during the 8 to 6 Ma period, suggesting an increase in terrigenous OM input. The BIT index for the U1456 Site samples is mostly ≤0.2, indicative of mainly marine OM input. Two late Miocene time intervals (8.27–7.79 Ma and 6.04–5.86 Ma) and a Pliocene sample (2.69 Ma) have BIT indices ≥0.5, suggesting high terrigenous sediment input. The $ACL_{(27\text{-}33)}$ varies between 28.9 and 30.1. The data suggest that the input of terrigenous OM is dominated by vegetation from warm regions during the last 10 Ma. Samples around 7.4 and 0.5 Ma show high input of terrigenous OM, dominated by vegetation from cooler climate. High precipitation levels in the period from ~2.6 to ~1.6 Ma are also clearly recorded by increasing terrigenous OM inputs, based on *n*-alkanes, steranes, and the BIT index. A eustatic fall in sea level may have increased terrigenous matter input into the basin. Nonetheless, variations in climate between the glacial-interglacial cycles are well-recognized as factors intensifying continental erosion and would also help increase terrigenous flux after ~3 Ma ago.

6.3. Pristane/Phytane (Pr/Ph) and oxicity of the depositional environment

To assess the relative abundance of pristane (2,6,10,14-tetramethylpentadecane; Pr) and phytane (2,6,10,14-tetramethylhexadecane; Ph) in marine sediments, the Pr/Ph, Pr/nC$_{17}$ and Ph/nC$_{18}$ ratios are used. These ratios are indicative of the oxicity of the depositional environment, and also provide information on thermal maturity and biodegradation of the samples (Volkman and Maxwell, 1986). The main source of Pr and Ph is the phytyl side chain of chlorophyll in phototrophic organisms and bacteriophyll from purple sulphur bacteria (Powell and McKirdy, 1973). Some marine organisms, including the calanoid copepods, are also considered as one of the biological sources (Blumer et al., 1964). In addition, Pr could be derived from anaerobic bacterial degradation (Rontani et al., 2010), thermal degradation (Lao et al., 1989) and clay catalysed degradation of the chlorophyll phytyl chain (Lao et al., 1989; Rontani et al., 2010). Ph can be produced through anaerobic biodegradation (Grossi et al., 1998) and clay catalysed thermal hydrogenation of the isoprenoid alkenes (Gelin et al., 1995), as well as by the thermal maturation of methanogenic bacteria (Rowland, 1990). In general, a Pr/Ph ratio <0.8 indicates an anoxic depositional environment, and a ratio higher than 3 indicates terrigenous organic matter input deposited under oxic conditions (Peters et al., 2005). The Pr/n-C$_{17}$ and Ph/n-C$_{18}$ ratios are used to characterise the biodegradation levels and thermal maturity of sediments (Peters and Moldowan, 1993). These ratios increase with an increasing biodegradation and thermal maturity of the sediments (Tissot et al., 1971).

Samples from the U1351 Site have Pr/Ph ratios that suggest an increase in oxicity of depositional environment (Fig. 2.4). The results are consistent with CPI$_{(22\text{-}32)}$, TAR and 1/P$_{aq}$ values that show increase of the terrigenous OM input with time.

Early Oligocene samples from the U1352 Site do not show any consistent pattern of the Pr/Ph ratio, with the depositional environment being interpreted as sub-oxic to oxic. The early Miocene samples show an increasing oxicity pattern which continues into the middle Miocene. This pattern is consistent with CPI$_{(22\text{-}32)}$, 1/P$_{aq}$, and TOC/TN results, and suggests a

gradual increase of terrigenous OM input during the recorded period. The changes in accumulation of OM during the early Oligocene and early Miocene can be attributed to the global sea level fluctuations of up to 30 meters (Van Sickel et al., 2004). The reconstructed tectonic activity of New Zealand for the same periods doesn't suggest any major activity in the area (Winkworth et al., 2002).

The middle Miocene samples from the U1352 Site have Pr/Ph ratios that indicate a suboxic depositional environment, except for the 15–12 Ma period where a strong oxic pattern is present. Samples with high Pr/Ph values also have a high TOC/TN (above 20), indicative of a high terrigenous OM input. From 11 Ma, the Pr/Ph ratios decrease, indicating a change towards sub-oxic conditions. This observation is supported by an increase of TAR, $CPI_{(22\text{-}32)}$, $1/P_{aq}$, and TOC/TN values. The fluctuations in oxicity of the depositional environment are consistent with global sea levels fluctuations during the middle Miocene (Van Sickel et al., 2004). Increasing terrigenous input from 14–12 Ma, together with high sedimentation rates at the same time, can be attributed to a significant land mass build-up in the South Island of New Zealand, related to an increase in convergence rates from ~20 Ma (Lu et al., 2005). The slow uplift of the western part of the South Island and the concomitant increase in the topographic gradient in the Canterbury Basin created an sub-oxic environment in the continental margin area and increased fast sedimentary input to the continental slope area. The middle Miocene increase in oxicity of the depositional environment recorded in the U1352 Site samples is correlating with the Haq et al. (1987) and Abreau et al. (1998) global sea level decrease during the same period, but are different to those proposed by Van Sickel et al. (2004). This variations in the oxicity could be influenced more by the local tectonic activity and uplift of the New Zealand South Island, rather than global climate change events.

The Pr/Ph ratios of the Site U1353 samples suggest an anoxic depositional environment, consistent with the low $CPI_{(22\text{-}32)}$ index and suggestive of high marine OM deposition. The results are also consistent with the TOC/TN and $1/P_{aq}$ interpretations. However, it is not

consistent with the TAR ratio, suggesting a relatively high terrigenous OM input. The fluctuations in oxicity of the depositional environment in New Zealand are consistent with global sea levels fluctuations during the middle Miocene (Van Sickel et al., 2004).

Most M0027A Site samples have Pr/Ph ratios close to or below 0.8, indicative of an anoxic depositional environment for the OM. One late Oligocene sample (23.11 Ma) has a Pr/Ph ratio of 1.46, suggesting a suboxic depositional environment, whilst another sample (18.05 Ma) has a Pr/Ph ratio of 5.2, indicating an oxic depositional environment. These data are consistent with TOC variations for this site that indicate a low sea level during this period. In contrast, the M0028A Site samples show a different depositional environment picture. While all three Aquitanian Stage samples are interpreted to have been deposited in an anoxic environment based on Pr/Ph, similar to the Site M0027A record, the 19.47 Ma sample from the M0028A Site has a Pr/Ph ratio of 15.6 and was thus deposited in a very oxic depositional environment. The samples from the second part of the Burdigalian Stage from the M0028A Site are interpreted to have been deposited a suboxic environment, with the exception of an oxic spike at 18.05 Ma, at a very similar time as when the Site M0027A samples show an oxic depositional environment. The middle Miocene period at the M0028A Site is characterised by indicators of an anoxic depositional environment, with only one sample at 14.34 Ma with Pr/Ph ratio value of 2.6.

These New Jersey samples show a correlation between global sea level fluctuations and the oxicity of the depositional environment. The 18 Ma oxicity spike recorded at both sites indicates an overlap with the global sea level decrease (Van Sickel et al., 2004). The 18 Ma increase in oxicity of the depositional environment is also recorded in U1352 Site Canterbury Basin samples, further supporting the idea of a global event. The 21 Ma spike in oxicity of the depositional environment of the New Jersey shelf is not correlated to a inferred sea level decrease, and could be due to a local increase in terrigenous input as a part of storm deposits or high river inputs.

The Pr/Ph ratio for the U1345 site samples is mostly <0.8, suggesting an anoxic depositional environment. One exception is for a period around 8 Ma, when Pr/Ph is higher (1.5-2.0), consistent with a more oxidising depositional environment (Fig. 3) (Powell and McKirdy, 1973). The Pr/Ph and TOC/TN data suggest strong but short-lived inputs of terrigenous OM around ~8.3 Ma.

6.4. Source of OM through hopane input

Oleanane, produced by angiosperms, originates in botulin or other pentacyclic triterpenoids (e.g. Whithead, 1973; Ekweozor and Udo, 1988). The oleanane/hopane ratio (the oleanane index) can be used to assess the relative abundance of angiosperm vegetation (Murray et al., 1994). The oleanane index for the 15–13 Ma interval and at 7 Ma shows an increase in angiosperm input for the samples from the U1352 and U1353 Sites in the Canterbury Basin. This increase is consistent with an increase in $CPI_{(22\text{-}32)}$ index and the TAR ratio, as discussed above, and hence can be attributed to an increase in land mass and plant coverage during these periods.

The presence of gammacerane in sediments is related to water-column stratification (Damsté et al., 1995). The amount of gammacerane increases in hypersaline environments. The origin of this biomarker is not known, but one of its precursors, tetrahymanol, is a membrane lipid found in some protozoa (Caspi et al., 1968; Ourisson et al., 1987). High values of the gammacerane/hopane ratio are indicative of marine carbonates and the virtual absence of gammacerane is typical of deltaic shales (Peters et al., 2005). Low sea levels for the New Zealand region around 13 Ma can be proposed based on the low values of the gammacerane/hopane ratio (Fig. 2.5E).

High C_{24} tetracyclic/C_{23} tricyclic terpane ratios (>0.6) are indicative of clastic marine sediments, whereas lower ratios are usually observed in carbonates and marls (Peters et al.,

2005). A high C_{23}/C_{21} tricyclic terpane ratio together with a low relative abundance of C_{24} tetracyclic terpane is indicative of marine OM input to the sediment. Based on these ratios, the U1351 Site samples in the Canterbury Basin have high marine OM input through the late Miocene, with only two samples at 6.60 Ma and 5.60 Ma having a C_{24} tetracyclic/C_{23} tricyclic terpane ratio <0.6, which indicates greater terrigenous OM input. These samples also have high C_{23}/C_{21} tricyclic terpane ratios, supporting the terrigenous OM input suggestion. The middle Miocene U1353 Site samples do not contain C_{24} tetracyclic terpanes, but the C_{23}/C_{21} tricyclic terpane ratio for this period suggest high terrigenous OM input.

A relatively stable uplift of the Southern Alps (Lu et al., 2005), causing an increase in vegetation cover together with a decrease in global temperatures from ~15 Ma (Zachos et al., 2001), can be proposed as a reason for low terrigenous input in the Canterbury Basin up to 11 Ma. The cooling event was followed by a constant increase in terrigenous OM input through the late Miocene, which could correlate to another increase in the land mass (Lu et al., 2005). The highest input of terrigenous OM was recorded around 6 Ma, based on TOC/TN data and other biomarker ratios. This spike can be attributed to an increase in the convergence rate between the Pacific and Australian plates to >7 mm yr around 6 Ma (Lu et al., 2005; Wood and Stagpoole, 2007), resulting in an increase in the elevation of the Southern Alps. This may have led to more angiosperm vegetation cover on the South Island.

6.5. Source of OM through the sterane input

Steranes are source-specific compounds containing 26 to 30 carbons in their structure. The C_{27} steranes are mainly derived from zooplankton, whereas C_{29} steranes are mainly derived from higher plants (Huang and Meinschein, 1979). The sources for C_{28} steranes are not fully identified, but some studies suggest that diatoms are rich in C_{28} steranes (Grantham and Wakefield, 1988). A C_{27}-C_{28}-C_{29} sterane ternary diagram has been used to determine the source of organic matter (Moldowan et al., 1985) and has also been used in oil-source

correlations . In addition, differences in sterane percentages for deltaic and continental shelf sediments have been reported (Meyers, 1997).

The samples from the outer continental shelf U1351 Site in the Canterbury Basin contain mixed OM input from deltaic-terrigenous and shallow marine sources, based on (Grantham and Wakefield, 1988) the sterane ternary diagram (Fig. 2.6). The U1352 Site samples steranes were mainly derived from shallow water or open marine organisms. The majority of the U1353 inner shelf Site samples have sterane compositions consistent with organic matter dominated by deltaic-terrigenous input. These data show steranes as good indicators of the site location relative to the shore line in the Canterbury Basin. The closer to a land mass, the higher the deltaic-terrigenous signal that the steranes record. In general, an open water sterane signal is present only in the outer continental shelf and continental slope sites, and not in the inner continental shelf samples. In contrast, the deltaic-terrigenous sterane signal is not present in the continental slope samples.

For the U1352 Site the early Oligocene and early Miocene samples have sterane distributions that suggest deposition of marine OM in an open marine environment. The middle Miocene samples show a shallow marine environment based on the steranes, and closer proximity to the shore line can be suggested for the ~16–14 Ma interval. The n-alkane data for the same interval shows an increased input of terrigenous OM, also arguably suggesting a shorter distance to the shore line, as does the high sedimentation rates at the time. The sterane data for the 12–10 Ma interval show higher input of marine OM, which is supported by the $CPI_{(22-32)}$ and $1/P_{aq}$ results. The late Miocene was previously characterised as having an increasing terrestrial OM input to the continental slope, compared to the middle Miocene, and the sterane signal supports this reconstruction, although the steranes do not have well identified sources (Moldowan et al., 1985).

The C_{30} sterane index is an index of 24-*n*-propylcholestanes relative to the other C_{27}-C_{30} identified steranes and is very specific for marine organic matter input (Seifert and Moldowan, 1978; Peters et al., 2005, for review). C_{30} sterane index values close to 1 are indicative of marine OM input. The early Oligocene samples from the U1352 Site have C_{30} sterane indices (Fig. 2.7C) that indicates significant marine OM input, which reduces through the early Miocene and then increases at the beginning of the middle Miocene. Another strong input of marine OM is recorded by the C_{30} sterane index at 14.57 Ma, followed by a significant decrease until the Pliocene (Table 2.4). These data are consistent with the previously suggested source interpretations for the Canterbury Basin.

The U1456 Site sterane distributions show variations in the OM input in the late Miocene period from 8.27–6.29 Ma, which is characterised by spasmodically enhanced terrigenous sediment contributions into the marine environment. This observation is supported by the high amounts of long chain *n*-alkanes and the high oleanane index that is indicative of angiosperm OM input during the same period (Whithead, 1973; Ekweozor and Udo, 1988; Murray et al., 1994; Murray et al., 1997), and is consistent with strong energy impulses from the Indus River region. The sediments deposited at other times have a C_{27}-C_{29} sterane signature characteristic of a mixed shallow water marine environment that can be explained by the slow movement of sediment from the main deltaic source of the Indus River towards the Laxmi Basin. This observation is supported by a significant increase in the C_{30} sterane index from 6.29 to 3.04 Ma, showing increased marine organic matter (Seifert and Moldowan, 1978; Peters et al., 2005).

6.6. Thermal maturity and biodegradation

The Pr/*n*-C_{17} and Ph/*n*-C_{18} ratios (Tissot et al., 1971) and various hopane and sterane ratios are commonly used for thermal maturity evaluation (Seifert and Moldowan, 1978; Stephens and Carroll, 1999; Nuzzo et al., 2012). The Pr/*n*-C_{17} and Ph/*n*-C_{18} ratios can also be

influenced by biodegradation (Tissot et al., 1971). C_{27} 17α-22,29,30-trisnorhopane (Tm) is less stable than C_{27} 18α-22,29,30-trisnorneohopane (Ts), and their relative abundance is usually measured by the Ts/(Ts+Tm) ratio. However, the sedimentation processes, early diagenesis, and variation in the source of OM can significantly alter Ts/(Ts+Tm) (Ourisson et al., 1984). The C_{31} 22S/(22S+22R) hopane epimer ratio increases with thermal maturity to an equilibrium between 0.57–0.62 which is reached at the start of oil generation (Seifert and Moldowan, 1980; Moldowan et al., 1986). The C_{30} 17β,21α(H) isomer (moretane) is less thermally stable than the C_{30} 17α,21β(H) hopane, and the C_{30} αβ/(αβ+βα) ratio increases with increasing thermal maturity (Mackenzie et al., 1980; Seifert and Moldowan, 1980). Maturity-related parameters can also be obtained from the isomerisation ratio of 20S/(20S+20R) C_{29} 5α,14α,17α(H) steranes, which equilibrates at 0.52-0.55 (Seifert and Moldowan, 1986). The ratio of C_{27} diasteranes to steranes increases with an increasing thermal maturity (Rubinstein et al., 1975; Peters et al., 2005). However, diasterane/sterane ratios can be increased due to oxidation processes or by clay catalysed reactions (Kirk and Shaw, 1975; Seifert and Moldowan, 1986).

All the biomarker ratios show a low thermal maturity for the analysed sediments, with some inferred increase in maturation with depth. No samples have reached the oil window. Most Pr/*n*-C_{17} and Ph/*n*-C_{18} ratios are relatively low for the U1351, U1352, and U1353 Sites (Table 2.2). The Pr/*n*-C_{17} and Ph/*n*-C_{18} ratios in the U1352 Site samples decrease somewhat with depth, indicating a small degree of increased thermal maturity influence on the OM.

The M0027A Site samples have Ph/*n*-C_{18} <2.0 and Pr/*n*-C_{17} <1 for all periods, except for one sample at 17.90 Ma with a Pr/*n*-C_{17} value of 5.9, possibly suggesting some short-term increase in biodegradation at that time that could have preferentially removed the n-alkane. The M0028A Site samples also have low Pr/*n*-C_{17} (< 1.5) and Ph/*n*-C_{18} (<2), suggesting that none of these samples are biodegraded. These ratios show a low thermal maturity for the New Jersey site samples.

Most U1352 Site samples have Ts/(Ts+Tm) ratios <0.4 suggesting a low thermal maturity. The 18 Ma and 15 Ma samples have high ratios (Fig. 2.5A), suggesting slightly enhanced thermal maturation. The C_{31} αβ 22S/(22S+22R) hopane ratio and the C_{30} αβ/(αβ+βα) ratio suggests a low thermal maturity of the U1352 Site samples (sub-oil window).

Maturity-related parameters can also be obtained from the isomerisation ratio of 20S/(20S+20R) C_{29} 5α,14α,17α(H) steranes, which equilibrates at 0.52-0.55 (Seifert and Moldowan, 1986). There is no correlation between the sterane 20S/(20S+20R) ratio and sample depth for the New Zealand samples (Fig. 2.5B). This supports the proposed low thermal maturity of these samples, and suggest that variations in the ratio are mainly related to the lithology and redox potential of the depositional environment (Kirk and Shaw, 1975; Seifert and Moldowan, 1986).

In addition, the ratio of C_{27} diasteranes to steranes increases with increasing thermal maturity (Rubinstein et al., 1975; Peters et al., 2005). The analysed samples from the U1352 Site in New Zealand do not show any correlation between ratio change and sample depth up to 32 Ma (Fig. 2.7A). However, the diasterane levels in sediments can be increased through the oxidation processes or during clay catalysed reactions (Kirk and Shaw, 1975; Seifert and Moldowan, 1986).

These biomarker ratios were also used to evaluate the thermal maturity of the U1456 Site samples. The low Ts/(Ts+Tm) ratios (<0.25) are indicative of low thermal maturity (Seifert and Moldowan, 1978; Stephens and Carroll, 1999; Nuzzo et al., 2012). Two samples at 10.15 Ma and 13.53 – 17.71 Ma show Ts/(Ts+Tm) ratio values >0.4 which probably influenced by the alterations in OM input source. The 22S/(22S+22R) C_{31} αβ hopane epimer ratios are mostly <0.4, suggest a low thermal maturity before the oil generation window for the site. Three samples at 7.79, 8.27, and 13.53-17.71 Ma have higher ratios (0.56, 0.55, and 0.57, respectively) than expected for the sample depth indication variation in OM input. A low

thermal maturity of the U1456 Site samples is supported by low 20S/(20S+20R) C_{29} 5α,14α,17α(H) sterane ratios (<0.61), which indicates that all the samples have not reached the oil generation window.

The *T*max (Espitalié, 1986) pyrolysis temperatures were calculated only for the New Zealand samples, and suggest a range of 400°C to 419°C for the U1351 Site samples, 406.5°C to 441.1°C for the U1352 Site, and 370 to 422 °C for the U1353 Site (Table 2.1; Fig. 2.2E). These *T*max values are consistent with thermal maturities prior to (U1351 and U1353 sites) and just into (deeper part of Site U1352) the oil window. In addition, the calculated reflectance (Rc) from the methylphenanthrene index was collected only for the New Zealand samples, and MaxT was calculated from Rc for only some samples dated between 12 and 4 Ma (Fig. 2.7E). The calculated Max*T* (Radke et al., 1986; Wang et al., 2005) for the U1351 Site show sediment temperature variations between 100ºC and 118 ºC. The Calculated Max*T* for the U1352 Site varies between 97ºC and 129ºC, without correlation to sample depth. The results indicate low levels of thermal maturation for the New Zealand samples, and thermal maturity levels stay below or just into the oil generation window.

The data collected from all three locations show low thermal maturity levels for all the analysed samples. The results are indicative of good preservation levels for the organic matter at all locations, and low levels of thermal alternation. The New Zealand samples have only reached the sub-oil generation window, or just into the oil generation window in the deeper parts of Site U1352. The New Jersey samples and the samples from the Indian Ocean contain organic matter that is below the oil generation window.

6.7. Reconstructed sea surface temperatures (SST)

For the SST reconstructions, only samples with a BIT index ≤0.5 were considered in this research. Therefore, the U1353 Site samples with BIT values >0.5 were not considered during the reconstructions.

The Eocene sample from the U1352 Site in the Canterbury Basin has a reconstructed SST based on the TEX^{H}_{86} parameter of 29.8 ºC, while the Oligocene SST is inferred to be in the range 21.5–25.6ºC (Fig. 3.4), with the latest Oligocene sample having the higher reconstructed SST (25.6ºC). These newly acquired New Zealand data are consistent with the reconstructed Oligocene SSTs from ODP site 511 (South Atlantic Ocean, Falkland Plateau) and DSDP Leg 26, Sites 250-252 (South Africa) (Miller et al., 2008; Liu et al., 2009; Pross et al., 2012). Moreover, temperature reconstructions for the Antarctic region in the early and middle Eocene suggest a warm tropical environment on that continent (Pross et al., 2012). The reconstructed late Eocene and early Oligocene SSTs in New Zealand show warm oceanic water temperatures above 20ºC, and are thus consistent with the proposed tropical environment for all the southern regions. Warm SSTs to the Eocene/Oligocene boundary were also recorded in global oxygen isotope records (Zachos et al., 2001; Zachos et al., 2008).

The early Miocene in New Zealand Site U1352 has high SSTs of 26.0ºC and 27.0ºC around 18 Ma, with a temperature decrease to 22.1ºC at 16.83 Ma, based on TEX^{H}_{86}. This decrease continues through the middle Miocene and reaches a minimum of 18.9ºC at 13.72 Ma. Similarly, the reconstructed SST based on the $U^{K`}_{37}$ index for the U1353 Site shows a decrease in temperature from 26.2ºC to 21.6ºC for the late Miocene to the end of the middle Miocene. A global climatic optimum and temperature increase at the early/middle Miocene boundary (Nelson and Cooke, 2001a), together with the increasing land mass of the New Zealand sub-continent based on an increase in sedimentation rates since the middle Miocene (Lu et al., 2005), suggest gradual intensification in the amount of land vegetation. Interpretation of global eustatic and climatic transformations suggest that cooler Neogene

seawater conditions were associated with (or accompanied by) a decrease in global sea levels (Zachos et al., 2001; Van Sickel et al., 2004). These data suggest an increase in SST for the 20–18 Ma period followed by SST decrease from the mid-Miocene Climatic Optimum. The early Miocene SST increase was not recorded in the global $\delta^{18}O$ reconstruction (Zachos et al., 2001). A similar SST decrease was recorded in the middle Miocene samples from the southwest Pacific (DSDP Leg 115, site 588; Flower and Kennett, 1994).

In the late Miocene period in the Canterbury Basin there was a decrease (Fig. 3.4) in SST from 19.8ºC at 11.92 Ma to 12.8ºC at 6.3 Ma, based on the U1352 Site samples. The U1351 Site samples show a decreasing SST trend from 22.4ºC to 18.3ºC during the 6.52 and 5.30 Ma period. The reconstructed SSTs for the Pliocene period in the Canterbury Basin are very variable (Fig. 3.4). The recorded temperatures fall in the range <10ºC for most of the period, except for the 3.65–3.24 Ma period where there are three SST values >10ºC.

From 10 Ma until the Holocene the reconstructed SST from New Zealand correlates well with the trend of global temperature decreases reconstructed from $\delta^{18}O$ (Zachos et al., 2001). Warm SSTs for this period were also recorded in the ODP 590 (south western Pacific) and ODP 763 (north eastern Indian Ocean) sites. For the ODP 590 site the alkenone proxy was used (Karas et al., 2011a), whereas for the ODP 793 site the SST was reconstructed using the Mg/Ca ratio (Karas et al., 2011b).

The New Jersey M0027A and M0028A site samples show a complex SST trend (Fig. 4.5), with the 19.28 Ma sample having a SST of 16.6ºC, followed by a SST increase to 20.5ºC at 17.83 Ma, and then an inferred rapid temperature drop to 15.1ºC at 16.94 Ma. A further temperature increase is suggested for the period between 16.52 and 15.69 Ma when SST values vary between 17ºC and 19ºC. Overall, a decrease in SST is seen from the early Miocene to the middle Miocene up to 16 Ma for the New Jersey samples. Our data is

consistent with the global Neogene cooling trend proposed in the literature (Zachos et al., 2001; Van Sickel et al., 2004; Lu et al., 2005).

Variations in lipid preservation in sediments can influence the reconstructed SST (Huguet et al., 2007; Kim et al., 2008; Seki et al., 2012). The iGDGT preservation in sediments can be by seasonal growth of *Thaumarchaeolata* (Huguet et al., 2011). The major growth of *Thaumarchaeolata* occurs in deeper water, so might influence the accumulation of iGDGTs above the mixed layer (Huguet et al., 2007; Kim et al., 2012; Seki et al., 2012). Moreover, the regional effect on each proxy must be considered during reconstructions (Tierney and Tingley, 2014, 2015).

The iGDGT-based SST reconstructions for the U1456 Site in the northern Indian Ocean indicate a slight decreasing temperature trend of 33.0°C to 30.5°C from 10.15 to 7.73 Ma. After 3 Ma the iGDGT-based SST is mostly stable around 28.6°C, with one significant temperature drop to 22.6°C at 1.60 Ma. The alkenone-based SST shows a temperature decrease from 28°C at 10.15 Ma to 25°C at 7.37 Ma , and a relatively stable SST from 6.04 to 1.07 Ma ago, averaging 28.6°C, similar to the iGDGT reconstructions. However, the SST based on alkenones decreases significantly to 23.9°C at 0.46 Ma ago, in contrast to the iGDGT SST reconstruction for this sample which is much higher (28.9°C). No significant temperature drop was recorded by the alkenone proxy at 1.6 Ma. The alkenone-based reconstructions yields lower SST estimates than those based on iGDGTs, which can be partly explained by the upper limit of the alkenone based calibration of 29°C (Sonzogni et al., 1997). The two SST proxies vary based on seasonal and depth interval variations (Kim et al., 2010; Leider et al., 2010).

One of the major factors in precipitation development is the sea-land thermal gradient (Webster et al., 1998). The SST reconstructions from the northern Indian Ocean suggest a slightly decreasing, but very warm SST, during the late Miocene (>30°C based on iGDGTs

and averaging ~27°C for the alkenone proxy). These results are consistent with data from the northern South China Sea (Wan et al., 2009) and global SST reconstructions based on $\delta^{18}O$ and Mg/Ca proxies (Müller et al., 1998; Zachos et al., 2001; Zachos et al., 2008). Temperature changes and increases in upwelling in the Indian Ocean during the late Miocene have been attributed to accumulation of Antarctic ice cover and development of the Antarctic Circumpolar current (Norris et al., 2013). Other studies have proposed that the modest sized permanent ice sheets in the Northern Hemisphere and the distribution of solar radiation are the main causes for the intensification of the monsoon in the late Miocene (Clemens et al., 1991). However, ice-temperature change models did not support such a correlation at that time (Cramer et al., 2011).

Variations in SST in the northern Indian Ocean since 3 Ma are consistent with existing reconstructions of the tropical ocean temperatures, which argue for significant control by glacial-interglacial cyclicity over precipitation patterns, with changing glaciation in the northern hemisphere (Beu et al., 1997; Zhisheng et al., 2001). These cycles were mainly developed because of the major changes in thermohaline circulation that followed closure of the Isthmus of Panama and onset of Northern Hemisphere glaciation with a decrease in atmospheric CO_2 content. Variations in magnetic sustainability suggest a strong influence of orbital forcing on Asian monsoon intensification, together with an increase in central Asian aridity levels (Clemens et al., 1991; Prell and Kutzbach, 1992; Zhisheng et al., 2001). All these observations support the strong influence of glacial cyclicity on the Asian monsoon during the last 3 million years.

6.8. Reconstructed mean annual air temperatures (MAAT)

The MAAT in the New Zealand region was reconstructed only for the last 18 million years (Fig. 4.5). The results suggest an air temperature variation between 2.4ºC and 11.1ºC during

the early and middle Miocene. The late Miocene samples have higher air temperatures from 21.4ºC to 32.6ºC. Two samples at 10.49 and 8.39 Ma have very low MAAT values of 8.0ºC and 7.1ºC, respectively. The reconstructed MAAT decreases rapidly below 10ºC during the Pliocene, with the majority of the Pliocene samples having MAAT records >2ºC. The Quaternary samples have relatively low MAAT temperatures between 15ºC and 2ºC. The temperatures decrease below 10ºC by 1.2 Ma, and rise back after 0.87 Ma. Temperatures reach their maximum at 0.43 Ma and gradually decrease to 2ºC until 0.10 Ma. The MAAT for the last 100 ka varies significantly.

The reconstructed MAAT for the New Jersey region show similar trends (Fig. 4.5). The MAAT for the M0027A Site shows temperature variations between 4.5ºC and 33.3ºC. The data show rapid MAAT decreases from 22.4ºC at 23.59 Ma to 4.5ºC at 20.74 Ma. The opposite trend is recorded at the M0028A Site for the 21.50 Ma sample that shows a very high temperature (34.4ºC). Warmer high latitude areas were proposed in North America (Wolfe, 1994b; Graham, 1999) and Beringia (Wolfe, 1994a) for the mid-Miocene Climatic Optimum. Warm temperatures for polar regions were also proposed (Bruch et al., 2006). General cooling through the Miocene from the mid-Miocene Climatic Optimum was recorded in global $\delta^{18}O$ records from ~15 Ma (Zachos et al., 2001). The reconstructed MAAT in this work partly contradicts the established global cooling trend. The MAAT continues to rise through the second part of middle Miocene and during the late Miocene, with only two major cooling events 10.49 and 8.39 Ma. The proposed temperature increase is not recorded by $\delta^{18}O$ or $\delta^{13}C$ data (Zachos et al., 2001; Zachos et al., 2008).

The relatively large calibration error for Eq. 9 (±5ºC) introduces a significant uncertainty for the MAAT estimates (Weijers et al., 2007; Schouten et al., 2013). Although the introduced temperature error is significant, it produces a better temperature evaluation than pollen or leaf based analysis where the potential biases are hard to evaluate (Schouten et al., 2013). Because

of the high analytical error, the exact MAAT evaluation is problematic and only general temperature trends can be discussed from the data.

6.9. Soil pH

Increasing precipitation increases the acidity of soils, because Ca and Mg ions are washed away from the system, leaving the soil more acidic. Soil pH can be estimated from the relative abundances of terrigenous lipids in a sample (Weijers et al., 2006). This biomarker signal is not sensitive enough to calibrate exact precipitation levels, but it is possible to evaluate the duration of the precipitation change based on the calculated pH (Weijers et al., 2006; Schouten et al., 2013).

The reconstructed soil pH for the Canterbury Basin in New Zealand shows a general trend of decreasing precipitation for the last 19 million years based on increasing soil pH (Fig. 4.5D). Some periods of higher rainfall in the Canterbury Basin can be inferred through a drop of soil pH from 6.9 at 13.72 Ma to 5.8 at 11.92 Ma, and from 7.8 at 3.60 Ma to 7.0 at 3.56 Ma. Another significant drop in soil pH from 7.9 to 6.7 is recorded from 0.235 to 0.003 Ma, with an increase in soil pH to 7.8 at 0.048 Ma dividing this period into two high precipitation periods with a short intervening dry interval. A significant jump in soil pH at 0.003 Ma to 8.4 suggests a rapid decrease in precipitation levels.

Reconstructed mean annual precipitation (MAP) in East Antarctica for the early Miocene, based on bulk geochemistry of marine siliciclastic sediments from drill cores on Antarctica's continental margin suggests an increase in MAP from 20 Ma to 15 Ma from 500 to 7590 mm, respectively (Passchier et al., 2013). The new soil pH data from the Canterbury Basin correlates with these reconstructions, confirming a gradual increase in precipitation levels from 16.83 Ma until the end of the early Miocene, and continuing further through the middle Miocene. The new soil pH data from the Canterbury Basin shows an inferred decrease in

precipitation from 11.92 Ma to 6.3 Ma. This is consistent with proposed decrease global rainfall decrease during the late Miocene (Flower and Kennett, 1994; Poage and Chamberlain, 2002; Retallack, 2004; Martin, 2006). In addition, the BIT index below 0.15 for most of the Canterbury Basin samples during the late Miocene supports low terrestrial OM runoff into the Pacific Ocean. At the same time, the MAAT data show a high temperature spike during the late Miocene, up to 32.6ºC. Such a temperature increase correlates well with a decrease of precipitation in New Zealand and partial aridification. This dry period has also been recorded in previous studies, based on the global atmospheric carbon dioxide evolution (Pagani et al., 1999), compound specific *n*-alkane records of $\delta^{13}C$ and δD in northern Japan (Seki et al., 2010), and pollen records preserved in speleothems from semiarid southern Australia (Sniderman et al., 2016).

The IODP 313 samples from New Jersey show a different soil pH pattern through the Miocene, with generally higher soil pH compared to the New Zealand data (Fig. 4.5D). The soil pH values concentrate in a narrow range between 7.8 and 8.6, thus suggesting no significant variation in precipitation in the region. The slow decrease in soil pH values through the first part of the early Miocene (from 21.50 to 18.61 Ma) suggests a gradual increase in precipitation levels. The following increase in soil pH to 8.6 at 15.90 Ma, might suggest a decrease in rain intensity in the New Jersey region. The soil pH then drops to 8.0 at 14.34 Ma and remains without significant changes until 11.02 Ma, indicating a precipitation increase back to the early Oligocene levels.

The early and middle Miocene soil pH values from New Jersey are higher than the soil pH values from New Zealand for the same period (Fig. 4.5D). This difference might indicate differences in type of terrigenous material eroded at the two sites. The New Zealand soil pH data shows fluctuations between 1.5 pH values, indicating significant variations in rainfall during the early and middle Miocene. In contrast, the New Jersey data for the same time period show less variability of 0.6 pH values. Both sites show the most significant soil pH

decrease during the mid-Miocene Climatic Optimum, suggesting that this event was associated with an increase in precipitation in both the north Atlantic and west Pacific margins. The rapid increase in precipitation in New Zealand between 13.72 and 11.92 Ma must have been influenced by local variations in evaporation patterns (Kennett et al., 1974; Pocknall, 1989).

Globally wetter conditions during the mid-Miocene Climatic Optimum (~18–14 Ma) have been widely discussed in the literature (e.g., Retallack, 2009; Wan et al., 2009; You et al., 2009; Bruch et al., 2011). The Serravallian Stage in Europe is associated with a decrease in precipitation caused by global cooling events (Shevenell et al., 2004). However, later studies based on a leaf fossil and pollen proxy did not find any significant precipitation decrease in Europe related to this cooling (Böhme et al., 2011). The newly acquired New Jersey data supports the later studies and shows no changes in precipitation for this period. The newly acquired New Zealand data for the Serravallian Stage show an increase in precipitation, consistent with flora proxy data collected in southern New Zealand (Reichgelt et al., 2015).

6.10. Synthesis

The organic data collected during this study provides a comprehensive climatic picture in three different locations during the second part of the Cenozoic Era. The biomarker proxies do not always provide the same climate picture for the region, but in the vast majority of cases they are well correlated with each other. A low thermal maturity of the OM in all three locations, the Canterbury Basin, the New Jersey continental shelf, and the Arabian Sea, is shown by Ts/(Ts+Tm), Pr/*n*-C_{17}, and Ph/*n*-C_{18}. Therefore, a paleoclimatic interpretation based on TOC, *n*-alkanes, isoprenoids, steranes, hopanes, alkenones, and GDGTs is proposed.

The Oligocene period in the Canterbury Basin is characterised by the dominance of the marine environment, with low terrigenous OM input, suggesting high global sea levels (Miller

et al., 2005) and low uplift of the New Zealand region above sea level (Winkworth et al., 2002). The C_{27}-C_{29} sterane distribution, the C_{30} sterane index and the BIT data support the open marine environmental reconstruction during the Oligocene. High Oligocene SSTs in the Canterbury Basin are consistent with other SSTs reconstructions for this period (Miller et al., 2008; Liu et al., 2009). Warm SST temperatures at the Eocene/Oligocene boundary were also recorded in global oxygen isotope records (Zachos et al., 2001; Zachos et al., 2008) and especially for the Antarctic region (Pross et al., 2012).

The New Jersey continental shelf data suggest an increasing terrigenous OM input trend for the Oligocene period, based on TOC, *n*-alkanes, isoprenoids, and GDGT data (the BIT index). The reconstructed MAAT shows relatively high air temperatures (>19ºC). No indication of a decrease in global sea level during the Oligocene is shown (Zachos et al., 2008; Millet et al., 2005). Therefore, these data suggest a strong influence of river sediment input.

The early Miocene data from the Canterbury Basin are consistent with a marine depositional environment. The interpretation is supported by *n*-alkanes, C_{27}-C_{29} sterane distributions, the C_{30} sterane index, and the low BIT index. The SST in the Canterbury Basin decreases through the early Miocene, but the MAAT continues to warm up. The continuous decrease in the SST contradicts the global $\delta^{18}O$ reconstructions for the 17–15 Ma period (Zachos et al., 2008; Miller et al., 2005) (Zachos et al., 2001 and references within) (Zachos et al., 2001 and references within) (Zachos et al., 2001 and references within). However, SST cooling can be attributed to the development of the Antarctic oceanic fronts during the Neogene (Lawver et al., 1992; Nelson and Cooke, 2001b). This would have caused a decrease in the SST around New Zealand from the early Miocene, as cooler subtropical paleo-currents and later on the cold intrusions of the sub-Antarctic currents started to influence the ocean temperature, especially around the east coast of New Zealand (Nelson and Cooke, 2001).

The warm MAAT for the New Zealand region contradicts the previously suggested cool early Miocene climate (Pockhall, 1989). However, palynological evidence supported by moisture availability and the spread of fire in the New Zealand area suggests a warm temperate climate for the early Miocene (Mildenhall et al., 2003; Pole, 2003). The differences between reconstructed MAAT and SST may be attributed to a delay in the influence of the cool water effect on air temperatures.

The early Miocene data from the New Jersey area are consistent with strong terrigenous OM inputs, based on the *n*-alkane, sterane, and BIT data sets. The reconstructed SST shows a decreasing temperature trend during the early Miocene. There is clear indication of coastal onlap associated with a major downward shift of the sea level for the New Jersey area from the early Miocene. This falling sea level exposed nearshore marine and coastal-plain depositional environments, and are consistent with the low global sea levels during the early Miocene that were proposed by Haq et al. (1987) and Van Sickel et al. (2004), that estimated a decrease in sea level just after 21 Ma. Abreu and Anderson (1998) also showed a global sea level decrease, with minimum sea levels during the early Miocene around 21 Ma and slightly after at 20 Ma.

The reconstructed temperature data from the Canterbury Basin and New Jersey Shelf show a decreasing SST trend for the early Miocene. This correlates with a global climatic optimum and temperature increase at the early/middle Miocene boundary, based on the $\delta^{18}O$ and $\delta^{13}C$ composition of calcareous microfossil shells (Shackleton and Kennett, 1975; Rohling and Cooke, 1999).

The middle Miocene reconstruction for the New Zealand region suggests an increasing terrigenous OM input, based on TOC, *n*-alkane, BIT, sterane, and terpane data. Moreover, the isoprenoid data shows an increasingly oxic depositional environment for the region. The fluctuations in oxicity of the depositional environment are consistent with global sea level

fluctuations during the middle Miocene (Van Sickel et al., 2004). Increasing terrigenous input from 14–12 Ma, together with high sedimentation rates at the same time, can be attributed to significant land mass build up of the South Island of New Zealand (Lu et al., 2005). The slow uplift of the western part of the South Island, and the resultant increase in the sloping gradient of the Canterbury Basin, created an anoxic environment in the continental margin area with high sedimentary input to the continental slope area.

The SST in the Canterbury Basin continued to decrease through the middle Miocene, which can be attributed to the influence of the cooler sub-Antarctic currents which started to influence the global ocean temperature (Nelson and Cooke, 2001). The MAAT in the South Island of New Zealand continued to be relatively warm. This correlates well with the established mid-Miocene Climatic Optimum reconstructions (Zachos et al., 2001; 2008). The MAAT in the New Zealand samples continued to rise through the second part of the middle Miocene. This temperature rise has also been recorded in the fossil studies of New Zealand vegetation (Mildenhall, 2003).

The New Jersey biomarker and geochemical data show high terrigenous OM input during the middle Miocene. The decrease in global sea level was followed by an increase in global sea level around 12 Ma, recorded in the TOC, *n*-alkane, isoprenoid, and BIT data sets. High sea levels have been proposed during the middle Miocene climatic optimum, when a decrease in ice sheet cover and an increase in global temperatures were recorded (Zachos et al., 2001; Miller et al., 2005; Zachos et al., 2008). The reconstructed SSTs in the New Jersey samples shows a decreasing SST trend from the early Miocene to the middle Miocene. This trend can also be seen through the temperature increase at the early/middle Miocene boundary based on the $\delta^{18}O$ and $\delta^{13}C$ composition of calcareous microfossil shells (Shackleton and Kennett, 1975; Rohling and Cooke, 1999).

Late Miocene sediments were only recovered for the New Zealand and Arabian Sea locations. The New Zealand data show an increase in terrigenous OM input through the late Miocene, indicating a further increase in the uplift of the Southern Alps, especially for the 7–5 Ma period (Lu et al., 2005; Wood and Stagpoole, 2007). A spike in the elevation of the Southern Alps around 6 Ma is recorded in the *n*-alkane, sterane, hopane, and BIT organic proxies. In addition, an increase in angiosperm vegetation is recorded, as is a partial increase in global sea level, based on sterane data for the 12–10 Ma period.

A decrease in SST during the late Miocene in the New Zealand area is also supported by the records from DSDP Site 593, southern Tasman Sea (Cooke et al., 2008). The late Miocene SST decrease can be correlated to an increase in ice sheet cover in southeast Greenland (Larsen et al., 1994), South America (Mercer and Sutter, 1982), and possible formation of ice sheets in Western Antarctica (Kennett, 1990). The continuous temperature decrease correlates to a global temperature decrease recorded by $\delta^{18}O$ (Zachos et al., 2001). A decrease in SST has been proposed for multiple locations across both hemispheres around the globe (Herbert et al., 2016). The DSDP Site 594, located in the Southern Pacific region (Herbert et al., 2016), shows a similar temperature decrease after 8 Ma.

The warm MAAT during the late Miocene period in New Zealand contradicts the proposed global late Neogene cooling (Herbert et al., 2016). However, the global cooling trend is not constant. Some studies have shown partial warming in the Arctic and Antarctic regions at the end of the late Miocene and into the Pliocene (Kennett, 1990; Thiede et al., 1998). The temperature fluctuations probably correlate to the pCO_2 changes in the late Miocene related to the orbital scale shifts, forcing climatic and ecosystem changes (Herbert et al., 2016). Rapid cooling in New Zealand during the Pliocene coincides with a large increase in ice sheet cover in Antarctica (Ross Sea), dated between 3.3 and 2.5 Ma (McKay et al., 2012).

One of the major factors in precipitation development is the sea-land thermal gradient (Webster et al., 1998). The SST reconstructions for the Indian Ocean region show warm SSTs during the late Miocene (>30°C based on iGDGTs, and averaging ~27°C for the alkenone proxy). These results are consistent with data from the northern South China Sea and global SST reconstructions based on $\delta^{18}O$ and Mg/Ca proxies. Temperature changes and increases in upwelling in the Indian Ocean during the late Miocene have been attributed to accumulation of Antarctic ice cover and development of the ACC (Norris et al., 2013). Other studies have proposed that the modest sized permanent ice sheets in the Northern Hemisphere and the distribution of solar radiation are the main causes for the intensification of the monsoon in the late Miocene (Clemens et al., 1991). However, ice-temperature change models do not support such a correlation at that time (Cramer et al., 2011).

Debate continues about the nature of the Asian monsoon in the Arabian Sea and its influence on the global climate. Some studies predict monsoon weakening between 10.15 and 3.09 Ma (Clift et al., 2008b), and after 8.27 Ma for the southern Asia area, while others argue for increasing summer rains over the same interval. Regardless of the direction of change, the closure of the Tethys Ocean together with the uplift of the Himalayas and the Tibetan Plateau have been linked to major alternations in monsoon intensity. The new observations in this thesis are consistent with no significant increase in precipitation between 10.15 and 8.26 Ma. This period was followed by an increase in summer monsoon levels, with an increase of the Indus River run-off for the eastern Arabian Sea region in the late Miocene (8.27–6.29 Ma), as recorded in the *n*-alkane (e.g., TAR and $1/P_{aq}$) and sterane data. These observations are supported by the compound specific, *n*-alakne $\delta^{13}C$ record. The increase in precipitation recorded by δD during the 8.27–6.29 Ma period also supports stronger Indus River runoff. The TOC/TN data and the Pr/Ph ratio also suggest strong but short-lived inputs of terrigenous OM around ~8.3 Ma. High precipitation levels in the period from ~2.6 Ma to ~1.6 Ma are also clearly recorded by increasing terrigenous OM inputs, based on *n*-alkanes, steranes, and the

BIT index. Falls in eustatic sea level may have increased terrigenous material input into the basin.

The development of the Asian monsoonal circulation may have occurred as early as the Eocene (Licht et al., 2014), but other studies argue for an intense phase beginning at the start of the Neogene (Clift et al., 2014). Some of these reconstructions have been informed by changes in eastern Asian vegetation patterns, as well as by chemical weathering proxies. Chemical weathering data from ODP Site 1146 in the South China Sea indicate a pattern of decreasing humidity from the middle Miocene to the early Pliocene, and a decrease in monsoon intensity (Steinke et al., 2010). The decline in chemical weathering intensity parallels a decrease of sedimentation rates on the Indus Fan, as well as a decline in chemical weathering and sedimentation rates at ODP Site 718 on the Bengal Fan (Cochran and Stow, 1987; Clift et al., 2008a; Clift et al., 2008b). In light of the regional character of these changes across the Himalayas and the Tibetan Plateau, it seems likely that they may reflect a common climate driver. The vegetation signal since 10.15 Ma at IODP Site U1456 is derived mainly from a continental source. Studies of Pakistan climate suggest a development of strong aridity and changes in precipitation patterns from 9 Ma (Quade et al., 1989). Sediment from the western Arabian Sea (ODP Site 722 drilling site) also show an increase in terrigenous sediment input from 8–6 Ma, although an increase in primary marine production was not detected because of poor carbonate preservation (Prell and Kutzbach, 1992; Zhisheng et al., 2001).

The new data indicate an increase in relative C_4 vegetation abundance for the western Himalaya region from ~10.15 ma until ~8.27 Ma, consistent with a regional decrease in precipitation. A strong increase in relative C_3 vegetation abundance from 8.27–7.5 Ma may be indicative of an increase in precipitation, consistent with an increase in Asian monsoon intensity. The aridity of the region increasing again after 7.5 Ma, with higher relative C_4 vegetation abundance. However, the δD results are more consistent with an increase in

precipitation from ~8.3 Ma to ~6.3 Ma. This is not supported by the local, Pakistani studies, which showed the development of strong aridity and changes in precipitation patterns from 9 Ma (Quade et al., 1989).

6.11. Future work

The research in this thesis shows good preservation of organic matter in continental shelf, continental slope, and deep water marine sediments. Good preservation of the organic compounds in marine sediments provides a unique opportunity for combining multiple proxies for understanding local and global climate variations during the Cenozoic. Recovered biomarkers show the strong influence of local tectonic activity on the accumulation of organic material in marine sediments. Therefore, biomarkers can be intensively used in research related to the influence of tectonic activity on the evolution of the continental shelf.

Additional studies of the cored sediments from the Atlantic, Pacific, and Indian oceans are require to confirm the observations made in this study. This study has only provide detailed discussion of the preserved biomarkers in three locations. Additional, geographically wider research is required to constrain the influence of eustasy on Cenozoic biomarkers. Higher resolution sampling is required to distinguish between different climatic mechanisms such as Milankovitch and orbital cycles. This study show that IODP cores provide a perfect research platform to tackle these research questions.

To provide a better correlation between different site locations, high sampling resolution should be used. Sediments with high TOC levels would be preferable for this type of research. Although preservation of the organic compounds varies between different sites, the same type of compounds should be checked for every site for better comparison. Multi proxy analyses, including heavy mineral studies and isotope analyses, should be carried out on the same samples, so as to provide information regarding the provenance of the sediments and possible sources of the organic matter.

6.12. References

Abreu, V.S., Anderson, J.B., 1998. Glacial eustasy during the Cenozoic: sequence stratigraphic implications. *AAPG Bulletin* 82, 1385-1400.

Albaigés, J., Grimalt, J., Bayona, J., Risebrough, R., De Lappe, B., Walker, W., 1984. Dissolved, particulate and sedimentary hydrocarbons in a deltaic environment. *Organic Geochemistry* 6, 237-248.

Barnes, M., Barnes, W., 1978. Organic compounds in lake sediments, Lakes. Springer, pp. 127-152.
Berner, R., 1990. Atmospheric carbon dioxide levels over Phanerozoic time. *Science* 249, 1382-1386.

Beu, A.G., Griffin, M., Maxwell, P., 1997. Opening of Drake Passage gateway and Late Miocene to Pleistocene cooling reflected in Southern Ocean molluscan dispersal: evidence from New Zealand and Argentina. *Tectonophysics* 281, 83-97.

Blair, N.E., Aller, R.C., 2012. The fate of terrestrial organic carbon in the marine environment. *Annual Review of Marine Science* 4, 401-423.

Blumer, M., Mullin, M.M., Thomas, D.W., 1964. Pristane in the marine environment. *Helgoländer Wissenschaftliche Meeresuntersuchungen* 10, 187-201.

Böhme, M., Winklhofer, M., Ilg, A., 2011. Miocene precipitation in Europe: temporal trends and spatial gradients. *Palaeogeography, Palaeoclimatology, Palaeoecology* 304, 212-218.

Bourbonniere, R., Meyers, P., 1996. Anthropogenic influences on hydrocarbon contents of sediments deposited in eastern Lake Ontario since 1800. *Environmental Geology* 28, 22-28.

Bray, E.E., Evans, E.D., 1961. Distribution of n-paraffins as a clue to recognition of source beds. *Geochimica et Cosmochimica Acta* 22, 2-15.

Bruch, A., Utescher, T., Mosbrugger, V., Gabrielyan, I., Ivanov, D., 2006. Late Miocene climate in the circum-Alpine realm—a quantitative analysis of terrestrial palaeofloras. *Palaeogeography, Palaeoclimatology, Palaeoecology* 238, 270-280.

Bruch, A.A., Utescher, T., Mosbrugger, V., 2011. Precipitation patterns in the Miocene of Central Europe and the development of continentality. *Palaeogeography, Palaeoclimatology, Palaeoecology* 304, 202-211.

Caspi, E., Zander, J.M., Greig, J.B., Mallory, F.B., Conner, R.L., Landrey, J.R., 1968. Evidence for a nonoxidative cyclization of squalene in the biosynthesis of tetrahymanol. *Journal of the American Chemical Society* 90, 3563-3564.

Clemens, S., Prell, W., Murray, D., Shimmield, G., Weedon, G., 1991. Forcing mechanisms of the Indian Ocean monsoon. *Nature* 353, 720-725.

Clift, P., Hodges, K., Heslop, D., Hannigan, R., Hoang, L., Calves, G., 2008a. Greater Himalayan exhumation triggered by Early Miocene monsoon intensification. *Nat Geosci* 1, 875-880.

Clift, P.D., Hodges, K.V., Heslop, D., Hannigan, R., Van Long, H., Calves, G., 2008b. Correlation of Himalayan exhumation rates and Asian monsoon intensity. *Nature Geosci* 1, 875-880.

Clift, P.D., Wan, S., Blusztajn, J., 2014. Reconstructing chemical weathering, physical erosion and monsoon intensity since 25Ma in the northern South China Sea: A review of competing proxies. *Earth-Science Reviews* 130, 86-102.

Cochran, J., Stow, D., 1987. 32. HIMALAYAN UPLIFT, SEA LEVEL, AND THE RECORD OF BENGAL FAN SEDIMENTATION AT THE ODP LEG 116 SITES1, Proceedings of the Ocean Drilling Program: Scientific results. The Program, p. 397.
Cooke, P.J., Nelson, C.S., Crundwell, M.P., 2008. Miocene isotope zones, paleotemperatures, and carbon maxima events at intermediate water-depth, Site 593, Southwest Pacific. *New Zealand Journal of Geology and Geophysics* 51, 1-22.

Cramer, B., Miller, K., Barrett, P., Wright, J., 2011. Late Cretaceous–Neogene trends in deep ocean temperature and continental ice volume: Reconciling records of benthic foraminiferal geochemistry (δ18O and Mg/Ca) with sea level history. *Journal of Geophysical Research: Oceans* 116.

Cranwell, P., 1984. Lipid geochemistry of sediments from Upton Broad, a small productive lake. *Organic Geochemistry* 7, 25-37.

Cranwell, P., Eglinton, G., Robinson, N., 1987. Lipids of aquatic organisms as potential contributors to lacustrine sediments—II. *Organic Geochemistry* 11, 513-527.

Damsté, J.S.S., Kenig, F., Koopmans, M.P., Köster, J., Schouten, S., Hayes, J., de Leeuw, J.W., 1995. Evidence for gammacerane as an indicator of water column stratification. *Geochimica et Cosmochimica Acta* 59, 1895-1900.

Dickens, A.F., Gélinas, Y., Masiello, C.A., Wakeham, S., Hedges, J.I., 2004. Reburial of fossil organic carbon in marine sediments. *Nature* 427, 336-339.

Eglinton, G., Hamilton, R.J., 1967. Leaf epicuticular waxes. *Science* 156, 1322-1335.

Ekweozor, C., Udo, O.T., 1988. The oleananes: Origin, maturation and limits of occurence in southern Nigeria sedimentary basins. *Organic Geochemistry* 13, 131-140.

Farquhar, G.D., Ehleringer, J.R., Hubick, K.T., 1989. Carbon isotope discrimination and photosynthesis. *Annual review of plant biology* 40, 503-537.

Ficken, K.J., Li, B., Swain, D., Eglinton, G., 2000. An n-alkane proxy for the sedimentary input of submerged/floating freshwater aquatic macrophytes. *Organic Geochemistry* 31, 745-749.

Flower, B.P., Kennett, J.P., 1994. The middle Miocene climatic transition: East Antarctic ice sheet development, deep ocean circulation and global carbon cycling. *Palaeogeography, Palaeoclimatology, Palaeoecology* 108, 537-555.

Fulthorpe, C.S., Hoyanagi, K., Crundwell, M.P., Dinarès-Turell, J., Ding, X., George, S.C., Hepp, D.A., Jaeger, J., Kawagata, S., Kemp, D.B., 2011. Expedition 317 summary.

Gelin, F., Damsté, J.S.S., Harrison, W.N., Maxwell, J.R., De Leeuw, J.W., 1995. Molecular indicators for palaeoenvironmental change in a Messinian evaporitic sequence (Vena del Gesso, Italy): III. Stratigraphic changes in the molecular structure of kerogen in a single marl bed as revealed by flash pyrolysis. *Organic Geochemistry* 23, 555-566.

Graham, A., 1999. Late Cretaceous and Cenozoic history of North American vegetation: north of Mexico. Oxford University Press on Demand.
Grantham, P.J., Wakefield, L.L., 1988. Variations in the sterane carbon number distributions of marine source rock derived crude oils through geological time. *Organic Geochemistry* 12, 61-73.

Grimalt, J., Albaigés, J., 1987. Sources and occurrence of C 12□ C 22 n-alkane distributions with even carbon-number preference in sedimentary environments. *Geochimica et Cosmochimica Acta* 51, 1379-1384.

Grossi, V., Hirschler, A., Raphel, D., Rontani, J.-F., De Leeuw, J., Bertrand, J.-C., 1998. Biotransformation pathways of phytol in recent anoxic sediments. *Organic Geochemistry* 29, 845-861.

Haq, B.U., Hardenbol, J., Vail, P.R., 1987. Chronology of fluctuating sea levels since the Triassic. *Science* 235, 1156-1167.

Hedges, J.I., Keil, R.G., 1995. Sedimentary organic matter preservation: an assessment and speculative synthesis. *Marine Chemistry* 49, 81-115.

Herbert, T.D., Lawrence, K.T., Tzanova, A., Peterson, L.C., Caballero-Gill, R., Kelly, C.S., 2016. Late Miocene global cooling and the rise of modern ecosystems. *Nature Geosci* 9, 843-847.

Hopmans, E.C., Weijers, J.W., Schefuß, E., Herfort, L., Damsté, J.S.S., Schouten, S., 2004. A novel proxy for terrestrial organic matter in sediments based on branched and isoprenoid tetraether lipids. *Earth and Planetary Science Letters* 224, 107-116.

Huang, W.-Y., Meinschein, W.G., 1979. Sterols as ecological indicators. *Geochimica et Cosmochimica Acta* 43, 739-745.

Huguet, C., Fietz, S., Stockhecke, M., Sturm, M., Anselmetti, F., Rosell-Mele, A., 2011. Biomarker seasonality study in lake van, Turkey. *Organic Geochemistry* 42, 1289-1298.

Huguet, C., Schimmelmann, A., Thunell, R., Lourens, L.J., Sinninghe Damsté, J.S., Schouten, S., 2007. A study of the TEX86 paleothermometer in the water column and sediments of the Santa Barbara Basin, California. *Paleoceanography* 22.

Karas, C., Nürnberg, D., Tiedemann, R., Garbe-Schönberg, D., 2011a. Pliocene climate change of the Southwest Pacific and the impact of ocean gateways. *Earth and Planetary Science Letters* 301, 117-124.

Karas, C., Nürnberg, D., Tiedemann, R., Garbe-Schönberg, D., 2011b. Pliocene Indonesian throughflow and Leeuwin current dynamics: implications for Indian Ocean polar heat flux. *Paleoceanography* 26.

Kennett, J., Houtz, R., Andrews, P., Edwards, A., Gostin, V., Hajos, M., Hampton, M., Jenkins, D., Margolis, S., Ovenshine, A., 1974. Development of the circum-Antarctic current. *Science* 186, 144-147.

Kennett, J.P., 1990. Latest Cretaceous to Cenozoic climate and oceanographic developments in the Weddell Sea, Antarcitca: An ocean-Drilling perspective, Proc. ODP, Sci. Results, pp. 937-960.
Kim, J.-H., Romero, O.E., Lohmann, G., Donner, B., Laepple, T., Haam, E., Damste, J.S.S., 2012. Pronounced subsurface cooling of North Atlantic waters off Northwest Africa during Dansgaard–Oeschger interstadials. *Earth and Planetary Science Letters* 339, 95-102.

Kim, J.-H., Schouten, S., Hopmans, E.C., Donner, B., Sinninghe Damsté, J.S., 2008. Global sediment core-top calibration of the TEX86 paleothermometer in the ocean. *Geochimica et Cosmochimica Acta* 72, 1154-1173.

Kim, J.-H., Van der Meer, J., Schouten, S., Helmke, P., Willmott, V., Sangiorgi, F., Koç, N., Hopmans, E.C., Damsté, J.S.S., 2010. New indices and calibrations derived from the distribution of crenarchaeal isoprenoid tetraether lipids: Implications for past sea surface temperature reconstructions. *Geochimica et Cosmochimica Acta* 74, 4639-4654.

Kirk, D.N., Shaw, P.M., 1975. Backbone rearrangements of steroidal 5-enes. *Journal of the Chemical Society, Perkin Transactions 1*, 2284-2294.

Knapp, A.N., Hastings, M.G., Sigman, D.M., Lipschultz, F., Galloway, J.N., 2010. The flux and isotopic composition of reduced and total nitrogen in Bermuda rain. *Marine Chemistry* 120, 83-89.

Lao, Y., Korth, J., Ellis, J., Crisp, P., 1989. Heterogeneous reactions of 1-pristene catalysed by clays under simulated geological conditions. *Organic Geochemistry* 14, 375-379.

Larsen, H., Saunders, A., Clift, P., Beget, J., Wei, W., Spezzaferri, S., Ali, J., Cambray, H., Demant, A., Fitton, G., 1994. Seven million years of glaciation in Greenland. *Science-AAAS-Weekly Paper Edition-including Guide to Scientific Information* 264, 952-954.

Lawver, L.A., Gahagan, L.M., Coffin, M.F., 1992. The development of paleoseaways around Antarctica. *The Antarctic Paleoenvironment: A Perspective on Global Change: Part One*, 7-30.

Leider, A., Hinrichs, K.-U., Mollenhauer, G., Versteegh, G.J., 2010. Core-top calibration of the lipid-based and TEX 86 temperature proxies on the southern Italian shelf (SW Adriatic Sea, Gulf of Taranto). *Earth and Planetary Science Letters* 300, 112-124.

Licht, A., Van Cappelle, M., Abels, H., Ladant, J.-B., Trabucho-Alexandre, J., France-Lanord, C., Donnadieu, Y., Vandenberghe, J., Rigaudier, T., Lécuyer, C., 2014. Asian monsoons in a late Eocene greenhouse world. *Nature* 513, 501-506.

Liu, Z., Pagani, M., Zinniker, D., DeConto, R., Huber, M., Brinkhuis, H., Shah, S.R., Leckie, R.M., Pearson, A., 2009. Global cooling during the Eocene-Oligocene climate transition. *Science* 323, 1187-1190.

Lu, H., Fulthorpe, C.S., Mann, P., Kominz, M.A., 2005. Miocene–Recent tectonic and climatic controls on sediment supply and sequence stratigraphy: Canterbury basin, New Zealand. *Basin Research* 17, 311-328.

Mackenzie, A., Patience, R., Maxwell, J., Vandenbroucke, M., Durand, B., 1980. Molecular parameters of maturation in the Toarcian shales, Paris Basin, France—I. Changes in the configurations of acyclic isoprenoid alkanes, steranes and triterpanes. *Geochimica et Cosmochimica Acta* 44, 1709-1721.

Martin, H., 2006. Cenozoic climatic change and the development of the arid vegetation in Australia. *Journal of Arid Environments* 66, 533-563.

McKay, R., Naish, T., Carter, L., Riesselman, C., Dunbar, R., Sjunneskog, C., Winter, D., Sangiorgi, F., Warren, C., Pagani, M., 2012. Antarctic and Southern Ocean influences on Late Pliocene global cooling. *Proceedings of the National Academy of Sciences* 109, 6423-6428.

Mercer, J.H., Sutter, J.F., 1982. Late Miocene—earliest Pliocene glaciation in southern Argentina: implications for global ice-sheet history. *Palaeogeography, Palaeoclimatology, Palaeoecology* 38, 185-206.

Meybeck, M., 1982. Carbon, nitrogen, and phosphorus transport by world rivers. *Am. J. Sci* 282, 401-450.

Meyers, P.A., 1997. Organic geochemical proxies of paleoceanographic, paleolimnologic, and paleoclimatic processes. *Organic Geochemistry* 27, 213-250.

Meyers, P.A., 2003. Applications of organic geochemistry to paleolimnological reconstructions: a summary of examples from the Laurentian Great Lakes. *Organic Geochemistry* 34, 261-289.

Meyers, P.A., Ishiwatari, R., 1993a. The Early Diagenesis of Organic Matter in Lacustrine Sediments, in: Engel, M., Macko, S. (Eds.), Organic Geochemistry. Springer US, pp. 185-209.
Meyers, P.A., Ishiwatari, R., 1993b. Lacustrine organic geochemistry—an overview of indicators of organic matter sources and diagenesis in lake sediments. *Organic Geochemistry* 20, 867-900.

Mildenhall, D., 2003. Deep-sea record of Pliocene and Pleistocene terrestrial palynomorphs from offshore eastern New Zealand (ODP Site 1123, Leg 181). *New Zealand Journal of Geology and Geophysics* 46, 343-361.

Mille, G., Asia, L., Guiliano, M., Malleret, L., Doumenq, P., 2007. Hydrocarbons in coastal sediments from the Mediterranean sea (Gulf of Fos area, France). *Marine Pollution Bulletin* 54, 566-575.

Miller, K.G., Browning, J.V., Aubry, M.-P., Wade, B.S., Katz, M.E., Kulpecz, A.A., Wright, J.D., 2008. Eocene–Oligocene global climate and sea-level changes: St. Stephens Quarry, Alabama. *Geological Society of America Bulletin* 120, 34-53.

Miller, K.G., Kominz, M.A., Browning, J.V., Wright, J.D., Mountain, G.S., Katz, M.E., Sugarman, P.J., Cramer, B.S., Christie-Blick, N., Pekar, S.F., 2005. The Phanerozoic record of global sea-level change. *Science* 310, 1293-1298.

Moldowan, J.M., Seifert, W.K., Gallegos, E.J., 1985. Relationship between petroleum composition and depositional environment of petroleum source rocks. *AAPG bulletin* 69, 1255-1268.

Moldowan, J.M., Sundararaman, P., Schoell, M., 1986. Sensitivity of biomarker properties to depositional environment and/or source input in the Lower Toarcian of SW-Germany. *Organic Geochemistry* 10, 915-926.

Müller, P.J., Kirst, G., Ruhland, G., Von Storch, I., Rosell-Melé, A., 1998. Calibration of the alkenone paleotemperature index U 37 K′ based on core-tops from the eastern South Atlantic and the global ocean (60 N-60 S). *Geochimica et Cosmochimica Acta* 62, 1757-1772.

Murray, A.P., Sosrowidjojo, I.B., Alexander, R., Kagi, R.I., Norgate, C.M., Summons, R.E., 1997. Oleananes in oils and sediments: Evidence of marine influence during early diagenesis? *Geochimica et Cosmochimica Acta* 61, 1261-1276.

Murray, A.P., Summons, R.E., Boreham, C.J., Dowling, L.M., 1994. Biomarker and n-alkane isotope profiles for Tertiary oils: relationship to source rock depositional setting. *Organic Geochemistry* 22, 521IN525-542IN526.

Nelson, C.S., Cooke, P.J., 2001a. History of oceanic front development in the New Zealand sector of the Southern Ocean during the Cenozoic—a synthesis. *New Zealand Journal of Geology and Geophysics* 44, 535-553.

Nelson, C.S., Cooke, P.J., 2001b. History of oceanic front development in the New Zealand sector of the Southern Ocean during the Cenozoic - a synthesis. *New Zealand Journal of Geology and Geophysics* 44, 535-553.

Nishimura, M., Baker, E.W., 1986. Possible origin of n-alkanes with a remarkable even-to-odd predominance in recent marine sediments. *Geochimica et Cosmochimica Acta* 50, 299-305.

Norris, R., Turner, S.K., Hull, P., Ridgwell, A., 2013. Marine ecosystem responses to Cenozoic global change. *Science* 341, 492-498.

Nuzzo, M., Elvert, M., Schmidt, M., Scholz, F., Reitz, A., Hinrichs, K.-U., Hensen, C., 2012. Impact of hot fluid advection on hydrocarbon gas production and seepage in mud volcano sediments of thick Cenozoic deltas. *Earth and Planetary Science Letters* 341, 139-157.

Ourisson, G., Albrecht, P., Rohmer, M., 1984. Microbial origin of fossil fuels. *Sci. Am.;(United States)* 251.

Ourisson, G., Rohmer, M., Poralla, K., 1987. Microbial lipids betrayed by their fossils. *Microbiological sciences* 4, 52-57.

Pagani, M., Arthur, M.A., Freeman, K.H., 1999. Miocene evolution of atmospheric carbon dioxide. *Paleoceanography* 14, 273-292.

Passchier, S., Bohaty, S., Jiménez-Espejo, F., Pross, J., Röhl, U., Flierdt, T., Escutia, C., Brinkhuis, H., 2013. Early Eocene to middle Miocene cooling and aridification of East Antarctica. *Geochemistry, Geophysics, Geosystems* 14, 1399-1410.

Peters, K.E., Moldowan, J.M., 1993. The biomarker guide : interpreting molecular fossils in petroleum and ancient sediments. Prentice Hall, Englewood Cliffs, N.J.
Peters, K.E., Walters, C.C., Moldowan, J.M., 2005. The biomarker guide, 2nd ed. Cambridge University Press, Cambridge, UK ; New York.
Poage, M., Chamberlain, C., 2002. Stable isotopic evidence for a pre-Middle Miocene rain shadow in the western Basin and Range: Implications for the paleotopography of the Sierra Nevada. *Tectonics* 21.

Pocknall, D.T., 1989. Late Eocene to Early Miocene vegetation and climate history of New Zealand. *Journal of the Royal Society of New Zealand* 19, 1-18.

Powell, T., McKirdy, D., 1973. Relationship between ratio of pristane to phytane, crude oil composition and geological environment in Australia. *Nature* 243, 37-39.

Prahl, F.G., Coble, P.G., 1994. Input and behavior of dissolved organic carbon in the Columbia River Estuary. *Changes in Fluxes in Estuaries: Implications from Science to Management*, 451-457.

Prahl, F.G., Ertel, J.R., Goni, M.A., Sparrow, M.A., Eversmeyer, B., 1994. Terrestrial Organic-Carbon Contributions to Sediments on the Washington Margin. *Geochimica et Cosmochimica Acta* 58, 3035-3048.

Prell, W., Kutzbach, J.E., 1992. Sensitivity of the Indian monsoon to forcing parameters and implications for ‘its evolution. *Nature* 360, 17.

Pross, J., Contreras, L., Bijl, P.K., Greenwood, D.R., Bohaty, S.M., Schouten, S., Bendle, J.A., Röhl, U., Tauxe, L., Raine, J.I., 2012. Persistent near-tropical warmth on the Antarctic continent during the early Eocene epoch. *Nature* 488, 73-77.

Quade, J., Cerling, T.E., Bowman, J.R., 1989. Development of Asian monsoon revealed by marked ecological shift during the latest Miocene in northern Pakistan. *Nature* 342, 163-166.

Radke, M., Welte, D., Willsch, H., 1986. Maturity parameters based on aromatic hydrocarbons: influence of the organic matter type. *Organic Geochemistry* 10, 51-63.

Reichgelt, T., Kennedy, E.M., Conran, J.G., Mildenhall, D.C., Lee, D.E., 2015. The early Miocene paleolake Manuherikia: vegetation heterogeneity and warm-temperate to subtropical climate in southern New Zealand. *Journal of Paleolimnology* 53, 349-365.

Retallack, G.J., 2004. Late Miocene climate and life on land in Oregon within a context of Neogene global change. *Palaeogeography, Palaeoclimatology, Palaeoecology* 214, 97-123.

Retallack, G.J., 2009. Refining a pedogenic-carbonate CO 2 paleobarometer to quantify a middle Miocene greenhouse spike. *Palaeogeography, Palaeoclimatology, Palaeoecology* 281, 57-65.

Rohling, E.J., Cooke, S., 1999. Stable oxygen and carbon isotopes in foraminiferal carbonate shells, Modern foraminifera. Springer, pp. 239-258.
Rontani, J.-F., Nassiry, M., Michotey, V., Guasco, S., Bonin, P., 2010. Formation of pristane from α-tocopherol under simulated anoxic sedimentary conditions: A combination of biotic and abiotic degradative processes. *Geochimica et Cosmochimica Acta* 74, 252-263.

Rowland, S., 1990. Production of acyclic isoprenoid hydrocarbons by laboratory maturation of methanogenic bacteria. *Organic Geochemistry* 15, 9-16.

Rubinstein, I., Sieskind, O., Albrecht, P., 1975. Rearranged sterenes in a shale: occurrence and simulated formation. *Journal of the Chemical Society, Perkin Transactions 1*, 1833-1836.

Saliot, A., 1981. Natural Hydrocarbons in Sea Water Alain Saliot. *Elsevier Oceanography Series* 31, 327-374.

Saliot, A., Denant, V., Bigot, M., 1998. Organic matter in large Chinese rivers and their estuaries: the Changjiang River and the Huanghe River. *Land-Sea Interaction in Chinese Coastal Zones. Ocean Press, Beijing*, 176-191.

Schouten, S., Hopmans, E.C., Damsté, J.S.S., 2004. The effect of maturity and depositional redox conditions on archaeal tetraether lipid palaeothermometry. *Organic Geochemistry* 35, 567-571.

Schouten, S., Hopmans, E.C., Damsté, J.S.S., 2013. The organic geochemistry of glycerol dialkyl glycerol tetraether lipids: a review. *Organic Geochemistry* 54, 19-61.

Seifert, W., Moldowan, J., 1986. Use of biological markers in petroleum exploration. *Methods in geochemistry and geophysics* 24, 261-290.

Seifert, W.K., Moldowan, J.M., 1978. Applications of steranes, terpanes and monoaromatics to the maturation, migration and source of crude oils. *Geochimica et Cosmochimica Acta* 42, 77-95.

Seifert, W.K., Moldowan, J.M., 1980. The effect of thermal stress on source-rock quality as measured by hopane stereochemistry. *Physics and Chemistry of the Earth* 12, 229-237.

Seki, O., Nakatsuka, T., Shibata, H., Kawamura, K., 2010. A compound-specific n-alkane δ13C and δD approach for assessing source and delivery processes of terrestrial organic matter within a forested watershed in northern Japan. *Geochimica et Cosmochimica Acta* 74, 599-613.

Seki, O., Schmidt, D.N., Schouten, S., Hopmans, E.C., Sinninghe Damsté, J.S., Pancost, R.D., 2012. Paleoceanographic changes in the Eastern Equatorial Pacific over the last 10 Myr. *Paleoceanography* 27.

Shackleton, N.J., Kennett, J.P., 1975. Paleotemperature history of the Cenozoic and the initiation of Antarctic glaciation: oxygen and carbon isotope analyses in DSDP Sites 277, 279, and 281. *Initial reports of the deep sea drilling project* 29, 743-755.

Shevenell, A.E., Kennett, J.P., Lea, D.W., 2004. Middle Miocene southern ocean cooling and Antarctic cryosphere expansion. *Science* 305, 1766-1770.

Simoneit, B.R., 1977. Diterpenoid compounds and other lipids in deep-sea sediments and their geochemical significance. *Geochimica et Cosmochimica Acta* 41, 463-476.

Sniderman, J.K., Woodhead, J.D., Hellstrom, J., Jordan, G.J., Drysdale, R.N., Tyler, J.J., Porch, N., 2016. Pliocene reversal of late Neogene aridification. *Proceedings of the National Academy of Sciences* 113, 1999-2004.

Sonzogni, C., Bard, E., Rostek, F., Dollfus, D., Rosell-Melé, A., Eglinton, G., 1997. Temperature and salinity effects on alkenone ratios measured in surface sediments from the Indian Ocean. *Quaternary Research* 47, 344-355.

Steinke, S., Groeneveld, J., Johnstone, H., Rendle-Bühring, R., 2010. East Asian summer monsoon weakening after 7.5 Ma: Evidence from combined planktonic foraminifera Mg/Ca and δ 18 O (ODP Site 1146; northern South China Sea). *Palaeogeography, Palaeoclimatology, Palaeoecology* 289, 33-43.

Stephens, N.P., Carroll, A.R., 1999. Salinity stratification in the Permian Phosphoria sea; a proposed paleoceanographic model. *Geology* 27, 899-902.

Sykes, R., 2004. Peat biomass and early diagenetic controls on the paraffinic oil potential of humic coals, Canterbury Basin, New Zealand. *Petroleum Geoscience* 10, 283-303.

Tesdal, J.-E., Galbraith, E., Kienast, M., 2013. Nitrogen isotopes in bulk marine sediment: linking seafloor observations with subseafloor records. *Biogeosciences* 10, 101.

Thiede, J., Winkler, A., Wolf-Welling, T., Eldholm, O., Myhre, A.M., Baumann, K.-H., Henrich, R., Stein, R., 1998. Late Cenozoic history of the polar North Atlantic: results from ocean drilling. *Quaternary Science Reviews* 17, 185-208.

Tierney, J.E., Tingley, M.P., 2014. A Bayesian, spatially-varying calibration model for the TEX 86 proxy. *Geochimica et Cosmochimica Acta* 127, 83-106.

Tierney, J.E., Tingley, M.P., 2015. A TEX86 surface sediment database and extended Bayesian calibration. *Scientific data* 2.

Tissot, B., Califet-Debyser, Y., Deroo, G., Oudin, J., 1971. Origin and evolution of hydrocarbons in early Toarcian shales, Paris Basin, France. *AAPG bulletin* 55, 2177-2193.

Van Sickel, W.A., Kominz, M.A., Miller, K.G., Browning, J.V., 2004. Late Cretaceous and Cenozoic sea-level estimates: backstripping analysis of borehole data, onshore New Jersey. *Basin Research* 16, 451-465.

Volkman, J.K., Maxwell, J.R., 1986. Acyclic isoprenoids as biological markers. *Methods in geochemistry and geophysics* 24, 1-42.

Wan, S., Kürschner, W.M., Clift, P.D., Li, A., Li, T., 2009. Extreme weathering/erosion during the Miocene Climatic Optimum: evidence from sediment record in the South China Sea. *Geophysical Research Letters* 36.

Wang, W., Zhou, Z.Y., Yu, P., 2005. Relations Between Vitrinite Reflectance, Peek Temperature and its Neighboring Temperature Variation Rate: A Comparison of Methods. *Chinese Journal of Geophysics* 48, 1443-1453.

Webster, P.J., Magana, V.O., Palmer, T., Shukla, J., Tomas, R., Yanai, M., Yasunari, T., 1998. Monsoons: Processes, predictability, and the prospects for prediction. *Journal of Geophysical Research: Oceans* 103, 14451-14510.

Weijers, J.W., Schouten, S., Spaargaren, O.C., Damsté, J.S.S., 2006. Occurrence and distribution of tetraether membrane lipids in soils: implications for the use of the TEX 86 proxy and the BIT index. *Organic Geochemistry* 37, 1680-1693.

Weijers, J.W.H., Schouten, S., Sluijs, A., Brinkhuis, H., Sinninghe Damsté, J.S., 2007. Warm arctic continents during the Palaeocene–Eocene thermal maximum. *Earth and Planetary Science Letters* 261, 230-238.

Whithead, J.M., 1973. The structure of petroleum pentacyclanes, in: Tissot, B.a., Bienner, F. (Eds.), Advances in Organic Geochemistry. Editions Technip, Paris, pp. 225-243.
Winkworth, R.C., Wagstaff, S.J., Glenny, D., Lockhart, P.J., 2002. Plant dispersal news from New Zealand. *Trends in Ecology & Evolution* 17, 514-520.

Wolfe, J.A., 1994a. An analysis of Neogene climates in Beringia. *Palaeogeography, Palaeoclimatology, Palaeoecology* 108, 207-216.

Wolfe, J.A., 1994b. Tertiary climatic changes at middle latitudes of western North America. *Palaeogeography, Palaeoclimatology, Palaeoecology* 108, 195-205.

Wood, R., Stagpoole, V., 2007. Validation of tectonic reconstructions by crustal volume balance: New Zealand through the Cenozoic. *Geological Society of America Bulletin* 119, 933-943.

You, Y., Huber, M., Müller, R., Poulsen, C., Ribbe, J., 2009. Simulation of the middle Miocene climate optimum. *Geophysical Research Letters* 36.

Youngblood, W., Blumer, M., 1973. Alkanes and alkenes in marine benthic algae. *Marine Biology* 21, 163-172.

Zachos, J., Pagani, M., Sloan, L., Thomas, E., Billups, K., 2001. Trends, rhythms, and aberrations in global climate 65 Ma to present. *Science* 292, 686-693.

Zachos, J.C., Dickens, G.R., Zeebe, R.E., 2008. An early Cenozoic perspective on greenhouse warming and carbon-cycle dynamics. *Nature* 451, 279-283.

Zhisheng, A., Kutzbach, J.E., Prell, W.L., Porter, S.C., 2001. Evolution of Asian monsoons and phased uplift of the Himalaya-Tibetan plateau since Late Miocene times. *Nature* 411, 62-66.

7.1. Appendix: chemical structure of analysed organic compounds and biomarkers

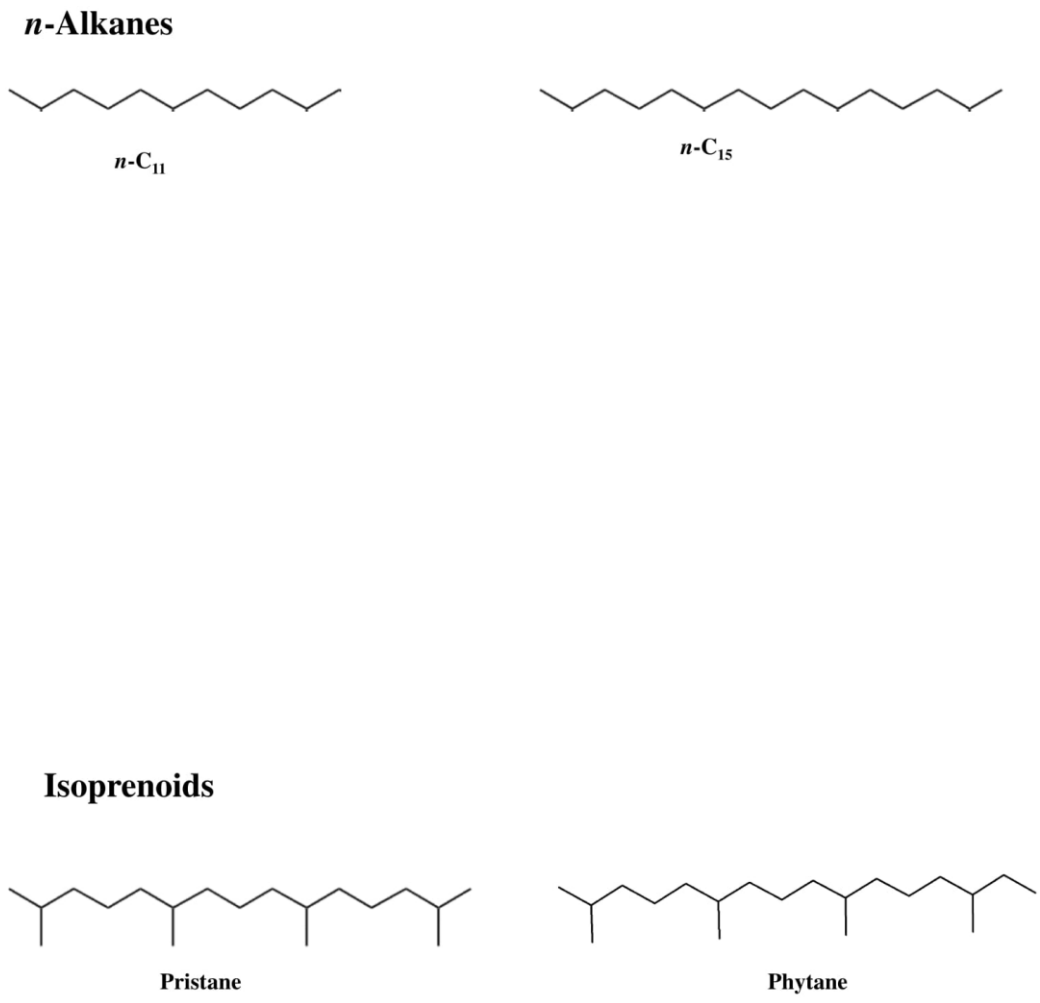

Fig. 7.1. 1: n-Alkanes and isoprenoids

Hopanes, tricyclic terpanes, and tetracyclic terpanes

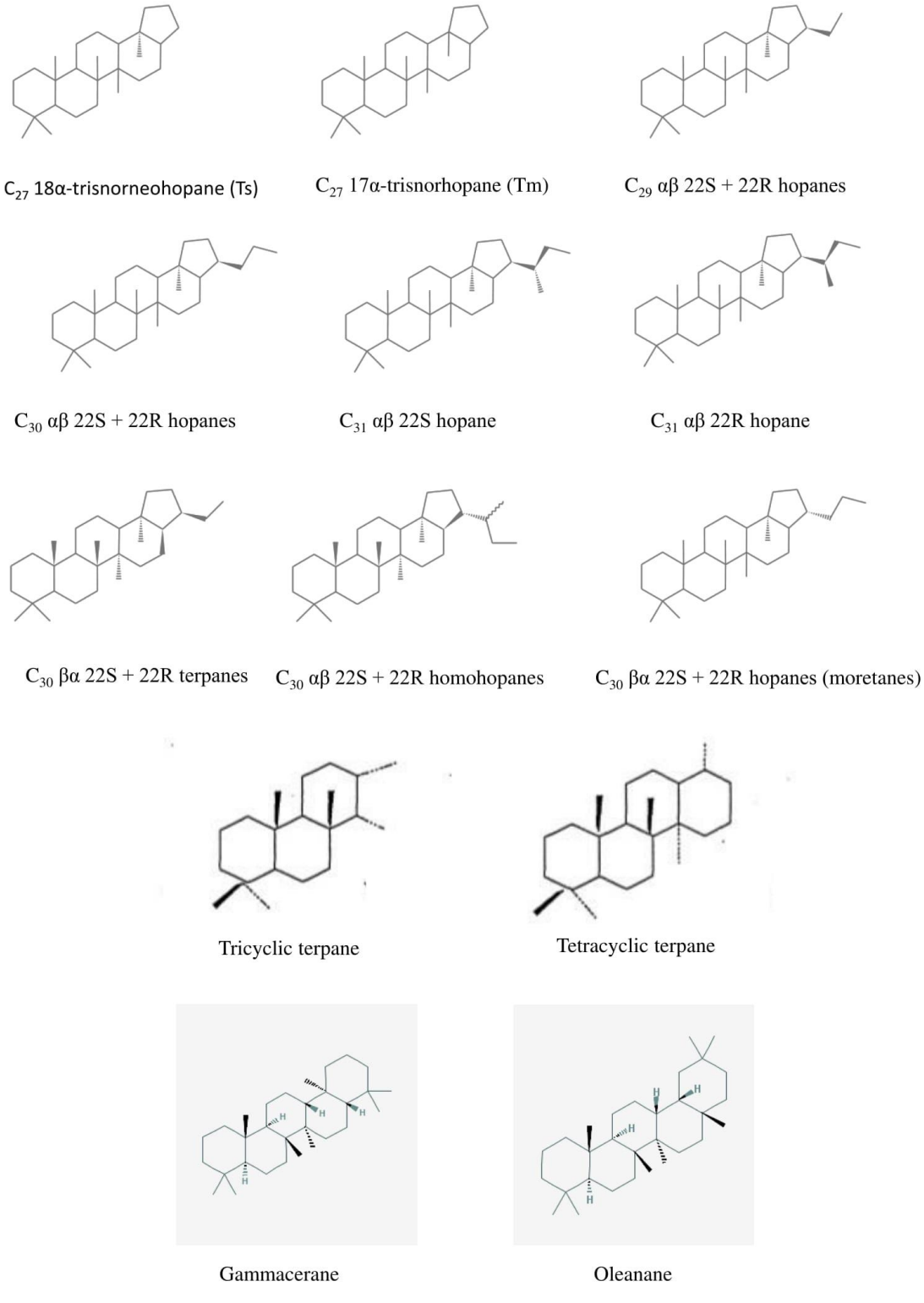

Fig. 7.1. 2: Hopanes, tricyclic terpanes, and tetracyclic terpanes

Steranes and diasteranes*

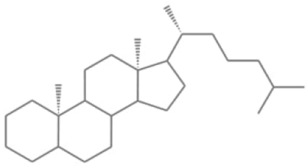

C_{27} 5α,14α,17α 20R sterane

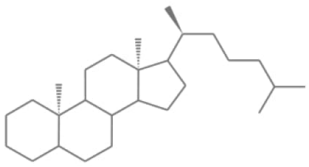

C_{27} 5α,14α,17α 20S sterane

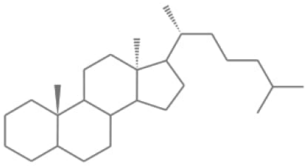

C_{27} 5α,14β,17 β 20R sterane

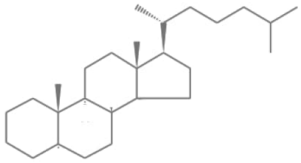

C_{27} 5α,14β,17 β 20S sterane

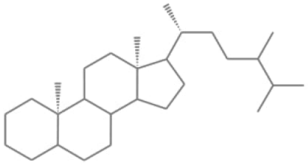

C_{28} 5α,14α,17α 20R sterane

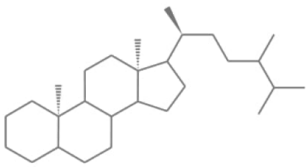

C_{28} 5α,14α,17α 20S sterane

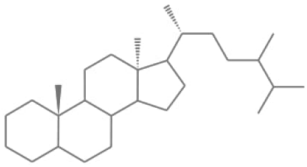

C_{28} 5α,14β,17 β 20R sterane

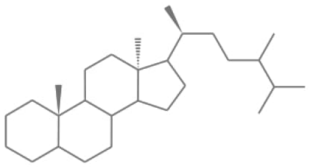

C_{28} 5α,14β,17 β 20S sterane

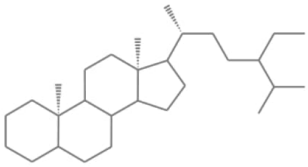

C_{29} 5α,14α,17α 20R sterane

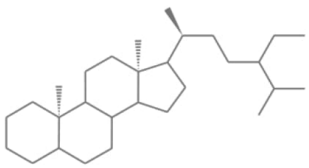

C_{29} 5α,14α,17α 20S sterane

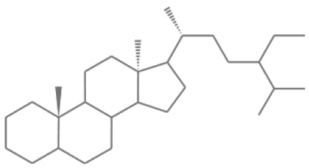

C_{29} 5α,14β,17 β 20R sterane

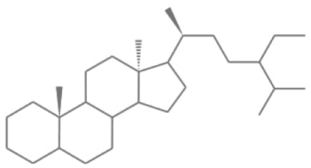

C_{29} 5α,14β,17 β 20S sterane

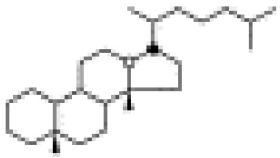

13α,17β 20S+20R diasterane

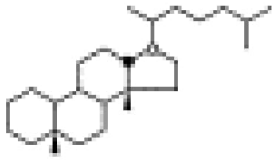

13β,17α 20S+20R diasterane

*Diasteranes (rearranged steranes) **-** The rearrangement involves migration of C-10 and C-13 methyl groups to C-5 and C-14 and is favored by acidic conditions, clay catalysis, and/or high temperatures.

Fig. 7.1. 3: Steranes and diasteranes

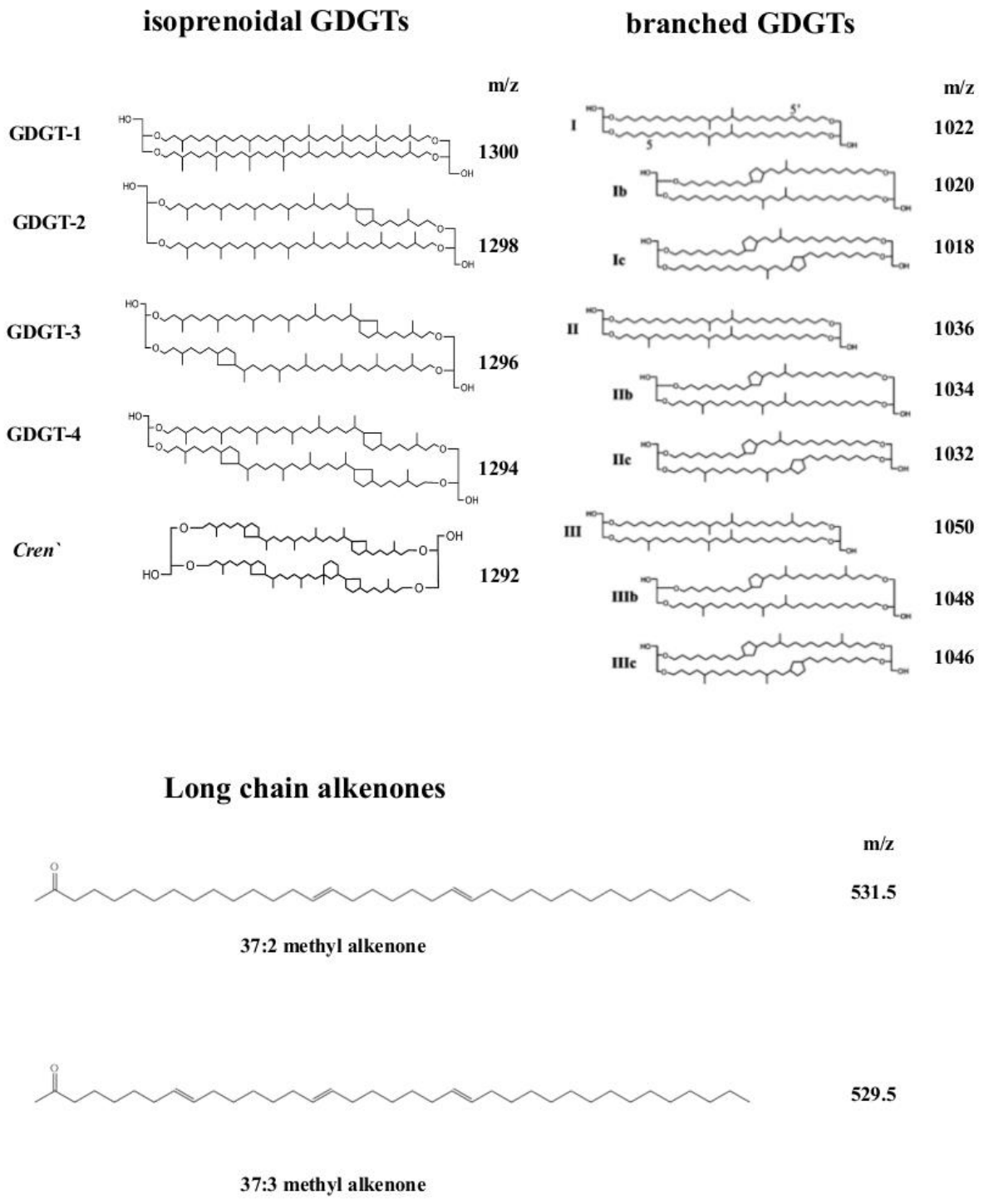

Fig. 7.1. 4: GDGTs and methyl alkenones

Polycyclic aromatic hydrocarbons (PAH)

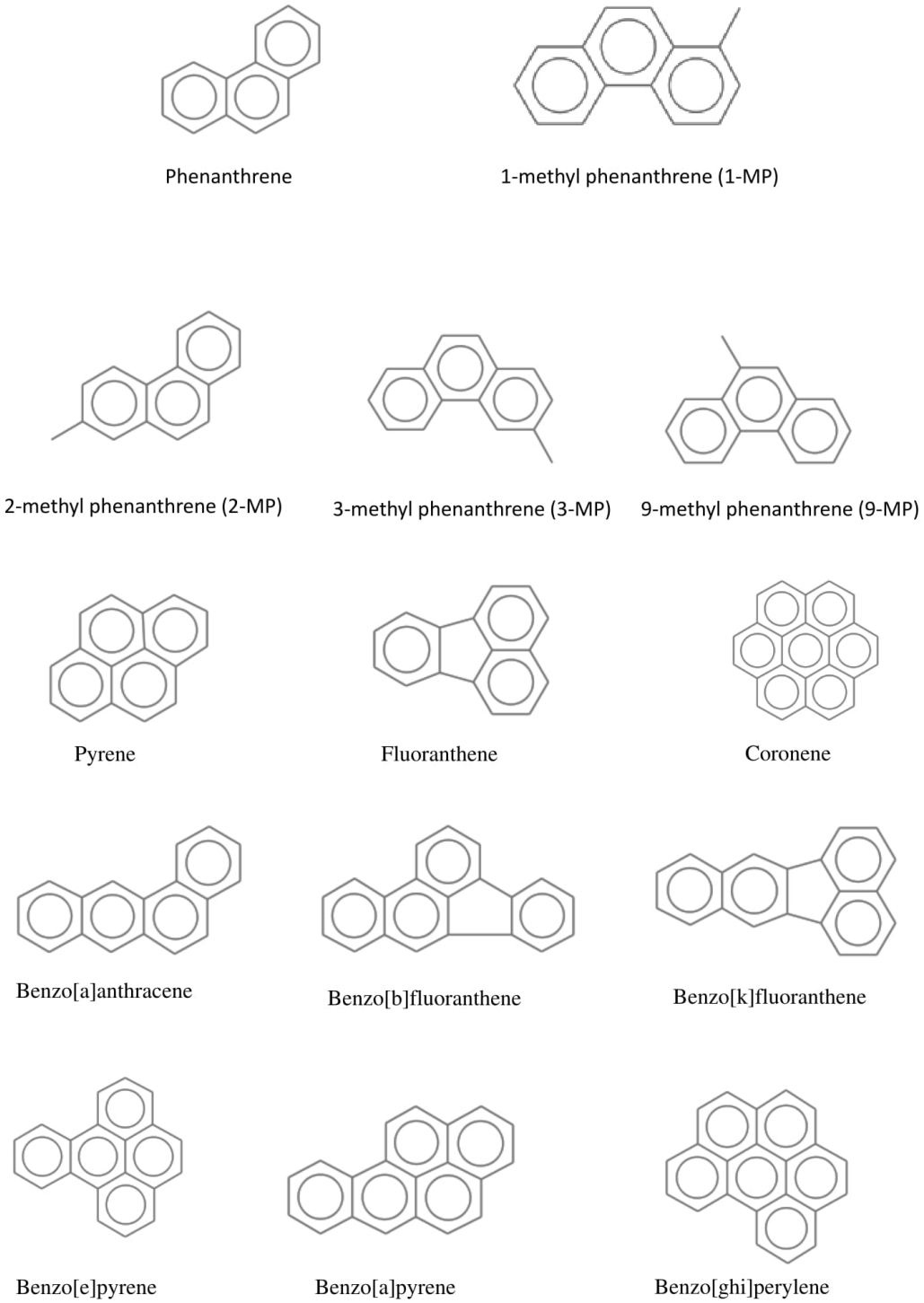

Fig. 7.1. 5: Polycyclic aromatic hydrocarbons (PAH)

7.2. Appendix: blanks

To insure lack of contamination of the results set of blank analyses was performed. Examples of the blank analyses are presented in this Appendix.

All organic solvents used during the extraction were analysed for organic contamination levels. From new bottle 100 ml of DCM, MeOH, and Hexane were concentrated to 100 µl. From the concentrated sample 1 µl was injected into GC-MS for organic analysis. The extraction was performed only when contamination levels were below the equipment detection limit (Fig. 7.2.1).

For the IODP 317 samples blank analysed involved solvent without sample that was run through all extraction stages. One blank sample was analysed for every eleven samples. The analysis was considering to be reliable when blank run showed no additional organic input during the extraction process (Fig. 7.2.2A). Some samples showed siloxane input into samples during the extraction (Fig. 7.2.2B). The siloxane derived to the sample from the pipette bulb used during the extraction or through the penetration of the GC-MS injection needle through the vial lid. Siloxane picks did not overlap any *n*-alkane or other biomarker picks in the analysed range. Therefore, this contamination was neglected during the analyses.

In addition, plastic wrap used for the sample storage was analysed (Fig. 7.2.2C). The results show presence of multiple sets of double and triple pics up to 50 min into analysis. These picks could overlap the *n*-alkane data in the same time period. In the samples were picks were identified their abundance was higher than the *n*-alkane signal. Therefore, the contamination was easily detected. These samples were not considered reliable for the discussion.

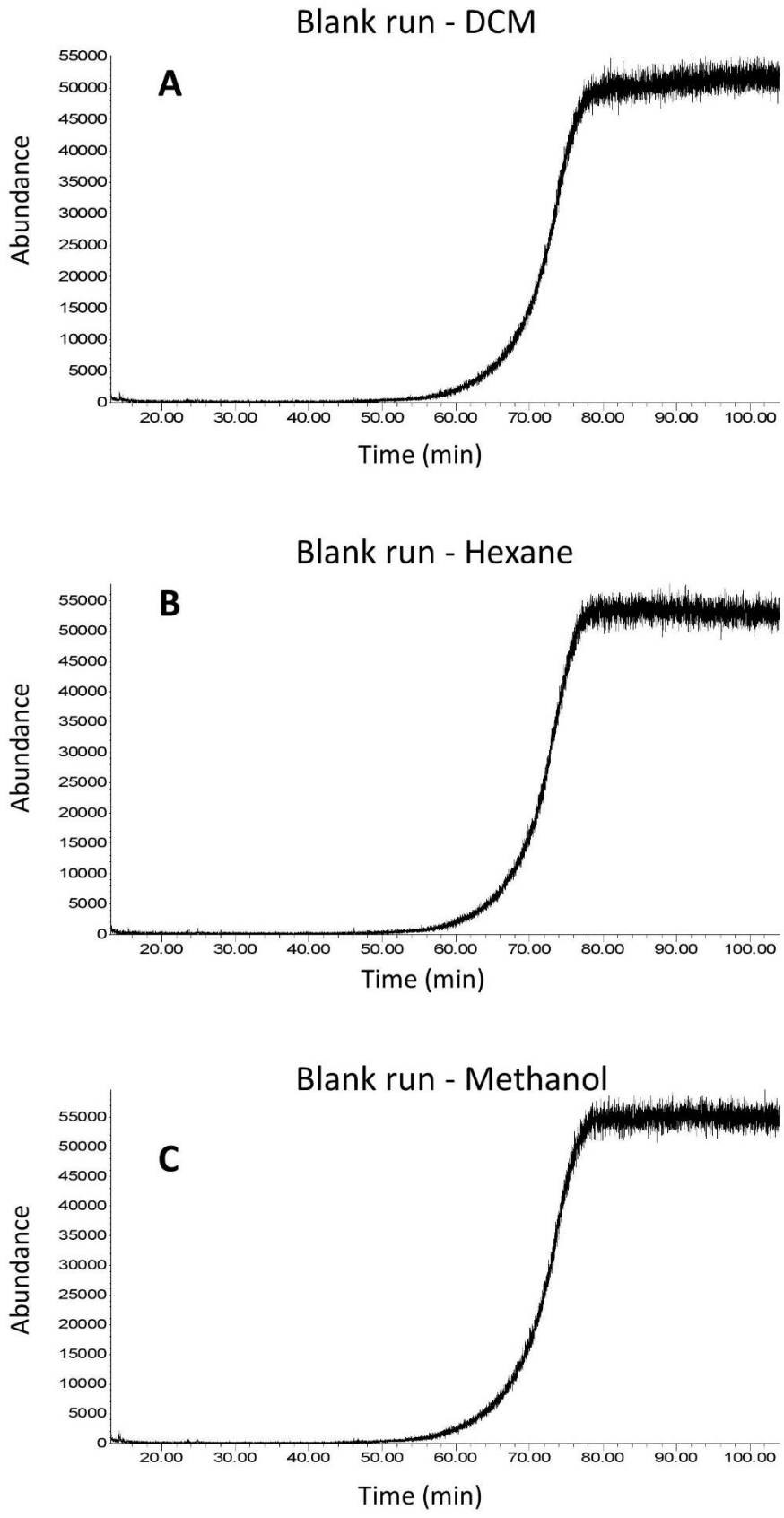

Fig. 7.2. 1: Solvent analysed where **A** – DCM, **B** – Hexane, and **C** – Methanol.

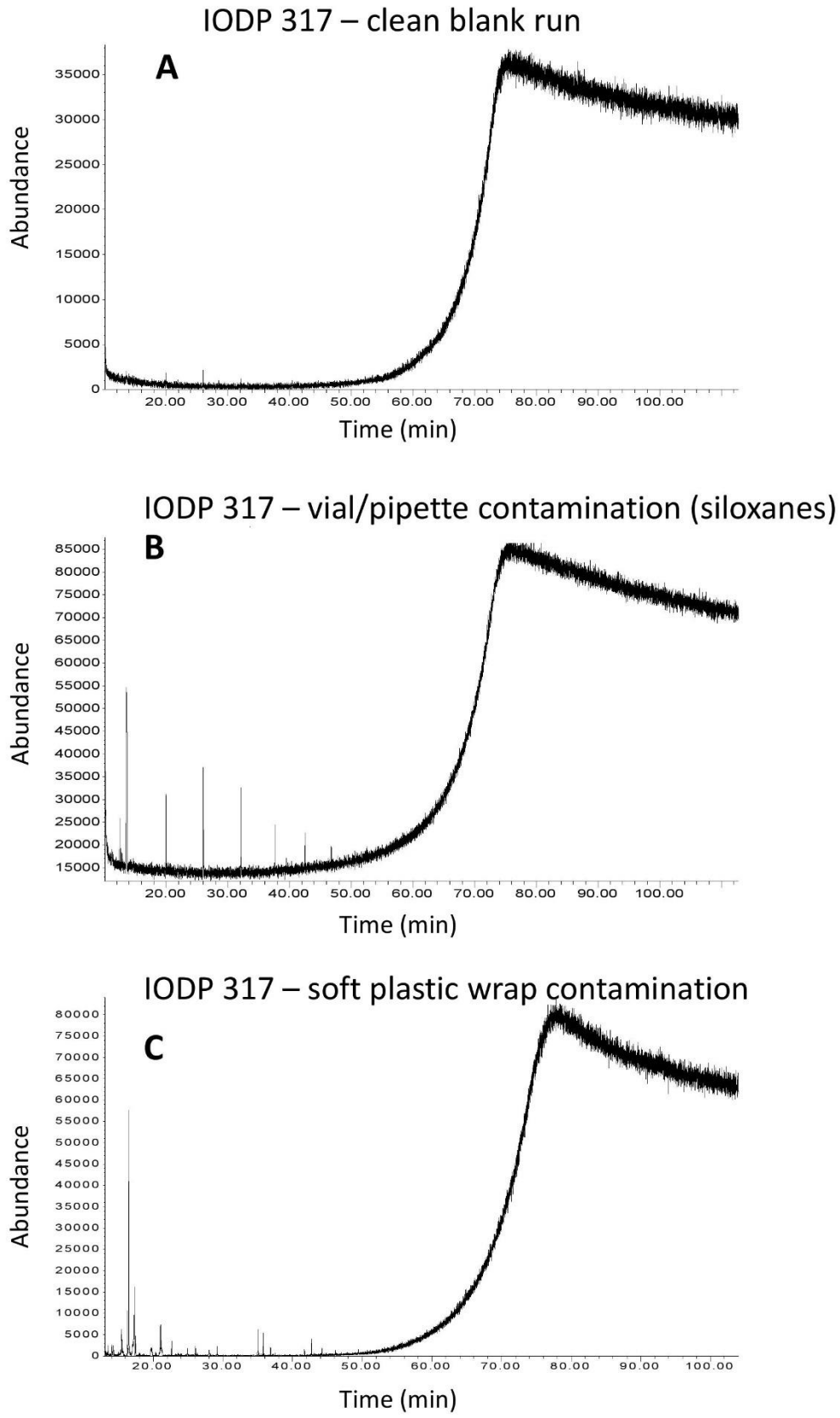

Fig. 7.2. 2: Results from the IODP 317 blank runs. **A** – solvent blank run; **B** – vial lid and pipette bulb analysis; **C** – sample plastic wrap analysis.

For the IODP 313 samples blank analyses involved solvent extraction without sample. One blank sample was analysed for every eleven samples. The analysis was considered to be reliable when blank run showed no additional organic input during the extraction process (Fig. 7.2.3B).

In addition, plastic wrap used for the sample storage was analysed (Fig. 7.2.3A). The results show presence of multiple sets of double and triple picks through all analytical run. These picks could overlap the *n*-alkane data in the samples. In the samples were picks were identified their abundance was higher than the *n*-alkane signal. Therefore, the contamination was easily detected. These samples were not considered reliable for the discussion.

Some blanks show high contamination of different short chain alkanes (up to C_9) in the sample (Fig. 7.2.3). After closer investigation, the same set of alkanes was identified in rotary evaporator system. Despite of high contamination levels the samples were consider to be reliable for *n*-alkane discussion in the range of C_{11} and higher.

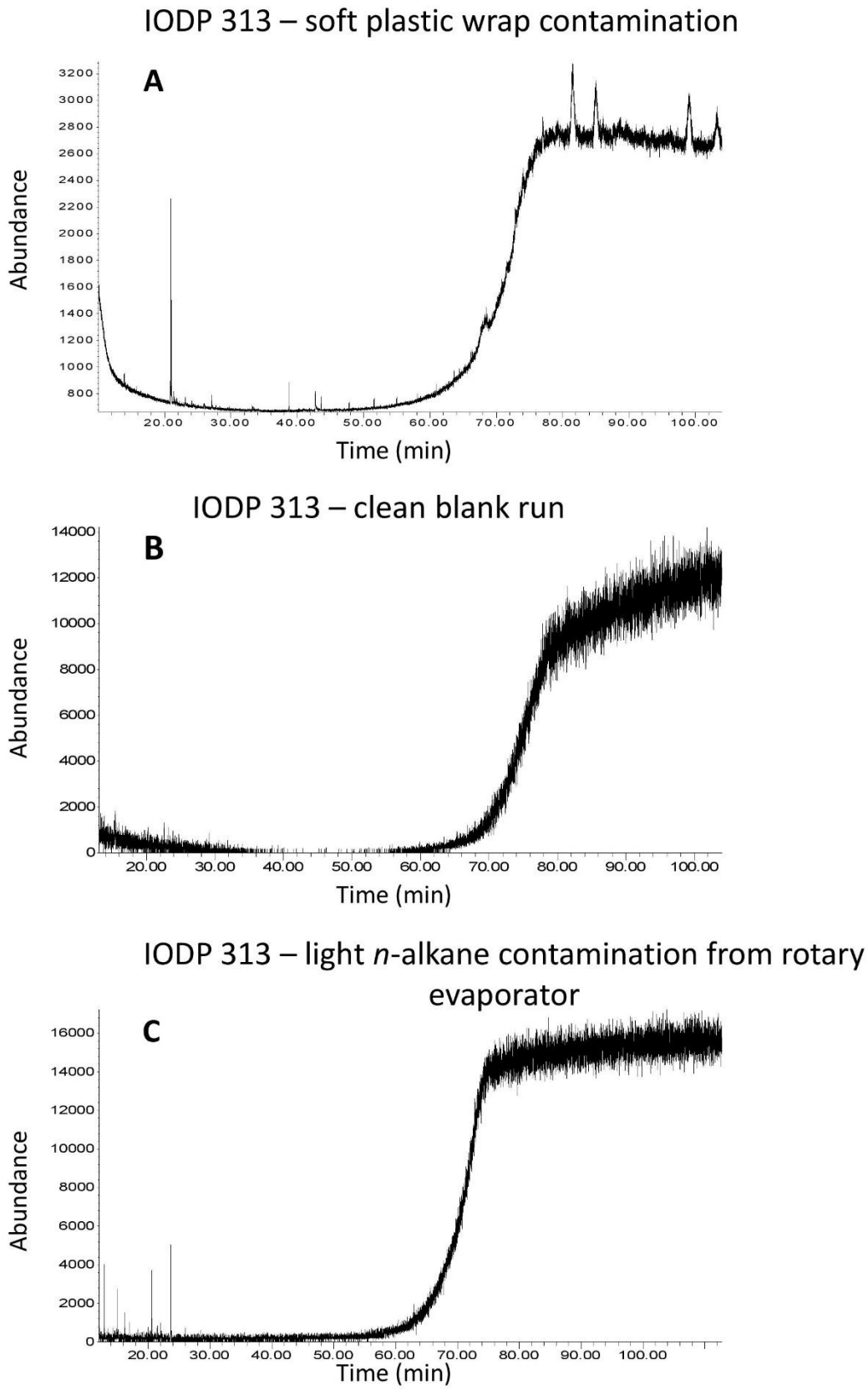

Fig. 7.2. 3: Results from the IODP 313 blank runs. **A** – sample plastic wrap analysis; **B** – solvent blank run; **C** – rotary evaporator light chain alkane input.

For the IODP 355 samples blank analyses involved solvent extraction without sample. One blank sample was analysed for every eleven samples. The analysis was considered to be reliable when blank run showed no additional organic input during the extraction process (Fig. 7.2.4C).

Some sedimentary samples were extracted on-board during the expedition. The sand used during the extraction process was analysed as well. In addition, every 11 samples a blank run was collected (Fig. 7.2.4.B). Only samples with sand blank contamination in the short alkanes (up to C_{10}) was consider to be reliable for analysis (Fig. 7.2.4A). The samples extracted in the laboratory when through the same blank check as IODP 317 and IODP 313 samples. Only samples with clean blank runs (Fig. 7.2.4C) were used in the discussion.

Plastic wrap used for the sample storage was analysed (Fig. 7.2.5). The results show presence of multiple sets of double and triple picks through all analytical run. These picks could overlap the *n*-alkane data in the samples. In the samples were picks were identified their abundance was higher than the *n*-alkane signal. Therefore, the contamination was easily detected. These samples were not considered reliable for the discussion.

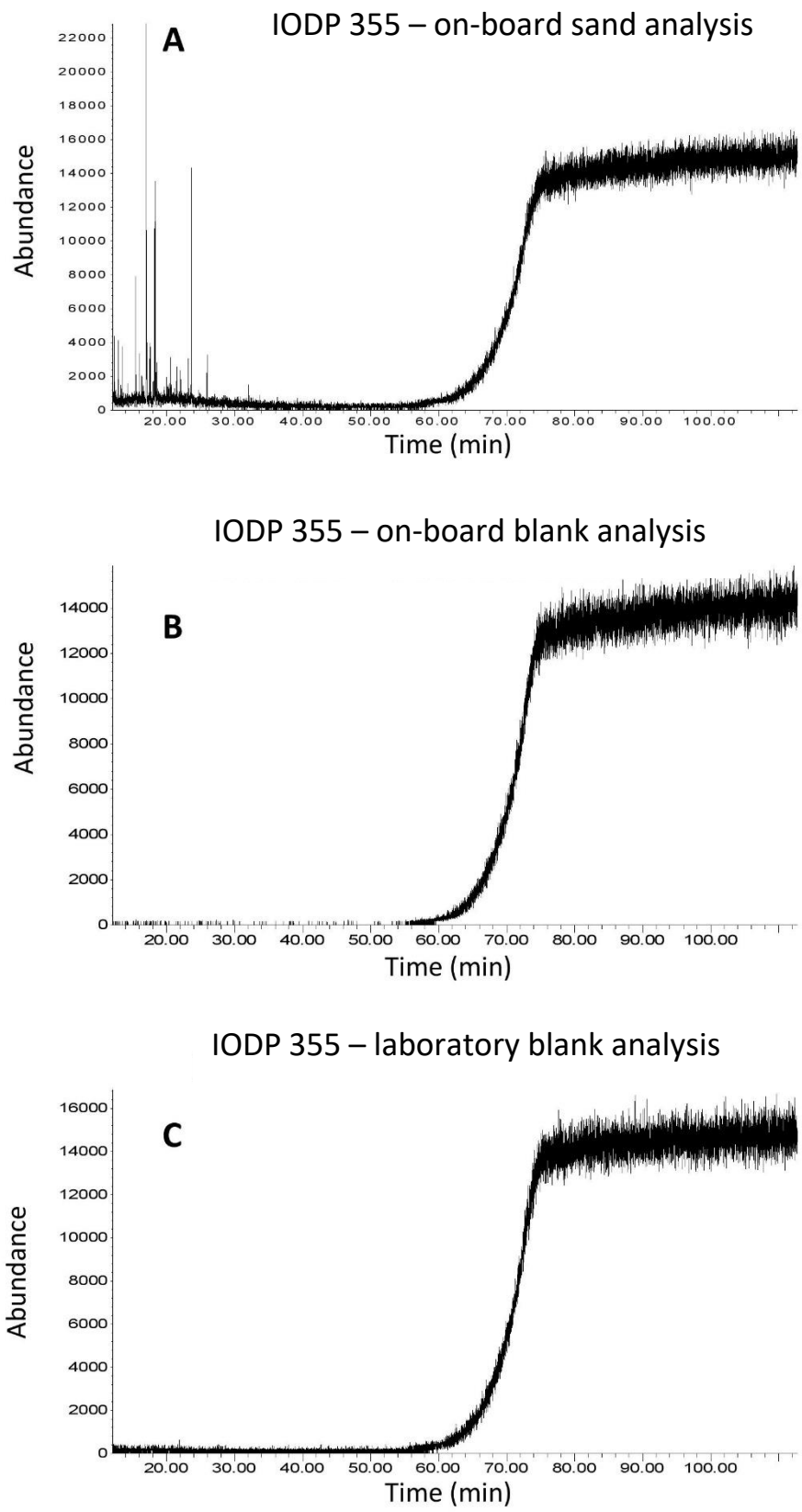

Fig. 7.2. 4: Results from the IODP 355 blank runs. A – blank run for on-board sand; B – blank run for on-board analysis; C – laboratory blank run.

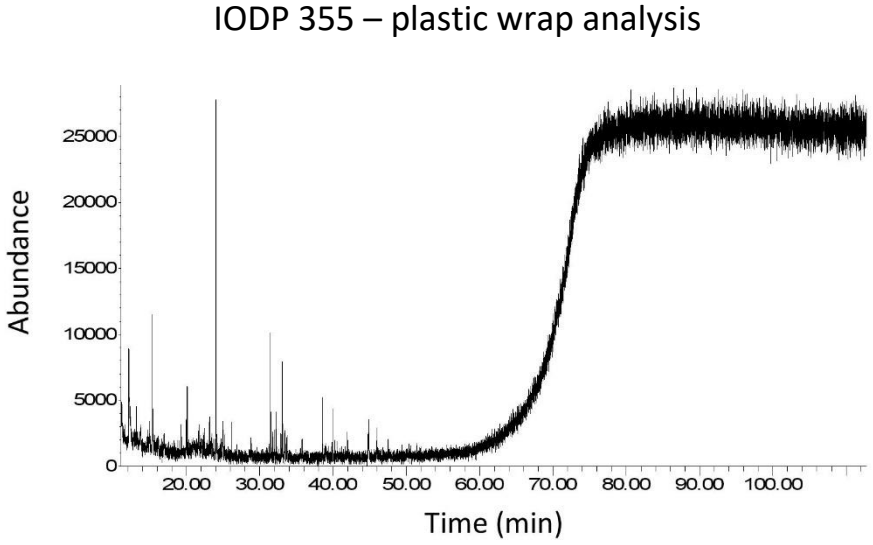

Fig. 7.2. 5: Results from the IODP 313 blank runs - sample plastic wrap analysis.

7.3.Appendix: conference presentations

The work discussed in a thesis is an outcome of collaborative research aiming to understand small part of the Earth's ocean-climate system. Sections of this thesis were presented at several local and international conferences. Accepted abstracts are presented below.

1. AOGC 2014 - the 18th Australian Organic Geochemistry Conference

Global Sea level changes or local tectonics? First Miocene biomarkers in cored sedimentary rocks from IODP Expedition 317, Canterbury Basin, New Zealand.

S. Bratenkov[1] & S.C. George[1]

1: Department of Earth and Planetary Sciences, Macquarie University,

North Ryde, Sydney, NSW 2109

Corresponding author email: Sophia.bratenkov@mq.edu.au

ABSTRACT

Integrated Ocean Drilling Program (IODP) Expedition 317 to the Canterbury Basin, on the eastern margin of the South Island of New Zealand, provided the opportunity to study sediment geochemistry in contrasting depositional settings, from mid-shelf to upper slope sedimentary rocks. The expedition recovered sediments from the Eocene to the Holocene. A particular research focus was on the sequence stratigraphy of the sedimentary package, which recorded a time when global sea level change was dominated by glacioeustasy. The main goal of this research was to provide the first organic geochemistry results for the cored Miocene sediments from this expedition. The comprehensive biomarker picture from these cores enables a better understanding of the organic matter origin and evolution in the Canterbury Basin, as well as the depositional and post-depositional processes involved.

Upper Eocene to Holocene sedimentary sequences were cored in a transect of three drilling sites on the continental shelf (Sites U1351, U1353 and U1354) and one on the continental slope (Site U1352). Overall, 72 samples were recovered from Miocene sediments in U1351, U1352 and U1353 for geochemical analysis including biomarker research. Thirteen of these were squeeze cakes, and the rest were cut spot samples.

Total organic carbon content for these samples is generally low (<1 wt. %), with only a few spot samples in U1352 having higher values. To determine the origin of the organic material, as well as the thermal maturity gradients in these three cores, hydrocarbons and biomarkers were extracted from 63 samples. All samples were solvent extracted using the Accelerated Solvent Extractor (ASE300), and the extractable organic matter (EOM) was fractionated into aliphatic hydrocarbons, aromatic hydrocarbons and polar compounds. Identification of organic compounds in the project was based mainly on gas chromatography-mass spectrometry (GC-MS). Relatively low amounts of EOM were detected. There is good preservation of C_{11} to C_{35} alkanes, with varying predominance of odd-over-even chain length long-chain n-alkanes ($CPI_{22\text{-}32}$) over the cores, with values between 0.2 and 4.8 (Figure 1). The Pr/Ph ratios (0.7-5.9) for all three cores indicate variable oxygenation conditions, from anoxic to oxic (Figure 1). Thermal maturities of the U1351 and U1352 core sediments were calculated using Pr/*n*-C_{17} (0.6-8.06) and Ph/*n*-C_{18} (0.3-2.8) ratios. These data indicate low thermal maturities (sub oil window) for all the Miocene cored samples. Some high Pr/*n*-C_{17} (e.g. 13.4) as well as high Ph/*n*-C_{18} (e.g. 3.8) ratios indicate possible biodegradation of the OM. Depositional environment was also determined by the abundance of C_{27}-C_{29} regular steranes in the samples, as well as the C_{30} sterane index and the C_{31}/C_{30} hopane ratio.

Varying inputs of organic matter were identified for the Miocene sediments in the cores. Acyclic biomarkers indicate probable marine biological input for the middle Miocene samples. Upper Miocene samples are predominantly defined by high terrigenous input. In addition, calculated wax indices for the Miocene sediments were between 0.1 – 2.8 for *n*-alkanes. These ratios suggest a primary marine depositional environment for the sediments, although the type of organic matter was likely often of terrestrial origin. The amount and distribution of the aromatic hydrocarbons suggest numerous origins of the organic matter, as well as diverse levels of biodegradation.

Current research provides a unique opportunity to explore the evolution of the biomarker input to marine sediments in the Canterbury Basin, New Zealand. These data may reflect changes in the OM input caused by changes in global sea level during the Early and Middle Miocene epochs. In addition, alteration in the sediment supply to the basin could have been triggered by the uplift of the Southern Alps during the Late Miocene period.

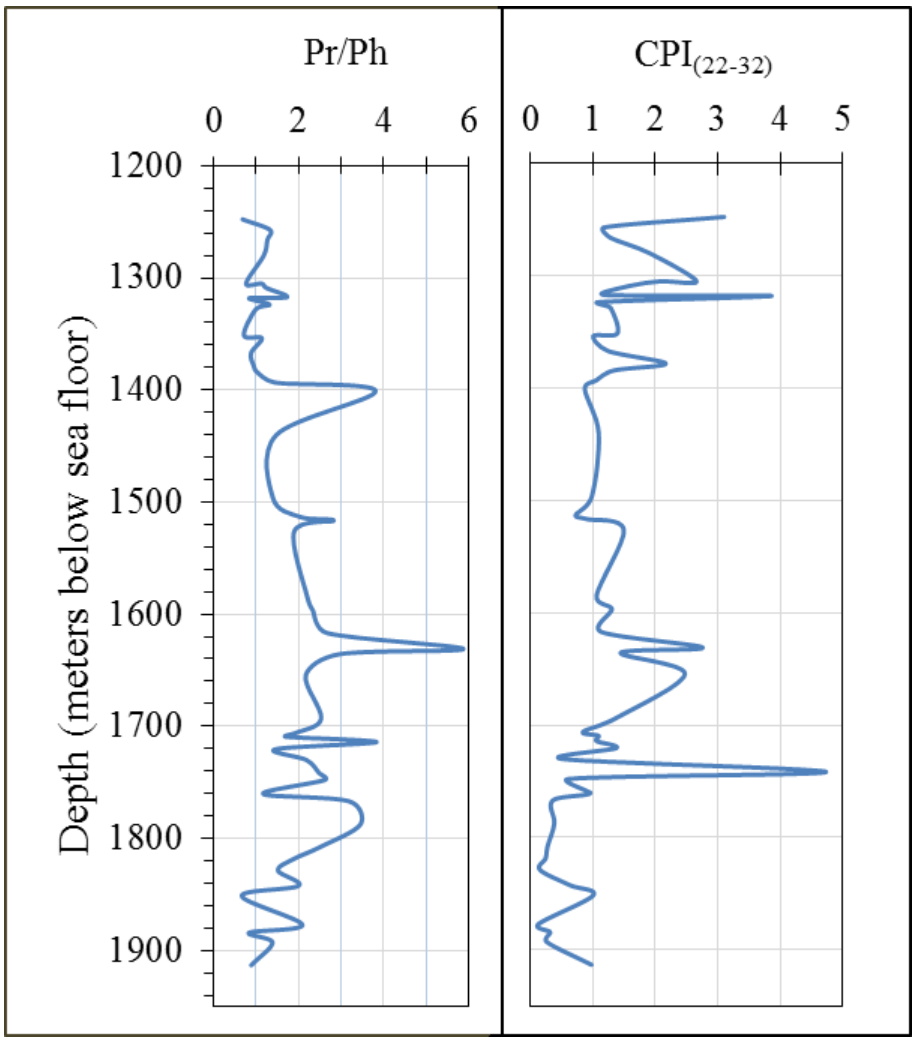

Figure 8: Oxicidy of depositional environment and organic matter input relative to depth in the continental slope core

2. TSOP2014 – The Society of Organic Petrology 34th Annual Meeting

Global Sea level changes or local tectonics? First Miocene biomarkers in cored sedimentary rocks from IODP Expedition 317, Canterbury Basin, New Zealand.

S. Bratenkov[1] & S.C. George[1]

1: Department of Earth and Planetary Sciences, Macquarie University

North Ryde, Sydney, NSW 2109

Corresponding author email: Sophia.bratenkov@mq.edu.au

ABSTRACT

Integrated Ocean Drilling Program (IODP) Expedition 317 to the Canterbury Basin, on the eastern margin of the South Island of New Zealand, provided the opportunity to study sediment geochemistry in contrasting depositional settings, from mid-shelf to upper slope sedimentary rocks. The expedition recovered sediments from the Eocene to the Holocene. A particular research focus was on the sequence stratigraphy of the sedimentary package, which recorded a time when global sea level change was dominated by glacioeustasy. The main goal of this research was to provide the first organic geochemistry results for the cored Miocene sediments from this expedition. The comprehensive biomarker picture from these cores enables a better understanding of the organic matter origin and evolution in the Canterbury Basin, as well as the depositional and post-depositional processes involved.

Upper Eocene to Holocene sedimentary sequences were cored in a transect of three drilling sites on the continental shelf (Sites U1351, U1353 and U1354) and one on the continental slope (Site U1352). Overall, 72 samples were recovered from Miocene sediments in U1351, U1352 and U1353 for geochemical analysis including biomarker research. Thirteen of these were squeeze cakes, and the rest were cut spot samples.

Total organic carbon content for these samples is generally low (<1 wt. %), with only a few spot samples in U1352 having higher values. To determine the origin of the organic material, as well as the thermal maturity gradients in these three cores, hydrocarbons and biomarkers were extracted from 63 samples. All samples were solvent extracted using the Accelerated Solvent Extractor (ASE300), and the extractable organic matter (EOM) was fractionated into aliphatic hydrocarbons, aromatic hydrocarbons and polar compounds. Identification of organic compounds in the project was based mainly on gas chromatography-mass spectrometry (GC-MS). Relatively low amounts of EOM were detected. There is good preservation of C_{11} to C_{35} alkanes, with a various predominance of odd-over-even chain length for long-chain n-alkanes ($CPI_{22\text{-}32}$) in different core depths with values between 0.8 and 3.9. The Pr/Ph ratios (0.6-5.9) for all three cores indicate variable oxygenation from anoxic to oxic conditions. Thermal maturities of the U1351 and U1352 core sediments were calculated using Pr/*n*-C_{17} (0.6-8.06) and Ph/*n*-C_{18} (0.3-2.8) ratios. These data indicate low thermal maturity with depth. High Pr/*n*-C_{17} (e.g. 13.4) as well as high Ph/*n*-C_{18} (e.g. 3.8) ratios indicate possible biodegradation of the OM. Depositional environment was also determined by the abundance of C_{27}-C_{29} regular steranes in the samples, as well as the C_{30} sterane index and the C_{31}/C_{30} hopane ratio.

Varying inputs of organic matter were identified for the Miocene sediments in the cores. Acyclic biomarkers indicate probable marine biological input for the middle Miocene samples. Upper Miocene samples predominantly were defined by high terrigenous input. In addition, calculated wax indices for the Miocene sediments were between 0.09-0.54 for n-alkanes. These ratios suggest a primary marine depositional environment for all the sediments, although the type of organic matter was likely often of terrestrial origin. The amount and distribution of the aromatic hydrocarbons suggest numerous origins of the organic matter, as well as diverse levels of biodegradation.

Current research provide a unique opportunity to explore evolution of the biomarker input to marine sediments in Canterbury Basin, New Zealand. These data may reflect changes in the OM input caused by alteration in the sediment supply to the basin triggered by the uplift of the Southern Alps.

Exploration of Miocene biomarkers in cored sedimentary rocks from IODP Expedition 317, Canterbury Basin, New Zealand

Sophia Bratenkov[1] and Simon C. George[1]

[1]Department of Earth and Planetary Sciences, Macquarie University, North Ryde, NSW 2109, Australia

Integrated Ocean Drilling Program (IODP) Expedition 317 to the Canterbury Basin, on the eastern margin of the South Island of New Zealand, provided the opportunity to study sediment geochemistry in contrasting depositional settings, from mid-shelf to upper slope sedimentary rocks. The expedition recovered sediments from the Eocene to the Holocene. A particular research focus was on the sequence stratigraphy of the sedimentary package, which recorded a time when global sea level change was dominated by glacioeustasy. The main goal of this research was to provide the first organic geochemistry results for the cored Miocene sediments from this expedition. The comprehensive biomarker picture from these cores enables a better understanding of the organic matter origin in the Canterbury Basin, as well as the depositional and post-depositional processes involved.

Upper Miocene to Holocene sedimentary sequences were cored in a transect of three drilling sites on the continental shelf (Sites U1354 and U1351) and one on the continental slope (Site U1352). Overall, 72 samples were recovered from Miocene sediments in U1351 and U1352 for geochemical analysis including biomarker research. Thirteen of these were squeeze cakes, and the rest were cut spot samples. Total organic carbon content for these samples is generally low (<1 wt %), with only a few spot samples in U1352 having higher values.

To determine the origin of the organic material, as well as the thermal maturity gradients in these three sites, hydrocarbons and biomarkers were extracted from 40 samples. Relatively low amounts of extractable organic matter (OM) were detected. There is good preservation of C_{11} to C_{34} alkanes, with a slight-moderate predominance of odd-over-even chain length for long-chain n-alkanes – the $CPI_{22\text{-}32}$ values are mainly between 1.09 and 1.77.

The Pr/Ph ratios (0.58-2.14) for all three cores indicate variable oxygenation from anoxic to suboxic conditions. Thermal maturities of the U1351 and U1352 core sediments were calculated using Pr/*n*-C_{17} (0.58-3.06) and Ph/*n*-C_{18} (0.3-1.9) ratios. These data indicate increasing thermal maturity with depth, as well as some possible biodegradation of the OM. Depositional environment can also be determined by the abundance of C_{27}-C_{29} regular steranes in the samples, as well as the C_{30} sterane index and the C_{31}/C_{30} hopane ratio.

Varying inputs of organic matter were identified for the Miocene sediments in the cores. Acyclic biomarkers indicate probable marine biological input for the middle Miocene samples. Upper Miocene samples predominantly were defined by high terrigenous input. In addition, calculated wax indices for the Miocene sediments were between 0.09-0.54 for n-alkanes. These ratios suggest a primary marine depositional environment for all the sediments, although the type of organic matter was likely often of terrestrial origin. The amount and distribution of the aromatic hydrocarbons suggest numerous origins of the organic matter, as well as diverse levels of biodegradation.

Preliminary results on the organic composition and thermal maturity of the Carboniferous Namoi Formation, northern NSW, Australia: a possible shale gas prospect?

Sophia Bratenkov[1] and Simon C. George[1]

[1]Department of Earth and Planetary Sciences, Macquarie University, North Ryde, NSW 2109, Australia

The Namoi Formation in the Werrie Syncline, north and west of Tamworth, is part of the well preserved Devonian-Carboniferous fore arc in the New England Fold Belt. The formation consists of olive-green mudstones with lenses of sandstone and oolitic limestone. Mudstone is the dominant rock in most parts of the sequence, which is between 640-914 meters thick. Thick, organic rich mudstones of sufficient thermal maturity are attracting plenty of attention as shale gas prospects, following the exponential take-up of shale gas in the USA. However, little has been published on the organic geochemistry of Palaeozoic sequences in NSW, excepting coal-related literature. The aim of this work is to present preliminary results from the first organic geochemistry research on the Devonian sediments at Keepit, northern NSW, Australia.

The organic matter (OM) from the Namoi Formation from different creeks in the Keepit area, Australia was solvent extracted. All five samples contain relatively low levels of OM (between 1.1-1.6 mg OM/g sediment). The results suggested good preservation of the aliphatic and aromatic hydrocarbon fractions, with no evidence of weathering or biodegradation. *n*-Alkanes from C_{15} to C_{36} are present in all samples, with strong long-chain carbon number predominance. The results suggest marine sources of OM with a low wax index (max 0.11) for *n*-alkanes, indicating low amounts of higher land plants. Carbon preference indices close to 1.0 values suggest the succession is highly thermally mature. A high thermal maturity is also indicated by the relatively low Pr/*n*-C_{17} (0.16-0.70) and Ph/*n*-C_{18} (0.48-1.51) ratios. Pr/Ph ratios between 0.71 and 0.76 indicate that the samples were deposited in an anoxic deposition environment. Some samples contains biomarkers suggestive of a marine depositional environment, including the C_{30} sterane index and the C_{31}/C_{30} hopane ratio. A bacterial source for some of the OM could be identified by the presence of tricyclic and tetracyclic terpanes.

Based on the distribution of aromatic hydrocarbons including alkylnaphthalenes and alkylphenanthrenes, the Namoi Formation samples are in the gas window. Based on calibration of the methylphenanthrene index (MPI) and other ratios with vitrinite reflectance, a calculated reflectance of about 2.1% was derived, which given a normal geothermal gradient would be equivalent to a maximum temperature for the formation during deepest burial of about 205°C, in the main part of the gas generating window. Various polynuclear aromatic hydrocarbons (PAH) were identified in the samples. A high thermal maturity is also supported by the dominance of PAHs over alkylated PAHs.

Based on these preliminary data, the Devonian Namoi Formation is a prospective shale gas source as it has been buried sufficiently to be well within the gas window. Where it is exposed at the surface gas will have been lost, but elsewhere it will be buried beneath other sediments and may still retain gas. Key exploration uncertainties include information on organic richness, lateral variation in thermal maturity, mineralogy, and porosity-permeability relationships.

5. IMOG2015 – International meeting of Organic Geochemists

Global sea level changes or local tectonics? First Miocene biomarkers in cored sedimentary rocks from IODP Expedition 317, Canterbury Basin, New Zealand

Sophia Bratenkov[1,*] and Simon C. George[1]

[1]Department of Earth and Planetary Sciences, Macquarie University, North Ryde, Sydney, NSW 2109 Australia

*(*corresponding author: sophia.bratenkov@mq.edu.au)*

The influence of global sea level (eustasy) and local tectonic changes on sedimentation processes in continental margin deposits is a fundamental part of sedimentary research. During the late Miocene to recent period global sea level change was dominated by glacioeustasy (Miller et al., 2005). Integrated Ocean Drilling Program (IODP) Expedition 317 to the Canterbury Basin, on the eastern margin of the South Island of New Zealand, provided a unique opportunity to study sediment geochemistry in contrasting depositional settings, from mid-shelf to upper slope, for the early Miocene to recent period.

Previous work suggested good preservation of low amounts of organic matter in some Miocene samples (George et al., 2011). The detected total organic carbon contents in Miocene samples was generally low (<1 wt. %), with only a few samples in U1352 having higher values (Expedition 317 Scientists, 2010). Here we report the first organic geochemical data for all Miocene sediments retrieved in IODP Expedition 317. Upper Eocene to Holocene sedimentary sequences were cored along a transect of the continental shelf (Sites U1351, U1353 and U1354) and the continental slope (Site U1352). Overall, 82 samples were recovered from Miocene sediments in U1351, U1352 and U1353 for geochemical and biomarker analysis. To determine the origin of the organic material, as well as the thermal maturity gradients in these three cores, all samples were solvent extracted using an Accelerated Solvent Extractor (ASE300), and the extractable organic matter (EOM) was fractionated into aliphatic hydrocarbons, aromatic hydrocarbons and polar compounds. The hydrocarbons were then analysed by GC-MS.

Relatively low amounts of EOM were detected in which good preservation of C_{11}–C_{35} alkanes was observed. The long-chain *n*-alkanes display varying odd-over-even predominance ($CPI_{22\text{-}32}$ = 0.2–4.8) while the pristane/phytane ratio (Pr/Ph = 0.7–5.9) indicates bottom water conditions ranged from anoxic to oxic (Fig. 1). Low thermal maturities (sub the start of the oil window) are suggested for all the Miocene core samples based on Pr/*n*-C_{17} (0.6–8.06) and Ph/*n*-C_{18} (0.3–2.8) ratios. Widely used hopane (Ts/(Ts+Tm)) and C_{29} ααα sterane (S/(S+R)) ratios support the low thermal maturity data.

The depositional environment was further constrained by relative abundances of the C_{27}–C_{29} regular steranes (Fig. 2), as well as the C_{30} sterane index, the oleanane index and the $C_{31}R/C_{30}$ hopane ratio. Predominantly the outer and inner continental shelf cores contain OM of shallow marine origin, whereas the continental slope core is dominated by OM of open marine origin. The distribution of aromatic hydrocarbons confirmed the diverse origins of the organic matter, and suggested various levels of biodegradation.

The biomarkers extracted from IODP Exp. 317 sediments provide the opportunity to explore the evolution of the organic input to marine sediments in the Canterbury Basin, New Zealand. These data may reflects changes in the OM input caused by global sea level fluctuations during the Early and Middle Miocene epochs. In addition, alteration in the sediment supply to the basin could have been triggered by local tectonics such as uplift of the Southern Alps during the Late Miocene.

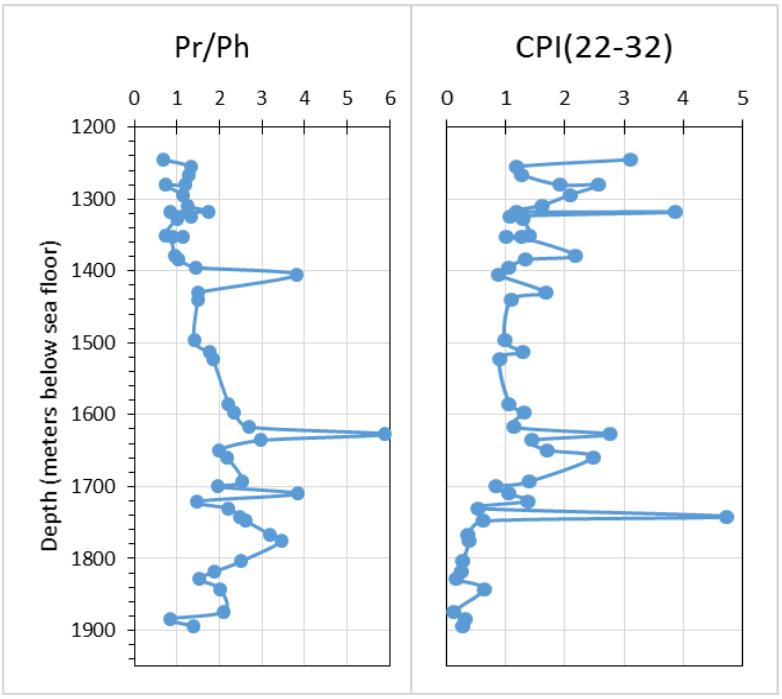

Fig. 1.Variation of pristane/phytane ratio and n-alkane carbon preference index with depth in the continental slope core

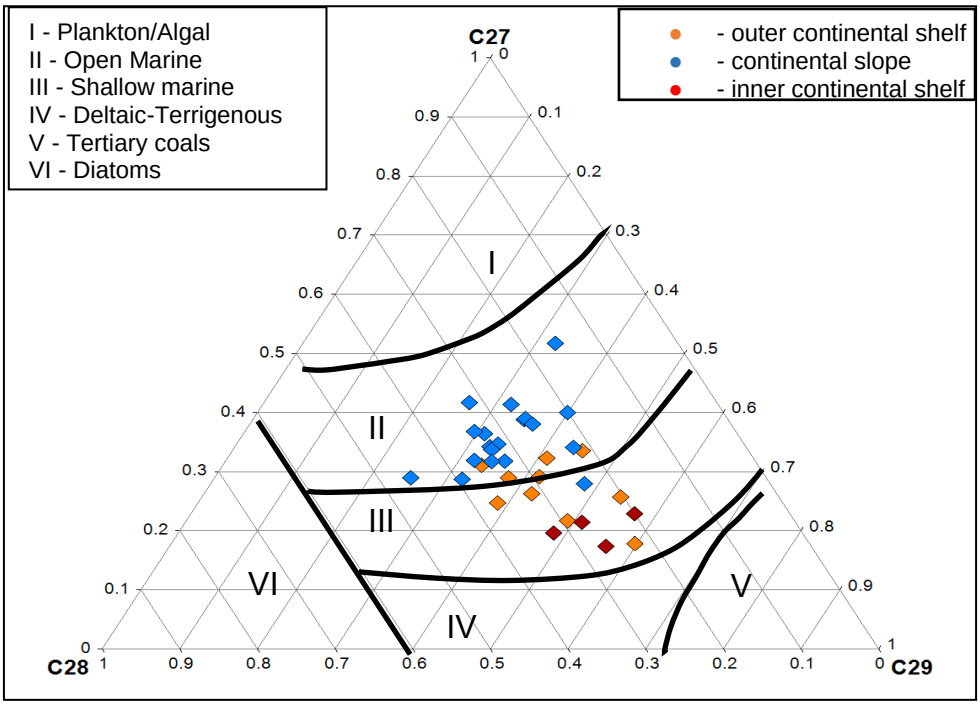

Fig. 2. Distribution of C_{27}, C_{28} and C_{29} steranes in Miocene samples in continental shelf and continental slope cores

References

Miller K.G., Kominz M.A., Browning J.V., Wright J. D., Mountain G.S., Katz M.E., Sugarman P.J., Cramer B. S., Christie-Blick N., Stephen F. Pekar S.F., The Phanerozoic Record of Global Sea-Level Change. Science 310(5752), 1293-1298.

Expedition 317 Scientists, 2010. Canterbury Basin Sea Level: Global and local controls on continental margin stratigraphy. IODP Prel. Rept., 317. doi:10.2204/iodp.pr.317.2010.

George, S.C., Lipp, J.S., Claypool, G.E., Yoshimura, T., and Expedition 317 Shipboard Scientific Party (2011). Organic carbon content and character of Holocene–Eocene sediments recovered during IODP Expedition 317, Canterbury Basin, New Zealand. In: *25th International Meeting on Organic Geochemistry*, Abstract Book, 18-23 September 2011. Interlaken. Poster-039, p. 186.

6. EGU2016 – European Geological Union Conference

Multi-proxy geochemical analyses of Indus Submarine Fan sediments sampled by IODP Expedition 355: implications for sediment provenance and palaeoclimate reconstructions

Sophia Bratenkov (1), Simon C. George (1), James Bendle (2), Hannah Liddy (3), Peter D. Clift (4), Dhananjai K. Pandey (5), Denise K. Kulhanek (6), Sergio Andò (7), Manish Tiwari (5), Boo-Keun Khim (8), Elizabeth Griffith (9), Stephan Steinke (10), Kenta Suzuki (11), Jongmin Lee (8), Kate Newton (2), Shubham Tripathi (5), and Expedition 355 Scientific Party

(1) Macquarie University, North Ryde, Sydney, NSW, Australia (sophia.bratenkov@mq.edu.au), (2) University of Birmingham, Edgbaston, United Kingdom, (3) University of Southern California, Los Angeles, CA, USA, (4) Louisiana State University, Baton Rouge, LA, USA, (5) National Centre for Antarctic and Ocean Research, Vasco da Gama, Goa, India, (6) Texas A&M University, College Station, TX, USA, (7) University of Milano Bicocca, Milan, Italy, (8) Pusan National University, Busan, Republic of Korea, (9) University of Texas at Arlington, Arlington, TX, USA, (10) MARUM, University of Bremen, Bremen, Germany, (11) Hokkaido University, Sapporo, Japan

The interplay between the development of the Asian summer monsoon and the growth of mountains in South and Central Asia is perhaps the most compelling example of the relationship between climate and the solid Earth. Understanding this relationship is crucial in the context of understanding past changes and for predicting future impacts in the Monsoon region. Both rapid and gradual mountain uplift influence the surrounding environments and regional climate. The sedimentary record of the Indus Fan offers a unique opportunity to study the climatic changes that occurred in South Asia and their link to the intensity of the erosion during the late Cenozoic. Although some paleoclimate reconstructions in the region can be partly addressed by studies onshore, the dominance of erosional processes in such a mountainous region ensures such records are fragmentary and limited in coverage. Thus ocean drilling is the best way to recover long sequences and to test the possible relations among mountain uplift, erosion, sediment deposition and climate (including carbon burial, chemical weathering and CO2 drawdown). The sediments and sedimentary rocks from the Indian continental margin, adjoining the Arabian Sea, were drilled during the International Ocean Discovery Program (IODP) Expedition 355. Drilling operations at Site U1456 penetrated through 1109.4 m of sediment and sedimentary rocks. The oldest sediment recovered at this site is dated to 13.5–17.7 Ma, with about 390 m of mass transport deposit. This study provides a multiproxy approach for palaeoenvironmental reconstructions in the Arabian Sea area. We use a wide variety of organic geochemical data coupled with inorganic chemistry, mineralogy, and isotopic analyses. For direct comparison among various data sets, we divided whole round residue from the interstitial water samples among different laboratories, with each receiving 50–300 g (dry mass). The preliminary results include initial sediment provenance data based on bulk petrography and heavy mineral analysis, geochemical data, isotope composition, and biomarker analysis. Preliminary organic geochemistry data suggest an increase of terrigenous organic matter input into sediment starting around 10.5 Ma, with a strong decrease in the last 1 Ma. Moreover, the detailed analyses of the glyceryl dialkyl glyceryl tetraether (GDGT) and alkenone lipids provide the first sea surface temperature (SST) reconstructions in the region. These data indicate decreasing SST from the Middle Miocene Climatic Optimum until today. This research provides an exceptional opportunity to apply a multiproxy approach to understand sediment provenance, erosional processes, and palaeoclimate evolution in the eastern Arabian Sea.

7. EGU2016 – European Geological Union Conference

Arabian Night and Sea Story – Biomarkers from a Giant Mass Transport Deposit.

Sophia Bratenkov (1), Denise K. Kulhanek (2), Peter D. Clift (3), and Simon C. George (1) (1) Macquarie University, North Ryde, Sydney, NSW, Australia (sophia.bratenkov@mq.edu.au), (2) Texas A&M University, College Station, Texas, USA, (3) Louisiana State University, Baton Rouge, LA, USA

The study of mass transport deposits (MTDs) is an important field of research due to the potential insights into catastrophic events in the past and modern geohazard threats (e.g. tsunamis). Submarine mass movements are very significant processes in sculpturing the structure of continental margins, particularly in their extent and magnitude that have consequences both in the modern day, as well as in the geological past. An understanding of the complex stratigraphy of a submarine mass transport deposit (MTD) might help in reconstructing the provenance and transport pathways of sedimentary material and thus give important insights into sedimentary dynamics and processes triggering specific events. Drilling operations during International Ocean Discovery Program (IODP) Expedition 355 Arabian Sea Monsoon, which took place during April and May, 2015 cored two sites in Laxmi Basin. Site U1456 was cored to 1109.4 m below seafloor (mbsf), with the oldest recovered rock dated to ~13.5-17.7 Ma. Site U1457 was cored to 1108.6 mbsf, with the oldest rock dated to ~62 Ma. At each site, we cored through ~330 m and ~190 m of MTD material. The MTD layers mainly consist of interbedded lithologies of dark grey claystone, light greenish calcarenite and calcilutite, and conglomerate/breccia, with ages based on calcareous nannofossil and foraminifer biostratigraphy ranging from the Eocene to early Miocene (Pandey et al., 2015). This MTD, known as Nataraja Slide, is the third largest MTD known from the geological record and the second largest on a passive margin. Calvés et al. (2015) identified a potential source area offshore Sourashstra on the Indian continental margin and invoked the single step mass movement model to explain the mechanism of emplacement. Initial shipboard work demonstrated the high variability in total organic carbon and total nitrogen levels in different layers within the MTD, which raises a number of questions related to the source and composition of the organic matter. Here we present the biomarker signature of the material based on gas chromatography-mass spectrometry (GC-MS) and high performance liquid chromatography-mass spectrometry (HPLC-MS) analyses. The purpose of this study is to understand the depositional and post-depositional processes of the sedimentary layers in the MTD. The unique opportunity of collaborative, multi-disciplinary data collection produced onboard the JOIDES Resolution, together with postcruise research, allows us to create a better understanding of the processes involved in creation of one of the largest known MTDs on Earth.

References:

Calvès, G., Huuse, M., Clift, P.D. and Brusset, S., 2015. Giant fossil mass wasting off the coast of West India: The Nataraja submarine slide. Earth and Planetary Science Letters, 432, pp.265-272.

Pandey, D.K., Clift, P.D., Kulhanek, D.K., et al., 2015. Expedition 355 Preliminary Report: Arabian Sea Monsoon. International Ocean Discovery Program. http://dx.doi.org/10.14379/iodp.pr.355.2015

8. EGU2016 – European Geological Union Conference

Combined heavy mineral and biomarker analysis in silt: a novel approach for provenance studies (Indus Fan, IODP Expedition 355)

Sergio Andò (1), Sophia Bratenkov (2), Annette Hahn (3), Simon George (2), Peter D. Clift (4), Eduardo Garzanti (1), and the Expedition 355 Scientists Team

(1) Department of Earth and Environmental Sciences, University of Milano-Bicocca, Milan, Italy (sergio.ando@unimib.it), (2) Department of Earth and Planetary Sciences, Macquarie University, Sydney, Australia, (3) MARUM, University of Bremen, Bremen, Germany, (4) Department of Geology and Geophysics, Louisiana State University, Baton Rouge, LA, USA

A high-resolution mineralogical study of Indus Fan turbiditic sediments cored during IODP Expedition 355 (Arabian Sea Monsoon) in the Laxmi Basin was carried out to investigate and quantify the different compositional signatures encoded in the sand, silt, and clay fractions. The turbidite deposits recovered at IODP Sites U1456 and U1457 in sedimentological Unit II were chosen as the best candidate for such a study. The integrated dataset presented here was obtained by coupling traditional and innovative bulk-sediment to single-grain analytical techniques, including bulk petrography, heavy-mineral and biomarker analyses on the same samples. Reliable quantitative results even in the medium to fine silt classes, which represent the dominant sediment sizes encountered in the recovered cores, were obtained by point-counting under the microscope, assisted by Micro-Raman spectroscopy (Andò et al., 2011; 2014). Preliminary data from the studied turbidites document rich and diverse heavy mineral assemblages in both the sand and silty-sand fractions. Heavy-mineral concentrations, as well as the number of mineral species, reach a maximum in sand and tend to decrease with grain size, becoming minimal in the clay fraction. Conversely, the biomarker analysis is generally focused on the finer sediment fractions and clay, where better preservation of biomarker compounds are obtained. The two approaches are thus complementary. Because biomarkers tend to be depleted in sand and heavy minerals in clay, the medium silt fraction represents the most suitable size window for the joint application of these two techniques. Comparing heavy-mineral assemblages with biomarkers allows us to evaluate both continental and marine inputs in turbidites and the hemipelagic deposits of the Indus Fan. This new methodological approach plays a key role in the identification of the effects of climate change on marine depositional environments and helps us to differentiate among the diverse Himalayan versus Indian Peninsular sources of detritus. Considered together, the organic and inorganic compositional fingerprints of sediments opens up a new frontier for future studies of the largely unexplored deep-marine sedimentary record.

Cited references

S. Andò, P. Vignola, E. Garzanti, 2011. Raman counting: a new method to determine provenance of silt. Rend. Fis. Acc. Lincei, 22: 327-347.

S. Andò, E. Garzanti, 2014. Raman spectroscopy in heavy-mineral studies. Geological Society, London, Special Publications, 386 (1), 395-412.

9. AOGC 2016 - the 19th Australian Organic Geochemistry Conference

Multi-proxy geochemical analyses of Indus Submarine Fan sediments sampled by IODP Expedition 355: implications for sediment provenance and palaeoclimate reconstructions

Sophia Aharonovich[1*], Simon C. Geroge[1], James Bendle[2], Hannah Liddy[3], Peter D. Clift[4], Dhananjai K. Pandey[5], Denise K. Kulhanek[6], Sergio Andò[7], Manish Tiwari[5], Boo-Keun Khim[8], Elizabeth Griffith[9], Stephan Steinke[10], Kenta Suzuki[11], Jongmin Lee[8], Kate Newton[2], Shubham Tripathi[5], and the Expedition 355 Scientific Party

[1] *Macquarie University, North Ryde, Sydney, NSW, Australia*

[2] *University of Birmingham, Edgbaston, United Kingdom*

[3] *University of Southern California, Los Angeles, CA, USA*

[4] *Louisiana State University, Baton Rouge, LA, USA*

[5] *National Centre for Antarctic and Ocean Research, Vasco da Gama, Goa, India*

[6] *Texas A&M University, College Station, TX, USA*

[7] *University of Milano Bicocca, Milan, Italy*

[8] *Pusan National University, Busan, Republic of Korea*

[9] *University of Texas at Arlington, Arlington, TX, USA*

[10] *MARUM, University of Bremen, Bremen, Germany*

[11] *Hokkaido University, Sapporo, Japan*

(corresponding author: sophia.aharonovich@mq.edu.au)*

The correlation between development of the Asian monsoon and continuing tectonic activity in the Himalaya and Tibetian Plateau is crucial to 70% of Earth's population. This correlation is perhaps the most compelling example of the relationship between climate and the solid Earth. To understand it the sediments and sedimentary rocks from the Laxmi Basin were drilled during the International Ocean Discovery Program (IODP) Expedition 355 – Arabian Seam Monsoon in 2015 (Pandey et al., 2015). Drilling operations at Site U1456 (Fig. 1) penetrated through 1109.4 m of sediments and sedimentary rocks, with the oldest sediment dated to 13.5–17.7 Ma.

Here we present the results of a multiproxy palaeoenvironmental study on samples from the IODP Site U1456. We use a wide variety of organic geochemical data coupled with bulk geochemistry, mineralogy, and isotopic analyses. For direct comparison between various data sets, we divided whole round residues from the interstitial water analyses (squeeze cakes) among ten laboratories, with each receiving 50–300 g (dry mass). These preliminary results include initial sediment provenance data based on bulk petrography and heavy mineral analyses, geochemical data, isotope compositions, and biomarker analyses.

The samples show a low extent of diagenesis and intrastratal dissolution of heavy minerals. Based on the amphibole-epidote assemblages and the volume percentage of heavy minerals (2-5%) a provenance from the orogenic Himalaya is suggested (Garzanti and Andò, 2007). The Indus River is interpreted to be the main source of sediment input into Laxmi Basin from ~ 8 Ma.

Preliminary organic geochemistry data suggest low levels of biodegradation and thermal maturity of the organic matter. The results indicate an increase of the terrigenous organic matter input into sediment starting around ~8 Ma, followed by a strong decrease in the last 1 Ma (Fig. 2). Moreover, the detailed compound specific isotope analyses suggest variation in the C3 vs. C4 vegetation cover in the area in the last 10 Ma. The recovered glycerol dialkyl glycerol tetraether (GDGT) and alkenone lipids provide the first sea surface temperature (SST) record for the eastern Arabian Sea (Fig. 2). The SST data based on the GDGT proxy suggest a decreasing temperature trend from the Middle Miocene Climatic Optimum. The alkenone based SST reconstruction shows no noticeable temperature trend. Possible reason for that could be an upper temperature limit of 29-30°C for this proxy (Conte et al., 2006).

This research provides an exceptional opportunity to apply a multiproxy approach for reconstruction of the provenance, the erosional processes, and the palaeoclimatic evolution in the eastern Arabian Sea region.

References:

Conte, M.H., Sicre, M.A., Rühlemann, C., Weber, J.C., Schulte, S., Schulz-Bull, D., Blanz, T., 2006. Global temperature calibration of the alkenone unsaturation index (UK′ 37) in surface waters and comparison with surface sediments. Geochemistry, Geophysics, Geosystems 7.

Garzanti, E., Andò, S., 2007. Chapter 20 Heavy Mineral Concentration in Modern Sands: Implications for Provenance Interpretation, in: Maria, A.M., David, T.W. (Eds.), Developments in Sedimentology. Elsevier, pp. 517-545.

Pandey, D.K., Clift, P.D., Kulhanek, D.K., et al., 2015. Expedition 355 Preliminary Report: Arabian Sea Monsoon. International Ocean Discovery Program. http://dx.doi.org/10.14379/iodp.pr.355.2015

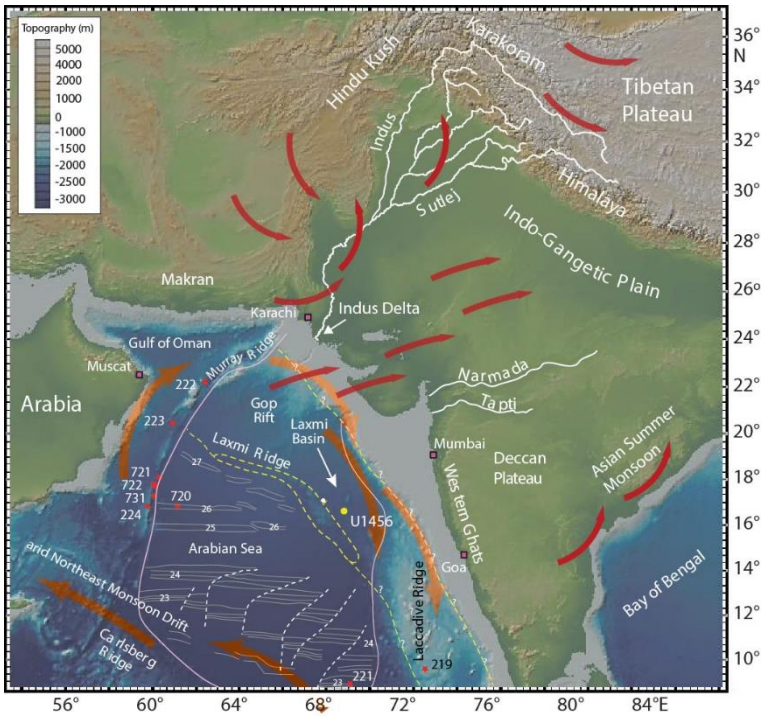

Fig. 9: IODP Expedition 355 drilling location, including modern currents (orange arrows) and summer monsoon (red arrows) directions.

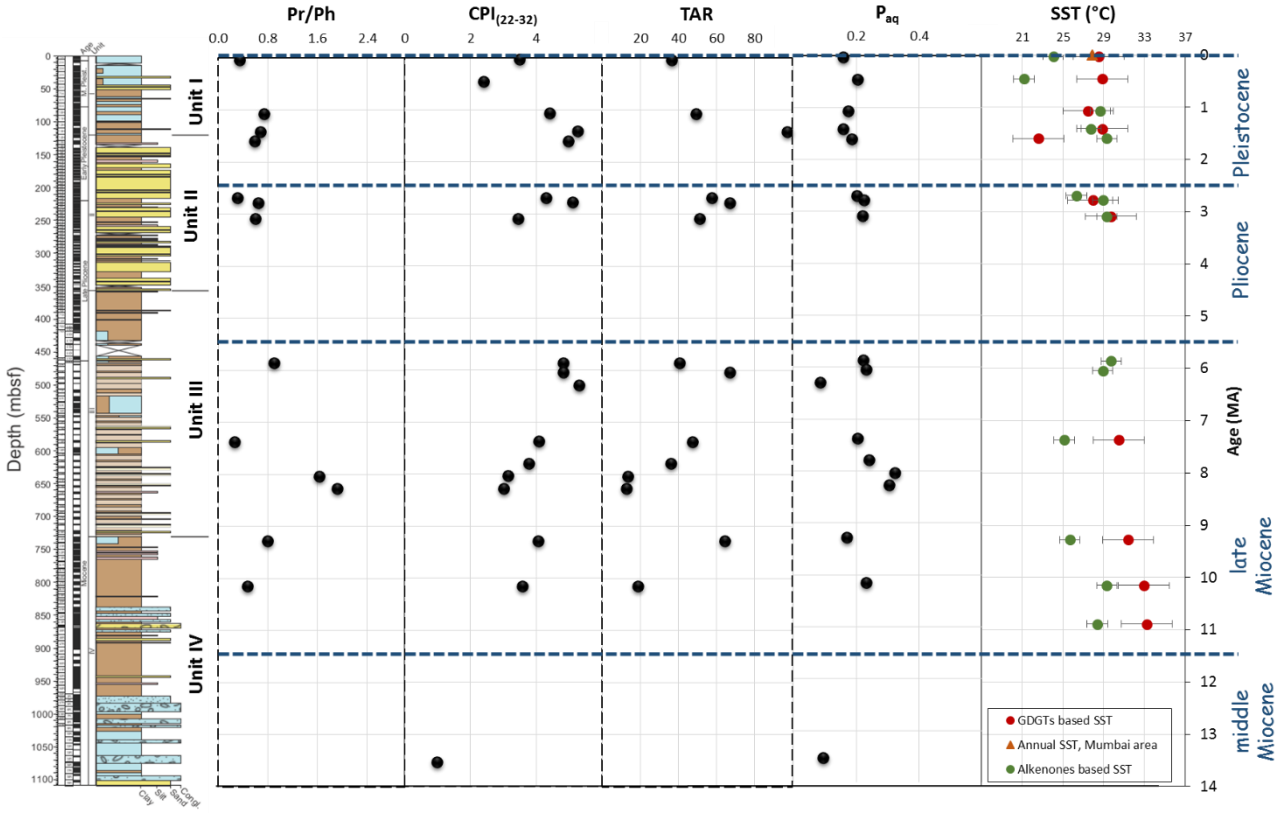

Fig.10: IODP Expedition 355 Site U1456 partial organic composition relative to lithology and geological periods where Pr-pristane, Ph-phytane, CPI – carbon preference index, TAR – terrigenous/aquatic ratio, and P_{aq} – submerged/floating aquatic macrophyte input vs. emergent and terrestrial plant input.

10. AOGC 2016 - the 19th Australian Organic Geochemistry Conference

SUB-MARINE MASS SLIDE AS A POTENTIAL BIOMARKER RESERVOIR: PRELIMINARY RESULTS FROM IODP EXPEDITION 355, ARABIAN SEA

Sophia Aharonovich[1*], Denise K. Kulhanek[2], Peter D. Clift[3], and Simon C. George[1]

[1]Macquarie University, North Ryde, Sydney, NSW, 2109, Australia

[2]Texas A&M University, College Station, Texas, 9547, USA

[3]Louisiana State University, Baton Rouge, LA, 70803, USA

(corresponding author: sophia.aharonovich@mq.edu.au)*

The study of mass transport deposits (MTDs) is an important field of research due to the potential insights into catastrophic events in the past and modern geohazard threats (e.g. tsunamis). Submarine mass movements are very significant processes in sculpturing the structure of continental margins, particularly in their extent and magnitude that have consequences both in the modern day as well as in the geological past. In addition, the high volume of many mass movements and the rapid burial of the sediments means that post-depositional alteration of the organic matter will be minimised, so preservation potential of any biomarkers is high. An understanding of the complex stratigraphy of a submarine mass transport deposit might help in reconstructing the provenance and transport pathways of the material and thus give important insights into sedimentary dynamics and processes triggering specific events.

Drilling operations during the International Ocean Discovery Program (IODP) Expedition 355 - Arabian Sea Monsoon took place during April and May 2015, with two cored sites in the Laxmi Basin (Pandey et al., 2015). Site U1456 was cored to 1109.4 m below seafloor (mbsf), with the oldest recovered rock dated to 13.5-17.7 Ma. Site U1457 was cored to 1108.6 mbsf, with the oldest rock dated to 62 Ma. The sites contain 330 m and 190 m of MTD material, respectively. The MTD layers mainly consist of interbedded lithologies of dark grey claystone, light greenish calcarenite and calcilutite, and conglomerate/breccia (Fig.1), with ages based on calcareous nannofossil and foraminifer biostratigraphy ranging from the Eocene to the early Miocene (Pandey et al., 2015). This MTD, known as the Nataraja Slide, is the third largest MTD known from the geological record, and the second largest on a passive margin. Calvés et al. (2015) identified a potential source area offshore of Sourashstra on the Indian continental margin, and invoked a single step mass movement model to explain the mechanism of emplacement.

The purpose of this study is to understand the depositional and post-depositional processes of the sedimentary layers in the MTD. Initial shipboard work demonstrated a high variability in total organic carbon (TOC) and total nitrogen (TN) levels in different depth within the MTD, might suggest multiple step mass movement model with some variations in deposited organic matter.

Here we present the biomarker signature of the material based on gas chromatography-mass spectrometry (GC-MS) and high performance liquid chromatography-mass spectrometry (HPLC-MS) analyses (Fig. 1 and 2). High carbon preference index values ($CPI_{22\text{-}32}$ >1.5) and high branched glycerol dialkyl glycerol tetraethers (GDGTs) index values – BIT>0.85, suggest high terrestrial lipid input with some variation in the oxicity of depositional environment through the MTD. A contribution of shallow marine biomarker input is suggested based on the sterane data. Sea surface temperature (SST) reconstruction based on the unsaturated alkenone index ($U^{K'}_{37}$) suggest very little variation through the MTD, with an average around 27.6°C. While the isoprenoid GDGTs based index (TEX^{H}_{86}) shows much diverse temperature range (22-30°C).

The unique opportunity of collaborative, multi-disciplinary data collection produced on-board the JOIDES Resolution, together with post-cruise research, allows us to create a better understanding of the processes involved in creation of one of the largest MTDs on Earth and its geological potential.

References

Calvès, G., Huuse, M., Clift, P.D. and Brusset, S., 2015. Giant fossil mass wasting off the coast of West India: The Nataraja submarine slide. *Earth and Planetary Science Letters*, *432*, pp.265-272.

Pandey, D.K., Clift, P.D., Kulhanek, D.K., et al., 2015. Expedition 355 Preliminary Report: Arabian Sea Monsoon. International Ocean Discovery Program. http://dx.doi.org/10.14379/iodp.pr.355.2015

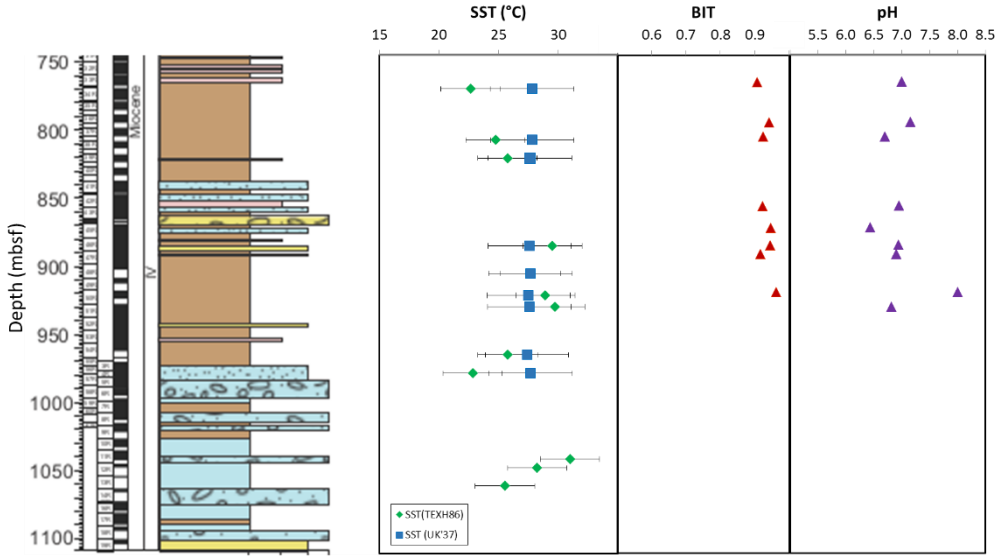

Fig. 1: IODP Expedition 355 Site U1456 unsaturated alkenones, isoprenoid GDGTs, and branched GDGTs data relative to the lithology of the mass transport deposit.

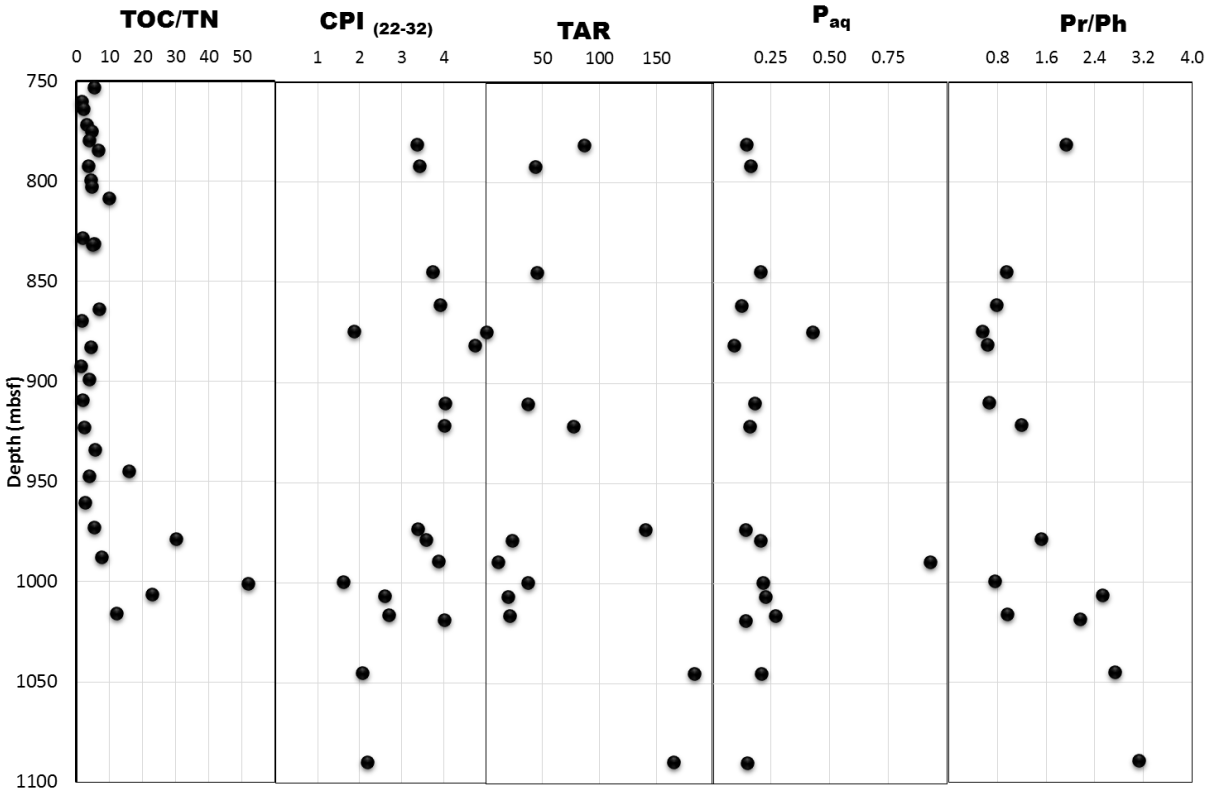

Fig. 2: IODP Expedition 355 organic composition of mass transit deposit from detected at the Site U1456 relative to the depth, where TAR – terrigenous/aquatic ratio, P_{aq} – submerged/floating aquatic macrophyte input vs. emergent and terrestrial input, Pr- pristane, and Ph – phytane.

7.4. **Appendix: Additional publications**

During my PhD I was involved in number of studies that were finalised in set of publications. Please see the change of the last name Bratenkov instead of Aharonovich.

Pandey, D. K., P. D. Clift, D. K. Kulhanek, S. Andò, J. A. P. Bendle, **S. Bratenkov**, E. M. Griffith et al. *Deep sea drilling in the Arabian Sea: Constraining tectonic-monsoon interactions in South Asia (Report)*. International Ocean Discovery Program, 2015.

1. Pandey, D.K., Clift, P.D., Kulhanek, D.K., Andò, S., Bendle, J.A.P., **Bratenkov, S.**, Griffith, E.M., Gurumurthy, G.P., Hahn, A., Iwai, M., Khim, B.-K., Kumar, A., Kumar, A.G., Liddy, H.M., Lu., H., Lyle, M.W., Mishra, R., Radhakrishna, T., Routledge, C.M., Saraswat, R., Saxena, R., Scardia, G., Sharma, G.K., Singh, A.D., Steinke, S., Suzuki, K., Tauxe, L., Tiwari, M., Xu, Z., and Yu, Z., 2015. *Expedition 355 Preliminary Report: Arabian Sea Monsoon.* International Ocean Discovery Program. http://dx.doi.org/10.14379/iodp.pr.355.2015

2. Pandey, D.K., Clift, P.D., Kulhanek, D.K., Andò, S., Bendle, J.A.P., **Bratenkov, S.**, and the Expedition 355 Scientists, 2016. *Arabian Sea Monsoon.* Proceedings of the International Ocean Discovery Program, 355: College Station, TX (International Ocean Discovery Program). **http://dx.doi.org/10.14379/iodp.proc.355.2016**

3. Pandey, D.K, Clift, P.D., Kulhanek, D.K, Andò, S., Bendle, J.A.P., **Bratenkov, S.**, Griffith, E.M., Gurumurthy, G.P., Hahn, A., Iwai, M., Khim, B.-K., Kumar, A., Kumar, A.G., Liddy, H.M., Lu, H., Lyle, M.W., Mishra, R., Radhakrishna, T., Routledge, C.M., Saraswat, R., Saxena, R., Scardia, G., Sharma, G.K., Singh, A.D., Steinke, S., Suzuki, K., Tauxe, L., Tiwari, M., Xu, Z., and Yu, Z., 2016. Expedition 355 summary. *In* Pandey, D.K., Clift, P.D., Kulhanek, D.K., and the Expedition 355 Scientists, *Arabian Sea Monsoon.* Proceedings of the International Ocean Discovery Program, 355: College Station, TX (International Ocean Discovery Program). **http://dx.doi.org/10.14379/iodp.proc.355.101.2016**

4. Pandey, D.K., Clift, P.D., Kulhanek, D.K., Andò, S., Bendle, J.A.P., **Bratenkov, S.**, Griffith, E.M., Gurumurthy, G.P., Hahn, A., Iwai, M., Khim, B.-K., Kumar, A., Kumar, A.G., Liddy, H.M., Lu, H., Lyle, M.W., Mishra, R., Radhakrishna, T., Routledge, C.M., Saraswat, R., Saxena, R., Scardia, G., Sharma, G.K., Singh, A.D., Steinke, S., Suzuki, K., Tauxe, L., Tiwari, M., Xu, Z., and Yu, Z., 2016. Expedition 355 methods. *In* Pandey, D.K., Clift, P.D., Kulhanek, D.K., and the Expedition 355 Scientists, *Arabian Sea Monsoon.* Proceedings of the International Ocean Discovery Program, 355: College Station, TX (International Ocean Discovery Program) **http://dx.doi.org/10.14379/iodp.proc.355.102.2016**

5. Pandey, D.K., Clift, P.D., Kulhanek, D.K., Andò, S., Bendle, J.A.P., **Bratenkov, S.**, Griffith, E.M., Gurumurthy, G.P., Hahn, A., Iwai, M., Khim, B.-K., Kumar, A., Kumar, A.G., Liddy, H.M., Lu, H., Lyle, M.W., Mishra, R., Radhakrishna, T., Routledge, C.M., Saraswat, R., Saxena, R., Scardia, G., Sharma, G.K., Singh, A.D., Steinke, S., Suzuki, K., Tauxe, L., Tiwari, M., Xu, Z., and Yu, Z., 2016. Site U1456. *In* Pandey, D.K., Clift, P.D., Kulhanek, D.K., and the Expedition 355 Scientists, *Arabian Sea Monsoon.* Proceedings of the International Ocean Discovery Program, 355: College Station, TX (International Ocean Discovery Program). **http://dx.doi.org/10.14379/iodp.proc.355.103.2016**

6. Pandey, D.K., Clift, P.D., Kulhanek, D.K., Andò, S., Bendle, J.A.P., **Bratenkov, S.**, Griffith, E.M., Gurumurthy, G.P., Hahn, A., Iwai, M., Khim, B.-K., Kumar, A., Kumar, A.G., Liddy, H.M., Lu, H., Lyle, M.W., Mishra, R., Radhakrishna, T., Routledge, C.M., Saraswat, R., Saxena, R., Scardia, G., Sharma, G.K., Singh, A.D., Steinke, S., Suzuki, K., Tauxe, L., Tiwari, M., Xu, Z., and Yu, Z., 2016. Site U1457. *In* Pandey, D.K., Clift, P.D., Kulhanek, D.K., and the Expedition 355 Scientists, *Arabian Sea Monsoon.* Proceedings of the International Ocean Discovery Program, 355: College Station, TX (International Ocean Discovery Program). **http://dx.doi.org/10.14379/iodp.proc.355.104.2016**

7. **Aharonovich, S.** and George, S.C., 2016. A possible shale gas prospect? First results of the organic composition and thermal maturity of the Carboniferous Namoi Formation, northern NSW, Australia. *Australian Journal of Earth Sciences*, *63*(6), pp.771-780.

Taylor & Francis
Taylor & Francis Group

Australian Journal of Earth Sciences
An International Geoscience Journal of the Geological Society of Australia

ISSN: 0812-0099 (Print) 1440-0952 (Online) Journal homepage: http://www.tandfonline.com/loi/taje20

A possible shale gas prospect? First results of the organic composition and thermal maturity of the Carboniferous Namoi Formation, northern NSW, Australia

S. Aharonovich & S. C. George

To cite this article: S. Aharonovich & S. C. George (2016) A possible shale gas prospect? First results of the organic composition and thermal maturity of the Carboniferous Namoi Formation, northern NSW, Australia, Australian Journal of Earth Sciences, 63:6, 771-780, DOI: 10.1080/08120099.2016.1247750

To link to this article: http://dx.doi.org/10.1080/08120099.2016.1247750

AUSTRALIAN JOURNAL OF EARTH SCIENCES, 2016
VOL. 63, NO. 6, 771–780
http://dx.doi.org/10.1080/08120099.2016.1247750

A possible shale gas prospect? First results of the organic composition and thermal maturity of the Carboniferous Namoi Formation, northern NSW, Australia

S. Aharonovich and S. C. George

Department of Earth and Planetary Sciences and Macquarie University Marine Research Centre, Macquarie University, Macquarie Park, NSW, 2109, Australia

ABSTRACT

The Namoi Formation in the Werrie Syncline, north and west of Tamworth, is part of the well-preserved Devonian–Carboniferous fore arc in the New England Fold Belt. The formation is between 640–914 m thick and consists of dominant olive-green mudstones with lenses of sandstone and oolitic limestone. To assess shale gas prospectivity, we analysed five outcrop samples from the Namoi Formation in the Keepit area. Well-preserved aliphatic and aromatic hydrocarbon fractions do not show evidence of weathering or biodegradation. *n*-Alkanes in all samples have a unimodal distribution maximising at C_{26} to C_{28}. Little odd-to-even *n*-alkane carbon number predominance and relatively low Pr/*n*-C_{17} and Ph/*n*-C_{18} ratios are consistent with a high thermal maturity. Based on the distribution of alkylnaphthalenes and alkylphenanthrenes, the Namoi Formation is in the gas window. Calibration of the methylphenanthrene index and ratio with vitrinite reflectance suggests a calculated reflectance around 2.1%, which given a normal geothermal gradient is equivalent to a maximum temperature of 205°C for the deepest burial of the formation. There is a dominance of parent polycyclic aromatic hydrocarbons (PAH) over alkylated PAHs, supporting a high thermal maturity. Some samples contain biomarkers suggestive of a marine depositional environment, including the C_{30} sterane index and the C_{31}/C_{30} hopane ratio. The Namoi Formation is a prospective shale-gas source, as it has been buried sufficiently to be well within the gas window. Where it is exposed at the surface gas will have been lost, but elsewhere it will be buried beneath other sediments and may still retain gas. Key exploration uncertainties include information on organic richness, lateral variation in thermal maturity, mineralogy, and porosity–permeability relationships.

ARTICLE HISTORY
Received 15 July 2016
Accepted 17 September 2016

KEYWORDS
shale gas; NSW; Australia; thermal maturity; biomarkers, Namoi Formation

Introduction

Natural gas is one of the most important global energy sources. Owing to environmental issues and technological developments, gas consumption for power generation is increasing in many regions around the world (BREE, 2012). During rapid economic growth following urbanisation, the global demand for gas-based energy is expected to grow (BREE, 2012), the switch to renewable sources notwithstanding (Leather, Bahadori, Nwaoha, & Wood, 2013). Indeed, owing to the significantly lower greenhouse gas impact of shale gas, for example, and compared with burning coal (Jenner & Lamadrid, 2013), gas will fill a role as a transitionary fuel as the world moves to a low- or zero-carbon emission economy (Jenner & Lamadrid, 2013; Moore, Horne, & Morrissey, 2014). From the beginning of the 21st century, technological developments such as horizontal drilling and hydraulic fracturing have raised the extraction efficiency of natural gas from shale formations to a new profitable level (IEA, 2009; Kinnaman, 2011).

After black and brown coal, natural gas is the third largest energy source in Australia. The volume of Australian proven natural gas reserves on 1 January 2012 was 133 trillion cubic feet (tcf), equivalent to 1.8% of global proven gas reserves (Wood, Nwaoha, & Towler, 2012). Based on International Energy Agency data, Australia contains 396 tcf of technically recoverable shale gas resources (IEA, 2012). The expected growth of Australian shale gas exploration will be exponential during the next decade, notwithstanding the current (2016) low price of oil and gas. Most conventional gas resources in Australia are located in western Australia in the Carnarvon, Browse and Bonaparte basins (Figure 1; Leather et al., 2013). Therefore, exploration of new basins with good shale gas potential is particularly important for eastern Australia to ease the possible predicted gas energy-supply constraints (Leather et al., 2013).

Shale gas is natural gas (mainly methane) that was trapped in its original source rock (Montgomery, Jarvie, Bowker, & Pollastro, 2005; Rogers, 2011). Gas is stored in shale gas reservoirs in fractures and pores, and absorbed on organic matter (Montgomery et al., 2005; Zhang, Ellis, Ruppel, Milliken, & Yang, 2012). High total organic carbon (TOC) levels together

CONTACT S. Aharonovich sophia.aharonovich@mq.edu.au
Editorial handling: Keyu Liu

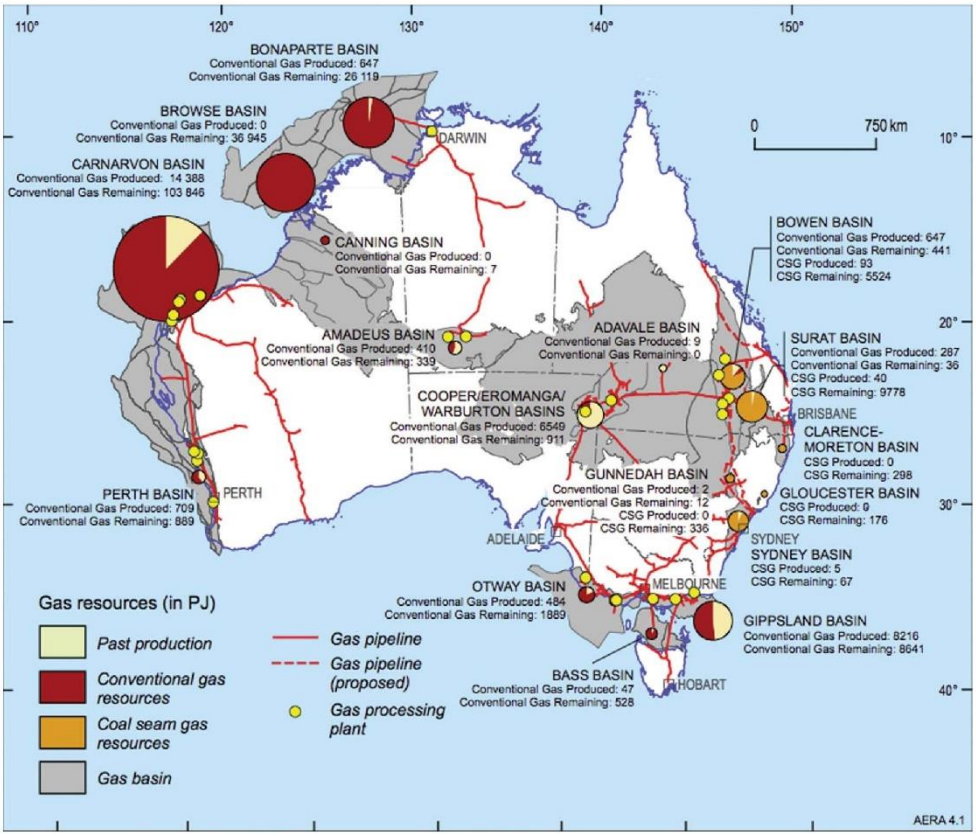

Figure 1. Location of the major gas basins in Australia (Geoscience Australia, 2011) including past production, conventional gas resources and coal seam gas resources. The gas pipelines (red lines), proposed gas pipelines (red dash line) and gas-processing plants (yellow points) are also presented.

with high thermal maturity of the organic matter (OM) increase absorption of the methane in shales (Zhang et al., 2012). Different types of OM are able to generate different amounts of methane (Jarvie, 2012). Based on US shale gas recovery results, the characteristics for shale gas occurrence should also include the following: (i) shale, siltstone or mudstone lithologies and mineralogy; (ii) TOC greater than 2 wt%; (iii) thickness of shales greater than 30 m; (iv) thermal maturity in the wet gas window (0.8–1.2% vitrinite reflectance equivalent [VRE]) or the dry gas window greater than 1.2% VRE; and (v) OM is not oxidised (Cook et al., 2013; Jarvie, 2012).

Organic geochemical analytical methods can help to characterise shale gas prospects and identify the production potential of the formation (Jarvie, Hill, Ruble, & Pollastro, 2007). Biomarker studies help to define source and thermal maturity, and can provide information about post-depositional processes that may have affected a formation (e.g. Peters, Walters, & Moldowan, 2005). Organic geochemical data can have a significant influence on the development of a shale reservoir, as well as providing important information related to environmental hazards of shale gas production in an area.

The Surat Basin in Queensland was recognised as a potential basin for shale gas development (Cook et al., 2013). The southern part of the Surat Basin is located in part of northern NSW and has not yet been studied for the presence of shale gas. Exploration for shale gas reservoirs in the developed areas in Australia will minimise facility and transportation costs, and allow Australia to stay competitive in the international energy market. The geographical location of the Namoi Formation will allow fast gas distribution to NSW and Queensland, two rapidly developing states. Moreover, increasing populations and constant development of the state's demands detailed environmental hazard analyses of any potential gas production in the region. This paper documents the first organic geochemistry study of the rocks from the Namoi Formation, Surat Basin, northern NSW, Australia. This research documents a high thermal maturity of the rocks, as

well as good organic preservation, and suggests that there could be potential development of the area as a shale gas prospect.

Experimental

Location and sampling

The Namoi Formation in the Werrie Syncline, Keepit, north and west of Tamworth, is part of the well-preserved Devonian–Carboniferous fore arc in the New England Fold Belt in the Surat Basin (Figure 2). The Devonian part of the basin was formed in a marine depositional environment; there was active submarine volcanism in the Early Devonian (Voisey & Williams, 1964). Most parts of the Carboniferous sequence consist dominantly of olive-green to brown, laminated, marine mudstones, with siltstones, fine-grained feldspatho-lithic sandstones and minor limestone, and is between 640 and 914 m thick (Voisey & Williams, 1964). Sea-level became progressively shallower during the Carboniferous, with predominant terrestrial sedimentation in the northern part of the basin (Leitch, 1974). The Namoi Formation is underlain by the Carboniferous Tulcumba Sandstone and is overlain by the Merlewood Formation, which is dominated by

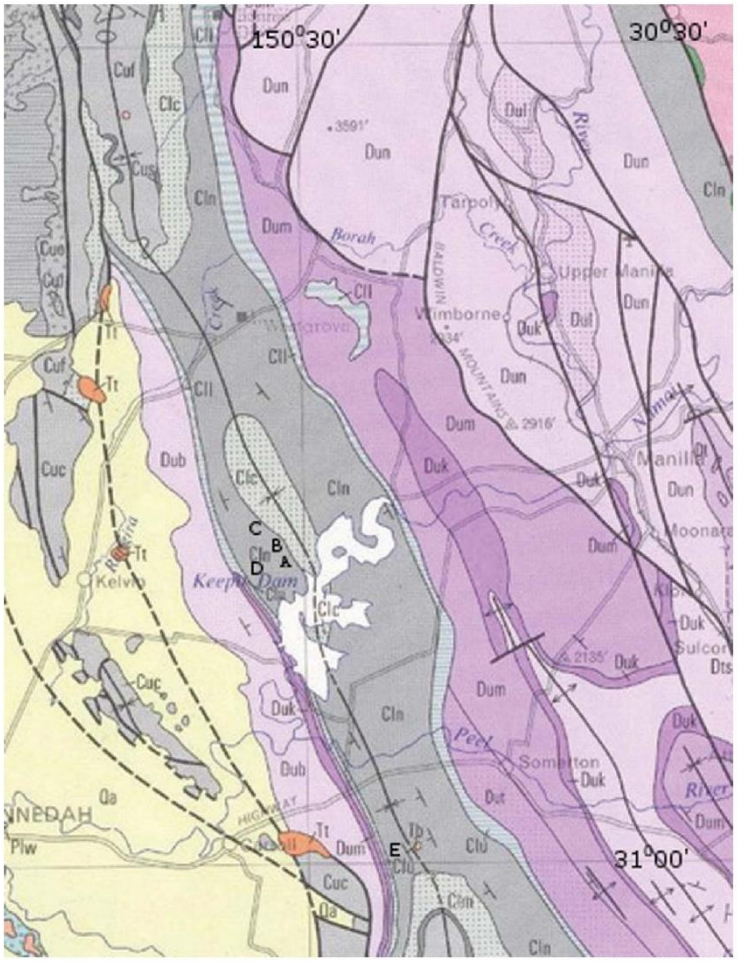

Figure 2. Modified geological map (Chesnut et al., 1973) of the Keepit Dam area, showing the sampling localities, where Cll, Luton Formation with Tulcumba Sandstone (Clt) and Tangaratta Formation (Cla); Cln, Namoi Formation; Clc, Caroda Formation; Dtz, Tamworth Group; Duk, Keepit Conglomerate; Dub, Baldwin Formation; Dum, Mandowa Mudstone; Pw, basaltic lava and tuff; Tl, basalt, dolerite; Qa, alluvium: clay, silt, sand, gravel; and green colour is serpentinite. Black lines indicate accurate geological boundary position, and dashed lines indicate the approximate ones.

Table 1. Descriptive information, organic richness, isoprenoids and *n*-alkane ratios for the Namoi Formation samples from Keepit.

Keepit sample ID	Latitude	Longitude	Description	TOC (wt%)	Extractability (mg OM/g rock)	Pr/Ph	Pr/nC_{17}	Ph/nC_{18}	$(C_{21}+C_{22})/(C_{28}+C_{29})$	$CPI_{(22-32)}$
A	30°49′38.24	150°27′23.84	Basal mudstone	0.11 ± 0.0055	0.05	0.67	0.83	0.63	0.08	0.98
B	30°50′15.84	150°28′29.24	Mudstone	0.17 ± 0.0085	0.04	0.89	0.62	0.42	0.10	1.03
C	30°49′3.46	150°28′2.78	Mudstone	0.19 ± 0.0095	0.03	0.89	0.74	0.61	0.11	0.99
D	31°1′48.13	150°30′36.07	Mudstone	0.21 ± 0.0105	0.05	0.76	0.68	0.59	0.08	1.00
E	30°49′36.72	150°28′19.78	Mudstone	0.16 ± 0.008	0.06	0.83	0.37	0.69	0.13	1.05

lithic sandstones and conglomerate (Voisey & Williams, 1964). The overlying lithology of the Surat Basin includes five formations of Lower and Middle Jurassic sandstones and coal measures (Othman & Ward, 1999). The Lower Cretaceous was marked by a transgression and mainly shallow marine sediments (Othman & Ward, 1999).

Five outcrop samples were taken from the creek banks in the Keepit area (Figure 2; Table 1). Before every sampling, about half a metre of rock was cleaned away to get to the part of the rock that was not in contact with modern vegetation. Samples were wrapped with aluminium foil and stored in plastic bags for delivery and storage. Five samples were taken in 2011, and an additional sample was taken in 2013. All samples were processed in the organic geochemistry laboratory at Macquarie University in 2013.

Pre-analysis cleaning and crushing, TOC determination, solvent extraction and fractionation

The outer layer of the samples (about 1 cm from each side) was removed, leaving only the inner part of the samples for analysis. After the cleaning process, the samples were crushed in a ceramic pestle and mortar to <250 μm grainsize.

TOC was determined on 12 mg of homogenised and sieved samples using a Shimadzu TOC 5000A total organic carbon analyser with ±5% of error range. Samples were sparged with CO_2-free oxygen for 2 min prior to analysis. The instrument was calibrated over an appropriate range using potassium hydrogen phthalate. The levels of total carbon (TC) and total inorganic carbon (TIC) were measured for every sample. The TOC level was calculated as the difference between TC and TIC measurements (Table 1).

About 50 g of crushed sample was mixed with pre-extracted and pre-baked sand (~1:1) and solvent extracted using dichloromethane (DCM): methanol (9:1) and an Accelerated Solvent Extractor (ASE300) at 1500 bar pressure. The solvent volume of the resulting extractable organic matter (EOM) was reduced by a Buchii rotary evaporator using a water bath temperature of 42°C and a vacuum of 420 bar.

To measure the amount of EOM the volume of the sample was reduced to 10 mL, and a 1 mL aliquot of the sample was taken and dried under a gentle flow of nitrogen in a pre-weighed vial, before re-weighing to derive extractability (mg/g; Table 1). The remaining 9/10th EOM aliquot was reduced to 0.1 mL and fractionated using two short (45 mm) silica columns. In the first stage, total hydrocarbons were eluted using *n*-hexane:DCM (4:1), and the polar compounds were recovered using DCM:methanol (1:1). In the second stage, the total hydrocarbon fraction was further separated into an aliphatic fraction (*n*-hexane) and an aromatic fraction (*n*-hexane:DCM, 4:1).

Gas chromatography-mass spectrometry

The aliphatic and aromatic fractions were analysed by gas chromatography-mass spectrometry (GC-MS) using an Agilent 6890 gas chromatograph interfaced to an Agilent Mass Selective Detector (5975B). The front inlet was set up in splitless mode at a temperature of 310°C, the interface was held at 310°C, and the MS source temperature was 280°C. The GC was equipped with a DB-5MS capillary column (60 m, 250 μm i.d., 0.25 μm film thickness) with 1.5 mL/min He carrier gas flow. The GC column oven temperature was programmed from 40°C (hold for 2 min) to 310°C at 4°C/min and held for 40.5 min. The MS was run using a scan method (*m/z* 50–550) and two selected ion monitoring methods. Biomarkers were analysed using *m/z* 177, 191, 205, 217, 218, 231 and 259 for steranes, diasteranes and terpanes, while aromatic hydrocarbons were analysed using *m/z* 128, 142, 178, 192, 202, 212, 216, 252, 300 and 314.

Results and discussion

Organic content

Extractability and TOC contents of the samples are presented in Table 1. The samples have relatively low extractability of the OM, up to 0.06 mg/g rock. Low TOC levels <0.25% suggest that this part of the Namoi Formation, which has been exposed on the surface at Keepit, is very lean. Based on the high thermal maturity (see below) of the Namoi Formation, it is suggested that a high percentage of the OM was converted into oil and gas during the maturation processes. The exposed part of the formation would have lost a significant portion of any stored gas during uplift and exposure at the surface.

n-*Alkanes and isoprenoids*

The distribution of *n*-alkanes (Figure 3a) provides valuable information regarding the source of the OM and the level of preservation. The Keepit samples have good preservation of long-chain *n*-alkanes between C_{20} and C_{36}, with a unimodal distribution maximising at *n*-C_{26} to *n*-C_{28} (Figure 5). There is little odd-over-even carbon number predominance, and the calculated Carbon Preference Index (CPI_{22-32}) is between 0.99 and 1.05 (Table 2), consistent with other parameters, which

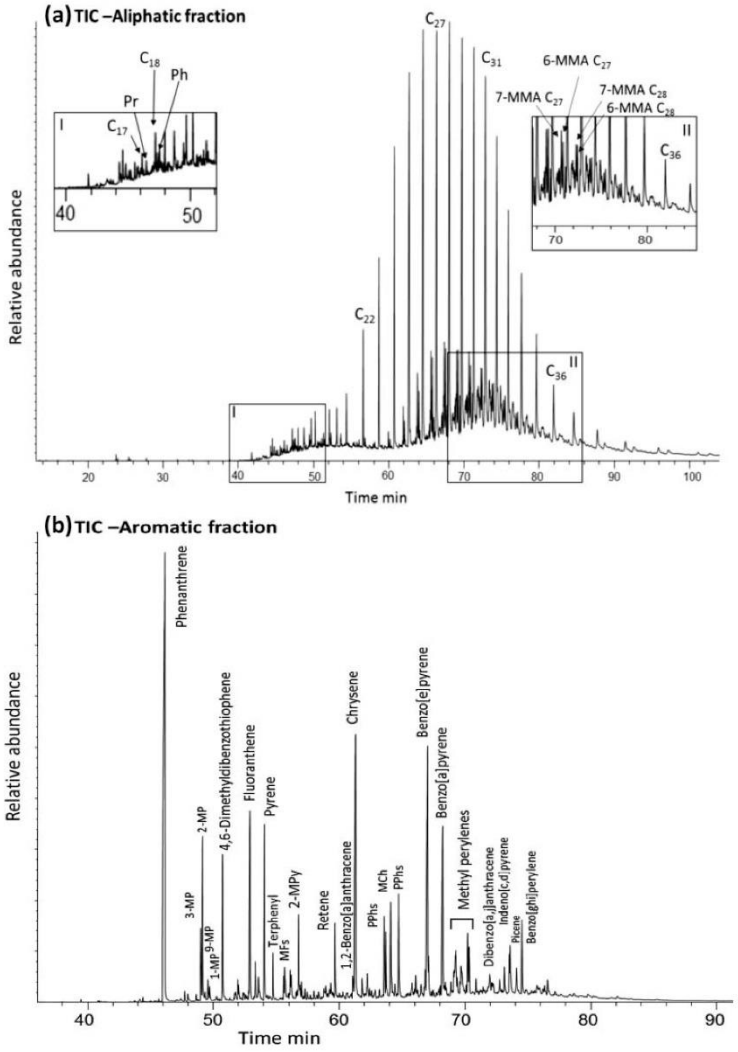

Figure 3. Total ion chromatograms of (a) the aliphatic hydrocarbon fraction of sample Keepit C, showing the distribution of *n*-alkanes (e.g. C_{27}), pristane (Pr), phytane (Ph) and monomethylalkanes (MMA); and (b) the aromatic hydrocarbon fraction of sample Keepit D. MP, methylphenanthrene; MFs, methylfluoranthene; MPy, methylpyrene; PPhs, phenylphenanthrenes; and MCh, methylchrysene.

indicate that the succession is highly thermally mature. The high abundance of waxy *n*-alkanes in the *n*-C_{25} to *n*-C_{31} range could be due to terrigenous OM input, but any original odd-over-even carbon number predominance is now lost. The absence of short- and mid-chain *n*-alkanes (up to C_{15}), and all other low-molecular-weight hydrocarbons also suggests a high thermal maturity for the Namoi Formation. Care was taken to avoid inadvertent loss of the low-molecular-weight portion of the EOM during evaporation (Ahmed & George, 2004), and furthermore the same loss was seen in all five samples. This suggest that some post-depositional process(es) may be involved in removal of these compounds, perhaps surficial weathering by wind or water after uplift. Biodegradation is unlikely to account for this removal, as there is no undifferentiated complex mixture, and the high-molecular-weight *n*-alkanes are well preserved.

Monomethylalkanes were identified in all samples in relatively high abundance (Figure 3a). Although these

Table 2. Sterane, diasterane and hopane ratios for the Namoi Formation samples from Keepit.

Keepit sample ID	Ts/(Ts+Tm)	C_{29} hopanes $\alpha\beta/(\alpha\beta+\beta\alpha)$	C_{30} hopanes $\alpha\beta/(\alpha\beta+\beta\alpha)$	C_{31} hopane $\alpha\beta$ S/(S+R)	C_{32} hopane $\alpha\beta$ S/(S+R)	C_{29}Ts/(C_{29}Ts+$C_{29}\alpha\beta$) hopane	C_{27}:C_{28}:C_{29} $\alpha\alpha\alpha$ steranes	C_{27} $\alpha\alpha\alpha$ steranes S/(S+R)	C_{29} steranes $\alpha\beta\beta/(\alpha\beta\beta+\alpha\alpha\alpha)$	$\alpha\beta\beta$ steranes/17α-hopanes	C_{27} $\beta\alpha$ diasteranes/C_{27} $\alpha\alpha\alpha$ steranes	C_{27}/C_{29} $\alpha\alpha\alpha$R steranes	C_{28}/C_{29} $\alpha\alpha\alpha$R steranes
A	0.46	0.90	–	0.52	0.59	0.18	28:28:44	0.47	0.48	2.4	0.78	0.66	0.64
B	0.50	0.85	0.82	0.55	0.55	0.15	26:29:45	0.47	0.48	3.2	0.78	0.57	0.64
C	0.44	0.89	0.89	0.53	0.50	0.16	32:24:44	0.44	0.42	3.0	0.56	0.72	0.54
D	0.52	–	0.91	0.58	0.58	0.15	29:30:41	0.45	0.50	2.3	0.64	0.71	0.75
E	0.54	–	0.86	0.58	0.59	0.17	32:33:35	0.53	0.51	2.0	1.02	0.90	0.94

compounds have commonly been reported in crude oils and source-rock extracts, their biological sources have not been unambiguously identified (Klomp, 1986; Peters et al., 2005). Cyanobacterial mats and endolithic cyanobacteria have been proposed to be a source of monomethylalkanes (e.g. Coates et al., 2014; Hoshino & George, 2015; Kenig et al., 1995). Monomethylalkanes have been reported as part of the surface lipids and waxes of insects (Nelson, 1978). Inorganic processes such as isomeric equilibrium (Klomp, 1986) and acid-catalysis of alkenes (Kissin, Feulmer, & Payne, 1986) have also been suggested as possible source of monomethylalkanes.

Pristane (2, 6, 10, 14-tetramethylpentadecane; Pr) and phytane (2, 6, 10, 14-tetramethylhexadecane; Ph) have commonly been identified in sediments and oils (Volkman, 1986), and may be derived from phototrophic organisms and bacteriophyll from purple sulfur bacteria (Powell & McKirdy, 1973). The relative abundance of Pr and Ph was suggested to be influenced by the oxicity of the depositional environment (Didyk, 1978). Pr/Ph < 0.8 is associated with anoxic depositional environments, whereas Pr/Ph > 3.0 usually correlates with oxic depositional environments or terrigenous plant input deposited under oxic or suboxic conditions (Didyk, 1978). The Keepit samples have Pr/Ph ratios of 0.65–0.9 (Table 2), suggestive of a reducing to suboxic depositional environment. The samples have relatively low Ph/*n*-C_{18} (0.4–0.7) and Pr/*n*-C_{17} (0.35–0.85) ratios (Table 2), consistent with a high thermal maturity (ten Haven, de Leeuw, Rullkotter, & Damste, 1987). The Pr/Ph ratio can be positively influenced by a high thermal maturity (Connan, 1974), but this would not change the above interpretation of oxicity (Table 2).

Biomarkers

Steranes, diasteranes and hopanes were identified in all the Keepit samples. Examples of biomarker distributions are shown in Figure 4a, b, and ratios are provided in Table 2.

C_{27}–C_{30} steranes and diasteranes were identified using the *m/z* 217 and 218 mass chromatograms in all samples with the abundance of steranes higher than diasteranes for all samples (Figure 4a; Table 2). Steranes are source-specific compounds; C_{27} steranes are commonly suggested to be derived mainly from zooplankton, whereas C_{29} steranes were originally suggested to be derived from higher plants (Huang & Meinschein, 1979). Diatoms, dinoflagellets and coccolithophorid sources are rich in C_{28} steranes (Falkowski et al., 2004), and the proportion of C_{28} steranes tends to increase in Mesozoic and Cenozoic rocks (e.g. Grantham & Wakefield, 1988). It is now known that there is more complexity in the origins of steranes (e.g. Volkman, 1986, 2005); for example, C_{29} sterols, the precursors of C_{29} steranes, have been identified in phytoplankton (Gagosian, 1976) and cyanobacterial mats (Volkman, 1986), and C_{29} steranes are also been found in green algal blooms (Kodner, Pearson, Summons, & Knoll, 2008).

Despite the multiple biological sources, the use of the C_{27}–C_{28}–C_{29} sterane ternary plot diagram to determine the source of the OM has previously proven to be effective (e.g. Huang & Meinschein, 1979; Moldowan, Seifert, & Gallegos, 1985; Wójcik-Tabol & Ślączka, 2015) and was also successfully used in oil–source correlations (Grantham & Wakefield, 1988). All the Keepit samples have a similar distribution of steranes, clustering closely in the middle of the sterane ternary diagram (Figure 6), which suggests a shallow to open marine environment for the source of the OM (Huang & Meinschein, 1979). The Keepit samples also contain small amounts of C_{30} *n*-propyl cholestanes, which are biomarkers for marine algae (Moldowan et al., 1985). C_{27}/C_{29} $\alpha\alpha\alpha$ and C_{28}/C_{29} $\alpha\alpha\alpha$ sterane ratios were calculated for all samples (Table 2) suggesting increasing diversification of zooplankton and phytoplankton assemblages (Moldowan et al., 1985).

The ratio of regular steranes [C_{27}, C_{28} and C_{29} $\alpha\alpha\alpha$ (20S+20R) and $\alpha\beta\beta$ (20S+20R)] to 17α-hopanes (C_{29}–C_{33} pseudohomologues) can provide information on the relative amounts of eukaryotic *vs* prokaryotic OM input. The Keepit samples have a high (2–3) sterane/hopane ratios for all samples (Table 2), suggestive of dominantly marine OM input from planktonic or benthic algae (Moldowan et al., 1985).

The C_{27} $\beta\alpha$ diasterane/C_{27} $\alpha\alpha\alpha$ sterane ratio provides further information on the source rock. In general, low values of the ratio are typical of carbonate or low clay content rocks, whereas high diasterane/sterane ratios indicate clay-rich and/or acid catalysed rocks (Moldowan et al., 1985; Peters et al., 2005). However, this ratio can be affected by increasing thermal maturation and/or heavy biodegradation (Seifert & Moldowan, 1978, 1979). All the Keepit samples have medium (0.56–1.02) C_{27} $\beta\alpha$ diasterane/$\alpha\alpha\alpha$ sterane ratios, consistent with anoxic clay-poor or carbonate source rock (Peters et al., 2005).

Maturity related parameters can also be obtained from the isomerisation ratio of C_{29} 5α, 14α,17α(H) steranes when the 20S/(20S+20R) isomerisation values vary between 0 and 0.52–0.55 at equilibrium (W. Seifert & Moldowan, 1986). The C_{29} $\alpha\alpha\alpha$ steranes S/(S+R) ratio for all samples is 0.44–0.53 (Table 2), suggesting that the steranes have not yet reached equilibrium. This result is supported by the C_{29} sterane

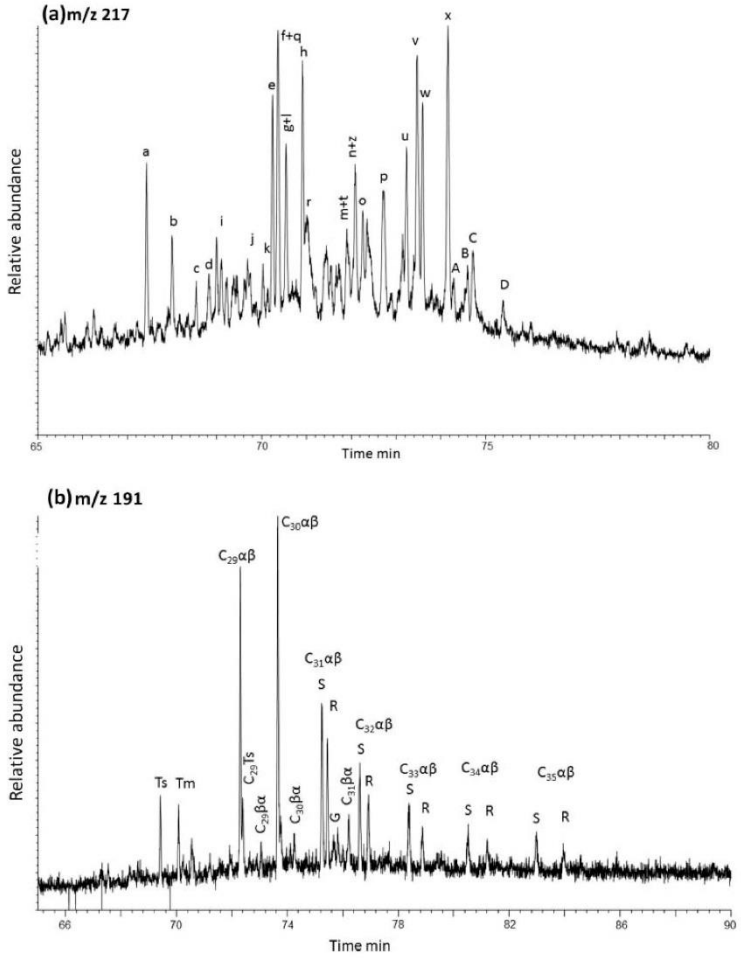

Figure 4. Partial *m/z* 217 (a) and 191 (b) mass chromatograms of the aliphatic hydrocarbon fraction of sample Keepit C, showing the distribution of steranes, diasteranes and hopanes. Biomarker peak assignments: a—C_{29} 13β(H),19α(H)-diacholestane (20S), b—C_{29} 13β(H),19α(H)-diacholestane (20R), c—C_{29} 13α (H),19β(H)-diacholestane (20S), d—C_{29} 13α (H),19β(H)-diacholestane (20R), i—C_{28} 24-methyl-13β(H),19α(H)-diacholestane (20S),(24S and 24R), j—C_{28} 24-methyl-13β(H),19α(H)-diacholestane (20R),(24S and 24R), k—C_{28} 13α(H),19β(H)-diacholestane (20S),(24R), e—C_{29} 5α(H),14α(H),19α(H)-cholestane (20S), f—C_{29}5α(H),14β(H),19β(H)-cholestane (20R), q—C_{29} 24-methyl-13β(H),19α(H)-diacholestane (20S), g—C_{29} 5α(H),14β(H),19β(H)-cholestane (20S), l—C_{28} 13α(H),19β(H)-diacholestane (20R),(24S and 24R), h—C_{29}5α(H),14α (H),19α(H)-cholestane (20R), r—C_{29} 24-methyl-13β(H),19α(H)-diacholestane (20R), m—C_{28} 24-methyl-5α(H),14α(H),19α(H)-cholestane (20S),(24S and 24R), t—C_{29} 24-methyl-13α(H),19β(H)-diacholestane (20R), n—C_{28} 5α(H),14β(H),19β(H)-cholestane (20S)(24S and 24R), z –, o—C_{28} 5α(H),14β(H),19β(H)-cholestane(20S),(24S and 24R), p—C_{28} 5α(H),14α(H),19α(H)-cholestane (20R), u—C_{29} 24-methyl-5α(H),14α(H),19α(H)-cholestane(20S), v—C_{29} 24-methyl-5α(H),14α(H),19α(H)-cholestane(20R), w—C_{29} 24-methyl-5α(H),14β(H),19β(H)-cholestane(20S), x—C_{29} 24-methyl-5α(H),14β(H),19β(H)-cholestane (20R), A—C_{30} 24-n-propyl-5α(H),14α(H),19α(H)-cholestane (20S), B—C_{30} 24-n-propyl-5α(H),14α(H),19α(H)-cholestane (20R), C—C_{30} 24-n-propyl-5α(H),14β(H),19β(H)-cholestane (20R), D—C_{30} 24-n-propyl-5α(H),14β(H),19β(H)-cholestane (20R), Ts—18α-22,29,30-trisnorneohopane, Tm—17α-22,29,30-trisnorhopane, $C_{29}\alpha\beta$—17α(H),21β(H)-30-norhopane, C_{29}Ts—18α(H)-30-norneohopane, $C_{30}\alpha\beta$—17α(H),21β(H)-hopane, $C_{30}\beta\alpha$—17β(H),21α(H)-hopane, $C_{31}\alpha\beta$S—17α(H),21β(H)-homohopane (22S), $C_{31}\alpha\beta$R—17α(H),21β(H)-homohopane (22R), G—gammacerane, $C_{31}\beta\alpha$—17β(H),21α(H)-homohopane (22S and 22R).

$\alpha\beta\beta/(\alpha\beta\beta+\ \alpha\alpha\alpha)$ ratio that varies from 0.42 to 0.51 (Table 2), which are values that also are not at thermal equilibrium.

Hopanes were identified using the *m/z* 191 mass chromatogram and are present in all the Keepit samples (Figure 4b). Bacteria are considered to be the main source of hopanes in the rocks (Ourisson, Albrecht, & Rohmer, 1984). C_{27} 17α-trisnorhopane (Tm) is a less thermally stable isomer than C_{27} 18α-trisnorneohopane (Ts) (K. W. Seifert & Moldowan, 1978), so the Ts/(Ts+Tm) ratio can be used as a maturity indicator. This ratio also depends on the source of the OM

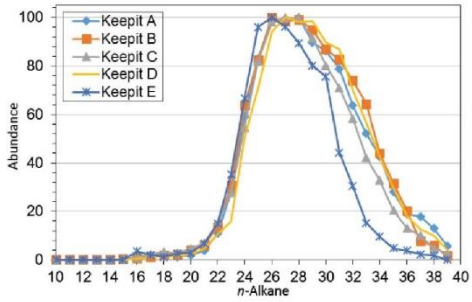

Figure 5. Distribution of *n*-alkanes in the Namoi Formation samples from Keepit.

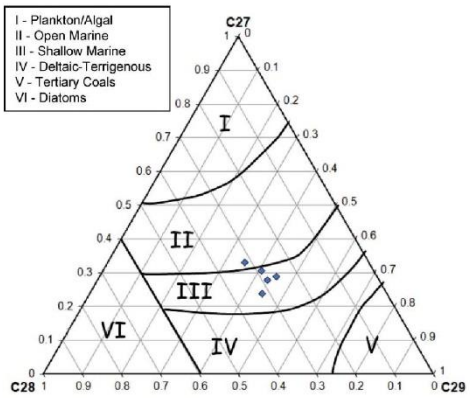

Figure 6. C_{27}, C_{28} and C_{29} $\alpha\alpha\alpha$ 20R sterane distributions for the Keepit samples (after Huang & Meinschein, 1979).

(Moldowan, Sundararaman, & Schoell, 1986), and can be influenced by clay-catalysed reactions. The Keepit samples have Ts/(Ts+Tm) ratios varying between 0.44 and 0.54 (Table 2) consistent with a moderate to high thermal maturity for the samples. Other hopane maturity parameters are the C_{29} and C_{30} hopane/moretane ratios [$\alpha\beta/(\alpha\beta+\beta\alpha)$] and the homohopane isomerisation ratios [22S/(22S+22R)], which are all close to thermal equilibrium values (0.95 and 0.6, respectively), suggesting that the Keepit samples are at least in the middle part of the oil window.

Aromatic hydrocarbons

The polycyclic aromatic hydrocarbons (PAH) that were identified include phenanthrene, pyrene, fluoranthene, benzo[a]anthracene, benzo[b]fluoranthene, benzo[k]fluoranthene, benzo[e]pyrene, benzo[a]pyrene, benzo[ghi]perylene and coronene. Combustion of various plant materials and fossil fuels has been suggested to be one of the major sources of higher-molecular-weight PAHs (e.g. Jiang, Alexander, Kagi, & Murray, 1998; Tan & Heit, 1981). For example, fluoranthene and pyrene have been suggested to be major combustion-derived PAHs (Killops & Massoud, 1992). The PAH are also abundant in highly over-matured samples (French et al., 2015), which is the more likely explanation in this instance, given the high thermal maturities indicated by other parameters. There is a dominance of parent polycyclic aromatic hydrocarbons (PAH) over alkylated PAHs, supporting a high thermal maturity.

The methylphenanthrene index (MPI_1) varies with thermal maturity (Radke, 1988; Radke, Welte, & Willsch, 1982) and for the Keepit samples has values between 0.10 and 0.37 (Table 3). The methylphenanthrene ratio (MPR; 2-/1-methylphenanthrene) is very high (6.6–10), consistent with highly matured OM. Together with the low MPI ratios, the high MPRs suggest the use of the following equation for calculated vitrinite reflectance (%R_c) (Radke & Welte, 1981):

$$\%R_c = (-0.6^{*}\mathrm{MPI}_1) + 2.3$$

Correlations between MPI and %R_c suggest that the Keepit samples are in the dry gas generation window, with ~%R_c for all samples between 2.1 and 2.2 based on MPI, and between 1.75 and 1.93 based on MPR (Table 3):

$$\%R_c = (0.99^{*}\log(\mathrm{MPR})) + 0.94$$

In order to derive a maximum paleotemperature (Max*T*), the following equation can be used (Wang et al., 2005):

$$\mathrm{Max}T = \frac{\ln\%R_c + 1.78}{0.0124}$$

The calculations based on MPI_1 index show a range of 203–209°C (Table 3) as the maximum temperature that the Namoi Formation in the Keepit area reached. The calculated Max*T*

Table 3. Aromatic hydrocarbon ratios for the Namoi Formation samples from Keepit. MP, methylphenanthrene; and MPI_1, {[(1.5(2-MP+3-MP)]/(phenanthrene+1-MP+9-MP)}.

Keepit sample ID	MPR (2-MP/1-MP)	MPI_1	%R_c (based on MPI_1)	Max*T* (based on MPI_1)	%R_c (based on MPR)	Max*T* (based on MPR)	Fluoranthene/(Fluoranthene+Pyrene)	2-Methylpyrene/(1-Methylpyrene+4-Methylpyrene)	Fluoranthene/methyl-Fluoranthene	Coronene/methyl-Coronene
A	6.7	0.10	2.2	209	1.8	189	0.19	–	5.4	10.5
B	8.5	0.37	2.1	203	1.9	194	0.22	3.3	1.6	5.1
C	–	0.11	2.2	208	–	–	0.20	–	–	–
D	10.0	0.25	2.2	205	1.9	197	0.51	25.1	5.0	–
E	9.9	0.25	2.2	205	1.9	196	0.41	4.3	–	–

based on the MPR ratio suggests a temperature range of 189–197°C (Table 3).

High ratios of parent PAHs to their methylated analogues (e.g. fluoranthene and methylfluoranthene) have been suggested to be diagnostic of samples with a high thermal maturity (French et al., 2015; Killops & Massoud, 1992). The fluoranthene/methylfluoranthene and coronene/methylcoronene ratios are >5, except for the Keepit B sample (1.6) (Table 3). These compounds were not identified in the Keepit C and E samples. These values are suggestive of high thermal maturities of the Keepit A, B and D samples; for example, the highly matured Archean samples reported by French et al. (2015) have values in this range. The fluoranthene/(fluoranthene+pyrene) ratio in all samples is lower than 0.51 (Table 3), also consistent with high levels of thermal stress in the rocks (Brault & Simoneit, 1989). Methylpyrenes were identified in the Keepit B, D and E samples (Table 3). Although the precursors of these compounds are unknown, the amount of 2-methylpyrene relative to the two other methylpyrene isomers increases in thermally mature samples (Garrigues, Soclo, Marniesse, & Ewald, 1987). The Keepit samples have a strong predominance of 2-methylpyrene (Table 3), consistent with a high thermal maturity.

Synthesis and conclusions

This paper provides the first preliminary data regarding the organic content and thermal maturity of the Carboniferous Namoi Formation mudstones in the Keepit area of NSW. The mudstones are organically lean (TOC <0.25%), partly owing to the high temperatures (>200°C) that they have been exposed to that led to the observed high thermal maturities. The results derived from GC-MS analysis indicate good levels of preservation of the organic compounds including high-molecular-weight *n*-alkanes. There is an absence of *n*-alkanes up to *n*-C_{15}, probably owing to the effects of weathering after uplift.

The sterane distribution in the samples suggests a shallow marine environment, and the high sterane/hopane ratios are consistent with a eukaryotic algae source, with limited terrigenous OM. The presence of hopanes indicate a bacterial OM input. Despite the possible influence of the high thermal maturity, the Pr/Ph ratio indicates an anoxic or suboxic depositional environment for the studied material.

The near unity CPI and the biomarker data are consistent with a thermal maturity at least in the mid oil window for all samples from the area. The aromatic hydrocarbons are more sensitive to higher thermal maturities than the biomarkers, and based on MPI and MPR a maximum temperature of over 200°C can be inferred for the Namoi Formation. These data suggest burial into the dry gas window, and the possibility of high levels of shale gas in any still buried sections with high organic content. Although no low-molecular-weight hydrocarbons are present in the outcrop samples, where the Namoi Formation is still buried below 200 m there may well be significant amounts of gas retained. Additional study is needed to more comprehensively evaluate the shale gas prospectivity of the area, including regional TOC and maturity variations, and investigation of the mineralogy and subsurface natural fracture patterns.

Acknowledgements

We would like to thank Dr Chris McRae for his help in calculation of the TOC levels in the Keepit samples. We would also like to thank Carl Peters and Amy Chen for help with the solvent extraction. Macquarie University is thanked for a PhD scholarship and research funds awarded to S.A.

Disclosure statement

No potential conflict of interest was reported by the authors.

References

Ahmed, M., & George, S. C. (2004). Changes in the molecular composition of crude oils during their preparation for GC and GC–MS analyses. *Organic Geochemistry, 35*, 137–155.

Brault, M., & Simoneit, B. (1989). Trace petroliferous organic matter associated with hydrothermal minerals from the Mid–Atlantic Ridge at the trans–Atlantic geotraverse 26° N site. *Journal of Geophysical Research: Oceans, 94*, 9791–9798.

BREE. (2012). *Australian Gas Resource Assessment 2012*. Canberra: Geoscience Australian and Bureau of Resources and Energy Economics.

Chesnut, W. S., Flood, R. H., & McKelvey, B. C. (1973). *Manilla 1:250 000 Geological Sheet SH/56-09* (1st ed.). Sydney, NSW: Geological Survey of New South Wales.

Coates, R. C., Podell, S., Korobeynikov, A., Lapidus, A., Pevzner, P., Sherman, D. H., … Gerwick, W. H. (2014). Characterization of cyanobacterial hydrocarbon composition and distribution of biosynthetic pathways. *PLoS One, 9*, e85140.

Connan, J. (1974). Diagenèse naturelle et diagenèse artificielle de la matière organique à éléments végétaux prédominants. In B. Tissot & F. Brienner (Eds.), *Advances in Organic Geochemistry* 1973 (pp. 73–95). Paris: Technip.

Cook, P., Beck, V., Brereton, D., Clark, R., Fisher, B., Kentish, S., … Williams, J. (2013). *Engineering energy: Unconventional gas production: A study of shale gas in Australia*. Melbourne Vic: ACOLA.

Didyk, B. (1978). Organic geochemical indicators of palaeoenvnonmental conditions of sedimentation. *Nature, 272*, 216–222.

Falkowski, P. G., Katz, M. E., Knoll, A. H., Quigg, A., Raven, J. A., Schofield, O., & Taylor, F. (2004). The evolution of modern eukaryotic phytoplankton. *Science, 305*, 354–360.

French, K. L., Hallmann, C., Hope, J. M., Schoon, P. L., Zumberge, J. A., Hoshino, Y., … Brocks, J. J. (2015). Reappraisal of hydrocarbon biomarkers in Archean rocks. *Proceedings of the National Academy of Sciences, 112*, 5915–5920.

Gagosian, R. B. (1976). A detailed vertical profile of sterols in the Sargasso Sea. *Limnology and Oceanography, 21*, 702–710.

Geoscience Australia. (2011). Retrieved from http://digsopen.minerals.nsw.gov.au/?rin=R00049263

Grantham, P. J., & Wakefield, L. L. (1988). Variations in the sterane carbon number distributions of marine source rock derived crude oils through geological time. *Organic Geochemistry, 12*, 61–73. doi:http://dx.doi.org/10.1016/0146-6380(88)90115-5

Garrigues, P., Soclo, H. H., Marniesse, M. P., & Ewald, M. (1987). Origin of polycyclic aromatic hydrocarbons (PAH) in recent sediments from the continental shelf of the «Golfe de Gascogne» (Atlantic Ocean) and in the Gironde Estuary. *International Journal of Environmental Analytical Chemistry, 28*, 121–131.

Hoshino, Y., & George, S. C. (2015). Cyanobacterial inhabitation on Archean rock surfaces in the Pilbara Craton, Western Australia. *Astrobiology, 15*, 559–574.

Huang, W.-Y., & Meinschein, W. G. (1979). Sterols as ecological indicators. *Geochimica et Cosmochimica Acta, 43*, 739–745. doi:http://dx.doi.org/10.1016/0016-7037(79)90257-6

IEA. (2009). *World energy outlook 2008*. Paris, France: International Energy Agency.

IEA. (2012). *World energy outlook 2011*. Paris, France: International Energy Agency.

Jarvie, D. M. (2012). Shale resource systems for oil and gas. Chapter 1, Part 2—Shale-oil resource systems. In J. A. Breyer (Ed.), Shale reservoirs—Giant resources for the 21st century (pp. 89–119) AAPG Memoir 97. Tulsa, Ok: AAPG.

Jarvie, D. M., Hill, R. J., Ruble, T. E., & Pollastro, R. M. (2007). Unconventional shale–gas systems: The Mississippian Barnett Shale of north-central Texas as one model for thermogenic shale-gas assessment. *AAPG Bulletin, 91*, 475–499.

Jenner, S., & Lamadrid, A. J. (2013). Shale gas vs. coal: Policy implications from environmental impact comparisons of shale gas, conventional gas, and coal on air, water, and land in the United States. *Energy Policy, 53*, 442–453. doi:http://dx.doi.org/10.1016/j.enpol.2012.11.010

Jiang, C., Alexander, R., Kagi, R. I., & Murray, A. P. (1998). Polycyclic aromatic hydrocarbons in ancient sediments and their relationships to palaeoclimate. *Organic Geochemistry, 29*, 1721–1735. doi:http://dx.doi.org/10.1016/S0146-6380(98)00083-7

Kenig, F., Damsté, J. S. S., Kock-van Dalen, A., Rijpstra, W. I. C., Huc, A. Y., & de Leeuw, J. W. (1995). Occurrence and origin of mono-, di-, and trimethylalkanes in modern and Holocene cyanobacterial mats from Abu Dhabi, United Arab Emirates. *Geochimica et Cosmochimica Acta, 59*, 2999–3015.

Killops, S., & Massoud, M. (1992). Polycyclic aromatic hydrocarbons of pyrolytic origin in ancient sediments: Evidence for Jurassic vegetation fires. *Organic Geochemistry, 18*, 1–7.

Kinnaman, T. C. (2011). The economic impact of shale gas extraction: A review of existing studies. *Ecological Economics, 70*, 1243–1249.

Kissin, Y., Feulmer, G., & Payne, W. (1986). Gas chromatographic analysis of polymethyl-substituted alkanes. *Journal of Chromatographic Science, 24*, 164–169.

Klomp, U. (1986). The chemical structure of a pronounced series of isoalkanes in South Oman crudes. *Organic Geochemistry, 10*, 807–814.

Kodner, R. B., Pearson, A., Summons, R. E., & Knoll, A. H. (2008). Sterols in red and green algae: Quantification, phylogeny, and relevance for the interpretation of geologic steranes. *Geobiology, 6*, 411–420.

Leather, D. T. B., Bahadori, A., Nwaoha, C., & Wood, D. A. (2013). A review of Australia's natural gas resources and their exploitation. *Journal of Natural Gas Science and Engineering, 10*, 68–88. doi:http://dx.doi.org/10.1016/j.jngse.2012.09.003

Leitch, E. (1974). The geological development of the southern part of the New England Fold Belt. *Journal of the Geological Society of Australia, 21*, 133–156.

Moldowan, J. M., Seifert, W. K., & Gallegos, E. J. (1985). Relationship between petroleum composition and depositional environment of petroleum source rocks. *AAPG Bulletin, 69*, 1255–1268.

Moldowan, J. M., Sundararaman, P., & Schoell, M. (1986). Sensitivity of biomarker properties to depositional environment and/or source input in the Lower Toarcian of SW-Germany. *Organic Geochemistry, 10*, 915–926.

Montgomery, S. L., Jarvie, D. M., Bowker, K. A., & Pollastro, R. M. (2005). Mississippian Barnett Shale, Fort Worth basin, north-central Texas: Gas-shale play with multi–trillion cubic foot potential. *AAPG Bulletin, 89*, 155–175.

Moore, T., Horne, R., & Morrissey, J. (2014). Zero emission housing: Policy development in Australia and comparisons with the EU, UK, USA and California. *Environmental Innovation and Societal Transitions, 11*, 25–45. doi:http://dx.doi.org/10.1016/j.eist.2013.12.003

Nelson, D. R. (1978). Long-chain methyl-branched hydrocarbons: Occurrence, biosynthesis, and function. In M. J. Beament, J. E. Treherne, & V. B. Wigglesworth (Eds.), *Advances in Insect Physiology* (Volume 13, pp. 1–33). London, Elsevier Academic Press.

Othman, R., & Ward, C. (1999). Stratigraphic correlations in the southern Bowen and northern Gunnedah Basins, northern New South Wales. Paper presented at the *Proceedings of 33rd Newcastle Symposium on Advances in the Study of the Sydney Basin* (pp. 23–30). Newcastle, NSW: Department of Geology, University of Newcastle.

Ourisson, G., Albrecht, P., & Rohmer, M. (1984). Microbial origin of fossil fuels. *Scientific American, 251*, 44–51.

Peters, K. E., Walters, C. C., & Moldowan, J. M. (2005). *The biomarker guide* (2nd ed.). Cambridge; New York, UK: Cambridge University Press.

Powell, T. G., & McKirdy, D. M. (1973). Relationship between ratio of pristane to phytane, crude oil composition and geological environment in Australia. *Nature, 243*, 37–39.

Radke, M. (1988). Application of aromatic compounds as maturity indicators in source rocks and crude oils. *Marine and Petroleum Geology, 5*, 224–236.

Radke, M., & Welte, D. (1981). The methylphenanthrene index (MPI): A maturity parameter based on aromatic hydrocarbons. *Advances in Organic Geochemistry, 1983*, 504–512.

Radke, M., Welte, D. H., & Willsch, H. (1982). Geochemical study on a well in the Western Canada Basin: Relation of the aromatic distribution pattern to maturity of organic matter. *Geochimica et Cosmochimica Acta, 46*, 1–10.

Rogers, H. (2011). Shale gas—the unfolding story. *Oxford Review of Economic Policy, 27*, 117–143.

Seifert, K. W., & Moldowan, J. M. (1978). Applications of steranes, terpanes and monoaromatics to the maturation, migration and source of crude oils. *Geochimica et Cosmochimica Acta, 42*, 77–95.

Seifert, W. K., & Moldowan, J. M. (1979). The effect of biodegradation on steranes and terpanes in crude oils. *Geochimica et Cosmochimica Acta, 43*, 111–126.

Seifert, W., & Moldowan, J. (1986). Use of biological markers in petroleum exploration. *Methods in Geochemistry and Geophysics, 24*, 261–290.

Tan, Y. L., & Heit, M. (1981). Biogenic and abiogenic polynuclear aromatic hydrocarbons in sediments from two remote Adirondack lakes. *Geochimica et Cosmochimica Acta, 45*, 2267–2279.

ten Haven, H. L., de Leeuw, J. W., Rullkotter, J., & Damste, J. S. S. (1987). Restricted utility of the pristane/phytane ratio as a palaeoenvironmental indicator. *Nature, 330*, 641–643.

Voisey, A., & Williams, K. (1964). The geology of the Carroll–Keepit–Rangari area of New South Wales. *Journal and Proceedings of the Royal Society of New South Wales, 97*, 65–72.

Volkman, J. K. (1986). A review of sterol markers for marine and terrigenous organic matter. *Organic Geochemistry, 9*, 83–99.

Volkman, J. K. (2005). Sterols and other triterpenoids: Source specificity and evolution of biosynthetic pathways. *Organic Geochemistry, 36*, 139–159.

Wang, W., Zhou, Z. Y. & Yu, P. (2005). Relations Between Vitrinite Reflectance, Peek Temperature and its Neighboring Temperature Variation Rate: A Comparison of Methods. *Chinese Journal of Geophysics, 48*, 1443–1453.

Wójcik-Tabol, P., & Ślączka, A. (2015). Are Early Cretaceous environmental changes recorded in deposits of the Western part of the Silesian Nappe? A geochemical approach. *Palaeogeography, Palaeoclimatology, Palaeoecology, 417*, 293–308. doi:http://dx.doi.org/10.1016/j.palaeo.2014.10.040

Wood, D. A., Nwaoha, C., & Towler, B. F. (2012). Gas-to-liquids (GTL): A review of an industry offering several routes for monetizing natural gas. *Journal of Natural Gas Science and Engineering, 9*, 196–208. doi:http://dx.doi.org/10.1016/j.jngse.2012.07.001

Zhang, T., Ellis, G. S., Ruppel, S. C., Milliken, K., & Yang, R. (2012). Effect of organic-matter type and thermal maturity on methane adsorption in shale-gas systems. *Organic Geochemistry, 47*, 120–131.